

# Parameterization of Stillinger-Weber Potential for Two-Dimensional Atomic Crystals

Jin-Wu Jiang\* and Yu-Ping Zhou

*Shanghai Institute of Applied Mathematics and Mechanics,  
Shanghai Key Laboratory of Mechanics in Energy Engineering,  
Shanghai University, Shanghai 200072, People's Republic of China*

(Dated: December 14, 2024)

## Abstract

We parametrize the Stillinger-Weber potential for 131 two-dimensional atomic crystals. Parameters for the Stillinger-Weber potential are obtained from the valence force field model following the analytic approach (Nanotechnology **26**, 315706 (2015)), in which the valence force constants are determined by the phonon spectrum. The Stillinger-Weber potential is an efficient nonlinear interaction, and is applicable for numerical simulations of nonlinear physical or mechanical processes. The supplemental resources for all simulations in the present work are available online in Ref. 1, including a fortran code to generate crystals' structures, files for molecular dynamics simulations using LAMMPS, files for phonon calculations with the Stillinger-Weber potential using GULP, and files for phonon calculations with the valence force field model using GULP.

PACS numbers: 78.20.Bh, 63.22.-m, 62.25.-g

Keywords: Layered Crystal, Stillinger-Weber Potential, Molecular Dynamics Simulation, Empirical Potential

## I. INTRODUCTION

The atomic interaction is of essential importance in the numerical investigation of most physical or mechanical processes. The present work provides parameters for the Stillinger-Weber (SW) empirical potential for 131 two-dimensional atomic crystal (TDACs). In practical applications, these layered materials are usually played as lego on atomic scale to construct the van der Waals heterostructures with comprehensive properties.<sup>2</sup> The computational cost of *ab initio* for the heterostructure will be substantially increased as compared with one individual atomic layer, because the unit cell for the heterostructure is typically very large resulting from the mismatch of the lattice constants of different layered components. The empirical potential will be a competitive alternative to help out this difficult situation, considering their high efficiency.

In the early stage before 1980s, the computation ability of the scientific community was quite limited. At that time, the valence force field (VFF) model was one popular empirical potential for the description of the atomic interaction, since the VFF model is linear and can be applied in the analytic derivation of most elastic quantities.<sup>3</sup> In this model, each VFF term corresponds to a particular motion style in the crystal. Hence, each parameter in the VFF model usually has clear physical essence, which is beneficial for the parameterization of this model. For instance, the bond stretching term in the VFF model is directly related to the frequency of the longitudinal optical phonon modes, so the force constant of the bond stretching term can be determined from the frequencies of the longitudinal optical phonon modes. The VFF model can thus serve as the starting point for developing atomic empirical potentials for different crystals.

While the VFF model is beneficial for the fastest numerical simulation, its strong limitation is the absence of nonlinear effect. Due to this limitation, the VFF model is not applicable to nonlinear phenomena, for which other potential models with nonlinear components are required. Some representative potential models are (in the order of their simulation costs) SW potential,<sup>4</sup> Tersoff potential,<sup>5</sup> Brenner potential,<sup>6</sup> *ab initio* approaches, and etc. The SW potential is one of the simplest potential forms with nonlinear effects included. An advanced feature for the SW potential is that it includes the nonlinear effect, and keeps the numerical simulation at a very fast level.

Considering its distinct advantages, the present article aims at providing the SW potential

for 131 TDACs. We will determine parameters for the SW potential from the VFF model, following the analytic approach proposed by one of the present author (J.W.J).<sup>7</sup> The VFF constants are fitted to the phonon spectrum or the elastic properties in the TDACs.

In this paper, we parametrize the SW potential for 131 TDACs. All structures discussed in the present work are listed in Tables I, II, III, IV, V, VI, VII, VIII, and IX. The supplemental materials are freely available online in Ref. 1, including a fortran code to generate crystals' structures, files for molecular dynamics simulations using LAMMPS, files for phonon calculations with the SW potential using GULP, and files for phonon calculations with the valence force field model using GULP.

TABLE I: 1H-MX<sub>2</sub>, with M as the transition metal and X as oxygen or dichalcogenide. The structure is shown in Fig. 1.

1H-ScO <sub>2</sub>	1H-ScS <sub>2</sub>	1H-ScSe <sub>2</sub>	1H-ScTe <sub>2</sub>	1H-TiTe <sub>2</sub>	1H-VO <sub>2</sub>	1H-VS <sub>2</sub>	1H-VSe <sub>2</sub>	1H-VTe <sub>2</sub>
1H-CrO <sub>2</sub>	1H-CrS <sub>2</sub>	1H-CrSe <sub>2</sub>	1H-CrTe <sub>2</sub>	1H-MnO <sub>2</sub>	1H-FeO <sub>2</sub>	1H-FeS <sub>2</sub>	1H-FeSe <sub>2</sub>	1H-FeTe <sub>2</sub>
1H-CoTe <sub>2</sub>	1H-NiS <sub>2</sub>	1H-NiSe <sub>2</sub>	1H-NiTe <sub>2</sub>	1H-NbS <sub>2</sub>	1H-NbSe <sub>2</sub>	1H-MoO <sub>2</sub>	1H-MoS <sub>2</sub>	1H-MoSe <sub>2</sub>
1H-MoTe <sub>2</sub>	1H-TaS <sub>2</sub>	1H-TaSe <sub>2</sub>	1H-WO <sub>2</sub>	1H-WS <sub>2</sub>	1H-WSe <sub>2</sub>	1H-WTe <sub>2</sub>		

TABLE II: 1T-MX<sub>2</sub>, with M as the transition metal and X as oxygen or dichalcogenide. The structure is shown in Fig. 71.

1T-ScO <sub>2</sub>	1T-ScS <sub>2</sub>	1T-ScSe <sub>2</sub>	1T-ScTe <sub>2</sub>	1T-TiS <sub>2</sub>	1T-TiSe <sub>2</sub>	1T-TiTe <sub>2</sub>	1T-VS <sub>2</sub>	1T-VSe <sub>2</sub>
1T-VTe <sub>2</sub>	1T-MnO <sub>2</sub>	1T-MnS <sub>2</sub>	1T-MnSe <sub>2</sub>	1T-MnTe <sub>2</sub>	1T-CoTe <sub>2</sub>	1T-NiO <sub>2</sub>	1T-NiS <sub>2</sub>	1T-NiSe <sub>2</sub>
1T-NiTe <sub>2</sub>	1T-ZrS <sub>2</sub>	1T-ZrSe <sub>2</sub>	1T-ZrTe <sub>2</sub>	1T-NbS <sub>2</sub>	1T-NbSe <sub>2</sub>	1T-NbTe <sub>2</sub>	1T-MoS <sub>2</sub>	1T-MoSe <sub>2</sub>
1T-MoTe <sub>2</sub>	1T-TcS <sub>2</sub>	1T-TcSe <sub>2</sub>	1T-TcTe <sub>2</sub>	1T-RhTe <sub>2</sub>	1T-PdS <sub>2</sub>	1T-PdSe <sub>2</sub>	1T-PdTe <sub>2</sub>	1T-SnS <sub>2</sub>
1T-SnSe <sub>2</sub>	1T-HfS <sub>2</sub>	1T-HfSe <sub>2</sub>	1T-HfTe <sub>2</sub>	1T-TaS <sub>2</sub>	1T-TaSe <sub>2</sub>	1T-TaTe <sub>2</sub>	1T-WS <sub>2</sub>	1T-WSe <sub>2</sub>
1T-WTe <sub>2</sub>	1T-ReS <sub>2</sub>	1T-ReSe <sub>2</sub>	1T-ReTe <sub>2</sub>	1T-IrTe <sub>2</sub>	1T-PtS <sub>2</sub>	1T-PtSe <sub>2</sub>	1T-PtTe <sub>2</sub>	

TABLE III: Puckered (p-) M, with M from group V. The structure is shown in Fig. 178 or Fig. 183.

black phosphorus	p-arsenene	p-antimonene	p-bismuthene
------------------	------------	--------------	--------------

TABLE IV: Puckered MX, with M from group IV and X from group VI. The structure is shown in Fig. 189.

p-SiTe	p-GeS	p-GeSe	p-SnS	p-SnSe
--------	-------	--------	-------	--------

TABLE V: Buckled (b-) M, with M from group IV or V. The structure is shown in Fig. 201.

silicene	germanene	stanene	indiene
blue phosphorus	b-arsenene	b-antimonene	b-bismuthene

## II. VFF MODEL AND SW POTENTIAL

### A. VFF model

The VFF model is one of the most widely used linear model for the description of atomic interactions.<sup>3</sup> The bond stretching and the angle bending are two typical motion styles for most covalent bonding materials. The bond stretching describes the energy variation for a bond due to a bond variation  $\Delta r = r - r_0$ , with  $r_0$  as the initial bond length. The angle bending gives the energy increment for an angle resulting from an angle variation  $\Delta\theta = \theta - \theta_0$ , with  $\theta_0$  as the initial angle. In the VFF model, the energy variations for the bond stretching and the angle bending are described by the following quadratic forms,

$$V_r = \frac{1}{2}K_r (\Delta r)^2, \quad (1)$$

$$V_\theta = \frac{1}{2}K_\theta (\Delta\theta)^2, \quad (2)$$

where  $K_r$  and  $K_\theta$  are two force constant parameters. These two potential expressions in Eqs. (1) and (2) are directly related to the optical phonon modes in the crystal. Hence, their force constant parameters  $K_r$  and  $K_\theta$  are usually determined by fitting to the phonon dispersion.

TABLE VI: Buckled MX, with M from group IV and X from group VI. The structure is shown in Fig. 218.

b-SiTe
--------

TABLE VII: Buckled MX, with both M and X from group IV, or M from group III and X from group V. The structure is shown in Fig. 218.

b-SnGe	b-SiGe	b-SnSi	b-InP	b-InAs	b-InSb	b-GaAs	b-GaP	b-AlSb
--------	--------	--------	-------	--------	--------	--------	-------	--------

TABLE VIII: Bi-buckled MX, with M from group III and X from group VI. The structure is shown in Fig. 239.

BO	AlO	GaO	InO
BS	AlS	GaS	InS
BSe	AlSe	GaSe	InSe
BTe	AlTe	GaTe	InTe

## B. SW potential

In the SW potential, energy increments for the bond stretching and angle bending are described by the following two-body and three-body forms,

$$V_2(r_{ij}) = A(B/r_{ij} - 1)e^{\rho/(r_{ij}-r_{max})}, \quad (3)$$

$$V_3(\theta_{ijk}) = Ke^{[\rho_1/(r_{ij}-r_{max12})+\rho_2/(r_{ik}-r_{max13})]}(\cos\theta_{ijk} - \cos\theta_0)^2 \quad (4)$$

where  $V_2$  corresponds to the bond stretching and  $V_3$  associates with the angle bending. The cut-offs  $r_{max}$ ,  $r_{max12}$  and  $r_{max13}$  are geometrically determined by the material's structure. There are five unknown geometrical parameters, i.e.,  $\rho$  and  $B$  in the two-body  $V_2$  term and  $\rho_1$ ,  $\rho_2$ , and  $\theta_0$  in the three-body  $V_3$  term, and two energy parameters  $A$  and  $K$ . There is a constraint among these parameters due to the equilibrium condition,<sup>7</sup>

$$\rho = \frac{-4B(d - r_{max})^2}{(Bd - d^5)}, \quad (5)$$

where  $d$  is the equilibrium bond length from experiments. Eq. (5) ensures that the bond has an equilibrium length of  $d$  and the  $V_2$  interaction for this bond is at the energy minimum state at the equilibrium configuration.

TABLE IX: Others.

borophene
-----------

The energy parameters  $A$  and  $K$  in the SW potential can be analytically derived from the VFF model as follows,

$$A = \frac{K_r}{\alpha e^{\rho/(d-r_{max})}}, \quad (6)$$

$$K = \frac{K_\theta}{2 \sin^2 \theta_0 e^{\rho_1/(d_1-r_{max12})+\rho_2/(d_2-r_{max13})}}, \quad (7)$$

where the coefficient  $\alpha$  in Eq. (6) is,

$$\begin{aligned} \alpha = & \left[ \frac{\rho}{(d-r_{max})^2} \right]^2 (B/d^4 - 1) \\ & + \left[ \frac{2\rho}{(d-r_{max})^3} \right] (B/d^4 - 1) \\ & + \left[ \frac{\rho}{(d-r_{max})^2} \right] \left( \frac{8B}{d^5} \right) + \left( \frac{20B}{d^6} \right). \end{aligned} \quad (8)$$

In some situations, the SW potential is also written into the following form,

$$V_2(r_{ij}) = \epsilon A_L \left( B_L \sigma^p r_{ij}^{-p} - \sigma^q r_{ij}^{-q} \right) e^{[\sigma/(r_{ij}-a\sigma)]}, \quad (9)$$

$$\begin{aligned} V_3(\theta_{ijk}) = & \epsilon \lambda e^{[\gamma\sigma/(r_{ij}-a\sigma)+\gamma\sigma/(r_{jk}-a\sigma)]} \\ & (\cos \theta_{ijk} - \cos \theta_0)^2. \end{aligned} \quad (10)$$

The parameters here can be determined by comparing the SW potential forms in Eqs. (9) and (10) with Eqs. (3) and (4). It is obvious that  $p = 4$  and  $q = 0$ . Eqs. (9) and (10) have two more parameters than Eqs. (3) and (4), so we can set  $\epsilon = 1.0$  eV and  $\gamma = 1.0$ . The other parameters in Eqs. (9) and (10) are related to these parameters in Eqs. (3) and (4) by the following equations

$$A_L = A, \quad (11)$$

$$\sigma = \rho, \quad (12)$$

$$B_L = B/\rho^4, \quad (13)$$

$$a = r_{max}/\rho, \quad (14)$$

$$\lambda = K. \quad (15)$$

The SW potential is implemented in GULP using Eqs. (3) and (4). The SW potential is implemented in LAMMPS using Eqs. (9) and (10).

In the rest of this article, we will develop the VFF model and the SW potential for layered crystals. The VFF model will be developed by fitting to the phonon dispersion from

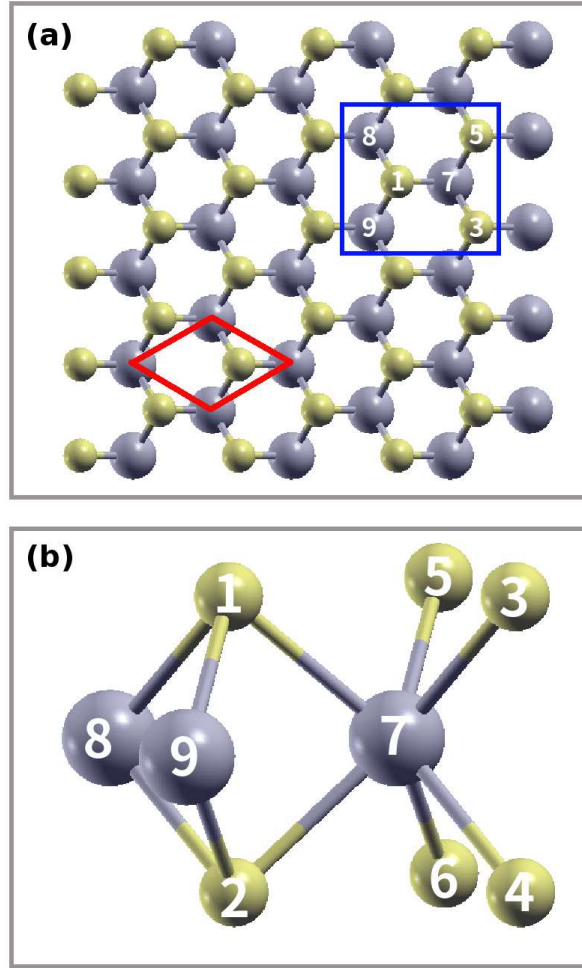


FIG. 1: (Color online) Configuration of the 1H-MX<sub>2</sub> in the 1H phase. (a) Top view. The unit cell is highlighted by a red parallelogram. (b) Enlarged view of atoms in the blue box in (a). Each M atom is surrounded by six X atoms, which are categorized into the top and bottom groups. Atoms X 1, 3, and 5 are from the top group, while atoms X 2, 4, and 6 are from the bottom group. M atoms are represented by larger gray balls. X atoms are represented by smaller yellow balls.

experiments or first-principles calculations. The SW potential will be developed following the above analytic parameterization approach. In this work, GULP<sup>8</sup> is used for the calculation of phonon dispersion and the fitting process, while LAMMPS<sup>9</sup> is used for molecular dynamics simulations. The OVITO<sup>10</sup> and XCRYSDEN<sup>11</sup> packages are used for visualization. All simulation scripts for GULP and LAMMPS are available online in Ref. 1.

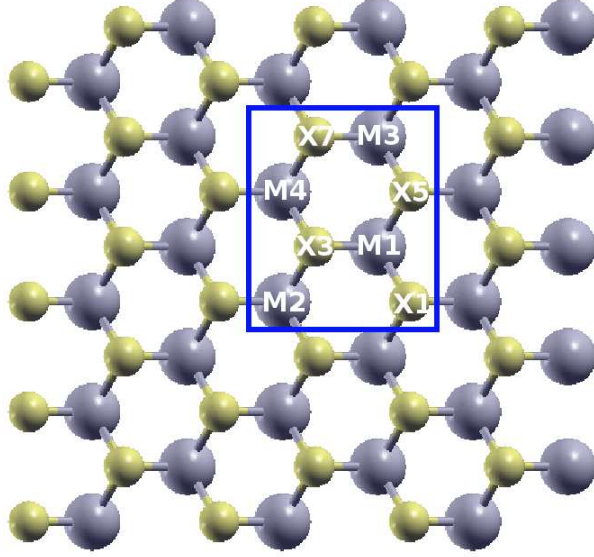


FIG. 2: (Color online) Twelve atom types are introduced to distinguish angles around each M atom for the single-layer 1H-MX<sub>2</sub>. Atoms X<sub>1</sub>, X<sub>3</sub>, X<sub>5</sub>, and X<sub>7</sub> are from the top layer. The other four atoms X<sub>2</sub>, X<sub>4</sub>, X<sub>6</sub>, and X<sub>8</sub> are from the bottom layer, which are not displayed in the figure.

TABLE X: The VFF model for single-layer 1H-ScO<sub>2</sub>. The second line gives an explicit expression for each VFF term. The third line is the force constant parameters. Parameters are in the unit of  $\frac{eV}{\text{\AA}^2}$  for the bond stretching interactions, and in the unit of eV for the angle bending interaction. The fourth line gives the initial bond length (in unit of  $\text{\AA}$ ) for the bond stretching interaction and the initial angle (in unit of degrees) for the angle bending interaction. The angle  $\theta_{ijk}$  has atom *i* as the apex.

VFF type	bond stretching		angle bending	
expression	$\frac{1}{2}K_{\text{Sc-O}}(\Delta r)^2$	$\frac{1}{2}K_{\text{Sc-O-O}}(\Delta\theta)^2$	$\frac{1}{2}K_{\text{Sc-O-O}'}(\Delta\theta)^2$	$\frac{1}{2}K_{\text{O-Sc-Sc}}(\Delta\theta)^2$
parameter	9.417	4.825	4.825	4.825
$r_0$ or $\theta_0$	2.090	98.222	58.398	98.222

### III. 1H-SCO<sub>2</sub>

Most existing theoretical studies on the single-layer 1H-ScO<sub>2</sub> are based on the first-principles calculations. In this section, we will develop the SW potential for the single-layer 1H-ScO<sub>2</sub>.

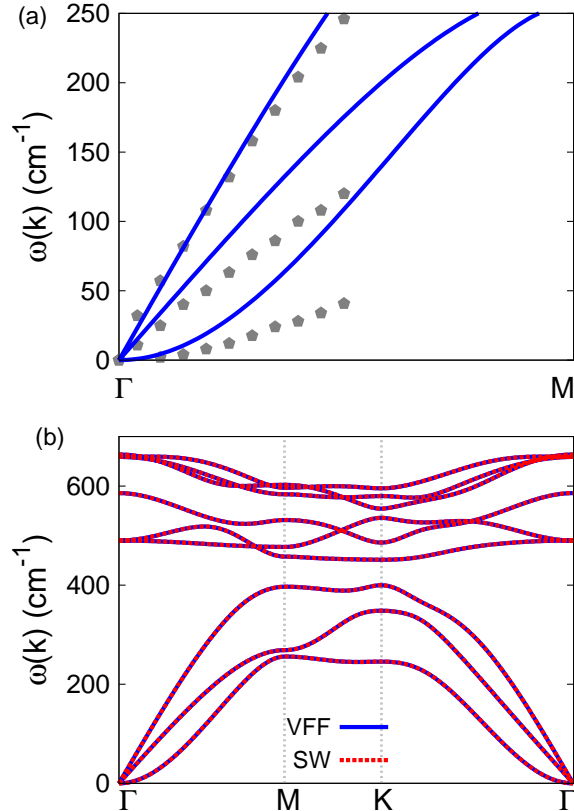


FIG. 3: (Color online) Phonon spectrum for single-layer 1H-ScO<sub>2</sub>. (a) Phonon dispersion along the  $\Gamma$ M direction in the Brillouin zone. The results from the VFF model (lines) are comparable with the *ab initio* results (pentagons) from Ref. 12. (b) The phonon dispersion from the SW potential is exactly the same as that from the VFF model.

TABLE XI: Two-body SW potential parameters for single-layer 1H-ScO<sub>2</sub> used by GULP<sup>8</sup> as expressed in Eq. (3).

	$A$ (eV)	$\rho$ ( $\text{\AA}$ )	$B$ ( $\text{\AA}^4$ )	$r_{\min}$ ( $\text{\AA}$ )	$r_{\max}$ ( $\text{\AA}$ )
Sc-O	7.506	1.380	9.540	0.0	2.939

The structure for the single-layer 1H-ScO<sub>2</sub> is shown in Fig. 1 (with M=Sc and X=O). Each Sc atom is surrounded by six O atoms. These O atoms are categorized into the top group (eg. atoms 1, 3, and 5) and bottom group (eg. atoms 2, 4, and 6). Each O atom is connected to three Sc atoms. The structural parameters are from the first-principles calculations,<sup>12</sup> including the lattice constant  $a = 3.16 \text{ \AA}$ , and the bond length  $d_{\text{Sc-O}} = 2.09 \text{ \AA}$ . The resultant

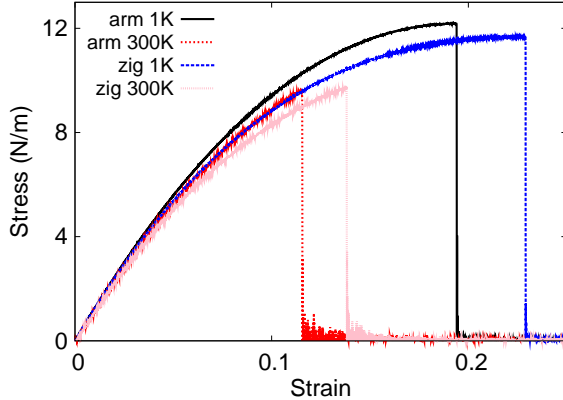


FIG. 4: (Color online) Stress-strain for single-layer 1H-ScO<sub>2</sub> of dimension 100 × 100 Å along the armchair and zigzag directions.

TABLE XII: Three-body SW potential parameters for single-layer 1H-ScO<sub>2</sub> used by GULP<sup>8</sup> as expressed in Eq. (4). The angle  $\theta_{ijk}$  in the first line indicates the bending energy for the angle with atom  $i$  as the apex.

	$K$ (eV)	$\theta_0$ (degree)	$\rho_1$ (Å)	$\rho_2$ (Å)	$r_{\min 12}$ (Å)	$r_{\max 12}$ (Å)	$r_{\min 13}$ (Å)	$r_{\max 13}$ (Å)	$r_{\min 23}$ (Å)	$r_{\max 23}$ (Å)
$\theta_{\text{Sc-O-O}}$	63.576	98.222	1.380	1.380	0.0	2.939	0.0	2.939	0.0	3.460
$\theta_{\text{Sc-O-O}'}$	85.850	58.398	1.380	1.380	0.0	2.939	0.0	2.939	0.0	3.460
$\theta_{\text{O-Sc-Sc}}$	63.576	98.222	1.380	1.380	0.0	2.939	0.0	2.939	0.0	3.460

angles are  $\theta_{\text{ScOO}} = \theta_{\text{OScSc}} = 98.222^\circ$  and  $\theta_{\text{ScOO}'} = 58.398^\circ$ , in which atoms O and O' are from different (top or bottom) group.

Table X shows four VFF terms for the single-layer 1H-ScO<sub>2</sub>, one of which is the bond stretching interaction shown by Eq. (1) while the other three terms are the angle bending interaction shown by Eq. (2). These force constant parameters are determined by fitting to the acoustic branches in the phonon dispersion along  $\Gamma\text{M}$  as shown in Fig. 3 (a). The *ab initio* calculations for the phonon dispersion are from Ref. 12. Fig. 3 (b) shows that the VFF model and the SW potential give exactly the same phonon dispersion, as the SW potential is derived from the VFF model.

The parameters for the two-body SW potential used by GULP are shown in Tab. XI. The parameters for the three-body SW potential used by GULP are shown in Tab. XII. Some representative parameters for the SW potential used by LAMMPS are listed in Tab. XIII.

TABLE XIII: SW potential parameters for single-layer 1H-ScO<sub>2</sub> used by LAMMPS<sup>9</sup> as expressed in Eqs. (9) and (10).

	$\epsilon$ (eV)	$\sigma$ (Å)	$a$	$\lambda$	$\gamma$	$\cos\theta_0$	$A_L$	$B_L$	$p$	$q$	tol
Sc <sub>1</sub> -O <sub>1</sub> -O <sub>1</sub>	1.000	1.380	2.129	0.000	1.000	0.000	7.506	2.627	4	0	0.0
Sc <sub>1</sub> -O <sub>1</sub> -O <sub>3</sub>	1.000	0.000	0.000	63.576	1.000	-0.143	0.000	0.000	4	0	0.0
Sc <sub>1</sub> -O <sub>1</sub> -O <sub>2</sub>	1.000	0.000	0.000	85.850	1.000	0.524	0.000	0.000	4	0	0.0
O <sub>1</sub> -Sc <sub>1</sub> -Sc <sub>3</sub>	1.000	0.000	0.000	63.576	1.000	-0.143	0.000	0.000	4	0	0.0

We note that twelve atom types have been introduced for the simulation of the single-layer 1H-ScO<sub>2</sub> using LAMMPS, because the angles around atom Sc in Fig. 1 (with M=Sc and X=O) are not distinguishable in LAMMPS. We have suggested two options to differentiate these angles by implementing some additional constraints in LAMMPS, which can be accomplished by modifying the source file of LAMMPS.<sup>13,14</sup> According to our experience, it is not so convenient for some users to implement these constraints and recompile the LAMMPS package. Hence, in the present work, we differentiate the angles by introducing more atom types, so it is not necessary to modify the LAMMPS package. Fig. 2 (with M=Sc and X=O) shows that, for 1H-ScO<sub>2</sub>, we can differentiate these angles around the Sc atom by assigning these six neighboring O atoms with different atom types. It can be found that twelve atom types are necessary for the purpose of differentiating all six neighbors around one Sc atom.

We use LAMMPS to perform MD simulations for the mechanical behavior of the single-layer 1H-ScO<sub>2</sub> under uniaxial tension at 1.0 K and 300.0 K. Fig. 4 shows the stress-strain curve for the tension of a single-layer 1H-ScO<sub>2</sub> of dimension  $100 \times 100$  Å. Periodic boundary conditions are applied in both armchair and zigzag directions. The single-layer 1H-ScO<sub>2</sub> is stretched uniaxially along the armchair or zigzag direction. The stress is calculated without involving the actual thickness of the quasi-two-dimensional structure of the single-layer 1H-ScO<sub>2</sub>. The Young's modulus can be obtained by a linear fitting of the stress-strain relation in the small strain range of [0, 0.01]. The Young's modulus are 126.3 N/m and 125.4 N/m along the armchair and zigzag directions, respectively. The Young's modulus is essentially isotropic in the armchair and zigzag directions. The Poisson's ratio from the VFF model and the SW potential is  $\nu_{xy} = \nu_{yx} = 0.16$ .

There is no available value for nonlinear quantities in the single-layer 1H-ScO<sub>2</sub>. We have

TABLE XIV: The VFF model for single-layer 1H-ScS<sub>2</sub>. The second line gives an explicit expression for each VFF term. The third line is the force constant parameters. Parameters are in the unit of  $\frac{\text{eV}}{\text{\AA}^2}$  for the bond stretching interactions, and in the unit of eV for the angle bending interaction. The fourth line gives the initial bond length (in unit of  $\text{\AA}$ ) for the bond stretching interaction and the initial angle (in unit of degrees) for the angle bending interaction. The angle  $\theta_{ijk}$  has atom  $i$  as the apex.

VFF type	bond stretching		angle bending	
expression	$\frac{1}{2}K_{\text{Sc-S}}(\Delta r)^2$	$\frac{1}{2}K_{\text{Sc-S-S}}(\Delta\theta)^2$	$\frac{1}{2}K_{\text{Sc-S-S}'}(\Delta\theta)^2$	$\frac{1}{2}K_{\text{S-Sc-S}}(\Delta\theta)^2$
parameter	5.192	2.027	2.027	2.027
$r_0$ or $\theta_0$	2.520	94.467	64.076	94.467

TABLE XV: Two-body SW potential parameters for single-layer 1H-ScS<sub>2</sub> used by GULP<sup>8</sup> as expressed in Eq. (3).

	$A$ (eV)	$\rho$ ( $\text{\AA}$ )	$B$ ( $\text{\AA}^4$ )	$r_{\text{min}}$ ( $\text{\AA}$ )	$r_{\text{max}}$ ( $\text{\AA}$ )
Sc-S	5.505	1.519	20.164	0.0	3.498

thus used the nonlinear parameter  $B = 0.5d^4$  in Eq. (5), which is close to the value of  $B$  in most materials. The value of the third order nonlinear elasticity  $D$  can be extracted by fitting the stress-strain relation to the function  $\sigma = E\epsilon + \frac{1}{2}D\epsilon^2$  with  $E$  as the Young's modulus. The values of  $D$  from the present SW potential are -652.8 N/m and -683.3 N/m along the armchair and zigzag directions, respectively. The ultimate stress is about  $12.2 \text{ Nm}^{-1}$  at the ultimate strain of 0.19 in the armchair direction at the low temperature of 1 K. The ultimate stress is about  $11.7 \text{ Nm}^{-1}$  at the ultimate strain of 0.23 in the zigzag direction at the low temperature of 1 K.

#### IV. 1H-SCS<sub>2</sub>

Most existing theoretical studies on the single-layer 1H-ScS<sub>2</sub> are based on the first-principles calculations. In this section, we will develop the SW potential for the single-layer 1H-ScS<sub>2</sub>.

The structure for the single-layer 1H-ScS<sub>2</sub> is shown in Fig. 1 (with M=Sc and X=S). Each

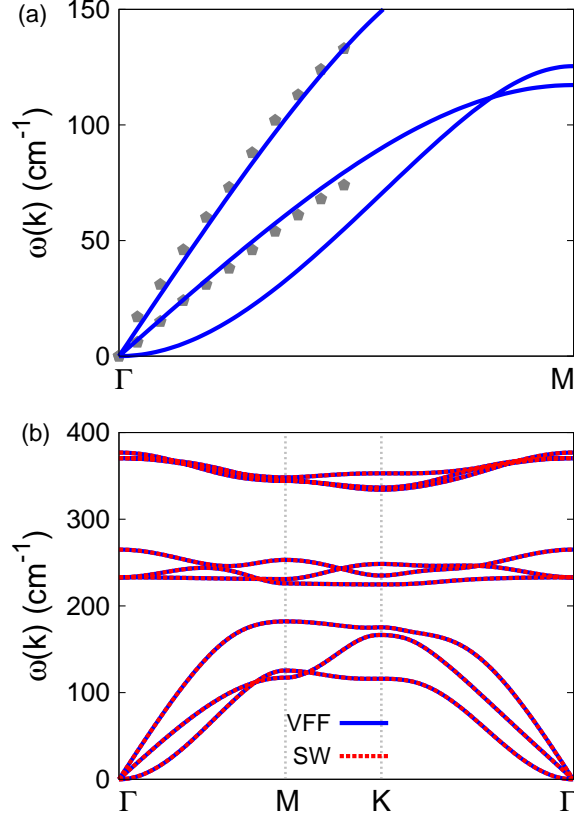


FIG. 5: (Color online) Phonon spectrum for single-layer 1H-ScS<sub>2</sub>. (a) Phonon dispersion along the  $\Gamma$ M direction in the Brillouin zone. The results from the VFF model (lines) are comparable with the *ab initio* results (pentagons) from Ref. 12. (b) The phonon dispersion from the SW potential is exactly the same as that from the VFF model.

Sc atom is surrounded by six S atoms. These S atoms are categorized into the top group (eg. atoms 1, 3, and 5) and bottom group (eg. atoms 2, 4, and 6). Each S atom is connected to three Sc atoms. The structural parameters are from the first-principles calculations,<sup>12</sup> including the lattice constant  $a = 3.70 \text{ \AA}$ , and the bond length  $d_{\text{Sc-S}} = 2.52 \text{ \AA}$ . The resultant angles are  $\theta_{\text{ScSS}} = \theta_{\text{SScSc}} = 94.467^\circ$  and  $\theta_{\text{ScSS}'} = 64.076^\circ$ , in which atoms S and S' are from different (top or bottom) group.

Table XIV shows four VFF terms for the single-layer 1H-ScS<sub>2</sub>, one of which is the bond stretching interaction shown by Eq. (1) while the other three terms are the angle bending interaction shown by Eq. (2). These force constant parameters are determined by fitting to the acoustic branches in the phonon dispersion along the  $\Gamma$ M as shown in Fig. 5 (a). The *ab*

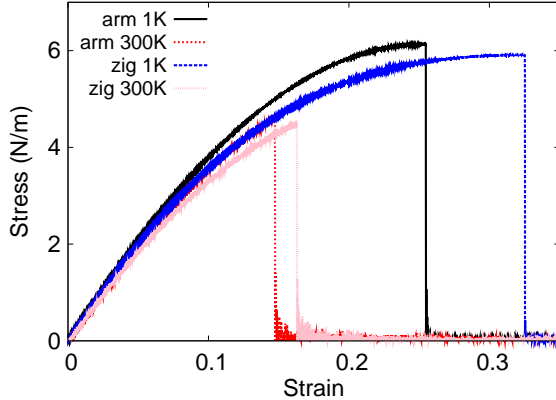


FIG. 6: (Color online) Stress-strain for single-layer 1H-ScS<sub>2</sub> of dimension  $100 \times 100 \text{ \AA}$  along the armchair and zigzag directions.

TABLE XVI: Three-body SW potential parameters for single-layer 1H-ScS<sub>2</sub> used by GULP<sup>8</sup> as expressed in Eq. (4). The angle  $\theta_{ijk}$  in the first line indicates the bending energy for the angle with atom  $i$  as the apex.

	$K$ (eV)	$\theta_0$ (degree)	$\rho_1$ (Å)	$\rho_2$ (Å)	$r_{\min 12}$ (Å)	$r_{\max 12}$ (Å)	$r_{\min 13}$ (Å)	$r_{\max 13}$ (Å)	$r_{\min 23}$ (Å)	$r_{\max 23}$ (Å)
$\theta_{\text{Sc-S-S}}$	22.768	94.467	1.519	1.519	0.0	3.498	0.0	3.498	0.0	4.132
$\theta_{\text{Sc-S-S}'}$	27.977	64.076	1.519	1.519	0.0	3.498	0.0	3.498	0.0	4.132
$\theta_{\text{S-Sc-Sc}}$	22.768	94.467	1.519	1.519	0.0	3.498	0.0	3.498	0.0	4.132

*initio* calculations for the phonon dispersion are from Ref. 12. Fig. 5 (b) shows that the VFF model and the SW potential give exactly the same phonon dispersion, as the SW potential is derived from the VFF model.

The parameters for the two-body SW potential used by GULP are shown in Tab. XV. The parameters for the three-body SW potential used by GULP are shown in Tab. XVI. Some representative parameters for the SW potential used by LAMMPS are listed in Tab. XVII. We note that twelve atom types have been introduced for the simulation of the single-layer 1H-ScS<sub>2</sub> using LAMMPS, because the angles around atom Sc in Fig. 1 (with M=Sc and X=S) are not distinguishable in LAMMPS. We have suggested two options to differentiate these angles by implementing some additional constraints in LAMMPS, which can be accomplished by modifying the source file of LAMMPS.<sup>13,14</sup> According to our experience, it is not so convenient for some users to implement these constraints and recompile the LAMMPS

TABLE XVII: SW potential parameters for single-layer 1H-ScS<sub>2</sub> used by LAMMPS<sup>9</sup> as expressed in Eqs. (9) and (10).

	$\epsilon$ (eV)	$\sigma$ (Å)	$a$	$\lambda$	$\gamma$	$\cos \theta_0$	$A_L$	$B_L$	$p$	$q$	tol
Sc <sub>1</sub> -S <sub>1</sub> -S <sub>1</sub>	1.000	1.519	2.303	0.000	1.000	0.000	5.505	3.784	4	0	0.0
Sc <sub>1</sub> -S <sub>1</sub> -S <sub>3</sub>	1.000	0.000	0.000	22.768	1.000	-0.078	0.000	0.000	4	0	0.0
Sc <sub>1</sub> -S <sub>1</sub> -S <sub>2</sub>	1.000	0.000	0.000	27.977	1.000	0.437	0.000	0.000	4	0	0.0
S <sub>1</sub> -Sc <sub>1</sub> -Sc <sub>3</sub>	1.000	0.000	0.000	22.768	1.000	-0.078	0.000	0.000	4	0	0.0

package. Hence, in the present work, we differentiate the angles by introducing more atom types, so it is not necessary to modify the LAMMPS package. Fig. 2 (with M=Sc and X=S) shows that, for 1H-ScS<sub>2</sub>, we can differentiate these angles around the Sc atom by assigning these six neighboring S atoms with different atom types. It can be found that twelve atom types are necessary for the purpose of differentiating all six neighbors around one Sc atom.

We use LAMMPS to perform MD simulations for the mechanical behavior of the single-layer 1H-ScS<sub>2</sub> under uniaxial tension at 1.0 K and 300.0 K. Fig. 6 shows the stress-strain curve for the tension of a single-layer 1H-ScS<sub>2</sub> of dimension  $100 \times 100$  Å. Periodic boundary conditions are applied in both armchair and zigzag directions. The single-layer 1H-ScS<sub>2</sub> is stretched uniaxially along the armchair or zigzag direction. The stress is calculated without involving the actual thickness of the quasi-two-dimensional structure of the single-layer 1H-ScS<sub>2</sub>. The Young's modulus can be obtained by a linear fitting of the stress-strain relation in the small strain range of  $[0, 0.01]$ . The Young's modulus are 43.8 N/m and 43.2 N/m along the armchair and zigzag directions, respectively. The Young's modulus is essentially isotropic in the armchair and zigzag directions. The Poisson's ratio from the VFF model and the SW potential is  $\nu_{xy} = \nu_{yx} = 0.30$ .

There is no available value for nonlinear quantities in the single-layer 1H-ScS<sub>2</sub>. We have thus used the nonlinear parameter  $B = 0.5d^4$  in Eq. (5), which is close to the value of  $B$  in most materials. The value of the third order nonlinear elasticity  $D$  can be extracted by fitting the stress-strain relation to the function  $\sigma = E\epsilon + \frac{1}{2}D\epsilon^2$  with  $E$  as the Young's modulus. The values of  $D$  from the present SW potential are -146.9 N/m and -159.1 N/m along the armchair and zigzag directions, respectively. The ultimate stress is about  $6.1 \text{ Nm}^{-1}$  at the ultimate strain of 0.25 in the armchair direction at the low temperature of 1 K. The

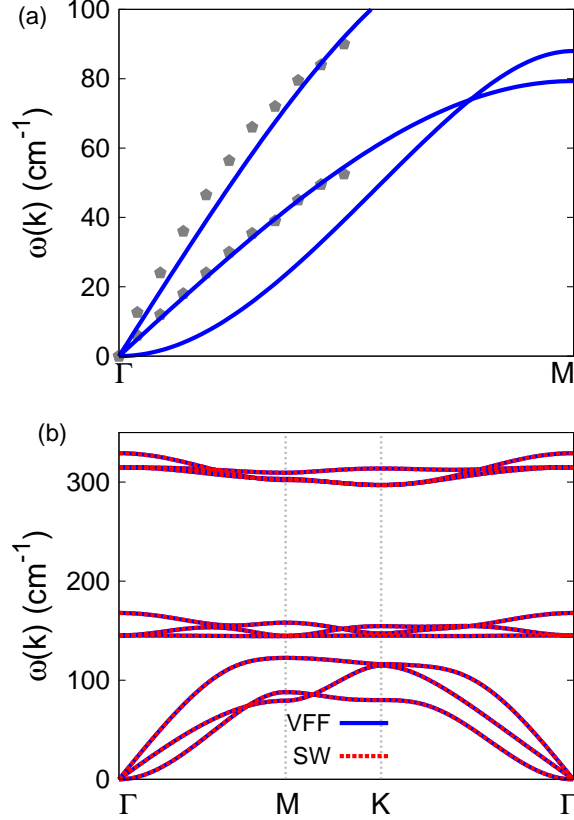


FIG. 7: (Color online) Phonon spectrum for single-layer 1H-ScSe<sub>2</sub>. (a) Phonon dispersion along the  $\Gamma$ M direction in the Brillouin zone. The results from the VFF model (lines) are comparable with the *ab initio* results (pentagons) from Ref. 12. (b) The phonon dispersion from the SW potential is exactly the same as that from the VFF model.

ultimate stress is about  $5.9 \text{ Nm}^{-1}$  at the ultimate strain of 0.32 in the zigzag direction at the low temperature of 1 K.

## V. 1H-SCSE<sub>2</sub>

Most existing theoretical studies on the single-layer 1H-ScSe<sub>2</sub> are based on the first-principles calculations. In this section, we will develop the SW potential for the single-layer 1H-ScSe<sub>2</sub>.

The structure for the single-layer 1H-ScSe<sub>2</sub> is shown in Fig. 1 (with M=Sc and X=Se). Each Sc atom is surrounded by six Se atoms. These Se atoms are categorized into the

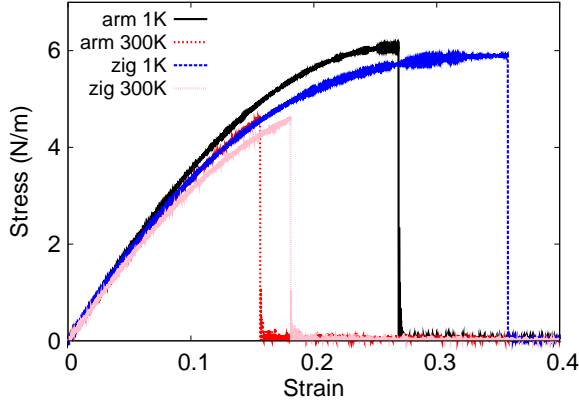


FIG. 8: (Color online) Stress-strain for single-layer 1H-ScSe<sub>2</sub> of dimension  $100 \times 100 \text{ \AA}$  along the armchair and zigzag directions.

TABLE XVIII: The VFF model for single-layer 1H-ScSe<sub>2</sub>. The second line gives an explicit expression for each VFF term. The third line is the force constant parameters. Parameters are in the unit of  $\frac{eV}{\text{\AA}^2}$  for the bond stretching interactions, and in the unit of eV for the angle bending interaction. The fourth line gives the initial bond length (in unit of  $\text{\AA}$ ) for the bond stretching interaction and the initial angle (in unit of degrees) for the angle bending interaction. The angle  $\theta_{ijk}$  has atom  $i$  as the apex.

VFF type	bond stretching	angle bending		
expression	$\frac{1}{2}K_{\text{Sc-Se}}(\Delta r)^2$	$\frac{1}{2}K_{\text{Sc-Se-Se}}(\Delta\theta)^2$	$\frac{1}{2}K_{\text{Sc-Se-Se'}}(\Delta\theta)^2$	$\frac{1}{2}K_{\text{Se-Sc-Sc}}(\Delta\theta)^2$
parameter	5.192	2.027	2.027	2.027
$r_0$ or $\theta_0$	2.650	92.859	66.432	92.859

top group (eg. atoms 1, 3, and 5) and bottom group (eg. atoms 2, 4, and 6). Each Se atom is connected to three Sc atoms. The structural parameters are from the first-principles calculations,<sup>12</sup> including the lattice constant  $a = 3.84 \text{ \AA}$ , and the bond length  $d_{\text{Sc-Se}} = 2.65 \text{ \AA}$ . The resultant angles are  $\theta_{\text{ScSeSe}} = \theta_{\text{SeScSc}} = 92.859^\circ$  and  $\theta_{\text{ScSeSe'}} = 66.432^\circ$ , in which atoms Se and Se' are from different (top or bottom) group.

Table XVIII shows four VFF terms for the single-layer 1H-ScSe<sub>2</sub>, one of which is the bond stretching interaction shown by Eq. (1) while the other three terms are the angle bending interaction shown by Eq. (2). These force constant parameters are determined by fitting to

TABLE XIX: Two-body SW potential parameters for single-layer 1H-ScSe<sub>2</sub> used by GULP<sup>8</sup> as expressed in Eq. (3).

	$A$ (eV)	$\rho$ (Å)	$B$ (Å <sup>4</sup> )	$r_{\min}$ (Å)	$r_{\max}$ (Å)
Sc-Se	5.853	1.533	24.658	0.0	3.658

TABLE XX: Three-body SW potential parameters for single-layer 1H-ScSe<sub>2</sub> used by GULP<sup>8</sup> as expressed in Eq. (4). The angle  $\theta_{ijk}$  in the first line indicates the bending energy for the angle with atom i as the apex.

	$K$ (eV)	$\theta_0$ (degree)	$\rho_1$ (Å)	$\rho_2$ (Å)	$r_{\min12}$ (Å)	$r_{\max12}$ (Å)	$r_{\min13}$ (Å)	$r_{\max13}$ (Å)	$r_{\min23}$ (Å)	$r_{\max23}$ (Å)
$\theta_{\text{Sc-Se-Se}}$	21.292	92.859	1.533	1.533	0.0	3.658	0.0	3.658	0.0	4.327
$\theta_{\text{Sc-Se-Se}'}$	25.280	66.432	1.533	1.533	0.0	3.658	0.0	3.658	0.0	4.327
$\theta_{\text{Se-Sc-Sc}}$	21.292	92.859	1.533	1.533	0.0	3.658	0.0	3.658	0.0	4.327

the acoustic branches in the phonon dispersion along the  $\Gamma\text{M}$  as shown in Fig. 7 (a). The *ab initio* calculations for the phonon dispersion are from Ref. 12. Fig. 7 (b) shows that the VFF model and the SW potential give exactly the same phonon dispersion, as the SW potential is derived from the VFF model.

The parameters for the two-body SW potential used by GULP are shown in Tab. XIX. The parameters for the three-body SW potential used by GULP are shown in Tab. XX. Some representative parameters for the SW potential used by LAMMPS are listed in Tab. XXI. We note that twelve atom types have been introduced for the simulation of the single-layer 1H-ScSe<sub>2</sub> using LAMMPS, because the angles around atom Sc in Fig. 1 (with M=Sc and

TABLE XXI: SW potential parameters for single-layer 1H-ScSe<sub>2</sub> used by LAMMPS<sup>9</sup> as expressed in Eqs. (9) and (10).

	$\epsilon$ (eV)	$\sigma$ (Å)	$a$	$\lambda$	$\gamma$	$\cos \theta_0$	$A_L$	$B_L$	$p$	$q$	tol
Sc <sub>1</sub> -Se <sub>1</sub> -Se <sub>1</sub>	1.000	1.533	2.386	0.000	1.000	0.000	5.853	4.464	4	0	0.0
Sc <sub>1</sub> -Se <sub>1</sub> -Se <sub>3</sub>	1.000	0.000	0.000	21.292	1.000	-0.050	0.000	0.000	4	0	0.0
Sc <sub>1</sub> -Se <sub>1</sub> -Se <sub>2</sub>	1.000	0.000	0.000	25.280	1.000	0.400	0.000	0.000	4	0	0.0
Se <sub>1</sub> -Sc <sub>1</sub> -Sc <sub>3</sub>	1.000	0.000	0.000	21.292	1.000	-0.050	0.000	0.000	4	0	0.0

X=Se) are not distinguishable in LAMMPS. We have suggested two options to differentiate these angles by implementing some additional constraints in LAMMPS, which can be accomplished by modifying the source file of LAMMPS.<sup>13,14</sup> According to our experience, it is not so convenient for some users to implement these constraints and recompile the LAMMPS package. Hence, in the present work, we differentiate the angles by introducing more atom types, so it is not necessary to modify the LAMMPS package. Fig. 2 (with M=Sc and X=Se) shows that, for 1H-ScSe<sub>2</sub>, we can differentiate these angles around the Sc atom by assigning these six neighboring Se atoms with different atom types. It can be found that twelve atom types are necessary for the purpose of differentiating all six neighbors around one Sc atom.

We use LAMMPS to perform MD simulations for the mechanical behavior of the single-layer 1H-ScSe<sub>2</sub> under uniaxial tension at 1.0 K and 300.0 K. Fig. 8 shows the stress-strain curve for the tension of a single-layer 1H-ScSe<sub>2</sub> of dimension 100 × 100 Å. Periodic boundary conditions are applied in both armchair and zigzag directions. The single-layer 1H-ScSe<sub>2</sub> is stretched uniaxially along the armchair or zigzag direction. The stress is calculated without involving the actual thickness of the quasi-two-dimensional structure of the single-layer 1H-ScSe<sub>2</sub>. The Young's modulus can be obtained by a linear fitting of the stress-strain relation in the small strain range of [0, 0.01]. The Young's modulus are 39.4 N/m and 39.9 N/m along the armchair and zigzag directions, respectively. The Young's modulus is essentially isotropic in the armchair and zigzag directions. The Poisson's ratio from the VFF model and the SW potential is  $\nu_{xy} = \nu_{yx} = 0.32$ .

There is no available value for nonlinear quantities in the single-layer 1H-ScSe<sub>2</sub>. We have thus used the nonlinear parameter  $B = 0.5d^4$  in Eq. (5), which is close to the value of  $B$  in most materials. The value of the third order nonlinear elasticity  $D$  can be extracted by fitting the stress-strain relation to the function  $\sigma = E\epsilon + \frac{1}{2}D\epsilon^2$  with  $E$  as the Young's modulus. The values of  $D$  from the present SW potential are -115.7 N/m and -135.7 N/m along the armchair and zigzag directions, respectively. The ultimate stress is about 6.1 Nm<sup>-1</sup> at the ultimate strain of 0.27 in the armchair direction at the low temperature of 1 K. The ultimate stress is about 5.9 Nm<sup>-1</sup> at the ultimate strain of 0.35 in the zigzag direction at the low temperature of 1 K.

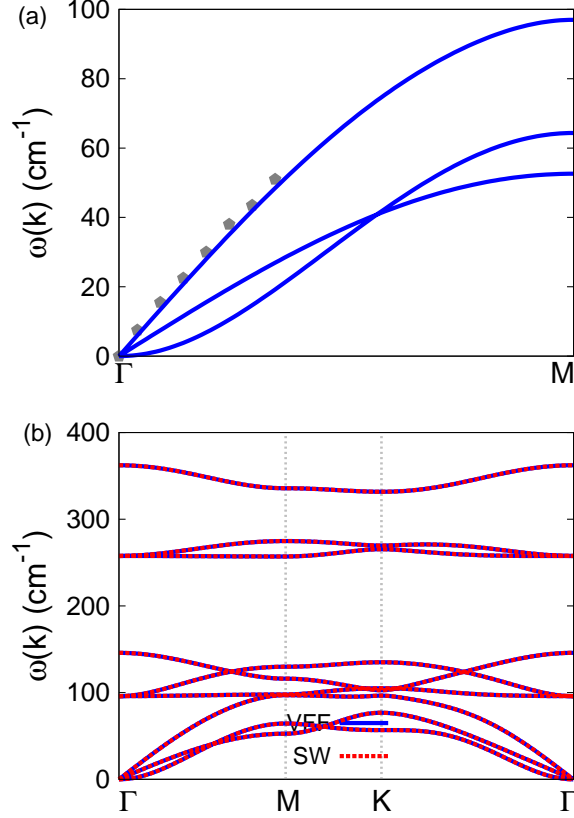


FIG. 9: (Color online) Phonon spectrum for single-layer 1H-ScTe<sub>2</sub>. (a) Phonon dispersion along the  $\Gamma$ M direction in the Brillouin zone. The results from the VFF model (lines) are comparable with the *ab initio* results (pentagons) from Ref. 12. (b) The phonon dispersion from the SW potential is exactly the same as that from the VFF model.

## VI. 1H-SCTE<sub>2</sub>

Most existing theoretical studies on the single-layer 1H-ScTe<sub>2</sub> are based on the first-principles calculations. In this section, we will develop the SW potential for the single-layer 1H-ScTe<sub>2</sub>.

The structure for the single-layer 1H-ScTe<sub>2</sub> is shown in Fig. 1 (with M=Sc and X=Te). Each Sc atom is surrounded by six Te atoms. These Te atoms are categorized into the top group (eg. atoms 1, 3, and 5) and bottom group (eg. atoms 2, 4, and 6). Each Te atom is connected to three Sc atoms. The structural parameters are from the first-principles calculations,<sup>12</sup> including the lattice constant  $a = 3.62 \text{ \AA}$ , and the bond length

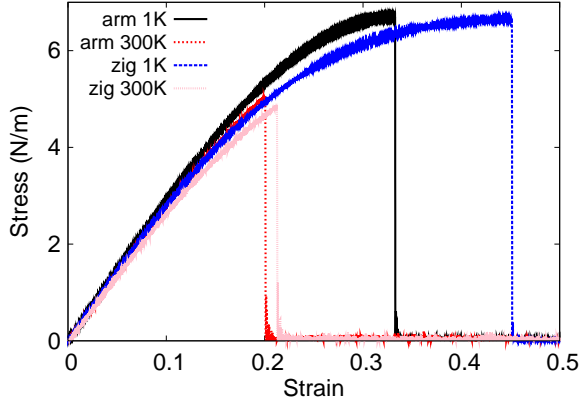


FIG. 10: (Color online) Stress-strain for single-layer 1H-ScTe<sub>2</sub> of dimension  $100 \times 100 \text{ \AA}$  along the armchair and zigzag directions.

TABLE XXII: The VFF model for single-layer 1H-ScTe<sub>2</sub>. The second line gives an explicit expression for each VFF term. The third line is the force constant parameters. Parameters are in the unit of  $\frac{eV}{\text{\AA}^2}$  for the bond stretching interactions, and in the unit of eV for the angle bending interaction. The fourth line gives the initial bond length (in unit of  $\text{\AA}$ ) for the bond stretching interaction and the initial angle (in unit of degrees) for the angle bending interaction. The angle  $\theta_{ijk}$  has atom  $i$  as the apex.

VFF type	bond stretching	angle bending		
expression	$\frac{1}{2}K_{\text{Sc-Te}}(\Delta r)^2$	$\frac{1}{2}K_{\text{Sc-Te-Te}}(\Delta\theta)^2$	$\frac{1}{2}K_{\text{Sc-Te-Te}'}(\Delta\theta)^2$	$\frac{1}{2}K_{\text{Te-Sc-Sc}}(\Delta\theta)^2$
parameter	5.192	2.027	2.027	2.027
$r_0$ or $\theta_0$	2.890	77.555	87.364	87.364

$d_{\text{Sc-Te}} = 2.89 \text{ \AA}$ . The resultant angles are  $\theta_{\text{ScTeTe}} = \theta_{\text{TeScSc}} = 77.555^\circ$  and  $\theta_{\text{ScTeTe}'} = 87.364^\circ$ , in which atoms Te and Te' are from different (top or bottom) group.

Table XXII shows four VFF terms for the single-layer 1H-ScTe<sub>2</sub>, one of which is the bond stretching interaction shown by Eq. (1) while the other three terms are the angle bending interaction shown by Eq. (2). These force constant parameters are determined by fitting to the acoustic branches in the phonon dispersion along the  $\Gamma\text{M}$  as shown in Fig. 9 (a). The *ab initio* calculations for the phonon dispersion are from Ref. 12. There is only one (longitudinal) acoustic branch available. We find that the VFF parameters can be chosen

TABLE XXIII: Two-body SW potential parameters for single-layer 1H-ScTe<sub>2</sub> used by GULP<sup>8</sup> as expressed in Eq. (3).

	$A$ (eV)	$\rho$ (Å)	$B$ (Å <sup>4</sup> )	$r_{\min}$ (Å)	$r_{\max}$ (Å)
Sc-Te	4.630	1.050	34.879	0.0	3.761

TABLE XXIV: Three-body SW potential parameters for single-layer 1H-ScTe<sub>2</sub> used by GULP<sup>8</sup> as expressed in Eq. (4). The angle  $\theta_{ijk}$  in the first line indicates the bending energy for the angle with atom i as the apex.

	$K$ (eV)	$\theta_0$ (degree)	$\rho_1$ (Å)	$\rho_2$ (Å)	$r_{\min12}$ (Å)	$r_{\max12}$ (Å)	$r_{\min13}$ (Å)	$r_{\max13}$ (Å)	$r_{\min23}$ (Å)	$r_{\max23}$ (Å)
$\theta_{\text{Sc-Te-Te}}$	11.848	77.555	1.050	1.050	0.0	3.761	0.0	3.761	0.0	4.504
$\theta_{\text{Sc-Te-Te}'}$	11.322	87.364	1.050	1.050	0.0	3.761	0.0	3.761	0.0	4.504
$\theta_{\text{Te-Sc-Sc}}$	11.848	77.555	1.050	1.050	0.0	3.761	0.0	3.761	0.0	4.504

to be the same as that of the 1H-ScSe<sub>2</sub>, from which the longitudinal acoustic branch agrees with the *ab initio* results as shown in Fig. 9 (a). It has also been shown that the VFF parameters can be the same for TaSe<sub>2</sub> and NbSe<sub>2</sub> of similar structure.<sup>15</sup> Fig. 9 (b) shows that the VFF model and the SW potential give exactly the same phonon dispersion, as the SW potential is derived from the VFF model.

The parameters for the two-body SW potential used by GULP are shown in Tab. XXIII. The parameters for the three-body SW potential used by GULP are shown in Tab. XXIV. Some representative parameters for the SW potential used by LAMMPS are listed in Tab. XXV. We note that twelve atom types have been introduced for the simulation of

TABLE XXV: SW potential parameters for single-layer 1H-ScTe<sub>2</sub> used by LAMMPS<sup>9</sup> as expressed in Eqs. (9) and (10).

	$\epsilon$ (eV)	$\sigma$ (Å)	$a$	$\lambda$	$\gamma$	$\cos\theta_0$	$A_L$	$B_L$	$p$	$q$	tol
Sc <sub>1</sub> -Te <sub>1</sub> -Te <sub>1</sub>	1.000	1.050	3.581	0.000	1.000	0.000	4.630	28.679	4	0	0.0
Sc <sub>1</sub> -Te <sub>1</sub> -Te <sub>3</sub>	1.000	0.000	0.000	11.848	1.000	0.216	0.000	0.000	4	0	0.0
Sc <sub>1</sub> -Te <sub>1</sub> -Te <sub>2</sub>	1.000	0.000	0.000	11.322	1.000	0.046	0.000	0.000	4	0	0.0
Te <sub>1</sub> -Sc <sub>1</sub> -Sc <sub>3</sub>	1.000	0.000	0.000	11.848	1.000	0.216	0.000	0.000	4	0	0.0

the single-layer 1H-ScTe<sub>2</sub> using LAMMPS, because the angles around atom Sc in Fig. 1 (with M=Sc and X=Te) are not distinguishable in LAMMPS. We have suggested two options to differentiate these angles by implementing some additional constraints in LAMMPS, which can be accomplished by modifying the source file of LAMMPS.<sup>13,14</sup> According to our experience, it is not so convenient for some users to implement these constraints and re-compile the LAMMPS package. Hence, in the present work, we differentiate the angles by introducing more atom types, so it is not necessary to modify the LAMMPS package. Fig. 2 (with M=Sc and X=Te) shows that, for 1H-ScTe<sub>2</sub>, we can differentiate these angles around the Sc atom by assigning these six neighboring Te atoms with different atom types. It can be found that twelve atom types are necessary for the purpose of differentiating all six neighbors around one Sc atom.

We use LAMMPS to perform MD simulations for the mechanical behavior of the single-layer 1H-ScTe<sub>2</sub> under uniaxial tension at 1.0 K and 300.0 K. Fig. 10 shows the stress-strain curve for the tension of a single-layer 1H-ScTe<sub>2</sub> of dimension 100 × 100 Å. Periodic boundary conditions are applied in both armchair and zigzag directions. The single-layer 1H-ScTe<sub>2</sub> is stretched uniaxially along the armchair or zigzag direction. The stress is calculated without involving the actual thickness of the quasi-two-dimensional structure of the single-layer 1H-ScTe<sub>2</sub>. The Young's modulus can be obtained by a linear fitting of the stress-strain relation in the small strain range of [0, 0.01]. The Young's modulus are 29.3 N/m and 28.8 N/m along the armchair and zigzag directions, respectively. The Young's modulus is essentially isotropic in the armchair and zigzag directions. The Poisson's ratio from the VFF model and the SW potential is  $\nu_{xy} = \nu_{yx} = 0.38$ .

There is no available value for nonlinear quantities in the single-layer 1H-ScTe<sub>2</sub>. We have thus used the nonlinear parameter  $B = 0.5d^4$  in Eq. (5), which is close to the value of  $B$  in most materials. The value of the third order nonlinear elasticity  $D$  can be extracted by fitting the stress-strain relation to the function  $\sigma = E\epsilon + \frac{1}{2}D\epsilon^2$  with  $E$  as the Young's modulus. The values of  $D$  from the present SW potential are -43.2 N/m and -59.3 N/m along the armchair and zigzag directions, respectively. The ultimate stress is about 6.7 Nm<sup>-1</sup> at the ultimate strain of 0.33 in the armchair direction at the low temperature of 1 K. The ultimate stress is about 6.7 Nm<sup>-1</sup> at the ultimate strain of 0.45 in the zigzag direction at the low temperature of 1 K.

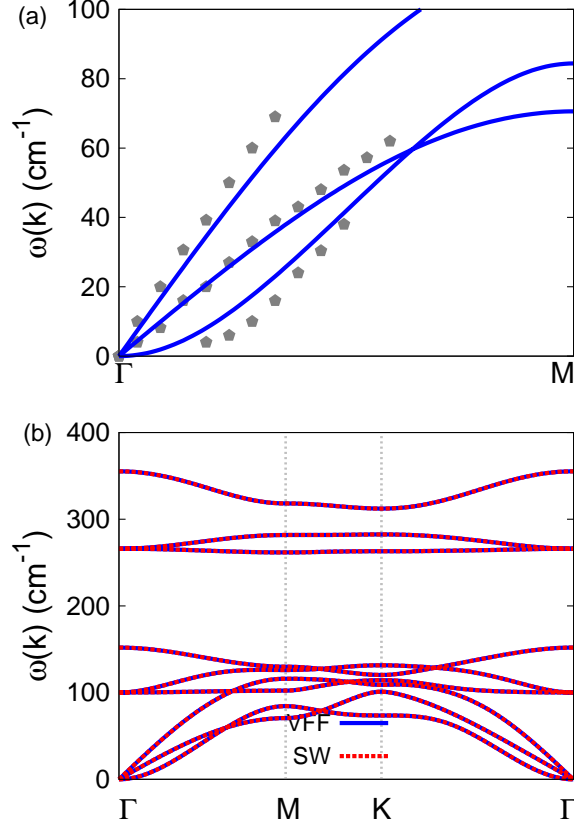


FIG. 11: (Color online) Phonon dispersion for single-layer 1H-TiTe<sub>2</sub>. (a) The VFF model is fitted to the three acoustic branches in the long wave limit along the  $\Gamma$ M direction. The *ab initio* results (gray pentagons) are from Ref. 12. (b) The VFF model (blue lines) and the SW potential (red lines) give the same phonon dispersion for single-layer 1H-TiTe<sub>2</sub> along  $\Gamma$ MK $\Gamma$ .

## VII. 1H-TITE<sub>2</sub>

Most existing theoretical studies on the single-layer 1H-TiTe<sub>2</sub> are based on the first-principles calculations. In this section, we will develop both VFF model and the SW potential for the single-layer 1H-TiTe<sub>2</sub>.

The structure for the single-layer 1H-TiTe<sub>2</sub> is shown in Fig. 1 (with M=Ti and X=Se). Each Ti atom is surrounded by six Te atoms. These Te atoms are categorized into the top group (eg. atoms 1, 3, and 5) and bottom group (eg. atoms 2, 4, and 6). Each Te atom is connected to three Ti atoms. The structural parameters are from Ref. 12, including the lattice constant  $a = 3.62$  Å, and the bond length  $d_{\text{Ti-Te}} = 2.75$  Å. The resultant angles

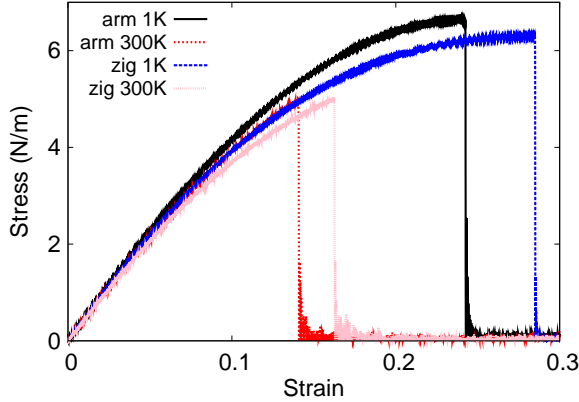


FIG. 12: (Color online) Stress-strain for single-layer 1H-TiTe<sub>2</sub> of dimension  $100 \times 100 \text{ \AA}$  along the armchair and zigzag directions.

TABLE XXVI: The VFF model for single-layer 1H-TiTe<sub>2</sub>. The second line gives an explicit expression for each VFF term. The third line is the force constant parameters. Parameters are in the unit of  $\frac{\text{eV}}{\text{\AA}^2}$  for the bond stretching interactions, and in the unit of eV for the angle bending interaction. The fourth line gives the initial bond length (in unit of  $\text{\AA}$ ) for the bond stretching interaction and the initial angle (in unit of degrees) for the angle bending interaction. The angle  $\theta_{ijk}$  has atom  $i$  as the apex.

VFF type	bond stretching	angle bending		
expression	$\frac{1}{2}K_{\text{Ti}-\text{Te}}(\Delta r)^2$	$\frac{1}{2}K_{\text{Ti}-\text{Te}-\text{Te}}(\Delta\theta)^2$	$\frac{1}{2}K_{\text{Ti}-\text{Te}-\text{Te}'}(\Delta\theta)^2$	$\frac{1}{2}K_{\text{Te}-\text{Ti}-\text{Ti}}(\Delta\theta)^2$
parameter	4.782	3.216	3.216	3.216
$r_0$ or $\theta_0$	2.750	82.323	81.071	82.323

are  $\theta_{\text{TiTeTe}} = \theta_{\text{TeTiTi}} = 82.323^\circ$  and  $\theta_{\text{TiTeTe}'} = 81.071^\circ$ , in which atoms Te and Te' are from different (top or bottom) group.

Table XXVI shows the VFF terms for the 1H-TiTe<sub>2</sub>, one of which is the bond stretching interaction shown by Eq. (1) while the other terms are the angle bending interaction shown by Eq. (2). These force constant parameters are determined by fitting to the three acoustic branches in the phonon dispersion along the  $\Gamma\text{M}$  as shown in Fig. 11 (a). The *ab initio* calculations for the phonon dispersion are from Ref. 12. Fig. 11 (b) shows that the VFF model and the SW potential give exactly the same phonon dispersion, as the SW potential

TABLE XXVII: Two-body SW potential parameters for single-layer 1H-TiTe<sub>2</sub> used by GULP<sup>8</sup> as expressed in Eq. (3).

	$A$ (eV)	$\rho$ (Å)	$B$ (Å <sup>4</sup> )	$r_{\min}$ (Å)	$r_{\max}$ (Å)
Ti-Te	4.414	1.173	28.596	0.0	3.648

TABLE XXVIII: Three-body SW potential parameters for single-layer 1H-TiTe<sub>2</sub> used by GULP<sup>8</sup> as expressed in Eq. (4). The angle  $\theta_{ijk}$  in the first line indicates the bending energy for the angle with atom  $i$  as the apex.

	$K$ (eV)	$\theta_0$ (degree)	$\rho_1$ (Å)	$\rho_2$ (Å)	$r_{\min12}$ (Å)	$r_{\max12}$ (Å)	$r_{\min13}$ (Å)	$r_{\max13}$ (Å)	$r_{\min23}$ (Å)	$r_{\max23}$ (Å)
$\theta_{\text{Ti-Te-Te}}$	22.321	82.323	1.173	1.173	0.0	3.648	0.0	3.648	0.0	4.354
$\theta_{\text{Ti-Te-Te}'}$	22.463	81.071	1.173	1.173	0.0	3.648	0.0	3.648	0.0	4.354
$\theta_{\text{Te-Ti-Ti}}$	11.321	82.323	1.173	1.173	0.0	3.648	0.0	3.648	0.0	4.354

is derived from the VFF model.

The parameters for the two-body SW potential used by GULP are shown in Tab. XXVII. The parameters for the three-body SW potential used by GULP are shown in Tab. XXVIII. Parameters for the SW potential used by LAMMPS are listed in Tab. XXIX. We note that twelve atom types have been introduced for the simulation of the single-layer 1H-TiTe<sub>2</sub> using LAMMPS, because the angles around atom Ti in Fig. 1 (with M=Ti and X=Te) are not distinguishable in LAMMPS. We have suggested two options to differentiate these angles by implementing some additional constraints in LAMMPS, which can be accomplished by modifying the source file of LAMMPS.<sup>13,14</sup> According to our experience, it is not so conve-

TABLE XXIX: SW potential parameters for single-layer 1H-TiTe<sub>2</sub> used by LAMMPS<sup>9</sup> as expressed in Eqs. (9) and (10). Atom types in the first column are displayed in Fig. 2 (with M=Ti and X=Te).

	$\epsilon$ (eV)	$\sigma$ (Å)	$a$	$\lambda$	$\gamma$	$\cos\theta_0$	$A_L$	$B_L$	$p$	$q$	tol
Ti <sub>1</sub> -Te <sub>1</sub> -Te <sub>1</sub>	1.000	1.173	3.110	0.000	1.000	0.000	4.414	15.100	4	0	0.0
Ti <sub>1</sub> -Te <sub>1</sub> -Te <sub>3</sub>	1.000	0.000	0.000	22.321	1.000	0.134	0.000	0.000	4	0	0.0
Ti <sub>1</sub> -Te <sub>1</sub> -Te <sub>2</sub>	1.000	0.000	0.000	22.463	1.000	0.155	0.000	0.000	4	0	0.0
Te <sub>1</sub> -Ti <sub>1</sub> -Ti <sub>3</sub>	1.000	0.000	0.000	22.321	1.000	0.134	0.000	0.000	4	0	0.0

nient for some users to implement these constraints and recompile the LAMMPS package. Hence, in the present work, we differentiate the angles by introducing more atom types, so it is not necessary to modify the LAMMPS package. Fig. 2 (with M=Ti and X=Te) shows that, for 1H-TiTe<sub>2</sub>, we can differentiate these angles around the Ti atom by assigning these six neighboring Te atoms with different atom types. It can be found that twelve atom types are necessary for the purpose of differentiating all six neighbors around one Ti atom.

We use LAMMPS to perform MD simulations for the mechanical behavior of the single-layer 1H-TiTe<sub>2</sub> under uniaxial tension at 1.0 K and 300.0 K. Fig. 12 shows the stress-strain curve for the tension of a single-layer 1H-TiTe<sub>2</sub> of dimension 100 × 100 Å. Periodic boundary conditions are applied in both armchair and zigzag directions. The single-layer 1H-TiTe<sub>2</sub> is stretched uniaxially along the armchair or zigzag direction. The stress is calculated without involving the actual thickness of the quasi-two-dimensional structure of the single-layer 1H-TiTe<sub>2</sub>. The Young's modulus can be obtained by a linear fitting of the stress-strain relation in the small strain range of [0, 0.01]. The Young's modulus are 47.9 N/m and 47.1 N/m along the armchair and zigzag directions, respectively. The Young's modulus is essentially isotropic in the armchair and zigzag directions. The Poisson's ratio from the VFF model and the SW potential is  $\nu_{xy} = \nu_{yx} = 0.29$ .

There is no available value for the nonlinear quantities in the single-layer 1H-TiTe<sub>2</sub>. We have thus used the nonlinear parameter  $B = 0.5d^4$  in Eq. (5), which is close to the value of  $B$  in most materials. The value of the third order nonlinear elasticity  $D$  can be extracted by fitting the stress-strain relation to the function  $\sigma = E\epsilon + \frac{1}{2}D\epsilon^2$  with  $E$  as the Young's modulus. The values of  $D$  from the present SW potential are -158.6 N/m and -176.3 N/m along the armchair and zigzag directions, respectively. The ultimate stress is about 6.6 Nm<sup>-1</sup> at the ultimate strain of 0.24 in the armchair direction at the low temperature of 1 K. The ultimate stress is about 6.3 Nm<sup>-1</sup> at the ultimate strain of 0.28 in the zigzag direction at the low temperature of 1 K.

### VIII. 1H-VO<sub>2</sub>

Most existing theoretical studies on the single-layer 1H-VO<sub>2</sub> are based on the first-principles calculations. In this section, we will develop the SW potential for the single-layer 1H-VO<sub>2</sub>.

TABLE XXX: The VFF model for single-layer 1H-VO<sub>2</sub>. The second line gives an explicit expression for each VFF term. The third line is the force constant parameters. Parameters are in the unit of  $\frac{eV}{\text{Å}^2}$  for the bond stretching interactions, and in the unit of eV for the angle bending interaction. The fourth line gives the initial bond length (in unit of Å) for the bond stretching interaction and the initial angle (in unit of degrees) for the angle bending interaction. The angle  $\theta_{ijk}$  has atom i as the apex.

VFF type	bond stretching	angle bending		
expression	$\frac{1}{2}K_{V-O}(\Delta r)^2$	$\frac{1}{2}K_{V-O-O}(\Delta\theta)^2$	$\frac{1}{2}K_{V-O-O'}(\Delta\theta)^2$	$\frac{1}{2}K_{O-V-V}(\Delta\theta)^2$
parameter	9.417	4.825	4.825	4.825
$r_0$ or $\theta_0$	1.920	89.356	71.436	89.356

TABLE XXXI: Two-body SW potential parameters for single-layer 1H-VO<sub>2</sub> used by GULP<sup>8</sup> as expressed in Eq. (3).

	$A$ (eV)	$\rho$ (Å)	$B$ (Å <sup>4</sup> )	$r_{\min}$ (Å)	$r_{\max}$ (Å)
V-O	5.105	1.011	6.795	0.0	2.617

TABLE XXXII: Three-body SW potential parameters for single-layer 1H-VO<sub>2</sub> used by GULP<sup>8</sup> as expressed in Eq. (4). The angle  $\theta_{ijk}$  in the first line indicates the bending energy for the angle with atom i as the apex.

	$K$ (eV)	$\theta_0$ (degree)	$\rho_1$ (Å)	$\rho_2$ (Å)	$r_{\min12}$ (Å)	$r_{\max12}$ (Å)	$r_{\min13}$ (Å)	$r_{\max13}$ (Å)	$r_{\min23}$ (Å)	$r_{\max23}$ (Å)
$\theta_{V-O-O}$	43.951	89.356	1.011	1.011	0.0	2.617	0.0	2.617	0.0	3.105
$\theta_{V-O-O'}$	48.902	71.436	1.011	1.011	0.0	2.617	0.0	2.617	0.0	3.105
$\theta_{O-V-V}$	43.951	89.356	1.011	1.011	0.0	2.617	0.0	2.617	0.0	3.105

TABLE XXXIII: SW potential parameters for single-layer 1H-VO<sub>2</sub> used by LAMMPS<sup>9</sup> as expressed in Eqs. (9) and (10).

	$\epsilon$ (eV)	$\sigma$ (Å)	$a$	$\lambda$	$\gamma$	$\cos\theta_0$	$A_L$	$B_L$	$p$	$q$	tol
V <sub>1</sub> -O <sub>1</sub> -O <sub>1</sub>	1.000	1.011	2.589	0.000	1.000	0.000	5.105	6.509	4	0	0.0
V <sub>1</sub> -O <sub>1</sub> -O <sub>3</sub>	1.000	0.000	0.000	43.951	1.000	0.011	0.000	0.000	4	0	0.0
V <sub>1</sub> -O <sub>1</sub> -O <sub>2</sub>	1.000	0.000	0.000	48.902	1.000	0.318	0.000	0.000	4	0	0.0
O <sub>1</sub> -V <sub>1</sub> -V <sub>3</sub>	1.000	0.000	0.000	43.951	1.000	0.011	0.000	0.000	4	0	0.0

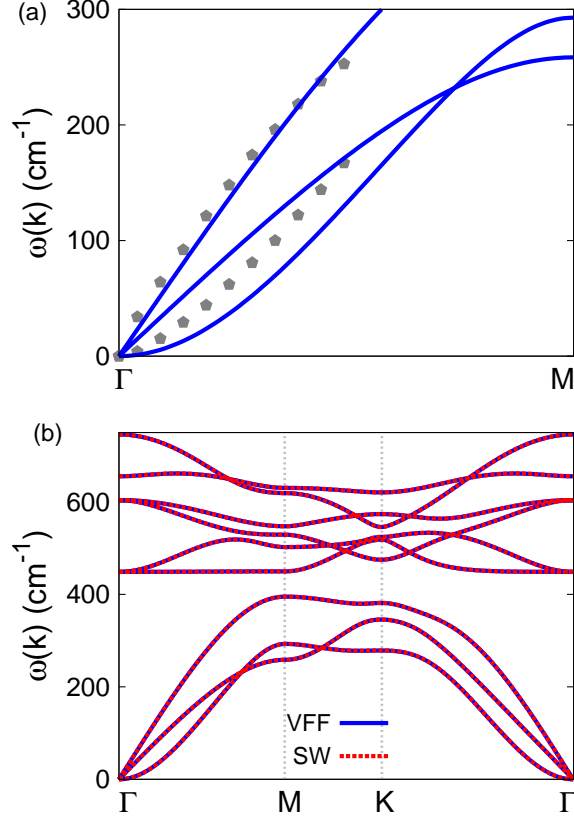


FIG. 13: (Color online) Phonon spectrum for single-layer 1H-VO<sub>2</sub>. (a) Phonon dispersion along the  $\Gamma$ M direction in the Brillouin zone. The results from the VFF model (lines) are comparable with the *ab initio* results (pentagons) from Ref. 12. (b) The phonon dispersion from the SW potential is exactly the same as that from the VFF model.

The structure for the single-layer 1H-VO<sub>2</sub> is shown in Fig. 1 (with M=V and X=O). Each V atom is surrounded by six O atoms. These O atoms are categorized into the top group (eg. atoms 1, 3, and 5) and bottom group (eg. atoms 2, 4, and 6). Each O atom is connected to three V atoms. The structural parameters are from the first-principles calculations,<sup>12</sup> including the lattice constant  $a = 2.70 \text{ \AA}$ , and the bond length  $d_{V-O} = 1.92 \text{ \AA}$ . The resultant angles are  $\theta_{VOO} = \theta_{OVV} = 89.356^\circ$  and  $\theta_{VOO'} = 71.436^\circ$ , in which atoms O and O' are from different (top or bottom) group.

Table XXX shows four VFF terms for the single-layer 1H-VO<sub>2</sub>, one of which is the bond stretching interaction shown by Eq. (1) while the other three terms are the angle bending interaction shown by Eq. (2). These force constant parameters are determined by fitting to

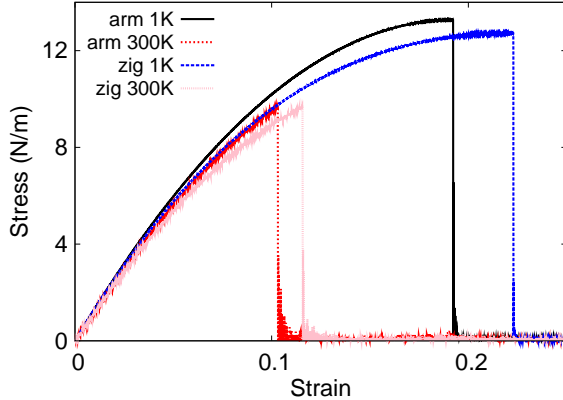


FIG. 14: (Color online) Stress-strain for single-layer 1H-VO<sub>2</sub> of dimension  $100 \times 100 \text{ \AA}$  along the armchair and zigzag directions.

the acoustic branches in the phonon dispersion along the  $\Gamma$ M as shown in Fig. 13 (a). The *ab initio* calculations for the phonon dispersion are from Ref. 12. Fig. 13 (b) shows that the VFF model and the SW potential give exactly the same phonon dispersion, as the SW potential is derived from the VFF model.

The parameters for the two-body SW potential used by GULP are shown in Tab. XXXI. The parameters for the three-body SW potential used by GULP are shown in Tab. XXXII. Some representative parameters for the SW potential used by LAMMPS are listed in Tab. XXXIII. We note that twelve atom types have been introduced for the simulation of the single-layer 1H-VO<sub>2</sub> using LAMMPS, because the angles around atom V in Fig. 1 (with M=V and X=O) are not distinguishable in LAMMPS. We have suggested two options to differentiate these angles by implementing some additional constraints in LAMMPS, which can be accomplished by modifying the source file of LAMMPS.<sup>13,14</sup> According to our experience, it is not so convenient for some users to implement these constraints and recompile the LAMMPS package. Hence, in the present work, we differentiate the angles by introducing more atom types, so it is not necessary to modify the LAMMPS package. Fig. 2 (with M=V and X=O) shows that, for 1H-VO<sub>2</sub>, we can differentiate these angles around the V atom by assigning these six neighboring O atoms with different atom types. It can be found that twelve atom types are necessary for the purpose of differentiating all six neighbors around one V atom.

We use LAMMPS to perform MD simulations for the mechanical behavior of the single-

layer 1H-VO<sub>2</sub> under uniaxial tension at 1.0 K and 300.0 K. Fig. 14 shows the stress-strain curve for the tension of a single-layer 1H-VO<sub>2</sub> of dimension 100 × 100 Å. Periodic boundary conditions are applied in both armchair and zigzag directions. The single-layer 1H-VO<sub>2</sub> is stretched uniaxially along the armchair or zigzag direction. The stress is calculated without involving the actual thickness of the quasi-two-dimensional structure of the single-layer 1H-VO<sub>2</sub>. The Young's modulus can be obtained by a linear fitting of the stress-strain relation in the small strain range of [0, 0.01]. The Young's modulus are 133.0 N/m and 132.9 N/m along the armchair and zigzag directions, respectively. The Young's modulus is essentially isotropic in the armchair and zigzag directions. The Poisson's ratio from the VFF model and the SW potential is  $\nu_{xy} = \nu_{yx} = 0.17$ .

There is no available value for nonlinear quantities in the single-layer 1H-VO<sub>2</sub>. We have thus used the nonlinear parameter  $B = 0.5d^4$  in Eq. (5), which is close to the value of  $B$  in most materials. The value of the third order nonlinear elasticity  $D$  can be extracted by fitting the stress-strain relation to the function  $\sigma = E\epsilon + \frac{1}{2}D\epsilon^2$  with  $E$  as the Young's modulus. The values of  $D$  from the present SW potential are -652.3 N/m and -705.8 N/m along the armchair and zigzag directions, respectively. The ultimate stress is about 13.3 Nm<sup>-1</sup> at the ultimate strain of 0.19 in the armchair direction at the low temperature of 1 K. The ultimate stress is about 12.7 Nm<sup>-1</sup> at the ultimate strain of 0.22 in the zigzag direction at the low temperature of 1 K.

## IX. 1H-VS<sub>2</sub>

Most existing theoretical studies on the single-layer 1H-VS<sub>2</sub> are based on the first-principles calculations. In this section, we will develop both VFF model and the SW potential for the single-layer 1H-VS<sub>2</sub>.

The structure for the single-layer 1H-VS<sub>2</sub> is shown in Fig. 1 (with M=V and X=S). Each V atom is surrounded by six S atoms. These S atoms are categorized into the top group (eg. atoms 1, 3, and 5) and bottom group (eg. atoms 2, 4, and 6). Each S atom is connected to three V atoms. The structural parameters are from Ref. 12, including the lattice constant  $a = 3.09$  Å, and the bond length  $d_{V-S} = 2.31$  Å. The resultant angles are  $\theta_{VSS} = \theta_{SVV} = 83.954^\circ$  and  $\theta_{VSS'} = 78.878^\circ$ , in which atoms S and S' are from different (top or bottom) group.

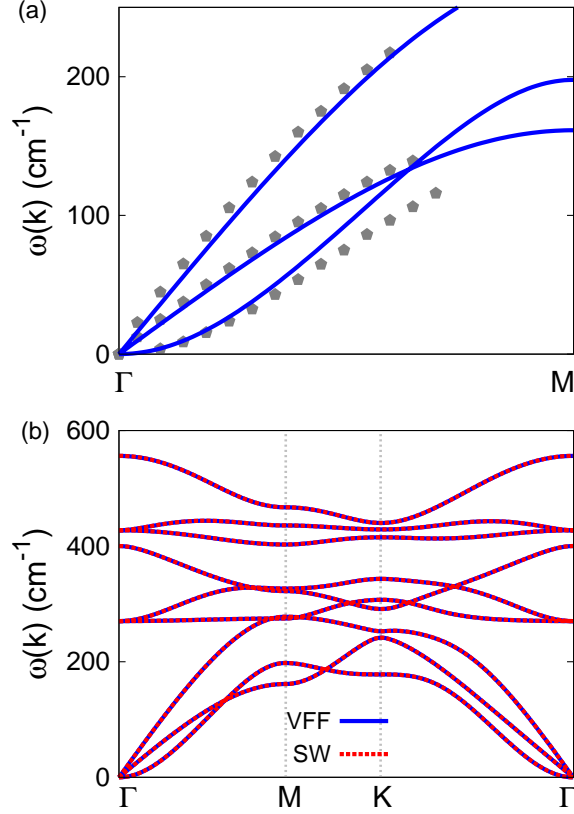


FIG. 15: (Color online) Phonon dispersion for single-layer 1H-VS<sub>2</sub>. (a) The VFF model is fitted to the three acoustic branches in the long wave limit along the  $\Gamma$ M direction. The *ab initio* results (gray pentagons) are from Ref. 16. (b) The VFF model (blue lines) and the SW potential (red lines) give the same phonon dispersion for single-layer 1H-VS<sub>2</sub> along  $\Gamma$ MKT.

Table XXXIV shows the VFF terms for the 1H-VS<sub>2</sub>, one of which is the bond stretching interaction shown by Eq. (1) while the other terms are the angle bending interaction shown by Eq. (2). These force constant parameters are determined by fitting to the three acoustic branches in the phonon dispersion along the  $\Gamma$ M as shown in Fig. 15 (a). The *ab initio* calculations for the phonon dispersion are from Ref. 16. The phonon dispersion can also be found in other *ab initio* calculations.<sup>12</sup> Fig. 15 (b) shows that the VFF model and the SW potential give exactly the same phonon dispersion, as the SW potential is derived from the VFF model.

The parameters for the two-body SW potential used by GULP are shown in Tab. XXXV. The parameters for the three-body SW potential used by GULP are shown in Tab. XXXVI.

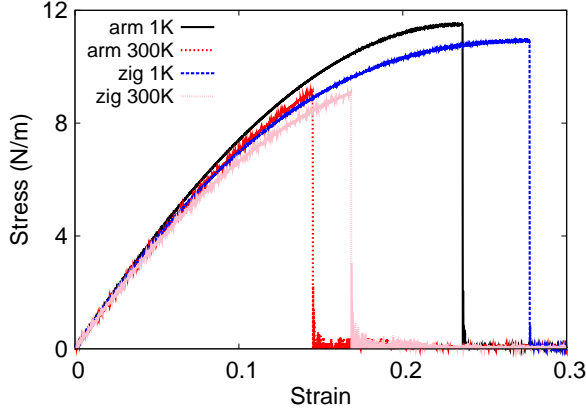


FIG. 16: (Color online) Stress-strain for single-layer 1H-VS<sub>2</sub> of dimension 100 × 100 Å along the armchair and zigzag directions.

TABLE XXXIV: The VFF model for single-layer 1H-VS<sub>2</sub>. The second line gives an explicit expression for each VFF term. The third line is the force constant parameters. Parameters are in the unit of  $\frac{eV}{\text{Å}^2}$  for the bond stretching interactions, and in the unit of eV for the angle bending interaction. The fourth line gives the initial bond length (in unit of Å) for the bond stretching interaction and the initial angle (in unit of degrees) for the angle bending interaction. The angle  $\theta_{ijk}$  has atom *i* as the apex.

VFF type	bond stretching	angle bending		
expression	$\frac{1}{2}K_{V-S}(\Delta r)^2$	$\frac{1}{2}K_{V-S-S}(\Delta\theta)^2$	$\frac{1}{2}K_{V-S-S'}(\Delta\theta)^2$	$\frac{1}{2}K_{S-V-V}(\Delta\theta)^2$
parameter	8.392	4.074	4.074	4.074
$r_0$ or $\theta_0$	2.310	83.954	78.878	83.954

Parameters for the SW potential used by LAMMPS are listed in Tab. XXXVII. We note that twelve atom types have been introduced for the simulation of the single-layer 1H-VS<sub>2</sub> using LAMMPS, because the angles around atom V in Fig. 1 (with M=V and X=S) are not distinguishable in LAMMPS. We have suggested two options to differentiate these angles by implementing some additional constraints in LAMMPS, which can be accomplished by modifying the source file of LAMMPS.<sup>13,14</sup> According to our experience, it is not so convenient for some users to implement these constraints and recompile the LAMMPS package. Hence, in the present work, we differentiate the angles by introducing more atom types, so

TABLE XXXV: Two-body SW potential parameters for single-layer 1H-VS<sub>2</sub> used by GULP<sup>8</sup> as expressed in Eq. (3).

	$A$ (eV)	$\rho$ (Å)	$B$ (Å <sup>4</sup> )	$r_{\min}$ (Å)	$r_{\max}$ (Å)
V-S	5.714	1.037	14.237	0.0	3.084

TABLE XXXVI: Three-body SW potential parameters for single-layer 1H-VS<sub>2</sub> used by GULP<sup>8</sup> as expressed in Eq. (4). The angle  $\theta_{ijk}$  in the first line indicates the bending energy for the angle with atom  $i$  as the apex.

	$K$ (eV)	$\theta_0$ (degree)	$\rho_1$ (Å)	$\rho_2$ (Å)	$r_{\min12}$ (Å)	$r_{\max12}$ (Å)	$r_{\min13}$ (Å)	$r_{\max13}$ (Å)	$r_{\min23}$ (Å)	$r_{\max23}$ (Å)
$\theta_{V-S-S}$	30.059	83.954	1.037	1.037	0.0	3.084	0.0	3.084	0.0	3.676
$\theta_{V-S-S'}$	30.874	78.878	1.037	1.037	0.0	3.084	0.0	3.084	0.0	3.676
$\theta_{S-V-V}$	30.059	83.954	1.037	1.037	0.0	3.084	0.0	3.084	0.0	3.676

it is not necessary to modify the LAMMPS package. Fig. 2 (with M=V and X=S) shows that, for 1H-VS<sub>2</sub>, we can differentiate these angles around the V atom by assigning these six neighboring S atoms with different atom types. It can be found that twelve atom types are necessary for the purpose of differentiating all six neighbors around one V atom.

We use LAMMPS to perform MD simulations for the mechanical behavior of the single-layer 1H-VS<sub>2</sub> under uniaxial tension at 1.0 K and 300.0 K. Fig. 16 shows the stress-strain curve for the tension of a single-layer 1H-VS<sub>2</sub> of dimension  $100 \times 100$  Å. Periodic boundary conditions are applied in both armchair and zigzag directions. The single-layer 1H-VS<sub>2</sub> is stretched uniaxially along the armchair or zigzag direction. The stress is calculated without

TABLE XXXVII: SW potential parameters for single-layer 1H-VS<sub>2</sub> used by LAMMPS<sup>9</sup> as expressed in Eqs. (9) and (10). Atom types in the first column are displayed in Fig. 2 (with M=V and X=S).

	$\epsilon$ (eV)	$\sigma$ (Å)	$a$	$\lambda$	$\gamma$	$\cos\theta_0$	$A_L$	$B_L$	$p$	$q$	tol
V <sub>1</sub> -S <sub>1</sub> -S <sub>1</sub>	1.000	1.037	2.973	0.000	1.000	0.000	5.714	12.294	4	0	0.0
V <sub>1</sub> -S <sub>1</sub> -S <sub>3</sub>	1.000	0.000	0.000	30.059	1.000	0.105	0.000	0.000	4	0	0.0
V <sub>1</sub> -S <sub>1</sub> -S <sub>2</sub>	1.000	0.000	0.000	30.874	1.000	0.193	0.000	0.000	4	0	0.0
S <sub>1</sub> -V <sub>1</sub> -V <sub>3</sub>	1.000	0.000	0.000	30.059	1.000	0.105	0.000	0.000	4	0	0.0

TABLE XXXVIII: The VFF model for single-layer 1H-VSe<sub>2</sub>. The second line gives an explicit expression for each VFF term. The third line is the force constant parameters. Parameters are in the unit of  $\frac{\text{eV}}{\text{Å}^2}$  for the bond stretching interactions, and in the unit of eV for the angle bending interaction. The fourth line gives the initial bond length (in unit of Å) for the bond stretching interaction and the initial angle (in unit of degrees) for the angle bending interaction. The angle  $\theta_{ijk}$  has atom *i* as the apex.

VFF type	bond stretching	angle bending		
expression	$\frac{1}{2}K_{\text{V-Se}}(\Delta r)^2$	$\frac{1}{2}K_{\text{V-Se-Se}}(\Delta\theta)^2$	$\frac{1}{2}K_{\text{V-Se-Se}'}(\Delta\theta)^2$	$\frac{1}{2}K_{\text{Se-V-V}}(\Delta\theta)^2$
parameter	6.492	4.716	4.716	4.716
$r_0$ or $\theta_0$	2.450	82.787	80.450	82.787

involving the actual thickness of the quasi-two-dimensional structure of the single-layer 1H-VS<sub>2</sub>. The Young's modulus can be obtained by a linear fitting of the stress-strain relation in the small strain range of [0, 0.01]. The Young's modulus are 86.5 N/m and 85.3 N/m along the armchair and zigzag directions, respectively. The Young's modulus is essentially isotropic in the armchair and zigzag directions. The Poisson's ratio from the VFF model and the SW potential is  $\nu_{xy} = \nu_{yx} = 0.28$ .

There is no available value for the nonlinear quantities in the single-layer 1H-VS<sub>2</sub>. We have thus used the nonlinear parameter  $B = 0.5d^4$  in Eq. (5), which is close to the value of  $B$  in most materials. The value of the third order nonlinear elasticity  $D$  can be extracted by fitting the stress-strain relation to the function  $\sigma = E\epsilon + \frac{1}{2}D\epsilon^2$  with  $E$  as the Young's modulus. The values of  $D$  from the present SW potential are -302.0 N/m and -334.7 N/m along the armchair and zigzag directions, respectively. The ultimate stress is about 11.5 Nm<sup>-1</sup> at the ultimate strain of 0.23 in the armchair direction at the low temperature of 1 K. The ultimate stress is about 10.9 Nm<sup>-1</sup> at the ultimate strain of 0.27 in the zigzag direction at the low temperature of 1 K.

## X. 1H-VSE<sub>2</sub>

Most existing theoretical studies on the single-layer 1H-VSe<sub>2</sub> are based on the first-principles calculations. In this section, we will develop both VFF model and the SW poten-

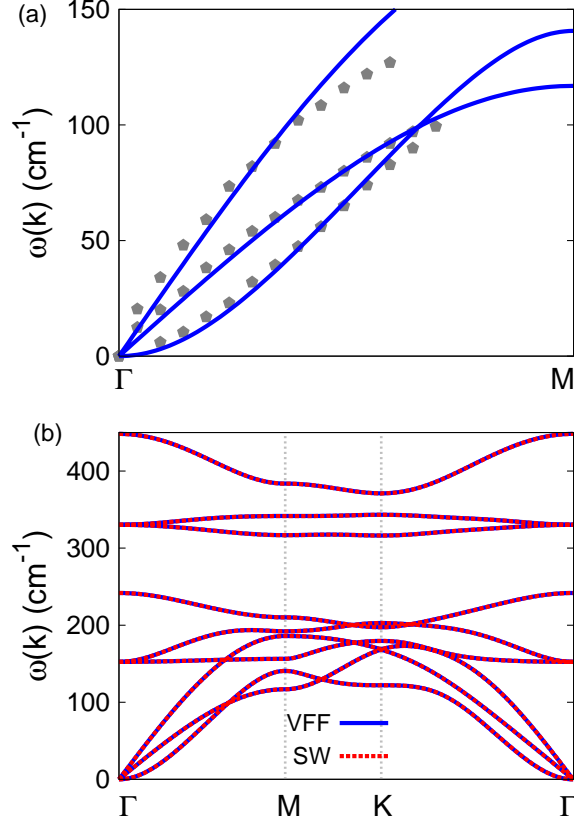


FIG. 17: (Color online) Phonon dispersion for single-layer 1H-VSe<sub>2</sub>. (a) The VFF model is fitted to the three acoustic branches in the long wave limit along the  $\Gamma\text{M}$  direction. The *ab initio* results (gray pentagons) are from Ref. 12. (b) The VFF model (blue lines) and the SW potential (red lines) give the same phonon dispersion for single-layer 1H-VSe<sub>2</sub> along  $\Gamma\text{MK}\Gamma$ .

TABLE XXXIX: Two-body SW potential parameters for single-layer 1H-VSe<sub>2</sub> used by GULP<sup>8</sup> as expressed in Eq. (3).

	$A$ (eV)	$\rho$ ( $\text{\AA}$ )	$B$ ( $\text{\AA}^4$ )	$r_{\min}$ ( $\text{\AA}$ )	$r_{\max}$ ( $\text{\AA}$ )
V-Se	4.817	1.061	18.015	0.0	3.256

tial for the single-layer 1H-VSe<sub>2</sub>.

The structure for the single-layer 1H-VSe<sub>2</sub> is shown in Fig. 1 (with M=V and X=Se). Each V atom is surrounded by six Se atoms. These Se atoms are categorized into the top group (eg. atoms 1, 3, and 5) and bottom group (eg. atoms 2, 4, and 6). Each Se atom is connected to three V atoms. The structural parameters are from Ref. 12, including the

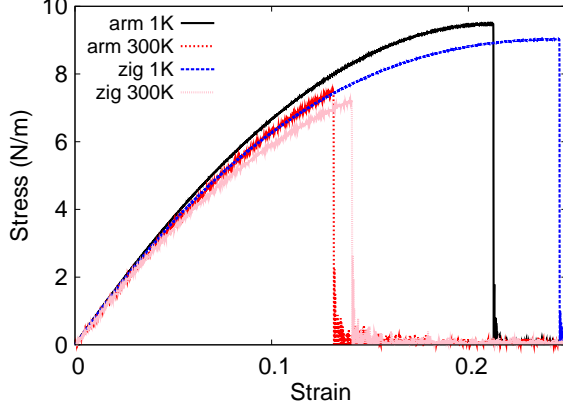


FIG. 18: (Color online) Stress-strain for single-layer 1H-VSe<sub>2</sub> of dimension 100 × 100 Å along the armchair and zigzag directions.

TABLE XL: Three-body SW potential parameters for single-layer 1H-VSe<sub>2</sub> used by GULP<sup>8</sup> as expressed in Eq. (4). The angle  $\theta_{ijk}$  in the first line indicates the bending energy for the angle with atom *i* as the apex.

	$K$ (eV)	$\theta_0$ (degree)	$\rho_1$ (Å)	$\rho_2$ (Å)	$r_{\min 12}$ (Å)	$r_{\max 12}$ (Å)	$r_{\min 13}$ (Å)	$r_{\max 13}$ (Å)	$r_{\min 23}$ (Å)	$r_{\max 23}$ (Å)
$\theta_{V-Se-Se}$	33.299	82.787	1.061	1.061	0.0	3.256	0.0	3.256	0.0	3.884
$\theta_{V-Se-Se'}$	33.702	80.450	1.061	1.061	0.0	3.256	0.0	3.256	0.0	3.884
$\theta_{Se-V-V}$	33.299	82.787	1.061	1.061	0.0	3.256	0.0	3.256	0.0	3.884

lattice constant  $a = 3.24$  Å, and the bond length  $d_{V-Se} = 2.45$  Å. The resultant angles are  $\theta_{VSeSe} = \theta_{SeVSe} = 82.787^\circ$  and  $\theta_{VSeSe'} = 80.450^\circ$ , in which atoms Se and Se' are from different (top or bottom) group.

Table XXXVIII shows the VFF terms for the 1H-VSe<sub>2</sub>, one of which is the bond stretching interaction shown by Eq. (1) while the other terms are the angle bending interaction shown by Eq. (2). These force constant parameters are determined by fitting to the three acoustic branches in the phonon dispersion along the  $\Gamma M$  as shown in Fig. 17 (a). The *ab initio* calculations for the phonon dispersion are from Ref. 12. Fig. 17 (b) shows that the VFF model and the SW potential give exactly the same phonon dispersion, as the SW potential is derived from the VFF model.

The parameters for the two-body SW potential used by GULP are shown in Tab. XXXIX. The parameters for the three-body SW potential used by GULP are shown in Tab. XL. Pa-

TABLE XLI: SW potential parameters for single-layer 1H-VSe<sub>2</sub> used by LAMMPS<sup>9</sup> as expressed in Eqs. (9) and (10). Atom types in the first column are displayed in Fig. 2 (with M=V and X=Se).

	$\epsilon$ (eV)	$\sigma$ (Å)	$a$	$\lambda$	$\gamma$	$\cos \theta_0$	$A_L$	$B_L$	$p$	$q$	tol
V <sub>1</sub> -Se <sub>1</sub> -Se <sub>1</sub>	1.000	1.061	3.070	0.000	1.000	0.000	4.817	14.236	4	0	0.0
V <sub>1</sub> -Se <sub>1</sub> -Se <sub>3</sub>	1.000	0.000	0.000	33.299	1.000	0.126	0.000	0.000	4	0	0.0
V <sub>1</sub> -Se <sub>1</sub> -Se <sub>2</sub>	1.000	0.000	0.000	33.702	1.000	0.166	0.000	0.000	4	0	0.0
Se <sub>1</sub> -V <sub>1</sub> -V <sub>3</sub>	1.000	0.000	0.000	33.299	1.000	0.126	0.000	0.000	4	0	0.0

parameters for the SW potential used by LAMMPS are listed in Tab. XLI. We note that twelve atom types have been introduced for the simulation of the single-layer 1H-VSe<sub>2</sub> using LAMMPS, because the angles around atom V in Fig. 1 (with M=V and X=Se) are not distinguishable in LAMMPS. We have suggested two options to differentiate these angles by implementing some additional constraints in LAMMPS, which can be accomplished by modifying the source file of LAMMPS.<sup>13,14</sup> According to our experience, it is not so convenient for some users to implement these constraints and recompile the LAMMPS package. Hence, in the present work, we differentiate the angles by introducing more atom types, so it is not necessary to modify the LAMMPS package. Fig. 2 (with M=V and X=Se) shows that, for 1H-VSe<sub>2</sub>, we can differentiate these angles around the V atom by assigning these six neighboring Se atoms with different atom types. It can be found that twelve atom types are necessary for the purpose of differentiating all six neighbors around one V atom.

We use LAMMPS to perform MD simulations for the mechanical behavior of the single-layer 1H-VSe<sub>2</sub> under uniaxial tension at 1.0 K and 300.0 K. Fig. 18 shows the stress-strain curve for the tension of a single-layer 1H-VSe<sub>2</sub> of dimension 100 × 100 Å. Periodic boundary conditions are applied in both armchair and zigzag directions. The single-layer 1H-VSe<sub>2</sub> is stretched uniaxially along the armchair or zigzag direction. The stress is calculated without involving the actual thickness of the quasi-two-dimensional structure of the single-layer 1H-VSe<sub>2</sub>. The Young's modulus can be obtained by a linear fitting of the stress-strain relation in the small strain range of [0, 0.01]. The Young's modulus are 81.7 N/m and 80.6 N/m along the armchair and zigzag directions, respectively. The Young's modulus is essentially isotropic in the armchair and zigzag directions. The Poisson's ratio from the VFF model and the SW potential is  $\nu_{xy} = \nu_{yx} = 0.23$ .

TABLE XLII: The VFF model for single-layer 1H-VTe<sub>2</sub>. The second line gives an explicit expression for each VFF term. The third line is the force constant parameters. Parameters are in the unit of  $\frac{\text{eV}}{\text{\AA}^2}$  for the bond stretching interactions, and in the unit of eV for the angle bending interaction. The fourth line gives the initial bond length (in unit of  $\text{\AA}$ ) for the bond stretching interaction and the initial angle (in unit of degrees) for the angle bending interaction. The angle  $\theta_{ijk}$  has atom  $i$  as the apex.

VFF type	bond stretching	angle bending		
expression	$\frac{1}{2}K_{\text{V-Te}}(\Delta r)^2$	$\frac{1}{2}K_{\text{V-Te-Te}}(\Delta\theta)^2$	$\frac{1}{2}K_{\text{V-Te-Te}'}(\Delta\theta)^2$	$\frac{1}{2}K_{\text{Te-V-V}}(\Delta\theta)^2$
parameter	6.371	4.384	4.384	4.384
$r_0$ or $\theta_0$	2.660	81.708	81.891	81.708

TABLE XLIII: Two-body SW potential parameters for single-layer 1H-VTe<sub>2</sub> used by GULP<sup>8</sup> as expressed in Eq. (3).

	$A$ (eV)	$\rho$ ( $\text{\AA}$ )	$B$ ( $\text{\AA}^4$ )	$r_{\text{min}}$ ( $\text{\AA}$ )	$r_{\text{max}}$ ( $\text{\AA}$ )
V-Te	5.410	1.112	25.032	0.0	3.520

There is no available value for the nonlinear quantities in the single-layer 1H-VSe<sub>2</sub>. We have thus used the nonlinear parameter  $B = 0.5d^4$  in Eq. (5), which is close to the value of  $B$  in most materials. The value of the third order nonlinear elasticity  $D$  can be extracted by fitting the stress-strain relation to the function  $\sigma = E\epsilon + \frac{1}{2}D\epsilon^2$  with  $E$  as the Young's modulus. The values of  $D$  from the present SW potential are -335.2 N/m and -363.3 N/m along the armchair and zigzag directions, respectively. The ultimate stress is about  $9.5 \text{ Nm}^{-1}$  at the ultimate strain of 0.21 in the armchair direction at the low temperature of 1 K. The ultimate stress is about  $9.0 \text{ Nm}^{-1}$  at the ultimate strain of 0.24 in the zigzag direction at the low temperature of 1 K.

## XI. 1H-VTE<sub>2</sub>

Most existing theoretical studies on the single-layer 1H-VTe<sub>2</sub> are based on the first-principles calculations. In this section, we will develop both VFF model and the SW potential for the single-layer 1H-VTe<sub>2</sub>.

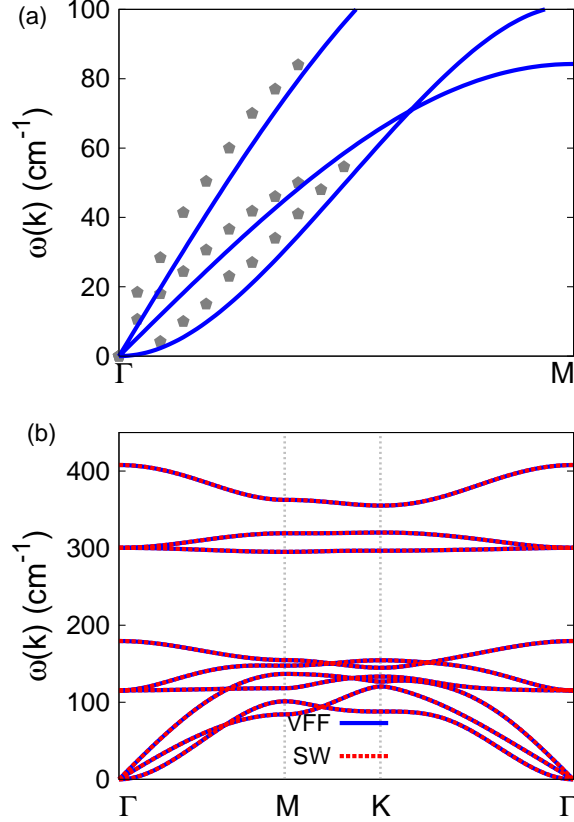


FIG. 19: (Color online) Phonon dispersion for single-layer 1H-VTe<sub>2</sub>. (a) The VFF model is fitted to the three acoustic branches in the long wave limit along the  $\Gamma\text{M}$  direction. The *ab initio* results (gray pentagons) are from Ref. 12. (b) The VFF model (blue lines) and the SW potential (red lines) give the same phonon dispersion for single-layer 1H-VTe<sub>2</sub> along  $\Gamma\text{MK}\Gamma$ .

The structure for the single-layer 1H-VTe<sub>2</sub> is shown in Fig. 1 (with M=V and X=Te). Each V atom is surrounded by six Te atoms. These Te atoms are categorized into the top group (eg. atoms 1, 3, and 5) and bottom group (eg. atoms 2, 4, and 6). Each Te atom is connected to three V atoms. The structural parameters are from Ref. 12, including the lattice constant  $a = 3.48 \text{ \AA}$ , and the bond length  $d_{\text{V-Te}} = 2.66 \text{ \AA}$ . The resultant angles are  $\theta_{\text{VTeTe}} = \theta_{\text{TeVV}} = 81.708^\circ$  and  $\theta_{\text{VTeTe}'} = 81.891^\circ$ , in which atoms Te and Te' are from different (top or bottom) group.

Table XLII shows the VFF terms for the 1H-VTe<sub>2</sub>, one of which is the bond stretching interaction shown by Eq. (1) while the other terms are the angle bending interaction shown by Eq. (2). These force constant parameters are determined by fitting to the three acoustic

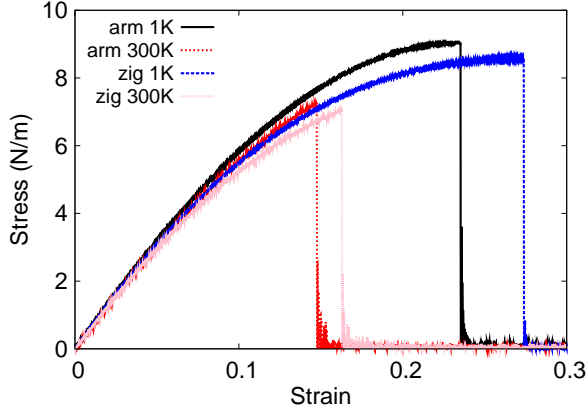


FIG. 20: (Color online) Stress-strain for single-layer 1H-VTe<sub>2</sub> of dimension 100 × 100 Å along the armchair and zigzag directions.

TABLE XLIV: Three-body SW potential parameters for single-layer 1H-VTe<sub>2</sub> used by GULP<sup>8</sup> as expressed in Eq. (4). The angle  $\theta_{ijk}$  in the first line indicates the bending energy for the angle with atom *i* as the apex.

	$K$ (eV)	$\theta_0$ (degree)	$\rho_1$ (Å)	$\rho_2$ (Å)	$r_{\min 12}$ (Å)	$r_{\max 12}$ (Å)	$r_{\min 13}$ (Å)	$r_{\max 13}$ (Å)	$r_{\min 23}$ (Å)	$r_{\max 23}$ (Å)
$\theta_{V-Te-Te}$	29.743	81.708	1.112	1.112	0.0	3.520	0.0	3.520	0.0	4.203
$\theta_{V-Te-Te'}$	29.716	81.891	1.112	1.112	0.0	3.520	0.0	3.520	0.0	4.203
$\theta_{Te-V-V}$	29.743	81.708	1.112	1.112	0.0	3.520	0.0	3.520	0.0	4.203

branches in the phonon dispersion along the  $\Gamma M$  as shown in Fig. 19 (a). The *ab initio* calculations for the phonon dispersion are from Ref. 12. Fig. 19 (b) shows that the VFF model and the SW potential give exactly the same phonon dispersion, as the SW potential is derived from the VFF model.

The parameters for the two-body SW potential used by GULP are shown in Tab. XLIII. The parameters for the three-body SW potential used by GULP are shown in Tab. XLIV. Parameters for the SW potential used by LAMMPS are listed in Tab. XLV. We note that twelve atom types have been introduced for the simulation of the single-layer 1H-VTe<sub>2</sub> using LAMMPS, because the angles around atom V in Fig. 1 (with M=V and X=Te) are not distinguishable in LAMMPS. We have suggested two options to differentiate these angles by implementing some additional constraints in LAMMPS, which can be accomplished by modifying the source file of LAMMPS.<sup>13,14</sup> According to our experience, it is not so conve-

TABLE XLV: SW potential parameters for single-layer 1H-VTe<sub>2</sub> used by LAMMPS<sup>9</sup> as expressed in Eqs. (9) and (10). Atom types in the first column are displayed in Fig. 2 (with M=V and X=Te).

	$\epsilon$ (eV)	$\sigma$ (Å)	$a$	$\lambda$	$\gamma$	$\cos \theta_0$	$A_L$	$B_L$	$p$	$q$	tol
V <sub>1</sub> -Te <sub>1</sub> -Te <sub>1</sub>	1.000	1.112	3.164	0.000	1.000	0.000	5.410	16.345	4	0	0.0
V <sub>1</sub> -Te <sub>1</sub> -Te <sub>3</sub>	1.000	0.000	0.000	29.743	1.000	0.144	0.000	0.000	4	0	0.0
V <sub>1</sub> -Te <sub>1</sub> -Te <sub>2</sub>	1.000	0.000	0.000	29.716	1.000	0.141	0.000	0.000	4	0	0.0
Te <sub>1</sub> -V <sub>1</sub> -V <sub>3</sub>	1.000	0.000	0.000	29.743	1.000	0.144	0.000	0.000	4	0	0.0

nient for some users to implement these constraints and recompile the LAMMPS package. Hence, in the present work, we differentiate the angles by introducing more atom types, so it is not necessary to modify the LAMMPS package. Fig. 2 (with M=V and X=Te) shows that, for 1H-VTe<sub>2</sub>, we can differentiate these angles around the V atom by assigning these six neighboring Te atoms with different atom types. It can be found that twelve atom types are necessary for the purpose of differentiating all six neighbors around one V atom.

We use LAMMPS to perform MD simulations for the mechanical behavior of the single-layer 1H-VTe<sub>2</sub> under uniaxial tension at 1.0 K and 300.0 K. Fig. 20 shows the stress-strain curve for the tension of a single-layer 1H-VTe<sub>2</sub> of dimension  $100 \times 100$  Å. Periodic boundary conditions are applied in both armchair and zigzag directions. The single-layer 1H-VTe<sub>2</sub> is stretched uniaxially along the armchair or zigzag direction. The stress is calculated without involving the actual thickness of the quasi-two-dimensional structure of the single-layer 1H-VTe<sub>2</sub>. The Young's modulus can be obtained by a linear fitting of the stress-strain relation in the small strain range of  $[0, 0.01]$ . The Young's modulus are 68.1 N/m and 66.8 N/m along the armchair and zigzag directions, respectively. The Young's modulus is essentially isotropic in the armchair and zigzag directions. The Poisson's ratio from the VFF model and the SW potential is  $\nu_{xy} = \nu_{yx} = 0.28$ .

There is no available value for the nonlinear quantities in the single-layer 1H-VTe<sub>2</sub>. We have thus used the nonlinear parameter  $B = 0.5d^4$  in Eq. (5), which is close to the value of  $B$  in most materials. The value of the third order nonlinear elasticity  $D$  can be extracted by fitting the stress-strain relation to the function  $\sigma = E\epsilon + \frac{1}{2}D\epsilon^2$  with  $E$  as the Young's modulus. The values of  $D$  from the present SW potential are -237.4 N/m and -260.4 N/m along the armchair and zigzag directions, respectively. The ultimate stress is about  $9.0 \text{ Nm}^{-1}$

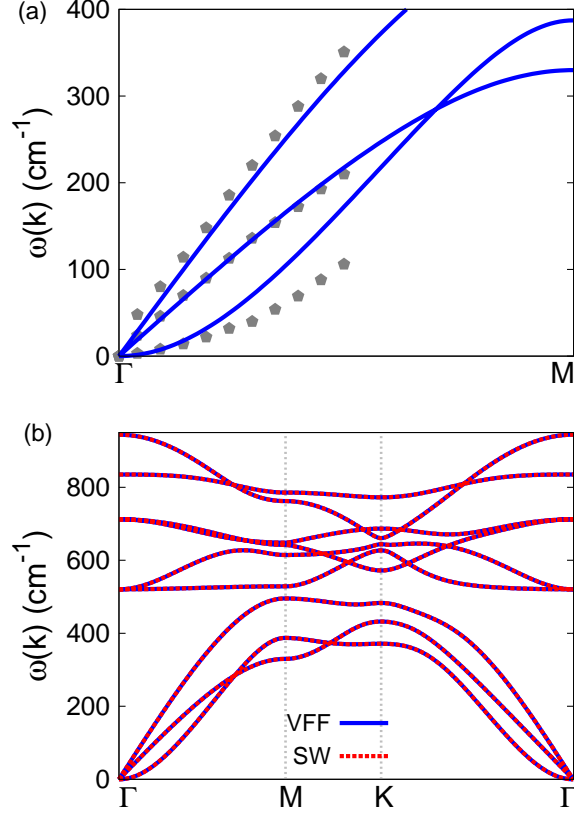


FIG. 21: (Color online) Phonon spectrum for single-layer 1H-CrO<sub>2</sub>. (a) Phonon dispersion along the  $\Gamma$ M direction in the Brillouin zone. The results from the VFF model (lines) are comparable with the *ab initio* results (pentagons) from Ref. 12. (b) The phonon dispersion from the SW potential is exactly the same as that from the VFF model.

at the ultimate strain of 0.23 in the armchair direction at the low temperature of 1 K. The ultimate stress is about  $8.6 \text{ Nm}^{-1}$  at the ultimate strain of 0.27 in the zigzag direction at the low temperature of 1 K.

## XII. 1H-CRO<sub>2</sub>

Most existing theoretical studies on the single-layer 1H-CrO<sub>2</sub> are based on the first-principles calculations. In this section, we will develop the SW potential for the single-layer 1H-CrO<sub>2</sub>.

The structure for the single-layer 1H-CrO<sub>2</sub> is shown in Fig. 1 (with M=Cr and X=O).

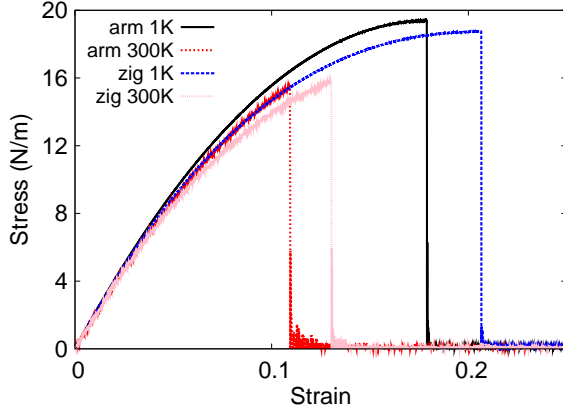


FIG. 22: (Color online) Stress-strain for single-layer 1H-CrO<sub>2</sub> of dimension  $100 \times 100 \text{ \AA}$  along the armchair and zigzag directions.

TABLE XLVI: The VFF model for single-layer 1H-CrO<sub>2</sub>. The second line gives an explicit expression for each VFF term. The third line is the force constant parameters. Parameters are in the unit of  $\frac{eV}{\text{\AA}^2}$  for the bond stretching interactions, and in the unit of eV for the angle bending interaction. The fourth line gives the initial bond length (in unit of  $\text{\AA}$ ) for the bond stretching interaction and the initial angle (in unit of degrees) for the angle bending interaction. The angle  $\theta_{ijk}$  has atom  $i$  as the apex.

VFF type	bond stretching		angle bending	
expression	$\frac{1}{2}K_{\text{Cr-O}}(\Delta r)^2$	$\frac{1}{2}K_{\text{Cr-O-O}}(\Delta\theta)^2$	$\frac{1}{2}K_{\text{Cr-O-O}'}(\Delta\theta)^2$	$\frac{1}{2}K_{\text{O-Cr-Cr}}(\Delta\theta)^2$
parameter	12.881	8.039	8.039	8.039
$r_0$ or $\theta_0$	1.880	86.655	75.194	86.655

Each Cr atom is surrounded by six O atoms. These O atoms are categorized into the top group (eg. atoms 1, 3, and 5) and bottom group (eg. atoms 2, 4, and 6). Each O atom is connected to three Cr atoms. The structural parameters are from the first-principles calculations,<sup>12</sup> including the lattice constant  $a = 2.58 \text{ \AA}$ , and the bond length  $d_{\text{Cr-O}} = 1.88 \text{ \AA}$ . The resultant angles are  $\theta_{\text{CrOO}} = \theta_{\text{OCrCr}} = 86.655^\circ$  and  $\theta_{\text{CrOO}'} = 75.194^\circ$ , in which atoms O and O' are from different (top or bottom) group.

Table XLVI shows four VFF terms for the single-layer 1H-CrO<sub>2</sub>, one of which is the bond stretching interaction shown by Eq. (1) while the other three terms are the angle bending

TABLE XLVII: Two-body SW potential parameters for single-layer 1H-CrO<sub>2</sub> used by GULP<sup>8</sup> as expressed in Eq. (3).

	$A$ (eV)	$\rho$ (Å)	$B$ (Å <sup>4</sup> )	$r_{\min}$ (Å)	$r_{\max}$ (Å)
Cr-O	6.343	0.916	6.246	0.0	2.536

TABLE XLVIII: Three-body SW potential parameters for single-layer 1H-CrO<sub>2</sub> used by GULP<sup>8</sup> as expressed in Eq. (4). The angle  $\theta_{ijk}$  in the first line indicates the bending energy for the angle with atom  $i$  as the apex.

	$K$ (eV)	$\theta_0$ (degree)	$\rho_1$ (Å)	$\rho_2$ (Å)	$r_{\min12}$ (Å)	$r_{\max12}$ (Å)	$r_{\min13}$ (Å)	$r_{\max13}$ (Å)	$r_{\min23}$ (Å)	$r_{\max23}$ (Å)
$\theta_{\text{Cr-O-O}}$	65.805	86.655	0.916	0.916	0.0	2.536	0.0	2.536	0.0	3.016
$\theta_{\text{Cr-O-O}'}$	70.163	75.194	0.916	0.916	0.0	2.536	0.0	2.536	0.0	3.016
$\theta_{\text{O-Cr-Cr}}$	65.805	86.655	0.916	0.916	0.0	2.536	0.0	2.536	0.0	3.016

interaction shown by Eq. (2). These force constant parameters are determined by fitting to the acoustic branches in the phonon dispersion along the  $\Gamma\text{M}$  as shown in Fig. 21 (a). The *ab initio* calculations for the phonon dispersion are from Ref. 12. Fig. 21 (b) shows that the VFF model and the SW potential give exactly the same phonon dispersion, as the SW potential is derived from the VFF model.

The parameters for the two-body SW potential used by GULP are shown in Tab. XLVII. The parameters for the three-body SW potential used by GULP are shown in Tab. XLVIII. Some representative parameters for the SW potential used by LAMMPS are listed in Tab. XLIX. We note that twelve atom types have been introduced for the simulation of

TABLE XLIX: SW potential parameters for single-layer 1H-CrO<sub>2</sub> used by LAMMPS<sup>9</sup> as expressed in Eqs. (9) and (10).

	$\epsilon$ (eV)	$\sigma$ (Å)	$a$	$\lambda$	$\gamma$	$\cos \theta_0$	$A_L$	$B_L$	$p$	$q$	tol
Cr <sub>1</sub> -O <sub>1</sub> -O <sub>1</sub>	1.000	0.916	2.769	0.000	1.000	0.000	6.242	8.871	4	0	0.0
Cr <sub>1</sub> -O <sub>1</sub> -O <sub>3</sub>	1.000	0.000	0.000	65.805	1.000	0.058	0.000	0.000	4	0	0.0
Cr <sub>1</sub> -O <sub>1</sub> -O <sub>2</sub>	1.000	0.000	0.000	70.163	1.000	0.256	0.000	0.000	4	0	0.0
O <sub>1</sub> -Cr <sub>1</sub> -Cr <sub>3</sub>	1.000	0.000	0.000	65.805	1.000	0.058	0.000	0.000	4	0	0.0

the single-layer 1H-CrO<sub>2</sub> using LAMMPS, because the angles around atom Cr in Fig. 1 (with M=Cr and X=O) are not distinguishable in LAMMPS. We have suggested two options to differentiate these angles by implementing some additional constraints in LAMMPS, which can be accomplished by modifying the source file of LAMMPS.<sup>13,14</sup> According to our experience, it is not so convenient for some users to implement these constraints and re-compile the LAMMPS package. Hence, in the present work, we differentiate the angles by introducing more atom types, so it is not necessary to modify the LAMMPS package. Fig. 2 (with M=Cr and X=O) shows that, for 1H-CrO<sub>2</sub>, we can differentiate these angles around the Cr atom by assigning these six neighboring O atoms with different atom types. It can be found that twelve atom types are necessary for the purpose of differentiating all six neighbors around one Cr atom.

We use LAMMPS to perform MD simulations for the mechanical behavior of the single-layer 1H-CrO<sub>2</sub> under uniaxial tension at 1.0 K and 300.0 K. Fig. 22 shows the stress-strain curve for the tension of a single-layer 1H-CrO<sub>2</sub> of dimension 100 × 100 Å. Periodic boundary conditions are applied in both armchair and zigzag directions. The single-layer 1H-CrO<sub>2</sub> is stretched uniaxially along the armchair or zigzag direction. The stress is calculated without involving the actual thickness of the quasi-two-dimensional structure of the single-layer 1H-CrO<sub>2</sub>. The Young's modulus can be obtained by a linear fitting of the stress-strain relation in the small strain range of [0, 0.01]. The Young's modulus are 210.6 N/m and 209.0 N/m along the armchair and zigzag directions, respectively. The Young's modulus is essentially isotropic in the armchair and zigzag directions. The Poisson's ratio from the VFF model and the SW potential is  $\nu_{xy} = \nu_{yx} = 0.13$ .

There is no available value for nonlinear quantities in the single-layer 1H-CrO<sub>2</sub>. We have thus used the nonlinear parameter  $B = 0.5d^4$  in Eq. (5), which is close to the value of  $B$  in most materials. The value of the third order nonlinear elasticity  $D$  can be extracted by fitting the stress-strain relation to the function  $\sigma = E\epsilon + \frac{1}{2}D\epsilon^2$  with  $E$  as the Young's modulus. The values of  $D$  from the present SW potential are -1127.7 N/m and -1185.8 N/m along the armchair and zigzag directions, respectively. The ultimate stress is about 19.4 Nm<sup>-1</sup> at the ultimate strain of 0.18 in the armchair direction at the low temperature of 1 K. The ultimate stress is about 18.7 Nm<sup>-1</sup> at the ultimate strain of 0.20 in the zigzag direction at the low temperature of 1 K.

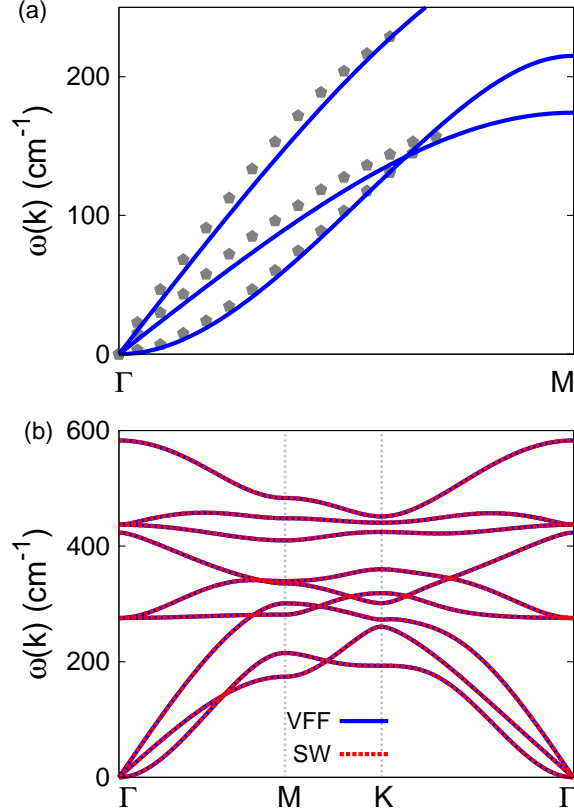


FIG. 23: (Color online) Phonon dispersion for single-layer 1H-CrS<sub>2</sub>. (a) The VFF model is fitted to the three acoustic branches in the long wave limit along the  $\Gamma$ M direction. The *ab initio* results (gray pentagons) are from Ref. 17. (b) The VFF model (blue lines) and the SW potential (red lines) give the same phonon dispersion for single-layer 1H-CrS<sub>2</sub> along  $\Gamma$ MKT $\Gamma$ .

### XIII. 1H-CrS<sub>2</sub>

Most existing theoretical studies on the single-layer 1H-CrS<sub>2</sub> are based on the first-principles calculations. In this section, we will develop both VFF model and the SW potential for the single-layer 1H-CrS<sub>2</sub>.

The structure for the single-layer 1H-CrS<sub>2</sub> is shown in Fig. 1 (with M=Cr and X=S). Each Cr atom is surrounded by six S atoms. These S atoms are categorized into the top group (eg. atoms 1, 3, and 5) and bottom group (eg. atoms 2, 4, and 6). Each S atom is connected to three Cr atoms. The structural parameters are from Ref. 17, including the lattice constant  $a = 2.99 \text{ \AA}$ , and the bond length  $d_{\text{Cr-S}} = 2.254 \text{ \AA}$ . The resultant angles are

TABLE L: The VFF model for single-layer 1H-CrS<sub>2</sub>. The second line gives an explicit expression for each VFF term. The third line is the force constant parameters. Parameters are in the unit of  $\frac{eV}{\text{Å}^2}$  for the bond stretching interactions, and in the unit of eV for the angle bending interaction. The fourth line gives the initial bond length (in unit of Å) for the bond stretching interaction and the initial angle (in unit of degrees) for the angle bending interaction. The angle  $\theta_{ijk}$  has atom i as the apex.

VFF type	bond stretching	angle bending		
expression	$\frac{1}{2}K_{Cr-S}(\Delta r)^2$	$\frac{1}{2}K_{Cr-S-S}(\Delta\theta)^2$	$\frac{1}{2}K_{Cr-S-S'}(\Delta\theta)^2$	$\frac{1}{2}K_{S-Cr-Cr}(\Delta\theta)^2$
parameter	8.752	4.614	4.614	4.614
$r_0$ or $\theta_0$	2.254	83.099	80.031	83.099

TABLE LI: Two-body SW potential parameters for single-layer 1HCrS<sub>2</sub> used by GULP<sup>8</sup> as expressed in Eq. (3).

	$A$ (eV)	$\rho$ (Å)	$B$ (Å <sup>4</sup> )	$r_{\min}$ (Å)	$r_{\max}$ (Å)
Cr-S	5.544	0.985	12.906	0.0	2.999

TABLE LII: Three-body SW potential parameters for single-layer 1H-CrS<sub>2</sub> used by GULP<sup>8</sup> as expressed in Eq. (4). The angle  $\theta_{ijk}$  in the first line indicates the bending energy for the angle with atom i as the apex.

	$K$ (eV)	$\theta_0$ (degree)	$\rho_1$ (Å)	$\rho_2$ (Å)	$r_{\min12}$ (Å)	$r_{\max12}$ (Å)	$r_{\min13}$ (Å)	$r_{\max13}$ (Å)	$r_{\min23}$ (Å)	$r_{\max23}$ (Å)
$\theta_{Cr-S-S}$	32.963	83.099	0.985	0.985	0.0	2.999	0.0	2.999	0.0	3.577
$\theta_{Cr-S-S'}$	33.491	80.031	0.985	0.985	0.0	2.999	0.0	2.999	0.0	3.577
$\theta_{S-Cr-Cr}$	32.963	83.099	0.985	0.985	0.0	2.999	0.0	2.999	0.0	3.577

TABLE LIII: SW potential parameters for single-layer 1H-CrS<sub>2</sub> used by LAMMPS<sup>9</sup> as expressed in Eqs. (9) and (10). Atom types in the first column are displayed in Fig. 2 (with M=Cr and X=S).

	$\epsilon$ (eV)	$\sigma$ (Å)	$a$	$\lambda$	$\gamma$	$\cos\theta_0$	$A_L$	$B_L$	$p$	$q$	tol
Cr <sub>1</sub> -S <sub>1</sub> -S <sub>1</sub>	1.000	0.985	3.043	0.000	1.000	0.000	5.544	13.683	4	0	0.0
Cr <sub>1</sub> -S <sub>1</sub> -S <sub>3</sub>	1.000	0.000	0.000	32.963	1.000	0.120	0.000	0.000	4	0	0.0
Cr <sub>1</sub> -S <sub>1</sub> -S <sub>2</sub>	1.000	0.000	0.000	33.491	1.000	0.173	0.000	0.000	4	0	0.0
S <sub>1</sub> -Cr <sub>1</sub> -Cr <sub>3</sub>	1.000	0.000	0.000	32.963	1.000	0.120	0.000	0.000	4	0	0.0

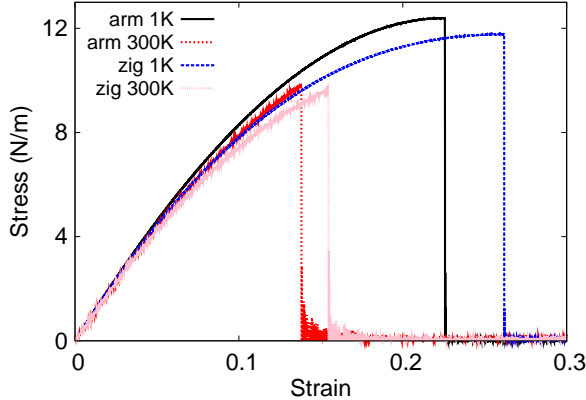


FIG. 24: (Color online) Stress-strain for single-layer 1H-CrS<sub>2</sub> of dimension 100 × 100 Å along the armchair and zigzag directions.

$\theta_{\text{CrSS}} = \theta_{\text{SCrCr}} = 83.099^\circ$  and  $\theta_{\text{CrSS}'} = 80.031^\circ$ , in which atoms S and S' are from different (top or bottom) group.

Table L shows four VFF terms for the 1H-CrS<sub>2</sub>, one of which is the bond stretching interaction shown by Eq. (1) while the other three terms are the angle bending interaction shown by Eq. (2). These force constant parameters are determined by fitting to the three acoustic branches in the phonon dispersion along the  $\Gamma\text{M}$  as shown in Fig. 23 (a). The *ab initio* calculations for the phonon dispersion are from Ref. 17. Similar phonon dispersion can also be found in other *ab initio* calculations.<sup>12</sup> Fig. 23 (b) shows that the VFF model and the SW potential give exactly the same phonon dispersion, as the SW potential is derived from the VFF model.

The parameters for the two-body SW potential used by GULP are shown in Tab. LI. The parameters for the three-body SW potential used by GULP are shown in Tab. LII. Parameters for the SW potential used by LAMMPS are listed in Tab. LIII. We note that twelve atom types have been introduced for the simulation of the single-layer 1H-CrS<sub>2</sub> using LAMMPS, because the angles around atom Cr in Fig. 1 (with M=Cr and X=S) are not distinguishable in LAMMPS. We have suggested two options to differentiate these angles by implementing some additional constraints in LAMMPS, which can be accomplished by modifying the source file of LAMMPS.<sup>13,14</sup> According to our experience, it is not so convenient for some users to implement these constraints and recompile the LAMMPS package. Hence, in the present work, we differentiate the angles by introducing more atom types, so

it is not necessary to modify the LAMMPS package. Fig. 2 (with M=Cr and X=S) shows that, for 1H-CrS<sub>2</sub>, we can differentiate these angles around the Cr atom by assigning these six neighboring S atoms with different atom types. It can be found that twelve atom types are necessary for the purpose of differentiating all six neighbors around one Cr atom.

We use LAMMPS to perform MD simulations for the mechanical behavior of the single-layer 1H-CrS<sub>2</sub> under uniaxial tension at 1.0 K and 300.0 K. Fig. 24 shows the stress-strain curve for the tension of a single-layer 1H-CrS<sub>2</sub> of dimension 100 × 100 Å. Periodic boundary conditions are applied in both armchair and zigzag directions. The single-layer 1H-CrS<sub>2</sub> is stretched uniaxially along the armchair or zigzag direction. The stress is calculated without involving the actual thickness of the quasi-two-dimensional structure of the single-layer 1H-CrS<sub>2</sub>. The Young's modulus can be obtained by a linear fitting of the stress-strain relation in the small strain range of [0, 0.01]. The Young's modulus are 98.4 N/m and 97.8 N/m along the armchair and zigzag directions, respectively. The Young's modulus is essentially isotropic in the armchair and zigzag directions. These values are in reasonably agreement with the *ab initio* results, eg. 112.0 N/m from Refs 18, or 111.9 N/m from Ref. 19. The Poisson's ratio from the VFF model and the SW potential is  $\nu_{xy} = \nu_{yx} = 0.26$ , which agrees with the *ab initio* value of 0.27.<sup>18,19</sup>

There is no available value for the nonlinear quantities in the single-layer 1H-CrS<sub>2</sub>. We have thus used the nonlinear parameter  $B = 0.5d^4$  in Eq. (5), which is close to the value of  $B$  in most materials. The value of the third order nonlinear elasticity  $D$  can be extracted by fitting the stress-strain relation to the function  $\sigma = E\epsilon + \frac{1}{2}D\epsilon^2$  with  $E$  as the Young's modulus. The values of  $D$  from the present SW potential are -364.8 N/m and -409.3 N/m along the armchair and zigzag directions, respectively. The ultimate stress is about 12.4 Nm<sup>-1</sup> at the ultimate strain of 0.22 in the armchair direction at the low temperature of 1 K. The ultimate stress is about 11.8 Nm<sup>-1</sup> at the ultimate strain of 0.26 in the zigzag direction at the low temperature of 1 K.

#### XIV. 1H-CRSE<sub>2</sub>

Most existing theoretical studies on the single-layer 1H-CrSe<sub>2</sub> are based on the first-principles calculations. In this section, we will develop both VFF model and the SW potential for the single-layer 1H-CrSe<sub>2</sub>.

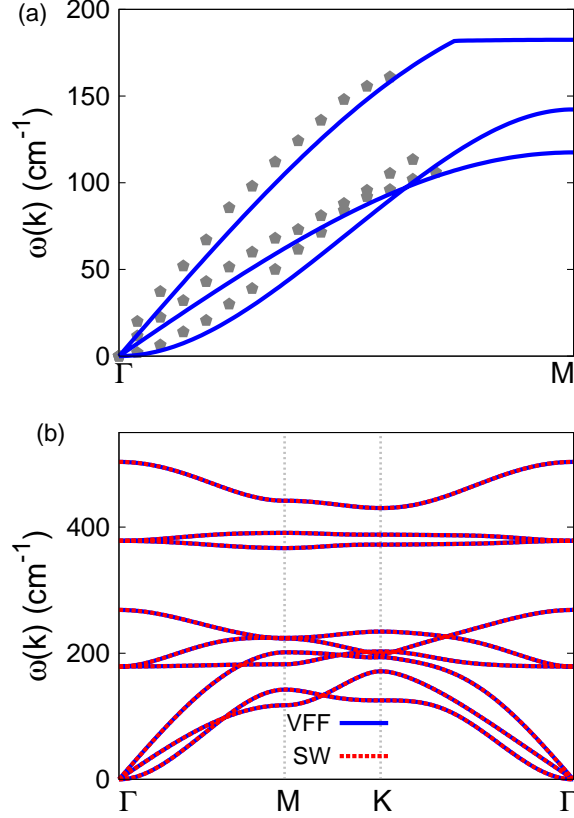


FIG. 25: (Color online) Phonon dispersion for single-layer 1H-CrSe<sub>2</sub>. (a) The VFF model is fitted to the three acoustic branches in the long wave limit along the  $\Gamma$ M direction. The *ab initio* results (gray pentagons) are from Ref. 12. (b) The VFF model (blue lines) and the SW potential (red lines) give the same phonon dispersion for single-layer 1H-CrSe<sub>2</sub> along  $\Gamma$ MK $\Gamma$ .

The structure for the single-layer 1H-CrSe<sub>2</sub> is shown in Fig. 1 (with M=Cr and X=Se). Each Cr atom is surrounded by six Se atoms. These Se atoms are categorized into the top group (eg. atoms 1, 3, and 5) and bottom group (eg. atoms 2, 4, and 6). Each Se atom is connected to three Cr atoms. The structural parameters are from Ref. 12, including the lattice constant  $a = 3.13 \text{ \AA}$ , and the bond length  $d_{\text{Cr-Se}} = 2.38 \text{ \AA}$ . The resultant angles are  $\theta_{\text{CrSeSe}} = \theta_{\text{SeCrCr}} = 82.229^\circ$  and  $\theta_{\text{CrSeSe}'} = 81.197^\circ$ , in which atoms Se and Se' are from different (top or bottom) group.

Table LIV shows four VFF terms for the 1H-CrSe<sub>2</sub>, one of which is the bond stretching interaction shown by Eq. (1) while the other three terms are the angle bending interaction shown by Eq. (2). These force constant parameters are determined by fitting to the three

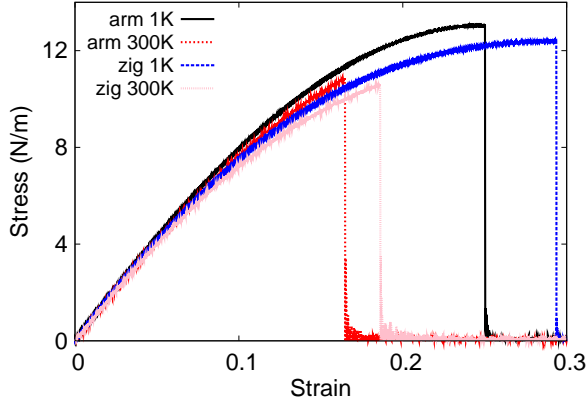


FIG. 26: (Color online) Stress-strain for single-layer 1H-CrSe<sub>2</sub> of dimension  $100 \times 100 \text{ \AA}$  along the armchair and zigzag directions.

TABLE LIV: The VFF model for single-layer 1H-CrSe<sub>2</sub>. The second line gives an explicit expression for each VFF term. The third line is the force constant parameters. Parameters are in the unit of  $\frac{eV}{\text{Å}^2}$  for the bond stretching interactions, and in the unit of eV for the angle bending interaction. The fourth line gives the initial bond length (in unit of Å) for the bond stretching interaction and the initial angle (in unit of degrees) for the angle bending interaction. The angle  $\theta_{ijk}$  has atom  $i$  as the apex.

VFF type	bond stretching	angle bending		
expression	$\frac{1}{2}K_{Cr-Se}(\Delta r)^2$	$\frac{1}{2}K_{Cr-Se-Se}(\Delta\theta)^2$	$\frac{1}{2}K_{Cr-Se-Se'}(\Delta\theta)^2$	$\frac{1}{2}K_{Se-Cr-Cr}(\Delta\theta)^2$
parameter	9.542	4.465	4.465	4.465
$r_0$ or $\theta_0$	2.380	82.229	81.197	82.229

acoustic branches in the phonon dispersion along the  $\Gamma M$  as shown in Fig. 25 (a). The *ab initio* calculations for the phonon dispersion are from Ref. 12. Fig. 25 (b) shows that the VFF model and the SW potential give exactly the same phonon dispersion, as the SW potential is derived from the VFF model.

The parameters for the two-body SW potential used by GULP are shown in Tab. LV. The parameters for the three-body SW potential used by GULP are shown in Tab. LVI. Parameters for the SW potential used by LAMMPS are listed in Tab. LVII. We note that twelve atom types have been introduced for the simulation of the single-layer 1H-CrSe<sub>2</sub> using LAMMPS, because the angles around atom Cr in Fig. 1 (with M=Cr and X=Se) are not

TABLE LV: Two-body SW potential parameters for single-layer 1H-CrSe<sub>2</sub> used by GULP<sup>8</sup> as expressed in Eq. (3).

	$A$ (eV)	$\rho$ (Å)	$B$ (Å <sup>4</sup> )	$r_{\min}$ (Å)	$r_{\max}$ (Å)
Cr-Se	6.581	1.012	16.043	0.0	3.156

TABLE LVI: Three-body SW potential parameters for single-layer 1H-CrSe<sub>2</sub> used by GULP<sup>8</sup> as expressed in Eq. (4). The angle  $\theta_{ijk}$  in the first line indicates the bending energy for the angle with atom i as the apex.

	$K$ (eV)	$\theta_0$ (degree)	$\rho_1$ (Å)	$\rho_2$ (Å)	$r_{\min12}$ (Å)	$r_{\max12}$ (Å)	$r_{\min13}$ (Å)	$r_{\max13}$ (Å)	$r_{\min23}$ (Å)	$r_{\max23}$ (Å)
$\theta_{\text{Cr-Se-Se}}$	30.881	82.229	1.012	1.012	0.0	3.156	0.0	3.156	0.0	3.767
$\theta_{\text{Cr-Se-Se}'}$	31.044	81.197	1.012	1.012	0.0	3.156	0.0	3.156	0.0	3.767
$\theta_{\text{Se-Cr-Cr}}$	30.881	82.229	1.012	1.012	0.0	3.156	0.0	3.156	0.0	3.767

distinguishable in LAMMPS. We have suggested two options to differentiate these angles by implementing some additional constraints in LAMMPS, which can be accomplished by modifying the source file of LAMMPS.<sup>13,14</sup> According to our experience, it is not so convenient for some users to implement these constraints and recompile the LAMMPS package. Hence, in the present work, we differentiate the angles by introducing more atom types, so it is not necessary to modify the LAMMPS package. Fig. 2 (with M=Cr and X=Se) shows that, for 1H-CrSe<sub>2</sub>, we can differentiate these angles around the Cr atom by assigning these six neighboring Se atoms with different atom types. It can be found that twelve atom types

TABLE LVII: SW potential parameters for single-layer 1H-CrSe<sub>2</sub> used by LAMMPS<sup>9</sup> as expressed in Eqs. (9) and (10). Atom types in the first column are displayed in Fig. 2 (with M=Cr and X=Se).

	$\epsilon$ (eV)	$\sigma$ (Å)	$a$	$\lambda$	$\gamma$	$\cos\theta_0$	$A_L$	$B_L$	$p$	$q$	tol
Cr <sub>1</sub> -Se <sub>1</sub> -Se <sub>1</sub>	1.000	1.012	3.118	0.000	1.000	0.000	6.581	15.284	4	0	0.0
Cr <sub>1</sub> -Se <sub>1</sub> -Se <sub>3</sub>	1.000	0.000	0.000	30.881	1.000	0.135	0.000	0.000	4	0	0.0
Cr <sub>1</sub> -Se <sub>1</sub> -Se <sub>2</sub>	1.000	0.000	0.000	31.044	1.000	0.153	0.000	0.000	4	0	0.0
Se <sub>1</sub> -Cr <sub>1</sub> -Cr <sub>3</sub>	1.000	0.000	0.000	30.881	1.000	0.135	0.000	0.000	4	0	0.0

are necessary for the purpose of differentiating all six neighbors around one Cr atom.

We use LAMMPS to perform MD simulations for the mechanical behavior of the single-layer 1H-CrSe<sub>2</sub> under uniaxial tension at 1.0 K and 300.0 K. Fig. 26 shows the stress-strain curve for the tension of a single-layer 1H-CrSe<sub>2</sub> of dimension 100 × 100 Å. Periodic boundary conditions are applied in both armchair and zigzag directions. The single-layer 1H-CrSe<sub>2</sub> is stretched uniaxially along the armchair or zigzag direction. The stress is calculated without involving the actual thickness of the quasi-two-dimensional structure of the single-layer 1H-CrSe<sub>2</sub>. The Young’s modulus can be obtained by a linear fitting of the stress-strain relation in the small strain range of [0, 0.01]. The Young’s modulus are 90.0 N/m and 89.0 N/m along the armchair and zigzag directions, respectively. The Young’s modulus is essentially isotropic in the armchair and zigzag directions. These values are in reasonably agreement with the *ab initio* results, eg. 88.0 N/m from Refs 18, or 87.9 N/m from Ref. 19. The Poisson’s ratio from the VFF model and the SW potential is  $\nu_{xy} = \nu_{yx} = 0.30$ , which agrees with the *ab initio* value of 0.30.<sup>18,19</sup>

There is no available value for the nonlinear quantities in the single-layer 1H-CrSe<sub>2</sub>. We have thus used the nonlinear parameter  $B = 0.5d^4$  in Eq. (5), which is close to the value of  $B$  in most two-dimensional atomic layered materials. The value of the third order nonlinear elasticity  $D$  can be extracted by fitting the stress-strain relation to the function  $\sigma = E\epsilon + \frac{1}{2}D\epsilon^2$  with  $E$  as the Young’s modulus. The values of  $D$  from the present SW potential are -279.6 N/m and -318.8 N/m along the armchair and zigzag directions, respectively. The ultimate stress is about 13.0 Nm<sup>-1</sup> at the ultimate strain of 0.25 in the armchair direction at the low temperature of 1 K. The ultimate stress is about 12.4 Nm<sup>-1</sup> at the ultimate strain of 0.29 in the zigzag direction at the low temperature of 1 K.

## XV. 1H-CRTE<sub>2</sub>

Most existing theoretical studies on the single-layer 1H-CrTe<sub>2</sub> are based on the first-principles calculations. In this section, we will develop both VFF model and the SW potential for the single-layer 1H-CrTe<sub>2</sub>.

The structure for the single-layer 1H-CrTe<sub>2</sub> is shown in Fig. 1 (with M=Cr and X=Te). Each Cr atom is surrounded by six Te atoms. These Te atoms are categorized into the top group (eg. atoms 1, 3, and 5) and bottom group (eg. atoms 2, 4, and 6). Each Te atom

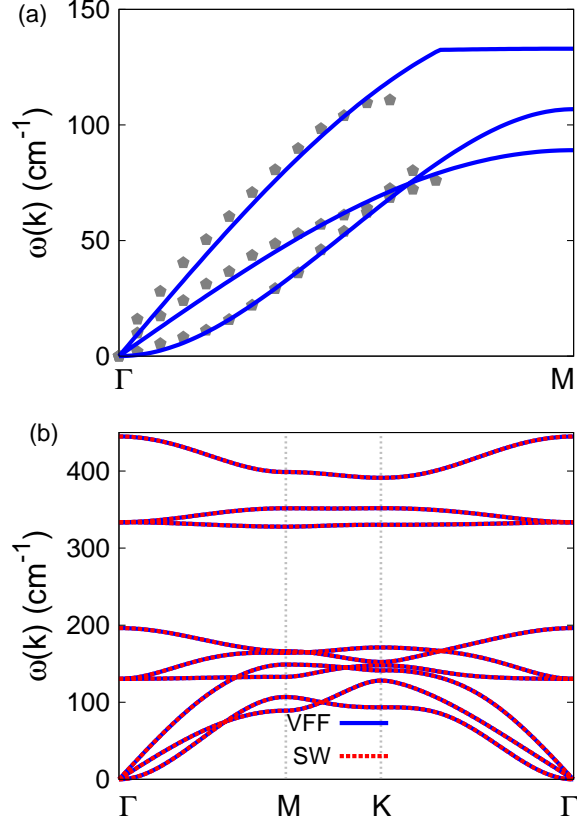


FIG. 27: (Color online) Phonon dispersion for single-layer 1H-CrTe<sub>2</sub>. (a) The VFF model is fitted to the three acoustic branches in the long wave limit along the  $\Gamma$ M direction. The *ab initio* results (gray pentagons) are from Ref. 12. (b) The VFF model (blue lines) and the SW potential (red lines) give the same phonon dispersion for single-layer 1H-CrTe<sub>2</sub> along  $\Gamma$ MKT $\Gamma$ .

is connected to three Cr atoms. The structural parameters are from Ref. 12, including the lattice constant  $a = 3.39$  Å, and the bond length  $d_{\text{Cr-Te}} = 2.58$  Å. The resultant angles are  $\theta_{\text{CrTeTe}} = \theta_{\text{TeCrCr}} = 82.139^\circ$  and  $\theta_{\text{CrTeTe}'} = 81.316^\circ$ , in which atoms Te and Te' are from different (top or bottom) group.

Table LVIII shows three VFF terms for the 1H-CrTe<sub>2</sub>, one of which is the bond stretching interaction shown by Eq. (1) while the other two terms are the angle bending interaction shown by Eq. (2). These force constant parameters are determined by fitting to the three acoustic branches in the phonon dispersion along the  $\Gamma$ M as shown in Fig. 27 (a). The *ab initio* calculations for the phonon dispersion are from Ref. 12. Fig. 27 (b) shows that the VFF model and the SW potential give exactly the same phonon dispersion, as the SW

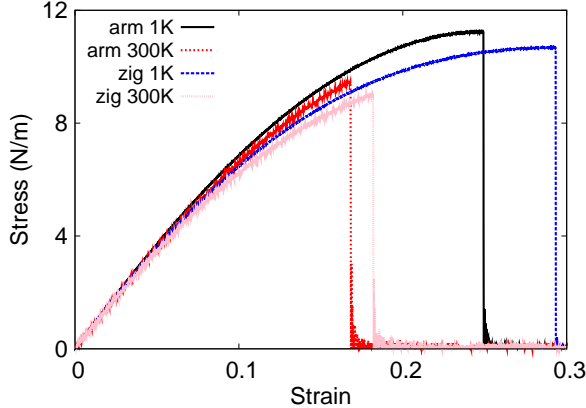


FIG. 28: (Color online) Stress-strain for single-layer 1H-CrTe<sub>2</sub> of dimension  $100 \times 100 \text{ \AA}$  along the armchair and zigzag directions.

TABLE LVIII: The VFF model for single-layer 1H-CrTe<sub>2</sub>. The second line gives an explicit expression for each VFF term. The third line is the force constant parameters. Parameters are in the unit of  $\frac{eV}{\text{Å}^2}$  for the bond stretching interactions, and in the unit of eV for the angle bending interaction. The fourth line gives the initial bond length (in unit of Å) for the bond stretching interaction and the initial angle (in unit of degrees) for the angle bending interaction. The angle  $\theta_{ijk}$  has atom *i* as the apex.

VFF type	bond stretching	angle bending		
expression	$\frac{1}{2}K_{Cr-Te}(\Delta r)^2$	$\frac{1}{2}K_{Cr-Te-Te}(\Delta\theta)^2$	$\frac{1}{2}K_{Cr-Te-Te'}(\Delta\theta)^2$	$\frac{1}{2}K_{Te-Cr-Cr}(\Delta\theta)^2$
parameter	8.197	4.543	4.543	4.543
$r_0$ or $\theta_0$	2.580	82.139	81.316	82.139

potential is derived from the VFF model.

The parameters for the two-body SW potential used by GULP are shown in Tab. LIX. The parameters for the three-body SW potential used by GULP are shown in Tab. LX. Parameters for the SW potential used by LAMMPS are listed in Tab. LXI. We note that twelve atom types have been introduced for the simulation of the single-layer 1H-CrTe<sub>2</sub> using LAMMPS, because the angles around atom Cr in Fig. 1 (with M=Cr and X=Te) are not distinguishable in LAMMPS. We have suggested two options to differentiate these angles by implementing some additional constraints in LAMMPS, which can be accomplished by

TABLE LIX: Two-body SW potential parameters for single-layer 1H-CrTe<sub>2</sub> used by GULP<sup>8</sup> as expressed in Eq. (3).

	$A$ (eV)	$\rho$ (Å)	$B$ (Å <sup>4</sup> )	$r_{\min}$ (Å)	$r_{\max}$ (Å)
Cr-Te	6.627	1.094	22.154	0.0	3.420

TABLE LX: Three-body SW potential parameters for single-layer 1H-CrTe<sub>2</sub> used by GULP<sup>8</sup> as expressed in Eq. (4). The angle  $\theta_{ijk}$  in the first line indicates the bending energy for the angle with atom i as the apex.

	$K$ (eV)	$\theta_0$ (degree)	$\rho_1$ (Å)	$\rho_2$ (Å)	$r_{\min12}$ (Å)	$r_{\max12}$ (Å)	$r_{\min13}$ (Å)	$r_{\max13}$ (Å)	$r_{\min23}$ (Å)	$r_{\max23}$ (Å)
$\theta_{\text{Cr-Te-Te}}$	31.316	82.139	1.094	1.094	0.0	3.420	0.0	3.420	0.0	4.082
$\theta_{\text{Cr-Te-Te}'}$	31.447	81.316	1.094	1.094	0.0	3.420	0.0	3.420	0.0	4.082
$\theta_{\text{Te-Cr-Cr}}$	31.316	82.139	1.094	1.094	0.0	3.420	0.0	3.420	0.0	4.082

modifying the source file of LAMMPS.<sup>13,14</sup> According to our experience, it is not so convenient for some users to implement these constraints and recompile the LAMMPS package. Hence, in the present work, we differentiate the angles by introducing more atom types, so it is not necessary to modify the LAMMPS package. Fig. 2 (with M=Cr and X=Te) shows that, for 1H-CrTe<sub>2</sub>, we can differentiate these angles around the Cr atom by assigning these six neighboring Te atoms with different atom types. It can be found that twelve atom types are necessary for the purpose of differentiating all six neighbors around one Cr atom.

We use LAMMPS to perform MD simulations for the mechanical behavior of the single-

TABLE LXI: SW potential parameters for single-layer 1H-CrTe<sub>2</sub> used by LAMMPS<sup>9</sup> as expressed in Eqs. (9) and (10). Atom types in the first column are displayed in Fig. 2 (with M=Cr and X=Te).

	$\epsilon$ (eV)	$\sigma$ (Å)	$a$	$\lambda$	$\gamma$	$\cos\theta_0$	$A_L$	$B_L$	$p$	$q$	tol
Cr <sub>1</sub> -Te <sub>1</sub> -Te <sub>1</sub>	1.000	1.094	3.126	0.000	1.000	0.000	6.627	15.461	4	0	0.0
Cr <sub>1</sub> -Te <sub>1</sub> -Te <sub>3</sub>	1.000	0.000	0.000	31.316	1.000	0.137	0.000	0.000	4	0	0.0
Cr <sub>1</sub> -Te <sub>1</sub> -Te <sub>2</sub>	1.000	0.000	0.000	31.447	1.000	0.151	0.000	0.000	4	0	0.0
Te <sub>1</sub> -Cr <sub>1</sub> -Cr <sub>3</sub>	1.000	0.000	0.000	31.316	1.000	0.137	0.000	0.000	4	0	0.0

layer 1H-CrTe<sub>2</sub> under uniaxial tension at 1.0 K and 300.0 K. Fig. 28 shows the stress-strain curve for the tension of a single-layer 1H-CrTe<sub>2</sub> of dimension  $100 \times 100 \text{ \AA}$ . Periodic boundary conditions are applied in both armchair and zigzag directions. The single-layer 1H-CrTe<sub>2</sub> is stretched uniaxially along the armchair or zigzag direction. The stress is calculated without involving the actual thickness of the quasi-two-dimensional structure of the single-layer 1H-CrTe<sub>2</sub>. The Young's modulus can be obtained by a linear fitting of the stress-strain relation in the small strain range of  $[0, 0.01]$ . The Young's modulus are 77.2 N/m and 76.4 N/m along the armchair and zigzag directions, respectively. The Young's modulus is essentially isotropic in the armchair and zigzag directions. These values are in reasonably agreement with the *ab initio* results, eg. 63.9 N/m from Refs 18 and 19. The Poisson's ratio from the VFF model and the SW potential is  $\nu_{xy} = \nu_{yx} = 0.30$ , which agrees with the *ab initio* value of 0.30.<sup>18,19</sup>

There is no available value for the nonlinear quantities in the single-layer 1H-CrTe<sub>2</sub>. We have thus used the nonlinear parameter  $B = 0.5d^4$  in Eq. (5), which is close to the value of  $B$  in most two-dimensional atomic layered materials. The value of the third order nonlinear elasticity  $D$  can be extracted by fitting the stress-strain relation to the function  $\sigma = E\epsilon + \frac{1}{2}D\epsilon^2$  with  $E$  as the Young's modulus. The values of  $D$  from the present SW potential are -237.1 N/m and -280.8 N/m along the armchair and zigzag directions, respectively. The ultimate stress is about  $11.2 \text{ Nm}^{-1}$  at the ultimate strain of 0.25 in the armchair direction at the low temperature of 1 K. The ultimate stress is about  $10.7 \text{ Nm}^{-1}$  at the ultimate strain of 0.29 in the zigzag direction at the low temperature of 1 K.

## XVI. 1H-MnO<sub>2</sub>

Most existing theoretical studies on the single-layer 1H-MnO<sub>2</sub> are based on the first-principles calculations. In this section, we will develop the SW potential for the single-layer 1H-MnO<sub>2</sub>.

The structure for the single-layer 1H-MnO<sub>2</sub> is shown in Fig. 1 (with M=Mn and X=O). Each Mn atom is surrounded by six O atoms. These O atoms are categorized into the top group (eg. atoms 1, 3, and 5) and bottom group (eg. atoms 2, 4, and 6). Each O atom is connected to three Mn atoms. The structural parameters are from the first-principles calculations,<sup>12</sup> including the lattice constant  $a = 2.61 \text{ \AA}$ , and the bond length

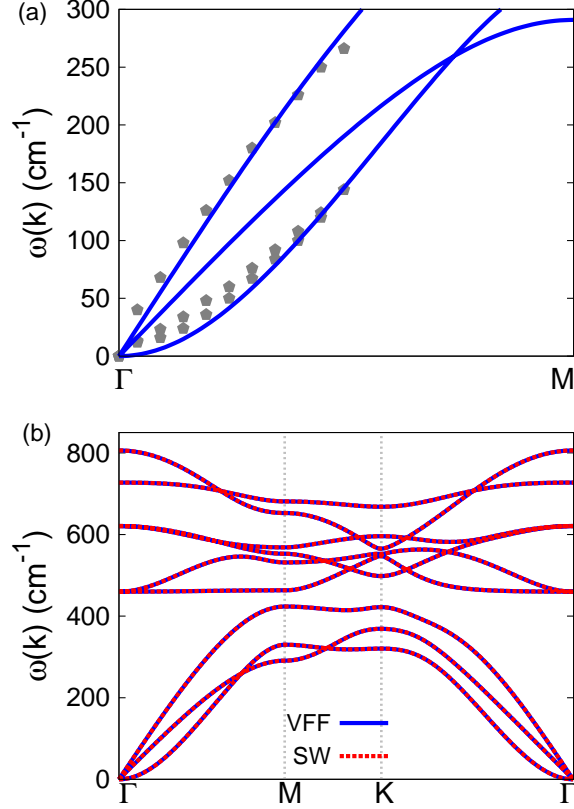


FIG. 29: (Color online) Phonon spectrum for single-layer 1H-MnO<sub>2</sub>. (a) Phonon dispersion along the  $\Gamma$ M direction in the Brillouin zone. The results from the VFF model (lines) are comparable with the *ab initio* results (pentagons) from Ref. 12. (b) The phonon dispersion from the SW potential is exactly the same as that from the VFF model.

$d_{\text{Mn-O}} = 1.87 \text{ \AA}$ . The resultant angles are  $\theta_{\text{MnOO}} = \theta_{\text{OMnMn}} = 88.511^\circ$  and  $\theta_{\text{MnOO}'} = 72.621^\circ$ , in which atoms O and O' are from different (top or bottom) group.

Table LXII shows four VFF terms for the single-layer 1H-MnO<sub>2</sub>, one of which is the bond stretching interaction shown by Eq. (1) while the other three terms are the angle bending interaction shown by Eq. (2). These force constant parameters are determined by fitting to the acoustic branches in the phonon dispersion along the  $\Gamma$ M as shown in Fig. 29 (a). The *ab initio* calculations for the phonon dispersion are from Ref. 12. Typically, the transverse acoustic branch has a linear dispersion, so is higher than the flexural branch. However, it can be seen that the transverse acoustic branch is close to the flexural branch, which should be due to the underestimation from the *ab initio* calculations. Fig. 29 (b) shows that the VFF

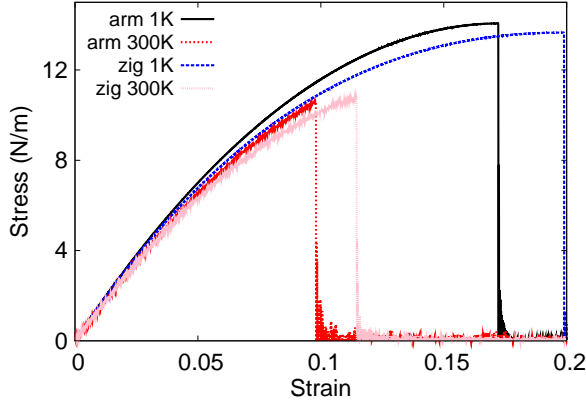


FIG. 30: (Color online) Stress-strain for single-layer 1H-MnO<sub>2</sub> of dimension  $100 \times 100 \text{ \AA}$  along the armchair and zigzag directions.

TABLE LXII: The VFF model for single-layer 1H-MnO<sub>2</sub>. The second line gives an explicit expression for each VFF term. The third line is the force constant parameters. Parameters are in the unit of  $\frac{eV}{\text{Å}^2}$  for the bond stretching interactions, and in the unit of eV for the angle bending interaction. The fourth line gives the initial bond length (in unit of Å) for the bond stretching interaction and the initial angle (in unit of degrees) for the angle bending interaction. The angle  $\theta_{ijk}$  has atom *i* as the apex.

VFF type	bond stretching	angle bending		
expression	$\frac{1}{2}K_{\text{Mn-O}}(\Delta r)^2$	$\frac{1}{2}K_{\text{Mn-O-O}}(\Delta\theta)^2$	$\frac{1}{2}K_{\text{Mn-O-O}'}(\Delta\theta)^2$	$\frac{1}{2}K_{\text{O-Mn-Mn}}(\Delta\theta)^2$
parameter	9.382	6.253	6.253	6.253
$r_0$ or $\theta_0$	1.870	88.511	72.621	88.511

model and the SW potential give exactly the same phonon dispersion, as the SW potential is derived from the VFF model.

The parameters for the two-body SW potential used by GULP are shown in Tab. LXIII. The parameters for the three-body SW potential used by GULP are shown in Tab. LXIV. Some representative parameters for the SW potential used by LAMMPS are listed in Tab. LXV. We note that twelve atom types have been introduced for the simulation of the single-layer 1H-MnO<sub>2</sub> using LAMMPS, because the angles around atom Mn in Fig. 1 (with M=Mn and X=O) are not distinguishable in LAMMPS. We have suggested two op-

TABLE LXIII: Two-body SW potential parameters for single-layer 1H-MnO<sub>2</sub> used by GULP<sup>8</sup> as expressed in Eq. (3).

	$A$ (eV)	$\rho$ (Å)	$B$ (Å <sup>4</sup> )	$r_{\min}$ (Å)	$r_{\max}$ (Å)
Mn-O	4.721	0.961	6.114	0.0	2.540

TABLE LXIV: Three-body SW potential parameters for single-layer 1H-MnO<sub>2</sub> used by GULP<sup>8</sup> as expressed in Eq. (4). The angle  $\theta_{ijk}$  in the first line indicates the bending energy for the angle with atom i as the apex.

	$K$ (eV)	$\theta_0$ (degree)	$\rho_1$ (Å)	$\rho_2$ (Å)	$r_{\min12}$ (Å)	$r_{\max12}$ (Å)	$r_{\min13}$ (Å)	$r_{\max13}$ (Å)	$r_{\min23}$ (Å)	$r_{\max23}$ (Å)
$\theta_{\text{Mn-O-O}}$	55.070	88.511	0.961	0.961	0.0	2.540	0.0	2.540	0.0	3.016
$\theta_{\text{Mn-O-O}'}$	60.424	72.621	0.961	0.961	0.0	2.540	0.0	2.540	0.0	3.016
$\theta_{\text{O-Mn-Mn}}$	55.070	88.511	0.961	0.961	0.0	2.540	0.0	2.540	0.0	3.016

tions to differentiate these angles by implementing some additional constraints in LAMMPS, which can be accomplished by modifying the source file of LAMMPS.<sup>13,14</sup> According to our experience, it is not so convenient for some users to implement these constraints and re-compile the LAMMPS package. Hence, in the present work, we differentiate the angles by introducing more atom types, so it is not necessary to modify the LAMMPS package. Fig. 2 (with M=Mn and X=O) shows that, for 1H-MnO<sub>2</sub>, we can differentiate these angles around the Mn atom by assigning these six neighboring O atoms with different atom types. It can be found that twelve atom types are necessary for the purpose of differentiating all six neighbors around one Mn atom.

TABLE LXV: SW potential parameters for single-layer 1H-MnO<sub>2</sub> used by LAMMPS<sup>9</sup> as expressed in Eqs. (9) and (10).

	$\epsilon$ (eV)	$\sigma$ (Å)	$a$	$\lambda$	$\gamma$	$\cos \theta_0$	$A_L$	$B_L$	$p$	$q$	tol
Mn <sub>1</sub> -O <sub>1</sub> -O <sub>1</sub>	1.000	0.961	2.643	0.000	1.000	0.000	4.721	7.158	4	0	0.0
Mn <sub>1</sub> -O <sub>1</sub> -O <sub>3</sub>	1.000	0.000	0.000	55.070	1.000	0.026	0.000	0.000	4	0	0.0
Mn <sub>1</sub> -O <sub>1</sub> -O <sub>2</sub>	1.000	0.000	0.000	60.424	1.000	0.299	0.000	0.000	4	0	0.0
O <sub>1</sub> -Mn <sub>1</sub> -Mn <sub>3</sub>	1.000	0.000	0.000	55.070	1.000	0.026	0.000	0.000	4	0	0.0

We use LAMMPS to perform MD simulations for the mechanical behavior of the single-layer 1H-MnO<sub>2</sub> under uniaxial tension at 1.0 K and 300.0 K. Fig. 30 shows the stress-strain curve for the tension of a single-layer 1H-MnO<sub>2</sub> of dimension 100 × 100 Å. Periodic boundary conditions are applied in both armchair and zigzag directions. The single-layer 1H-MnO<sub>2</sub> is stretched uniaxially along the armchair or zigzag direction. The stress is calculated without involving the actual thickness of the quasi-two-dimensional structure of the single-layer 1H-MnO<sub>2</sub>. The Young's modulus can be obtained by a linear fitting of the stress-strain relation in the small strain range of [0, 0.01]. The Young's modulus are 161.1 N/m and 160.2 N/m along the armchair and zigzag directions, respectively. The Young's modulus is essentially isotropic in the armchair and zigzag directions. The Poisson's ratio from the VFF model and the SW potential is  $\nu_{xy} = \nu_{yx} = 0.10$ .

There is no available value for nonlinear quantities in the single-layer 1H-MnO<sub>2</sub>. We have thus used the nonlinear parameter  $B = 0.5d^4$  in Eq. (5), which is close to the value of  $B$  in most materials. The value of the third order nonlinear elasticity  $D$  can be extracted by fitting the stress-strain relation to the function  $\sigma = E\epsilon + \frac{1}{2}D\epsilon^2$  with  $E$  as the Young's modulus. The values of  $D$  from the present SW potential are -915.9 N/m and -957.1 N/m along the armchair and zigzag directions, respectively. The ultimate stress is about 14.1 Nm<sup>-1</sup> at the ultimate strain of 0.17 in the armchair direction at the low temperature of 1 K. The ultimate stress is about 13.7 Nm<sup>-1</sup> at the ultimate strain of 0.20 in the zigzag direction at the low temperature of 1 K.

## XVII. 1H-FeO<sub>2</sub>

Most existing theoretical studies on the single-layer 1H-FeO<sub>2</sub> are based on the first-principles calculations. In this section, we will develop the SW potential for the single-layer 1H-FeO<sub>2</sub>.

The structure for the single-layer 1H-FeO<sub>2</sub> is shown in Fig. 1 (with M=Fe and X=O). Each Fe atom is surrounded by six O atoms. These O atoms are categorized into the top group (eg. atoms 1, 3, and 5) and bottom group (eg. atoms 2, 4, and 6). Each O atom is connected to three Fe atoms. The structural parameters are from the first-principles calculations,<sup>12</sup> including the lattice constant  $a = 2.62$  Å, and the bond length  $d_{\text{Fe-O}} = 1.88$  Å. The resultant angles are  $\theta_{\text{FeOO}} = \theta_{\text{OFeFe}} = 88.343^\circ$  and  $\theta_{\text{FeOO}'} = 72.856^\circ$ , in which atoms O and O' are

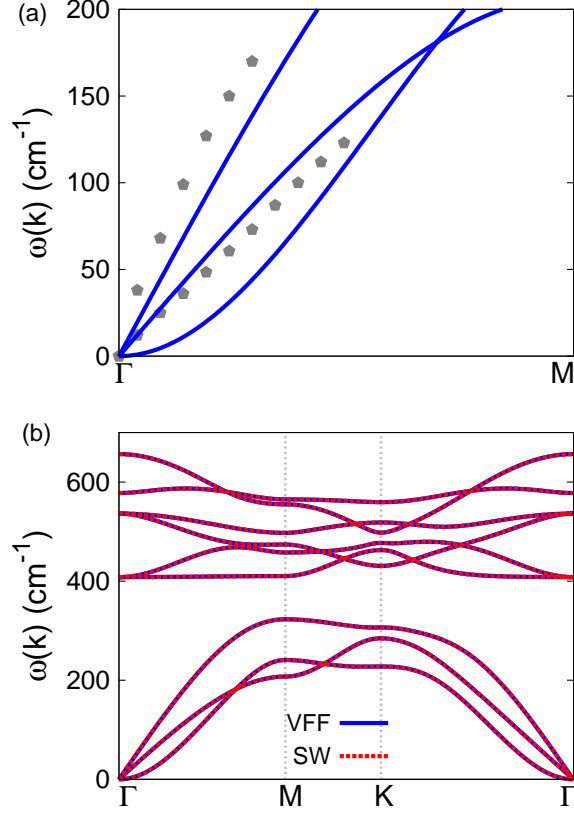


FIG. 31: (Color online) Phonon spectrum for single-layer 1H-FeO<sub>2</sub>. (a) Phonon dispersion along the  $\Gamma$ M direction in the Brillouin zone. The results from the VFF model (lines) are comparable with the *ab initio* results (pentagons) from Ref. 12. (b) The phonon dispersion from the SW potential is exactly the same as that from the VFF model.

from different (top or bottom) group.

Table LXVI shows four VFF terms for the single-layer 1H-FeO<sub>2</sub>, one of which is the bond stretching interaction shown by Eq. (1) while the other three terms are the angle bending interaction shown by Eq. (2). These force constant parameters are determined by fitting to the three acoustic branches in the phonon dispersion along the  $\Gamma$ M as shown in Fig. 31 (a). The *ab initio* calculations for the phonon dispersion are from Ref. 12. Fig. 31 (b) shows that the VFF model and the SW potential give exactly the same phonon dispersion, as the SW potential is derived from the VFF model.

The parameters for the two-body SW potential used by GULP are shown in Tab. LXVII. The parameters for the three-body SW potential used by GULP are shown in Tab. LXVIII.

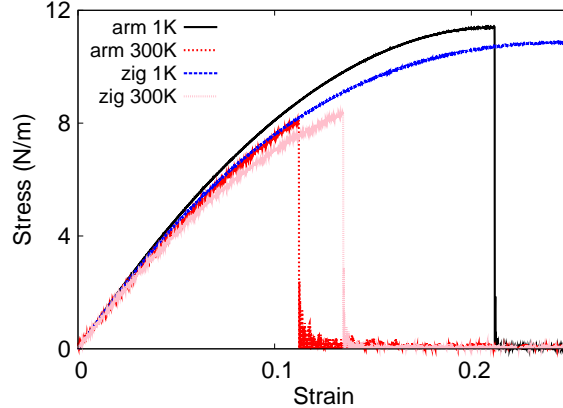


FIG. 32: (Color online) Stress-strain for single-layer 1H-FeO<sub>2</sub> of dimension 100 × 100 Å along the armchair and zigzag directions.

TABLE LXVI: The VFF model for single-layer 1H-FeO<sub>2</sub>. The second line gives an explicit expression for each VFF term. The third line is the force constant parameters. Parameters are in the unit of  $\frac{eV}{\text{Å}^2}$  for the bond stretching interactions, and in the unit of eV for the angle bending interaction. The fourth line gives the initial bond length (in unit of Å) for the bond stretching interaction and the initial angle (in unit of degrees) for the angle bending interaction. The angle  $\theta_{ijk}$  has atom *i* as the apex.

VFF type	bond stretching	angle bending		
expression	$\frac{1}{2}K_{\text{Fe-O}}(\Delta r)^2$	$\frac{1}{2}K_{\text{Fe-O-O}}(\Delta\theta)^2$	$\frac{1}{2}K_{\text{Fe-O-O}'}(\Delta\theta)^2$	$\frac{1}{2}K_{\text{O-Fe-Fe}}(\Delta\theta)^2$
parameter	8.377	3.213	3.213	3.213
$r_0$ or $\theta_0$	1.880	88.343	72.856	88.343

Some representative parameters for the SW potential used by LAMMPS are listed in Tab. LXIX. We note that twelve atom types have been introduced for the simulation of the single-layer 1H-FeO<sub>2</sub> using LAMMPS, because the angles around atom Fe in Fig. 1 (with M=Fe and X=O) are not distinguishable in LAMMPS. We have suggested two options to differentiate these angles by implementing some additional constraints in LAMMPS, which can be accomplished by modifying the source file of LAMMPS.<sup>13,14</sup> According to our experience, it is not so convenient for some users to implement these constraints and recompile the LAMMPS package. Hence, in the present work, we differentiate the angles by introducing

TABLE LXVII: Two-body SW potential parameters for single-layer 1H-FeO<sub>2</sub> used by GULP<sup>8</sup> as expressed in Eq. (3).

	$A$ (eV)	$\rho$ (Å)	$B$ (Å <sup>4</sup> )	$r_{\min}$ (Å)	$r_{\max}$ (Å)
Fe-O	4.242	0.962	6.246	0.0	2.552

TABLE LXVIII: Three-body SW potential parameters for single-layer 1H-FeO<sub>2</sub> used by GULP<sup>8</sup> as expressed in Eq. (4). The angle  $\theta_{ijk}$  in the first line indicates the bending energy for the angle with atom  $i$  as the apex.

	$K$ (eV)	$\theta_0$ (degree)	$\rho_1$ (Å)	$\rho_2$ (Å)	$r_{\min12}$ (Å)	$r_{\max12}$ (Å)	$r_{\min13}$ (Å)	$r_{\max13}$ (Å)	$r_{\min23}$ (Å)	$r_{\max23}$ (Å)
$\theta_{\text{Fe-O-O}}$	28.105	88.343	0.962	0.962	0.0	2.552	0.0	2.552	0.0	3.031
$\theta_{\text{Fe-O-O}'}$	30.754	72.856	0.962	0.962	0.0	2.552	0.0	2.552	0.0	3.031
$\theta_{\text{O-Fe-Fe}}$	28.105	88.343	0.962	0.962	0.0	2.552	0.0	2.552	0.0	3.031

more atom types, so it is not necessary to modify the LAMMPS package. Fig. 2 (with M=Fe and X=O) shows that, for 1H-FeO<sub>2</sub>, we can differentiate these angles around the Fe atom by assigning these six neighboring O atoms with different atom types. It can be found that twelve atom types are necessary for the purpose of differentiating all six neighbors around one Fe atom.

We use LAMMPS to perform MD simulations for the mechanical behavior of the single-layer 1H-FeO<sub>2</sub> under uniaxial tension at 1.0 K and 300.0 K. Fig. 32 shows the stress-strain curve for the tension of a single-layer 1H-FeO<sub>2</sub> of dimension  $100 \times 100$  Å. Periodic boundary conditions are applied in both armchair and zigzag directions. The single-layer 1H-FeO<sub>2</sub> is

TABLE LXIX: SW potential parameters for single-layer 1H-FeO<sub>2</sub> used by LAMMPS<sup>9</sup> as expressed in Eqs. (9) and (10).

	$\epsilon$ (eV)	$\sigma$ (Å)	$a$	$\lambda$	$\gamma$	$\cos \theta_0$	$A_L$	$B_L$	$p$	$q$	tol
Fe <sub>1</sub> -O <sub>1</sub> -O <sub>1</sub>	1.000	0.962	2.654	0.000	1.000	0.000	4.242	7.298	4	0	0.0
Fe <sub>1</sub> -O <sub>1</sub> -O <sub>3</sub>	1.000	0.000	0.000	28.105	1.000	0.029	0.000	0.000	4	0	0.0
Fe <sub>1</sub> -O <sub>1</sub> -O <sub>2</sub>	1.000	0.000	0.000	30.754	1.000	0.295	0.000	0.000	4	0	0.0
O <sub>1</sub> -Fe <sub>1</sub> -Fe <sub>3</sub>	1.000	0.000	0.000	28.105	1.000	0.029	0.000	0.000	4	0	0.0

TABLE LXX: The VFF model for single-layer 1H-FeS<sub>2</sub>. The second line gives an explicit expression for each VFF term. The third line is the force constant parameters. Parameters are in the unit of  $\frac{\text{eV}}{\text{Å}^2}$  for the bond stretching interactions, and in the unit of eV for the angle bending interaction. The fourth line gives the initial bond length (in unit of Å) for the bond stretching interaction and the initial angle (in unit of degrees) for the angle bending interaction. The angle  $\theta_{ijk}$  has atom  $i$  as the apex.

VFF type	bond stretching		angle bending	
expression	$\frac{1}{2}K_{\text{Fe-S}}(\Delta r)^2$	$\frac{1}{2}K_{\text{Fe-S-S}}(\Delta\theta)^2$	$\frac{1}{2}K_{\text{Fe-S-S'}}(\Delta\theta)^2$	$\frac{1}{2}K_{\text{S-Fe-Fe}}(\Delta\theta)^2$
parameter	6.338	3.964	3.964	3.964
$r_0$ or $\theta_0$	2.220	87.132	74.537	87.132

stretched uniaxially along the armchair or zigzag direction. The stress is calculated without involving the actual thickness of the quasi-two-dimensional structure of the single-layer 1H-FeO<sub>2</sub>. The Young's modulus can be obtained by a linear fitting of the stress-strain relation in the small strain range of  $[0, 0.01]$ . The Young's modulus are 100.2 N/m and 99.3 N/m along the armchair and zigzag directions, respectively. The Young's modulus is essentially isotropic in the armchair and zigzag directions. The Poisson's ratio from the VFF model and the SW potential is  $\nu_{xy} = \nu_{yx} = 0.23$ .

There is no available value for nonlinear quantities in the single-layer 1H-FeO<sub>2</sub>. We have thus used the nonlinear parameter  $B = 0.5d^4$  in Eq. (5), which is close to the value of  $B$  in most materials. The value of the third order nonlinear elasticity  $D$  can be extracted by fitting the stress-strain relation to the function  $\sigma = E\epsilon + \frac{1}{2}D\epsilon^2$  with  $E$  as the Young's modulus. The values of  $D$  from the present SW potential are -423.4 N/m and -460.2 N/m along the armchair and zigzag directions, respectively. The ultimate stress is about 11.4 Nm<sup>-1</sup> at the ultimate strain of 0.21 in the armchair direction at the low temperature of 1 K. The ultimate stress is about 10.9 Nm<sup>-1</sup> at the ultimate strain of 0.25 in the zigzag direction at the low temperature of 1 K.

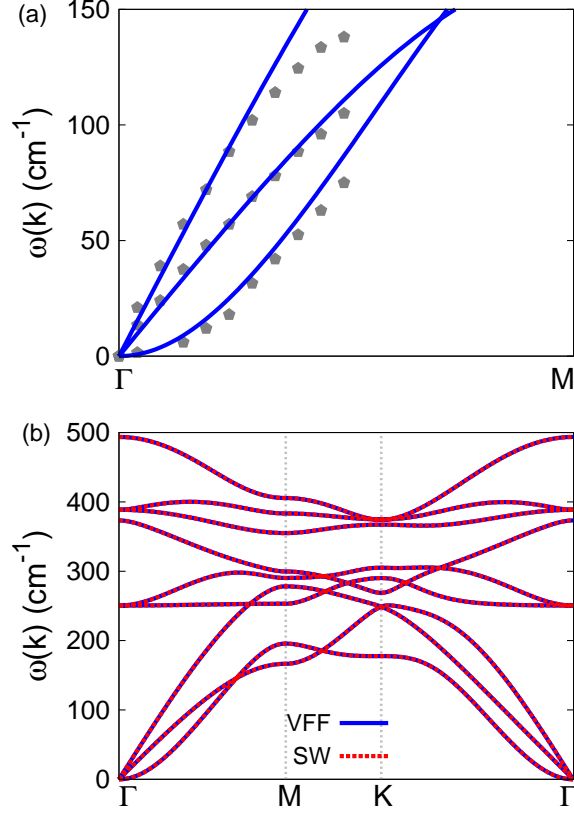


FIG. 33: (Color online) Phonon spectrum for single-layer 1H-FeS<sub>2</sub>. (a) Phonon dispersion along the  $\Gamma$ M direction in the Brillouin zone. The results from the VFF model (lines) are comparable with the *ab initio* results (pentagons) from Ref. 12. (b) The phonon dispersion from the SW potential is exactly the same as that from the VFF model.

TABLE LXXI: Two-body SW potential parameters for single-layer 1H-FeS<sub>2</sub> used by GULP<sup>8</sup> as expressed in Eq. (3).

	$A$ (eV)	$\rho$ ( $\text{\AA}$ )	$B$ ( $\text{\AA}^4$ )	$r_{\min}$ ( $\text{\AA}$ )	$r_{\max}$ ( $\text{\AA}$ )
Fe-S	4.337	1.097	12.145	0.0	3.000

## XVIII. 1H-FES<sub>2</sub>

Most existing theoretical studies on the single-layer 1H-FeS<sub>2</sub> are based on the first-principles calculations. In this section, we will develop the SW potential for the single-layer 1H-FeS<sub>2</sub>.

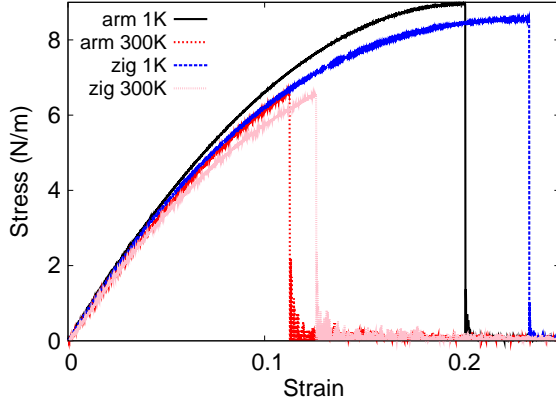


FIG. 34: (Color online) Stress-strain for single-layer 1H-FeS<sub>2</sub> of dimension 100 × 100 Å along the armchair and zigzag directions.

TABLE LXXII: Three-body SW potential parameters for single-layer 1H-FeS<sub>2</sub> used by GULP<sup>8</sup> as expressed in Eq. (4). The angle  $\theta_{ijk}$  in the first line indicates the bending energy for the angle with atom *i* as the apex.

	$K$ (eV)	$\theta_0$ (degree)	$\rho_1$ (Å)	$\rho_2$ (Å)	$r_{\min 12}$ (Å)	$r_{\max 12}$ (Å)	$r_{\min 13}$ (Å)	$r_{\max 13}$ (Å)	$r_{\min 23}$ (Å)	$r_{\max 23}$ (Å)
$\theta_{\text{Fe-S-S}}$	33.060	87.132	1.097	1.097	0.0	3.000	0.0	3.000	0.0	3.567
$\theta_{\text{Fe-S-S}'}$	35.501	74.537	1.097	1.097	0.0	3.000	0.0	3.000	0.0	3.567
$\theta_{\text{S-Fe-Fe}}$	33.060	87.132	1.097	1.097	0.0	3.000	0.0	3.000	0.0	3.567

The structure for the single-layer 1H-FeS<sub>2</sub> is shown in Fig. 1 (with M=Fe and X=S). Each Fe atom is surrounded by six S atoms. These S atoms are categorized into the top group (eg. atoms 1, 3, and 5) and bottom group (eg. atoms 2, 4, and 6). Each S atom is connected to three Fe atoms. The structural parameters are from the first-principles calculations,<sup>12</sup> including the lattice constant  $a = 3.06$  Å, and the bond length  $d_{\text{Fe-S}} = 2.22$  Å. The resultant angles are  $\theta_{\text{FeSS}} = \theta_{\text{SFeFe}} = 87.132^\circ$  and  $\theta_{\text{FeSS}'} = 74.537^\circ$ , in which atoms S and S' are from different (top or bottom) group.

Table LXX shows four VFF terms for the single-layer 1H-FeS<sub>2</sub>, one of which is the bond stretching interaction shown by Eq. (1) while the other three terms are the angle bending interaction shown by Eq. (2). These force constant parameters are determined by fitting to the three acoustic branches in the phonon dispersion along the  $\Gamma\text{M}$  as shown in Fig. 33 (a). The *ab initio* calculations for the phonon dispersion are from Ref. 12. Fig. 33 (b) shows that

TABLE LXXIII: SW potential parameters for single-layer 1H-FeS<sub>2</sub> used by LAMMPS<sup>9</sup> as expressed in Eqs. (9) and (10).

	$\epsilon$ (eV)	$\sigma$ (Å)	$a$	$\lambda$	$\gamma$	$\cos\theta_0$	$A_L$	$B_L$	$p$	$q$	tol
Fe <sub>1</sub> -S <sub>1</sub> -S <sub>1</sub>	1.000	1.097	2.735	0.000	1.000	0.000	4.337	8.338	4	0	0.0
Fe <sub>1</sub> -S <sub>1</sub> -S <sub>3</sub>	1.000	0.000	0.000	33.060	1.000	0.050	0.000	0.000	4	0	0.0
Fe <sub>1</sub> -S <sub>1</sub> -S <sub>2</sub>	1.000	0.000	0.000	35.501	1.000	0.267	0.000	0.000	4	0	0.0
S <sub>1</sub> -Fe <sub>1</sub> -Fe <sub>3</sub>	1.000	0.000	0.000	33.060	1.000	0.050	0.000	0.000	4	0	0.0

the VFF model and the SW potential give exactly the same phonon dispersion, as the SW potential is derived from the VFF model.

The parameters for the two-body SW potential used by GULP are shown in Tab. LXXI. The parameters for the three-body SW potential used by GULP are shown in Tab. LXXII. Some representative parameters for the SW potential used by LAMMPS are listed in Tab. LXXIII. We note that twelve atom types have been introduced for the simulation of the single-layer 1H-FeS<sub>2</sub> using LAMMPS, because the angles around atom Fe in Fig. 1 (with M=Fe and X=S) are not distinguishable in LAMMPS. We have suggested two options to differentiate these angles by implementing some additional constraints in LAMMPS, which can be accomplished by modifying the source file of LAMMPS.<sup>13,14</sup> According to our experience, it is not so convenient for some users to implement these constraints and recompile the LAMMPS package. Hence, in the present work, we differentiate the angles by introducing more atom types, so it is not necessary to modify the LAMMPS package. Fig. 2 (with M=Fe and X=S) shows that, for 1H-FeS<sub>2</sub>, we can differentiate these angles around the Fe atom by assigning these six neighboring S atoms with different atom types. It can be found that twelve atom types are necessary for the purpose of differentiating all six neighbors around one Fe atom.

We use LAMMPS to perform MD simulations for the mechanical behavior of the single-layer 1H-FeS<sub>2</sub> under uniaxial tension at 1.0 K and 300.0 K. Fig. 34 shows the stress-strain curve for the tension of a single-layer 1H-FeS<sub>2</sub> of dimension 100 × 100 Å. Periodic boundary conditions are applied in both armchair and zigzag directions. The single-layer 1H-FeS<sub>2</sub> is stretched uniaxially along the armchair or zigzag direction. The stress is calculated without involving the actual thickness of the quasi-two-dimensional structure of the single-layer 1H-

TABLE LXXIV: The VFF model for single-layer 1H-FeSe<sub>2</sub>. The second line gives an explicit expression for each VFF term. The third line is the force constant parameters. Parameters are in the unit of  $\frac{\text{eV}}{\text{Å}^2}$  for the bond stretching interactions, and in the unit of eV for the angle bending interaction. The fourth line gives the initial bond length (in unit of Å) for the bond stretching interaction and the initial angle (in unit of degrees) for the angle bending interaction. The angle  $\theta_{ijk}$  has atom i as the apex.

VFF type	bond stretching	angle bending		
expression	$\frac{1}{2}K_{\text{Fe-Se}}(\Delta r)^2$	$\frac{1}{2}K_{\text{Fe-Se-Se}}(\Delta\theta)^2$	$\frac{1}{2}K_{\text{Fe-Se-Se}'}(\Delta\theta)^2$	$\frac{1}{2}K_{\text{Se-Fe-Fe}}(\Delta\theta)^2$
parameter	6.338	3.964	3.964	3.964
$r_0$ or $\theta_0$	2.350	86.488	75.424	86.488

FeS<sub>2</sub>. The Young's modulus can be obtained by a linear fitting of the stress-strain relation in the small strain range of [0, 0.01]. The Young's modulus are 83.6 N/m and 83.4 N/m along the armchair and zigzag directions, respectively. The Young's modulus is essentially isotropic in the armchair and zigzag directions. The Poisson's ratio from the VFF model and the SW potential is  $\nu_{xy} = \nu_{yx} = 0.20$ .

There is no available value for nonlinear quantities in the single-layer 1H-FeS<sub>2</sub>. We have thus used the nonlinear parameter  $B = 0.5d^4$  in Eq. (5), which is close to the value of  $B$  in most materials. The value of the third order nonlinear elasticity  $D$  can be extracted by fitting the stress-strain relation to the function  $\sigma = E\epsilon + \frac{1}{2}D\epsilon^2$  with  $E$  as the Young's modulus. The values of  $D$  from the present SW potential are -377.5 N/m and -412.7 N/m along the armchair and zigzag directions, respectively. The ultimate stress is about 9.0 Nm<sup>-1</sup> at the ultimate strain of 0.20 in the armchair direction at the low temperature of 1 K. The ultimate stress is about 8.6 Nm<sup>-1</sup> at the ultimate strain of 0.23 in the zigzag direction at the low temperature of 1 K.

## XIX. 1H-FESE<sub>2</sub>

Most existing theoretical studies on the single-layer 1H-FeSe<sub>2</sub> are based on the first-principles calculations. In this section, we will develop the SW potential for the single-layer 1H-FeSe<sub>2</sub>.

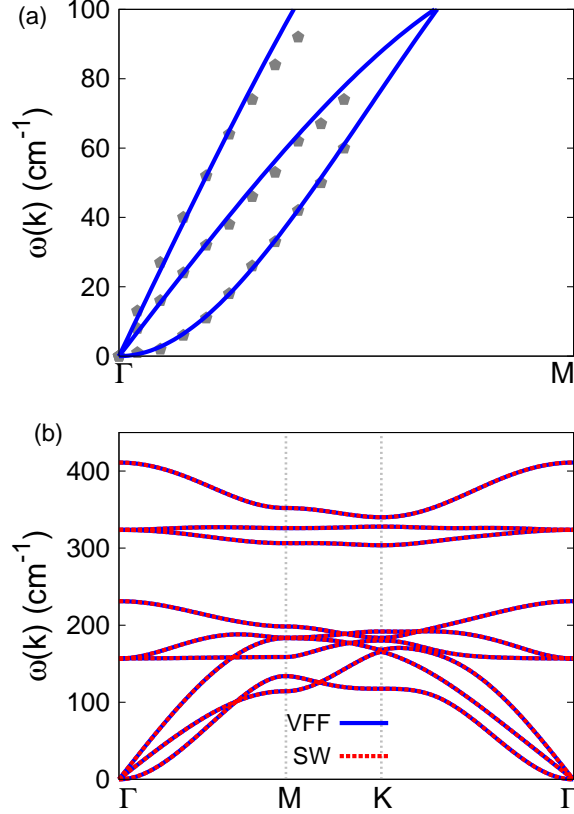


FIG. 35: (Color online) Phonon spectrum for single-layer 1H-FeSe<sub>2</sub>. (a) Phonon dispersion along the  $\Gamma$ M direction in the Brillouin zone. The results from the VFF model (lines) are comparable with the *ab initio* results (pentagons) from Ref. 12. (b) The phonon dispersion from the SW potential is exactly the same as that from the VFF model.

TABLE LXXV: Two-body SW potential parameters for single-layer 1H-FeSe<sub>2</sub> used by GULP<sup>8</sup> as expressed in Eq. (3).

	$A$ (eV)	$\rho$ ( $\text{\AA}$ )	$B$ ( $\text{\AA}^4$ )	$r_{\min}$ ( $\text{\AA}$ )	$r_{\max}$ ( $\text{\AA}$ )
Fe-Se	4.778	1.139	15.249	0.0	3.168

The structure for the single-layer 1H-FeSe<sub>2</sub> is shown in Fig. 1 (with M=Fe and X=Se). Each Fe atom is surrounded by six Se atoms. These Se atoms are categorized into the top group (eg. atoms 1, 3, and 5) and bottom group (eg. atoms 2, 4, and 6). Each Se atom is connected to three Fe atoms. The structural parameters are from the first-principles calculations,<sup>12</sup> including the lattice constant  $a = 3.22 \text{ \AA}$ , and the bond length

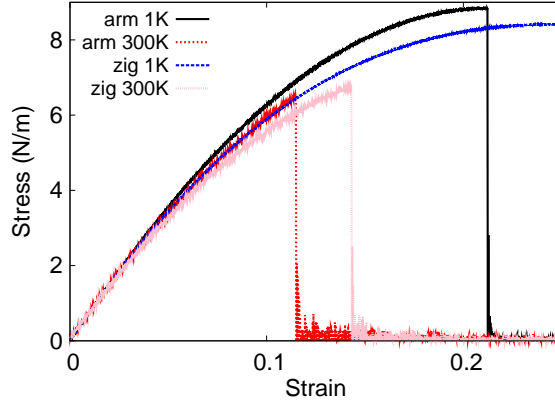


FIG. 36: (Color online) Stress-strain for single-layer 1H-FeSe<sub>2</sub> of dimension  $100 \times 100 \text{ \AA}$  along the armchair and zigzag directions.

TABLE LXXVI: Three-body SW potential parameters for single-layer 1H-FeSe<sub>2</sub> used by GULP<sup>8</sup> as expressed in Eq. (4). The angle  $\theta_{ijk}$  in the first line indicates the bending energy for the angle with atom  $i$  as the apex.

	$K$ (eV)	$\theta_0$ (degree)	$\rho_1$ (Å)	$\rho_2$ (Å)	$r_{\min 12}$ (Å)	$r_{\max 12}$ (Å)	$r_{\min 13}$ (Å)	$r_{\max 13}$ (Å)	$r_{\min 23}$ (Å)	$r_{\max 23}$ (Å)
$\theta_{\text{Fe-Se-Se}}$	32.235	86.488	1.139	1.139	0.0	3.168	0.0	3.168	0.0	3.768
$\theta_{\text{Fe-Se-Se}'}$	34.286	75.424	1.139	1.139	0.0	3.168	0.0	3.168	0.0	3.768
$\theta_{\text{Se-Fe-Fe}}$	32.235	86.488	1.139	1.139	0.0	3.168	0.0	3.168	0.0	3.768

$d_{\text{Fe-Se}} = 2.35 \text{ \AA}$ . The resultant angles are  $\theta_{\text{FeSeSe}} = \theta_{\text{SeFeFe}} = 86.488^\circ$  and  $\theta_{\text{FeSeSe}'} = 75.424^\circ$ , in which atoms Se and Se' are from different (top or bottom) group.

Table LXXIV shows four VFF terms for the single-layer 1H-FeSe<sub>2</sub>, one of which is the bond stretching interaction shown by Eq. (1) while the other three terms are the angle bending interaction shown by Eq. (2). These force constant parameters are determined by fitting to the three acoustic branches in the phonon dispersion along the  $\Gamma\text{M}$  as shown in Fig. 35 (a). The *ab initio* calculations for the phonon dispersion are from Ref. 12. Fig. 35 (b) shows that the VFF model and the SW potential give exactly the same phonon dispersion, as the SW potential is derived from the VFF model.

The parameters for the two-body SW potential used by GULP are shown in Tab. LXXV. The parameters for the three-body SW potential used by GULP are shown in Tab. LXXVI. Some representative parameters for the SW potential used by LAMMPS are listed in

TABLE LXXVII: SW potential parameters for single-layer 1H-FeSe<sub>2</sub> used by LAMMPS<sup>9</sup> as expressed in Eqs. (9) and (10).

	$\epsilon$ (eV)	$\sigma$ (Å)	$a$	$\lambda$	$\gamma$	$\cos \theta_0$	$A_L$	$B_L$	$p$	$q$	tol
Fe <sub>1</sub> -Se <sub>1</sub> -Se <sub>1</sub>	1.000	1.139	2.781	0.000	1.000	0.000	4.778	9.049	4	0	0.0
Fe <sub>1</sub> -Se <sub>1</sub> -Se <sub>3</sub>	1.000	0.000	0.000	32.235	1.000	0.061	0.000	0.000	4	0	0.0
Fe <sub>1</sub> -Se <sub>1</sub> -Se <sub>2</sub>	1.000	0.000	0.000	34.286	1.000	0.252	0.000	0.000	4	0	0.0
Se <sub>1</sub> -Fe <sub>1</sub> -Fe <sub>3</sub>	1.000	0.000	0.000	32.235	1.000	0.061	0.000	0.000	4	0	0.0

Tab. LXXVII. We note that twelve atom types have been introduced for the simulation of the single-layer 1H-FeSe<sub>2</sub> using LAMMPS, because the angles around atom Fe in Fig. 1 (with M=Fe and X=Se) are not distinguishable in LAMMPS. We have suggested two options to differentiate these angles by implementing some additional constraints in LAMMPS, which can be accomplished by modifying the source file of LAMMPS.<sup>13,14</sup> According to our experience, it is not so convenient for some users to implement these constraints and recompile the LAMMPS package. Hence, in the present work, we differentiate the angles by introducing more atom types, so it is not necessary to modify the LAMMPS package. Fig. 2 (with M=Fe and X=Se) shows that, for 1H-FeSe<sub>2</sub>, we can differentiate these angles around the Fe atom by assigning these six neighboring Se atoms with different atom types. It can be found that twelve atom types are necessary for the purpose of differentiating all six neighbors around one Fe atom.

We use LAMMPS to perform MD simulations for the mechanical behavior of the single-layer 1H-FeSe<sub>2</sub> under uniaxial tension at 1.0 K and 300.0 K. Fig. 36 shows the stress-strain curve for the tension of a single-layer 1H-FeSe<sub>2</sub> of dimension 100 × 100 Å. Periodic boundary conditions are applied in both armchair and zigzag directions. The single-layer 1H-FeSe<sub>2</sub> is stretched uniaxially along the armchair or zigzag direction. The stress is calculated without involving the actual thickness of the quasi-two-dimensional structure of the single-layer 1H-FeSe<sub>2</sub>. The Young's modulus can be obtained by a linear fitting of the stress-strain relation in the small strain range of [0, 0.01]. The Young's modulus are 77.3 N/m and 77.4 N/m along the armchair and zigzag directions, respectively. The Young's modulus is essentially isotropic in the armchair and zigzag directions. The Poisson's ratio from the VFF model and the SW potential is  $\nu_{xy} = \nu_{yx} = 0.23$ .

TABLE LXXVIII: The VFF model for single-layer 1H-FeTe<sub>2</sub>. The second line gives an explicit expression for each VFF term. The third line is the force constant parameters. Parameters are in the unit of  $\frac{\text{eV}}{\text{Å}^2}$  for the bond stretching interactions, and in the unit of eV for the angle bending interaction. The fourth line gives the initial bond length (in unit of Å) for the bond stretching interaction and the initial angle (in unit of degrees) for the angle bending interaction. The angle  $\theta_{ijk}$  has atom i as the apex.

VFF type	bond stretching	angle bending		
expression	$\frac{1}{2}K_{\text{Fe-Te}}(\Delta r)^2$	$\frac{1}{2}K_{\text{Fe-Te-Te}}(\Delta\theta)^2$	$\frac{1}{2}K_{\text{Fe-Te-Te}'}(\Delta\theta)^2$	$\frac{1}{2}K_{\text{Te-Fe-Fe}}(\Delta\theta)^2$
parameter	6.338	3.964	3.964	3.964
$r_0$ or $\theta_0$	2.530	86.904	74.851	86.904

TABLE LXXIX: Two-body SW potential parameters for single-layer 1H-FeTe<sub>2</sub> used by GULP<sup>8</sup> as expressed in Eq. (3).

	$A$ (eV)	$\rho$ (Å)	$B$ (Å <sup>4</sup> )	$r_{\text{min}}$ (Å)	$r_{\text{max}}$ (Å)
Fe-Te	5.599	1.242	20.486	0.0	3.416

There is no available value for nonlinear quantities in the single-layer 1H-FeSe<sub>2</sub>. We have thus used the nonlinear parameter  $B = 0.5d^4$  in Eq. (5), which is close to the value of  $B$  in most materials. The value of the third order nonlinear elasticity  $D$  can be extracted by fitting the stress-strain relation to the function  $\sigma = E\epsilon + \frac{1}{2}D\epsilon^2$  with  $E$  as the Young's modulus. The values of  $D$  from the present SW potential are -323.8 N/m and -360.8 N/m along the armchair and zigzag directions, respectively. The ultimate stress is about 8.8 Nm<sup>-1</sup> at the ultimate strain of 0.21 in the armchair direction at the low temperature of 1 K. The ultimate stress is about 8.4 Nm<sup>-1</sup> at the ultimate strain of 0.25 in the zigzag direction at the low temperature of 1 K.

## XX. 1H-FETE<sub>2</sub>

Most existing theoretical studies on the single-layer 1H-FeTe<sub>2</sub> are based on the first-principles calculations. In this section, we will develop the SW potential for the single-layer 1H-FeTe<sub>2</sub>.

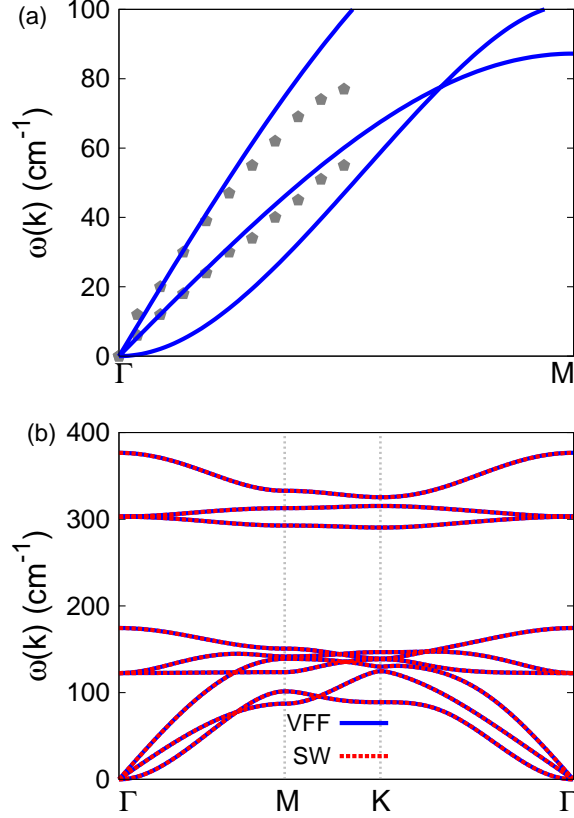


FIG. 37: (Color online) Phonon spectrum for single-layer 1H-FeTe<sub>2</sub>. (a) Phonon dispersion along the  $\Gamma$ M direction in the Brillouin zone. The results from the VFF model (lines) are comparable with the *ab initio* results (pentagons) from Ref. 12. (b) The phonon dispersion from the SW potential is exactly the same as that from the VFF model.

The structure for the single-layer 1H-FeTe<sub>2</sub> is shown in Fig. 1 (with M=Fe and X=Te). Each Fe atom is surrounded by six Te atoms. These Te atoms are categorized into the top group (eg. atoms 1, 3, and 5) and bottom group (eg. atoms 2, 4, and 6). Each Te atom is connected to three Fe atoms. The structural parameters are from the first-principles calculations,<sup>12</sup> including the lattice constant  $a = 3.48 \text{ \AA}$ , and the bond length  $d_{\text{Fe-Te}} = 2.53 \text{ \AA}$ . The resultant angles are  $\theta_{\text{FeTeTe}} = \theta_{\text{TeFeFe}} = 86.904^\circ$  and  $\theta_{\text{FeTeTe}'} = 74.851^\circ$ , in which atoms Te and Te' are from different (top or bottom) group.

Table LXXVIII shows four VFF terms for the single-layer 1H-FeTe<sub>2</sub>, one of which is the bond stretching interaction shown by Eq. (1) while the other three terms are the angle bending interaction shown by Eq. (2). These force constant parameters are determined

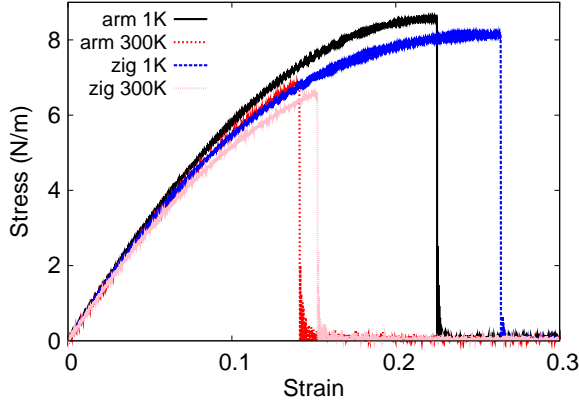


FIG. 38: (Color online) Stress-strain for single-layer 1H-FeTe<sub>2</sub> of dimension  $100 \times 100 \text{ \AA}$  along the armchair and zigzag directions.

TABLE LXXX: Three-body SW potential parameters for single-layer 1H-FeTe<sub>2</sub> used by GULP<sup>8</sup> as expressed in Eq. (4). The angle  $\theta_{ijk}$  in the first line indicates the bending energy for the angle with atom  $i$  as the apex.

	$K$ (eV)	$\theta_0$ (degree)	$\rho_1$ (Å)	$\rho_2$ (Å)	$r_{\min 12}$ (Å)	$r_{\max 12}$ (Å)	$r_{\min 13}$ (Å)	$r_{\max 13}$ (Å)	$r_{\min 23}$ (Å)	$r_{\max 23}$ (Å)
$\theta_{\text{Fe-Te-Te}}$	32.766	86.904	1.242	1.242	0.0	3.416	0.0	3.416	0.0	4.062
$\theta_{\text{Fe-Te-Te}'}$	35.065	74.851	1.242	1.242	0.0	3.416	0.0	3.416	0.0	4.062
$\theta_{\text{Te-Fe-Fe}}$	32.766	86.904	1.242	1.242	0.0	3.416	0.0	3.416	0.0	4.062

by fitting to the two in-plane acoustic branches in the phonon dispersion along the  $\Gamma\text{M}$  as shown in Fig. 37 (a). The *ab initio* calculations for the phonon dispersion are from Ref. 12. Fig. 37 (b) shows that the VFF model and the SW potential give exactly the same phonon dispersion, as the SW potential is derived from the VFF model.

The parameters for the two-body SW potential used by GULP are shown in Tab. LXXIX. The parameters for the three-body SW potential used by GULP are shown in Tab. LXXX. Some representative parameters for the SW potential used by LAMMPS are listed in Tab. LXXXI. We note that twelve atom types have been introduced for the simulation of the single-layer 1H-FeTe<sub>2</sub> using LAMMPS, because the angles around atom Fe in Fig. 1 (with  $M=\text{Fe}$  and  $X=\text{Te}$ ) are not distinguishable in LAMMPS. We have suggested two options to differentiate these angles by implementing some additional constraints in LAMMPS, which can be accomplished by modifying the source file of LAMMPS.<sup>13,14</sup> According to our

TABLE LXXXI: SW potential parameters for single-layer 1H-FeTe<sub>2</sub> used by LAMMPS<sup>9</sup> as expressed in Eqs. (9) and (10).

	$\epsilon$ (eV)	$\sigma$ (Å)	$a$	$\lambda$	$\gamma$	$\cos \theta_0$	$A_L$	$B_L$	$p$	$q$	tol
Fe <sub>1</sub> -Te <sub>1</sub> -Te <sub>1</sub>	1.000	1.242	2.751	0.000	1.000	0.000	5.599	8.615	4	0	0.0
Fe <sub>1</sub> -Te <sub>1</sub> -Te <sub>3</sub>	1.000	0.000	0.000	32.766	1.000	0.054	0.000	0.000	4	0	0.0
Fe <sub>1</sub> -Te <sub>1</sub> -Te <sub>2</sub>	1.000	0.000	0.000	35.065	1.000	0.261	0.000	0.000	4	0	0.0
Te <sub>1</sub> -Fe <sub>1</sub> -Fe <sub>3</sub>	1.000	0.000	0.000	32.766	1.000	0.054	0.000	0.000	4	0	0.0

experience, it is not so convenient for some users to implement these constraints and re-compile the LAMMPS package. Hence, in the present work, we differentiate the angles by introducing more atom types, so it is not necessary to modify the LAMMPS package. Fig. 2 (with M=Fe and X=Te) shows that, for 1H-FeTe<sub>2</sub>, we can differentiate these angles around the Fe atom by assigning these six neighboring Te atoms with different atom types. It can be found that twelve atom types are necessary for the purpose of differentiating all six neighbors around one Fe atom.

We use LAMMPS to perform MD simulations for the mechanical behavior of the single-layer 1H-FeTe<sub>2</sub> under uniaxial tension at 1.0 K and 300.0 K. Fig. 38 shows the stress-strain curve for the tension of a single-layer 1H-FeTe<sub>2</sub> of dimension  $100 \times 100$  Å. Periodic boundary conditions are applied in both armchair and zigzag directions. The single-layer 1H-FeTe<sub>2</sub> is stretched uniaxially along the armchair or zigzag direction. The stress is calculated without involving the actual thickness of the quasi-two-dimensional structure of the single-layer 1H-FeTe<sub>2</sub>. The Young's modulus can be obtained by a linear fitting of the stress-strain relation in the small strain range of [0, 0.01]. The Young's modulus are 69.6 N/m and 69.8 N/m along the armchair and zigzag directions, respectively. The Young's modulus is essentially isotropic in the armchair and zigzag directions. The Poisson's ratio from the VFF model and the SW potential is  $\nu_{xy} = \nu_{yx} = 0.25$ .

There is no available value for nonlinear quantities in the single-layer 1H-FeTe<sub>2</sub>. We have thus used the nonlinear parameter  $B = 0.5d^4$  in Eq. (5), which is close to the value of  $B$  in most materials. The value of the third order nonlinear elasticity  $D$  can be extracted by fitting the stress-strain relation to the function  $\sigma = E\epsilon + \frac{1}{2}D\epsilon^2$  with  $E$  as the Young's modulus. The values of  $D$  from the present SW potential are -267.5 N/m and -302.8 N/m

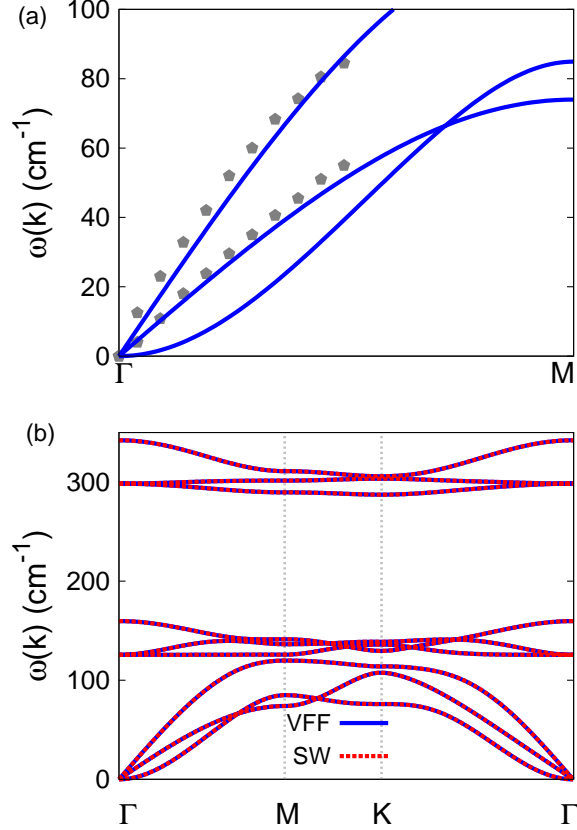


FIG. 39: (Color online) Phonon spectrum for single-layer 1H-CoTe<sub>2</sub>. (a) Phonon dispersion along the  $\Gamma$ M direction in the Brillouin zone. The results from the VFF model (lines) are comparable with the *ab initio* results (pentagons) from Ref. 12. (b) The phonon dispersion from the SW potential is exactly the same as that from the VFF model.

along the armchair and zigzag directions, respectively. The ultimate stress is about  $8.6 \text{ Nm}^{-1}$  at the ultimate strain of 0.22 in the armchair direction at the low temperature of 1 K. The ultimate stress is about  $8.1 \text{ Nm}^{-1}$  at the ultimate strain of 0.26 in the zigzag direction at the low temperature of 1 K.

## XXI. 1H-COTE<sub>2</sub>

Most existing theoretical studies on the single-layer 1H-CoTe<sub>2</sub> are based on the first-principles calculations. In this section, we will develop the SW potential for the single-layer 1H-CoTe<sub>2</sub>.

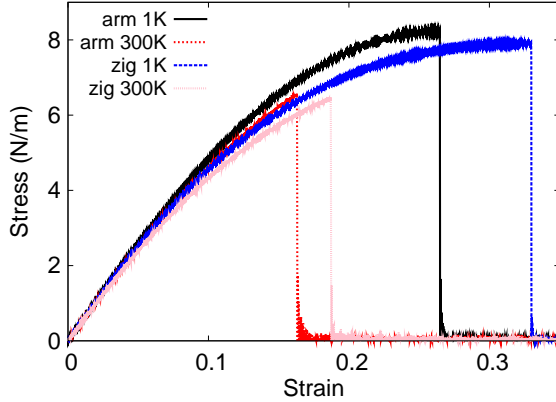


FIG. 40: (Color online) Stress-strain for single-layer 1H-CoTe<sub>2</sub> of dimension  $100 \times 100 \text{ \AA}$  along the armchair and zigzag directions.

TABLE LXXXII: The VFF model for single-layer 1H-CoTe<sub>2</sub>. The second line gives an explicit expression for each VFF term. The third line is the force constant parameters. Parameters are in the unit of  $\frac{\text{eV}}{\text{Å}^2}$  for the bond stretching interactions, and in the unit of eV for the angle bending interaction. The fourth line gives the initial bond length (in unit of Å) for the bond stretching interaction and the initial angle (in unit of degrees) for the angle bending interaction. The angle  $\theta_{ijk}$  has atom *i* as the apex.

VFF type	bond stretching	angle bending		
expression	$\frac{1}{2}K_{\text{Co-Te}}(\Delta r)^2$	$\frac{1}{2}K_{\text{Co-Te-Te}}(\Delta\theta)^2$	$\frac{1}{2}K_{\text{Co-Te-Te'}}(\Delta\theta)^2$	$\frac{1}{2}K_{\text{Te-Co-Co}}(\Delta\theta)^2$
parameter	6.712	2.656	2.656	2.656
$r_0$ or $\theta_0$	2.510	89.046	71.873	89.046

The structure for the single-layer 1H-CoTe<sub>2</sub> is shown in Fig. 1 (with M=Co and X=Te). Each Co atom is surrounded by six Te atoms. These Te atoms are categorized into the top group (eg. atoms 1, 3, and 5) and bottom group (eg. atoms 2, 4, and 6). Each Te atom is connected to three Co atoms. The structural parameters are from the first-principles calculations,<sup>12</sup> including the lattice constant  $a = 3.52 \text{ \AA}$ , and the bond length  $d_{\text{Co-Te}} = 2.51 \text{ \AA}$ . The resultant angles are  $\theta_{\text{CoTeTe}} = \theta_{\text{TeCoCo}} = 89.046^\circ$  and  $\theta_{\text{CoTeTe'}} = 71.873^\circ$ , in which atoms Te and Te' are from different (top or bottom) group.

Table LXXXII shows four VFF terms for the single-layer 1H-CoTe<sub>2</sub>, one of which is the

TABLE LXXXIII: Two-body SW potential parameters for single-layer 1H-CoTe<sub>2</sub> used by GULP<sup>8</sup> as expressed in Eq. (3).

	$A$ (eV)	$\rho$ (Å)	$B$ (Å <sup>4</sup> )	$r_{\min}$ (Å)	$r_{\max}$ (Å)
Co-Te	6.169	1.310	19.846	0.0	3.417

TABLE LXXXIV: Three-body SW potential parameters for single-layer 1H-CoTe<sub>2</sub> used by GULP<sup>8</sup> as expressed in Eq. (4). The angle  $\theta_{ijk}$  in the first line indicates the bending energy for the angle with atom  $i$  as the apex.

	$K$ (eV)	$\theta_0$ (degree)	$\rho_1$ (Å)	$\rho_2$ (Å)	$r_{\min12}$ (Å)	$r_{\max12}$ (Å)	$r_{\min13}$ (Å)	$r_{\max13}$ (Å)	$r_{\min23}$ (Å)	$r_{\max23}$ (Å)
$\theta_{\text{Co-Te-Te}}$	23.895	89.046	1.310	1.310	0.0	3.417	0.0	3.417	0.0	4.055
$\theta_{\text{Co-Te-Te}'}$	26.449	71.873	1.310	1.310	0.0	3.417	0.0	3.417	0.0	4.055
$\theta_{\text{Te-Co-Co}}$	23.895	89.046	1.310	1.310	0.0	3.417	0.0	3.417	0.0	4.055

bond stretching interaction shown by Eq. (1) while the other three terms are the angle bending interaction shown by Eq. (2). These force constant parameters are determined by fitting to the acoustic branches in the phonon dispersion along the  $\Gamma\text{M}$  as shown in Fig. 39 (a). The *ab initio* calculations for the phonon dispersion are from Ref. 12. Fig. 39 (b) shows that the VFF model and the SW potential give exactly the same phonon dispersion, as the SW potential is derived from the VFF model.

The parameters for the two-body SW potential used by GULP are shown in Tab. LXXXIII. The parameters for the three-body SW potential used by GULP are shown in Tab. LXXXIV. Some representative parameters for the SW potential used by LAMMPS

TABLE LXXXV: SW potential parameters for single-layer 1H-CoTe<sub>2</sub> used by LAMMPS<sup>9</sup> as expressed in Eqs. (9) and (10).

	$\epsilon$ (eV)	$\sigma$ (Å)	$a$	$\lambda$	$\gamma$	$\cos \theta_0$	$A_L$	$B_L$	$p$	$q$	tol
Co <sub>1</sub> -Te <sub>1</sub> -Te <sub>1</sub>	1.000	1.310	2.608	0.000	1.000	0.000	6.169	6.739	4	0	0.0
Co <sub>1</sub> -Te <sub>1</sub> -Te <sub>3</sub>	1.000	0.000	0.000	23.895	1.000	0.017	0.000	0.000	4	0	0.0
Co <sub>1</sub> -Te <sub>1</sub> -Te <sub>2</sub>	1.000	0.000	0.000	26.449	1.000	0.311	0.000	0.000	4	0	0.0
Te <sub>1</sub> -Co <sub>1</sub> -Co <sub>3</sub>	1.000	0.000	0.000	23.895	1.000	0.017	0.000	0.000	4	0	0.0

are listed in Tab. LXXXV. We note that twelve atom types have been introduced for the simulation of the single-layer 1H-CoTe<sub>2</sub> using LAMMPS, because the angles around atom Co in Fig. 1 (with M=Co and X=Te) are not distinguishable in LAMMPS. We have suggested two options to differentiate these angles by implementing some additional constraints in LAMMPS, which can be accomplished by modifying the source file of LAMMPS.<sup>13,14</sup> According to our experience, it is not so convenient for some users to implement these constraints and recompile the LAMMPS package. Hence, in the present work, we differentiate the angles by introducing more atom types, so it is not necessary to modify the LAMMPS package. Fig. 2 (with M=Co and X=Te) shows that, for 1H-CoTe<sub>2</sub>, we can differentiate these angles around the Co atom by assigning these six neighboring Te atoms with different atom types. It can be found that twelve atom types are necessary for the purpose of differentiating all six neighbors around one Co atom.

We use LAMMPS to perform MD simulations for the mechanical behavior of the single-layer 1H-CoTe<sub>2</sub> under uniaxial tension at 1.0 K and 300.0 K. Fig. 40 shows the stress-strain curve for the tension of a single-layer 1H-CoTe<sub>2</sub> of dimension 100 × 100 Å. Periodic boundary conditions are applied in both armchair and zigzag directions. The single-layer 1H-CoTe<sub>2</sub> is stretched uniaxially along the armchair or zigzag direction. The stress is calculated without involving the actual thickness of the quasi-two-dimensional structure of the single-layer 1H-CoTe<sub>2</sub>. The Young's modulus can be obtained by a linear fitting of the stress-strain relation in the small strain range of [0, 0.01]. The Young's modulus are 53.7 N/m and 54.3 N/m along the armchair and zigzag directions, respectively. The Young's modulus is essentially isotropic in the armchair and zigzag directions. The Poisson's ratio from the VFF model and the SW potential is  $\nu_{xy} = \nu_{yx} = 0.32$ .

There is no available value for nonlinear quantities in the single-layer 1H-CoTe<sub>2</sub>. We have thus used the nonlinear parameter  $B = 0.5d^4$  in Eq. (5), which is close to the value of  $B$  in most materials. The value of the third order nonlinear elasticity  $D$  can be extracted by fitting the stress-strain relation to the function  $\sigma = E\epsilon + \frac{1}{2}D\epsilon^2$  with  $E$  as the Young's modulus. The values of  $D$  from the present SW potential are -157.2 N/m and -187.9 N/m along the armchair and zigzag directions, respectively. The ultimate stress is about 8.2 Nm<sup>-1</sup> at the ultimate strain of 0.26 in the armchair direction at the low temperature of 1 K. The ultimate stress is about 7.9 Nm<sup>-1</sup> at the ultimate strain of 0.33 in the zigzag direction at the low temperature of 1 K.

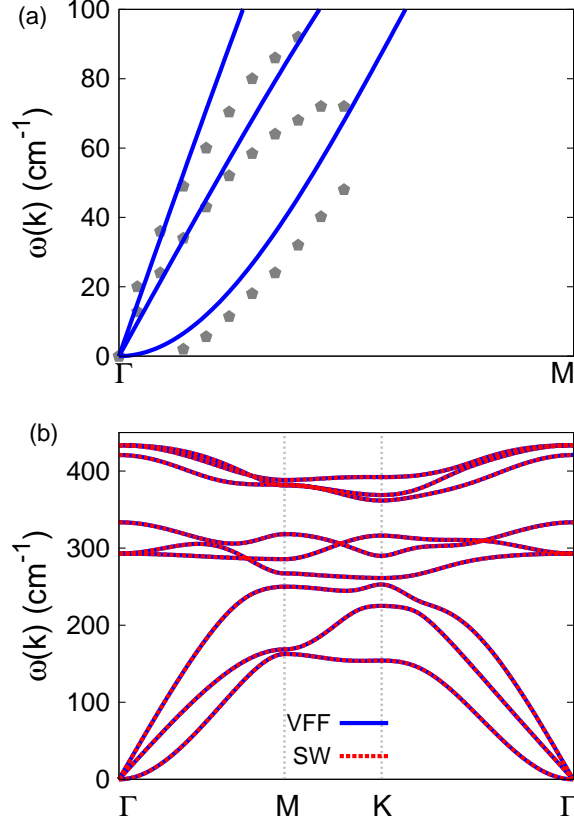


FIG. 41: (Color online) Phonon spectrum for single-layer 1H-NiS<sub>2</sub>. (a) Phonon dispersion along the  $\Gamma$ M direction in the Brillouin zone. The results from the VFF model (lines) are comparable with the *ab initio* results (pentagons) from Ref. 12. (b) The phonon dispersion from the SW potential is exactly the same as that from the VFF model.

## XXII. 1H-NIS<sub>2</sub>

Most existing theoretical studies on the single-layer 1H-NiS<sub>2</sub> are based on the first-principles calculations. In this section, we will develop the SW potential for the single-layer 1H-NiS<sub>2</sub>.

The structure for the single-layer 1H-NiS<sub>2</sub> is shown in Fig. 1 (with M=Ni and X=S). Each Ni atom is surrounded by six S atoms. These S atoms are categorized into the top group (eg. atoms 1, 3, and 5) and bottom group (eg. atoms 2, 4, and 6). Each S atom is connected to three Ni atoms. The structural parameters are from the first-principles calculations,<sup>12</sup> including the lattice constant  $a = 3.40 \text{ \AA}$ , and the bond length  $d_{\text{Ni-S}} = 2.24 \text{ \AA}$ . The resultant

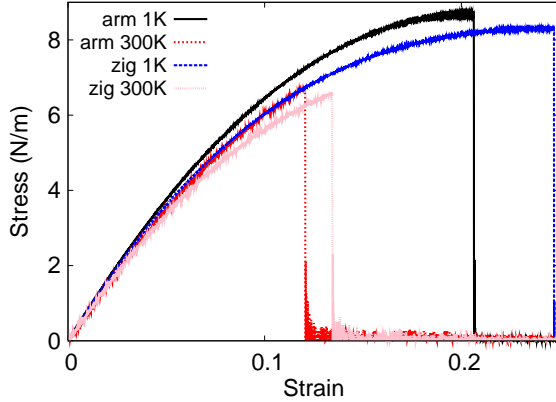


FIG. 42: (Color online) Stress-strain for single-layer 1H-NiS<sub>2</sub> of dimension 100 × 100 Å along the armchair and zigzag directions.

TABLE LXXXVI: The VFF model for single-layer 1H-NiS<sub>2</sub>. The second line gives an explicit expression for each VFF term. The third line is the force constant parameters. Parameters are in the unit of  $\frac{eV}{\text{Å}^2}$  for the bond stretching interactions, and in the unit of eV for the angle bending interaction. The fourth line gives the initial bond length (in unit of Å) for the bond stretching interaction and the initial angle (in unit of degrees) for the angle bending interaction. The angle  $\theta_{ijk}$  has atom i as the apex.

VFF type	bond stretching	angle bending		
expression	$\frac{1}{2}K_{\text{Ni-S}}(\Delta r)^2$	$\frac{1}{2}K_{\text{Ni-S-S}}(\Delta\theta)^2$	$\frac{1}{2}K_{\text{Ni-S-S'}}(\Delta\theta)^2$	$\frac{1}{2}K_{\text{S-Ni-Ni}}(\Delta\theta)^2$
parameter	6.933	3.418	3.418	3.418
$r_0$ or $\theta_0$	2.240	98.740	57.593	98.740

angles are  $\theta_{\text{NiSS}} = \theta_{\text{S Ni Ni}} = 98.740^\circ$  and  $\theta_{\text{NiSS'}} = 57.593^\circ$ , in which atoms S and S' are from different (top or bottom) group.

Table LXXXVI shows four VFF terms for the single-layer 1H-NiS<sub>2</sub>, one of which is the bond stretching interaction shown by Eq. (1) while the other three terms are the angle bending interaction shown by Eq. (2). These force constant parameters are determined by fitting to the acoustic branches in the phonon dispersion along the  $\Gamma\text{M}$  as shown in Fig. 41 (a). The *ab initio* calculations for the phonon dispersion are from Ref. 12. Fig. 41 (b) shows that the VFF model and the SW potential give exactly the same phonon dispersion, as the SW

TABLE LXXXVII: Two-body SW potential parameters for single-layer 1H-NiS<sub>2</sub> used by GULP<sup>8</sup> as expressed in Eq. (3).

	$A$ (eV)	$\rho$ (Å)	$B$ (Å <sup>4</sup> )	$r_{\min}$ (Å)	$r_{\max}$ (Å)
Ni-S	6.425	1.498	12.588	0.0	3.156

TABLE LXXXVIII: Three-body SW potential parameters for single-layer 1H-NiS<sub>2</sub> used by GULP<sup>8</sup> as expressed in Eq. (4). The angle  $\theta_{ijk}$  in the first line indicates the bending energy for the angle with atom  $i$  as the apex.

	$K$ (eV)	$\theta_0$ (degree)	$\rho_1$ (Å)	$\rho_2$ (Å)	$r_{\min12}$ (Å)	$r_{\max12}$ (Å)	$r_{\min13}$ (Å)	$r_{\max13}$ (Å)	$r_{\min23}$ (Å)	$r_{\max23}$ (Å)
$\theta_{\text{Ni-S-S}}$	46.062	98.740	1.498	1.498	0.0	3.156	0.0	3.156	0.0	3.713
$\theta_{\text{Ni-S-S}'}$	63.130	57.593	1.498	1.498	0.0	3.156	0.0	3.156	0.0	3.713
$\theta_{\text{S-Ni-Ni}}$	46.062	98.740	1.498	1.498	0.0	3.156	0.0	3.156	0.0	3.713

potential is derived from the VFF model.

The parameters for the two-body SW potential used by GULP are shown in Tab. LXXXVII. The parameters for the three-body SW potential used by GULP are shown in Tab. LXXXVIII. Some representative parameters for the SW potential used by LAMMPS are listed in Tab. LXXXIX. We note that twelve atom types have been introduced for the simulation of the single-layer 1H-NiS<sub>2</sub> using LAMMPS, because the angles around atom Ni in Fig. 1 (with M=Ni and X=S) are not distinguishable in LAMMPS. We have suggested two options to differentiate these angles by implementing some additional constraints in LAMMPS, which can be accomplished by modifying the source file of LAMMPS.<sup>13,14</sup>

TABLE LXXXIX: SW potential parameters for single-layer 1H-NiS<sub>2</sub> used by LAMMPS<sup>9</sup> as expressed in Eqs. (9) and (10).

	$\epsilon$ (eV)	$\sigma$ (Å)	$a$	$\lambda$	$\gamma$	$\cos\theta_0$	$A_L$	$B_L$	$p$	$q$	tol
Ni <sub>1</sub> -S <sub>1</sub> -S <sub>1</sub>	1.000	1.498	2.107	0.000	1.000	0.000	6.425	2.502	4	0	0.0
Ni <sub>1</sub> -S <sub>1</sub> -S <sub>3</sub>	1.000	0.000	0.000	46.062	1.000	-0.152	0.000	0.000	4	0	0.0
Ni <sub>1</sub> -S <sub>1</sub> -S <sub>2</sub>	1.000	0.000	0.000	63.130	1.000	0.536	0.000	0.000	4	0	0.0
S <sub>1</sub> -Ni <sub>1</sub> -Ni <sub>3</sub>	1.000	0.000	0.000	46.062	1.000	-0.152	0.000	0.000	4	0	0.0

According to our experience, it is not so convenient for some users to implement these constraints and recompile the LAMMPS package. Hence, in the present work, we differentiate the angles by introducing more atom types, so it is not necessary to modify the LAMMPS package. Fig. 2 (with M=Ni and X=S) shows that, for 1H-NiS<sub>2</sub>, we can differentiate these angles around the Ni atom by assigning these six neighboring S atoms with different atom types. It can be found that twelve atom types are necessary for the purpose of differentiating all six neighbors around one Ni atom.

We use LAMMPS to perform MD simulations for the mechanical behavior of the single-layer 1H-NiS<sub>2</sub> under uniaxial tension at 1.0 K and 300.0 K. Fig. 42 shows the stress-strain curve for the tension of a single-layer 1H-NiS<sub>2</sub> of dimension  $100 \times 100 \text{ \AA}$ . Periodic boundary conditions are applied in both armchair and zigzag directions. The single-layer 1H-NiS<sub>2</sub> is stretched uniaxially along the armchair or zigzag direction. The stress is calculated without involving the actual thickness of the quasi-two-dimensional structure of the single-layer 1H-NiS<sub>2</sub>. The Young's modulus can be obtained by a linear fitting of the stress-strain relation in the small strain range of  $[0, 0.01]$ . The Young's modulus are 84.0 N/m and 82.5 N/m along the armchair and zigzag directions, respectively. The Young's modulus is essentially isotropic in the armchair and zigzag directions. The Poisson's ratio from the VFF model and the SW potential is  $\nu_{xy} = \nu_{yx} = 0.19$ .

There is no available value for nonlinear quantities in the single-layer 1H-NiS<sub>2</sub>. We have thus used the nonlinear parameter  $B = 0.5d^4$  in Eq. (5), which is close to the value of  $B$  in most materials. The value of the third order nonlinear elasticity  $D$  can be extracted by fitting the stress-strain relation to the function  $\sigma = E\epsilon + \frac{1}{2}D\epsilon^2$  with  $E$  as the Young's modulus. The values of  $D$  from the present SW potential are -403.2 N/m and -414.8 N/m along the armchair and zigzag directions, respectively. The ultimate stress is about  $8.7 \text{ Nm}^{-1}$  at the ultimate strain of 0.20 in the armchair direction at the low temperature of 1 K. The ultimate stress is about  $8.3 \text{ Nm}^{-1}$  at the ultimate strain of 0.24 in the zigzag direction at the low temperature of 1 K.

### XXIII. 1H-NiSe<sub>2</sub>

Most existing theoretical studies on the single-layer 1H-NiSe<sub>2</sub> are based on the first-principles calculations. In this section, we will develop the SW potential for the single-layer

TABLE XC: The VFF model for single-layer 1H-NiSe<sub>2</sub>. The second line gives an explicit expression for each VFF term. The third line is the force constant parameters. Parameters are in the unit of  $\frac{\text{eV}}{\text{\AA}^2}$  for the bond stretching interactions, and in the unit of eV for the angle bending interaction. The fourth line gives the initial bond length (in unit of  $\text{\AA}$ ) for the bond stretching interaction and the initial angle (in unit of degrees) for the angle bending interaction. The angle  $\theta_{ijk}$  has atom  $i$  as the apex.

VFF type	bond stretching	angle bending		
expression	$\frac{1}{2}K_{\text{Ni-Se}}(\Delta r)^2$	$\frac{1}{2}K_{\text{Ni-Se-Se}}(\Delta\theta)^2$	$\frac{1}{2}K_{\text{Ni-Se-Se'}}(\Delta\theta)^2$	$\frac{1}{2}K_{\text{Se-Ni-Ni}}(\Delta\theta)^2$
parameter	4.823	2.171	2.171	2.171
$r_0$ or $\theta_0$	2.350	90.228	70.206	90.228

TABLE XCI: Two-body SW potential parameters for single-layer 1H-NiSe<sub>2</sub> used by GULP<sup>8</sup> as expressed in Eq. (3).

	$A$ (eV)	$\rho$ ( $\text{\AA}$ )	$B$ ( $\text{\AA}^4$ )	$r_{\min}$ ( $\text{\AA}$ )	$r_{\max}$ ( $\text{\AA}$ )
Ni-Se	4.004	1.267	15.249	0.0	3.213

TABLE XCII: Three-body SW potential parameters for single-layer 1H-NiSe<sub>2</sub> used by GULP<sup>8</sup> as expressed in Eq. (4). The angle  $\theta_{ijk}$  in the first line indicates the bending energy for the angle with atom  $i$  as the apex.

	$K$ (eV)	$\theta_0$ (degree)	$\rho_1$ ( $\text{\AA}$ )	$\rho_2$ ( $\text{\AA}$ )	$r_{\min12}$ ( $\text{\AA}$ )	$r_{\max12}$ ( $\text{\AA}$ )	$r_{\min13}$ ( $\text{\AA}$ )	$r_{\max13}$ ( $\text{\AA}$ )	$r_{\min23}$ ( $\text{\AA}$ )	$r_{\max23}$ ( $\text{\AA}$ )
$\theta_{\text{Ni-Se-Se}}$	20.479	90.228	1.267	1.267	0.0	3.213	0.0	3.213	0.0	3.809
$\theta_{\text{Ni-Se-Se'}}$	23.132	70.206	1.267	1.267	0.0	3.213	0.0	3.213	0.0	3.809
$\theta_{\text{Se-Ni-Ni}}$	20.479	90.228	1.267	1.267	0.0	3.213	0.0	3.213	0.0	3.809

TABLE XCIII: SW potential parameters for single-layer 1H-NiSe<sub>2</sub> used by LAMMPS<sup>9</sup> as expressed in Eqs. (9) and (10).

	$\epsilon$ (eV)	$\sigma$ ( $\text{\AA}$ )	$a$	$\lambda$	$\gamma$	$\cos\theta_0$	$A_L$	$B_L$	$p$	$q$	tol
Ni <sub>1</sub> -Se <sub>1</sub> -Se <sub>1</sub>	1.000	1.267	2.535	0.000	1.000	0.000	4.004	5.913	4	0	0.0
Ni <sub>1</sub> -Se <sub>1</sub> -Se <sub>3</sub>	1.000	0.000	0.000	20.479	1.000	-0.004	0.000	0.000	4	0	0.0
Ni <sub>1</sub> -Se <sub>1</sub> -Se <sub>2</sub>	1.000	0.000	0.000	23.132	1.000	0.339	0.000	0.000	4	0	0.0
Se <sub>1</sub> -Ni <sub>1</sub> -Ni <sub>3</sub>	1.000	0.000	0.000	20.479	1.000	-0.004	0.000	0.000	4	0	0.0

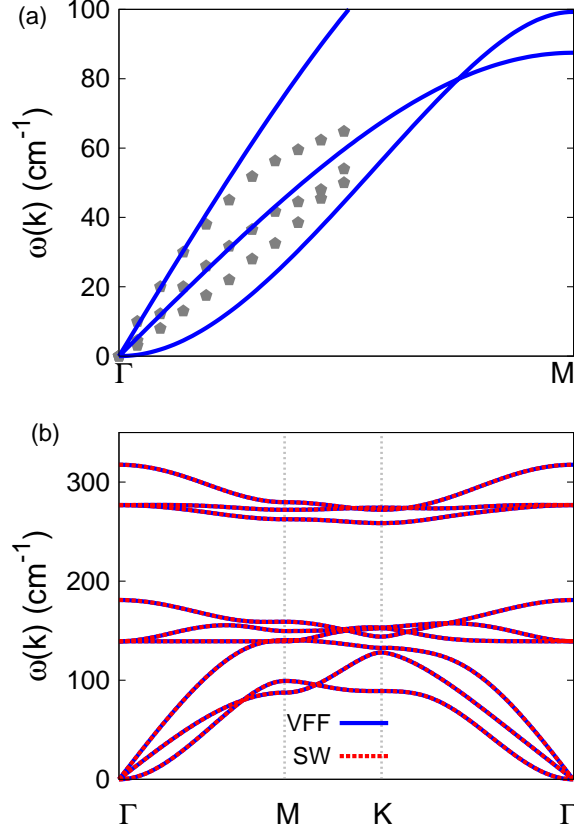


FIG. 43: (Color online) Phonon spectrum for single-layer 1H-NiSe<sub>2</sub>. (a) Phonon dispersion along the  $\Gamma$ M direction in the Brillouin zone. The results from the VFF model (lines) are comparable with the *ab initio* results (pentagons) from Ref. 12. (b) The phonon dispersion from the SW potential is exactly the same as that from the VFF model.

1H-NiSe<sub>2</sub>.

The structure for the single-layer 1H-NiSe<sub>2</sub> is shown in Fig. 1 (with M=Ni and X=Se). Each Ni atom is surrounded by six Se atoms. These Se atoms are categorized into the top group (eg. atoms 1, 3, and 5) and bottom group (eg. atoms 2, 4, and 6). Each Se atom is connected to three Ni atoms. The structural parameters are from the first-principles calculations,<sup>12</sup> including the lattice constant  $a = 3.33 \text{ \AA}$ , and the bond length  $d_{\text{Ni-Se}} = 2.35 \text{ \AA}$ . The resultant angles are  $\theta_{\text{NiSeSe}} = \theta_{\text{SeNiNi}} = 90.228^\circ$  and  $\theta_{\text{NiSeSe}'} = 70.206^\circ$ , in which atoms Se and Se' are from different (top or bottom) group.

Table XC shows four VFF terms for the single-layer 1H-NiSe<sub>2</sub>, one of which is the bond stretching interaction shown by Eq. (1) while the other three terms are the angle bending

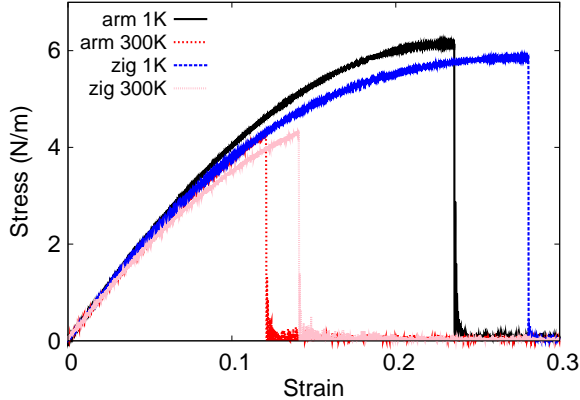


FIG. 44: (Color online) Stress-strain for single-layer 1H-NiSe<sub>2</sub> of dimension  $100 \times 100 \text{ \AA}$  along the armchair and zigzag directions.

interaction shown by Eq. (2). These force constant parameters are determined by fitting to the acoustic branches in the phonon dispersion along the  $\Gamma\text{M}$  as shown in Fig. 43 (a). The *ab initio* calculations for the phonon dispersion are from Ref. 12. The lowest acoustic branch (flexural mode) is almost linear in the *ab initio* calculations, which may due to the violation of the rigid rotational invariance.<sup>20</sup> Fig. 43 (b) shows that the VFF model and the SW potential give exactly the same phonon dispersion, as the SW potential is derived from the VFF model.

The parameters for the two-body SW potential used by GULP are shown in Tab. XCI. The parameters for the three-body SW potential used by GULP are shown in Tab. XCII. Some representative parameters for the SW potential used by LAMMPS are listed in Tab. XCIII. We note that twelve atom types have been introduced for the simulation of the single-layer 1H-NiSe<sub>2</sub> using LAMMPS, because the angles around atom Ni in Fig. 1 (with M=Ni and X=Se) are not distinguishable in LAMMPS. We have suggested two options to differentiate these angles by implementing some additional constraints in LAMMPS, which can be accomplished by modifying the source file of LAMMPS.<sup>13,14</sup> According to our experience, it is not so convenient for some users to implement these constraints and recompile the LAMMPS package. Hence, in the present work, we differentiate the angles by introducing more atom types, so it is not necessary to modify the LAMMPS package. Fig. 2 (with M=Ni and X=Se) shows that, for 1H-NiSe<sub>2</sub>, we can differentiate these angles around the Ni atom by assigning these six neighboring Se atoms with different atom types. It can be found that

twelve atom types are necessary for the purpose of differentiating all six neighbors around one Ni atom.

We use LAMMPS to perform MD simulations for the mechanical behavior of the single-layer 1H-NiSe<sub>2</sub> under uniaxial tension at 1.0 K and 300.0 K. Fig. 44 shows the stress-strain curve for the tension of a single-layer 1H-NiSe<sub>2</sub> of dimension 100 × 100 Å. Periodic boundary conditions are applied in both armchair and zigzag directions. The single-layer 1H-NiSe<sub>2</sub> is stretched uniaxially along the armchair or zigzag direction. The stress is calculated without involving the actual thickness of the quasi-two-dimensional structure of the single-layer 1H-NiSe<sub>2</sub>. The Young's modulus can be obtained by a linear fitting of the stress-strain relation in the small strain range of [0, 0.01]. The Young's modulus are 47.6 N/m and 47.8 N/m along the armchair and zigzag directions, respectively. The Young's modulus is essentially isotropic in the armchair and zigzag directions. The Poisson's ratio from the VFF model and the SW potential is  $\nu_{xy} = \nu_{yx} = 0.27$ .

There is no available value for nonlinear quantities in the single-layer 1H-NiSe<sub>2</sub>. We have thus used the nonlinear parameter  $B = 0.5d^4$  in Eq. (5), which is close to the value of  $B$  in most materials. The value of the third order nonlinear elasticity  $D$  can be extracted by fitting the stress-strain relation to the function  $\sigma = E\epsilon + \frac{1}{2}D\epsilon^2$  with  $E$  as the Young's modulus. The values of  $D$  from the present SW potential are -173.9 N/m and -197.6 N/m along the armchair and zigzag directions, respectively. The ultimate stress is about 6.1 Nm<sup>-1</sup> at the ultimate strain of 0.23 in the armchair direction at the low temperature of 1 K. The ultimate stress is about 5.9 Nm<sup>-1</sup> at the ultimate strain of 0.28 in the zigzag direction at the low temperature of 1 K.

#### XXIV. 1H-NITE<sub>2</sub>

Most existing theoretical studies on the single-layer 1H-NiTe<sub>2</sub> are based on the first-principles calculations. In this section, we will develop the SW potential for the single-layer 1H-NiTe<sub>2</sub>.

The structure for the single-layer 1H-NiTe<sub>2</sub> is shown in Fig. 1 (with M=Ni and X=Te). Each Ni atom is surrounded by six Te atoms. These Te atoms are categorized into the top group (eg. atoms 1, 3, and 5) and bottom group (eg. atoms 2, 4, and 6). Each Te atom is connected to three Ni atoms. The structural parameters are from the first-

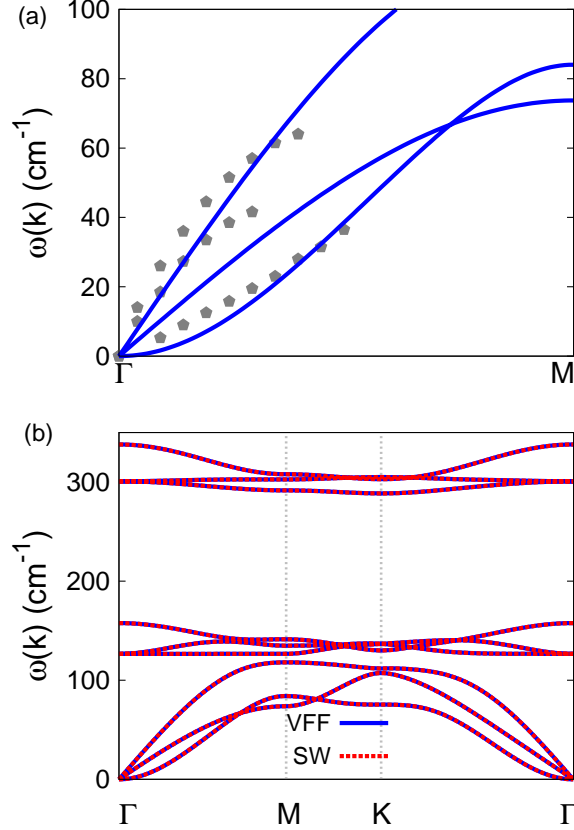


FIG. 45: (Color online) Phonon spectrum for single-layer 1H-NiTe<sub>2</sub>. (a) Phonon dispersion along the  $\Gamma$ M direction in the Brillouin zone. The results from the VFF model (lines) are comparable with the *ab initio* results (pentagons) from Ref. 12. (b) The phonon dispersion from the SW potential is exactly the same as that from the VFF model.

principles calculations,<sup>12</sup> including the lattice constant  $a = 3.59 \text{ \AA}$ , and the bond length  $d_{\text{Ni-Te}} = 2.54 \text{ \AA}$ . The resultant angles are  $\theta_{\text{NiTeTe}} = \theta_{\text{TeNiNi}} = 89.933^\circ$  and  $\theta_{\text{NiTeTe}'} = 70.624^\circ$ , in which atoms Te and Te' are from different (top or bottom) group.

Table XCIV shows four VFF terms for the single-layer 1H-NiTe<sub>2</sub>, one of which is the bond stretching interaction shown by Eq. (1) while the other three terms are the angle bending interaction shown by Eq. (2). These force constant parameters are determined by fitting to the acoustic branches in the phonon dispersion along the  $\Gamma$ M as shown in Fig. 45 (a). The *ab initio* calculations for the phonon dispersion are from Ref. 12. The lowest acoustic branch (flexural mode) is almost linear in the *ab initio* calculations, which may due to the violation of the rigid rotational invariance.<sup>20</sup> The transverse acoustic branch is very close

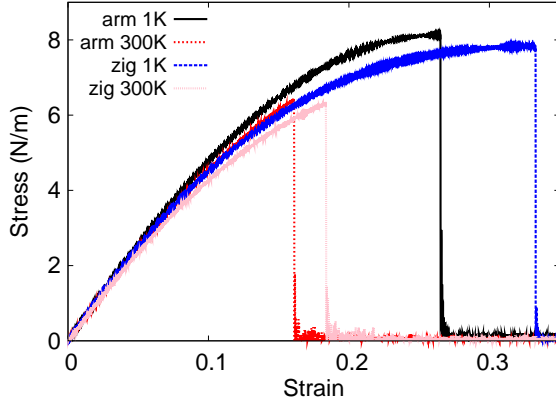


FIG. 46: (Color online) Stress-strain for single-layer 1H-NiTe<sub>2</sub> of dimension  $100 \times 100 \text{ \AA}$  along the armchair and zigzag directions.

TABLE XCIV: The VFF model for single-layer 1H-NiTe<sub>2</sub>. The second line gives an explicit expression for each VFF term. The third line is the force constant parameters. Parameters are in the unit of  $\frac{eV}{\text{Å}^2}$  for the bond stretching interactions, and in the unit of eV for the angle bending interaction. The fourth line gives the initial bond length (in unit of Å) for the bond stretching interaction and the initial angle (in unit of degrees) for the angle bending interaction. The angle  $\theta_{ijk}$  has atom *i* as the apex.

VFF type	bond stretching	angle bending		
expression	$\frac{1}{2}K_{\text{Ni-Te}}(\Delta r)^2$	$\frac{1}{2}K_{\text{Ni-Te-Te}}(\Delta\theta)^2$	$\frac{1}{2}K_{\text{Ni-Te-Te}'}(\Delta\theta)^2$	$\frac{1}{2}K_{\text{Te-Ni-Ni}}(\Delta\theta)^2$
parameter	6.712	2.656	2.656	2.656
$r_0$ or $\theta_0$	2.540	89.933	70.624	89.933

to the longitudinal acoustic branch in the *ab initio* calculations. Fig. 45 (b) shows that the VFF model and the SW potential give exactly the same phonon dispersion, as the SW potential is derived from the VFF model.

The parameters for the two-body SW potential used by GULP are shown in Tab. XCV. The parameters for the three-body SW potential used by GULP are shown in Tab. XCVI. Some representative parameters for the SW potential used by LAMMPS are listed in Tab. XCVII. We note that twelve atom types have been introduced for the simulation of the single-layer 1H-NiTe<sub>2</sub> using LAMMPS, because the angles around atom Ni in Fig. 1 (with

TABLE XCV: Two-body SW potential parameters for single-layer 1H-NiTe<sub>2</sub> used by GULP<sup>8</sup> as expressed in Eq. (3).

	$A$ (eV)	$\rho$ (Å)	$B$ (Å <sup>4</sup> )	$r_{\min}$ (Å)	$r_{\max}$ (Å)
Ni-Te	6.461	1.359	20.812	0.0	3.469

TABLE XCVI: Three-body SW potential parameters for single-layer 1H-NiTe<sub>2</sub> used by GULP<sup>8</sup> as expressed in Eq. (4). The angle  $\theta_{ijk}$  in the first line indicates the bending energy for the angle with atom  $i$  as the apex.

	$K$ (eV)	$\theta_0$ (degree)	$\rho_1$ (Å)	$\rho_2$ (Å)	$r_{\min12}$ (Å)	$r_{\max12}$ (Å)	$r_{\min13}$ (Å)	$r_{\max13}$ (Å)	$r_{\min23}$ (Å)	$r_{\max23}$ (Å)
$\theta_{\text{Ni-Te-Te}}$	24.759	89.933	1.359	1.359	0.0	3.469	0.0	3.469	0.0	4.114
$\theta_{\text{Ni-Te-Te}'}$	27.821	70.624	1.359	1.359	0.0	3.469	0.0	3.469	0.0	4.114
$\theta_{\text{Te-Ni-Ni}}$	24.759	89.933	1.359	1.359	0.0	3.469	0.0	3.469	0.0	4.114

M=Ni and X=Te) are not distinguishable in LAMMPS. We have suggested two options to differentiate these angles by implementing some additional constraints in LAMMPS, which can be accomplished by modifying the source file of LAMMPS.<sup>13,14</sup> According to our experience, it is not so convenient for some users to implement these constraints and recompile the LAMMPS package. Hence, in the present work, we differentiate the angles by introducing more atom types, so it is not necessary to modify the LAMMPS package. Fig. 2 (with M=Ni and X=Te) shows that, for 1H-NiTe<sub>2</sub>, we can differentiate these angles around the Ni atom by assigning these six neighboring Te atoms with different atom types. It can be found that twelve atom types are necessary for the purpose of differentiating all six neighbors around one Ni atom.

TABLE XCVII: SW potential parameters for single-layer 1H-NiTe<sub>2</sub> used by LAMMPS<sup>9</sup> as expressed in Eqs. (9) and (10).

	$\epsilon$ (eV)	$\sigma$ (Å)	$a$	$\lambda$	$\gamma$	$\cos \theta_0$	$A_L$	$B_L$	$p$	$q$	tol
Ni <sub>1</sub> -Te <sub>1</sub> -Te <sub>1</sub>	1.000	1.359	2.553	0.000	1.000	0.000	6.461	6.107	4	0	0.0
Ni <sub>1</sub> -Te <sub>1</sub> -Te <sub>3</sub>	1.000	0.000	0.000	24.759	1.000	0.001	0.000	0.000	4	0	0.0
Ni <sub>1</sub> -Te <sub>1</sub> -Te <sub>2</sub>	1.000	0.000	0.000	27.821	1.000	0.332	0.000	0.000	4	0	0.0
Te <sub>1</sub> -Ni <sub>1</sub> -Ni <sub>3</sub>	1.000	0.000	0.000	24.759	1.000	0.001	0.000	0.000	4	0	0.0

We use LAMMPS to perform MD simulations for the mechanical behavior of the single-layer 1H-NiTe<sub>2</sub> under uniaxial tension at 1.0 K and 300.0 K. Fig. 46 shows the stress-strain curve for the tension of a single-layer 1H-NiTe<sub>2</sub> of dimension 100 × 100 Å. Periodic boundary conditions are applied in both armchair and zigzag directions. The single-layer 1H-NiTe<sub>2</sub> is stretched uniaxially along the armchair or zigzag direction. The stress is calculated without involving the actual thickness of the quasi-two-dimensional structure of the single-layer 1H-NiTe<sub>2</sub>. The Young's modulus can be obtained by a linear fitting of the stress-strain relation in the small strain range of [0, 0.01]. The Young's modulus are 53.2 N/m and 53.6 N/m along the armchair and zigzag directions, respectively. The Young's modulus is essentially isotropic in the armchair and zigzag directions. The Poisson's ratio from the VFF model and the SW potential is  $\nu_{xy} = \nu_{yx} = 0.32$ .

There is no available value for nonlinear quantities in the single-layer 1H-NiTe<sub>2</sub>. We have thus used the nonlinear parameter  $B = 0.5d^4$  in Eq. (5), which is close to the value of  $B$  in most materials. The value of the third order nonlinear elasticity  $D$  can be extracted by fitting the stress-strain relation to the function  $\sigma = E\epsilon + \frac{1}{2}D\epsilon^2$  with  $E$  as the Young's modulus. The values of  $D$  from the present SW potential are -156.6 N/m and -184.8 N/m along the armchair and zigzag directions, respectively. The ultimate stress is about 8.1 Nm<sup>-1</sup> at the ultimate strain of 0.26 in the armchair direction at the low temperature of 1 K. The ultimate stress is about 7.8 Nm<sup>-1</sup> at the ultimate strain of 0.33 in the zigzag direction at the low temperature of 1 K.

## XXV. 1H-NbS<sub>2</sub>

In 1983, the VFF model was developed to investigate the lattice dynamical properties in the bulk 2H-NbS<sub>2</sub>.<sup>21</sup> In this section, we will develop the SW potential for the single-layer 1H-NbS<sub>2</sub>.

The structure for the single-layer 1H-NbS<sub>2</sub> is shown in Fig. 1 (with M=Nb and X=S). Each Nb atom is surrounded by six S atoms. These S atoms are categorized into the top group (eg. atoms 1, 3, and 5) and bottom group (eg. atoms 2, 4, and 6). Each S atom is connected to three Nb atoms. The structural parameters are from Ref. 21, including the lattice constant  $a = 3.31$  Å, and the bond length  $d_{\text{Nb-S}} = 2.47$  Å. The resultant angles are  $\theta_{\text{NbSS}} = \theta_{\text{SNbNb}} = 84.140^\circ$  and  $\theta_{\text{NbSS}'} = 78.626^\circ$ , in which atoms S and S' are from different

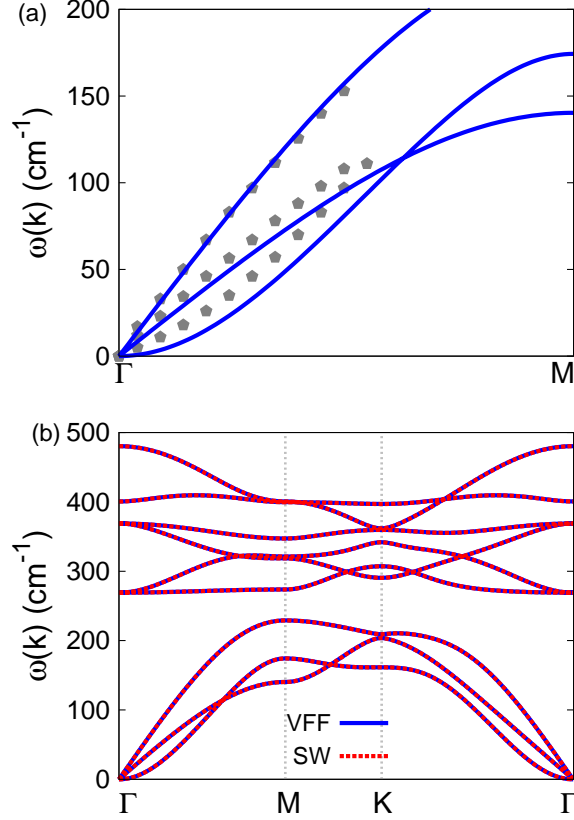


FIG. 47: (Color online) Phonon dispersion for single-layer 1H-NbS<sub>2</sub>. (a) The VFF model is fitted to the three acoustic branches in the long wave limit along the  $\Gamma$ M direction. The theoretical results (gray pentagons) are from Ref. 21. The blue lines are from the present VFF model. (b) The VFF model (blue lines) and the SW potential (red lines) give the same phonon dispersion for single-layer 1H-NbS<sub>2</sub> along  $\Gamma$ MK $\Gamma$ .

(top or bottom) group.

Table XCVIII shows four VFF terms for the 1H-NbS<sub>2</sub>, one of which is the bond stretching interaction shown by Eq. (1) while the other three terms are the angle bending interaction shown by Eq. (2). These force constant parameters are determined by fitting to the three acoustic branches in the phonon dispersion along the  $\Gamma$ M as shown in Fig. 47 (a). The theoretical phonon frequencies (gray pentagons) are from Ref. 21, which are the phonon dispersion of bulk 2H-NbS<sub>2</sub>. We have used these phonon frequencies as the phonon dispersion of the single-layer 1H-NbS<sub>2</sub>, as the inter-layer interaction in the bulk 2H-NbS<sub>2</sub> only induces weak effects on the two inplane acoustic branches. The inter-layer coupling will

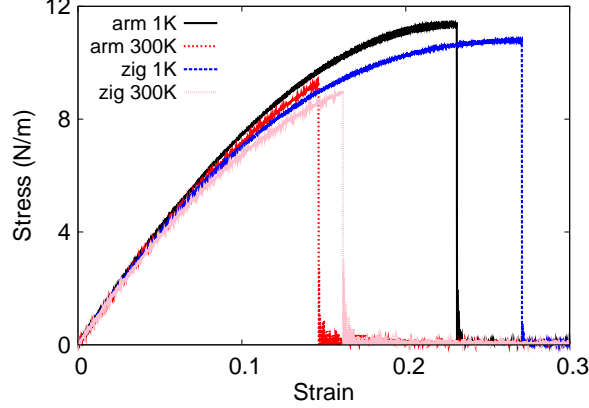


FIG. 48: (Color online) Stress-strain for single-layer 1H-NbS<sub>2</sub> of dimension 100 × 100 Å along the armchair and zigzag directions.

TABLE XCVIII: The VFF model for single-layer 1H-NbS<sub>2</sub>. The second line gives an explicit expression for each VFF term. The third line is the force constant parameters. Parameters are in the unit of  $\frac{eV}{\text{Å}^2}$  for the bond stretching interactions, and in the unit of eV for the angle bending interaction. The fourth line gives the initial bond length (in unit of Å) for the bond stretching interaction and the initial angle (in unit of degrees) for the angle bending interaction. The angle  $\theta_{ijk}$  has atom *i* as the apex.

VFF type	bond stretching	angle bending		
expression	$\frac{1}{2}K_{Nb-S}(\Delta r)^2$	$\frac{1}{2}K_{Nb-S-S}(\Delta\theta)^2$	$\frac{1}{2}K_{Nb-S-S'}(\Delta\theta)^2$	$\frac{1}{2}K_{S-Nb-Nb}(\Delta\theta)^2$
parameter	8.230	4.811	4.811	4.811
$r_0$ or $\theta_0$	2.470	84.140	78.626	84.140

strengthen the out-of-plane acoustic branch (flexural branch), so the flexural branch from the present VFF model (blue line) is lower than the theoretical results for bulk 2H-NbS<sub>2</sub> (gray pentagons). Fig. 47 (b) shows that the VFF model and the SW potential give exactly the same phonon dispersion, as the SW potential is derived from the VFF model.

The parameters for the two-body SW potential used by GULP are shown in Tab. XCIX. The parameters for the three-body SW potential used by GULP are shown in Tab. C. Parameters for the SW potential used by LAMMPS are listed in Tab. CI. We note that twelve atom types have been introduced for the simulation of the single-layer 1H-NbS<sub>2</sub> us-

TABLE XCIX: Two-body SW potential parameters for single-layer 1H-NbS<sub>2</sub> used by GULP<sup>8</sup> as expressed in Eq. (3).

	$A$ (eV)	$\rho$ (Å)	$B$ (Å <sup>4</sup> )	$r_{\min}$ (Å)	$r_{\max}$ (Å)
Nb-S	6.439	1.116	18.610	0.0	3.300

TABLE C: Three-body SW potential parameters for single-layer 1H-NbS<sub>2</sub> used by GULP<sup>8</sup> as expressed in Eq. (4). The angle  $\theta_{ijk}$  in the first line indicates the bending energy for the angle with atom i as the apex.

	$K$ (eV)	$\theta_0$ (degree)	$\rho_1$ (Å)	$\rho_2$ (Å)	$r_{\min12}$ (Å)	$r_{\max12}$ (Å)	$r_{\min13}$ (Å)	$r_{\max13}$ (Å)	$r_{\min23}$ (Å)	$r_{\max23}$ (Å)
$\theta_{\text{Nb-S-S}}$	35.748	84.140	1.116	1.116	0.0	3.300	0.0	3.300	0.0	3.933
$\theta_{\text{Nb-S-S}'}$	36.807	78.626	1.116	1.116	0.0	3.300	0.0	3.300	0.0	3.933
$\theta_{\text{S-Nb-Nb}}$	35.748	84.140	1.116	1.116	0.0	3.300	0.0	3.300	0.0	3.933

ing LAMMPS, because the angles around atom Nb in Fig. 1 (with M=Nb and X=S) are not distinguishable in LAMMPS. We have suggested two options to differentiate these angles by implementing some additional constraints in LAMMPS, which can be accomplished by modifying the source file of LAMMPS.<sup>13,14</sup> According to our experience, it is not so convenient for some users to implement these constraints and recompile the LAMMPS package. Hence, in the present work, we differentiate the angles by introducing more atom types, so it is not necessary to modify the LAMMPS package. Fig. 2 (with M=Nb and X=S) shows that, for 1H-NbS<sub>2</sub>, we can differentiate these angles around the Nb atom by assigning these six neighboring S atoms with different atom types. It can be found that twelve atom types

TABLE CI: SW potential parameters for single-layer 1H-NbS<sub>2</sub> used by LAMMPS<sup>9</sup> as expressed in Eqs. (9) and (10). Atom types in the first column are displayed in Fig. 2 (with M=Nb and X=S).

	$\epsilon$ (eV)	$\sigma$ (Å)	$a$	$\lambda$	$\gamma$	$\cos\theta_0$	$A_L$	$B_L$	$p$	$q$	tol
Nb <sub>1</sub> -S <sub>1</sub> -S <sub>1</sub>	1.000	1.116	2.958	0.000	1.000	0.000	6.439	12.014	4	0	0.0
Nb <sub>1</sub> -S <sub>1</sub> -S <sub>3</sub>	1.000	0.000	0.000	35.748	1.000	0.102	0.000	0.000	4	0	0.0
Nb <sub>1</sub> -S <sub>1</sub> -S <sub>2</sub>	1.000	0.000	0.000	36.807	1.000	0.197	0.000	0.000	4	0	0.0
S <sub>1</sub> -Nb <sub>1</sub> -Nb <sub>3</sub>	1.000	0.000	0.000	35.748	1.000	0.102	0.000	0.000	4	0	0.0

are necessary for the purpose of differentiating all six neighbors around one Nb atom.

We use LAMMPS to perform MD simulations for the mechanical behavior of the single-layer 1H-NbS<sub>2</sub> under uniaxial tension at 1.0 K and 300.0 K. Fig. 48 shows the stress-strain curve for the tension of a single-layer 1H-NbS<sub>2</sub> of dimension 100 × 100 Å. Periodic boundary conditions are applied in both armchair and zigzag directions. The single-layer 1H-NbS<sub>2</sub> is stretched uniaxially along the armchair or zigzag direction. The stress is calculated without involving the actual thickness of the quasi-two-dimensional structure of the single-layer 1H-NbS<sub>2</sub>. The Young's modulus can be obtained by a linear fitting of the stress-strain relation in the small strain range of [0, 0.01]. The Young's modulus are 87.7 N/m and 87.2 N/m along the armchair and zigzag directions, respectively. The Young's modulus is essentially isotropic in the armchair and zigzag directions. The Poisson's ratio from the VFF model and the SW potential is  $\nu_{xy} = \nu_{yx} = 0.27$ .

There is no available value for the nonlinear quantities in the single-layer 1H-NbS<sub>2</sub>. We have thus used the nonlinear parameter  $B = 0.5d^4$  in Eq. (5), which is close to the value of  $B$  in most materials. The value of the third order nonlinear elasticity  $D$  can be extracted by fitting the stress-strain relation to the function  $\sigma = E\epsilon + \frac{1}{2}D\epsilon^2$  with  $E$  as the Young's modulus. The values of  $D$  from the present SW potential are -315.3 N/m and -355.1 N/m along the armchair and zigzag directions, respectively. The ultimate stress is about 11.4 Nm<sup>-1</sup> at the ultimate strain of 0.23 in the armchair direction at the low temperature of 1 K. The ultimate stress is about 10.8 Nm<sup>-1</sup> at the ultimate strain of 0.27 in the zigzag direction at the low temperature of 1 K.

## XXVI. 1H-NbSe<sub>2</sub>

In 1983, the VFF model was developed to investigate the lattice dynamical properties in the bulk 2H-NbSe<sub>2</sub>.<sup>15,21</sup> In this section, we will develop the SW potential for the single-layer 1H-NbSe<sub>2</sub>.

The structure for the single-layer 1H-NbSe<sub>2</sub> is shown in Fig. 1 (with M=Nb and X=Se). Each Nb atom is surrounded by six Se atoms. These Se atoms are categorized into the top group (eg. atoms 1, 3, and 5) and bottom group (eg. atoms 2, 4, and 6). Each Se atom is connected to three Nb atoms. The structural parameters are from Ref. 21, including the lattice constant  $a = 3.45$  Å, and the bond length  $d_{\text{Nb-Se}} = 2.60$  Å. The resultant angles

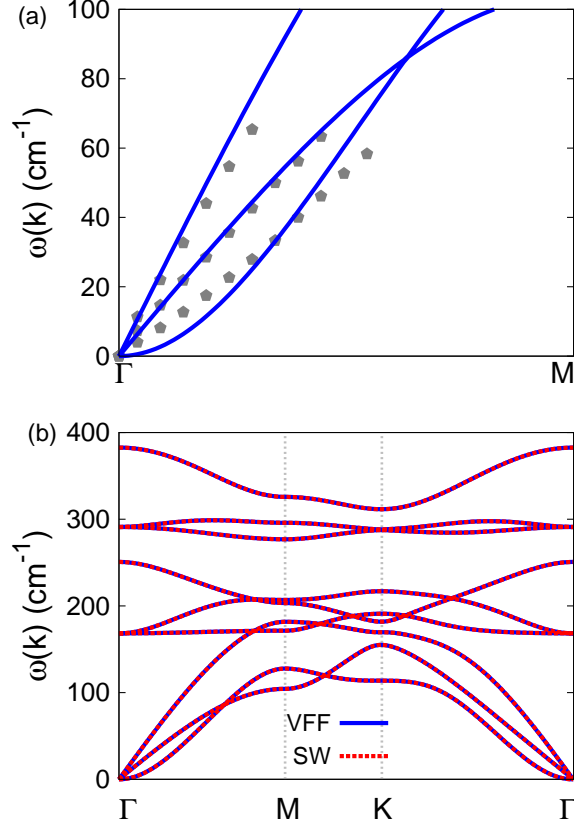


FIG. 49: (Color online) Phonon dispersion for single-layer 1H-NbSe<sub>2</sub>. (a) The VFF model is fitted to the three acoustic branches in the long wave limit along the  $\Gamma$ M direction. The theoretical results (gray pentagons) are from Ref. 15. The blue lines are from the present VFF model. (b) The VFF model (blue lines) and the SW potential (red lines) give the same phonon dispersion for single-layer 1H-NbSe<sub>2</sub> along  $\Gamma$ MK $\Gamma$ .

are  $\theta_{\text{NbSeSe}} = \theta_{\text{SNbNb}} = 83.129^\circ$  and  $\theta_{\text{NbSeSe}'} = 79.990^\circ$ , in which atoms Se and Se' are from different (top or bottom) group.

Table CII shows four VFF terms for the 1H-NbSe<sub>2</sub>, one of which is the bond stretching interaction shown by Eq. (1) while the other three terms are the angle bending interaction shown by Eq. (2). These force constant parameters are determined by fitting to the three acoustic branches in the phonon dispersion along the  $\Gamma$ M as shown in Fig. 49 (a). The theoretical phonon frequencies (gray pentagons) are from Ref. 21, which are the phonon dispersion of bulk 2H-NbSe<sub>2</sub>. We have used these phonon frequencies as the phonon dispersion of the single-layer 1H-NbSe<sub>2</sub>, as the inter-layer interaction in the bulk 2H-NbSe<sub>2</sub> only

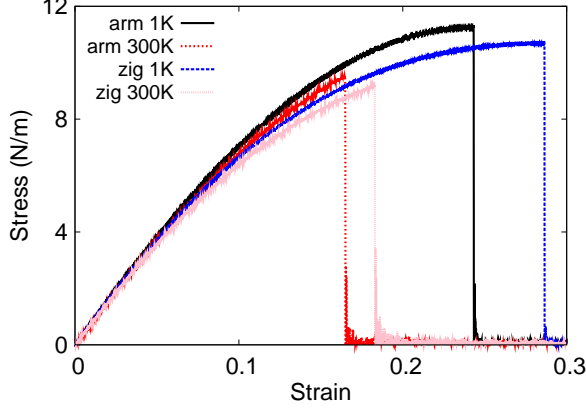


FIG. 50: (Color online) Stress-strain for single-layer 1H-NbSe<sub>2</sub> of dimension  $100 \times 100 \text{ \AA}$  along the armchair and zigzag directions.

TABLE CII: The VFF model for single-layer 1H-NbSe<sub>2</sub>. The second line gives an explicit expression for each VFF term. The third line is the force constant parameters. Parameters are in the unit of  $\frac{eV}{\text{Å}^2}$  for the bond stretching interactions, and in the unit of eV for the angle bending interaction. The fourth line gives the initial bond length (in unit of Å) for the bond stretching interaction and the initial angle (in unit of degrees) for the angle bending interaction. The angle  $\theta_{ijk}$  has atom  $i$  as the apex.

VFF type	bond stretching	angle bending		
expression	$\frac{1}{2}K_{\text{Nb-Se}}(\Delta r)^2$	$\frac{1}{2}K_{\text{Nb-Se-Se}}(\Delta\theta)^2$	$\frac{1}{2}K_{\text{Nb-Se-Se'}}(\Delta\theta)^2$	$\frac{1}{2}K_{\text{Se-Nb-Nb}}(\Delta\theta)^2$
parameter	8.230	4.811	4.811	4.811
$r_0$ or $\theta_0$	2.600	83.129	79.990	83.129

induces weak effects on the two inplane acoustic branches. The inter-layer coupling will strengthen the out-of-plane acoustic branch (flexural branch), so the flexural branch from the present VFF model (blue line) is lower than the theoretical results for bulk 2H-NbSe<sub>2</sub> (gray pentagons). It turns out that the VFF parameters for the single-layer 1H-NbSe<sub>2</sub> are the same as the single-layer NbS<sub>2</sub>. The phonon dispersion for single-layer 1H-NbSe<sub>2</sub> was also shown in Ref. 12. Fig. 49 (b) shows that the VFF model and the SW potential give exactly the same phonon dispersion, as the SW potential is derived from the VFF model.

The parameters for the two-body SW potential used by GULP are shown in Tab. CIII. The parameters for the three-body SW potential used by GULP are shown in Tab. CIV.

TABLE CIII: Two-body SW potential parameters for single-layer 1H-NbSe<sub>2</sub> used by GULP<sup>8</sup> as expressed in Eq. (3).

	$A$ (eV)	$\rho$ (Å)	$B$ (Å <sup>4</sup> )	$r_{\min}$ (Å)	$r_{\max}$ (Å)
Nb-Se	6.942	1.138	22.849	0.0	3.460

TABLE CIV: Three-body SW potential parameters for single-layer 1H-NbSe<sub>2</sub> used by GULP<sup>8</sup> as expressed in Eq. (4). The angle  $\theta_{ijk}$  in the first line indicates the bending energy for the angle with atom i as the apex.

	$K$ (eV)	$\theta_0$ (degree)	$\rho_1$ (Å)	$\rho_2$ (Å)	$r_{\min12}$ (Å)	$r_{\max12}$ (Å)	$r_{\min13}$ (Å)	$r_{\max13}$ (Å)	$r_{\min23}$ (Å)	$r_{\max23}$ (Å)
$\theta_{\text{Nb-Se-Se}}$	34.409	83.129	1.138	1.138	0.0	3.460	0.0	3.460	0.0	4.127
$\theta_{\text{Nb-Se-Se}'}$	34.973	79.990	1.138	1.138	0.0	3.460	0.0	3.460	0.0	4.127
$\theta_{\text{Se-Nb-Nb}}$	34.409	83.129	1.138	1.138	0.0	3.460	0.0	3.460	0.0	4.127

Parameters for the SW potential used by LAMMPS are listed in Tab. CV. We note that twelve atom types have been introduced for the simulation of the single-layer 1H-NbSe<sub>2</sub> using LAMMPS, because the angles around atom Nb in Fig. 1 (with M=Nb and X=Se) are not distinguishable in LAMMPS. We have suggested two options to differentiate these angles by implementing some additional constraints in LAMMPS, which can be accomplished by modifying the source file of LAMMPS.<sup>13,14</sup> According to our experience, it is not so convenient for some users to implement these constraints and recompile the LAMMPS package. Hence, in the present work, we differentiate the angles by introducing more atom types, so

TABLE CV: SW potential parameters for single-layer 1H-NbSe<sub>2</sub> used by LAMMPS<sup>9</sup> as expressed in Eqs. (9) and (10). Atom types in the first column are displayed in Fig. 2 (with M=Nb and X=Se).

	$\epsilon$ (eV)	$\sigma$ (Å)	$a$	$\lambda$	$\gamma$	$\cos \theta_0$	$A_L$	$B_L$	$p$	$q$	tol
Nb <sub>1</sub> -Se <sub>1</sub> -Se <sub>1</sub>	1.000	1.138	3.041	0.000	1.000	0.000	6.942	13.631	4	0	0.0
Nb <sub>1</sub> -Se <sub>1</sub> -Se <sub>3</sub>	1.000	0.000	0.000	34.409	1.000	0.120	0.000	0.000	4	0	0.0
Nb <sub>1</sub> -Se <sub>1</sub> -Se <sub>2</sub>	1.000	0.000	0.000	34.973	1.000	0.174	0.000	0.000	4	0	0.0
Se <sub>1</sub> -Nb <sub>1</sub> -Nb <sub>3</sub>	1.000	0.000	0.000	34.409	1.000	0.120	0.000	0.000	4	0	0.0

it is not necessary to modify the LAMMPS package. Fig. 2 (with M=Nb and X=Se) shows that, for 1H-NbSe<sub>2</sub>, we can differentiate these angles around the Nb atom by assigning these six neighboring Se atoms with different atom types. It can be found that twelve atom types are necessary for the purpose of differentiating all six neighbors around one Nb atom.

We use LAMMPS to perform MD simulations for the mechanical behavior of the single-layer 1H-NbSe<sub>2</sub> under uniaxial tension at 1.0 K and 300.0 K. Fig. 50 shows the stress-strain curve for the tension of a single-layer 1H-NbSe<sub>2</sub> of dimension 100 × 100 Å. Periodic boundary conditions are applied in both armchair and zigzag directions. The single-layer 1H-NbSe<sub>2</sub> is stretched uniaxially along the armchair or zigzag direction. The stress is calculated without involving the actual thickness of the quasi-two-dimensional structure of the single-layer 1H-NbSe<sub>2</sub>. The Young's modulus can be obtained by a linear fitting of the stress-strain relation in the small strain range of [0, 0.01]. The Young's modulus are 80.2 N/m and 80.7 N/m along the armchair and zigzag directions, respectively. The Young's modulus is essentially isotropic in the armchair and zigzag directions. The Poisson's ratio from the VFF model and the SW potential is  $\nu_{xy} = \nu_{yx} = 0.29$ .

There is no available value for the nonlinear quantities in the single-layer 1H-NbSe<sub>2</sub>. We have thus used the nonlinear parameter  $B = 0.5d^4$  in Eq. (5), which is close to the value of  $B$  in most materials. The value of the third order nonlinear elasticity  $D$  can be extracted by fitting the stress-strain relation to the function  $\sigma = E\epsilon + \frac{1}{2}D\epsilon^2$  with  $E$  as the Young's modulus. The values of  $D$  from the present SW potential are -258.8 N/m and -306.1 N/m along the armchair and zigzag directions, respectively. The ultimate stress is about 11.2 Nm<sup>-1</sup> at the ultimate strain of 0.24 in the armchair direction at the low temperature of 1 K. The ultimate stress is about 10.7 Nm<sup>-1</sup> at the ultimate strain of 0.28 in the zigzag direction at the low temperature of 1 K.

## XXVII. 1H-MOO<sub>2</sub>

Most existing theoretical studies on the single-layer 1H-MoO<sub>2</sub> are based on the first-principles calculations. In this section, we will develop the SW potential for the single-layer 1H-MoO<sub>2</sub>.

The structure for the single-layer 1H-MoO<sub>2</sub> is shown in Fig. 1 (with M=Mo and X=O). Each Mo atom is surrounded by six O atoms. These O atoms are categorized into the

TABLE CVI: The VFF model for single-layer 1H-MoO<sub>2</sub>. The second line gives an explicit expression for each VFF term. The third line is the force constant parameters. Parameters are in the unit of  $\frac{eV}{\text{Å}^2}$  for the bond stretching interactions, and in the unit of eV for the angle bending interaction. The fourth line gives the initial bond length (in unit of Å) for the bond stretching interaction and the initial angle (in unit of degrees) for the angle bending interaction. The angle  $\theta_{ijk}$  has atom *i* as the apex.

VFF type	bond stretching	angle bending		
expression	$\frac{1}{2}K_{\text{Mo-O}}(\Delta r)^2$	$\frac{1}{2}K_{\text{Mo-O-O}}(\Delta\theta)^2$	$\frac{1}{2}K_{\text{Mo-O-O}'}(\Delta\theta)^2$	$\frac{1}{2}K_{\text{O-Mo-Mo}}(\Delta\theta)^2$
parameter	14.622	8.410	8.410	8.410
$r_0$ or $\theta_0$	2.000	88.054	73.258	88.054

TABLE CVII: Two-body SW potential parameters for single-layer 1H-MoO<sub>2</sub> used by GULP<sup>8</sup> as expressed in Eq. (3).

	$A$ (eV)	$\rho$ (Å)	$B$ (Å <sup>4</sup> )	$r_{\min}$ (Å)	$r_{\max}$ (Å)
Mo-O	8.317	1.015	8.000	0.0	2.712

TABLE CVIII: Three-body SW potential parameters for single-layer 1H-MoO<sub>2</sub> used by GULP<sup>8</sup> as expressed in Eq. (4). The angle  $\theta_{ijk}$  in the first line indicates the bending energy for the angle with atom *i* as the apex.

	$K$ (eV)	$\theta_0$ (degree)	$\rho_1$ (Å)	$\rho_2$ (Å)	$r_{\min12}$ (Å)	$r_{\max12}$ (Å)	$r_{\min13}$ (Å)	$r_{\max13}$ (Å)	$r_{\min23}$ (Å)	$r_{\max23}$ (Å)
$\theta_{\text{Mo-O-O}}$	72.735	88.054	1.015	1.015	0.0	2.712	0.0	2.712	0.0	3.222
$\theta_{\text{Mo-O-O}'}$	79.226	73.258	1.015	1.015	0.0	2.712	0.0	2.712	0.0	3.222
$\theta_{\text{O-Mo-Mo}}$	72.735	88.054	1.015	1.015	0.0	2.712	0.0	2.712	0.0	3.222

TABLE CIX: SW potential parameters for single-layer 1H-MoO<sub>2</sub> used by LAMMPS<sup>9</sup> as expressed in Eqs. (9) and (10).

	$\epsilon$ (eV)	$\sigma$ (Å)	$a$	$\lambda$	$\gamma$	$\cos\theta_0$	$A_L$	$B_L$	$p$	$q$	tol
Mo <sub>1</sub> -O <sub>1</sub> -O <sub>1</sub>	1.000	1.015	2.673	0.000	1.000	0.000	8.317	7.541	4	0	0.0
Mo <sub>1</sub> -O <sub>1</sub> -O <sub>3</sub>	1.000	0.000	0.000	72.735	1.000	0.034	0.000	0.000	4	0	0.0
Mo <sub>1</sub> -O <sub>1</sub> -O <sub>2</sub>	1.000	0.000	0.000	79.226	1.000	0.288	0.000	0.000	4	0	0.0
O <sub>1</sub> -Mo <sub>1</sub> -Mo <sub>3</sub>	1.000	0.000	0.000	72.735	1.000	0.034	0.000	0.000	4	0	0.0

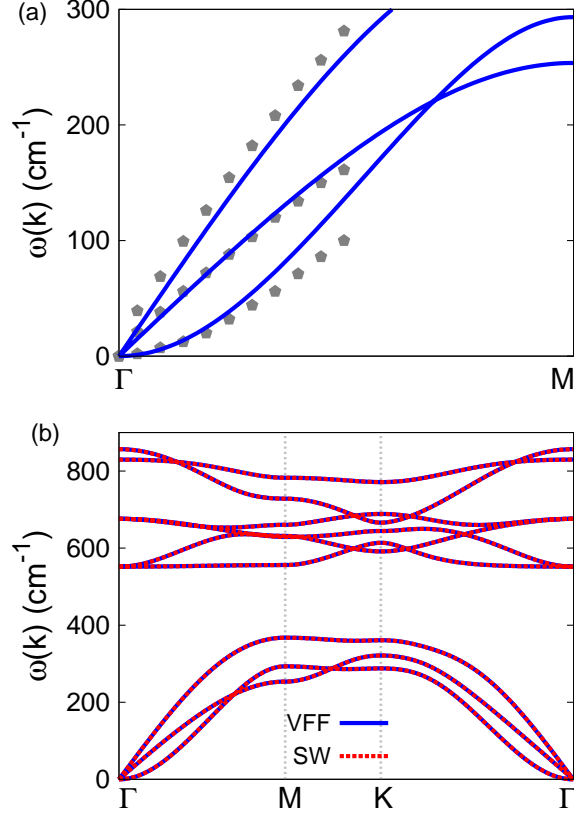


FIG. 51: (Color online) Phonon spectrum for single-layer 1H-MoO<sub>2</sub>. (a) Phonon dispersion along the  $\Gamma$ M direction in the Brillouin zone. The results from the VFF model (lines) are comparable with the *ab initio* results (pentagons) from Ref. 12. (b) The phonon dispersion from the SW potential is exactly the same as that from the VFF model.

top group (eg. atoms 1, 3, and 5) and bottom group (eg. atoms 2, 4, and 6). Each O atom is connected to three Mo atoms. The structural parameters are from the first-principles calculations,<sup>12</sup> including the lattice constant  $a = 2.78 \text{ \AA}$ , and the bond length  $d_{\text{Mo-O}} = 2.00 \text{ \AA}$ . The resultant angles are  $\theta_{\text{MoOO}} = \theta_{\text{OMoMo}} = 88.054^\circ$  and  $\theta_{\text{MoOO}'} = 73.258^\circ$ , in which atoms O and O' are from different (top or bottom) group.

Table CVI shows four VFF terms for the single-layer 1H-MoO<sub>2</sub>, one of which is the bond stretching interaction shown by Eq. (1) while the other three terms are the angle bending interaction shown by Eq. (2). These force constant parameters are determined by fitting to the acoustic branches in the phonon dispersion along the  $\Gamma$ M as shown in Fig. 51 (a). The *ab initio* calculations for the phonon dispersion are from Ref. 12. Fig. 51 (b) shows that

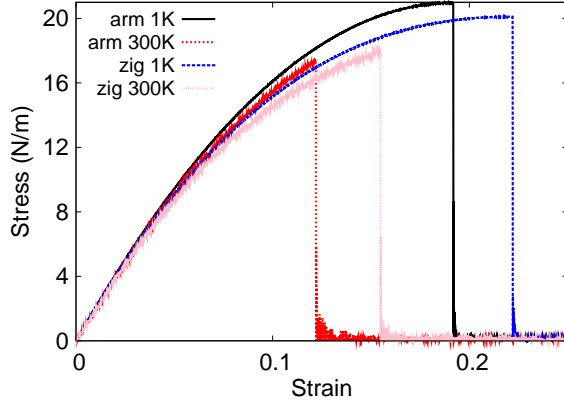


FIG. 52: (Color online) Stress-strain for single-layer 1H-MoO<sub>2</sub> of dimension  $100 \times 100 \text{ \AA}$  along the armchair and zigzag directions.

the VFF model and the SW potential give exactly the same phonon dispersion, as the SW potential is derived from the VFF model.

The parameters for the two-body SW potential used by GULP are shown in Tab. CVII. The parameters for the three-body SW potential used by GULP are shown in Tab. CVIII. Some representative parameters for the SW potential used by LAMMPS are listed in Tab. CIX. We note that twelve atom types have been introduced for the simulation of the single-layer 1H-MoO<sub>2</sub> using LAMMPS, because the angles around atom Mo in Fig. 1 (with M=Mo and X=O) are not distinguishable in LAMMPS. We have suggested two options to differentiate these angles by implementing some additional constraints in LAMMPS, which can be accomplished by modifying the source file of LAMMPS.<sup>13,14</sup> According to our experience, it is not so convenient for some users to implement these constraints and re-compile the LAMMPS package. Hence, in the present work, we differentiate the angles by introducing more atom types, so it is not necessary to modify the LAMMPS package. Fig. 2 (with M=Mo and X=O) shows that, for 1H-MoO<sub>2</sub>, we can differentiate these angles around the Mo atom by assigning these six neighboring O atoms with different atom types. It can be found that twelve atom types are necessary for the purpose of differentiating all six neighbors around one Mo atom.

We use LAMMPS to perform MD simulations for the mechanical behavior of the single-layer 1H-MoO<sub>2</sub> under uniaxial tension at 1.0 K and 300.0 K. Fig. 52 shows the stress-strain curve for the tension of a single-layer 1H-MoO<sub>2</sub> of dimension  $100 \times 100 \text{ \AA}$ . Periodic boundary

TABLE CX: The VFF model parameters for single-layer 1H-MoS<sub>2</sub> from Ref. 22. The second line gives the expression for each VFF term. Parameters are in the unit of  $\frac{eV}{\text{Å}^2}$  for the bond stretching interactions, and in the unit of eV for the angle bending interaction. The fourth line gives the initial bond length (in unit of Å) for the bond stretching interaction and the initial angle (in unit of degrees) for the angle bending interaction. The angle  $\theta_{ijk}$  has atom i as the apex.

VFF type	bond stretching	angle bending	
expression	$\frac{1}{2}K_{Mo-S} (\Delta r_{Mo-S})^2$	$\frac{1}{2}K_{MoSS} (\Delta \theta_{MoSS})^2$	$\frac{1}{2}K_{SMoMo} (\Delta \theta_{SMoMo})^2$
parameter	8.640	5.316	4.891
$r_0$ or $\theta_0$	2.382	80.581	80.581

conditions are applied in both armchair and zigzag directions. The single-layer 1H-MoO<sub>2</sub> is stretched uniaxially along the armchair or zigzag direction. The stress is calculated without involving the actual thickness of the quasi-two-dimensional structure of the single-layer 1H-MoO<sub>2</sub>. The Young's modulus can be obtained by a linear fitting of the stress-strain relation in the small strain range of [0, 0.01]. The Young's modulus are 210.0 N/m and 209.3 N/m along the armchair and zigzag directions, respectively. The Young's modulus is essentially isotropic in the armchair and zigzag directions. The Poisson's ratio from the VFF model and the SW potential is  $\nu_{xy} = \nu_{yx} = 0.17$ .

There is no available value for nonlinear quantities in the single-layer 1H-MoO<sub>2</sub>. We have thus used the nonlinear parameter  $B = 0.5d^4$  in Eq. (5), which is close to the value of  $B$  in most materials. The value of the third order nonlinear elasticity  $D$  can be extracted by fitting the stress-strain relation to the function  $\sigma = E\epsilon + \frac{1}{2}D\epsilon^2$  with  $E$  as the Young's modulus. The values of  $D$  from the present SW potential are -1027.8 N/m and -1106.8 N/m along the armchair and zigzag directions, respectively. The ultimate stress is about 21.0 Nm<sup>-1</sup> at the ultimate strain of 0.19 in the armchair direction at the low temperature of 1 K. The ultimate stress is about 20.1 Nm<sup>-1</sup> at the ultimate strain of 0.22 in the zigzag direction at the low temperature of 1 K.

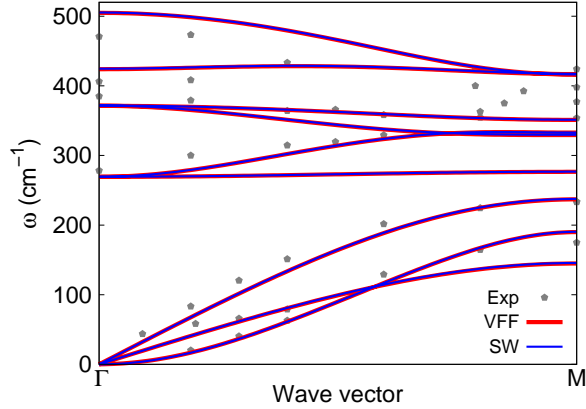


FIG. 53: (Color online) Phonon spectrum for single-layer 1H-MoS<sub>2</sub>. Phonon dispersion along the  $\Gamma$ M direction in the Brillouin zone. The results from the VFF model (lines) are comparable with the experiment data (pentagons) from Ref. 22. The phonon dispersion from the SW potential is exactly the same as that from the VFF model.

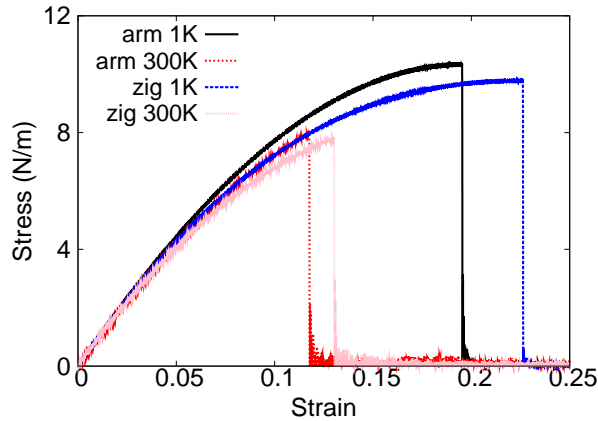


FIG. 54: (Color online) Stress-strain for single-layer 1H-MoS<sub>2</sub> of dimension  $100 \times 100 \text{ \AA}$  along the armchair and zigzag directions.

## XXVIII. 1H-MOS<sub>2</sub>

Several potentials have been proposed to describe the interaction for the single-layer 1H-MoS<sub>2</sub>. In 1975, Wakabayashi et al. developed a VFF model to calculate the phonon spectrum of the bulk 2H-MoS<sub>2</sub>.<sup>22</sup> In 2009, Liang et al. parameterized a bond-order potential for 1H-MoS<sub>2</sub>,<sup>23</sup> which is based on the bond order concept underlying the Brenner potential.<sup>6</sup>

TABLE CXI: Two-body SW potential parameters for single-layer 1H-MoS<sub>2</sub> used by GULP<sup>8</sup> as expressed in Eq. (3).

	$A$ (eV)	$\rho$ (Å)	$B$ (Å <sup>4</sup> )	$r_{\min}$ (Å)	$r_{\max}$ (Å)
$r_{\text{Mo-S}}$	6.918	1.252	17.771	0.0	3.16

TABLE CXII: Three-body SW potential parameters for single-layer 1H-MoS<sub>2</sub> used by GULP<sup>8</sup> as expressed in Eq. (4). The angle  $\theta_{ijk}$  in the first line indicates the bending energy for the angle with atom  $i$  as the apex.

	$K$ (eV)	$\theta_0$ (degree)	$\rho_1$ (Å)	$\rho_2$ (Å)	$r_{\min 12}$ (Å)	$r_{\max 12}$ (Å)	$r_{\min 13}$ (Å)	$r_{\max 13}$ (Å)	$r_{\min 23}$ (Å)	$r_{\max 23}$ (Å)
$\theta_{\text{MoSS}}$	67.883	81.788	1.252	1.252	0.0	3.16	0.0	3.16	0.0	3.78
$\theta_{\text{SMoMo}}$	62.449	81.788	1.252	1.252	0.0	3.16	0.0	3.16	0.0	4.27

A separate force field model was parameterized in 2010 for MD simulations of bulk 2H-MoS<sub>2</sub>.<sup>24</sup> The present author (J.W.J.) and his collaborators parameterized the SW potential for 1H-MoS<sub>2</sub> in 2013,<sup>13</sup> which was improved by one of the present author (J.W.J.) in 2015.<sup>7</sup> Recently, another set of parameters for the SW potential were proposed for the single-layer 1H-MoS<sub>2</sub>.<sup>25</sup>

We show the VFF model and the SW potential for single-layer 1H-MoS<sub>2</sub> in this section. These potentials have been developed in previous works. The VFF model presented here is from Ref. 22, while the SW potential presented in this section is from Ref. 7.

The structural parameters for the single-layer 1H-MoS<sub>2</sub> are from the first-principles calculations as shown in Fig. 1 (with M=Mo and X=S).<sup>26</sup> The Mo atom layer in the single-layer

TABLE CXIII: SW potential parameters for single-layer 1H-MoS<sub>2</sub> used by LAMMPS<sup>9</sup> as expressed in Eqs. (9) and (10). Atom types in the first column are displayed in Fig. 2 (with M=Mo and X=S).

	$\epsilon$ (eV)	$\sigma$ (Å)	$a$	$\lambda$	$\gamma$	$\cos \theta_0$	$A_L$	$B_L$	$p$	$q$	tol
Mo <sub>1</sub> -S <sub>1</sub> -S <sub>1</sub>	1.000	1.252	2.523	0.000	1.000	0.000	6.918	7.223	4	0	0.0
Mo <sub>1</sub> -S <sub>1</sub> -S <sub>3</sub>	1.000	0.000	0.000	67.883	1.000	0.143	0.000	0.000	4	0	0.0
S <sub>1</sub> -Mo <sub>1</sub> -Mo <sub>3</sub>	1.000	0.000	0.000	62.449	1.000	0.143	0.000	0.000	4	0	0.0

1H-MoS<sub>2</sub> is sandwiched by two S atom layers. Accordingly, each Mo atom is surrounded by six S atoms, while each S atom is connected to three Mo atoms. The bond length between neighboring Mo and S atoms is  $d = 2.382 \text{ \AA}$ , and the angles are  $\theta_{\text{MoSS}} = 80.581^\circ$  and  $\theta_{\text{SMoMo}} = 80.581^\circ$ .

The VFF model for single-layer 1H-MoS<sub>2</sub> is from Ref. 22, which is able to describe the phonon spectrum and the sound velocity accurately. We have listed the first three leading force constants for single-layer 1H-MoS<sub>2</sub> in Tab. CX, neglecting other weak interaction terms. The SW potential parameters for single-layer 1H-MoS<sub>2</sub> used by GULP are listed in Tabs. CXI and CXII. The SW potential parameters for single-layer 1H-MoS<sub>2</sub> used by LAMMPS<sup>9</sup> are listed in Tab. CXIII. We note that twelve atom types have been introduced for the simulation of the single-layer 1H-MoS<sub>2</sub> using LAMMPS, because the angles around atom Mo in Fig. 1 (with M=Mo and X=S) are not distinguishable in LAMMPS. We have suggested two options to differentiate these angles by implementing some additional constraints in LAMMPS, which can be accomplished by modifying the source file of LAMMPS.<sup>13,14</sup> According to our experience, it is not so convenient for some users to implement these constraints and recompile the LAMMPS package. Hence, in the present work, we differentiate the angles by introducing more atom types, so it is not necessary to modify the LAMMPS package. Fig. 2 (with M=Mo and X=S) shows that, for 1H-MoS<sub>2</sub>, we can differentiate these angles around the Mo atom by assigning these six neighboring S atoms with different atom types. It can be found that twelve atom types are necessary for the purpose of differentiating all six neighbors around one Mo atom.

We use GULP to compute the phonon dispersion for the single-layer 1H-MoS<sub>2</sub> as shown in Fig. 53. The results from the VFF model are quite comparable with the experiment data. The phonon dispersion from the SW potential is the same as that from the VFF model, which indicates that the SW potential has fully inherited the linear portion of the interaction from the VFF model.

We use LAMMPS to perform MD simulations for the mechanical behavior of the single-layer 1H-MoS<sub>2</sub> under uniaxial tension at 1.0 K and 300.0 K. Fig. 54 shows the stress-strain curve during the tension of a single-layer 1H-MoS<sub>2</sub> of dimension  $100 \times 100 \text{ \AA}$ . Periodic boundary conditions are applied in both armchair and zigzag directions. The single-layer 1H-MoS<sub>2</sub> is stretched uniaxially along the armchair or zigzag direction. The stress is calculated without involving the actual thickness of the quasi-two-dimensional structure of the single-

TABLE CXIV: The VFF model for single-layer 1H-MoSe<sub>2</sub>. The second line gives an explicit expression for each VFF term. The third line is the force constant parameters. Parameters are in the unit of  $\frac{\text{eV}}{\text{\AA}^2}$  for the bond stretching interactions, and in the unit of eV for the angle bending interaction. The fourth line gives the initial bond length (in unit of \AA) for the bond stretching interaction and the initial angle (in unit of degrees) for the angle bending interaction. The angle  $\theta_{ijk}$  has atom i as the apex.

VFF type	bond stretching	angle bending		
expression	$\frac{1}{2}K_{Mo-Se}(\Delta r)^2$	$\frac{1}{2}K_{Mo-Se-Se}(\Delta\theta)^2$	$\frac{1}{2}K_{Mo-Se-Se'}(\Delta\theta)^2$	$\frac{1}{2}K_{Se-Mo-Mo}(\Delta\theta)^2$
parameter	7.928	6.945	6.945	5.782
$r_0$ or $\theta_0$	2.528	82.119	81.343	82.119

TABLE CXV: Two-body SW potential parameters for single-layer 1H-MoSe<sub>2</sub> used by GULP<sup>8</sup> as expressed in Eq. (3).

	$A$ (eV)	$\rho$ (\AA)	$B$ (\AA <sup>4</sup> )	$r_{\min}$ (\AA)	$r_{\max}$ (\AA)
Mo-Se	5.737	0.913	18.787	0.0	3.351

layer 1H-MoS<sub>2</sub>. The Young's modulus can be obtained by a linear fitting of the stress-strain relation in the small strain range of [0, 0.01]. The Young's modulus are 97 N/m and 96 N/m along the armchair and zigzag directions, respectively. The Young's modulus is isotropic in the armchair and zigzag directions. These values are in considerable agreement with the experimental results, eg.  $120 \pm 30$  N/m from Refs 27,28, or  $180 \pm 60$  N/m from Ref. 29. The third-order nonlinear elastic constant  $D$  can be obtained by fitting the stress-strain relation to  $\sigma = E\epsilon + \frac{1}{2}D\epsilon^2$  with  $E$  as the Young's modulus. The values of  $D$  are -418 N/m and -461 N/m along the armchair and zigzag directions, respectively. The Poisson's ratio from the VFF model and the SW potential is  $\nu_{xy} = \nu_{yx} = 0.27$ .

## XXIX. 1H-MOSE<sub>2</sub>

There is a recent parameter set for the SW potential in the single-layer 1H-MoSe<sub>2</sub>.<sup>25</sup> In this section, we will develop both VFF model and the SW potential for the single-layer 1H-MoSe<sub>2</sub>.

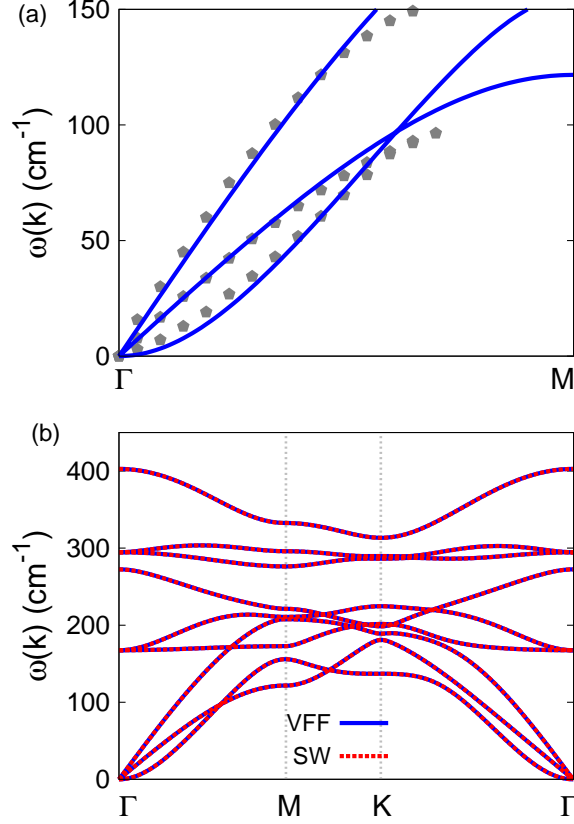


FIG. 55: (Color online) Phonon dispersion for single-layer 1H-MoSe<sub>2</sub>. (a) The VFF model is fitted to the three acoustic branches in the long wave limit along the  $\Gamma$ M direction. The *ab initio* results (gray pentagons) are from Ref. 30. (b) The VFF model (blue lines) and the SW potential (red lines) give the same phonon dispersion for single-layer 1H-MoSe<sub>2</sub> along  $\Gamma$ MK $\Gamma$ .

The structure for the single-layer 1H-MoSe<sub>2</sub> is shown in Fig. 1 (with M=Mo and X=Se). Each Mo atom is surrounded by six Se atoms. These Se atoms are categorized into the top group (eg. atoms 1, 3, and 5) and bottom group (eg. atoms 2, 4, and 6). Each Se atom is connected to three Mo atoms. The structural parameters are from Ref. 30, including the lattice constant  $a = 3.321 \text{ \AA}$ , and the bond length  $d_{\text{Mo-Se}} = 2.528 \text{ \AA}$ . The resultant angles are  $\theta_{\text{MoSeSe}} = \theta_{\text{SeMoMo}} = 82.119^\circ$  and  $\theta_{\text{MoSeSe}'} = 81.343^\circ$ , in which atoms Se and Se' are from different (top or bottom) group.

Table CXIV shows four VFF terms for the 1H-MoSe<sub>2</sub>, one of which is the bond stretching interaction shown by Eq. (1) while the other three terms are the angle bending interaction shown by Eq. (2). These force constant parameters are determined by fitting to the three

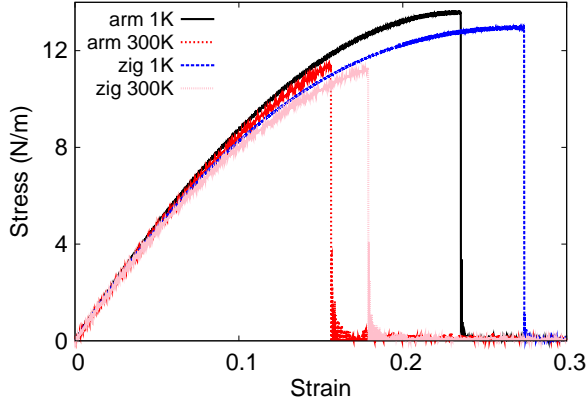


FIG. 56: (Color online) Stress-strain for single-layer 1H-MoSe<sub>2</sub> of dimension  $100 \times 100 \text{ \AA}$  along the armchair and zigzag directions.

TABLE CXVI: Three-body SW potential parameters for single-layer 1H-MoSe<sub>2</sub> used by GULP<sup>8</sup> as expressed in Eq. (4). The angle  $\theta_{ijk}$  in the first line indicates the bending energy for the angle with atom  $i$  as the apex.

	$K$ (eV)	$\theta_0$ (degree)	$\rho_1$ (Å)	$\rho_2$ (Å)	$r_{\min 12}$ (Å)	$r_{\max 12}$ (Å)	$r_{\min 13}$ (Å)	$r_{\max 13}$ (Å)	$r_{\min 23}$ (Å)	$r_{\max 23}$ (Å)
$\theta_{\text{Mo-Se-Se}}$	32.526	82.119	0.913	0.913	0.0	3.351	0.0	3.351	0.0	4.000
$\theta_{\text{Mo-Se-Se}'}$	32.654	81.343	0.913	0.913	0.0	3.351	0.0	3.351	0.0	4.000
$\theta_{\text{Se-Mo-Mo}}$	27.079	82.119	0.913	0.913	0.0	3.351	0.0	3.351	0.0	4.000

acoustic branches in the phonon dispersion along the  $\Gamma\text{M}$  as shown in Fig. 55 (a). The *ab initio* calculations for the phonon dispersion are from Ref. 30. Similar phonon dispersion can also be found in other *ab initio* calculations.<sup>12,31–34</sup> Fig. 55 (b) shows that the VFF model and the SW potential give exactly the same phonon dispersion, as the SW potential is derived from the VFF model.

The parameters for the two-body SW potential used by GULP are shown in Tab. CXV. The parameters for the three-body SW potential used by GULP are shown in Tab. CXVI. Parameters for the SW potential used by LAMMPS are listed in Tab. CXVII. We note that twelve atom types have been introduced for the simulation of the single-layer 1H-MoSe<sub>2</sub> using LAMMPS, because the angles around atom Mo in Fig. 1 (with  $\text{M}=\text{Mo}$  and  $\text{X}=\text{Se}$ ) are not distinguishable in LAMMPS. We have suggested two options to differentiate these angles by implementing some additional constraints in LAMMPS, which can be accomplished by

TABLE CXVII: SW potential parameters for single-layer 1H-MoSe<sub>2</sub> used by LAMMPS<sup>9</sup> as expressed in Eqs. (9) and (10). Atom types in the first column are displayed in Fig. 2 (with M=Mo and X=Se).

	$\epsilon$ (eV)	$\sigma$ (Å)	$a$	$\lambda$	$\gamma$	$\cos \theta_0$	$A_L$	$B_L$	$p$	$q$	tol
Mo <sub>1</sub> -Se <sub>1</sub> -Se <sub>1</sub>	1.000	0.913	3.672	0.000	1.000	0.000	5.737	27.084	4	0	0.0
Mo <sub>1</sub> -Se <sub>1</sub> -Se <sub>3</sub>	1.000	0.000	0.000	32.526	1.000	0.137	0.000	0.000	4	0	0.0
Mo <sub>1</sub> -Se <sub>1</sub> -Se <sub>2</sub>	1.000	0.000	0.000	32.654	1.000	0.151	0.000	0.000	4	0	0.0
Se <sub>1</sub> -Mo <sub>1</sub> -Mo <sub>3</sub>	1.000	0.000	0.000	27.079	1.000	0.137	0.000	0.000	4	0	0.0

modifying the source file of LAMMPS.<sup>13,14</sup> According to our experience, it is not so convenient for some users to implement these constraints and recompile the LAMMPS package. Hence, in the present work, we differentiate the angles by introducing more atom types, so it is not necessary to modify the LAMMPS package. Fig. 2 (with M=Mo and X=Se) shows that, for 1H-MoSe<sub>2</sub>, we can differentiate these angles around the Mo atom by assigning these six neighboring Se atoms with different atom types. It can be found that twelve atom types are necessary for the purpose of differentiating all six neighbors around one Mo atom.

We use LAMMPS to perform MD simulations for the mechanical behavior of the single-layer 1H-MoSe<sub>2</sub> under uniaxial tension at 1.0 K and 300.0 K. Fig. 56 shows the stress-strain curve during the tension of a single-layer 1H-MoSe<sub>2</sub> of dimension  $100 \times 100$  Å. Periodic boundary conditions are applied in both armchair and zigzag directions. The single-layer 1H-MoSe<sub>2</sub> is stretched uniaxially along the armchair or zigzag direction. The stress is calculated without involving the actual thickness of the quasi-two-dimensional structure of the single-layer 1H-MoSe<sub>2</sub>. The Young's modulus can be obtained by a linear fitting of the stress-strain relation in the small strain range of  $[0, 0.01]$ . The Young's modulus are 103.0 N/m and 101.8 N/m along the armchair and zigzag directions, respectively. The Young's modulus is essentially isotropic in the armchair and zigzag directions. These values are in considerable agreement with the experimental results, eg. 103.9 N/m from Refs 18, or 113.9 N/m from Ref. 35. The Poisson's ratio from the VFF model and the SW potential is  $\nu_{xy} = \nu_{yx} = 0.24$ , which agrees quite well with the *ab initio* value of 0.23.<sup>18</sup>

We have determined the nonlinear parameter to be  $B = 0.46d^4$  in Eq. (5) by fitting to the third-order nonlinear elastic constant  $D$  from the *ab initio* calculations.<sup>35</sup> We have extracted

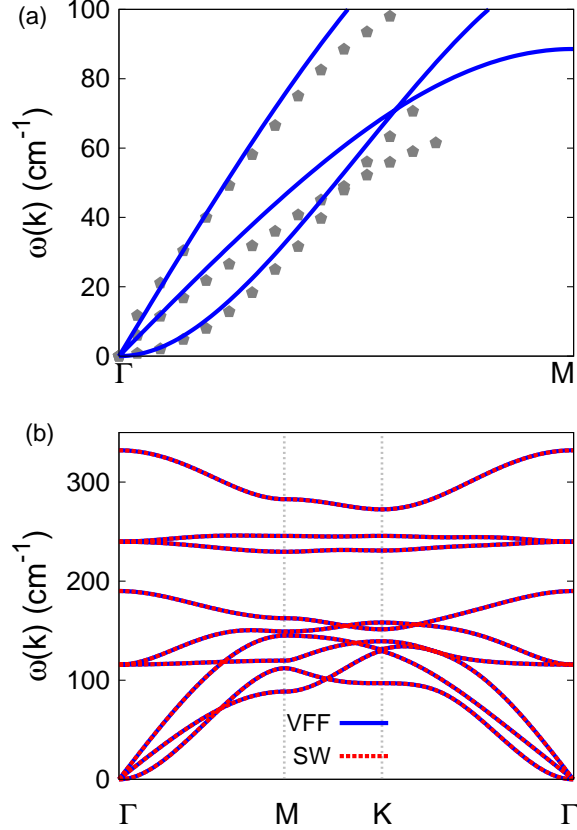


FIG. 57: (Color online) Phonon dispersion for single-layer 1H-MoTe<sub>2</sub>. (a) The VFF model is fitted to the three acoustic branches in the long wave limit along the  $\Gamma\text{M}$  direction. The *ab initio* results (gray pentagons) are from Ref. 36. (b) The VFF model (blue lines) and the SW potential (red lines) give the same phonon dispersion for single-layer 1H-MoTe<sub>2</sub> along  $\Gamma\text{MK}\Gamma$ .

the value of  $D = -383.7 \text{ N/m}$  by fitting the stress-strain relation along the armchair direction in the *ab initio* calculations to the function  $\sigma = E\epsilon + \frac{1}{2}D\epsilon^2$  with  $E$  as the Young's modulus. The values of  $D$  from the present SW potential are  $-365.4 \text{ N/m}$  and  $-402.4 \text{ N/m}$  along the armchair and zigzag directions, respectively. The ultimate stress is about  $13.6 \text{ Nm}^{-1}$  at the ultimate strain of 0.23 in the armchair direction at the low temperature of 1 K. The ultimate stress is about  $13.0 \text{ Nm}^{-1}$  at the ultimate strain of 0.27 in the zigzag direction at the low temperature of 1 K.

TABLE CXVIII: The VFF model for single-layer 1H-MoTe<sub>2</sub>. The second line gives an explicit expression for each VFF term. The third line is the force constant parameters. Parameters are in the unit of  $\frac{eV}{\text{Å}^2}$  for the bond stretching interactions, and in the unit of eV for the angle bending interaction. The fourth line gives the initial bond length (in unit of Å) for the bond stretching interaction and the initial angle (in unit of degrees) for the angle bending interaction. The angle  $\theta_{ijk}$  has atom i as the apex.

VFF type	bond stretching	angle bending		
expression	$\frac{1}{2}K_{\text{Mo-Te}}(\Delta r)^2$	$\frac{1}{2}K_{\text{Mo-Te-Te}}(\Delta\theta)^2$	$\frac{1}{2}K_{\text{Mo-Te-Te}'}(\Delta\theta)^2$	$\frac{1}{2}K_{\text{Te-Mo-Mo}}(\Delta\theta)^2$
parameter	6.317	6.184	6.184	5.225
$r_0$ or $\theta_0$	2.730	81.111	82.686	81.111

TABLE CXIX: Two-body SW potential parameters for single-layer 1H-MoTe<sub>2</sub> used by GULP<sup>8</sup> as expressed in Eq. (3).

	$A$ (eV)	$\rho$ (Å)	$B$ (Å <sup>4</sup> )	$r_{\min}$ (Å)	$r_{\max}$ (Å)
Mo-Te	5.086	0.880	24.440	0.0	3.604

TABLE CXX: Three-body SW potential parameters for single-layer 1H-MoTe<sub>2</sub> used by GULP<sup>8</sup> as expressed in Eq. (4). The angle  $\theta_{ijk}$  in the first line indicates the bending energy for the angle with atom i as the apex.

	$K$ (eV)	$\theta_0$ (degree)	$\rho_1$ (Å)	$\rho_2$ (Å)	$r_{\min12}$ (Å)	$r_{\max12}$ (Å)	$r_{\min13}$ (Å)	$r_{\max13}$ (Å)	$r_{\min23}$ (Å)	$r_{\max23}$ (Å)
$\theta_{\text{Mo-Te-Te}}$	23.705	81.111	0.880	0.880	0.0	3.604	0.0	3.604	0.0	4.305
$\theta_{\text{Mo-Te-Te}'}$	23.520	82.686	0.880	0.880	0.0	3.604	0.0	3.604	0.0	4.305
$\theta_{\text{Te-Mo-Mo}}$	20.029	81.111	0.880	0.880	0.0	3.604	0.0	3.604	0.0	4.305

TABLE CXXI: SW potential parameters for single-layer 1H-MoTe<sub>2</sub> used by LAMMPS<sup>9</sup> as expressed in Eqs. (9) and (10). Atom types in the first column are displayed in Fig. 2 (with M=Mo and X=Te).

	$\epsilon$ (eV)	$\sigma$ (Å)	$a$	$\lambda$	$\gamma$	$\cos\theta_0$	$A_L$	$B_L$	$p$	$q$	tol
Mo <sub>1</sub> -Te <sub>1</sub> -Te <sub>1</sub>	1.000	0.900	4.016	0.000	1.000	0.000	5.169	37.250	4	0	0.0
Mo <sub>1</sub> -Te <sub>1</sub> -Te <sub>3</sub>	1.000	0.000	0.000	24.163	1.000	0.143	0.000	0.000	4	0	0.0
Te <sub>1</sub> -Mo <sub>1</sub> -Mo <sub>3</sub>	1.000	0.000	0.000	20.416	1.000	0.143	0.000	0.000	4	0	0.0

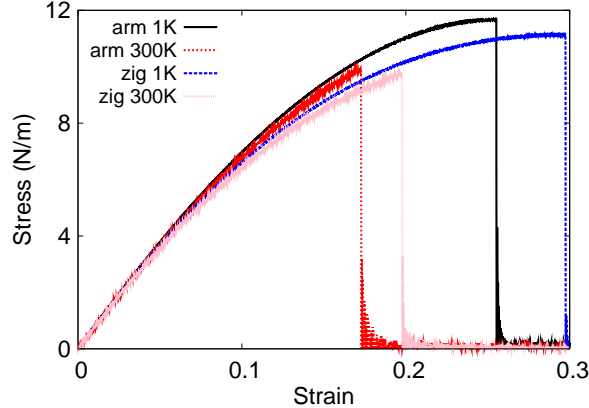


FIG. 58: (Color online) Stress-strain for single-layer 1H-MoTe<sub>2</sub> of dimension  $100 \times 100 \text{ \AA}$  along the armchair and zigzag directions.

### XXX. 1H-MOTE<sub>2</sub>

Most existing theoretical studies on the single-layer 1H-MoTe<sub>2</sub> are based on the first-principles calculations. In this section, we will develop both VFF model and the SW potential for the single-layer 1H-MoTe<sub>2</sub>.

The structure for the single-layer 1H-MoTe<sub>2</sub> is shown in Fig. 1 (with M=Mo and X=Te). Each Mo atom is surrounded by six Te atoms. These Te atoms are categorized into the top group (eg. atoms 1, 3, and 5) and bottom group (eg. atoms 2, 4, and 6). Each Te atom is connected to three Mo atoms. The structural parameters are from Ref. 36, including the lattice constant  $a = 3.55 \text{ \AA}$ , and the bond length  $d_{\text{Mo-Te}} = 2.73 \text{ \AA}$ . The resultant angles are  $\theta_{\text{MoTeTe}} = \theta_{\text{TeMoMo}} = 81.111^\circ$  and  $\theta_{\text{MoTeTe}'} = 82.686^\circ$ , in which atoms Te and Te' are from different (top or bottom) group.

Table CXVIII shows four VFF terms for the 1H-MoTe<sub>2</sub>, one of which is the bond stretching interaction shown by Eq. (1) while the other three terms are the angle bending interaction shown by Eq. (2). These force constant parameters are determined by fitting to the three acoustic branches in the phonon dispersion along the  $\Gamma\text{M}$  as shown in Fig. 57 (a). The *ab initio* calculations for the phonon dispersion are from Ref. 36. Similar phonon dispersion can also be found in other *ab initio* calculations.<sup>12,34,37</sup> Fig. 57 (b) shows that the VFF model and the SW potential give exactly the same phonon dispersion, as the SW potential is derived from the VFF model.

The parameters for the two-body SW potential used by GULP are shown in Tab. CXIX. The parameters for the three-body SW potential used by GULP are shown in Tab. CXX. Parameters for the SW potential used by LAMMPS are listed in Tab. CXXI. We note that twelve atom types have been introduced for the simulation of the single-layer 1H-MoTe<sub>2</sub> using LAMMPS, because the angles around atom Mo in Fig. 1 (with M=Mo and X=Te) are not distinguishable in LAMMPS. We have suggested two options to differentiate these angles by implementing some additional constraints in LAMMPS, which can be accomplished by modifying the source file of LAMMPS.<sup>13,14</sup> According to our experience, it is not so convenient for some users to implement these constraints and recompile the LAMMPS package. Hence, in the present work, we differentiate the angles by introducing more atom types, so it is not necessary to modify the LAMMPS package. Fig. 2 (with M=Mo and X=Te) shows that, for 1H-MoTe<sub>2</sub>, we can differentiate these angles around the Mo atom by assigning these six neighboring Te atoms with different atom types. It can be found that twelve atom types are necessary for the purpose of differentiating all six neighbors around one Mo atom.

We use LAMMPS to perform MD simulations for the mechanical behavior of the single-layer 1H-MoTe<sub>2</sub> under uniaxial tension at 1.0 K and 300.0 K. Fig. 58 shows the stress-strain curve for the tension of a single-layer 1H-MoTe<sub>2</sub> of dimension 100 × 100 Å. Periodic boundary conditions are applied in both armchair and zigzag directions. The single-layer 1H-MoTe<sub>2</sub> is stretched uniaxially along the armchair or zigzag direction. The stress is calculated without involving the actual thickness of the quasi-two-dimensional structure of the single-layer 1H-MoTe<sub>2</sub>. The Young's modulus can be obtained by a linear fitting of the stress-strain relation in the small strain range of [0, 0.01]. The Young's modulus are 79.8 N/m and 78.5 N/m along the armchair and zigzag directions, respectively. The Young's modulus is essentially isotropic in the armchair and zigzag directions. These values are in considerable agreement with the experimental results, eg. 79.4 N/m from Refs 18, or 87.0 N/m from Ref. 35. The Poisson's ratio from the VFF model and the SW potential is  $\nu_{xy} = \nu_{yx} = 0.25$ , which agrees with the *ab initio* value of 0.24.<sup>18</sup>

We have determined the nonlinear parameter to be  $B = 0.44d^4$  in Eq. (5) by fitting to the third-order nonlinear elastic constant  $D$  from the *ab initio* calculations.<sup>35</sup> We have extracted the value of  $D = -278.2$  N/m by fitting the stress-strain relation along the armchair direction in the *ab initio* calculations to the function  $\sigma = E\epsilon + \frac{1}{2}D\epsilon^2$  with  $E$  as the Young's modulus. The values of  $D$  from the present SW potential are -250.5 N/m and -276.6 N/m along the

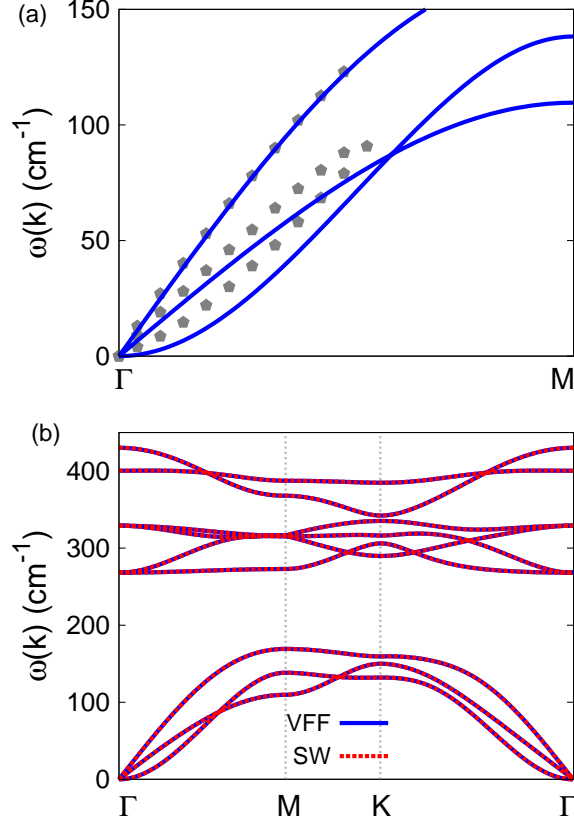


FIG. 59: (Color online) Phonon dispersion for single-layer 1H-TaS<sub>2</sub>. (a) The VFF model is fitted to the three acoustic branches in the long wave limit along the  $\Gamma$ M direction. The theoretical results (gray pentagons) are from Ref. 21. The blue lines are from the present VFF model. (b) The VFF model (blue lines) and the SW potential (red lines) give the same phonon dispersion for single-layer 1H-TaS<sub>2</sub> along  $\Gamma$ MK $\Gamma$ .

armchair and zigzag directions, respectively. The ultimate stress is about  $11.7 \text{ Nm}^{-1}$  at the ultimate strain of 0.25 in the armchair direction at the low temperature of 1 K. The ultimate stress is about  $11.1 \text{ Nm}^{-1}$  at the ultimate strain of 0.29 in the zigzag direction at the low temperature of 1 K.

### XXXI. 1H-TAS<sub>2</sub>

In 1983, the VFF model was developed to investigate the lattice dynamical properties in the bulk 2H-TaS<sub>2</sub>.<sup>21</sup> In this section, we will develop the SW potential for the single-layer

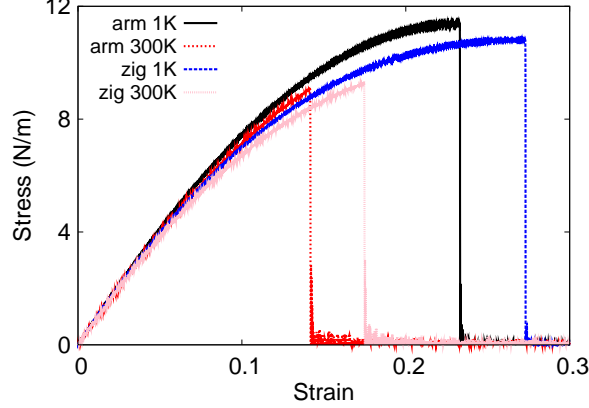


FIG. 60: (Color online) Stress-strain for single-layer 1H-TaS<sub>2</sub> of dimension 100 × 100 Å along the armchair and zigzag directions.

TABLE CXXII: The VFF model for single-layer 1H-TaS<sub>2</sub>. The second line gives an explicit expression for each VFF term. The third line is the force constant parameters. Parameters are in the unit of  $\frac{eV}{\text{Å}^2}$  for the bond stretching interactions, and in the unit of eV for the angle bending interaction. The fourth line gives the initial bond length (in unit of Å) for the bond stretching interaction and the initial angle (in unit of degrees) for the angle bending interaction. The angle  $\theta_{ijk}$  has atom *i* as the apex.

VFF type	bond stretching	angle bending		
expression	$\frac{1}{2}K_{\text{Ta-S}}(\Delta r)^2$	$\frac{1}{2}K_{\text{Ta-S-S}}(\Delta\theta)^2$	$\frac{1}{2}K_{\text{Ta-S-S}'}(\Delta\theta)^2$	$\frac{1}{2}K_{\text{S-Ta-Ta}}(\Delta\theta)^2$
parameter	8.230	4.811	4.811	4.811
$r_0$ or $\theta_0$	2.480	83.879	78.979	83.879

1H-TaS<sub>2</sub>.

The structure for the single-layer 1H-TaS<sub>2</sub> is shown in Fig. 1 (with M=Ta and X=S). Each Ta atom is surrounded by six S atoms. These S atoms are categorized into the top group (eg. atoms 1, 3, and 5) and bottom group (eg. atoms 2, 4, and 6). Each S atom is connected to three Ta atoms. The structural parameters are from Ref. 21, including the lattice constant  $a = 3.315$  Å, and the bond length  $d_{\text{Ta-S}} = 2.48$  Å. The resultant angles are  $\theta_{\text{TaSS}} = \theta_{\text{STaTa}} = 83.879^\circ$  and  $\theta_{\text{TaSS}'} = 78.979^\circ$ , in which atoms S and S' are from different (top or bottom) group.

TABLE CXXIII: Two-body SW potential parameters for single-layer 1H-TaS<sub>2</sub> used by GULP<sup>8</sup> as expressed in Eq. (3).

	$A$ (eV)	$\rho$ (Å)	$B$ (Å <sup>4</sup> )	$r_{\min}$ (Å)	$r_{\max}$ (Å)
Ta-S	6.446	1.111	18.914	0.0	3.310

TABLE CXXIV: Three-body SW potential parameters for single-layer 1H-TaS<sub>2</sub> used by GULP<sup>8</sup> as expressed in Eq. (4). The angle  $\theta_{ijk}$  in the first line indicates the bending energy for the angle with atom  $i$  as the apex.

	$K$ (eV)	$\theta_0$ (degree)	$\rho_1$ (Å)	$\rho_2$ (Å)	$r_{\min12}$ (Å)	$r_{\max12}$ (Å)	$r_{\min13}$ (Å)	$r_{\max13}$ (Å)	$r_{\min23}$ (Å)	$r_{\max23}$ (Å)
$\theta_{\text{Ta-S-S}}$	35.396	83.879	1.111	1.111	0.0	3.310	0.0	3.310	0.0	3.945
$\theta_{\text{Ta-S-S}'}$	36.321	78.979	1.111	1.111	0.0	3.310	0.0	3.310	0.0	3.945
$\theta_{\text{S-Ta-Ta}}$	35.396	83.879	1.111	1.111	0.0	3.310	0.0	3.310	0.0	3.945

Table CXXII shows the VFF terms for the 1H-TaS<sub>2</sub>, one of which is the bond stretching interaction shown by Eq. (1) while the others are the angle bending interaction shown by Eq. (2). These force constant parameters are determined by fitting to the three acoustic branches in the phonon dispersion along the  $\Gamma\text{M}$  as shown in Fig. 59 (a). The theoretical phonon frequencies (gray pentagons) are from Ref. 21, which are the phonon dispersion of bulk 2H-TaS<sub>2</sub>. We have used these phonon frequencies as the phonon dispersion of the single-layer 1H-TaS<sub>2</sub>, as the inter-layer interaction in the bulk 2H-TaS<sub>2</sub> only induces weak effects on the two inplane acoustic branches. The inter-layer coupling will strengthen the out-of-plane acoustic (flexural) branch, so the flexural branch from the present VFF model

TABLE CXXV: SW potential parameters for single-layer 1H-TaS<sub>2</sub> used by LAMMPS<sup>9</sup> as expressed in Eqs. (9) and (10). Atom types in the first column are displayed in Fig. 2 (with M=Ta and X=S).

	$\epsilon$ (eV)	$\sigma$ (Å)	$a$	$\lambda$	$\gamma$	$\cos \theta_0$	$A_L$	$B_L$	$p$	$q$	tol
Ta <sub>1</sub> -S <sub>1</sub> -S <sub>1</sub>	1.000	1.111	2.979	0.000	1.000	0.000	6.446	12.408	4	0	0.0
Ta <sub>1</sub> -S <sub>1</sub> -S <sub>3</sub>	1.000	0.000	0.000	35.396	1.000	0.107	0.000	0.000	4	0	0.0
Ta <sub>1</sub> -S <sub>1</sub> -S <sub>2</sub>	1.000	0.000	0.000	36.321	1.000	0.191	0.000	0.000	4	0	0.0
S <sub>1</sub> -Ta <sub>1</sub> -Ta <sub>3</sub>	1.000	0.000	0.000	35.396	1.000	0.107	0.000	0.000	4	0	0.0

(blue line) is lower than the theoretical results for bulk 2H-TaS<sub>2</sub> (gray pentagons). Fig. 59 (b) shows that the VFF model and the SW potential give exactly the same phonon dispersion, as the SW potential is derived from the VFF model.

The parameters for the two-body SW potential used by GULP are shown in Tab. CXXIII. The parameters for the three-body SW potential used by GULP are shown in Tab. CXXIV. Parameters for the SW potential used by LAMMPS are listed in Tab. CXXV. We note that twelve atom types have been introduced for the simulation of the single-layer 1H-TaS<sub>2</sub> using LAMMPS, because the angles around atom Ta in Fig. 1 (with M=Ta and X=S) are not distinguishable in LAMMPS. We have suggested two options to differentiate these angles by implementing some additional constraints in LAMMPS, which can be accomplished by modifying the source file of LAMMPS.<sup>13,14</sup> According to our experience, it is not so convenient for some users to implement these constraints and recompile the LAMMPS package. Hence, in the present work, we differentiate the angles by introducing more atom types, so it is not necessary to modify the LAMMPS package. Fig. 2 (with M=Ta and X=S) shows that, for 1H-TaS<sub>2</sub>, we can differentiate these angles around the Ta atom by assigning these six neighboring S atoms with different atom types. It can be found that twelve atom types are necessary for the purpose of differentiating all six neighbors around one Ta atom.

We use LAMMPS to perform MD simulations for the mechanical behavior of the single-layer 1H-TaS<sub>2</sub> under uniaxial tension at 1.0 K and 300.0 K. Fig. 60 shows the stress-strain curve for the tension of a single-layer 1H-TaS<sub>2</sub> of dimension 100 × 100 Å. Periodic boundary conditions are applied in both armchair and zigzag directions. The single-layer 1H-TaS<sub>2</sub> is stretched uniaxially along the armchair or zigzag direction. The stress is calculated without involving the actual thickness of the quasi-two-dimensional structure of the single-layer 1H-TaS<sub>2</sub>. The Young's modulus can be obtained by a linear fitting of the stress-strain relation in the small strain range of [0, 0.01]. The Young's modulus is 87.4 N/m and 86.6 N/m along the armchair and zigzag directions, respectively. The Poisson's ratio from the VFF model and the SW potential is  $\nu_{xy} = \nu_{yx} = 0.27$ .

There is no available value for the nonlinear quantities in the single-layer 1H-TaS<sub>2</sub>. We have thus used the nonlinear parameter  $B = 0.5d^4$  in Eq. (5), which is close to the value of  $B$  in most materials. The value of the third order nonlinear elasticity  $D$  can be extracted by fitting the stress-strain relation to the function  $\sigma = E\epsilon + \frac{1}{2}D\epsilon^2$  with  $E$  as the Young's modulus. The values of  $D$  from the present SW potential are -313.0 N/m and -349.3 N/m along

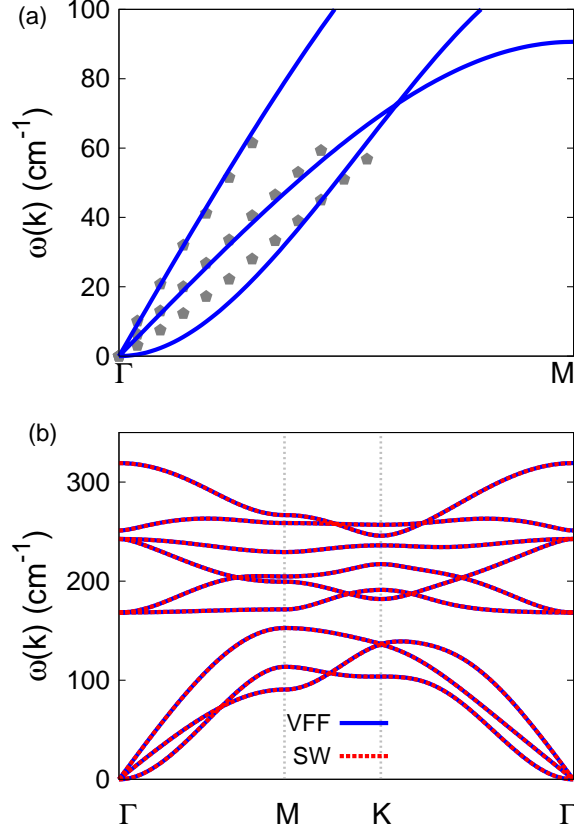


FIG. 61: (Color online) Phonon dispersion for single-layer 1H-TaSe<sub>2</sub>. (a) The VFF model is fitted to the three acoustic branches in the long wave limit along the  $\Gamma$ M direction. The theoretical results (gray pentagons) are from Ref. 15. The blue lines are from the present VFF model. (b) The VFF model (blue lines) and the SW potential (red lines) give the same phonon dispersion for single-layer 1H-TaSe<sub>2</sub> along  $\Gamma$ MK $\Gamma$ .

the armchair and zigzag directions, respectively. The ultimate stress is about  $11.4 \text{ Nm}^{-1}$  at the ultimate strain of 0.23 in the armchair direction at the low temperature of 1 K. The ultimate stress is about  $10.8 \text{ Nm}^{-1}$  at the ultimate strain of 0.27 in the zigzag direction at the low temperature of 1 K.

### XXXII. 1H-TASE<sub>2</sub>

The VFF model was developed to investigate the lattice dynamical properties in the bulk 2H-TaSe<sub>2</sub>.<sup>15,21</sup> In this section, we will develop the SW potential for the single-layer 1H-TaSe<sub>2</sub>.

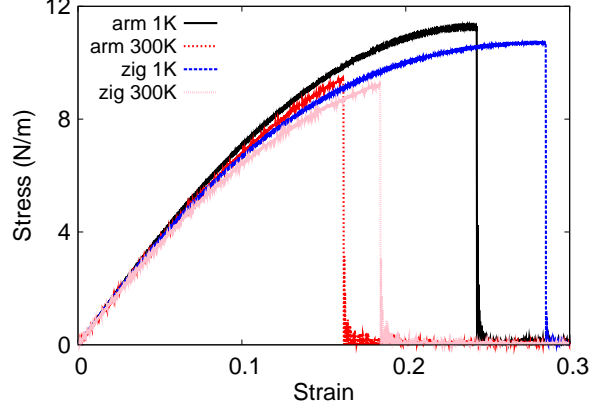


FIG. 62: (Color online) Stress-strain for single-layer 1H-TaSe<sub>2</sub> of dimension  $100 \times 100 \text{ \AA}$  along the armchair and zigzag directions.

TABLE CXXVI: The VFF model for single-layer 1H-TaSe<sub>2</sub>. The second line gives an explicit expression for each VFF term. The third line is the force constant parameters. Parameters are in the unit of  $\frac{eV}{\text{Å}^2}$  for the bond stretching interactions, and in the unit of eV for the angle bending interaction. The fourth line gives the initial bond length (in unit of Å) for the bond stretching interaction and the initial angle (in unit of degrees) for the angle bending interaction. The angle  $\theta_{ijk}$  has atom *i* as the apex.

VFF type	bond stretching	angle bending		
expression	$\frac{1}{2}K_{\text{Ta-Se}}(\Delta r)^2$	$\frac{1}{2}K_{\text{Ta-Se-Se}}(\Delta\theta)^2$	$\frac{1}{2}K_{\text{Ta-Se-Se}'}(\Delta\theta)^2$	$\frac{1}{2}K_{\text{Se-Ta-Ta}}(\Delta\theta)^2$
parameter	8.230	4.811	4.811	4.811
$r_0$ or $\theta_0$	2.590	83.107	80.019	83.107

The structure for the single-layer 1H-TaSe<sub>2</sub> is shown in Fig. 1 (with M=Ta and X=Se). Each Ta atom is surrounded by six Se atoms. These Se atoms are categorized into the top group (eg. atoms 1, 3, and 5) and bottom group (eg. atoms 2, 4, and 6). Each Se atom is connected to three Ta atoms. The structural parameters are from Ref. 21, including the lattice constant  $a = 3.436 \text{ \AA}$ , and the bond length  $d_{\text{Ta-Se}} = 2.59 \text{ \AA}$ . The resultant angles are  $\theta_{\text{TaSeSe}} = \theta_{\text{SeTaTa}} = 83.107^\circ$  and  $\theta_{\text{TaSeSe}'} = 80.019^\circ$ , in which atoms Se and Se' are from different (top or bottom) group.

Table CXXVI shows the VFF terms for the 1H-TaSe<sub>2</sub>, one of which is the bond stretching

TABLE CXXVII: Two-body SW potential parameters for single-layer 1H-TaSe<sub>2</sub> used by GULP<sup>8</sup> as expressed in Eq. (3).

	$A$ (eV)	$\rho$ (Å)	$B$ (Å <sup>4</sup> )	$r_{\min}$ (Å)	$r_{\max}$ (Å)
Ta-Se	6.885	1.133	22.499	0.0	3.446

TABLE CXXVIII: Three-body SW potential parameters for single-layer 1H-TaSe<sub>2</sub> used by GULP<sup>8</sup> as expressed in Eq. (4). The angle  $\theta_{ijk}$  in the first line indicates the bending energy for the angle with atom  $i$  as the apex.

	$K$ (eV)	$\theta_0$ (degree)	$\rho_1$ (Å)	$\rho_2$ (Å)	$r_{\min12}$ (Å)	$r_{\max12}$ (Å)	$r_{\min13}$ (Å)	$r_{\max13}$ (Å)	$r_{\min23}$ (Å)	$r_{\max23}$ (Å)
$\theta_{\text{Ta-Se-Se}}$	34.381	83.107	1.133	1.133	0.0	3.446	0.0	3.446	0.0	4.111
$\theta_{\text{Ta-Se-Se}'}$	34.936	80.019	1.133	1.133	0.0	3.446	0.0	3.446	0.0	4.111
$\theta_{\text{Se-Ta-Ta}}$	34.381	83.107	1.133	1.133	0.0	3.446	0.0	3.446	0.0	4.111

interaction shown by Eq. (1) while the others are the angle bending interaction shown by Eq. (2). These force constant parameters are determined by fitting to the three acoustic branches in the phonon dispersion along the  $\Gamma\text{M}$  as shown in Fig. 61 (a). The theoretical phonon frequencies (gray pentagons) are from Ref. 21, which are the phonon dispersion of bulk 2H-TaSe<sub>2</sub>. We have used these phonon frequencies as the phonon dispersion of the single-layer 1H-TaSe<sub>2</sub>, as the inter-layer interaction in the bulk 2H-TaSe<sub>2</sub> only induces weak effects on the two in-plane acoustic branches. The inter-layer coupling will strengthen the out-of-plane acoustic branch (flexural branch), so the flexural branch from the present VFF

TABLE CXXIX: SW potential parameters for single-layer 1H-TaSe<sub>2</sub> used by LAMMPS<sup>9</sup> as expressed in Eqs. (9) and (10). Atom types in the first column are displayed in Fig. 2 (with M=Ta and X=Se).

	$\epsilon$ (eV)	$\sigma$ (Å)	$a$	$\lambda$	$\gamma$	$\cos\theta_0$	$A_L$	$B_L$	$p$	$q$	tol
Ta <sub>1</sub> -Se <sub>1</sub> -Se <sub>1</sub>	1.000	1.133	3.043	0.000	1.000	0.000	6.885	13.668	4	0	0.0
Ta <sub>1</sub> -Se <sub>1</sub> -Se <sub>3</sub>	1.000	0.000	0.000	34.381	1.000	0.120	0.000	0.000	4	0	0.0
Ta <sub>1</sub> -Se <sub>1</sub> -Se <sub>2</sub>	1.000	0.000	0.000	34.936	1.000	0.173	0.000	0.000	4	0	0.0
Se <sub>1</sub> -Ta <sub>1</sub> -Ta <sub>3</sub>	1.000	0.000	0.000	34.381	1.000	0.120	0.000	0.000	4	0	0.0

model (blue line) is lower than the theoretical results for bulk 2H-TaSe<sub>2</sub> (gray pentagons). Fig. 61 (b) shows that the VFF model and the SW potential give exactly the same phonon dispersion, as the SW potential is derived from the VFF model.

The parameters for the two-body SW potential used by GULP are shown in Tab. CXXVII. The parameters for the three-body SW potential used by GULP are shown in Tab. CXXVIII. Parameters for the SW potential used by LAMMPS are listed in Tab. CXXIX. We note that twelve atom types have been introduced for the simulation of the single-layer 1H-TaSe<sub>2</sub> using LAMMPS, because the angles around atom Ta in Fig. 1 (with M=Ta and X=Se) are not distinguishable in LAMMPS. We have suggested two options to differentiate these angles by implementing some additional constraints in LAMMPS, which can be accomplished by modifying the source file of LAMMPS.<sup>13,14</sup> According to our experience, it is not so convenient for some users to implement these constraints and recompile the LAMMPS package. Hence, in the present work, we differentiate the angles by introducing more atom types, so it is not necessary to modify the LAMMPS package. Fig. 2 (with M=Ta and X=Se) shows that, for 1H-TaSe<sub>2</sub>, we can differentiate these angles around the Ta atom by assigning these six neighboring Se atoms with different atom types. It can be found that twelve atom types are necessary for the purpose of differentiating all six neighbors around one Ta atom.

We use LAMMPS to perform MD simulations for the mechanical behavior of the single-layer 1H-TaSe<sub>2</sub> under uniaxial tension at 1.0 K and 300.0 K. Fig. 62 shows the stress-strain curve for the tension of a single-layer 1H-TaSe<sub>2</sub> of dimension 100 × 100 Å. Periodic boundary conditions are applied in both armchair and zigzag directions. The single-layer 1H-TaSe<sub>2</sub> is stretched uniaxially along the armchair or zigzag direction. The stress is calculated without involving the actual thickness of the quasi-two-dimensional structure of the single-layer 1H-TaSe<sub>2</sub>. The Young's modulus can be obtained by a linear fitting of the stress-strain relation in the small strain range of [0, 0.01]. The Young's modulus are 80.8 N/m and 81.1 N/m along the armchair and zigzag directions, respectively. The Young's modulus is essentially isotropic in the armchair and zigzag directions. The Poisson's ratio from the VFF model and the SW potential is  $\nu_{xy} = \nu_{yx} = 0.29$ .

There is no available value for the nonlinear quantities in the single-layer 1H-TaSe<sub>2</sub>. We have thus used the nonlinear parameter  $B = 0.5d^4$  in Eq. (5), which is close to the value of  $B$  in most materials. The value of the third order nonlinear elasticity  $D$  can be extracted by fitting the stress-strain relation to the function  $\sigma = E\epsilon + \frac{1}{2}D\epsilon^2$  with  $E$  as

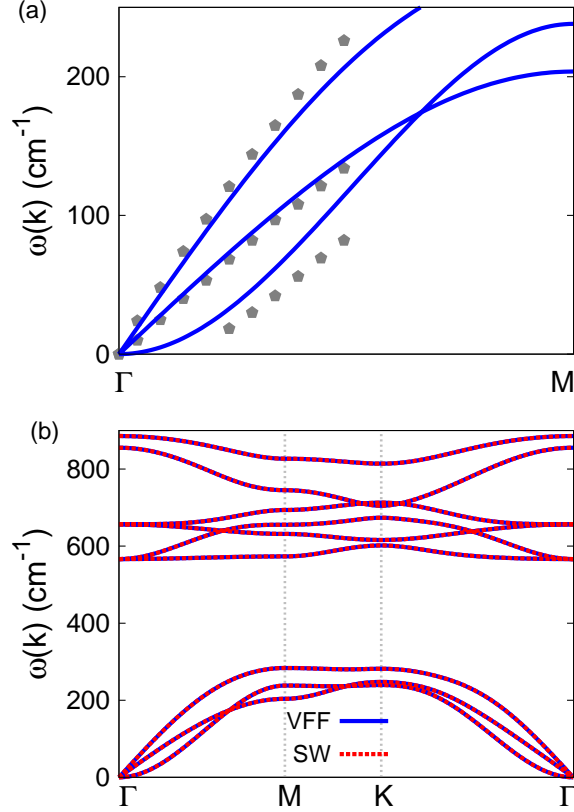


FIG. 63: (Color online) Phonon spectrum for single-layer 1H-WO<sub>2</sub>. (a) Phonon dispersion along the FM direction in the Brillouin zone. The results from the VFF model (lines) are comparable with the *ab initio* results (pentagons) from Ref. 12. (b) The phonon dispersion from the SW potential is exactly the same as that from the VFF model.

the Young's modulus. The values of  $D$  from the present SW potential are -263.3 N/m and -308.6 N/m along the armchair and zigzag directions, respectively. The ultimate stress is about 11.3 Nm<sup>-1</sup> at the ultimate strain of 0.24 in the armchair direction at the low temperature of 1 K. The ultimate stress is about 10.7 Nm<sup>-1</sup> at the ultimate strain of 0.28 in the zigzag direction at the low temperature of 1 K.

### XXXIII. 1H-WO<sub>2</sub>

Most existing theoretical studies on the single-layer 1H-WO<sub>2</sub> are based on the first-principles calculations. In this section, we will develop the SW potential for the single-layer

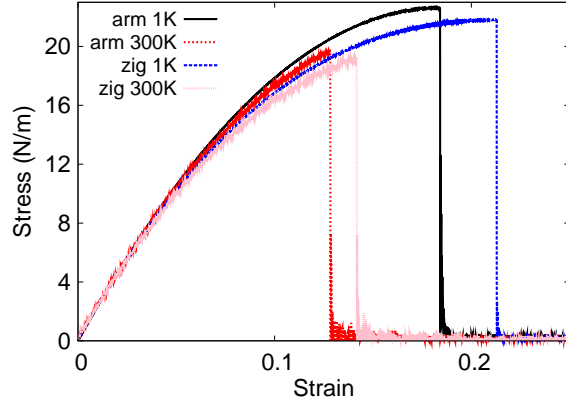


FIG. 64: (Color online) Stress-strain for single-layer 1H-WO<sub>2</sub> of dimension 100 × 100 Å along the armchair and zigzag directions.

TABLE CXXX: The VFF model for single-layer 1H-WO<sub>2</sub>. The second line gives an explicit expression for each VFF term. The third line is the force constant parameters. Parameters are in the unit of  $\frac{eV}{\text{Å}^2}$  for the bond stretching interactions, and in the unit of eV for the angle bending interaction. The fourth line gives the initial bond length (in unit of Å) for the bond stretching interaction and the initial angle (in unit of degrees) for the angle bending interaction. The angle  $\theta_{ijk}$  has atom i as the apex.

VFF type	bond stretching	angle bending		
expression	$\frac{1}{2}K_{W-O}(\Delta r)^2$	$\frac{1}{2}K_{W-O-O}(\Delta\theta)^2$	$\frac{1}{2}K_{W-O-O'}(\Delta\theta)^2$	$\frac{1}{2}K_{O-W-W}(\Delta\theta)^2$
parameter	15.318	10.276	10.276	10.276
$r_0$ or $\theta_0$	2.030	87.206	74.435	87.206

1H-WO<sub>2</sub>.

The structure for the single-layer 1H-WO<sub>2</sub> is shown in Fig. 1 (with M=W and X=O). Each W atom is surrounded by six O atoms. These O atoms are categorized into the top group (eg. atoms 1, 3, and 5) and bottom group (eg. atoms 2, 4, and 6). Each O atom is connected to three W atoms. The structural parameters are from the first-principles calculations,<sup>12</sup> including the lattice constant  $a = 2.80$  Å, and the bond length  $d_{W-O} = 2.03$  Å. The resultant angles are  $\theta_{WOO} = \theta_{OWW} = 87.206^\circ$  and  $\theta_{WOO'} = 74.435^\circ$ , in which atoms O and O' are from different (top or bottom) group.

TABLE CXXXI: Two-body SW potential parameters for single-layer 1H-WO<sub>2</sub> used by GULP<sup>8</sup> as expressed in Eq. (3).

	$A$ (eV)	$\rho$ (Å)	$B$ (Å <sup>4</sup> )	$r_{\min}$ (Å)	$r_{\max}$ (Å)
W-O	8.781	1.005	8.491	0.0	2.744

TABLE CXXXII: Three-body SW potential parameters for single-layer 1H-WO<sub>2</sub> used by GULP<sup>8</sup> as expressed in Eq. (4). The angle  $\theta_{ijk}$  in the first line indicates the bending energy for the angle with atom  $i$  as the apex.

	$K$ (eV)	$\theta_0$ (degree)	$\rho_1$ (Å)	$\rho_2$ (Å)	$r_{\min12}$ (Å)	$r_{\max12}$ (Å)	$r_{\min13}$ (Å)	$r_{\max13}$ (Å)	$r_{\min23}$ (Å)	$r_{\max23}$ (Å)
$\theta_{W-O-O}$	85.955	87.206	1.005	1.005	0.0	2.744	0.0	2.744	0.0	3.262
$\theta_{W-O-O'}$	92.404	74.435	1.005	1.005	0.0	2.744	0.0	2.744	0.0	3.262
$\theta_{O-W-W}$	85.955	87.206	1.005	1.005	0.0	2.744	0.0	2.744	0.0	3.262

Table CXXX shows four VFF terms for the single-layer 1H-WO<sub>2</sub>, one of which is the bond stretching interaction shown by Eq. (1) while the other three terms are the angle bending interaction shown by Eq. (2). These force constant parameters are determined by fitting to the acoustic branches in the phonon dispersion along the  $\Gamma$ M as shown in Fig. 63 (a). The *ab initio* calculations for the phonon dispersion are from Ref. 12. Fig. 63 (b) shows that the VFF model and the SW potential give exactly the same phonon dispersion, as the SW potential is derived from the VFF model.

The parameters for the two-body SW potential used by GULP are shown in Tab. CXXXI. The parameters for the three-body SW potential used by GULP are shown in Tab. CXXXII.

TABLE CXXXIII: SW potential parameters for single-layer 1H-WO<sub>2</sub> used by LAMMPS<sup>9</sup> as expressed in Eqs. (9) and (10).

	$\epsilon$ (eV)	$\sigma$ (Å)	$a$	$\lambda$	$\gamma$	$\cos \theta_0$	$A_L$	$B_L$	$p$	$q$	tol
W <sub>1</sub> -O <sub>1</sub> -O <sub>1</sub>	1.000	1.005	2.730	0.000	1.000	0.000	8.781	8.316	4	0	0.0
W <sub>1</sub> -O <sub>1</sub> -O <sub>3</sub>	1.000	0.000	0.000	85.955	1.000	0.049	0.000	0.000	4	0	0.0
W <sub>1</sub> -O <sub>1</sub> -O <sub>2</sub>	1.000	0.000	0.000	92.404	1.000	0.268	0.000	0.000	4	0	0.0
O <sub>1</sub> -W <sub>1</sub> -W <sub>3</sub>	1.000	0.000	0.000	85.955	1.000	0.049	0.000	0.000	4	0	0.0

Some representative parameters for the SW potential used by LAMMPS are listed in Tab. CXXXIII. We note that twelve atom types have been introduced for the simulation of the single-layer 1H-WO<sub>2</sub> using LAMMPS, because the angles around atom W in Fig. 1 (with M=W and X=O) are not distinguishable in LAMMPS. We have suggested two options to differentiate these angles by implementing some additional constraints in LAMMPS, which can be accomplished by modifying the source file of LAMMPS.<sup>13,14</sup> According to our experience, it is not so convenient for some users to implement these constraints and recompile the LAMMPS package. Hence, in the present work, we differentiate the angles by introducing more atom types, so it is not necessary to modify the LAMMPS package. Fig. 2 (with M=W and X=O) shows that, for 1H-WO<sub>2</sub>, we can differentiate these angles around the W atom by assigning these six neighboring O atoms with different atom types. It can be found that twelve atom types are necessary for the purpose of differentiating all six neighbors around one W atom.

We use LAMMPS to perform MD simulations for the mechanical behavior of the single-layer 1H-WO<sub>2</sub> under uniaxial tension at 1.0 K and 300.0 K. Fig. 64 shows the stress-strain curve for the tension of a single-layer 1H-WO<sub>2</sub> of dimension 100 × 100 Å. Periodic boundary conditions are applied in both armchair and zigzag directions. The single-layer 1H-WO<sub>2</sub> is stretched uniaxially along the armchair or zigzag direction. The stress is calculated without involving the actual thickness of the quasi-two-dimensional structure of the single-layer 1H-WO<sub>2</sub>. The Young's modulus can be obtained by a linear fitting of the stress-strain relation in the small strain range of [0, 0.01]. The Young's modulus are 237.1 N/m and 237.2 N/m along the armchair and zigzag directions, respectively. The Young's modulus is essentially isotropic in the armchair and zigzag directions. The Poisson's ratio from the VFF model and the SW potential is  $\nu_{xy} = \nu_{yx} = 0.15$ .

There is no available value for nonlinear quantities in the single-layer 1H-WO<sub>2</sub>. We have thus used the nonlinear parameter  $B = 0.5d^4$  in Eq. (5), which is close to the value of  $B$  in most materials. The value of the third order nonlinear elasticity  $D$  can be extracted by fitting the stress-strain relation to the function  $\sigma = E\epsilon + \frac{1}{2}D\epsilon^2$  with  $E$  as the Young's modulus. The values of  $D$  from the present SW potential are -1218.0 N/m and -1312.9 N/m along the armchair and zigzag directions, respectively. The ultimate stress is about 22.6 Nm<sup>-1</sup> at the ultimate strain of 0.18 in the armchair direction at the low temperature of 1 K. The ultimate stress is about 21.8 Nm<sup>-1</sup> at the ultimate strain of 0.21 in the zigzag direction at

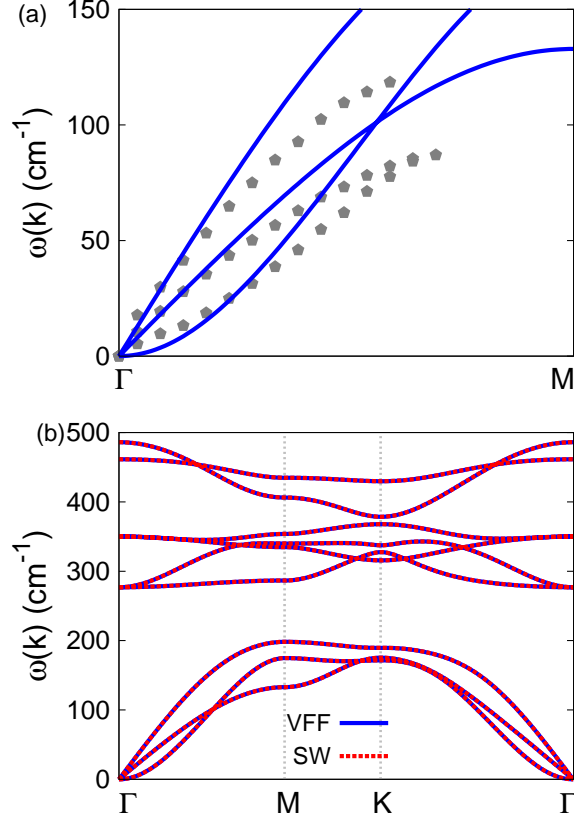


FIG. 65: (Color online) Phonon dispersion for single-layer 1H-WS<sub>2</sub>. (a) The VFF model is fitted to the three acoustic branches in the long wave limit along the  $\Gamma$ M direction. The *ab initio* results (gray pentagons) are from Ref. 31. (b) The VFF model (blue lines) and the SW potential (red lines) give the same phonon dispersion for single-layer 1H-WS<sub>2</sub> along  $\Gamma$ MK $\Gamma$ .

the low temperature of 1 K.

#### XXXIV. 1H-WS<sub>2</sub>

Most existing theoretical studies on the single-layer 1H-WS<sub>2</sub> are based on the first-principles calculations. In this section, we will develop both VFF model and the SW potential for the single-layer 1H-WS<sub>2</sub>.

The structure for the single-layer 1H-WS<sub>2</sub> is shown in Fig. 1 (with M=W and X=S). Each W atom is surrounded by six S atoms. These S atoms are categorized into the top group (eg. atoms 1, 3, and 5) and bottom group (eg. atoms 2, 4, and 6). Each S atom

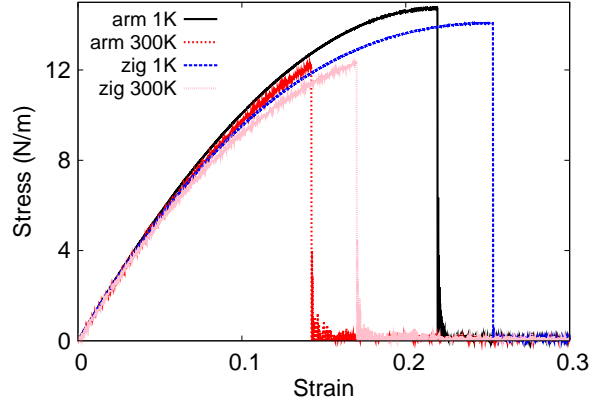


FIG. 66: (Color online) Stress-strain for single-layer 1H-WS<sub>2</sub> of dimension 100 × 100 Å along the armchair and zigzag directions.

TABLE CXXXIV: The VFF model for single-layer 1H-WS<sub>2</sub>. The second line gives an explicit expression for each VFF term. The third line is the force constant parameters. Parameters are in the unit of  $\frac{eV}{\text{Å}^2}$  for the bond stretching interactions, and in the unit of eV for the angle bending interaction. The fourth line gives the initial bond length (in unit of Å) for the bond stretching interaction and the initial angle (in unit of degrees) for the angle bending interaction. The angle  $\theta_{ijk}$  has atom *i* as the apex.

VFF type	bond stretching	angle bending		
expression	$\frac{1}{2}K_{W-S}(\Delta r)^2$	$\frac{1}{2}K_{W-S-S}(\Delta\theta)^2$	$\frac{1}{2}K_{W-S-S'}(\Delta\theta)^2$	$\frac{1}{2}K_{S-W-W}(\Delta\theta)^2$
parameter	8.701	7.421	7.421	6.607
$r_0$ or $\theta_0$	2.390	81.811	81.755	81.811

is connected to three W atoms. The structural parameters are from Ref. 12, including the lattice constant  $a = 3.13$  Å, and the bond length  $d_{W-S} = 2.39$  Å. The resultant angles are  $\theta_{WSS} = \theta_{SWW} = 81.811^\circ$  and  $\theta_{WSS'} = 81.755^\circ$ , in which atoms S and S' are from different (top or bottom) group.

Table CXXXIV shows the VFF terms for the 1H-WS<sub>2</sub>, one of which is the bond stretching interaction shown by Eq. (1) while the other terms are the angle bending interaction shown by Eq. (2). These force constant parameters are determined by fitting to the three acoustic branches in the phonon dispersion along the  $\Gamma M$  as shown in Fig. 65 (a). The *ab initio*

TABLE CXXXV: Two-body SW potential parameters for single-layer 1H-WS<sub>2</sub> used by GULP<sup>8</sup> as expressed in Eq. (3).

	$A$ (eV)	$\rho$ (Å)	$B$ (Å <sup>4</sup> )	$r_{\min}$ (Å)	$r_{\max}$ (Å)
W-S	5.664	0.889	15.335	0.0	3.164

TABLE CXXXVI: Three-body SW potential parameters for single-layer 1H-WS<sub>2</sub> used by GULP<sup>8</sup> as expressed in Eq. (4). The angle  $\theta_{ijk}$  in the first line indicates the bending energy for the angle with atom  $i$  as the apex.

	$K$ (eV)	$\theta_0$ (degree)	$\rho_1$ (Å)	$\rho_2$ (Å)	$r_{\min12}$ (Å)	$r_{\max12}$ (Å)	$r_{\min13}$ (Å)	$r_{\max13}$ (Å)	$r_{\min23}$ (Å)	$r_{\max23}$ (Å)
$\theta_{W-S-S}$	37.687	81.811	0.889	0.889	0.0	3.164	0.0	3.164	0.0	3.778
$\theta_{W-S-S'}$	37.697	81.755	0.889	0.889	0.0	3.164	0.0	3.164	0.0	3.778
$\theta_{S-W-W}$	33.553	81.811	0.889	0.889	0.0	3.164	0.0	3.164	0.0	3.778

calculations for the phonon dispersion are from Ref. 31. Similar phonon dispersion can also be found in other *ab initio* calculations.<sup>12,26,34,38,39</sup> Fig. 65 (b) shows that the VFF model and the SW potential give exactly the same phonon dispersion, as the SW potential is derived from the VFF model.

The parameters for the two-body SW potential used by GULP are shown in Tab. CXXXV. The parameters for the three-body SW potential used by GULP are shown in Tab. CXXXVI. Parameters for the SW potential used by LAMMPS are listed in Tab. CXXXVII. We note that twelve atom types have been introduced for the simulation of the single-layer 1H-WS<sub>2</sub>

TABLE CXXXVII: SW potential parameters for single-layer 1H-WS<sub>2</sub> used by LAMMPS<sup>9</sup> as expressed in Eqs. (9) and (10). Atom types in the first column are displayed in Fig. 2 (with M=W and X=S).

	$\epsilon$ (eV)	$\sigma$ (Å)	$a$	$\lambda$	$\gamma$	$\cos \theta_0$	$A_L$	$B_L$	$p$	$q$	tol
W <sub>1</sub> -S <sub>1</sub> -S <sub>1</sub>	1.000	0.889	3.558	0.000	1.000	0.000	5.664	24.525	4	0	0.0
W <sub>1</sub> -S <sub>1</sub> -S <sub>3</sub>	1.000	0.000	0.000	37.687	1.000	0.142	0.000	0.000	4	0	0.0
W <sub>1</sub> -S <sub>1</sub> -S <sub>2</sub>	1.000	0.000	0.000	37.697	1.000	0.143	0.000	0.000	4	0	0.0
S <sub>1</sub> -W <sub>1</sub> -W <sub>3</sub>	1.000	0.000	0.000	33.553	1.000	0.142	0.000	0.000	4	0	0.0

using LAMMPS, because the angles around atom W in Fig. 1 (with M=W and X=S) are not distinguishable in LAMMPS. We have suggested two options to differentiate these angles by implementing some additional constraints in LAMMPS, which can be accomplished by modifying the source file of LAMMPS.<sup>13,14</sup> According to our experience, it is not so convenient for some users to implement these constraints and recompile the LAMMPS package. Hence, in the present work, we differentiate the angles by introducing more atom types, so it is not necessary to modify the LAMMPS package. Fig. 2 (with M=W and X=S) shows that, for 1H-WS<sub>2</sub>, we can differentiate these angles around the W atom by assigning these six neighboring S atoms with different atom types. It can be found that twelve atom types are necessary for the purpose of differentiating all six neighbors around one W atom.

We use LAMMPS to perform MD simulations for the mechanical behavior of the single-layer 1H-WS<sub>2</sub> under uniaxial tension at 1.0 K and 300.0 K. Fig. 66 shows the stress-strain curve for the tension of a single-layer 1H-WS<sub>2</sub> of dimension 100 × 100 Å. Periodic boundary conditions are applied in both armchair and zigzag directions. The single-layer 1H-WS<sub>2</sub> is stretched uniaxially along the armchair or zigzag direction. The stress is calculated without involving the actual thickness of the quasi-two-dimensional structure of the single-layer 1H-WS<sub>2</sub>. The Young's modulus can be obtained by a linear fitting of the stress-strain relation in the small strain range of [0, 0.01]. The Young's modulus are 121.5 N/m along both armchair and zigzag directions. These values are in reasonably agreement with the *ab initio* results, eg. 139.6 N/m from Ref. 18, or 148.5 N/m from Ref. 35. The Poisson's ratio from the VFF model and the SW potential is  $\nu_{xy} = \nu_{yx} = 0.21$ , which agrees with the *ab initio* value of 0.22.<sup>18</sup>

We have determined the nonlinear parameter to be  $B = 0.47d^4$  in Eq. (5) by fitting to the third-order nonlinear elastic constant  $D$  from the *ab initio* calculations.<sup>35</sup> We have extracted the value of  $D = -502.9$  N/m by fitting the stress-strain relation along the armchair direction in the *ab initio* calculations to the function  $\sigma = E\epsilon + \frac{1}{2}D\epsilon^2$  with  $E$  as the Young's modulus. The values of  $D$  from the present SW potential are -472.8 N/m and -529.6 N/m along the armchair and zigzag directions, respectively. The ultimate stress is about 14.7 Nm<sup>-1</sup> at the ultimate strain of 0.22 in the armchair direction at the low temperature of 1 K. The ultimate stress is about 14.1 Nm<sup>-1</sup> at the ultimate strain of 0.25 in the zigzag direction at the low temperature of 1 K.

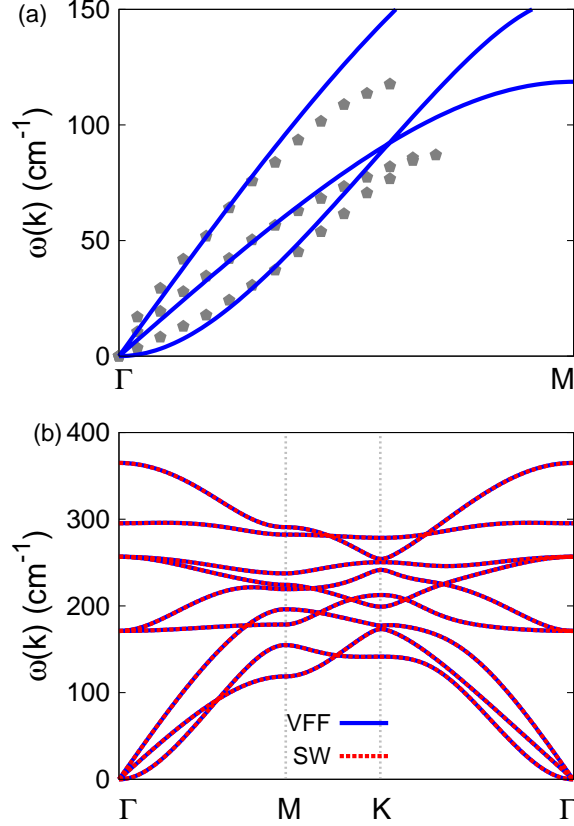


FIG. 67: (Color online) Phonon dispersion for single-layer 1H-WSe<sub>2</sub>. (a) The VFF model is fitted to the three acoustic branches in the long wave limit along the  $\Gamma$ M direction. The *ab initio* results (gray pentagons) are from Ref. 31. (b) The VFF model (blue lines) and the SW potential (red lines) give the same phonon dispersion for single-layer 1H-WSe<sub>2</sub> along  $\Gamma$ MK $\Gamma$ .

### XXXV. 1H-WSe<sub>2</sub>

Most existing theoretical studies on the single-layer 1H-WSe<sub>2</sub> are based on the first-principles calculations. Norouzzadeh and Singh provided one set of parameters for the SW potential for the single-layer 1H-WSe<sub>2</sub>.<sup>40</sup> In this section, we will develop both VFF model and the SW potential for the single-layer 1H-WSe<sub>2</sub>.

The structure for the single-layer 1H-WSe<sub>2</sub> is shown in Fig. 1 (with M=W and X=Se). Each W atom is surrounded by six Se atoms. These Se atoms are categorized into the top group (eg. atoms 1, 3, and 5) and bottom group (eg. atoms 2, 4, and 6). Each Se atom is connected to three W atoms. The structural parameters are from Ref. 12, including the

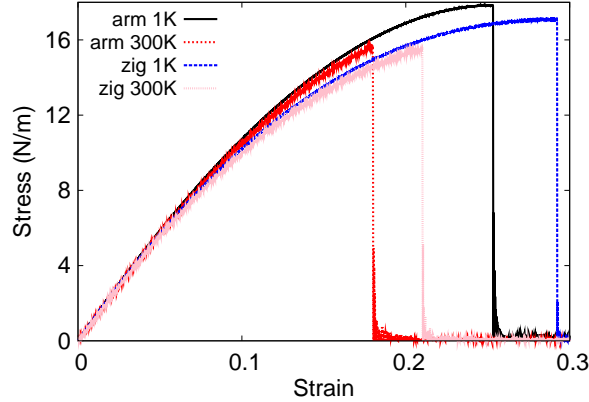


FIG. 68: (Color online) Stress-strain for single-layer 1H-WSe<sub>2</sub> of dimension 100 × 100 Å along the armchair and zigzag directions.

TABLE CXXXVIII: The VFF model for single-layer 1H-WSe<sub>2</sub>. The second line gives an explicit expression for each VFF term. The third line is the force constant parameters. Parameters are in the unit of  $\frac{eV}{\text{Å}^2}$  for the bond stretching interactions, and in the unit of eV for the angle bending interaction. The fourth line gives the initial bond length (in unit of Å) for the bond stretching interaction and the initial angle (in unit of degrees) for the angle bending interaction. The angle  $\theta_{ijk}$  has atom *i* as the apex.

VFF type	bond stretching	angle bending		
expression	$\frac{1}{2}K_{W-Se}(\Delta r)^2$	$\frac{1}{2}K_{W-Se-Se}(\Delta\theta)^2$	$\frac{1}{2}K_{W-Se-Se'}(\Delta\theta)^2$	$\frac{1}{2}K_{Se-W-W}(\Delta\theta)^2$
parameter	8.286	8.513	8.513	7.719
$r_0$ or $\theta_0$	2.510	80.693	83.140	80.693

lattice constant  $a = 3.25$  Å, and the bond length  $d_{W-Se} = 2.51$  Å. The resultant angles are  $\theta_{WSeSe} = \theta_{SeWW} = 80.693^\circ$  and  $\theta_{WSeSe'} = 83.240^\circ$ , in which atoms Se and Se' are from different (top or bottom) group.

Table CXXXVIII shows three VFF terms for the 1H-WSe<sub>2</sub>, one of which is the bond stretching interaction shown by Eq. (1) while the other two terms are the angle bending interaction shown by Eq. (2). These force constant parameters are determined by fitting to the three acoustic branches in the phonon dispersion along the  $\Gamma M$  as shown in Fig. 67 (a). The *ab initio* calculations for the phonon dispersion are from Ref. 31. Similar phonon

TABLE CXXXIX: Two-body SW potential parameters for single-layer 1H-WSe<sub>2</sub> used by GULP<sup>8</sup> as expressed in Eq. (3).

	$A$ (eV)	$\rho$ (Å)	$B$ (Å <sup>4</sup> )	$r_{\min}$ (Å)	$r_{\max}$ (Å)
W-Se	5.476	0.706	16.273	0.0	3.308

TABLE CXL: Three-body SW potential parameters for single-layer 1H-WSe<sub>2</sub> used by GULP<sup>8</sup> as expressed in Eq. (4). The angle  $\theta_{ijk}$  in the first line indicates the bending energy for the angle with atom i as the apex.

	$K$ (eV)	$\theta_0$ (degree)	$\rho_1$ (Å)	$\rho_2$ (Å)	$r_{\min12}$ (Å)	$r_{\max12}$ (Å)	$r_{\min13}$ (Å)	$r_{\max13}$ (Å)	$r_{\min23}$ (Å)	$r_{\max23}$ (Å)
$\theta_{W-Se-Se}$	25.607	80.693	0.706	0.706	0.0	3.308	0.0	3.308	0.0	3.953
$\theta_{W-Se-Se'}$	25.287	83.240	0.706	0.706	0.0	3.308	0.0	3.308	0.0	3.953
$\theta_{Se-W-W}$	23.218	80.693	0.706	0.706	0.0	3.308	0.0	3.308	0.0	3.953

dispersion can also be found in other *ab initio* calculations.<sup>12,33,34,39,41</sup> Fig. 67 (b) shows that the VFF model and the SW potential give exactly the same phonon dispersion, as the SW potential is derived from the VFF model.

The parameters for the two-body SW potential used by GULP are shown in Tab. CXXXIX. The parameters for the three-body SW potential used by GULP are shown in Tab. CXL. Parameters for the SW potential used by LAMMPS are listed in Tab. CXLI. We note that twelve atom types have been introduced for the simulation of the single-layer 1H-WSe<sub>2</sub> using LAMMPS, because the angles around atom W in Fig. 1 (with M=W and X=Se) are not distinguishable in LAMMPS. We have suggested two options to differenti-

TABLE CXLI: SW potential parameters for single-layer 1H-WSe<sub>2</sub> used by LAMMPS<sup>9</sup> as expressed in Eqs. (9) and (10). Atom types in the first column are displayed in Fig. 2 (with M=W and X=Se).

	$\epsilon$ (eV)	$\sigma$ (Å)	$a$	$\lambda$	$\gamma$	$\cos \theta_0$	$A_L$	$B_L$	$p$	$q$	tol
W <sub>1</sub> -Se <sub>1</sub> -Se <sub>1</sub>	1.000	0.706	4.689	0.000	1.000	0.000	5.476	65.662	4	0	0.0
W <sub>1</sub> -Se <sub>1</sub> -Se <sub>3</sub>	1.000	0.000	0.000	25.607	1.000	0.162	0.000	0.000	4	0	0.0
W <sub>1</sub> -Se <sub>1</sub> -Se <sub>2</sub>	1.000	0.000	0.000	25.287	1.000	0.118	0.000	0.000	4	0	0.0
Se <sub>1</sub> -W <sub>1</sub> -W <sub>3</sub>	1.000	0.000	0.000	23.218	1.000	0.162	0.000	0.000	4	0	0.0

ate these angles by implementing some additional constraints in LAMMPS, which can be accomplished by modifying the source file of LAMMPS.<sup>13,14</sup> According to our experience, it is not so convenient for some users to implement these constraints and recompile the LAMMPS package. Hence, in the present work, we differentiate the angles by introducing more atom types, so it is not necessary to modify the LAMMPS package. Fig. 2 (with M=W and X=Se) shows that, for 1H-WSe<sub>2</sub>, we can differentiate these angles around the W atom by assigning these six neighboring Se atoms with different atom types. It can be found that twelve atom types are necessary for the purpose of differentiating all six neighbors around one W atom.

We use LAMMPS to perform MD simulations for the mechanical behavior of the single-layer 1H-WSe<sub>2</sub> under uniaxial tension at 1.0 K and 300.0 K. Fig. 68 shows the stress-strain curve for the tension of a single-layer 1H-WSe<sub>2</sub> of dimension 100 × 100 Å. Periodic boundary conditions are applied in both armchair and zigzag directions. The single-layer 1H-WSe<sub>2</sub> is stretched uniaxially along the armchair or zigzag direction. The stress is calculated without involving the actual thickness of the quasi-two-dimensional structure of the single-layer 1H-WSe<sub>2</sub>. The Young's modulus can be obtained by a linear fitting of the stress-strain relation in the small strain range of [0, 0.01]. The Young's modulus are 124.1 N/m and 123.0 N/m along the armchair and zigzag directions, respectively. The Young's modulus is essentially isotropic in the armchair and zigzag directions. These values are in reasonably agreement with the *ab initio* results, eg. 116.0 N/m from Ref. 18, or 126.2 N/m from Ref. 35. The Poisson's ratio from the VFF model and the SW potential is  $\nu_{xy} = \nu_{yx} = 0.20$ , which agrees with the *ab initio* value of 0.19.<sup>18</sup>

We have determined the nonlinear parameter to be  $B = 0.41d^4$  in Eq. (5) by fitting to the third-order nonlinear elastic constant  $D$  from the *ab initio* calculations.<sup>35</sup> We have extracted the value of  $D = -413.1$  N/m by fitting the stress-strain relation along the armchair direction in the *ab initio* calculations to the function  $\sigma = E\epsilon + \frac{1}{2}D\epsilon^2$  with  $E$  as the Young's modulus. The values of  $D$  from the present SW potential are -400.4 N/m and -444.3 N/m along the armchair and zigzag directions, respectively. The ultimate stress is about 17.8 Nm<sup>-1</sup> at the ultimate strain of 0.25 in the armchair direction at the low temperature of 1 K. The ultimate stress is about 17.1 Nm<sup>-1</sup> at the ultimate strain of 0.29 in the zigzag direction at the low temperature of 1 K.

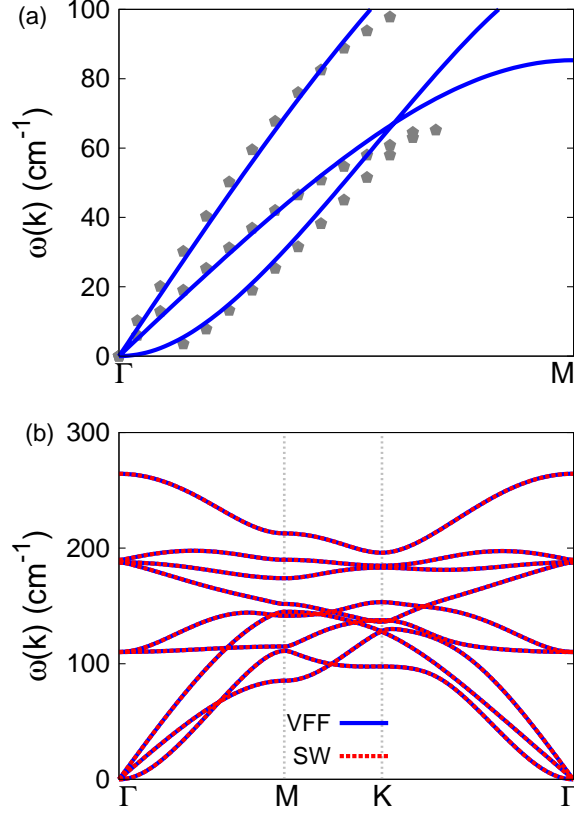


FIG. 69: (Color online) Phonon dispersion for single-layer 1H-WTe<sub>2</sub>. (a) The VFF model is fitted to the three acoustic branches in the long wave limit along the  $\Gamma$ M direction. The *ab initio* results (gray pentagons) are from Ref. 42. (b) The VFF model (blue lines) and the SW potential (red lines) give the same phonon dispersion for single-layer 1H-WTe<sub>2</sub> along  $\Gamma$ MK $\Gamma$ .

### XXXVI. 1H-WTe<sub>2</sub>

Most existing theoretical studies on the single-layer 1H-WTe<sub>2</sub> are based on the first-principles calculations. In this section, we will develop both VFF model and the SW potential for the single-layer 1H-WTe<sub>2</sub>.

The bulk WTe<sub>2</sub> has the trigonally coordinated H phase structure.<sup>43</sup> However, it has been predicted that the structure of the single-layer WTe<sub>2</sub> can be either the trigonally coordinated H phase<sup>12</sup> or the octahedrally coordinated  $T_d$  phase,<sup>44–47</sup> with  $T_d$  phase as the more stable structure.<sup>42</sup> We will thus consider both phases in the present paper. This section is devoted to the H phase for the WTe<sub>2</sub> (1H-WTe<sub>2</sub>), while the SW potential for the  $T_d$ -WTe<sub>2</sub> (1T-WTe<sub>2</sub>)

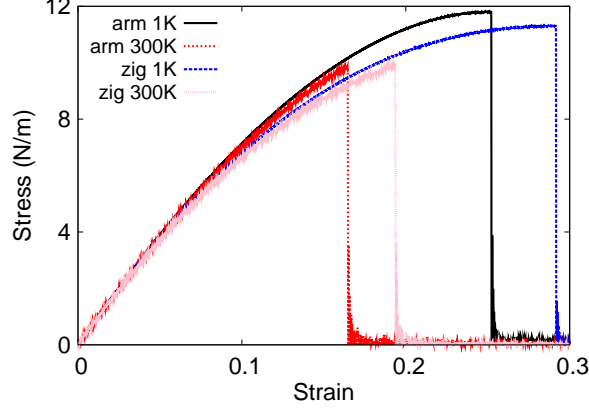


FIG. 70: (Color online) Stress-strain for single-layer 1H-WTe<sub>2</sub> of dimension  $100 \times 100 \text{ \AA}$  along the armchair and zigzag directions.

TABLE CXLII: The VFF model for single-layer 1H-WTe<sub>2</sub>. The second line gives an explicit expression for each VFF term. The third line is the force constant parameters. Parameters are in the unit of  $\frac{eV}{\text{Å}^2}$  for the bond stretching interactions, and in the unit of eV for the angle bending interaction. The fourth line gives the initial bond length (in unit of Å) for the bond stretching interaction and the initial angle (in unit of degrees) for the angle bending interaction. The angle  $\theta_{ijk}$  has atom *i* as the apex.

VFF type	bond stretching	angle bending		
expression	$\frac{1}{2}K_{W-Te}(\Delta r)^2$	$\frac{1}{2}K_{W-Te-Te}(\Delta\theta)^2$	$\frac{1}{2}K_{W-Te-Te'}(\Delta\theta)^2$	$\frac{1}{2}K_{Te-W-W}(\Delta\theta)^2$
parameter	5.483	7.016	7.016	5.718
$r_0$ or $\theta_0$	2.730	81.111	82.686	81.111

is presented in another section.

The structure for the single-layer 1H-WTe<sub>2</sub> is shown in Fig. 1 (with M=W and X=Te). Each W atom is surrounded by six Te atoms. These Te atoms are categorized into the top group (eg. atoms 1, 3, and 5) and bottom group (eg. atoms 2, 4, and 6). Each Te atom is connected to three W atoms. The structural parameters are from Ref. 42, including the lattice constant  $a = 3.55 \text{ \AA}$ , and the bond length  $d_{W-Te} = 2.73 \text{ \AA}$ . The resultant angles are  $\theta_{WTeTe} = \theta_{TeWW} = 81.111^\circ$  and  $\theta_{WTeTe'} = 82.686^\circ$ , in which atoms Te and Te' are from different (top or bottom) group.

TABLE CXLIII: Two-body SW potential parameters for single-layer 1H-WTe<sub>2</sub> used by GULP<sup>8</sup> as expressed in Eq. (3).

	$A$ (eV)	$\rho$ (Å)	$B$ (Å <sup>4</sup> )	$r_{\min}$ (Å)	$r_{\max}$ (Å)
W-Te	4.326	0.778	22.774	0.0	3.604

TABLE CXLIV: Three-body SW potential parameters for single-layer 1H-WTe<sub>2</sub> used by GULP<sup>8</sup> as expressed in Eq. (4). The angle  $\theta_{ijk}$  in the first line indicates the bending energy for the angle with atom  $i$  as the apex.

	$K$ (eV)	$\theta_0$ (degree)	$\rho_1$ (Å)	$\rho_2$ (Å)	$r_{\min12}$ (Å)	$r_{\max12}$ (Å)	$r_{\min13}$ (Å)	$r_{\max13}$ (Å)	$r_{\min23}$ (Å)	$r_{\max23}$ (Å)
$\theta_{W-Te-Te}$	21.313	81.111	0.778	0.778	0.0	3.604	0.0	3.604	0.0	4.305
$\theta_{W-Te-Te'}$	21.147	82.686	0.778	0.778	0.0	3.604	0.0	3.604	0.0	4.305
$\theta_{Te-W-W}$	17.370	81.111	0.778	0.778	0.0	3.604	0.0	3.604	0.0	4.305

Table CXLII shows the VFF terms for the 1H-WTe<sub>2</sub>, one of which is the bond stretching interaction shown by Eq. (1) while the other terms are the angle bending interaction shown by Eq. (2). These force constant parameters are determined by fitting to the three acoustic branches in the phonon dispersion along the  $\Gamma M$  as shown in Fig. 69 (a). The *ab initio* calculations for the phonon dispersion are from Ref. 42. Similar phonon dispersion can also be found in other *ab initio* calculations.<sup>12</sup> Fig. 69 (b) shows that the VFF model and the SW potential give exactly the same phonon dispersion, as the SW potential is derived from the VFF model.

The parameters for the two-body SW potential used by GULP are shown in Tab. CXLIII.

TABLE CXLV: SW potential parameters for single-layer 1H-WTe<sub>2</sub> used by LAMMPS<sup>9</sup> as expressed in Eqs. (9) and (10). Atom types in the first column are displayed in Fig. 2 (with M=W and X=Te).

	$\epsilon$ (eV)	$\sigma$ (Å)	$a$	$\lambda$	$\gamma$	$\cos \theta_0$	$A_L$	$B_L$	$p$	$q$	tol
W <sub>1</sub> -Te <sub>1</sub> -Te <sub>1</sub>	1.000	0.778	4.632	0.000	1.000	0.000	4.326	62.148	4	0	0.0
W <sub>1</sub> -Te <sub>1</sub> -Te <sub>3</sub>	1.000	0.000	0.000	21.313	1.000	0.155	0.000	0.000	4	0	0.0
W <sub>1</sub> -Te <sub>1</sub> -Te <sub>2</sub>	1.000	0.000	0.000	21.147	1.000	0.127	0.000	0.000	4	0	0.0
Te <sub>1</sub> -W <sub>1</sub> -W <sub>3</sub>	1.000	0.000	0.000	17.370	1.000	0.155	0.000	0.000	4	0	0.0

The parameters for the three-body SW potential used by GULP are shown in Tab. CXLIV. Parameters for the SW potential used by LAMMPS are listed in Tab. CXLV. We note that twelve atom types have been introduced for the simulation of the single-layer 1H-WTe<sub>2</sub> using LAMMPS, because the angles around atom W in Fig. 1 (with M=W and X=Te) are not distinguishable in LAMMPS. We have suggested two options to differentiate these angles by implementing some additional constraints in LAMMPS, which can be accomplished by modifying the source file of LAMMPS.<sup>13,14</sup> According to our experience, it is not so convenient for some users to implement these constraints and recompile the LAMMPS package. Hence, in the present work, we differentiate the angles by introducing more atom types, so it is not necessary to modify the LAMMPS package. Fig. 2 (with M=W and X=Te) shows that, for 1H-WTe<sub>2</sub>, we can differentiate these angles around the W atom by assigning these six neighboring Te atoms with different atom types. It can be found that twelve atom types are necessary for the purpose of differentiating all six neighbors around one W atom.

We use LAMMPS to perform MD simulations for the mechanical behavior of the single-layer 1H-WTe<sub>2</sub> under uniaxial tension at 1.0 K and 300.0 K. Fig. 70 shows the stress-strain curve for the tension of a single-layer 1H-WTe<sub>2</sub> of dimension 100 × 100 Å. Periodic boundary conditions are applied in both armchair and zigzag directions. The single-layer 1H-WTe<sub>2</sub> is stretched uniaxially along the armchair or zigzag direction. The stress is calculated without involving the actual thickness of the quasi-two-dimensional structure of the single-layer 1H-WTe<sub>2</sub>. The Young's modulus can be obtained by a linear fitting of the stress-strain relation in the small strain range of [0, 0.01]. The Young's modulus are 82.7 N/m and 81.9 N/m along the armchair and zigzag directions, respectively. The Young's modulus is essentially isotropic in the armchair and zigzag directions. These values are in reasonably agreement with the *ab initio* results, eg. 86.4 N/m from Ref. 18, or 93.9 N/m from Ref. 35. The Poisson's ratio from the VFF model and the SW potential is  $\nu_{xy} = \nu_{yx} = 0.20$ , which agrees with the *ab initio* value of 0.18.<sup>18</sup>

We have determined the nonlinear parameter to be  $B = 0.41d^4$  in Eq. (5) by fitting to the third-order nonlinear elastic constant  $D$  from the *ab initio* calculations.<sup>35</sup> We have extracted the value of  $D = -280.3$  N/m by fitting the stress-strain relation along the armchair direction in the *ab initio* calculations to the function  $\sigma = E\epsilon + \frac{1}{2}D\epsilon^2$  with  $E$  as the Young's modulus. The values of  $D$  from the present SW potential are -269.4 N/m and -297.9 N/m along the armchair and zigzag directions, respectively. The ultimate stress is about 11.8 Nm<sup>-1</sup> at the

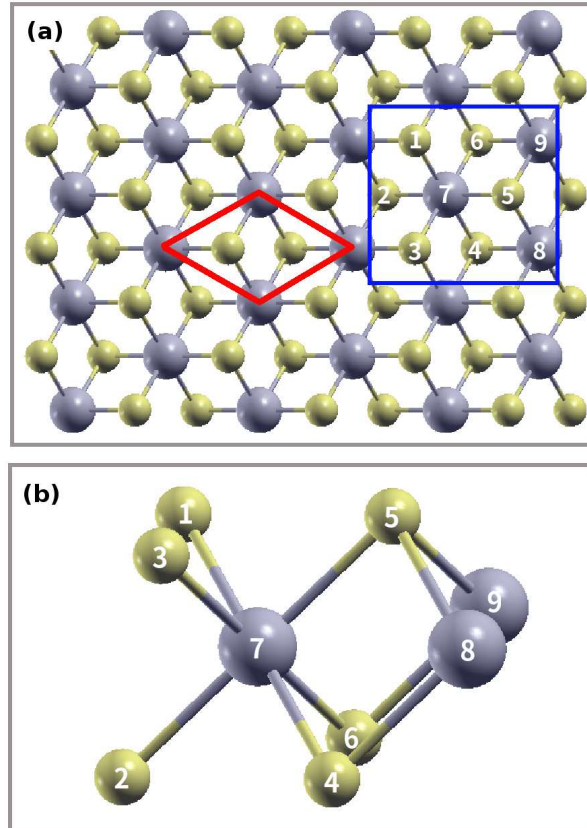


FIG. 71: (Color online) Configuration of the 1T-MX<sub>2</sub> in the 1T phase. (a) Top view. The unit cell is highlighted by a red parallelogram. The armchair direction is defined to be along the horizontal direction. The zigzag direction is along the vertical direction. (b) Enlarged view of atoms in the blue box in (a). Each M atom is surrounded by six X atoms, which are categorized into the top and bottom groups. Atoms X 1, 3, and 5 are from the top group, while atoms X 2, 4, and 6 are from the bottom group. M atoms are represented by larger gray balls. X atoms are represented by smaller yellow balls.

ultimate strain of 0.25 in the armchair direction at the low temperature of 1 K. The ultimate stress is about  $11.3 \text{ Nm}^{-1}$  at the ultimate strain of 0.29 in the zigzag direction at the low temperature of 1 K.

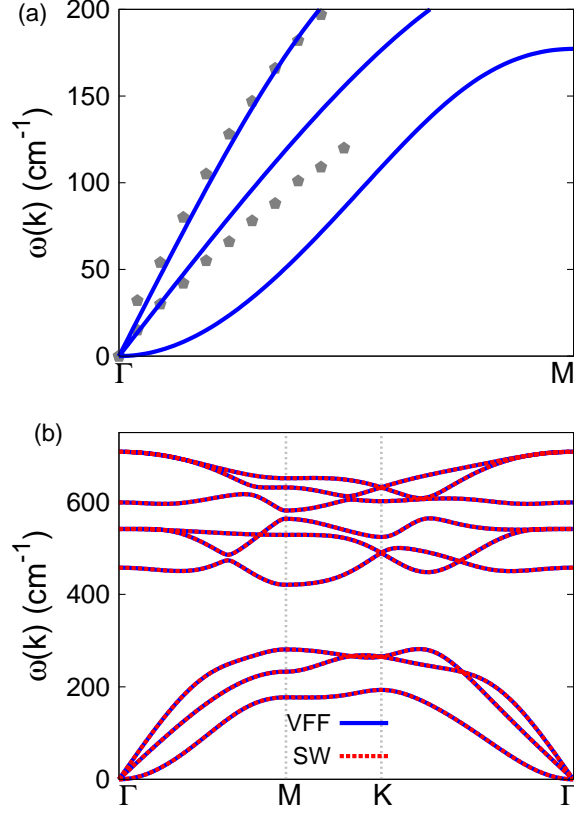


FIG. 72: (Color online) Phonon spectrum for single-layer 1T-ScO<sub>2</sub>. (a) Phonon dispersion along the  $\Gamma$ M direction in the Brillouin zone. The results from the VFF model (lines) are comparable with the *ab initio* results (pentagons) from Ref. 12. (b) The phonon dispersion from the SW potential is exactly the same as that from the VFF model.

### XXXVII. 1T-SCO<sub>2</sub>

Most existing theoretical studies on the single-layer 1T-ScO<sub>2</sub> are based on the first-principles calculations. In this section, we will develop the SW potential for the single-layer 1T-ScO<sub>2</sub>.

The structure for the single-layer 1T-ScO<sub>2</sub> is shown in Fig. 71 (with M=Sc and X=O). Each Ni atom is surrounded by six O atoms. These O atoms are categorized into the top group (eg. atoms 1, 3, and 5) and bottom group (eg. atoms 2, 4, and 6). Each O atom is connected to three Sc atoms. The structural parameters are from the first-principles calculations,<sup>12</sup> including the lattice constant  $a = 3.22 \text{ \AA}$  and the bond length  $d_{\text{Sc-O}} = 2.07 \text{ \AA}$ .

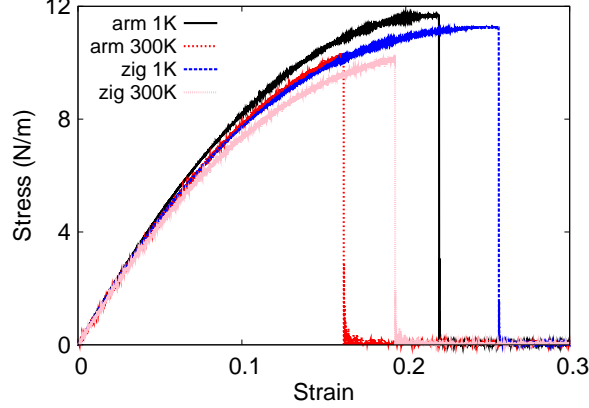


FIG. 73: (Color online) Stress-strain for single-layer 1T-ScO<sub>2</sub> of dimension 100 × 100 Å along the armchair and zigzag directions.

TABLE CXLVI: The VFF model for single-layer 1T-ScO<sub>2</sub>. The second line gives an explicit expression for each VFF term. The third line is the force constant parameters. Parameters are in the unit of  $\frac{eV}{\text{Å}^2}$  for the bond stretching interactions, and in the unit of eV for the angle bending interaction. The fourth line gives the initial bond length (in unit of Å) for the bond stretching interaction and the initial angle (in unit of degrees) for the angle bending interaction. The angle  $\theta_{ijk}$  has atom *i* as the apex.

VFF type	bond stretching	angle bending	
expression	$\frac{1}{2}K_{\text{Sc-O}}(\Delta r)^2$	$\frac{1}{2}K_{\text{Sc-O-O}}(\Delta\theta)^2$	$\frac{1}{2}K_{\text{O-Sc-Sc}}(\Delta\theta)^2$
parameter	11.926	3.258	3.258
$r_0$ or $\theta_0$	2.07	102.115	102.115

The resultant angles are  $\theta_{\text{ScOO}} = 102.115^\circ$  with O atoms from the same (top or bottom) group, and  $\theta_{\text{OScSc}} = 102.115^\circ$ .

Table CXLVI shows three VFF terms for the single-layer 1T-ScO<sub>2</sub>, one of which is the bond stretching interaction shown by Eq. (1) while the other two terms are the angle bending interaction shown by Eq. (2). We note that the angle bending term  $K_{\text{Sc-O-O}}$  is for the angle  $\theta_{\text{Sc-O-O}}$  with both O atoms from the same (top or bottom) group. These force constant parameters are determined by fitting to the two in-plane acoustic branches in the phonon dispersion along the  $\Gamma\text{M}$  as shown in Fig. 72 (a). The *ab initio* calculations for the phonon

TABLE CXLVII: Two-body SW potential parameters for single-layer 1T-ScO<sub>2</sub> used by GULP<sup>8</sup> as expressed in Eq. (3).

	$A$ (eV)	$\rho$ (Å)	$B$ (Å <sup>4</sup> )	$r_{\min}$ (Å)	$r_{\max}$ (Å)
Sc-O	10.187	1.493	9.180	0.0	2.949

TABLE CXLVIII: Three-body SW potential parameters for single-layer 1T-ScO<sub>2</sub> used by GULP<sup>8</sup> as expressed in Eq. (4). The angle  $\theta_{ijk}$  in the first line indicates the bending energy for the angle with atom  $i$  as the apex.

	$K$ (eV)	$\theta_0$ (degree)	$\rho_1$ (Å)	$\rho_2$ (Å)	$r_{\min12}$ (Å)	$r_{\max12}$ (Å)	$r_{\min13}$ (Å)	$r_{\max13}$ (Å)	$r_{\min23}$ (Å)	$r_{\max23}$ (Å)
$\theta_{\text{Sc-O-O}}$	50.913	102.115	1.493	1.493	0.0	2.949	0.0	2.949	0.0	4.399
$\theta_{\text{O-Sc-Sc}}$	50.913	102.115	1.493	1.493	0.0	2.949	0.0	2.949	0.0	4.399

dispersion are from Ref. 12. Fig. 72 (b) shows that the VFF model and the SW potential give exactly the same phonon dispersion, as the SW potential is derived from the VFF model.

The parameters for the two-body SW potential used by GULP are shown in Tab. CXLVII. The parameters for the three-body SW potential used by GULP are shown in Tab. CXLVIII. Some representative parameters for the SW potential used by LAMMPS are listed in Tab. CXLIX.

We use LAMMPS to perform MD simulations for the mechanical behavior of the single-layer 1T-ScO<sub>2</sub> under uniaxial tension at 1.0 K and 300.0 K. Fig. 73 shows the stress-strain curve for the tension of a single-layer 1T-ScO<sub>2</sub> of dimension  $100 \times 100$  Å. Periodic boundary conditions are applied in both armchair and zigzag directions. The single-layer 1T-ScO<sub>2</sub> is stretched uniaxially along the armchair or zigzag direction. The stress is calculated without involving the actual thickness of the quasi-two-dimensional structure of the single-layer 1T-ScO<sub>2</sub>. The Young's modulus can be obtained by a linear fitting of the stress-strain relation in the small strain range of  $[0, 0.01]$ . The Young's modulus are 100.9 N/m and 100.4 N/m

TABLE CXLIX: SW potential parameters for single-layer 1T-ScO<sub>2</sub> used by LAMMPS<sup>9</sup> as expressed in Eqs. (9) and (10).

	$\epsilon$ (eV)	$\sigma$ (Å)	$a$	$\lambda$	$\gamma$	$\cos \theta_0$	$A_L$	$B_L$	$p$	$q$	tol
Sc-O <sub>1</sub> -O <sub>1</sub>	1.000	1.493	1.975	50.913	1.000	-0.210	10.187	1.847	4	0	0.0

TABLE CL: The VFF model for single-layer 1T-ScS<sub>2</sub>. The second line gives an explicit expression for each VFF term. The third line is the force constant parameters. Parameters are in the unit of  $\frac{\text{eV}}{\text{\AA}^2}$  for the bond stretching interactions, and in the unit of eV for the angle bending interaction. The fourth line gives the initial bond length (in unit of  $\text{\AA}$ ) for the bond stretching interaction and the initial angle (in unit of degrees) for the angle bending interaction. The angle  $\theta_{ijk}$  has atom  $i$  as the apex.

VFF type	bond stretching	angle bending	
expression	$\frac{1}{2}K_{\text{Sc-S}}(\Delta r)^2$	$\frac{1}{2}K_{\text{Sc-S-S}}(\Delta\theta)^2$	$\frac{1}{2}K_{\text{S-Sc-S}}(\Delta\theta)^2$
parameter	3.512	1.593	1.593
$r_0$ or $\theta_0$	2.50	92.771	92.771

TABLE CLI: Two-body SW potential parameters for single-layer 1T-ScS<sub>2</sub> used by GULP<sup>8</sup> as expressed in Eq. (3).

	$A$ (eV)	$\rho$ ( $\text{\AA}$ )	$B$ ( $\text{\AA}^4$ )	$r_{\text{min}}$ ( $\text{\AA}$ )	$r_{\text{max}}$ ( $\text{\AA}$ )
Sc-S	3.516	1.443	19.531	0.0	3.450

along the armchair and zigzag directions, respectively. The Young's modulus is essentially isotropic in the armchair and zigzag directions. The Poisson's ratio from the VFF model and the SW potential is  $\nu_{xy} = \nu_{yx} = 0.15$ .

There is no available value for nonlinear quantities in the single-layer 1T-ScO<sub>2</sub>. We have thus used the nonlinear parameter  $B = 0.5d^4$  in Eq. (5), which is close to the value of  $B$  in most materials. The value of the third order nonlinear elasticity  $D$  can be extracted by fitting the stress-strain relation to the function  $\sigma = E\epsilon + \frac{1}{2}D\epsilon^2$  with  $E$  as the Young's modulus. The values of  $D$  from the present SW potential are -422.4 N/m and -453.7 N/m along the armchair and zigzag directions, respectively. The ultimate stress is about 11.7 Nm<sup>-1</sup> at the ultimate strain of 0.22 in the armchair direction at the low temperature of 1 K. The ultimate stress is about 11.3 Nm<sup>-1</sup> at the ultimate strain of 0.25 in the zigzag direction at the low temperature of 1 K.

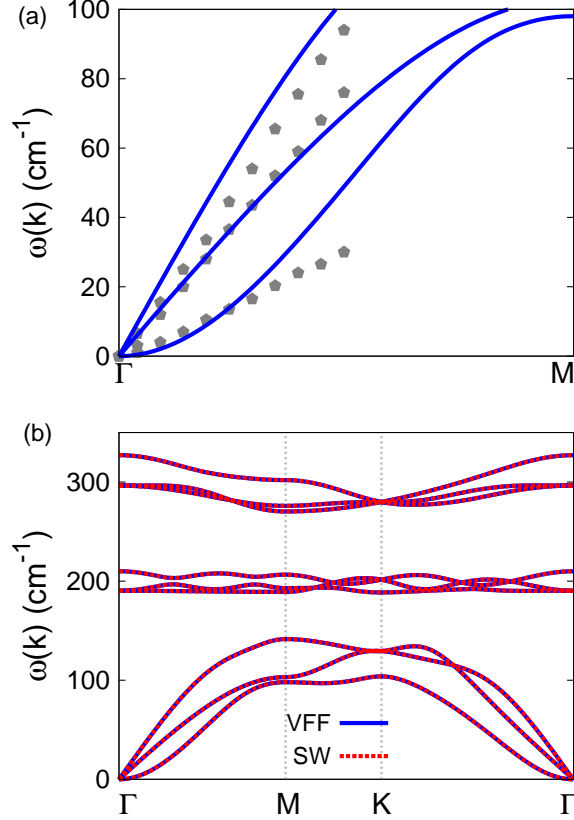


FIG. 74: (Color online) Phonon spectrum for single-layer 1T-ScS<sub>2</sub>. (a) Phonon dispersion along the  $\Gamma$ M direction in the Brillouin zone. The results from the VFF model (lines) are comparable with the *ab initio* results (pentagons) from Ref. 12. (b) The phonon dispersion from the SW potential is exactly the same as that from the VFF model.

### XXXVIII. 1T-SCS<sub>2</sub>

Most existing theoretical studies on the single-layer 1T-ScS<sub>2</sub> are based on the first-principles calculations. In this section, we will develop the SW potential for the single-layer 1T-ScS<sub>2</sub>.

The structure for the single-layer 1T-ScS<sub>2</sub> is shown in Fig. 71 (with M=Sc and X=S). Each Sc atom is surrounded by six S atoms. These S atoms are categorized into the top group (eg. atoms 1, 3, and 5) and bottom group (eg. atoms 2, 4, and 6). Each S atom is connected to three Sc atoms. The structural parameters are from the first-principles calculations,<sup>12</sup> including the lattice constant  $a = 3.62 \text{ \AA}$ , and the bond length  $d_{\text{Sc-S}} = 2.50 \text{ \AA}$ . The resultant

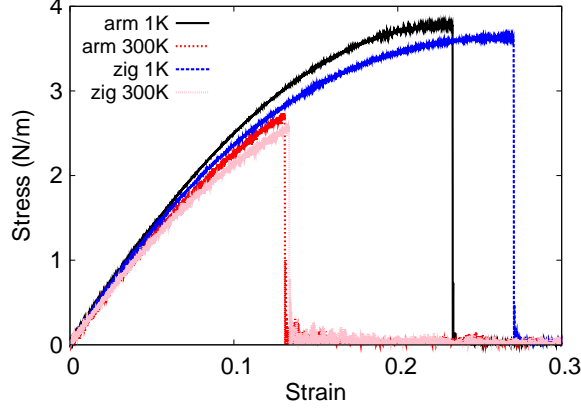


FIG. 75: (Color online) Stress-strain for single-layer 1T-ScS<sub>2</sub> of dimension 100 × 100 Å along the armchair and zigzag directions.

TABLE CLII: Three-body SW potential parameters for single-layer 1T-ScS<sub>2</sub> used by GULP<sup>8</sup> as expressed in Eq. (4). The angle  $\theta_{ijk}$  in the first line indicates the bending energy for the angle with atom  $i$  as the apex.

	$K$ (eV)	$\theta_0$ (degree)	$\rho_1$ (Å)	$\rho_2$ (Å)	$r_{\min 12}$ (Å)	$r_{\max 12}$ (Å)	$r_{\min 13}$ (Å)	$r_{\max 13}$ (Å)	$r_{\min 23}$ (Å)	$r_{\max 23}$ (Å)
$\theta_{\text{Sc-S-S}}$	16.674	92.771	1.443	1.443	0.0	3.450	0.0	3.450	0.0	4.945
$\theta_{\text{S-Sc-Sc}}$	16.674	92.771	1.443	1.443	0.0	3.450	0.0	3.450	0.0	4.945

angle is  $\theta_{\text{SScSc}} = 92.771^\circ$  and  $\theta_{\text{ScSS}} = 92.771^\circ$  with S atoms from the same (top or bottom) group.

Table CL shows three VFF terms for the single-layer 1T-ScS<sub>2</sub>, one of which is the bond stretching interaction shown by Eq. (1) while the other two terms are the angle bending interaction shown by Eq. (2). We note that the angle bending term  $K_{\text{Sc-S-S}}$  is for the angle  $\theta_{\text{Sc-S-S}}$  with both S atoms from the same (top or bottom) group. These force constant parameters are determined by fitting to the three acoustic branches in the phonon dispersion

TABLE CLIII: SW potential parameters for single-layer 1T-ScS<sub>2</sub> used by LAMMPS<sup>9</sup> as expressed in Eqs. (9) and (10).

	$\epsilon$ (eV)	$\sigma$ (Å)	$a$	$\lambda$	$\gamma$	$\cos \theta_0$	$A_L$	$B_L$	$p$	$q$	tol
Sc-S <sub>1</sub> -S <sub>1</sub>	1.000	1.443	2.390	16.674	1.000	-0.048	3.516	4.504	4	0	0.0

along the  $\Gamma M$  as shown in Fig. 74 (a). The *ab initio* calculations for the phonon dispersion are from Ref. 12. Fig. 74 (b) shows that the VFF model and the SW potential give exactly the same phonon dispersion, as the SW potential is derived from the VFF model.

The parameters for the two-body SW potential used by GULP are shown in Tab. CLI. The parameters for the three-body SW potential used by GULP are shown in Tab. CLII. Some representative parameters for the SW potential used by LAMMPS are listed in Tab. CLIII.

We use LAMMPS to perform MD simulations for the mechanical behavior of the single-layer 1T-ScS<sub>2</sub> under uniaxial tension at 1.0 K and 300.0 K. Fig. 75 shows the stress-strain curve for the tension of a single-layer 1T-ScS<sub>2</sub> of dimension  $100 \times 100$  Å. Periodic boundary conditions are applied in both armchair and zigzag directions. The single-layer 1T-ScS<sub>2</sub> is stretched uniaxially along the armchair or zigzag direction. The stress is calculated without involving the actual thickness of the quasi-two-dimensional structure of the single-layer 1T-ScS<sub>2</sub>. The Young's modulus can be obtained by a linear fitting of the stress-strain relation in the small strain range of  $[0, 0.01]$ . The Young's modulus are 30.0 N/m and 29.9 N/m along the armchair and zigzag directions, respectively. The Young's modulus is essentially isotropic in the armchair and zigzag directions. The Poisson's ratio from the VFF model and the SW potential is  $\nu_{xy} = \nu_{yx} = 0.17$ .

There is no available value for nonlinear quantities in the single-layer 1T-ScS<sub>2</sub>. We have thus used the nonlinear parameter  $B = 0.5d^4$  in Eq. (5), which is close to the value of  $B$  in most materials. The value of the third order nonlinear elasticity  $D$  can be extracted by fitting the stress-strain relation to the function  $\sigma = E\epsilon + \frac{1}{2}D\epsilon^2$  with  $E$  as the Young's modulus. The values of  $D$  from the present SW potential are -113.7 N/m and -124.6 N/m along the armchair and zigzag directions, respectively. The ultimate stress is about  $3.8 \text{ Nm}^{-1}$  at the ultimate strain of 0.23 in the armchair direction at the low temperature of 1 K. The ultimate stress is about  $3.6 \text{ Nm}^{-1}$  at the ultimate strain of 0.27 in the zigzag direction at the low temperature of 1 K.

### XXXIX. 1T-SCSE<sub>2</sub>

Most existing theoretical studies on the single-layer 1T-ScSe<sub>2</sub> are based on the first-principles calculations. In this section, we will develop the SW potential for the single-layer 1T-ScSe<sub>2</sub>.

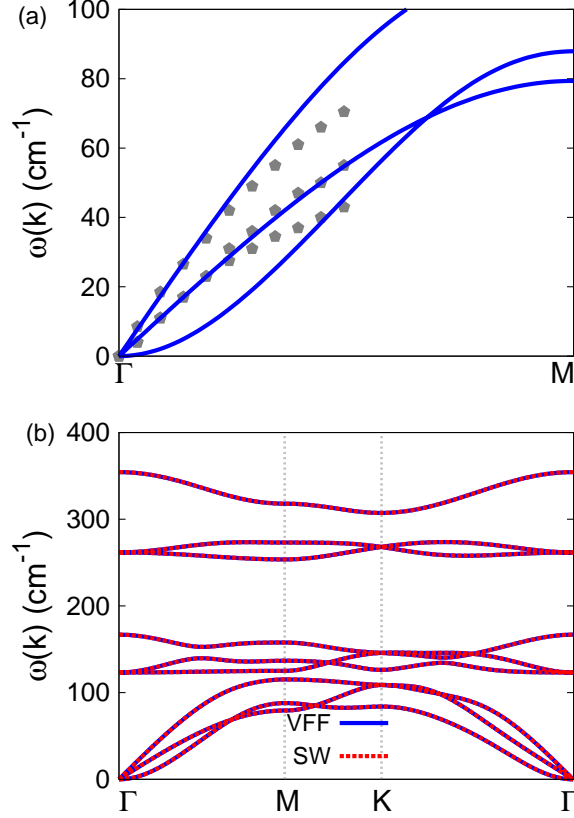


FIG. 76: (Color online) Phonon spectrum for single-layer 1T-ScSe<sub>2</sub>. (a) Phonon dispersion along the  $\Gamma$ M direction in the Brillouin zone. The results from the VFF model (lines) are comparable with the *ab initio* results (pentagons) from Ref. 12. (b) The phonon dispersion from the SW potential is exactly the same as that from the VFF model.

The structure for the single-layer 1T-ScSe<sub>2</sub> is shown in Fig. 71 (with M=Sc and X=Se). Each Sc atom is surrounded by six Se atoms. These Se atoms are categorized into the top group (eg. atoms 1, 3, and 5) and bottom group (eg. atoms 2, 4, and 6). Each Se atom is connected to three Sc atoms. The structural parameters are from the first-principles calculations,<sup>12</sup> including the lattice constant  $a = 3.52 \text{ \AA}$ , and the bond length  $d_{\text{Sc-Se}} = 2.64 \text{ \AA}$ . The resultant angle is  $\theta_{\text{SeScSc}} = 83.621^\circ$  and  $\theta_{\text{ScSeSe}} = 83.621^\circ$  with Se atoms from the same (top or bottom) group.

Table CLIV shows three VFF terms for the single-layer 1T-ScSe<sub>2</sub>, one of which is the bond stretching interaction shown by Eq. (1) while the other two terms are the angle bending interaction shown by Eq. (2). We note that the angle bending term  $K_{\text{Sc-Se-Se}}$  is for the angle

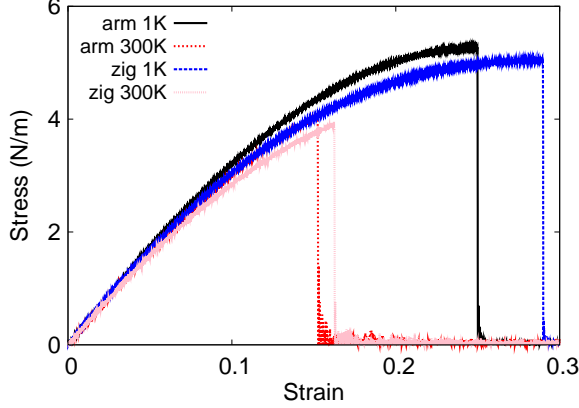


FIG. 77: (Color online) Stress-strain for single-layer 1T-ScSe<sub>2</sub> of dimension  $100 \times 100 \text{ \AA}$  along the armchair and zigzag directions.

TABLE CLIV: The VFF model for single-layer 1T-ScSe<sub>2</sub>. The second line gives an explicit expression for each VFF term. The third line is the force constant parameters. Parameters are in the unit of  $\frac{eV}{\text{\AA}^2}$  for the bond stretching interactions, and in the unit of eV for the angle bending interaction. The fourth line gives the initial bond length (in unit of  $\text{\AA}$ ) for the bond stretching interaction and the initial angle (in unit of degrees) for the angle bending interaction. The angle  $\theta_{ijk}$  has atom  $i$  as the apex.

VFF type	bond stretching	angle bending	
expression	$\frac{1}{2}K_{\text{Sc-Se}}(\Delta r)^2$	$\frac{1}{2}K_{\text{Sc-Se-Se}}(\Delta\theta)^2$	$\frac{1}{2}K_{\text{Se-Sc-Sc}}(\Delta\theta)^2$
parameter	4.407	2.399	2.399
$r_0$ or $\theta_0$	2.64	83.621	83.621

$\theta_{\text{Sc-Se-Se}}$  with both Se atoms from the same (top or bottom) group. These force constant parameters are determined by fitting to the three acoustic branches in the phonon dispersion along the  $\Gamma\text{M}$  as shown in Fig. 76 (a). The *ab initio* calculations for the phonon dispersion are from Ref. 12. We note that the lowest-frequency branch around the  $\Gamma$  point from the VFF model is lower than the *ab initio* results. This branch is the flexural branch, which should be a quadratic dispersion. However, the *ab initio* calculations give a linear dispersion for the flexural branch due to the violation of the rigid rotational invariance in the first-principles package,<sup>20</sup> so *ab initio* calculations typically overestimate the frequency of this

TABLE CLV: Two-body SW potential parameters for single-layer 1T-ScSe<sub>2</sub> used by GULP<sup>8</sup> as expressed in Eq. (3).

	$A$ (eV)	$\rho$ (Å)	$B$ (Å <sup>4</sup> )	$r_{\min}$ (Å)	$r_{\max}$ (Å)
Sc-Se	3.884	1.173	24.288	0.0	3.520

TABLE CLVI: Three-body SW potential parameters for single-layer 1T-ScSe<sub>2</sub> used by GULP<sup>8</sup> as expressed in Eq. (4). The angle  $\theta_{ijk}$  in the first line indicates the bending energy for the angle with atom  $i$  as the apex.

	$K$ (eV)	$\theta_0$ (degree)	$\rho_1$ (Å)	$\rho_2$ (Å)	$r_{\min12}$ (Å)	$r_{\max12}$ (Å)	$r_{\min13}$ (Å)	$r_{\max13}$ (Å)	$r_{\min23}$ (Å)	$r_{\max23}$ (Å)
$\theta_{\text{Sc-Se-Se}}$	17.479	83.621	1.173	1.173	0.0	3.520	0.0	3.520	0.0	4.808
$\theta_{\text{Se-Sc-Sc}}$	17.479	83.621	1.173	1.173	0.0	3.520	0.0	3.520	0.0	4.808

branch. Fig. 76 (b) shows that the VFF model and the SW potential give exactly the same phonon dispersion, as the SW potential is derived from the VFF model.

The parameters for the two-body SW potential used by GULP are shown in Tab. CLV. The parameters for the three-body SW potential used by GULP are shown in Tab. CLVI. Some representative parameters for the SW potential used by LAMMPS are listed in Tab. CLVII.

We use LAMMPS to perform MD simulations for the mechanical behavior of the single-layer 1T-ScSe<sub>2</sub> under uniaxial tension at 1.0 K and 300.0 K. Fig. 77 shows the stress-strain curve for the tension of a single-layer 1T-ScSe<sub>2</sub> of dimension  $100 \times 100$  Å. Periodic boundary conditions are applied in both armchair and zigzag directions. The single-layer 1T-ScSe<sub>2</sub> is stretched uniaxially along the armchair or zigzag direction. The stress is calculated without involving the actual thickness of the quasi-two-dimensional structure of the single-layer 1T-ScSe<sub>2</sub>. The Young's modulus can be obtained by a linear fitting of the stress-strain relation in the small strain range of  $[0, 0.01]$ . The Young's modulus are 36.4 N/m and 36.3 N/m

TABLE CLVII: SW potential parameters for single-layer 1T-ScSe<sub>2</sub> used by LAMMPS<sup>9</sup> as expressed in Eqs. (9) and (10).

	$\epsilon$ (eV)	$\sigma$ (Å)	$a$	$\lambda$	$\gamma$	$\cos \theta_0$	$A_L$	$B_L$	$p$	$q$	tol
Sc-Se <sub>1</sub> -Se <sub>1</sub>	1.000	1.173	3.000	17.479	1.000	0.111	3.884	12.814	4	0	0.0

TABLE CLVIII: The VFF model for single-layer 1T-ScTe<sub>2</sub>. The second line gives an explicit expression for each VFF term. The third line is the force constant parameters. Parameters are in the unit of  $\frac{\text{eV}}{\text{Å}^2}$  for the bond stretching interactions, and in the unit of eV for the angle bending interaction. The fourth line gives the initial bond length (in unit of Å) for the bond stretching interaction and the initial angle (in unit of degrees) for the angle bending interaction. The angle  $\theta_{ijk}$  has atom *i* as the apex.

VFF type	bond stretching	angle bending	
expression	$\frac{1}{2}K_{\text{Sc-Te}}(\Delta r)^2$	$\frac{1}{2}K_{\text{Sc-Te-Te}}(\Delta\theta)^2$	$\frac{1}{2}K_{\text{Te-Sc-Sc}}(\Delta\theta)^2$
parameter	4.407	2.399	2.399
$r_0$ or $\theta_0$	2.85	81.481	81.481

TABLE CLIX: Two-body SW potential parameters for single-layer 1T-ScTe<sub>2</sub> used by GULP<sup>8</sup> as expressed in Eq. (3).

	$A$ (eV)	$\rho$ (Å)	$B$ (Å <sup>4</sup> )	$r_{\text{min}}$ (Å)	$r_{\text{max}}$ (Å)
Sc-Te	4.269	1.183	32.988	0.0	3.768

along the armchair and zigzag directions, respectively. The Young's modulus is essentially isotropic in the armchair and zigzag directions. The Poisson's ratio from the VFF model and the SW potential is  $\nu_{xy} = \nu_{yx} = 0.20$ .

There is no available value for nonlinear quantities in the single-layer 1T-ScSe<sub>2</sub>. We have thus used the nonlinear parameter  $B = 0.5d^4$  in Eq. (5), which is close to the value of  $B$  in most materials. The value of the third order nonlinear elasticity  $D$  can be extracted by fitting the stress-strain relation to the function  $\sigma = E\epsilon + \frac{1}{2}D\epsilon^2$  with  $E$  as the Young's modulus. The values of  $D$  from the present SW potential are -113.7 N/m and -130.3 N/m along the armchair and zigzag directions, respectively. The ultimate stress is about 5.3 Nm<sup>-1</sup> at the ultimate strain of 0.25 in the armchair direction at the low temperature of 1 K. The ultimate stress is about 5.0 Nm<sup>-1</sup> at the ultimate strain of 0.29 in the zigzag direction at the low temperature of 1 K.

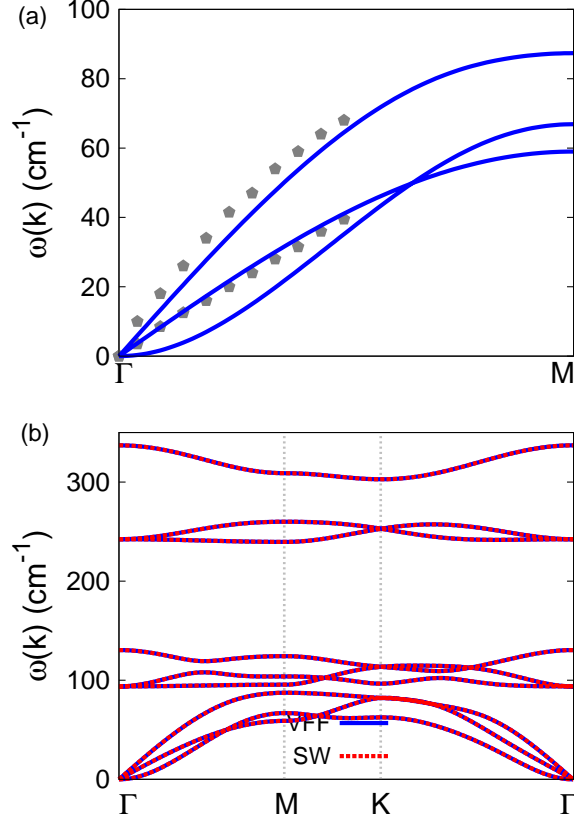


FIG. 78: (Color online) Phonon spectrum for single-layer 1T-ScTe<sub>2</sub>. (a) Phonon dispersion along the  $\Gamma$ M direction in the Brillouin zone. The results from the VFF model (lines) are comparable with the *ab initio* results (pentagons) from Ref. 12. (b) The phonon dispersion from the SW potential is exactly the same as that from the VFF model.

## **XL. 1T-SCTE<sub>2</sub>**

Most existing theoretical studies on the single-layer 1T-ScTe<sub>2</sub> are based on the first-principles calculations. In this section, we will develop the SW potential for the single-layer 1T-ScTe<sub>2</sub>.

The structure for the single-layer 1T-ScTe<sub>2</sub> is shown in Fig. 71 (with M=Sc and X=Te). Each Sc atom is surrounded by six Te atoms. These Te atoms are categorized into the top group (eg. atoms 1, 3, and 5) and bottom group (eg. atoms 2, 4, and 6). Each Te atom is connected to three Sc atoms. The structural parameters are from the first-principles calculations,<sup>12</sup> including the lattice constant  $a = 3.72 \text{ \AA}$ , and the bond length

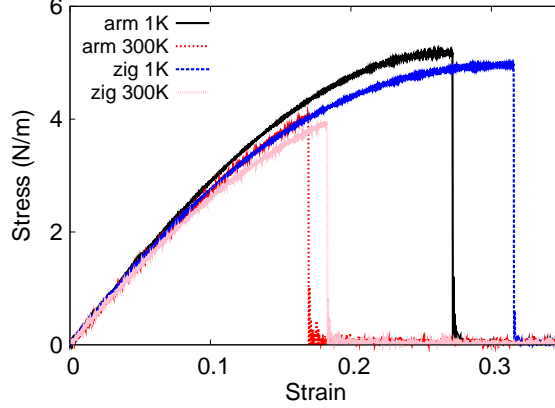


FIG. 79: (Color online) Stress-strain for single-layer 1T-ScTe<sub>2</sub> of dimension 100 × 100 Å along the armchair and zigzag directions.

TABLE CLX: Three-body SW potential parameters for single-layer 1T-ScTe<sub>2</sub> used by GULP<sup>8</sup> as expressed in Eq. (4). The angle  $\theta_{ijk}$  in the first line indicates the bending energy for the angle with atom i as the apex.

	$K$ (eV)	$\theta_0$ (degree)	$\rho_1$ (Å)	$\rho_2$ (Å)	$r_{\min 12}$ (Å)	$r_{\max 12}$ (Å)	$r_{\min 13}$ (Å)	$r_{\max 13}$ (Å)	$r_{\min 23}$ (Å)	$r_{\max 23}$ (Å)
$\theta_{\text{Sc-Te-Te}}$	16.139	81.481	1.183	1.183	0.0	3.768	0.0	3.768	0.0	5.082
$\theta_{\text{Te-Sc-Sc}}$	16.139	81.481	1.183	1.183	0.0	3.768	0.0	3.768	0.0	5.082

$d_{\text{Sc-Te}} = 2.85$  Å. The resultant angle is  $\theta_{\text{TeScSc}} = 81.481^\circ$  and  $\theta_{\text{ScTeTe}} = 81.481^\circ$  with Se atoms from the same (top or bottom) group.

Table CLVIII shows three VFF terms for the single-layer 1T-ScTe<sub>2</sub>, one of which is the bond stretching interaction shown by Eq. (1) while the other two terms are the angle bending interaction shown by Eq. (2). We note that the angle bending term  $K_{\text{Sc-Te-Te}}$  is for the angle  $\theta_{\text{Sc-Te-Te}}$  with both Te atoms from the same (top or bottom) group. These force constant parameters are determined by fitting to the two in-plane acoustic branches in the

TABLE CLXI: SW potential parameters for single-layer 1T-ScTe<sub>2</sub> used by LAMMPS<sup>9</sup> as expressed in Eqs. (9) and (10).

	$\epsilon$ (eV)	$\sigma$ (Å)	$a$	$\lambda$	$\gamma$	$\cos \theta_0$	$A_L$	$B_L$	$p$	$q$	tol
Sc-Te <sub>1</sub> -Te <sub>1</sub>	1.000	1.183	3.185	16.139	1.000	0.148	4.269	16.841	4	0	0.0

phonon dispersion along the  $\Gamma$ M as shown in Fig. 78 (a). The *ab initio* calculations for the phonon dispersion are from Ref. 12. Fig. 78 (b) shows that the VFF model and the SW potential give exactly the same phonon dispersion, as the SW potential is derived from the VFF model.

The parameters for the two-body SW potential used by GULP are shown in Tab. CLIX. The parameters for the three-body SW potential used by GULP are shown in Tab. CLX. Some representative parameters for the SW potential used by LAMMPS are listed in Tab. CLXI.

We use LAMMPS to perform MD simulations for the mechanical behavior of the single-layer 1T-ScTe<sub>2</sub> under uniaxial tension at 1.0 K and 300.0 K. Fig. 79 shows the stress-strain curve for the tension of a single-layer 1T-ScTe<sub>2</sub> of dimension  $100 \times 100$  Å. Periodic boundary conditions are applied in both armchair and zigzag directions. The single-layer 1T-ScTe<sub>2</sub> is stretched uniaxially along the armchair or zigzag direction. The stress is calculated without involving the actual thickness of the quasi-two-dimensional structure of the single-layer 1T-ScTe<sub>2</sub>. The Young's modulus can be obtained by a linear fitting of the stress-strain relation in the small strain range of  $[0, 0.01]$ . The Young's modulus are 31.4 N/m and 31.3 N/m along the armchair and zigzag directions, respectively. The Young's modulus is essentially isotropic in the armchair and zigzag directions. The Poisson's ratio from the VFF model and the SW potential is  $\nu_{xy} = \nu_{yx} = 0.22$ .

There is no available value for nonlinear quantities in the single-layer 1T-ScTe<sub>2</sub>. We have thus used the nonlinear parameter  $B = 0.5d^4$  in Eq. (5), which is close to the value of  $B$  in most materials. The value of the third order nonlinear elasticity  $D$  can be extracted by fitting the stress-strain relation to the function  $\sigma = E\epsilon + \frac{1}{2}D\epsilon^2$  with  $E$  as the Young's modulus. The values of  $D$  from the present SW potential are -81.2 N/m and -96.7 N/m along the armchair and zigzag directions, respectively. The ultimate stress is about  $5.2 \text{ Nm}^{-1}$  at the ultimate strain of 0.27 in the armchair direction at the low temperature of 1 K. The ultimate stress is about  $5.0 \text{ Nm}^{-1}$  at the ultimate strain of 0.31 in the zigzag direction at the low temperature of 1 K.

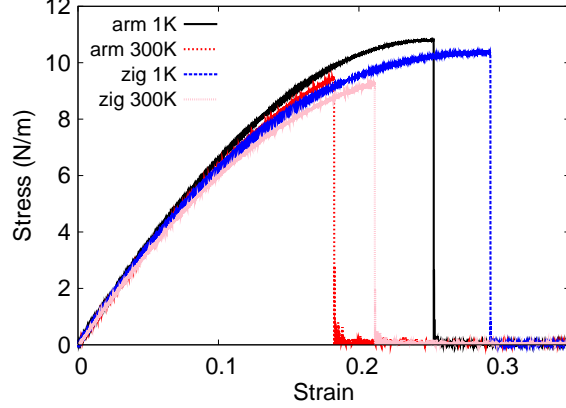


FIG. 80: (Color online) Stress-strain for single-layer 1T-TiS<sub>2</sub> of dimension  $100 \times 100 \text{ \AA}$  along the armchair and zigzag directions.

TABLE CLXII: The VFF model for single-layer 1T-TiS<sub>2</sub>. The second line gives an explicit expression for each VFF term. The third line is the force constant parameters. Parameters are in the unit of  $\frac{\text{eV}}{\text{Å}^2}$  for the bond stretching interactions, and in the unit of eV for the angle bending interaction. The fourth line gives the initial bond length (in unit of Å) for the bond stretching interaction and the initial angle (in unit of degrees) for the angle bending interaction. The angle  $\theta_{ijk}$  has atom *i* as the apex.

VFF type	bond stretching	angle bending	
expression	$\frac{1}{2}K_{\text{Ti-S}}(\Delta r)^2$	$\frac{1}{2}K_{\text{Ti-S-S}}(\Delta\theta)^2$	$\frac{1}{2}K_{\text{S-Ti-Ti}}(\Delta\theta)^2$
parameter	9.815	3.754	3.754
$r_0$ or $\theta_0$	2.390	87.984	87.984

## XLI. 1T-TIS<sub>2</sub>

Most existing theoretical studies on the single-layer 1T-TiS<sub>2</sub> are based on the first-principles calculations. In this section, we will develop the SW potential for the single-layer 1T-TiS<sub>2</sub>.

The structure for the single-layer 1T-TiS<sub>2</sub> is shown in Fig. 71 (with M=Ti and X=S). Each Ti atom is surrounded by six S atoms. These S atoms are categorized into the top group (eg. atoms 1, 3, and 5) and bottom group (eg. atoms 2, 4, and 6). Each S atom is connected to three Ti atoms. The structural parameters are from the first-principles

TABLE CLXIII: Two-body SW potential parameters for single-layer 1T-TiS<sub>2</sub> used by GULP<sup>8</sup> as expressed in Eq. (3).

	$A$ (eV)	$\rho$ (Å)	$B$ (Å <sup>4</sup> )	$r_{\min}$ (Å)	$r_{\max}$ (Å)
Ti-S	7.958	1.210	16.314	0.0	3.240

TABLE CLXIV: Three-body SW potential parameters for single-layer 1T-TiS<sub>2</sub> used by GULP<sup>8</sup> as expressed in Eq. (4). The angle  $\theta_{ijk}$  in the first line indicates the bending energy for the angle with atom i as the apex.

	$K$ (eV)	$\theta_0$ (degree)	$\rho_1$ (Å)	$\rho_2$ (Å)	$r_{\min12}$ (Å)	$r_{\max12}$ (Å)	$r_{\min13}$ (Å)	$r_{\max13}$ (Å)	$r_{\min23}$ (Å)	$r_{\max23}$ (Å)
$\theta_{\text{Ti-S-S}}$	32.377	87.984	1.210	1.210	0.0	3.240	0.0	3.240	0.0	4.535
$\theta_{\text{S-Ti-Ti}}$	32.377	87.984	1.210	1.210	0.0	3.240	0.0	3.240	0.0	4.535

calculations,<sup>12</sup> including the lattice constant  $a = 3.32$  Å and the bond length  $d_{\text{Ti-S}} = 2.39$  Å. The resultant angles are  $\theta_{\text{TiSS}} = 87.984^\circ$  with S atoms from the same (top or bottom) group, and  $\theta_{\text{STiTi}} = 87.984^\circ$ .

Table CLXII shows three VFF terms for the single-layer 1T-TiS<sub>2</sub>, one of which is the bond stretching interaction shown by Eq. (1) while the other two terms are the angle bending interaction shown by Eq. (2). We note that the angle bending term  $K_{\text{Ti-S-S}}$  is for the angle  $\theta_{\text{Ti-S-S}}$  with both S atoms from the same (top or bottom) group. We find that there are actually only two parameters in the VFF model, so we can determine their value by fitting to the Young's modulus and the Poisson's ratio of the system. The *ab initio* calculations have predicted the Young's modulus to be 85 N/m and the Poisson's ratio as 0.20.<sup>48</sup>

The parameters for the two-body SW potential used by GULP are shown in Tab. CLXIII. The parameters for the three-body SW potential used by GULP are shown in Tab. CLXIV. Some representative parameters for the SW potential used by LAMMPS are listed in Tab. CLXV.

TABLE CLXV: SW potential parameters for single-layer 1T-TiS<sub>2</sub> used by LAMMPS<sup>9</sup> as expressed in Eqs. (9) and (10).

	$\epsilon$ (eV)	$\sigma$ (Å)	$a$	$\lambda$	$\gamma$	$\cos \theta_0$	$A_L$	$B_L$	$p$	$q$	tol
Ti-S-S	1.000	1.210	2.677	32.377	1.000	0.035	7.958	7.602	4	0	0.0

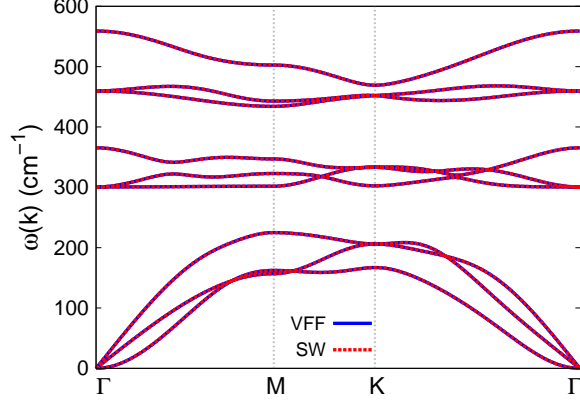


FIG. 81: (Color online) Phonon spectrum for single-layer 1T-TiS<sub>2</sub> along the  $\Gamma$ MK $\Gamma$  direction in the Brillouin zone. The phonon dispersion from the SW potential is exactly the same as that from the VFF model.

We use LAMMPS to perform MD simulations for the mechanical behavior of the single-layer 1T-TiS<sub>2</sub> under uniaxial tension at 1.0 K and 300.0 K. Fig. 80 shows the stress-strain curve for the tension of a single-layer 1T-TiS<sub>2</sub> of dimension  $100 \times 100$  Å. Periodic boundary conditions are applied in both armchair and zigzag directions. The single-layer 1T-TiS<sub>2</sub> is stretched uniaxially along the armchair or zigzag direction. The stress is calculated without involving the actual thickness of the quasi-two-dimensional structure of the single-layer 1T-TiS<sub>2</sub>. The Young's modulus can be obtained by a linear fitting of the stress-strain relation in the small strain range of  $[0, 0.01]$ . The Young's modulus are 75.0 N/m and 74.6 N/m along the armchair and zigzag directions, respectively. The Young's modulus is essentially isotropic in the armchair and zigzag directions. The Poisson's ratio from the VFF model and the SW potential is  $\nu_{xy} = \nu_{yx} = 0.20$ . The fitted Young's modulus value is about 10% smaller than the *ab initio* result of 85 N/m,<sup>48</sup> as only short-range interactions are considered in the present work. The long-range interactions are ignored, which typically leads to about 10% underestimation for the value of the Young's modulus.

There is no available value for nonlinear quantities in the single-layer 1T-TiS<sub>2</sub>. We have thus used the nonlinear parameter  $B = 0.5d^4$  in Eq. (5), which is close to the value of  $B$  in most materials. The value of the third order nonlinear elasticity  $D$  can be extracted by fitting the stress-strain relation to the function  $\sigma = E\epsilon + \frac{1}{2}D\epsilon^2$  with  $E$  as the Young's modulus. The values of  $D$  from the present SW potential are -220.8 N/m and -264.4 N/m along the

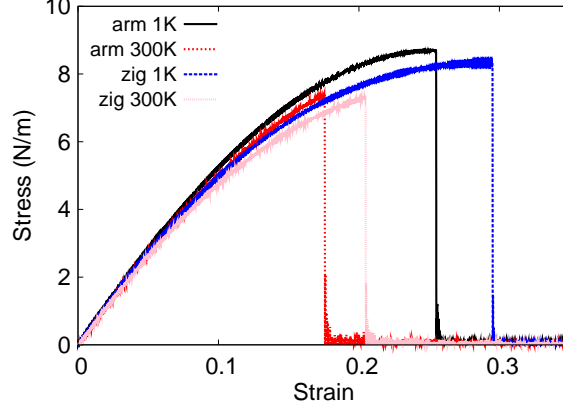


FIG. 82: (Color online) Stress-strain for single-layer 1T-TiSe<sub>2</sub> of dimension  $100 \times 100 \text{ \AA}$  along the armchair and zigzag directions.

TABLE CLXVI: The VFF model for single-layer 1T-TiSe<sub>2</sub>. The second line gives an explicit expression for each VFF term. The third line is the force constant parameters. Parameters are in the unit of  $\frac{\text{eV}}{\text{\AA}^2}$  for the bond stretching interactions, and in the unit of eV for the angle bending interaction. The fourth line gives the initial bond length (in unit of  $\text{\AA}$ ) for the bond stretching interaction and the initial angle (in unit of degrees) for the angle bending interaction. The angle  $\theta_{ijk}$  has atom  $i$  as the apex.

VFF type	bond stretching	angle bending	
expression	$\frac{1}{2}K_{\text{Ti-Se}}(\Delta r)^2$	$\frac{1}{2}K_{\text{Ti-Se-Se}}(\Delta\theta)^2$	$\frac{1}{2}K_{\text{Se-Ti-Ti}}(\Delta\theta)^2$
parameter	7.712	3.363	3.363
$r_0$ or $\theta_0$	2.510	86.199	86.199

armchair and zigzag directions, respectively. The ultimate stress is about  $10.8 \text{ Nm}^{-1}$  at the ultimate strain of 0.25 in the armchair direction at the low temperature of 1 K. The ultimate stress is about  $10.4 \text{ Nm}^{-1}$  at the ultimate strain of 0.29 in the zigzag direction at the low temperature of 1 K.

Fig. 81 shows that the VFF model and the SW potential give exactly the same phonon dispersion, as the SW potential is derived from the VFF model.

TABLE CLXVII: Two-body SW potential parameters for single-layer 1T-TiSe<sub>2</sub> used by GULP<sup>8</sup> as expressed in Eq. (3).

	$A$ (eV)	$\rho$ (Å)	$B$ (Å <sup>4</sup> )	$r_{\min}$ (Å)	$r_{\max}$ (Å)
Ti-Se	6.582	1.207	19.846	0.0	3.380

TABLE CLXVIII: Three-body SW potential parameters for single-layer 1T-TiSe<sub>2</sub> used by GULP<sup>8</sup> as expressed in Eq. (4). The angle  $\theta_{ijk}$  in the first line indicates the bending energy for the angle with atom  $i$  as the apex.

	$K$ (eV)	$\theta_0$ (degree)	$\rho_1$ (Å)	$\rho_2$ (Å)	$r_{\min12}$ (Å)	$r_{\max12}$ (Å)	$r_{\min13}$ (Å)	$r_{\max13}$ (Å)	$r_{\min23}$ (Å)	$r_{\max23}$ (Å)
$\theta_{\text{Ti-Se-Se}}$	27.044	86.199	1.207	1.207	0.0	3.380	0.0	3.380	0.0	4.685
$\theta_{\text{Se-Ti-Ti}}$	27.044	86.199	1.207	1.207	0.0	3.380	0.0	3.380	0.0	4.685

## XLII. 1T-TiSe<sub>2</sub>

Most existing theoretical studies on the single-layer 1T-TiSe<sub>2</sub> are based on the first-principles calculations. In this section, we will develop the SW potential for the single-layer 1T-TiSe<sub>2</sub>.

The structure for the single-layer 1T-TiSe<sub>2</sub> is shown in Fig. 71 (with M=Ti and X=Se). Each Ti atom is surrounded by six Se atoms. These Se atoms are categorized into the top group (eg. atoms 1, 3, and 5) and bottom group (eg. atoms 2, 4, and 6). Each Se atom is connected to three Ti atoms. The structural parameters are from the first-principles calculations,<sup>12</sup> including the lattice constant  $a = 3.43$  Å and the bond length  $d_{\text{Ti-Se}} = 2.51$  Å. The resultant angles are  $\theta_{\text{TiSeSe}} = 86.199^\circ$  with Se atoms from the same (top or bottom) group, and  $\theta_{\text{SeTiTi}} = 86.199^\circ$ .

Table CLXVI shows three VFF terms for the single-layer 1T-TiSe<sub>2</sub>, one of which is the bond stretching interaction shown by Eq. (1) while the other two terms are the angle bending

TABLE CLXIX: SW potential parameters for single-layer 1T-TiSe<sub>2</sub> used by LAMMPS<sup>9</sup> as expressed in Eqs. (9) and (10).

	$\epsilon$ (eV)	$\sigma$ (Å)	$a$	$\lambda$	$\gamma$	$\cos \theta_0$	$A_L$	$B_L$	$p$	$q$	tol
Ti-Se-Se	1.000	1.207	2.801	27.044	1.000	0.066	6.582	9.362	4	0	0.0

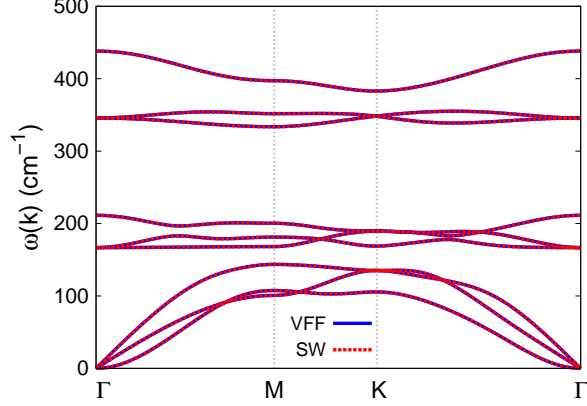


FIG. 83: (Color online) Phonon spectrum for single-layer 1T-TiSe<sub>2</sub> along the  $\Gamma$ MK $\Gamma$  direction in the Brillouin zone. The phonon dispersion from the SW potential is exactly the same as that from the VFF model.

interaction shown by Eq. (2). We note that the angle bending term  $K_{\text{Ti-Se-Se}}$  is for the angle  $\theta_{\text{Ti-Se-Se}}$  with both Se atoms from the same (top or bottom) group. We find that there are actually only two parameters in the VFF model, so we can determine their value by fitting to the Young's modulus and the Poisson's ratio of the system. The *ab initio* calculations have predicted the Young's modulus to be 70 N/m and the Poisson's ratio as 0.20.<sup>48</sup>

The parameters for the two-body SW potential used by GULP are shown in Tab. CLXVII. The parameters for the three-body SW potential used by GULP are shown in Tab. CLXVIII. Some representative parameters for the SW potential used by LAMMPS are listed in Tab. CLXIX.

We use LAMMPS to perform MD simulations for the mechanical behavior of the single-layer 1T-TiSe<sub>2</sub> under uniaxial tension at 1.0 K and 300.0 K. Fig. 82 shows the stress-strain curve for the tension of a single-layer 1T-TiSe<sub>2</sub> of dimension  $100 \times 100 \text{ \AA}$ . Periodic boundary conditions are applied in both armchair and zigzag directions. The single-layer 1T-TiSe<sub>2</sub> is stretched uniaxially along the armchair or zigzag direction. The stress is calculated without involving the actual thickness of the quasi-two-dimensional structure of the single-layer 1T-TiSe<sub>2</sub>. The Young's modulus can be obtained by a linear fitting of the stress-strain relation in the small strain range of  $[0, 0.01]$ . The Young's modulus are 59.2 N/m and 58.9 N/m along the armchair and zigzag directions, respectively. The Young's modulus is essentially isotropic in the armchair and zigzag directions. The Poisson's ratio from the VFF model

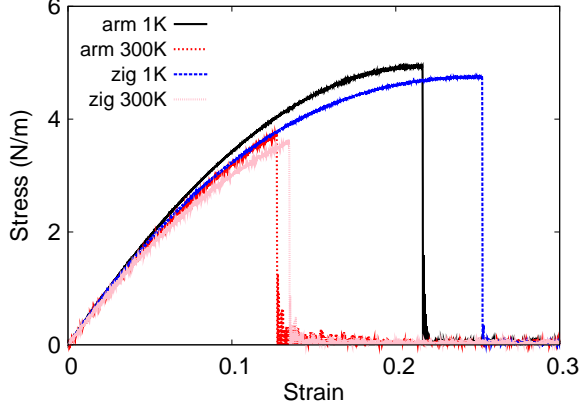


FIG. 84: (Color online) Stress-strain for single-layer 1T-TiTe<sub>2</sub> of dimension  $100 \times 100 \text{ \AA}$  along the armchair and zigzag directions.

and the SW potential is  $\nu_{xy} = \nu_{yx} = 0.20$ . The fitted Young's modulus value is about 10% smaller than the *ab initio* result of  $70 \text{ N/m}$ ,<sup>48</sup> as only short-range interactions are considered in the present work. The long-range interactions are ignored, which typically leads to about 10% underestimation for the value of the Young's modulus.

There is no available value for nonlinear quantities in the single-layer 1T-TiSe<sub>2</sub>. We have thus used the nonlinear parameter  $B = 0.5d^4$  in Eq. (5), which is close to the value of  $B$  in most materials. The value of the third order nonlinear elasticity  $D$  can be extracted by fitting the stress-strain relation to the function  $\sigma = E\epsilon + \frac{1}{2}D\epsilon^2$  with  $E$  as the Young's modulus. The values of  $D$  from the present SW potential are  $-166.5 \text{ N/m}$  and  $-201.6 \text{ N/m}$  along the armchair and zigzag directions, respectively. The ultimate stress is about  $8.7 \text{ Nm}^{-1}$  at the ultimate strain of 0.25 in the armchair direction at the low temperature of 1 K. The ultimate stress is about  $8.3 \text{ Nm}^{-1}$  at the ultimate strain of 0.29 in the zigzag direction at the low temperature of 1 K.

Fig. 83 shows that the VFF model and the SW potential give exactly the same phonon dispersion, as the SW potential is derived from the VFF model.

### XLIII. 1T-TITE<sub>2</sub>

Most existing theoretical studies on the single-layer 1T-TiTe<sub>2</sub> are based on the first-principles calculations. In this section, we will develop the SW potential for the single-layer

TABLE CLXX: The VFF model for single-layer 1T-TiTe<sub>2</sub>. The second line gives an explicit expression for each VFF term. The third line is the force constant parameters. Parameters are in the unit of  $\frac{\text{eV}}{\text{Å}^2}$  for the bond stretching interactions, and in the unit of eV for the angle bending interaction. The fourth line gives the initial bond length (in unit of Å) for the bond stretching interaction and the initial angle (in unit of degrees) for the angle bending interaction. The angle  $\theta_{ijk}$  has atom i as the apex.

VFF type	bond stretching	angle bending	
expression	$\frac{1}{2}K_{\text{Ti-Te}}(\Delta r)^2$	$\frac{1}{2}K_{\text{Ti-Te-Te}}(\Delta\theta)^2$	$\frac{1}{2}K_{\text{Te-Ti-Ti}}(\Delta\theta)^2$
parameter	3.758	3.217	3.217
$r_0$ or $\theta_0$	2.730	83.621	83.621

TABLE CLXXI: Two-body SW potential parameters for single-layer 1T-TiTe<sub>2</sub> used by GULP<sup>8</sup> as expressed in Eq. (3).

	$A$ (eV)	$\rho$ (Å)	$B$ (Å <sup>4</sup> )	$r_{\min}$ (Å)	$r_{\max}$ (Å)
Ti-Te	3.542	1.213	27.773	0.0	3.640

1T-TiTe<sub>2</sub>.

The structure for the single-layer 1T-TiTe<sub>2</sub> is shown in Fig. 71 (with M=Ti and X=Te). Each Ti atom is surrounded by six Te atoms. These Te atoms are categorized into the top group (eg. atoms 1, 3, and 5) and bottom group (eg. atoms 2, 4, and 6). Each Te atom is connected to three Ti atoms. The structural parameters are from the first-principles calculations,<sup>12</sup> including the lattice constant  $a = 3.64$  Å and the bond length  $d_{\text{Ti-Te}} = 2.73$  Å. The resultant angles are  $\theta_{\text{TiTeTe}} = 83.621^\circ$  with Te atoms from the same (top or bottom)

TABLE CLXXII: Three-body SW potential parameters for single-layer 1T-TiTe<sub>2</sub> used by GULP<sup>8</sup> as expressed in Eq. (4). The angle  $\theta_{ijk}$  in the first line indicates the bending energy for the angle with atom i as the apex.

	$K$ (eV)	$\theta_0$ (degree)	$\rho_1$ (Å)	$\rho_2$ (Å)	$r_{\min12}$ (Å)	$r_{\max12}$ (Å)	$r_{\min13}$ (Å)	$r_{\max13}$ (Å)	$r_{\min23}$ (Å)	$r_{\max23}$ (Å)
$\theta_{\text{Ti-Te-Te}}$	23.439	83.621	1.213	1.213	0.0	3.640	0.0	3.640	0.0	4.972
$\theta_{\text{Te-Ti-Ti}}$	23.439	83.621	1.213	1.213	0.0	3.640	0.0	3.640	0.0	4.972

TABLE CLXXIII: SW potential parameters for single-layer 1T-TiTe<sub>2</sub> used by LAMMPS<sup>9</sup> as expressed in Eqs. (9) and (10).

	$\epsilon$ (eV)	$\sigma$ (Å)	$a$	$\lambda$	$\gamma$	$\cos \theta_0$	$A_L$	$B_L$	$p$	$q$	tol
Ti-Te-Te	1.000	1.213	3.000	23.439	1.000	0.111	3.542	12.814	4	0	0.0

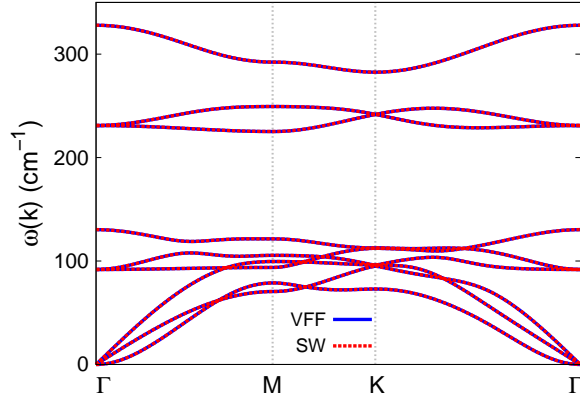


FIG. 85: (Color online) Phonon spectrum for single-layer 1T-TiTe<sub>2</sub> along the  $\Gamma$ MK $\Gamma$  direction in the Brillouin zone. The phonon dispersion from the SW potential is exactly the same as that from the VFF model.

group, and  $\theta_{\text{TeTiTi}} = 83.621^\circ$ .

Table CLXX shows three VFF terms for the single-layer 1T-TiTe<sub>2</sub>, one of which is the bond stretching interaction shown by Eq. (1) while the other two terms are the angle bending interaction shown by Eq. (2). We note that the angle bending term  $K_{\text{Ti-Te-Te}}$  is for the angle  $\theta_{\text{Ti-Te-Te}}$  with both Te atoms from the same (top or bottom) group. We find that there are actually only two parameters in the VFF model, so we can determine their value by fitting to the Young's modulus and the Poisson's ratio of the system. The *ab initio* calculations have predicted the Young's modulus to be 46 N/m and the Poisson's ratio as 0.15.<sup>48</sup>

The parameters for the two-body SW potential used by GULP are shown in Tab. CLXXI. The parameters for the three-body SW potential used by GULP are shown in Tab. CLXXII. Some representative parameters for the SW potential used by LAMMPS are listed in Tab. CLXXIII.

We use LAMMPS to perform MD simulations for the mechanical behavior of the single-layer 1T-TiTe<sub>2</sub> under uniaxial tension at 1.0 K and 300.0 K. Fig. 84 shows the stress-strain

curve for the tension of a single-layer 1T-TiTe<sub>2</sub> of dimension  $100 \times 100 \text{ \AA}$ . Periodic boundary conditions are applied in both armchair and zigzag directions. The single-layer 1T-TiTe<sub>2</sub> is stretched uniaxially along the armchair or zigzag direction. The stress is calculated without involving the actual thickness of the quasi-two-dimensional structure of the single-layer 1T-TiTe<sub>2</sub>. The Young's modulus can be obtained by a linear fitting of the stress-strain relation in the small strain range of  $[0, 0.01]$ . The Young's modulus are 41.4 N/m and 41.2 N/m along the armchair and zigzag directions, respectively. The Young's modulus is essentially isotropic in the armchair and zigzag directions. The Poisson's ratio from the VFF model and the SW potential is  $\nu_{xy} = \nu_{yx} = 0.15$ . The fitted Young's modulus value is about 10% smaller than the *ab initio* result of 46 N/m,<sup>48</sup> as only short-range interactions are considered in the present work. The long-range interactions are ignored, which typically leads to about 10% underestimation for the value of the Young's modulus.

There is no available value for nonlinear quantities in the single-layer 1T-TiTe<sub>2</sub>. We have thus used the nonlinear parameter  $B = 0.5d^4$  in Eq. (5), which is close to the value of  $B$  in most materials. The value of the third order nonlinear elasticity  $D$  can be extracted by fitting the stress-strain relation to the function  $\sigma = E\epsilon + \frac{1}{2}D\epsilon^2$  with  $E$  as the Young's modulus. The values of  $D$  from the present SW potential are -161.3 N/m and -181.4 N/m along the armchair and zigzag directions, respectively. The ultimate stress is about  $4.9 \text{ Nm}^{-1}$  at the ultimate strain of 0.22 in the armchair direction at the low temperature of 1 K. The ultimate stress is about  $4.7 \text{ Nm}^{-1}$  at the ultimate strain of 0.25 in the zigzag direction at the low temperature of 1 K.

Fig. 85 shows that the VFF model and the SW potential give exactly the same phonon dispersion, as the SW potential is derived from the VFF model.

#### **XLIV. 1T-VS<sub>2</sub>**

Most existing theoretical studies on the single-layer 1T-VS<sub>2</sub> are based on the first-principles calculations. In this section, we will develop the SW potential for the single-layer 1T-VS<sub>2</sub>.

The structure for the single-layer 1T-VS<sub>2</sub> is shown in Fig. 71 (with M=V and X=S). Each V atom is surrounded by six S atoms. These S atoms are categorized into the top group (eg. atoms 1, 3, and 5) and bottom group (eg. atoms 2, 4, and 6). Each S atom

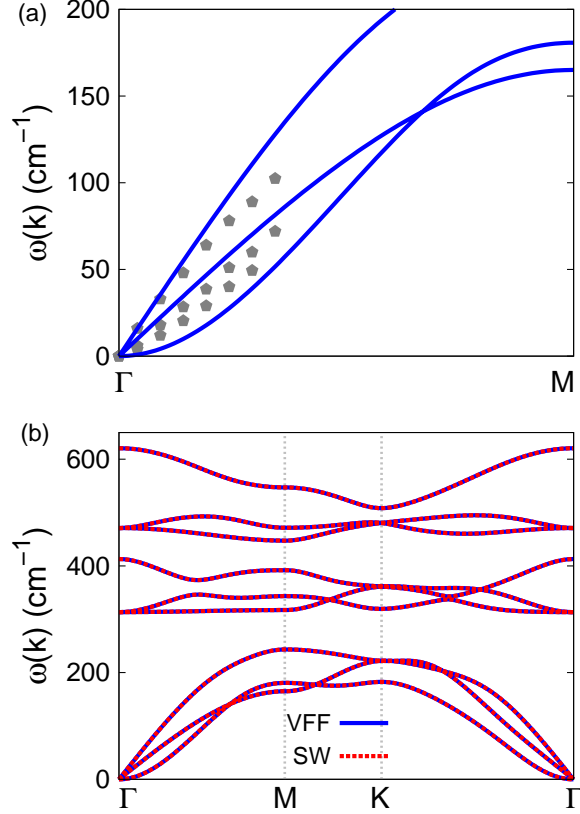


FIG. 86: (Color online) Phonon spectrum for single-layer 1T-VS<sub>2</sub>. (a) Phonon dispersion along the  $\Gamma$ M direction in the Brillouin zone. The results from the VFF model (lines) are comparable with the *ab initio* results (pentagons) from Ref. 12. (b) The phonon dispersion from the SW potential is exactly the same as that from the VFF model.

is connected to three V atoms. The structural parameters are from the first-principles calculations,<sup>12</sup> including the lattice constant  $a = 3.10 \text{ \AA}$  and the bond length  $d_{V-S} = 2.31 \text{ \AA}$ . The resultant angles are  $\theta_{VSS} = 84.288^\circ$  with S atoms from the same (top or bottom) group, and  $\theta_{SVV} = 84.288^\circ$ .

Table CLXXIV shows three VFF terms for the single-layer 1T-VS<sub>2</sub>, one of which is the bond stretching interaction shown by Eq. (1) while the other two terms are the angle bending interaction shown by Eq. (2). We note that the angle bending term  $K_{V-S-S}$  is for the angle  $\theta_{V-S-S}$  with both S atoms from the same (top or bottom) group. These force constant parameters are determined by fitting to the three acoustic branches in the phonon dispersion along the  $\Gamma$ M as shown in Fig. 86 (a). The *ab initio* calculations for the phonon

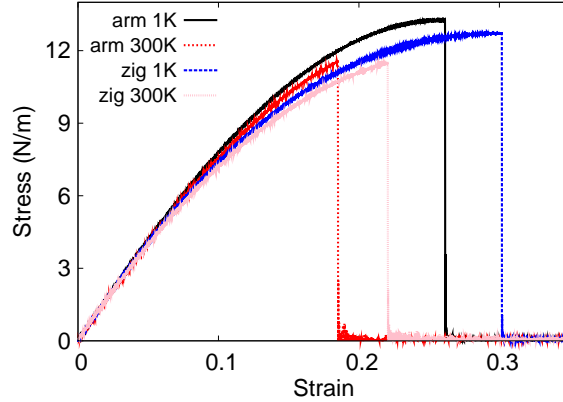


FIG. 87: (Color online) Stress-strain for single-layer 1T-VS<sub>2</sub> of dimension 100 × 100 Å along the armchair and zigzag directions.

TABLE CLXXIV: The VFF model for single-layer 1T-VS<sub>2</sub>. The second line gives an explicit expression for each VFF term. The third line is the force constant parameters. Parameters are in the unit of  $\frac{eV}{\text{Å}^2}$  for the bond stretching interactions, and in the unit of eV for the angle bending interaction. The fourth line gives the initial bond length (in unit of Å) for the bond stretching interaction and the initial angle (in unit of degrees) for the angle bending interaction. The angle  $\theta_{ijk}$  has atom *i* as the apex.

VFF type	bond stretching	angle bending	
expression	$\frac{1}{2}K_{V-S}(\Delta r)^2$	$\frac{1}{2}K_{V-S-S}(\Delta\theta)^2$	$\frac{1}{2}K_{S-V-V}(\Delta\theta)^2$
parameter	11.562	4.237	4.237
$r_0$ or $\theta_0$	2.310	84.288	84.288

dispersion are from Ref. 12. The lowest acoustic branch (flexural mode) is linear and very close to the inplane transverse acoustic branch in the *ab initio* calculations, which may due to the violation of the rigid rotational invariance.<sup>20</sup> Fig. 86 (b) shows that the VFF model and the SW potential give exactly the same phonon dispersion, as the SW potential is derived from the VFF model.

The parameters for the two-body SW potential used by GULP are shown in Tab. CLXXV. The parameters for the three-body SW potential used by GULP are shown in Tab. CLXXVI. Some representative parameters for the SW potential used by LAMMPS are listed in

TABLE CLXXV: Two-body SW potential parameters for single-layer 1T-VS<sub>2</sub> used by GULP<sup>8</sup> as expressed in Eq. (3).

	$A$ (eV)	$\rho$ (Å)	$B$ (Å <sup>4</sup> )	$r_{\min}$ (Å)	$r_{\max}$ (Å)
V-S	7.943	1.048	14.237	0.0	3.088

TABLE CLXXVI: Three-body SW potential parameters for single-layer 1T-VS<sub>2</sub> used by GULP<sup>8</sup> as expressed in Eq. (4). The angle  $\theta_{ijk}$  in the first line indicates the bending energy for the angle with atom  $i$  as the apex.

	$K$ (eV)	$\theta_0$ (degree)	$\rho_1$ (Å)	$\rho_2$ (Å)	$r_{\min12}$ (Å)	$r_{\max12}$ (Å)	$r_{\min13}$ (Å)	$r_{\max13}$ (Å)	$r_{\min23}$ (Å)	$r_{\max23}$ (Å)
$\theta_{V-S-S}$	31.659	84.288	1.048	1.048	0.0	3.088	0.0	3.088	0.0	4.235
$\theta_{S-V-V}$	31.659	84.288	1.048	1.048	0.0	3.088	0.0	3.088	0.0	4.235

Tab. CLXXVII.

We use LAMMPS to perform MD simulations for the mechanical behavior of the single-layer 1T-VS<sub>2</sub> under uniaxial tension at 1.0 K and 300.0 K. Fig. 87 shows the stress-strain curve for the tension of a single-layer 1T-VS<sub>2</sub> of dimension  $100 \times 100$  Å. Periodic boundary conditions are applied in both armchair and zigzag directions. The single-layer 1T-VS<sub>2</sub> is stretched uniaxially along the armchair or zigzag direction. The stress is calculated without involving the actual thickness of the quasi-two-dimensional structure of the single-layer 1T-VS<sub>2</sub>. The Young's modulus can be obtained by a linear fitting of the stress-strain relation in the small strain range of  $[0, 0.01]$ . The Young's modulus are 87.1 N/m and 86.8 N/m along the armchair and zigzag directions, respectively. The Young's modulus is essentially isotropic in the armchair and zigzag directions. The Poisson's ratio from the VFF model and the SW potential is  $\nu_{xy} = \nu_{yx} = 0.21$ .

There is no available value for nonlinear quantities in the single-layer 1T-VS<sub>2</sub>. We have thus used the nonlinear parameter  $B = 0.5d^4$  in Eq. (5), which is close to the value of  $B$  in

TABLE CLXXVII: SW potential parameters for single-layer 1T-VS<sub>2</sub> used by LAMMPS<sup>9</sup> as expressed in Eqs. (9) and (10).

	$\epsilon$ (eV)	$\sigma$ (Å)	$a$	$\lambda$	$\gamma$	$\cos \theta_0$	$A_L$	$B_L$	$p$	$q$	tol
V-S <sub>1</sub> -S <sub>1</sub>	1.000	1.048	2.946	31.659	1.000	0.100	7.943	11.797	4	0	0.0

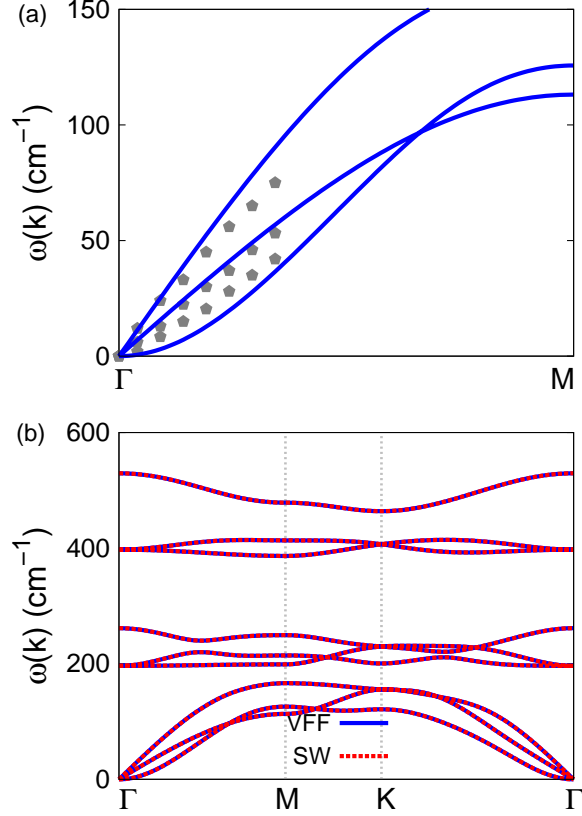


FIG. 88: (Color online) Phonon spectrum for single-layer 1T-VSe<sub>2</sub>. (a) Phonon dispersion along the  $\Gamma$ M direction in the Brillouin zone. The results from the VFF model (lines) are comparable with the experiment data (pentagons) from Ref. 12. (b) The phonon dispersion from the SW potential is exactly the same as that from the VFF model.

most materials. The value of the third order nonlinear elasticity  $D$  can be extracted by fitting the stress-strain relation to the function  $\sigma = E\epsilon + \frac{1}{2}D\epsilon^2$  with  $E$  as the Young's modulus. The values of  $D$  from the present SW potential are -230.5 N/m and -283.6 N/m along the armchair and zigzag directions, respectively. The ultimate stress is about  $13.3 \text{ Nm}^{-1}$  at the ultimate strain of 0.26 in the armchair direction at the low temperature of 1 K. The ultimate stress is about  $12.7 \text{ Nm}^{-1}$  at the ultimate strain of 0.30 in the zigzag direction at the low temperature of 1 K.

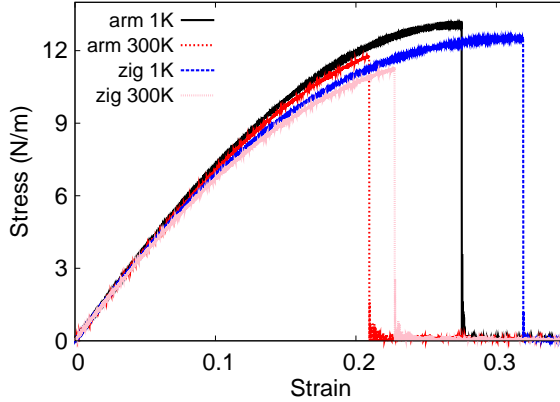


FIG. 89: (Color online) Stress-strain for single-layer 1T-VSe<sub>2</sub> of dimension 100 × 100 Å along the armchair and zigzag directions.

TABLE CLXXVIII: The VFF model for single-layer 1T-VSe<sub>2</sub>. The second line gives an explicit expression for each VFF term. The third line is the force constant parameters. Parameters are in the unit of  $\frac{eV}{\text{Å}^2}$  for the bond stretching interactions, and in the unit of eV for the angle bending interaction. The fourth line gives the initial bond length (in unit of Å) for the bond stretching interaction and the initial angle (in unit of degrees) for the angle bending interaction. The angle  $\theta_{ijk}$  has atom *i* as the apex.

VFF type	bond stretching	angle bending	
expression	$\frac{1}{2}K_{V-Se}(\Delta r)^2$	$\frac{1}{2}K_{V-Se-Se}(\Delta\theta)^2$	$\frac{1}{2}K_{Se-V-V}(\Delta\theta)^2$
parameter	11.562	4.237	4.237
$r_0$ or $\theta_0$	2.440	83.201	83.201

#### XLV. 1T-VSE<sub>2</sub>

Most existing theoretical studies on the single-layer 1T-VSe<sub>2</sub> are based on the first-principles calculations. In this section, we will develop the SW potential for the single-layer 1T-VSe<sub>2</sub>.

The structure for the single-layer 1T-VSe<sub>2</sub> is shown in Fig. 71 (with M=V and X=Se). Each V atom is surrounded by six Se atoms. These Se atoms are categorized into the top group (eg. atoms 1, 3, and 5) and bottom group (eg. atoms 2, 4, and 6). Each Se atom is connected to three V atoms. The structural parameters are from the first-principles

TABLE CLXXIX: Two-body SW potential parameters for single-layer 1T-VSe<sub>2</sub> used by GULP<sup>8</sup> as expressed in Eq. (3).

	$A$ (eV)	$\rho$ (Å)	$B$ (Å <sup>4</sup> )	$r_{\min}$ (Å)	$r_{\max}$ (Å)
V-Se	8.606	1.070	17.723	0.0	3.248

TABLE CLXXX: Three-body SW potential parameters for single-layer 1T-VSe<sub>2</sub> used by GULP<sup>8</sup> as expressed in Eq. (4). The angle  $\theta_{ijk}$  in the first line indicates the bending energy for the angle with atom  $i$  as the apex.

	$K$ (eV)	$\theta_0$ (degree)	$\rho_1$ (Å)	$\rho_2$ (Å)	$r_{\min12}$ (Å)	$r_{\max12}$ (Å)	$r_{\min13}$ (Å)	$r_{\max13}$ (Å)	$r_{\min23}$ (Å)	$r_{\max23}$ (Å)
$\theta_{V-Se-Se}$	30.387	83.201	1.070	1.070	0.0	3.248	0.0	3.248	0.0	4.426
$\theta_{Se-V-V}$	30.387	83.201	1.070	1.070	0.0	3.248	0.0	3.248	0.0	4.426

calculations,<sup>12</sup> including the lattice constant  $a = 3.24$  Å and the bond length  $d_{V-Se} = 2.44$  Å. The resultant angles are  $\theta_{VSeSe} = 83.201^\circ$  with Se atoms from the same (top or bottom) group, and  $\theta_{SeVV} = 83.201^\circ$ .

Table CLXXVIII shows three VFF terms for the single-layer 1T-VSe<sub>2</sub>, one of which is the bond stretching interaction shown by Eq. (1) while the other two terms are the angle bending interaction shown by Eq. (2). We note that the angle bending term  $K_{V-Se-Se}$  is for the angle  $\theta_{V-Se-Se}$  with both Se atoms from the same (top or bottom) group. These force constant parameters are determined by fitting to the three acoustic branches in the phonon dispersion along the  $\Gamma M$  as shown in Fig. 88 (a). The *ab initio* calculations for the phonon dispersion are from Ref. 12. The lowest acoustic branch (flexural mode) is almost linear in the *ab initio* calculations, which may due to the violation of the rigid rotational invariance.<sup>20</sup> Fig. 88 (b) shows that the VFF model and the SW potential give exactly the same phonon dispersion, as the SW potential is derived from the VFF model.

The parameters for the two-body SW potential used by GULP are shown in

TABLE CLXXXI: SW potential parameters for single-layer 1T-VSe<sub>2</sub> used by LAMMPS<sup>9</sup> as expressed in Eqs. (9) and (10).

	$\epsilon$ (eV)	$\sigma$ (Å)	$a$	$\lambda$	$\gamma$	$\cos \theta_0$	$A_L$	$B_L$	$p$	$q$	tol
V-Se <sub>1</sub> -Se <sub>1</sub>	1.000	1.070	3.035	30.387	1.000	0.118	8.606	13.507	4	0	0.0

Tab. CLXXIX. The parameters for the three-body SW potential used by GULP are shown in Tab. CLXXX. Some representative parameters for the SW potential used by LAMMPS are listed in Tab. CLXXXI.

We use LAMMPS to perform MD simulations for the mechanical behavior of the single-layer 1T-VSe<sub>2</sub> under uniaxial tension at 1.0 K and 300.0 K. Fig. 89 shows the stress-strain curve for the tension of a single-layer 1T-VSe<sub>2</sub> of dimension 100 × 100 Å. Periodic boundary conditions are applied in both armchair and zigzag directions. The single-layer 1T-VSe<sub>2</sub> is stretched uniaxially along the armchair or zigzag direction. The stress is calculated without involving the actual thickness of the quasi-two-dimensional structure of the single-layer 1T-VSe<sub>2</sub>. The Young's modulus can be obtained by a linear fitting of the stress-strain relation in the small strain range of [0, 0.01]. The Young's modulus are 78.4 N/m and 78.1 N/m along the armchair and zigzag directions, respectively. The Young's modulus is essentially isotropic in the armchair and zigzag directions. The Poisson's ratio from the VFF model and the SW potential is  $\nu_{xy} = \nu_{yx} = 0.22$ .

There is no available value for nonlinear quantities in the single-layer 1T-VSe<sub>2</sub>. We have thus used the nonlinear parameter  $B = 0.5d^4$  in Eq. (5), which is close to the value of  $B$  in most materials. The value of the third order nonlinear elasticity  $D$  can be extracted by fitting the stress-strain relation to the function  $\sigma = E\epsilon + \frac{1}{2}D\epsilon^2$  with  $E$  as the Young's modulus. The values of  $D$  from the present SW potential are -168.5 N/m and -218.6 N/m along the armchair and zigzag directions, respectively. The ultimate stress is about 13.1 Nm<sup>-1</sup> at the ultimate strain of 0.27 in the armchair direction at the low temperature of 1 K. The ultimate stress is about 12.5 Nm<sup>-1</sup> at the ultimate strain of 0.32 in the zigzag direction at the low temperature of 1 K.

## XLVI. 1T-VTe<sub>2</sub>

Most existing theoretical studies on the single-layer 1T-VTe<sub>2</sub> are based on the first-principles calculations. In this section, we will develop the SW potential for the single-layer 1T-VTe<sub>2</sub>.

The structure for the single-layer 1T-VTe<sub>2</sub> is shown in Fig. 71 (with M=V and X=Te). Each V atom is surrounded by six Te atoms. These Te atoms are categorized into the top group (eg. atoms 1, 3, and 5) and bottom group (eg. atoms 2, 4, and 6). Each Te

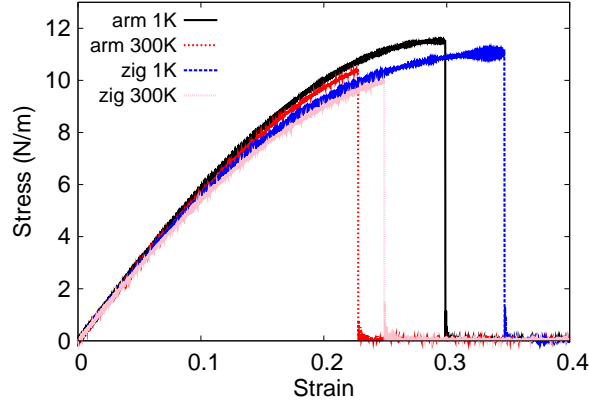


FIG. 90: (Color online) Stress-strain for single-layer 1T-VTe<sub>2</sub> of dimension  $100 \times 100 \text{ \AA}$  along the armchair and zigzag directions.

TABLE CLXXXII: The VFF model for single-layer 1T-VTe<sub>2</sub>. The second line gives an explicit expression for each VFF term. The third line is the force constant parameters. Parameters are in the unit of  $\frac{\text{eV}}{\text{\AA}^2}$  for the bond stretching interactions, and in the unit of eV for the angle bending interaction. The fourth line gives the initial bond length (in unit of  $\text{\AA}$ ) for the bond stretching interaction and the initial angle (in unit of degrees) for the angle bending interaction. The angle  $\theta_{ijk}$  has atom  $i$  as the apex.

VFF type	bond stretching	angle bending	
expression	$\frac{1}{2}K_{\text{V-Te}}(\Delta r)^2$	$\frac{1}{2}K_{\text{V-Te-Te}}(\Delta\theta)^2$	$\frac{1}{2}K_{\text{Te-V-V}}(\Delta\theta)^2$
parameter	10.476	3.814	3.814
$r_0$ or $\theta_0$	2.640	81.885	81.885

atom is connected to three V atoms. The structural parameters are from the first-principles calculations,<sup>12</sup> including the lattice constant  $a = 3.46 \text{ \AA}$  and the bond length  $d_{\text{V-Te}} = 2.64 \text{ \AA}$ . The resultant angles are  $\theta_{\text{VTeTe}} = 81.885^\circ$  with Te atoms from the same (top or bottom) group, and  $\theta_{\text{TeVV}} = 81.885^\circ$ .

Table CLXXXII shows three VFF terms for the single-layer 1T-VTe<sub>2</sub>, one of which is the bond stretching interaction shown by Eq. (1) while the other two terms are the angle bending interaction shown by Eq. (2). We note that the angle bending term  $K_{\text{V-Te-Te}}$  is for the angle  $\theta_{\text{V-Te-Te}}$  with both Te atoms from the same (top or bottom) group. We find

TABLE CLXXXIII: Two-body SW potential parameters for single-layer 1T-VTe<sub>2</sub> used by GULP<sup>8</sup> as expressed in Eq. (3).

	$A$ (eV)	$\rho$ (Å)	$B$ (Å <sup>4</sup> )	$r_{\min}$ (Å)	$r_{\max}$ (Å)
V-Te	8.805	1.110	24.288	0.0	3.496

TABLE CLXXXIV: Three-body SW potential parameters for single-layer 1T-VTe<sub>2</sub> used by GULP<sup>8</sup> as expressed in Eq. (4). The angle  $\theta_{ijk}$  in the first line indicates the bending energy for the angle with atom  $i$  as the apex.

	$K$ (eV)	$\theta_0$ (degree)	$\rho_1$ (Å)	$\rho_2$ (Å)	$r_{\min12}$ (Å)	$r_{\max12}$ (Å)	$r_{\min13}$ (Å)	$r_{\max13}$ (Å)	$r_{\min23}$ (Å)	$r_{\max23}$ (Å)
$\theta_{V-Te-Te}$	26.043	81.885	1.110	1.110	0.0	3.496	0.0	3.496	0.0	4.726
$\theta_{Te-V-V}$	26.043	81.885	1.110	1.110	0.0	3.496	0.0	3.496	0.0	4.726

that there are actually only two parameters in the VFF model, so we can determine their value by fitting to the Young's modulus and the Poisson's ratio of the system. The *ab initio* calculations have predicted the Young's modulus to be 67 N/m and the Poisson's ratio as 0.24.<sup>48</sup>

The parameters for the two-body SW potential used by GULP are shown in Tab. CLXXXIII. The parameters for the three-body SW potential used by GULP are shown in Tab. CLXXXIV. Some representative parameters for the SW potential used by LAMMPS are listed in Tab. CLXXXV.

We use LAMMPS to perform MD simulations for the mechanical behavior of the single-layer 1T-VTe<sub>2</sub> under uniaxial tension at 1.0 K and 300.0 K. Fig. 90 shows the stress-strain curve for the tension of a single-layer 1T-VTe<sub>2</sub> of dimension  $100 \times 100$  Å. Periodic boundary conditions are applied in both armchair and zigzag directions. The single-layer 1T-VTe<sub>2</sub> is stretched uniaxially along the armchair or zigzag direction. The stress is calculated without involving the actual thickness of the quasi-two-dimensional structure of the single-layer 1T-

TABLE CLXXXV: SW potential parameters for single-layer 1T-VTe<sub>2</sub> used by LAMMPS<sup>9</sup> as expressed in Eqs. (9) and (10).

	$\epsilon$ (eV)	$\sigma$ (Å)	$a$	$\lambda$	$\gamma$	$\cos \theta_0$	$A_L$	$B_L$	$p$	$q$	tol
V-Te <sub>1</sub> -Te <sub>1</sub>	1.000	1.110	3.149	26.043	1.000	0.141	8.805	15.980	4	0	0.0

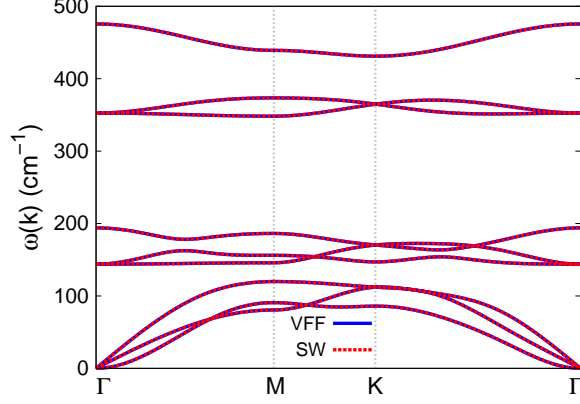


FIG. 91: (Color online) Phonon spectrum for single-layer 1T-VTe<sub>2</sub> along the  $\Gamma$ MK $\Gamma$  direction in the Brillouin zone. The phonon dispersion from the SW potential is exactly the same as that from the VFF model.

VTe<sub>2</sub>. The Young's modulus can be obtained by a linear fitting of the stress-strain relation in the small strain range of  $[0, 0.01]$ . The Young's modulus are 61.2 N/m and 61.0 N/m along the armchair and zigzag directions, respectively. The Young's modulus is essentially isotropic in the armchair and zigzag directions. The Poisson's ratio from the VFF model and the SW potential is  $\nu_{xy} = \nu_{yx} = 0.24$ . The fitted Young's modulus value is about 10% smaller than the *ab initio* result of 67 N/m,<sup>48</sup> as only short-range interactions are considered in the present work. The long-range interactions are ignored, which typically leads to about 10% underestimation for the value of the Young's modulus.

There is no available value for nonlinear quantities in the single-layer 1T-VTe<sub>2</sub>. We have thus used the nonlinear parameter  $B = 0.5d^4$  in Eq. (5), which is close to the value of  $B$  in most materials. The value of the third order nonlinear elasticity  $D$  can be extracted by fitting the stress-strain relation to the function  $\sigma = E\epsilon + \frac{1}{2}D\epsilon^2$  with  $E$  as the Young's modulus. The values of  $D$  from the present SW potential are -95.8 N/m and -135.6 N/m along the armchair and zigzag directions, respectively. The ultimate stress is about 11.5 Nm<sup>-1</sup> at the ultimate strain of 0.30 in the armchair direction at the low temperature of 1 K. The ultimate stress is about 11.0 Nm<sup>-1</sup> at the ultimate strain of 0.34 in the zigzag direction at the low temperature of 1 K.

Fig. 91 shows that the VFF model and the SW potential give exactly the same phonon dispersion, as the SW potential is derived from the VFF model.

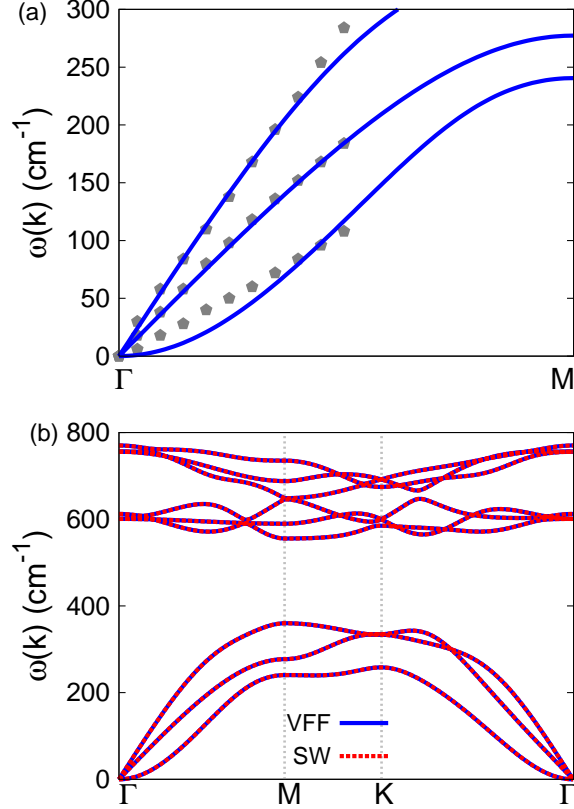


FIG. 92: (Color online) Phonon spectrum for single-layer 1T-MnO<sub>2</sub>. (a) Phonon dispersion along the  $\Gamma$ M direction in the Brillouin zone. The results from the VFF model (lines) are comparable with the *ab initio* results (pentagons) from Ref. 12. (b) The phonon dispersion from the SW potential is exactly the same as that from the VFF model.

## XLVII. 1T-MNO<sub>2</sub>

Most existing theoretical studies on the single-layer 1T-MnO<sub>2</sub> are based on the first-principles calculations. In this section, we will develop the SW potential for the single-layer 1T-MnO<sub>2</sub>.

The structure for the single-layer 1T-MnO<sub>2</sub> is shown in Fig. 71 (with M=Mn and X=O). Each Mn atom is surrounded by six O atoms. These O atoms are categorized into the top group (eg. atoms 1, 3, and 5) and bottom group (eg. atoms 2, 4, and 6). Each O atom is connected to three Mn atoms. The structural parameters are from the first-principles calculations,<sup>12</sup> including the lattice constant  $a = 2.82 \text{ \AA}$  and the bond length

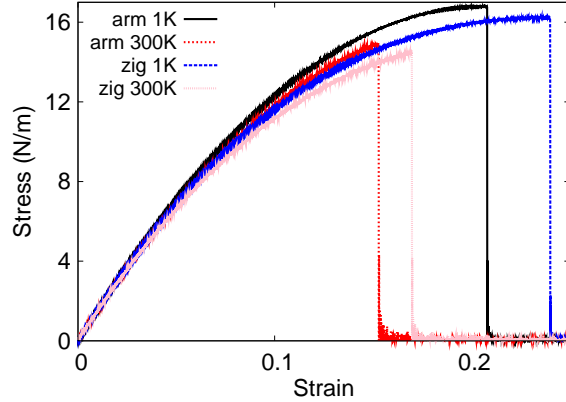


FIG. 93: (Color online) Stress-strain for single-layer 1T-MnO<sub>2</sub> of dimension  $100 \times 100 \text{ \AA}$  along the armchair and zigzag directions.

TABLE CLXXXVI: The VFF model for single-layer 1T-MnO<sub>2</sub>. The second line gives an explicit expression for each VFF term. The third line is the force constant parameters. Parameters are in the unit of  $\frac{\text{eV}}{\text{\AA}^2}$  for the bond stretching interactions, and in the unit of eV for the angle bending interaction. The fourth line gives the initial bond length (in unit of  $\text{\AA}$ ) for the bond stretching interaction and the initial angle (in unit of degrees) for the angle bending interaction. The angle  $\theta_{ijk}$  has atom  $i$  as the apex.

VFF type	bond stretching	angle bending	
expression	$\frac{1}{2}K_{\text{Mn-O}}(\Delta r)^2$	$\frac{1}{2}K_{\text{Mn-O-O}}(\Delta\theta)^2$	$\frac{1}{2}K_{\text{O-Mn-Mn}}(\Delta\theta)^2$
parameter	15.371	4.822	4.822
$r_0$ or $\theta_0$	1.88	97.181	97.181

$d_{\text{Mn-O}} = 1.88 \text{ \AA}$ . The resultant angles are  $\theta_{\text{MnOO}} = 97.181^\circ$  with O atoms from the same (top or bottom) group, and  $\theta_{\text{OMnMn}} = 97.181^\circ$ .

Table CLXXXVI shows three VFF terms for the single-layer 1T-MnO<sub>2</sub>, one of which is the bond stretching interaction shown by Eq. (1) while the other two terms are the angle bending interaction shown by Eq. (2). We note that the angle bending term  $K_{\text{Mn-O-O}}$  is for the angle  $\theta_{\text{Mn-O-O}}$  with both O atoms from the same (top or bottom) group. These force constant parameters are determined by fitting to the two in-plane acoustic branches in the phonon dispersion along the  $\Gamma\text{M}$  as shown in Fig. 92 (a). The *ab initio* calculations for the

TABLE CLXXXVII: Two-body SW potential parameters for single-layer 1T-MnO<sub>2</sub> used by GULP<sup>8</sup> as expressed in Eq. (3).

	$A$ (eV)	$\rho$ (Å)	$B$ (Å <sup>4</sup> )	$r_{\min}$ (Å)	$r_{\max}$ (Å)
Mn-O	9.675	1.212	6.246	0.0	2.635

TABLE CLXXXVIII: Three-body SW potential parameters for single-layer 1T-MnO<sub>2</sub> used by GULP<sup>8</sup> as expressed in Eq. (4). The angle  $\theta_{ijk}$  in the first line indicates the bending energy for the angle with atom  $i$  as the apex.

	$K$ (eV)	$\theta_0$ (degree)	$\rho_1$ (Å)	$\rho_2$ (Å)	$r_{\min12}$ (Å)	$r_{\max12}$ (Å)	$r_{\min13}$ (Å)	$r_{\max13}$ (Å)	$r_{\min23}$ (Å)	$r_{\max23}$ (Å)
$\theta_{\text{Mn-O-O}}$	60.755	97.181	1.212	1.212	0.0	2.635	0.0	2.635	0.0	3.852
$\theta_{\text{O-Mn-Mn}}$	60.755	97.181	1.212	1.212	0.0	2.635	0.0	2.635	0.0	3.852

phonon dispersion are from Ref. 12. Fig. 92 (b) shows that the VFF model and the SW potential give exactly the same phonon dispersion, as the SW potential is derived from the VFF model.

The parameters for the two-body SW potential used by GULP are shown in Tab. CLXXXVII. The parameters for the three-body SW potential used by GULP are shown in Tab. CLXXXVIII. Some representative parameters for the SW potential used by LAMMPS are listed in Tab. CLXXXIX.

We use LAMMPS to perform MD simulations for the mechanical behavior of the single-layer 1T-MnO<sub>2</sub> under uniaxial tension at 1.0 K and 300.0 K. Fig. 93 shows the stress-strain curve for the tension of a single-layer 1T-MnO<sub>2</sub> of dimension  $100 \times 100$  Å. Periodic boundary conditions are applied in both armchair and zigzag directions. The single-layer 1T-MnO<sub>2</sub> is stretched uniaxially along the armchair or zigzag direction. The stress is calculated without involving the actual thickness of the quasi-two-dimensional structure of the single-layer 1T-MnO<sub>2</sub>. The Young's modulus can be obtained by a linear fitting of the stress-strain relation

TABLE CLXXXIX: SW potential parameters for single-layer 1T-MnO<sub>2</sub> used by LAMMPS<sup>9</sup> as expressed in Eqs. (9) and (10).

	$\epsilon$ (eV)	$\sigma$ (Å)	$a$	$\lambda$	$\gamma$	$\cos \theta_0$	$A_L$	$B_L$	$p$	$q$	tol
Mn-O <sub>1</sub> -O <sub>1</sub>	1.000	1.212	2.175	60.755	1.000	-0.125	9.675	2.899	4	0	0.0

TABLE CXC: The VFF model for single-layer 1T-MnS<sub>2</sub>. The second line gives an explicit expression for each VFF term. The third line is the force constant parameters. Parameters are in the unit of  $\frac{eV}{\text{Å}^2}$  for the bond stretching interactions, and in the unit of eV for the angle bending interaction. The fourth line gives the initial bond length (in unit of Å) for the bond stretching interaction and the initial angle (in unit of degrees) for the angle bending interaction. The angle  $\theta_{ijk}$  has atom  $i$  as the apex.

VFF type	bond stretching	angle bending	
expression	$\frac{1}{2}K_{\text{Mn-S}}(\Delta r)^2$	$\frac{1}{2}K_{\text{Mn-S-S}}(\Delta\theta)^2$	$\frac{1}{2}K_{\text{S-Mn-Mn}}(\Delta\theta)^2$
parameter	4.407	2.399	2.399
$r_0$ or $\theta_0$	2.27	86.822	86.822

in the small strain range of  $[0, 0.01]$ . The Young's modulus are 156.3 N/m and 155.4 N/m along the armchair and zigzag directions, respectively. The Young's modulus is essentially isotropic in the armchair and zigzag directions. The Poisson's ratio from the VFF model and the SW potential is  $\nu_{xy} = \nu_{yx} = 0.12$ .

There is no available value for nonlinear quantities in the single-layer 1T-MnO<sub>2</sub>. We have thus used the nonlinear parameter  $B = 0.5d^4$  in Eq. (5), which is close to the value of  $B$  in most materials. The value of the third order nonlinear elasticity  $D$  can be extracted by fitting the stress-strain relation to the function  $\sigma = E\epsilon + \frac{1}{2}D\epsilon^2$  with  $E$  as the Young's modulus. The values of  $D$  from the present SW potential are -711.7 N/m and -756.1 N/m along the armchair and zigzag directions, respectively. The ultimate stress is about 16.8 Nm<sup>-1</sup> at the ultimate strain of 0.21 in the armchair direction at the low temperature of 1 K. The ultimate stress is about 16.2 Nm<sup>-1</sup> at the ultimate strain of 0.24 in the zigzag direction at the low temperature of 1 K.

### XLVIII. 1T-MNS<sub>2</sub>

Most existing theoretical studies on the single-layer 1T-MnS<sub>2</sub> are based on the first-principles calculations. In this section, we will develop the SW potential for the single-layer 1T-MnS<sub>2</sub>.

The structure for the single-layer 1T-MnS<sub>2</sub> is shown in Fig. 71 (with M=Mn and X=S).

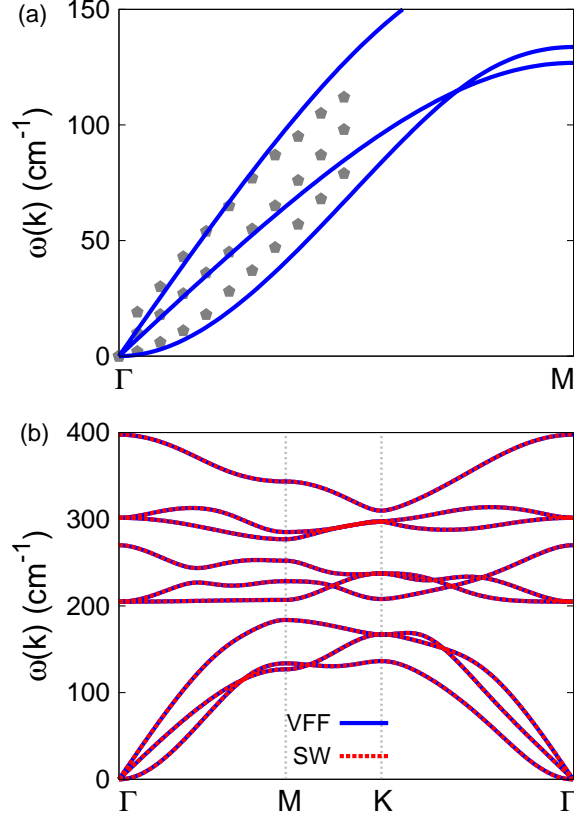


FIG. 94: (Color online) Phonon spectrum for single-layer 1T-MnS<sub>2</sub>. (a) Phonon dispersion along the  $\Gamma$ M direction in the Brillouin zone. The results from the VFF model (lines) are comparable with the *ab initio* results (pentagons) from Ref. 12. (b) The phonon dispersion from the SW potential is exactly the same as that from the VFF model.

TABLE CXCI: Two-body SW potential parameters for single-layer 1T-MnS<sub>2</sub> used by GULP<sup>8</sup> as expressed in Eq. (3).

	$A$ (eV)	$\rho$ ( $\text{\AA}$ )	$B$ ( $\text{\AA}^4$ )	$r_{\min}$ ( $\text{\AA}$ )	$r_{\max}$ ( $\text{\AA}$ )
Mn-S	3.127	1.111	13.276	0.0	3.064

Each Mn atom is surrounded by six S atoms. These S atoms are categorized into the top group (eg. atoms 1, 3, and 5) and bottom group (eg. atoms 2, 4, and 6). Each S atom is connected to three Mn atoms. The structural parameters are from the first-principles calculations,<sup>12</sup> including the lattice constant  $a = 3.12 \text{ \AA}$  and the bond length  $d_{\text{Mn-S}} = 2.27 \text{ \AA}$ . The resultant angles are  $\theta_{\text{MnSS}} = 86.822^\circ$  with S atoms from the same (top or bottom) group,

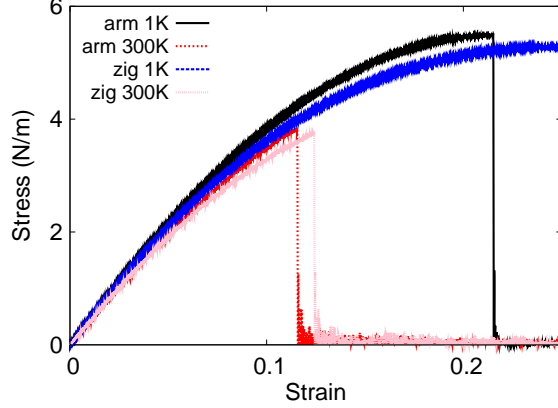


FIG. 95: (Color online) Stress-strain for single-layer 1T-MnS<sub>2</sub> of dimension  $100 \times 100 \text{ \AA}$  along the armchair and zigzag directions.

TABLE CXCI: Three-body SW potential parameters for single-layer 1T-MnS<sub>2</sub> used by GULP<sup>8</sup> as expressed in Eq. (4). The angle  $\theta_{ijk}$  in the first line indicates the bending energy for the angle with atom  $i$  as the apex.

	$K$ (eV)	$\theta_0$ (degree)	$\rho_1$ (Å)	$\rho_2$ (Å)	$r_{\min 12}$ (Å)	$r_{\max 12}$ (Å)	$r_{\min 13}$ (Å)	$r_{\max 13}$ (Å)	$r_{\min 23}$ (Å)	$r_{\max 23}$ (Å)
$\theta_{\text{Mn-S-S}}$	19.765	86.822	1.111	1.111	0.0	3.064	0.0	3.064	0.0	4.262
$\theta_{\text{S-Mn-Mn}}$	19.765	86.822	1.111	1.111	0.0	3.064	0.0	3.064	0.0	4.262

and  $\theta_{\text{SMnMn}} = 86.822^\circ$ .

Table CXC shows three VFF terms for the single-layer 1T-MnS<sub>2</sub>, one of which is the bond stretching interaction shown by Eq. (1) while the other two terms are the angle bending interaction shown by Eq. (2). We note that the angle bending term  $K_{\text{Mn-S-S}}$  is for the angle  $\theta_{\text{Mn-S-S}}$  with both S atoms from the same (top or bottom) group. These force constant parameters are determined by fitting to the acoustic branches in the phonon dispersion along the  $\Gamma\text{M}$  as shown in Fig. 94 (a). The *ab initio* calculations for the phonon dispersion

TABLE CXCI: SW potential parameters for single-layer 1T-MnS<sub>2</sub> used by LAMMPS<sup>9</sup> as expressed in Eqs. (9) and (10).

	$\epsilon$ (eV)	$\sigma$ (Å)	$a$	$\lambda$	$\gamma$	$\cos \theta_0$	$A_L$	$B_L$	$p$	$q$	tol
Mn-S <sub>1</sub> -S <sub>1</sub>	1.000	1.111	2.757	19.765	1.000	0.055	3.127	8.700	4	0	0.0

are from Ref. 12. Fig. 94 (b) shows that the VFF model and the SW potential give exactly the same phonon dispersion, as the SW potential is derived from the VFF model.

The parameters for the two-body SW potential used by GULP are shown in Tab. CXCI. The parameters for the three-body SW potential used by GULP are shown in Tab. CXCII. Some representative parameters for the SW potential used by LAMMPS are listed in Tab. CXCIII.

We use LAMMPS to perform MD simulations for the mechanical behavior of the single-layer 1T-MnS<sub>2</sub> under uniaxial tension at 1.0 K and 300.0 K. Fig. 95 shows the stress-strain curve for the tension of a single-layer 1T-MnS<sub>2</sub> of dimension 100 × 100 Å. Periodic boundary conditions are applied in both armchair and zigzag directions. The single-layer 1T-MnS<sub>2</sub> is stretched uniaxially along the armchair or zigzag direction. The stress is calculated without involving the actual thickness of the quasi-two-dimensional structure of the single-layer 1T-MnS<sub>2</sub>. The Young's modulus can be obtained by a linear fitting of the stress-strain relation in the small strain range of [0, 0.01]. The Young's modulus are 47.1 N/m and 46.8 N/m along the armchair and zigzag directions, respectively. The Young's modulus is essentially isotropic in the armchair and zigzag directions. The Poisson's ratio from the VFF model and the SW potential is  $\nu_{xy} = \nu_{yx} = 0.15$ .

There is no available value for nonlinear quantities in the single-layer 1T-MnS<sub>2</sub>. We have thus used the nonlinear parameter  $B = 0.5d^4$  in Eq. (5), which is close to the value of  $B$  in most materials. The value of the third order nonlinear elasticity  $D$  can be extracted by fitting the stress-strain relation to the function  $\sigma = E\epsilon + \frac{1}{2}D\epsilon^2$  with  $E$  as the Young's modulus. The values of  $D$  from the present SW potential are -193.8 N/m and -210.1 N/m along the armchair and zigzag directions, respectively. The ultimate stress is about 5.5 Nm<sup>-1</sup> at the ultimate strain of 0.21 in the armchair direction at the low temperature of 1 K. The ultimate stress is about 5.3 Nm<sup>-1</sup> at the ultimate strain of 0.25 in the zigzag direction at the low temperature of 1 K.

## XLIX. 1T-MNSE<sub>2</sub>

Most existing theoretical studies on the single-layer 1T-MnSe<sub>2</sub> are based on the first-principles calculations. In this section, we will develop the SW potential for the single-layer 1T-MnSe<sub>2</sub>.

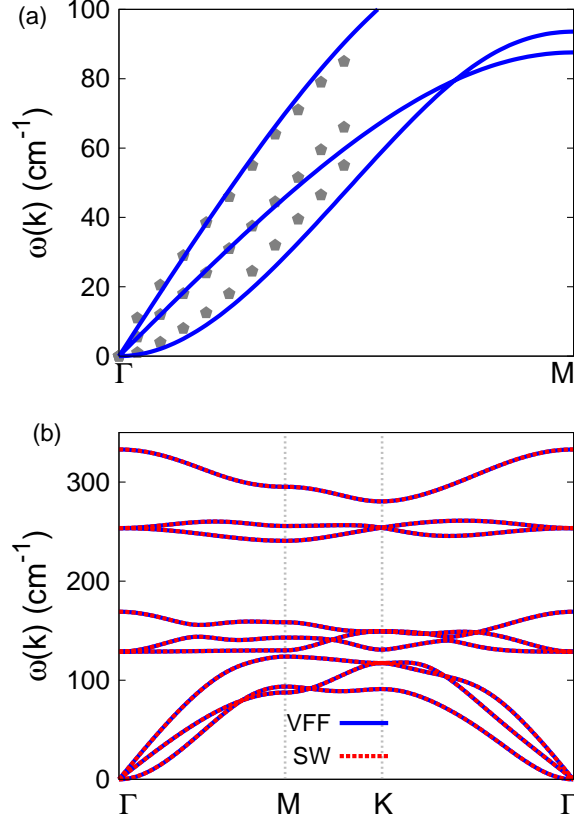


FIG. 96: (Color online) Phonon spectrum for single-layer 1T-MnSe<sub>2</sub>. (a) Phonon dispersion along the  $\Gamma$ M direction in the Brillouin zone. The results from the VFF model (lines) are comparable with the *ab initio* results (pentagons) from Ref. 12. (b) The phonon dispersion from the SW potential is exactly the same as that from the VFF model.

The structure for the single-layer 1T-MnSe<sub>2</sub> is shown in Fig. 71 (with M=Mn and X=Se). Each Mn atom is surrounded by six Se atoms. These Se atoms are categorized into the top group (eg. atoms 1, 3, and 5) and bottom group (eg. atoms 2, 4, and 6). Each Se atom is connected to three Mn atoms. The structural parameters are from the first-principles calculations,<sup>12</sup> including the lattice constant  $a = 3.27 \text{ \AA}$  and the bond length  $d_{\text{Mn-Se}} = 2.39 \text{ \AA}$ . The resultant angles are  $\theta_{\text{MnSeSe}} = 86.330^\circ$  with Se atoms from the same (top or bottom) group, and  $\theta_{\text{SeMnMn}} = 86.330^\circ$ .

Table CXCIV shows three VFF terms for the single-layer 1T-MnSe<sub>2</sub>, one of which is the bond stretching interaction shown by Eq. (1) while the other two terms are the angle bending interaction shown by Eq. (2). We note that the angle bending term  $K_{\text{Mn-Se-Se}}$  is

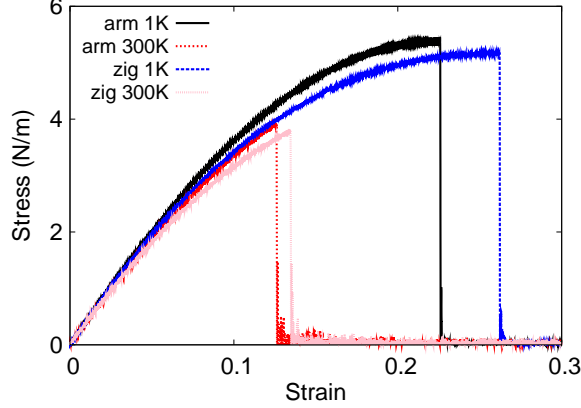


FIG. 97: (Color online) Stress-strain for single-layer 1T-MnSe<sub>2</sub> of dimension  $100 \times 100 \text{ \AA}$  along the armchair and zigzag directions.

TABLE CXCIV: The VFF model for single-layer 1T-MnSe<sub>2</sub>. The second line gives an explicit expression for each VFF term. The third line is the force constant parameters. Parameters are in the unit of  $\frac{\text{eV}}{\text{Å}^2}$  for the bond stretching interactions, and in the unit of eV for the angle bending interaction. The fourth line gives the initial bond length (in unit of Å) for the bond stretching interaction and the initial angle (in unit of degrees) for the angle bending interaction. The angle  $\theta_{ijk}$  has atom  $i$  as the apex.

VFF type	bond stretching	angle bending	
expression	$\frac{1}{2}K_{\text{Mn-Se}}(\Delta r)^2$	$\frac{1}{2}K_{\text{Mn-Se-Se}}(\Delta\theta)^2$	$\frac{1}{2}K_{\text{Se-Mn-Mn}}(\Delta\theta)^2$
parameter	4.407	2.399	2.399
$r_0$ or $\theta_0$	2.39	86.330	86.330

for the angle  $\theta_{\text{Mn-Se-Se}}$  with both Se atoms from the same (top or bottom) group. These force constant parameters are determined by fitting to the acoustic branches in the phonon dispersion along the  $\Gamma\text{M}$  as shown in Fig. 96 (a). The *ab initio* calculations for the phonon dispersion are from Ref. 12. Fig. 96 (b) shows that the VFF model and the SW potential give exactly the same phonon dispersion, as the SW potential is derived from the VFF model.

The parameters for the two-body SW potential used by GULP are shown in Tab. CXCIV. The parameters for the three-body SW potential used by GULP are shown in Tab. CXCVI. Some representative parameters for the SW potential used by LAMMPS are listed in

TABLE CXCIV: Two-body SW potential parameters for single-layer 1T-MnSe<sub>2</sub> used by GULP<sup>8</sup> as expressed in Eq. (3).

	$A$ (eV)	$\rho$ (Å)	$B$ (Å <sup>4</sup> )	$r_{\min}$ (Å)	$r_{\max}$ (Å)
Mn-Se	3.422	1.153	16.314	0.0	3.220

TABLE CXCV: Three-body SW potential parameters for single-layer 1T-MnSe<sub>2</sub> used by GULP<sup>8</sup> as expressed in Eq. (4). The angle  $\theta_{ijk}$  in the first line indicates the bending energy for the angle with atom  $i$  as the apex.

	$K$ (eV)	$\theta_0$ (degree)	$\rho_1$ (Å)	$\rho_2$ (Å)	$r_{\min12}$ (Å)	$r_{\max12}$ (Å)	$r_{\min13}$ (Å)	$r_{\max13}$ (Å)	$r_{\min23}$ (Å)	$r_{\max23}$ (Å)
$\theta_{\text{Mn-Se-Se}}$	19.390	86.330	1.153	1.153	0.0	3.220	0.0	3.220	0.0	4.467
$\theta_{\text{Se-Mn-Mn}}$	19.390	86.330	1.153	1.153	0.0	3.220	0.0	3.220	0.0	4.467

Tab. CXCVI.

We use LAMMPS to perform MD simulations for the mechanical behavior of the single-layer 1T-MnSe<sub>2</sub> under uniaxial tension at 1.0 K and 300.0 K. Fig. 97 shows the stress-strain curve for the tension of a single-layer 1T-MnSe<sub>2</sub> of dimension  $100 \times 100$  Å. Periodic boundary conditions are applied in both armchair and zigzag directions. The single-layer 1T-MnSe<sub>2</sub> is stretched uniaxially along the armchair or zigzag direction. The stress is calculated without involving the actual thickness of the quasi-two-dimensional structure of the single-layer 1T-MnSe<sub>2</sub>. The Young's modulus can be obtained by a linear fitting of the stress-strain relation in the small strain range of  $[0, 0.01]$ . The Young's modulus are 43.2 N/m and 42.9 N/m along the armchair and zigzag directions, respectively. The Young's modulus is essentially isotropic in the armchair and zigzag directions. The Poisson's ratio from the VFF model and the SW potential is  $\nu_{xy} = \nu_{yx} = 0.17$ .

There is no available value for nonlinear quantities in the single-layer 1T-MnSe<sub>2</sub>. We have thus used the nonlinear parameter  $B = 0.5d^4$  in Eq. (5), which is close to the value of

TABLE CXCVII: SW potential parameters for single-layer 1T-MnSe<sub>2</sub> used by LAMMPS<sup>9</sup> as expressed in Eqs. (9) and (10).

	$\epsilon$ (eV)	$\sigma$ (Å)	$a$	$\lambda$	$\gamma$	$\cos \theta_0$	$A_L$	$B_L$	$p$	$q$	tol
Mn-Se <sub>1</sub> -Se <sub>1</sub>	1.000	1.153	2.792	19.390	1.000	0.064	3.422	9.219	4	0	0.0

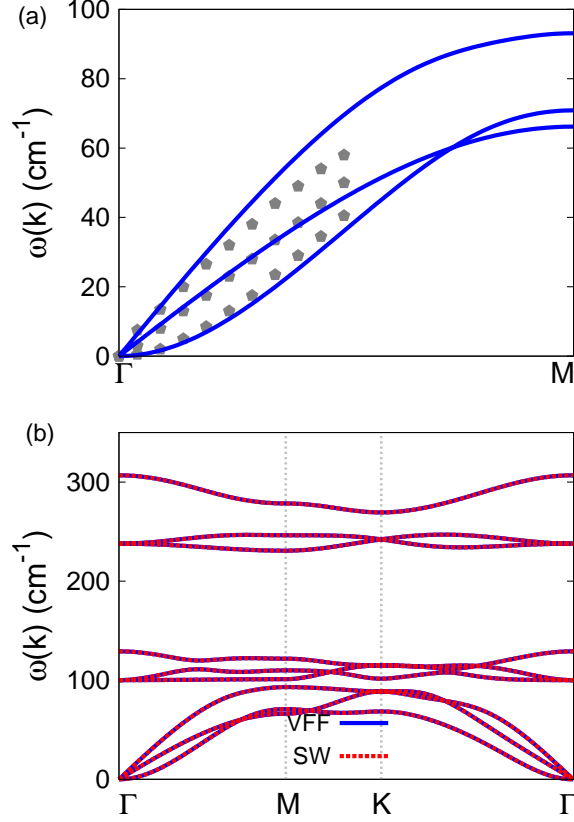


FIG. 98: (Color online) Phonon spectrum for single-layer 1T-MnTe<sub>2</sub>. (a) Phonon dispersion along the  $\Gamma$ M direction in the Brillouin zone. The results from the VFF model (lines) are comparable with the *ab initio* results (pentagons) from Ref. 12. (b) The phonon dispersion from the SW potential is exactly the same as that from the VFF model.

$B$  in most materials. The value of the third order nonlinear elasticity  $D$  can be extracted by fitting the stress-strain relation to the function  $\sigma = E\epsilon + \frac{1}{2}D\epsilon^2$  with  $E$  as the Young's modulus. The values of  $D$  from the present SW potential are -163.4 N/m and -179.4 N/m along the armchair and zigzag directions, respectively. The ultimate stress is about 5.4 Nm<sup>-1</sup> at the ultimate strain of 0.22 in the armchair direction at the low temperature of 1 K. The ultimate stress is about 5.2 Nm<sup>-1</sup> at the ultimate strain of 0.26 in the zigzag direction at the low temperature of 1 K.

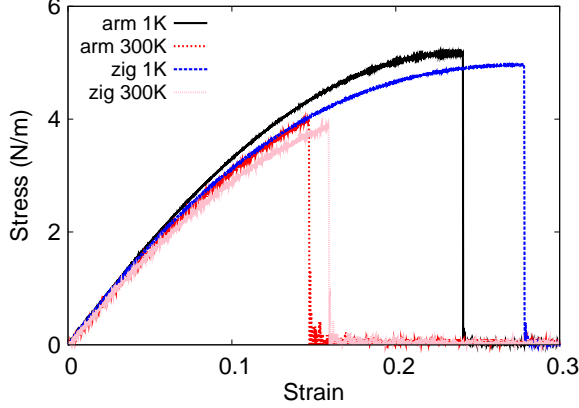


FIG. 99: (Color online) Stress-strain for single-layer 1T-MnTe<sub>2</sub> of dimension  $100 \times 100 \text{ \AA}$  along the armchair and zigzag directions.

TABLE CXCVIII: The VFF model for single-layer 1T-MnTe<sub>2</sub>. The second line gives an explicit expression for each VFF term. The third line is the force constant parameters. Parameters are in the unit of  $\frac{\text{eV}}{\text{Å}^2}$  for the bond stretching interactions, and in the unit of eV for the angle bending interaction. The fourth line gives the initial bond length (in unit of Å) for the bond stretching interaction and the initial angle (in unit of degrees) for the angle bending interaction. The angle  $\theta_{ijk}$  has atom  $i$  as the apex.

VFF type	bond stretching	angle bending	
expression	$\frac{1}{2}K_{\text{Mn-Te}}(\Delta r)^2$	$\frac{1}{2}K_{\text{Mn-Te-Te}}(\Delta\theta)^2$	$\frac{1}{2}K_{\text{Te-Mn-Mn}}(\Delta\theta)^2$
parameter	4.407	2.399	2.399
$r_0$ or $\theta_0$	2.59	86.219	86.219

## L. 1T-MNTE<sub>2</sub>

Most existing theoretical studies on the single-layer 1T-MnTe<sub>2</sub> are based on the first-principles calculations. In this section, we will develop the SW potential for the single-layer 1T-MnTe<sub>2</sub>.

The structure for the single-layer 1T-MnTe<sub>2</sub> is shown in Fig. 71 (with M=Mn and X=Te). Each Mn atom is surrounded by six Te atoms. These Te atoms are categorized into the top group (eg. atoms 1, 3, and 5) and bottom group (eg. atoms 2, 4, and 6). Each Te atom is connected to three Mn atoms. The structural parameters are from the first-

TABLE CXCIX: Two-body SW potential parameters for single-layer 1T-MnTe<sub>2</sub> used by GULP<sup>8</sup> as expressed in Eq. (3).

	$A$ (eV)	$\rho$ (Å)	$B$ (Å <sup>4</sup> )	$r_{\min}$ (Å)	$r_{\max}$ (Å)
Mn-Te	4.007	1.246	22.499	0.0	3.488

TABLE CC: Three-body SW potential parameters for single-layer 1T-MnTe<sub>2</sub> used by GULP<sup>8</sup> as expressed in Eq. (4). The angle  $\theta_{ijk}$  in the first line indicates the bending energy for the angle with atom  $i$  as the apex.

	$K$ (eV)	$\theta_0$ (degree)	$\rho_1$ (Å)	$\rho_2$ (Å)	$r_{\min12}$ (Å)	$r_{\max12}$ (Å)	$r_{\min13}$ (Å)	$r_{\max13}$ (Å)	$r_{\min23}$ (Å)	$r_{\max23}$ (Å)
$\theta_{\text{Mn-Te-Te}}$	19.307	86.219	1.246	1.246	0.0	3.488	0.0	3.488	0.0	4.836
$\theta_{\text{Te-Mn-Mn}}$	19.307	86.219	1.246	1.246	0.0	3.488	0.0	3.488	0.0	4.836

principles calculations,<sup>12</sup> including the lattice constant  $a = 3.54$  Å and the bond length  $d_{\text{Mn-Te}} = 2.59$  Å. The resultant angles are  $\theta_{\text{MnTeTe}} = 86.219^\circ$  with Te atoms from the same (top or bottom) group, and  $\theta_{\text{TeMnMn}} = 86.219^\circ$ .

Table CXCVIII shows three VFF terms for the single-layer 1T-MnTe<sub>2</sub>, one of which is the bond stretching interaction shown by Eq. (1) while the other two terms are the angle bending interaction shown by Eq. (2). We note that the angle bending term  $K_{\text{Mn-Te-Te}}$  is for the angle  $\theta_{\text{Mn-Te-Te}}$  with both Se atoms from the same (top or bottom) group. These force constant parameters are determined by fitting to the acoustic branches in the phonon dispersion along the  $\Gamma\text{M}$  as shown in Fig. 98 (a). The *ab initio* calculations for the phonon dispersion are from Ref. 12. Fig. 98 (b) shows that the VFF model and the SW potential give exactly the same phonon dispersion, as the SW potential is derived from the VFF model.

The parameters for the two-body SW potential used by GULP are shown in Tab. CXCIX. The parameters for the three-body SW potential used by GULP are shown in Tab. CC. Some representative parameters for the SW potential used by LAMMPS are listed in Tab. CCI.

TABLE CCI: SW potential parameters for single-layer 1T-MnTe<sub>2</sub> used by LAMMPS<sup>9</sup> as expressed in Eqs. (9) and (10).

	$\epsilon$ (eV)	$\sigma$ (Å)	$a$	$\lambda$	$\gamma$	$\cos \theta_0$	$A_L$	$B_L$	$p$	$q$	tol
Mn-Te <sub>1</sub> -Te <sub>1</sub>	1.000	1.246	2.800	19.307	1.000	0.066	4.007	9.340	4	0	0.0

We use LAMMPS to perform MD simulations for the mechanical behavior of the single-layer 1T-MnTe<sub>2</sub> under uniaxial tension at 1.0 K and 300.0 K. Fig. 99 shows the stress-strain curve for the tension of a single-layer 1T-MnTe<sub>2</sub> of dimension 100×100 Å. Periodic boundary conditions are applied in both armchair and zigzag directions. The single-layer 1T-MnTe<sub>2</sub> is stretched uniaxially along the armchair or zigzag direction. The stress is calculated without involving the actual thickness of the quasi-two-dimensional structure of the single-layer 1T-MnTe<sub>2</sub>. The Young’s modulus can be obtained by a linear fitting of the stress-strain relation in the small strain range of [0, 0.01]. The Young’s modulus are 38.5 N/m and 38.4 N/m along the armchair and zigzag directions, respectively. The Young’s modulus is essentially isotropic in the armchair and zigzag directions. The Poisson’s ratio from the VFF model and the SW potential is  $\nu_{xy} = \nu_{yx} = 0.19$ .

There is no available value for nonlinear quantities in the single-layer 1T-MnTe<sub>2</sub>. We have thus used the nonlinear parameter  $B = 0.5d^4$  in Eq. (5), which is close to the value of  $B$  in most materials. The value of the third order nonlinear elasticity  $D$  can be extracted by fitting the stress-strain relation to the function  $\sigma = E\epsilon + \frac{1}{2}D\epsilon^2$  with  $E$  as the Young’s modulus. The values of  $D$  from the present SW potential are -133.5 N/m and -149.5 N/m along the armchair and zigzag directions, respectively. The ultimate stress is about 5.2 Nm<sup>-1</sup> at the ultimate strain of 0.24 in the armchair direction at the low temperature of 1 K. The ultimate stress is about 5.0 Nm<sup>-1</sup> at the ultimate strain of 0.28 in the zigzag direction at the low temperature of 1 K.

## LI. 1T-COTE<sub>2</sub>

Most existing theoretical studies on the single-layer 1T-CoTe<sub>2</sub> are based on the first-principles calculations. In this section, we will develop the SW potential for the single-layer 1T-CoTe<sub>2</sub>.

The structure for the single-layer 1T-CoTe<sub>2</sub> is shown in Fig. 71 (with M=Co and X=Te). Each Co atom is surrounded by six Te atoms. These Te atoms are categorized into the top group (eg. atoms 1, 3, and 5) and bottom group (eg. atoms 2, 4, and 6). Each Te atom is connected to three Co atoms. The structural parameters are from the first-principles calculations,<sup>48</sup> including the lattice constant  $a = 3.5983$  Å, and the bond length  $d_{\text{Co-Te}} = 2.5117$  Å, which is derived from the angle  $\theta_{\text{TeCoCo}} = 91.5^\circ$ . The other angle is

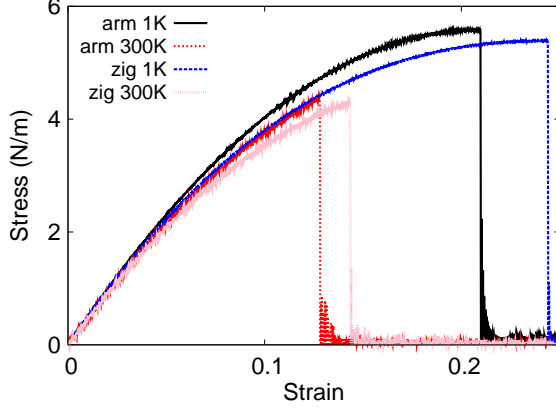


FIG. 100: (Color online) Stress-strain for single-layer 1T-CoTe<sub>2</sub> of dimension  $100 \times 100 \text{ \AA}$  along the armchair and zigzag directions.

TABLE CCII: The VFF model for single-layer 1T-CoTe<sub>2</sub>. The second line gives an explicit expression for each VFF term. The third line is the force constant parameters. Parameters are in the unit of  $\frac{eV}{\text{Å}^2}$  for the bond stretching interactions, and in the unit of eV for the angle bending interaction. The fourth line gives the initial bond length (in unit of Å) for the bond stretching interaction and the initial angle (in unit of degrees) for the angle bending interaction. The angle  $\theta_{ijk}$  has atom  $i$  as the apex.

VFF type	bond stretching	angle bending	
expression	$\frac{1}{2}K_{\text{Co-Te}}(\Delta r)^2$	$\frac{1}{2}K_{\text{Co-Te-Te}}(\Delta\theta)^2$	$\frac{1}{2}K_{\text{Te-Co-Co}}(\Delta\theta)^2$
parameter	4.726	3.035	3.035
$r_0$ or $\theta_0$	2.512	91.501	91.501

$\theta_{\text{CoTeTe}} = 91.5^\circ$  with Te atoms from the same (top or bottom) group.

Table CCII shows three VFF terms for the single-layer 1T-CoTe<sub>2</sub>, one of which is the bond stretching interaction shown by Eq. (1) while the other two terms are the angle bending interaction shown by Eq. (2). We note that the angle bending term  $K_{\text{Co-Te-Te}}$  is for the angle  $\theta_{\text{Co-Te-Te}}$  with both Te atoms from the same (top or bottom) group. We find that there are actually only two parameters in the VFF model, so we can determine their value by fitting to the Young's modulus and the Poisson's ratio of the system. The *ab initio* calculations have predicted the Young's modulus to be 59 N/m and the Poisson's ratio as

TABLE CCIII: Two-body SW potential parameters for single-layer 1T-CoTe<sub>2</sub> used by GULP<sup>8</sup> as expressed in Eq. (3).

	$A$ (eV)	$\rho$ (Å)	$B$ (Å <sup>4</sup> )	$r_{\min}$ (Å)	$r_{\max}$ (Å)
Co-Te	4.628	1.402	19.899	0.0	3.450

TABLE CCIV: Three-body SW potential parameters for single-layer 1T-CoTe<sub>2</sub> used by GULP<sup>8</sup> as expressed in Eq. (4). The angle  $\theta_{ijk}$  in the first line indicates the bending energy for the angle with atom  $i$  as the apex.

	$K$ (eV)	$\theta_0$ (degree)	$\rho_1$ (Å)	$\rho_2$ (Å)	$r_{\min12}$ (Å)	$r_{\max12}$ (Å)	$r_{\min13}$ (Å)	$r_{\max13}$ (Å)	$r_{\min23}$ (Å)	$r_{\max23}$ (Å)
$\theta_{\text{Co-Te-Te}}$	30.149	91.501	1.402	1.402	0.0	3.450	0.0	3.450	0.0	4.915
$\theta_{\text{Te-Co-Co}}$	30.149	91.501	1.402	1.402	0.0	3.450	0.0	3.450	0.0	4.915

0.14.<sup>48</sup>

The parameters for the two-body SW potential used by GULP are shown in Tab. CCIII. The parameters for the three-body SW potential used by GULP are shown in Tab. CCIV. Some representative parameters for the SW potential used by LAMMPS are listed in Tab. CCV.

We use LAMMPS to perform MD simulations for the mechanical behavior of the single-layer 1T-CoTe<sub>2</sub> under uniaxial tension at 1.0 K and 300.0 K. Fig. 100 shows the stress-strain curve for the tension of a single-layer 1T-CoTe<sub>2</sub> of dimension  $100 \times 100$  Å. Periodic boundary conditions are applied in both armchair and zigzag directions. The single-layer 1T-CoTe<sub>2</sub> is stretched uniaxially along the armchair or zigzag direction. The stress is calculated without involving the actual thickness of the quasi-two-dimensional structure of the single-layer 1T-CoTe<sub>2</sub>. The Young's modulus can be obtained by a linear fitting of the stress-strain relation in the small strain range of  $[0, 0.01]$ . The Young's modulus are 50.5 N/m and 50.3 N/m along the armchair and zigzag directions, respectively. The Young's modulus is essentially

TABLE CCV: SW potential parameters for single-layer 1T-CoTe<sub>2</sub> used by LAMMPS<sup>9</sup> as expressed in Eqs. (9) and (10).

	$\epsilon$ (eV)	$\sigma$ (Å)	$a$	$\lambda$	$\gamma$	$\cos \theta_0$	$A_L$	$B_L$	$p$	$q$	tol
Co-Te <sub>1</sub> -Te <sub>1</sub>	1.000	1.402	2.461	30.149	1.000	-0.026	4.628	5.151	4	0	0.0

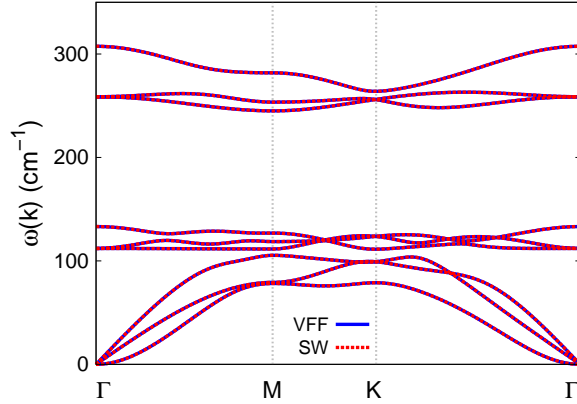


FIG. 101: (Color online) Phonon spectrum for single-layer 1T-CoTe<sub>2</sub> along the  $\Gamma$ MK $\Gamma$  direction in the Brillouin zone. The phonon dispersion from the SW potential is exactly the same as that from the VFF model.

isotropic in the armchair and zigzag directions. The Poisson's ratio from the VFF model and the SW potential is  $\nu_{xy} = \nu_{yx} = 0.13$ . The fitted Young's modulus value is about 10% smaller than the *ab initio* result of 59 N/m,<sup>48</sup> as only short-range interactions are considered in the present work. The long-range interactions are ignored, which typically leads to about 10% underestimation for the value of the Young's modulus.

There is no available value for nonlinear quantities in the single-layer 1T-CoTe<sub>2</sub>. We have thus used the nonlinear parameter  $B = 0.5d^4$  in Eq. (5), which is close to the value of  $B$  in most materials. The value of the third order nonlinear elasticity  $D$  can be extracted by fitting the stress-strain relation to the function  $\sigma = E\epsilon + \frac{1}{2}D\epsilon^2$  with  $E$  as the Young's modulus. The values of  $D$  from the present SW potential are -221.5 N/m and -238.3 N/m along the armchair and zigzag directions, respectively. The ultimate stress is about 5.6 Nm<sup>-1</sup> at the ultimate strain of 0.21 in the armchair direction at the low temperature of 1 K. The ultimate stress is about 5.4 Nm<sup>-1</sup> at the ultimate strain of 0.24 in the zigzag direction at the low temperature of 1 K.

Fig. 101 shows that the VFF model and the SW potential give exactly the same phonon dispersion, as the SW potential is derived from the VFF model.

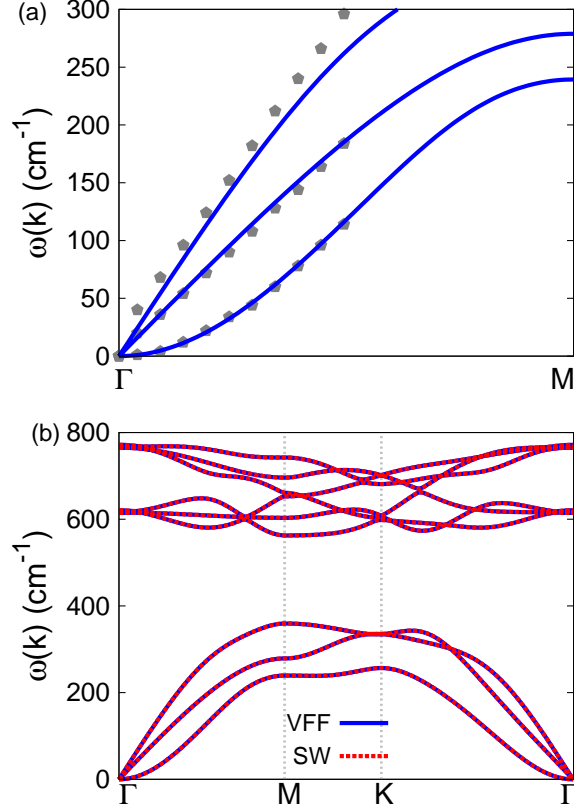


FIG. 102: (Color online) Phonon spectrum for single-layer 1T-NiO<sub>2</sub>. (a) Phonon dispersion along the  $\Gamma$ M direction in the Brillouin zone. The results from the VFF model (lines) are comparable with the *ab initio* results (pentagons) from Ref. 12. (b) The phonon dispersion from the SW potential is exactly the same as that from the VFF model.

### LII. 1T-NiO<sub>2</sub>

Most existing theoretical studies on the single-layer 1T-NiO<sub>2</sub> are based on the first-principles calculations. In this section, we will develop the SW potential for the single-layer 1T-NiO<sub>2</sub>.

The structure for the single-layer 1T-NiO<sub>2</sub> is shown in Fig. 71 (with M=Ni and X=O). Each Ni atom is surrounded by six O atoms. These O atoms are categorized into the top group (eg. atoms 1, 3, and 5) and bottom group (eg. atoms 2, 4, and 6). Each O atom is connected to three Ni atoms. The structural parameters are from the first-principles calculations,<sup>12</sup> including the lattice constant  $a = 2.77 \text{ \AA}$  and the bond length  $d_{\text{Ni-O}} = 1.84 \text{ \AA}$ .

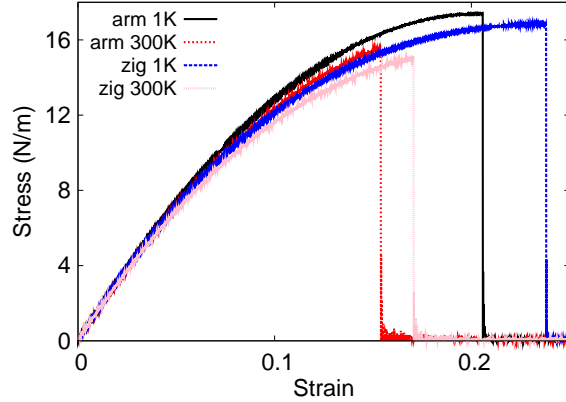


FIG. 103: (Color online) Stress-strain for single-layer 1T-NiO<sub>2</sub> of dimension  $100 \times 100 \text{ \AA}$  along the armchair and zigzag directions.

TABLE CCVI: The VFF model for single-layer 1T-NiO<sub>2</sub>. The second line gives an explicit expression for each VFF term. The third line is the force constant parameters. Parameters are in the unit of  $\frac{eV}{\text{Å}^2}$  for the bond stretching interactions, and in the unit of eV for the angle bending interaction. The fourth line gives the initial bond length (in unit of Å) for the bond stretching interaction and the initial angle (in unit of degrees) for the angle bending interaction. The angle  $\theta_{ijk}$  has atom *i* as the apex.

VFF type	bond stretching	angle bending	
expression	$\frac{1}{2}K_{\text{Ni-O}}(\Delta r)^2$	$\frac{1}{2}K_{\text{Ni-O-O}}(\Delta\theta)^2$	$\frac{1}{2}K_{\text{O-Ni-Ni}}(\Delta\theta)^2$
parameter	15.925	4.847	4.847
$r_0$ or $\theta_0$		97.653	97.653

The resultant angles are  $\theta_{\text{NiOO}} = 97.653^\circ$  with O atoms from the same (top or bottom) group, and  $\theta_{\text{ONiNi}} = 97.653^\circ$ .

Table CCVI shows three VFF terms for the single-layer 1T-NiO<sub>2</sub>, one of which is the bond stretching interaction shown by Eq. (1) while the other two terms are the angle bending interaction shown by Eq. (2). We note that the angle bending term  $K_{\text{Ni-O-O}}$  is for the angle  $\theta_{\text{Ni-O-O}}$  with both O atoms from the same (top or bottom) group. These force constant parameters are determined by fitting to the two in-plane acoustic branches in the phonon dispersion along the  $\Gamma\text{M}$  as shown in Fig. 102 (a). The *ab initio* calculations for the phonon

TABLE CCVII: Two-body SW potential parameters for single-layer 1T-NiO<sub>2</sub> used by GULP<sup>8</sup> as expressed in Eq. (3).

	$A$ (eV)	$\rho$ (Å)	$B$ (Å <sup>4</sup> )	$r_{\min}$ (Å)	$r_{\max}$ (Å)
Ni-O	9.709	1.199	5.731	0.0	2.583

TABLE CCVIII: Three-body SW potential parameters for single-layer 1T-NiO<sub>2</sub> used by GULP<sup>8</sup> as expressed in Eq. (4). The angle  $\theta_{ijk}$  in the first line indicates the bending energy for the angle with atom  $i$  as the apex.

	$K$ (eV)	$\theta_0$ (degree)	$\rho_1$ (Å)	$\rho_2$ (Å)	$r_{\min12}$ (Å)	$r_{\max12}$ (Å)	$r_{\min13}$ (Å)	$r_{\max13}$ (Å)	$r_{\min23}$ (Å)	$r_{\max23}$ (Å)
$\theta_{\text{Ni-O-O}}$	62.317	97.653	1.199	1.199	0.0	2.583	0.0	2.583	0.0	3.784
$\theta_{\text{O-Ni-Ni}}$	62.317	97.653	1.199	1.199	0.0	2.583	0.0	2.583	0.0	3.784

dispersion are from Ref. 12. Fig. 102 (b) shows that the VFF model and the SW potential give exactly the same phonon dispersion, as the SW potential is derived from the VFF model.

The parameters for the two-body SW potential used by GULP are shown in Tab. CCVII. The parameters for the three-body SW potential used by GULP are shown in Tab. CCVIII. Some representative parameters for the SW potential used by LAMMPS are listed in Tab. CCIX.

We use LAMMPS to perform MD simulations for the mechanical behavior of the single-layer 1T-NiO<sub>2</sub> under uniaxial tension at 1.0 K and 300.0 K. Fig. 103 shows the stress-strain curve for the tension of a single-layer 1T-NiO<sub>2</sub> of dimension  $100 \times 100$  Å. Periodic boundary conditions are applied in both armchair and zigzag directions. The single-layer 1T-NiO<sub>2</sub> is stretched uniaxially along the armchair or zigzag direction. The stress is calculated without involving the actual thickness of the quasi-two-dimensional structure of the single-layer 1T-NiO<sub>2</sub>. The Young's modulus can be obtained by a linear fitting of the stress-strain relation

TABLE CCIX: SW potential parameters for single-layer 1T-NiO<sub>2</sub> used by LAMMPS<sup>9</sup> as expressed in Eqs. (9) and (10).

	$\epsilon$ (eV)	$\sigma$ (Å)	$a$	$\lambda$	$\gamma$	$\cos \theta_0$	$A_L$	$B_L$	$p$	$q$	tol
Ni-O <sub>1</sub> -O <sub>1</sub>	1.000	1.199	2.154	62.317	1.000	-0.133	9.709	2.772	4	0	0.0

TABLE CCX: The VFF model for single-layer 1T-NiS<sub>2</sub>. The second line gives an explicit expression for each VFF term. The third line is the force constant parameters. Parameters are in the unit of  $\frac{\text{eV}}{\text{Å}^2}$  for the bond stretching interactions, and in the unit of eV for the angle bending interaction. The fourth line gives the initial bond length (in unit of Å) for the bond stretching interaction and the initial angle (in unit of degrees) for the angle bending interaction. The angle  $\theta_{ijk}$  has atom  $i$  as the apex.

VFF type	bond stretching	angle bending	
expression	$\frac{1}{2}K_{\text{Ni-S}}(\Delta r)^2$	$\frac{1}{2}K_{\text{Ni-S-S}}(\Delta\theta)^2$	$\frac{1}{2}K_{\text{S-Ni-Ni}}(\Delta\theta)^2$
parameter	9.385	2.952	2.952
$r_0$ or $\theta_0$	2.232	96.000	96.000

in the small strain range of  $[0, 0.01]$ . The Young's modulus are 163.3 N/m and 162.4 N/m along the armchair and zigzag directions, respectively. The Young's modulus is essentially isotropic in the armchair and zigzag directions. The Poisson's ratio from the VFF model and the SW potential is  $\nu_{xy} = \nu_{yx} = 0.12$ .

There is no available value for nonlinear quantities in the single-layer 1T-NiO<sub>2</sub>. We have thus used the nonlinear parameter  $B = 0.5d^4$  in Eq. (5), which is close to the value of  $B$  in most materials. The value of the third order nonlinear elasticity  $D$  can be extracted by fitting the stress-strain relation to the function  $\sigma = E\epsilon + \frac{1}{2}D\epsilon^2$  with  $E$  as the Young's modulus. The values of  $D$  from the present SW potential are -748.7 N/m and -796.0 N/m along the armchair and zigzag directions, respectively. The ultimate stress is about 17.4 Nm<sup>-1</sup> at the ultimate strain of 0.20 in the armchair direction at the low temperature of 1 K. The ultimate stress is about 16.8 Nm<sup>-1</sup> at the ultimate strain of 0.24 in the zigzag direction at the low temperature of 1 K.

### LIII. 1T-NIS<sub>2</sub>

Most existing theoretical studies on the single-layer 1T-NiS<sub>2</sub> are based on the first-principles calculations. In this section, we will develop the SW potential for the single-layer 1T-NiS<sub>2</sub>.

The structure for the single-layer 1T-NiS<sub>2</sub> is shown in Fig. 71 (with M=Ni and X=S).

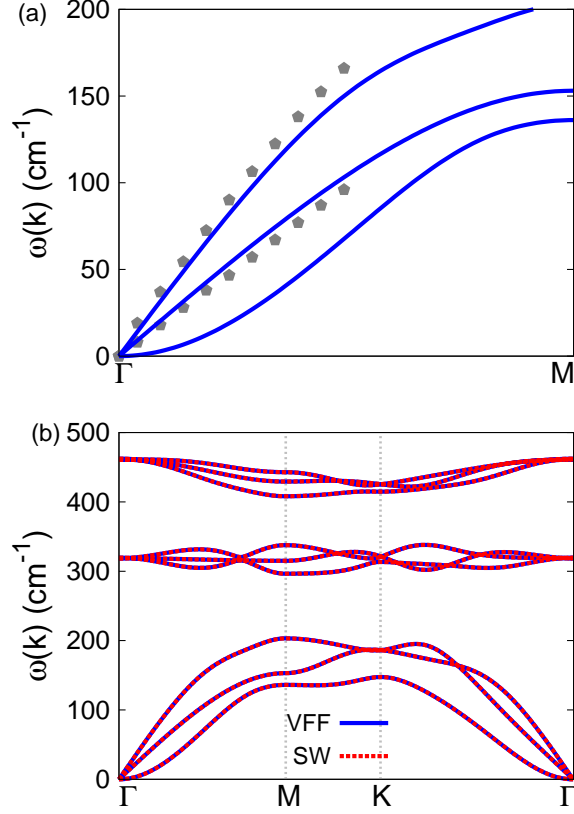


FIG. 104: (Color online) Phonon spectrum for single-layer 1T-NiS<sub>2</sub>. (a) Phonon dispersion along the  $\Gamma$ M direction in the Brillouin zone. The results from the VFF model (lines) are comparable with the *ab initio* results (pentagons) from Ref. 12. (b) The phonon dispersion from the SW potential is exactly the same as that from the VFF model.

TABLE CCXI: Two-body SW potential parameters for single-layer 1T-NiS<sub>2</sub> used by GULP<sup>8</sup> as expressed in Eq. (3).

	$A$ (eV)	$\rho$ ( $\text{\AA}$ )	$B$ ( $\text{\AA}^4$ )	$r_{\min}$ ( $\text{\AA}$ )	$r_{\max}$ ( $\text{\AA}$ )
Ni-S	8.098	1.398	12.409	0.0	3.115

Each Ni atom is surrounded by six S atoms. These S atoms are categorized into the top group (eg. atoms 1, 3, and 5) and bottom group (eg. atoms 2, 4, and 6). Each S atom is connected to three Ni atoms. The structural parameters are from the first-principles calculations,<sup>48</sup> including the lattice constant  $a = 3.3174 \text{ \AA}$ , and the bond length  $d_{\text{Ni-S}} = 2.2320 \text{ \AA}$ , which is derived from the angle  $\theta_{\text{S Ni Ni}} = 96^\circ$ . The other angle is  $\theta_{\text{Ni S S}} = 96^\circ$  with S atoms from the

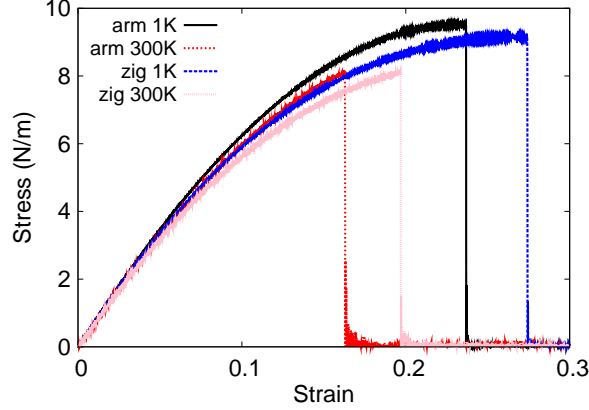


FIG. 105: (Color online) Stress-strain for single-layer 1T-NiS<sub>2</sub> of dimension 100 × 100 Å along the armchair and zigzag directions.

TABLE CCXII: Three-body SW potential parameters for single-layer 1T-NiS<sub>2</sub> used by GULP<sup>8</sup> as expressed in Eq. (4). The angle  $\theta_{ijk}$  in the first line indicates the bending energy for the angle with atom  $i$  as the apex.

	$K$ (eV)	$\theta_0$ (degree)	$\rho_1$ (Å)	$\rho_2$ (Å)	$r_{\min 12}$ (Å)	$r_{\max 12}$ (Å)	$r_{\min 13}$ (Å)	$r_{\max 13}$ (Å)	$r_{\min 23}$ (Å)	$r_{\max 23}$ (Å)
$\theta_{\text{Ni-S-S}}$	35.372	96.000	1.398	1.398	0.0	3.115	0.0	3.115	0.0	4.532
$\theta_{\text{S-Ni-Ni}}$	35.372	96.000	1.398	1.398	0.0	3.115	0.0	3.115	0.0	4.532

same (top or bottom) group.

Table CCX shows three VFF terms for the single-layer 1T-NiS<sub>2</sub>, one of which is the bond stretching interaction shown by Eq. (1) while the other two terms are the angle bending interaction shown by Eq. (2). We note that the angle bending term  $K_{\text{Ni-S-S}}$  is for the angle  $\theta_{\text{Ni-S-S}}$  with both S atoms from the same (top or bottom) group. These force constant parameters are determined by fitting to the two in-plane acoustic branches in the phonon dispersion along the  $\Gamma\text{M}$  as shown in Fig. 104 (a). The *ab initio* calculations for the phonon

TABLE CCXIII: SW potential parameters for single-layer 1T-NiS<sub>2</sub> used by LAMMPS<sup>9</sup> as expressed in Eqs. (9) and (10).

	$\epsilon$ (eV)	$\sigma$ (Å)	$a$	$\lambda$	$\gamma$	$\cos \theta_0$	$A_L$	$B_L$	$p$	$q$	tol
Ni-S <sub>1</sub> -S <sub>1</sub>	1.000	1.398	2.228	35.372	1.000	-0.105	8.098	3.249	4	0	0.0

dispersion are from Ref. 12. Fig. 104 (b) shows that the VFF model and the SW potential give exactly the same phonon dispersion, as the SW potential is derived from the VFF model.

The parameters for the two-body SW potential used by GULP are shown in Tab. CCXI. The parameters for the three-body SW potential used by GULP are shown in Tab. CCXII. Some representative parameters for the SW potential used by LAMMPS are listed in Tab. CCXIII.

We use LAMMPS to perform MD simulations for the mechanical behavior of the single-layer 1T-NiS<sub>2</sub> under uniaxial tension at 1.0 K and 300.0 K. Fig. 105 shows the stress-strain curve for the tension of a single-layer 1T-NiS<sub>2</sub> of dimension  $100 \times 100 \text{ \AA}$ . Periodic boundary conditions are applied in both armchair and zigzag directions. The single-layer 1T-NiS<sub>2</sub> is stretched uniaxially along the armchair or zigzag direction. The stress is calculated without involving the actual thickness of the quasi-two-dimensional structure of the single-layer 1T-NiS<sub>2</sub>. The Young's modulus can be obtained by a linear fitting of the stress-strain relation in the small strain range of  $[0, 0.01]$ . The Young's modulus are 74.2 N/m and 73.9 N/m along the armchair and zigzag directions, respectively. The Young's modulus is essentially isotropic in the armchair and zigzag directions. The Poisson's ratio from the VFF model and the SW potential is  $\nu_{xy} = \nu_{yx} = 0.17$ .

There is no available value for nonlinear quantities in the single-layer 1T-NiS<sub>2</sub>. We have thus used the nonlinear parameter  $B = 0.5d^4$  in Eq. (5), which is close to the value of  $B$  in most materials. The value of the third order nonlinear elasticity  $D$  can be extracted by fitting the stress-strain relation to the function  $\sigma = E\epsilon + \frac{1}{2}D\epsilon^2$  with  $E$  as the Young's modulus. The values of  $D$  from the present SW potential are -274.5 N/m and -301.4 N/m along the armchair and zigzag directions, respectively. The ultimate stress is about  $9.5 \text{ Nm}^{-1}$  at the ultimate strain of 0.23 in the armchair direction at the low temperature of 1 K. The ultimate stress is about  $9.2 \text{ Nm}^{-1}$  at the ultimate strain of 0.27 in the zigzag direction at the low temperature of 1 K.

#### LIV. 1T-NiSe<sub>2</sub>

Most existing theoretical studies on the single-layer 1T-NiSe<sub>2</sub> are based on the first-principles calculations. In this section, we will develop the SW potential for the single-layer

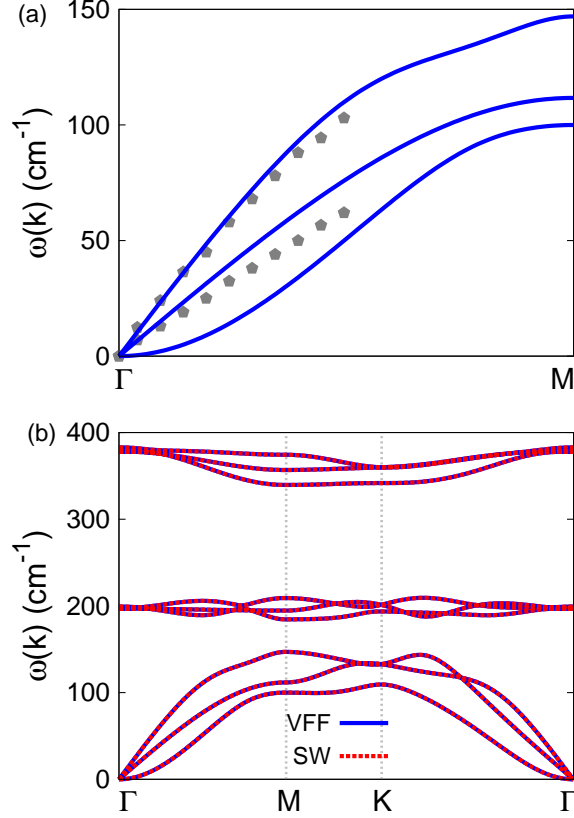


FIG. 106: (Color online) Phonon spectrum for single-layer 1T-NiSe<sub>2</sub>. (a) Phonon dispersion along the  $\Gamma$ M direction in the Brillouin zone. The results from the VFF model (lines) are comparable with the *ab initio* results (pentagons) from Ref. 12. (b) The phonon dispersion from the SW potential is exactly the same as that from the VFF model.

1T-NiSe<sub>2</sub>.

The structure for the single-layer 1T-NiSe<sub>2</sub> is shown in Fig. 71 (with M=Ni and X=Se). Each Ni atom is surrounded by six Se atoms. These Se atoms are categorized into the top group (eg. atoms 1, 3, and 5) and bottom group (eg. atoms 2, 4, and 6). Each Se atom is connected to three Ni atoms. The structural parameters are from the first-principles calculations,<sup>48</sup> including the lattice constant  $a = 3.4712 \text{ \AA}$ , and the bond length  $d_{\text{Ni-Se}} = 2.3392 \text{ \AA}$ , which is derived from the angle  $\theta_{\text{SeNiNi}} = 95.8^\circ$ . The other angle is  $\theta_{\text{NiSeSe}} = 95.8^\circ$  with Se atoms from the same (top or bottom) group.

Table CCXIV shows three VFF terms for the single-layer 1T-NiSe<sub>2</sub>, one of which is the bond stretching interaction shown by Eq. (1) while the other two terms are the angle

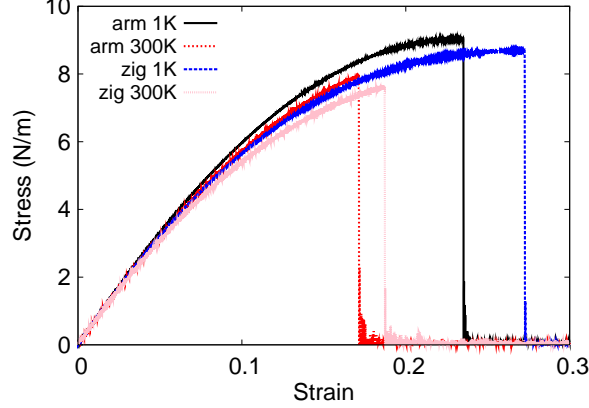


FIG. 107: (Color online) Stress-strain for single-layer 1T-NiSe<sub>2</sub> of dimension  $100 \times 100 \text{ \AA}$  along the armchair and zigzag directions.

TABLE CCXIV: The VFF model for single-layer 1T-NiSe<sub>2</sub>. The second line gives an explicit expression for each VFF term. The third line is the force constant parameters. Parameters are in the unit of  $\frac{eV}{\text{Å}^2}$  for the bond stretching interactions, and in the unit of eV for the angle bending interaction. The fourth line gives the initial bond length (in unit of Å) for the bond stretching interaction and the initial angle (in unit of degrees) for the angle bending interaction. The angle  $\theta_{ijk}$  has atom *i* as the apex.

VFF type	bond stretching	angle bending	
expression	$\frac{1}{2}K_{\text{Ni-Se}}(\Delta r)^2$	$\frac{1}{2}K_{\text{Ni-Se-Se}}(\Delta\theta)^2$	$\frac{1}{2}K_{\text{Se-Ni-Ni}}(\Delta\theta)^2$
parameter	8.814	3.149	3.149
$r_0$ or $\theta_0$	2.339	95.798	95.798

bending interaction shown by Eq. (2). We note that the angle bending term  $K_{\text{Ni-Se-Se}}$  is for the angle  $\theta_{\text{Ni-Se-Se}}$  with both Se atoms from the same (top or bottom) group. These force constant parameters are determined by fitting to the two in-plane acoustic branches in the phonon dispersion along the  $\Gamma\text{M}$  as shown in Fig. 106 (a). The *ab initio* calculations for the phonon dispersion are from Ref. 12. Fig. 106 (b) shows that the VFF model and the SW potential give exactly the same phonon dispersion, as the SW potential is derived from the VFF model.

The parameters for the two-body SW potential used by GULP are shown in Tab. CCXV.

TABLE CCXV: Two-body SW potential parameters for single-layer 1T-NiSe<sub>2</sub> used by GULP<sup>8</sup> as expressed in Eq. (3).

	$A$ (eV)	$\rho$ (Å)	$B$ (Å <sup>4</sup> )	$r_{\min}$ (Å)	$r_{\max}$ (Å)
Ni-Se	8.313	1.458	14.971	0.0	3.263

TABLE CCXVI: Three-body SW potential parameters for single-layer 1T-NiSe<sub>2</sub> used by GULP<sup>8</sup> as expressed in Eq. (4). The angle  $\theta_{ijk}$  in the first line indicates the bending energy for the angle with atom  $i$  as the apex.

	$K$ (eV)	$\theta_0$ (degree)	$\rho_1$ (Å)	$\rho_2$ (Å)	$r_{\min12}$ (Å)	$r_{\max12}$ (Å)	$r_{\min13}$ (Å)	$r_{\max13}$ (Å)	$r_{\min23}$ (Å)	$r_{\max23}$ (Å)
$\theta_{\text{Ni-Se-Se}}$	37.407	95.798	1.458	1.458	0.0	3.263	0.0	3.263	0.0	4.742
$\theta_{\text{Se-Ni-Ni}}$	37.407	95.798	1.458	1.458	0.0	3.263	0.0	3.263	0.0	4.742

The parameters for the three-body SW potential used by GULP are shown in Tab. CCXVI. Some representative parameters for the SW potential used by LAMMPS are listed in Tab. CCXVII.

We use LAMMPS to perform MD simulations for the mechanical behavior of the single-layer 1T-NiSe<sub>2</sub> under uniaxial tension at 1.0 K and 300.0 K. Fig. 107 shows the stress-strain curve for the tension of a single-layer 1T-NiSe<sub>2</sub> of dimension  $100 \times 100$  Å. Periodic boundary conditions are applied in both armchair and zigzag directions. The single-layer 1T-NiSe<sub>2</sub> is stretched uniaxially along the armchair or zigzag direction. The stress is calculated without involving the actual thickness of the quasi-two-dimensional structure of the single-layer 1T-NiSe<sub>2</sub>. The Young's modulus can be obtained by a linear fitting of the stress-strain relation in the small strain range of  $[0, 0.01]$ . The Young's modulus are 70.9 N/m and 70.6 N/m along the armchair and zigzag directions, respectively. The Young's modulus is essentially isotropic in the armchair and zigzag directions. The Poisson's ratio from the VFF model and the SW potential is  $\nu_{xy} = \nu_{yx} = 0.17$ .

TABLE CCXVII: SW potential parameters for single-layer 1T-NiSe<sub>2</sub> used by LAMMPS<sup>9</sup> as expressed in Eqs. (9) and (10).

	$\epsilon$ (eV)	$\sigma$ (Å)	$a$	$\lambda$	$\gamma$	$\cos \theta_0$	$A_L$	$B_L$	$p$	$q$	tol
Ni-Se <sub>1</sub> -Se <sub>1</sub>	1.000	1.458	2.238	37.407	1.000	-0.101	8.313	3.315	4	0	0.0

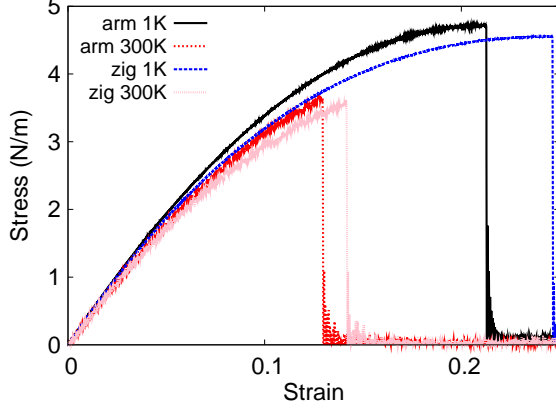


FIG. 108: (Color online) Stress-strain for single-layer 1T-NiTe<sub>2</sub> of dimension  $100 \times 100 \text{ \AA}$  along the armchair and zigzag directions.

There is no available value for nonlinear quantities in the single-layer 1T-NiSe<sub>2</sub>. We have thus used the nonlinear parameter  $B = 0.5d^4$  in Eq. (5), which is close to the value of  $B$  in most materials. The value of the third order nonlinear elasticity  $D$  can be extracted by fitting the stress-strain relation to the function  $\sigma = E\epsilon + \frac{1}{2}D\epsilon^2$  with  $E$  as the Young's modulus. The values of  $D$  from the present SW potential are  $-263.7 \text{ N/m}$  and  $-289.5 \text{ N/m}$  along the armchair and zigzag directions, respectively. The ultimate stress is about  $9.0 \text{ Nm}^{-1}$  at the ultimate strain of 0.23 in the armchair direction at the low temperature of 1 K. The ultimate stress is about  $8.7 \text{ Nm}^{-1}$  at the ultimate strain of 0.27 in the zigzag direction at the low temperature of 1 K.

#### LV. 1T-NITE<sub>2</sub>

Most existing theoretical studies on the single-layer 1T-NiTe<sub>2</sub> are based on the first-principles calculations. In this section, we will develop the SW potential for the single-layer 1T-NiTe<sub>2</sub>.

The structure for the single-layer 1T-NiTe<sub>2</sub> is shown in Fig. 71 (with M=Ni and X=Te). Each Ni atom is surrounded by six Te atoms. These Te atoms are categorized into the top group (eg. atoms 1, 3, and 5) and bottom group (eg. atoms 2, 4, and 6). Each Te atom is connected to three Ni atoms. The structural parameters are from the first-principles calculations,<sup>48</sup> including the lattice constant  $a = 3.7248 \text{ \AA}$ , and the bond length

TABLE CCXVIII: The VFF model for single-layer 1T-NiTe<sub>2</sub>. The second line gives an explicit expression for each VFF term. The third line is the force constant parameters. Parameters are in the unit of  $\frac{\text{eV}}{\text{\AA}^2}$  for the bond stretching interactions, and in the unit of eV for the angle bending interaction. The fourth line gives the initial bond length (in unit of  $\text{\AA}$ ) for the bond stretching interaction and the initial angle (in unit of degrees) for the angle bending interaction. The angle  $\theta_{ijk}$  has atom i as the apex.

VFF type	bond stretching	angle bending	
expression	$\frac{1}{2}K_{\text{Ni-Te}}(\Delta r)^2$	$\frac{1}{2}K_{\text{Ni-Te-Te}}(\Delta\theta)^2$	$\frac{1}{2}K_{\text{Te-Ni-Ni}}(\Delta\theta)^2$
parameter	4.230	2.429	2.429
$r_0$ or $\theta_0$	2.532	94.702	94.702
or $\theta_0$	2.635	95.999	95.999

TABLE CCXIX: Two-body SW potential parameters for single-layer 1T-NiTe<sub>2</sub> used by GULP<sup>8</sup> as expressed in Eq. (3).

	$A$ (eV)	$\rho$ ( $\text{\AA}$ )	$B$ ( $\text{\AA}^4$ )	$r_{\text{min}}$ ( $\text{\AA}$ )	$r_{\text{max}}$ ( $\text{\AA}$ )
Ni-Te	4.554	1.536	20.554	0.0	3.518

TABLE CCXX: Three-body SW potential parameters for single-layer 1T-NiTe<sub>2</sub> used by GULP<sup>8</sup> as expressed in Eq. (4). The angle  $\theta_{ijk}$  in the first line indicates the bending energy for the angle with atom i as the apex.

	$K$ (eV)	$\theta_0$ (degree)	$\rho_1$ ( $\text{\AA}$ )	$\rho_2$ ( $\text{\AA}$ )	$r_{\text{min}12}$ ( $\text{\AA}$ )	$r_{\text{max}12}$ ( $\text{\AA}$ )	$r_{\text{min}13}$ ( $\text{\AA}$ )	$r_{\text{max}13}$ ( $\text{\AA}$ )	$r_{\text{min}23}$ ( $\text{\AA}$ )	$r_{\text{max}23}$ ( $\text{\AA}$ )
$\theta_{\text{Ni-Te-Te}}$	27.553	94.702	1.536	1.536	0.0	3.518	0.0	3.518	0.0	5.088
$\theta_{\text{Te-Ni-Ni}}$	27.553	94.702	1.536	1.536	0.0	3.518	0.0	3.518	0.0	5.088

TABLE CCXXI: SW potential parameters for single-layer 1T-NiTe<sub>2</sub> used by LAMMPS<sup>9</sup> as expressed in Eqs. (9) and (10).

	$\epsilon$ (eV)	$\sigma$ ( $\text{\AA}$ )	$a$	$\lambda$	$\gamma$	$\cos\theta_0$	$A_L$	$B_L$	$p$	$q$	tol
Ni-Te <sub>1</sub> -Te <sub>1</sub>	1.000	1.536	2.291	27.553	1.000	-0.082	4.554	3.696	4	0	0.0

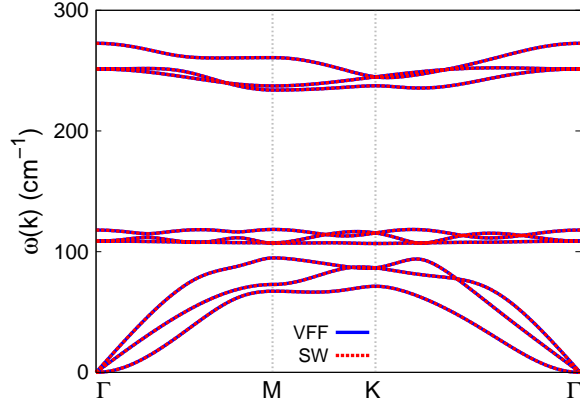


FIG. 109: (Color online) Phonon spectrum for single-layer 1T-NiTe<sub>2</sub> along the  $\Gamma$ MK $\Gamma$  direction in the Brillouin zone. The phonon dispersion from the SW potential is exactly the same as that from the VFF model.

$d_{\text{Ni-Te}} = 2.5321 \text{ \AA}$ , which is derived from the angle  $\theta_{\text{TeNiNi}} = 94.7^\circ$ . The other angle is  $\theta_{\text{NiTeTe}} = 94.7^\circ$  with Te atoms from the same (top or bottom) group.

Table CCXVIII shows three VFF terms for the single-layer 1T-NiTe<sub>2</sub>, one of which is the bond stretching interaction shown by Eq. (1) while the other two terms are the angle bending interaction shown by Eq. (2). We note that the angle bending term  $K_{\text{Ni-Te-Te}}$  is for the angle  $\theta_{\text{Ni-Te-Te}}$  with both Te atoms from the same (top or bottom) group. We find that there are actually only two parameters in the VFF model, so we can determine their value by fitting to the Young's modulus and the Poisson's ratio of the system. The *ab initio* calculations have predicted the Young's modulus to be 44 N/m and the Poisson's ratio as 0.14.<sup>48</sup>

The parameters for the two-body SW potential used by GULP are shown in Tab. CCXIX. The parameters for the three-body SW potential used by GULP are shown in Tab. CCXX. Some representative parameters for the SW potential used by LAMMPS are listed in Tab. CCXXI.

We use LAMMPS to perform MD simulations for the mechanical behavior of the single-layer 1T-NiTe<sub>2</sub> under uniaxial tension at 1.0 K and 300.0 K. Fig. 108 shows the stress-strain curve for the tension of a single-layer 1T-NiTe<sub>2</sub> of dimension  $100 \times 100 \text{ \AA}$ . Periodic boundary conditions are applied in both armchair and zigzag directions. The single-layer 1T-NiTe<sub>2</sub> is stretched uniaxially along the armchair or zigzag direction. The stress is calculated without

TABLE CCXXII: The VFF model for single-layer 1T-ZrS<sub>2</sub>. The second line gives an explicit expression for each VFF term. The third line is the force constant parameters. Parameters are in the unit of  $\frac{\text{eV}}{\text{Å}^2}$  for the bond stretching interactions, and in the unit of eV for the angle bending interaction. The fourth line gives the initial bond length (in unit of Å) for the bond stretching interaction and the initial angle (in unit of degrees) for the angle bending interaction. The angle  $\theta_{ijk}$  has atom i as the apex.

VFF type	bond stretching	angle bending	
expression	$\frac{1}{2}K_{\text{Zr-S}}(\Delta r)^2$	$\frac{1}{2}K_{\text{Zr-S-S}}(\Delta\theta)^2$	$\frac{1}{2}K_{\text{S-Zr-Zr}}(\Delta\theta)^2$
parameter	7.930	4.283	4.283
$r_0$ or $\theta_0$	2.580	91.305	91.305

involving the actual thickness of the quasi-two-dimensional structure of the single-layer 1T-NiTe<sub>2</sub>. The Young's modulus can be obtained by a linear fitting of the stress-strain relation in the small strain range of [0, 0.01]. The Young's modulus are 42.6 N/m and 42.4 N/m along the armchair and zigzag directions, respectively. The Young's modulus is essentially isotropic in the armchair and zigzag directions. The Poisson's ratio from the VFF model and the SW potential is  $\nu_{xy} = \nu_{yx} = 0.14$ .

There is no available value for nonlinear quantities in the single-layer 1T-NiTe<sub>2</sub>. We have thus used the nonlinear parameter  $B = 0.5d^4$  in Eq. (5), which is close to the value of  $B$  in most materials. The value of the third order nonlinear elasticity  $D$  can be extracted by fitting the stress-strain relation to the function  $\sigma = E\epsilon + \frac{1}{2}D\epsilon^2$  with  $E$  as the Young's modulus. The values of  $D$  from the present SW potential are -187.6 N/m and -200.6 N/m along the armchair and zigzag directions, respectively. The ultimate stress is about 4.7 Nm<sup>-1</sup> at the ultimate strain of 0.21 in the armchair direction at the low temperature of 1 K. The ultimate stress is about 4.6 Nm<sup>-1</sup> at the ultimate strain of 0.24 in the zigzag direction at the low temperature of 1 K.

Fig. 109 shows that the VFF model and the SW potential give exactly the same phonon dispersion, as the SW potential is derived from the VFF model.

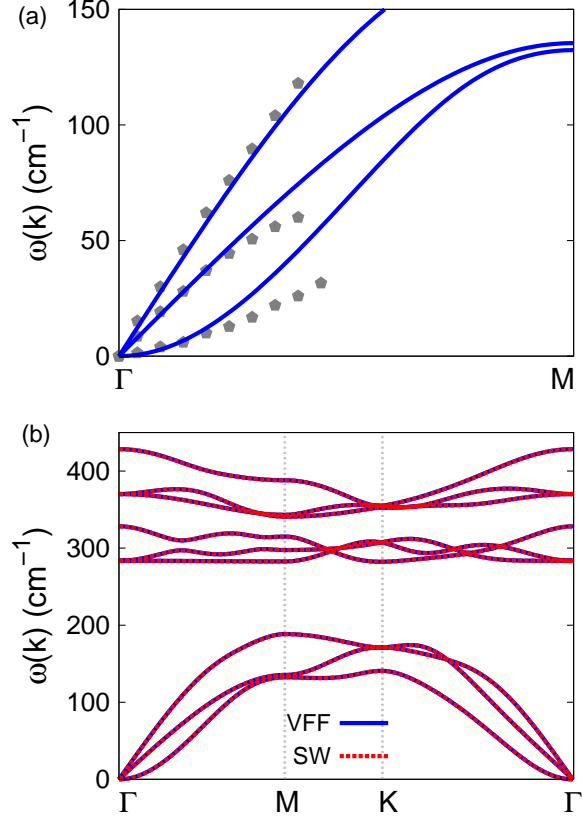


FIG. 110: (Color online) Phonon spectrum for single-layer 1T-ZrS<sub>2</sub>. (a) Phonon dispersion along the  $\Gamma$ M direction in the Brillouin zone. The results from the VFF model (lines) are comparable with the experiment data (pentagons) from Ref. 38. (b) The phonon dispersion from the SW potential is exactly the same as that from the VFF model.

TABLE CCXXIII: Two-body SW potential parameters for single-layer 1T-ZrS<sub>2</sub> used by GULP<sup>8</sup> as expressed in Eq. (3).

	$A$ (eV)	$\rho$ ( $\text{\AA}$ )	$B$ ( $\text{\AA}^4$ )	$r_{\min}$ ( $\text{\AA}$ )	$r_{\max}$ ( $\text{\AA}$ )
Zr-S	8.149	1.432	22.154	0.0	3.541

## LVI. 1T-ZRS<sub>2</sub>

Most existing theoretical studies on the single-layer 1T-ZrS<sub>2</sub> are based on the first-principles calculations. In this section, we will develop the SW potential for the single-layer 1T-ZrS<sub>2</sub>.

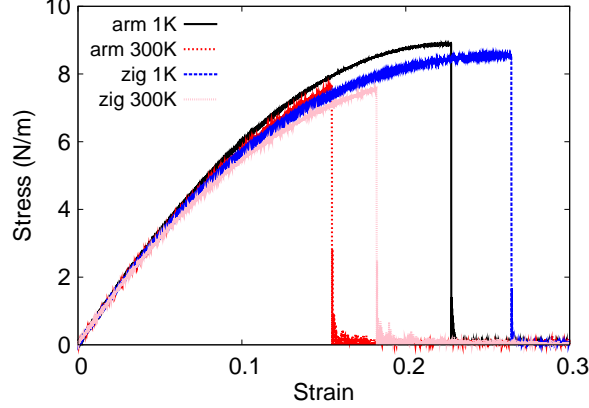


FIG. 111: (Color online) Stress-strain for single-layer 1T-ZrS<sub>2</sub> of dimension 100 × 100 Å along the armchair and zigzag directions.

TABLE CCXXIV: Three-body SW potential parameters for single-layer 1T-ZrS<sub>2</sub> used by GULP<sup>8</sup> as expressed in Eq. (4). The angle  $\theta_{ijk}$  in the first line indicates the bending energy for the angle with atom i as the apex.

	$K$ (eV)	$\theta_0$ (degree)	$\rho_1$ (Å)	$\rho_2$ (Å)	$r_{\min 12}$ (Å)	$r_{\max 12}$ (Å)	$r_{\min 13}$ (Å)	$r_{\max 13}$ (Å)	$r_{\min 23}$ (Å)	$r_{\max 23}$ (Å)
$\theta_{\text{Zr-S-S}}$	42.170	91.305	1.432	1.432	0.0	3.541	0.0	3.541	0.0	5.041
$\theta_{\text{S-Zr-Zr}}$	42.170	91.305	1.432	1.432	0.0	3.541	0.0	3.541	0.0	5.041

The structure for the single-layer 1T-ZrS<sub>2</sub> is shown in Fig. 71 (with M=Zr and X=S). Each Zr atom is surrounded by six S atoms. These S atoms are categorized into the top group (eg. atoms 1, 3, and 5) and bottom group (eg. atoms 2, 4, and 6). Each S atom is connected to three Zr atoms. The structural parameters are from the first-principles calculations,<sup>49</sup> including the lattice constant  $a = 3.690$  Å and the bond length  $d_{\text{Zr-S}} = 2.58$  Å. The resultant angles are  $\theta_{\text{ZrSS}} = 91.305^\circ$  with S atoms from the same (top or bottom) group, and

TABLE CCXXV: SW potential parameters for single-layer 1T-ZrS<sub>2</sub> used by LAMMPS<sup>9</sup> as expressed in Eqs. (9) and (10).

	$\epsilon$ (eV)	$\sigma$ (Å)	$a$	$\lambda$	$\gamma$	$\cos \theta_0$	$A_L$	$B_L$	$p$	$q$	tol
Zr-S1-S1	1.000	1.432	2.473	42.177	1.000	-0.023	8.149	5.268	4	0	0.0
S1-Zr-Zr	1.000	1.432	2.473	42.177	1.000	-0.023	8.149	5.268	4	0	0.0

$$\theta_{\text{SZrZr}} = 91.305^\circ.$$

Table [CCXXII](#) shows three VFF terms for the single-layer 1T-ZrS<sub>2</sub>, one of which is the bond stretching interaction shown by Eq. (1) while the other two terms are the angle bending interaction shown by Eq. (2). We note that the angle bending term  $K_{\text{Zr-S-S}}$  is for the angle  $\theta_{\text{Zr-S-S}}$  with both S atoms from the same (top or bottom) group. These force constant parameters are determined by fitting to the three acoustic branches in the phonon dispersion along the  $\Gamma\text{M}$  as shown in Fig. [110](#) (a). The *ab initio* calculations for the phonon dispersion are from Ref. 38. Similar phonon dispersion can also be found in other *ab initio* calculations.<sup>34</sup> Fig. [110](#) (b) shows that the VFF model and the SW potential give exactly the same phonon dispersion, as the SW potential is derived from the VFF model.

The parameters for the two-body SW potential used by GULP are shown in Tab. [CCXXIII](#). The parameters for the three-body SW potential used by GULP are shown in Tab. [CCXXIV](#). Some representative parameters for the SW potential used by LAMMPS are listed in Tab. [CCXXV](#).

We use LAMMPS to perform MD simulations for the mechanical behavior of the single-layer 1T-ZrS<sub>2</sub> under uniaxial tension at 1.0 K and 300.0 K. Fig. [111](#) shows the stress-strain curve for the tension of a single-layer 1T-ZrS<sub>2</sub> of dimension  $100 \times 100$  Å. Periodic boundary conditions are applied in both armchair and zigzag directions. The single-layer 1T-ZrS<sub>2</sub> is stretched uniaxially along the armchair or zigzag direction. The stress is calculated without involving the actual thickness of the quasi-two-dimensional structure of the single-layer 1T-ZrS<sub>2</sub>. The Young's modulus can be obtained by a linear fitting of the stress-strain relation in the small strain range of  $[0, 0.01]$ . The Young's modulus are 71.8 N/m and 71.5 N/m along the armchair and zigzag directions, respectively. The Young's modulus is essentially isotropic in the armchair and zigzag directions. These values are close to the *ab initio* results at 0 K temperature, eg. 75.74 Nm<sup>-1</sup> in Ref. 49. The Poisson's ratio from the VFF model and the SW potential is  $\nu_{xy} = \nu_{yx} = 0.16$ , which are comparable with the *ab initio* result<sup>49</sup> of 0.22.

There is no available value for nonlinear quantities in the single-layer 1T-ZrS<sub>2</sub>. We have thus used the nonlinear parameter  $B = 0.5d^4$  in Eq. (5), which is close to the value of  $B$  in most materials. The value of the third order nonlinear elasticity  $D$  can be extracted by fitting the stress-strain relation to the function  $\sigma = E\epsilon + \frac{1}{2}D\epsilon^2$  with  $E$  as the Young's modulus. The values of  $D$  from the present SW potential are -268.9 N/m and -305.2 N/m

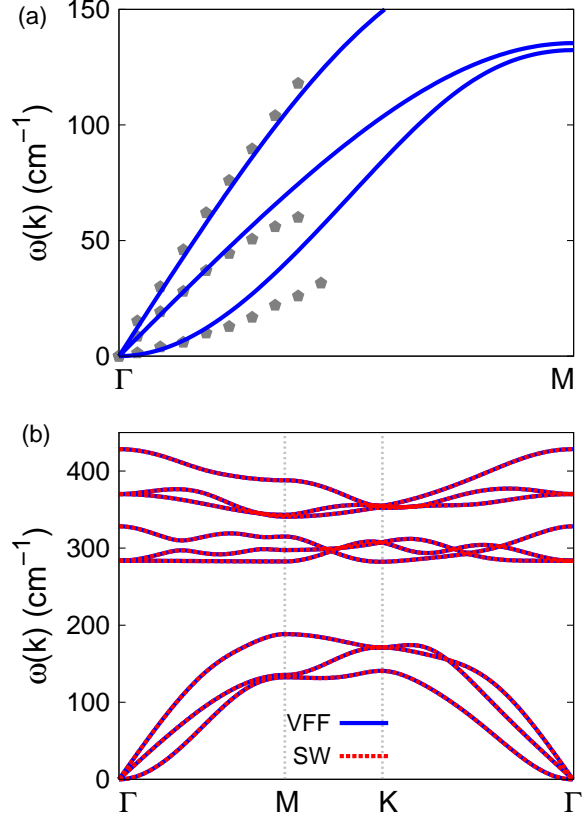


FIG. 112: (Color online) Phonon spectrum for single-layer 1T-ZrSe<sub>2</sub>. (a) Phonon dispersion along the  $\Gamma$ M direction in the Brillouin zone. The results from the VFF model (lines) are comparable with the experiment data (pentagons) from Ref. 50. (b) The phonon dispersion from the SW potential is exactly the same as that from the VFF model.

along the armchair and zigzag directions, respectively. The ultimate stress is about  $8.9 \text{ Nm}^{-1}$  at the ultimate strain of 0.23 in the armchair direction at the low temperature of 1 K. The ultimate stress is about  $8.5 \text{ Nm}^{-1}$  at the ultimate strain of 0.26 in the zigzag direction at the low temperature of 1 K.

## LVII. 1T-ZRSE<sub>2</sub>

Most existing theoretical studies on the single-layer 1T-ZrSe<sub>2</sub> are based on the first-principles calculations. In this section, we will develop the SW potential for the single-layer 1T-ZrSe<sub>2</sub>.

TABLE CCXXVI: The VFF model for single-layer 1T-ZrSe<sub>2</sub>. The second line gives an explicit expression for each VFF term. The third line is the force constant parameters. Parameters are in the unit of  $\frac{\text{eV}}{\text{Å}^2}$  for the bond stretching interactions, and in the unit of eV for the angle bending interaction. The fourth line gives the initial bond length (in unit of Å) for the bond stretching interaction and the initial angle (in unit of degrees) for the angle bending interaction. The angle  $\theta_{ijk}$  has atom i as the apex.

VFF type	bond stretching	angle bending	
expression	$\frac{1}{2}K_{\text{Zr-Se}}(\Delta r)^2$	$\frac{1}{2}K_{\text{Zr-Se-Se}}(\Delta\theta)^2$	$\frac{1}{2}K_{\text{Se-Zr-Zr}}(\Delta\theta)^2$
parameter	7.930	4.283	4.283
$r_0$ or $\theta_0$	2.667	88.058	88.058

TABLE CCXXVII: Two-body SW potential parameters for single-layer 1T-ZrSe<sub>2</sub> used by GULP<sup>8</sup> as expressed in Eq. (3).

	$A$ (eV)	$\rho$ (Å)	$B$ (Å <sup>4</sup> )	$r_{\text{min}}$ (Å)	$r_{\text{max}}$ (Å)
Zr-Se	8.022	1.354	25.297	0.0	3.617

TABLE CCXXVIII: Three-body SW potential parameters for single-layer 1T-ZrSe<sub>2</sub> used by GULP<sup>8</sup> as expressed in Eq. (4). The angle  $\theta_{ijk}$  in the first line indicates the bending energy for the angle with atom i as the apex.

	$K$ (eV)	$\theta_0$ (degree)	$\rho_1$ (Å)	$\rho_2$ (Å)	$r_{\text{min}12}$ (Å)	$r_{\text{max}12}$ (Å)	$r_{\text{min}13}$ (Å)	$r_{\text{max}13}$ (Å)	$r_{\text{min}23}$ (Å)	$r_{\text{max}23}$ (Å)
$\theta_{\text{Zr-Se-Se}}$	37.051	88.058	1.354	1.354	0.0	3.617	0.0	3.617	0.0	5.064
$\theta_{\text{Se-Zr-Zr}}$	37.051	88.058	1.354	1.354	0.0	3.617	0.0	3.617	0.0	5.064

TABLE CCXXIX: SW potential parameters for single-layer 1T-ZrSe<sub>2</sub> used by LAMMPS<sup>9</sup> as expressed in Eqs. (9) and (10).

	$\epsilon$ (eV)	$\sigma$ (Å)	$a$	$\lambda$	$\gamma$	$\cos\theta_0$	$A_L$	$B_L$	$p$	$q$	tol
Zr-Se-Se	1.000	1.354	2.671	37.051	1.000	0.034	8.022	7.527	4	0	0.0
Se-Zr-Zr	1.000	1.354	2.671	37.051	1.000	0.034	8.022	7.527	4	0	0.0

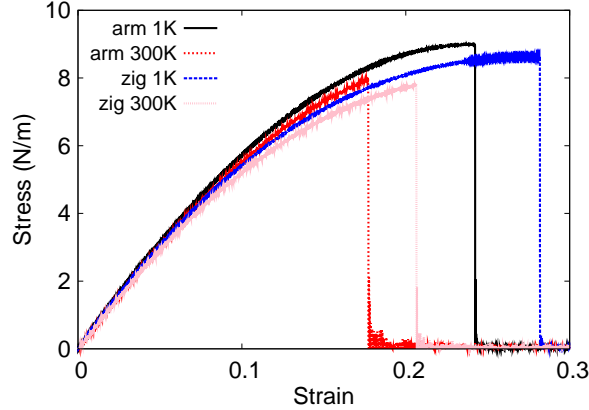


FIG. 113: (Color online) Stress-strain for single-layer 1T-ZrSe<sub>2</sub> of dimension  $100 \times 100 \text{ \AA}$  along the armchair and zigzag directions.

The structure for the single-layer 1T-ZrSe<sub>2</sub> is shown in Fig. 71 (with M=Zr and X=Se). Each Zr atom is surrounded by six Se atoms. These Se atoms are categorized into the top group (eg. atoms 1, 3, and 5) and bottom group (eg. atoms 2, 4, and 6). Each Se atom is connected to three Zr atoms. The structural parameters are from the first-principles calculations,<sup>51</sup> including the lattice constant  $a = 3.707 \text{ \AA}$ , and the position of the Se atom with respect to the Zr atomic plane  $h = 1.591 \text{ \AA}$ . The resultant angles are  $\theta_{\text{ZrSeSe}} = 88.058^\circ$  with Se atoms from the same (top or bottom) group, and  $\theta_{\text{SeZrZr}} = 88.058^\circ$ .

Table CCXXVI shows three VFF terms for the single-layer 1T-ZrSe<sub>2</sub>, one of which is the bond stretching interaction shown by Eq. (1) while the other two terms are the angle bending interaction shown by Eq. (2). We note that the angle bending term  $K_{\text{Zr-Se-Se}}$  is for the angle  $\theta_{\text{Zr-Se-Se}}$  with both Se atoms from the same (top or bottom) group. These force constant parameters are determined by fitting to the three acoustic branches in the phonon dispersion along the  $\Gamma\text{M}$  as shown in Fig. 112 (a). The *ab initio* calculations for the phonon dispersion are from Ref. 50. Similar phonon dispersion can also be found in other *ab initio* calculations.<sup>34</sup> Fig. 112 (b) shows that the VFF model and the SW potential give exactly the same phonon dispersion, as the SW potential is derived from the VFF model.

The parameters for the two-body SW potential used by GULP are shown in Tab. CCXXVII. The parameters for the three-body SW potential used by GULP are shown in Tab. CCXXVIII. Some representative parameters for the SW potential used by LAMMPS are listed in Tab. CCXXIX.

We use LAMMPS to perform MD simulations for the mechanical behavior of the single-layer 1T-ZrSe<sub>2</sub> under uniaxial tension at 1.0 K and 300.0 K. Fig. 113 shows the stress-strain curve for the tension of a single-layer 1T-ZrSe<sub>2</sub> of dimension 100 × 100 Å. Periodic boundary conditions are applied in both armchair and zigzag directions. The single-layer 1T-ZrSe<sub>2</sub> is stretched uniaxially along the armchair or zigzag direction. The stress is calculated without involving the actual thickness of the quasi-two-dimensional structure of the single-layer 1T-ZrSe<sub>2</sub>. The Young's modulus can be obtained by a linear fitting of the stress-strain relation in the small strain range of [0, 0.01]. The Young's modulus are 66.7 N/m and 66.4 N/m along the armchair and zigzag directions, respectively. The Young's modulus is essentially isotropic in the armchair and zigzag directions. The Poisson's ratio from the VFF model and the SW potential is  $\nu_{xy} = \nu_{yx} = 0.19$ .

There is no available value for nonlinear quantities in the single-layer 1T-ZrSe<sub>2</sub>. We have thus used the nonlinear parameter  $B = 0.5d^4$  in Eq. (5), which is close to the value of  $B$  in most materials. The value of the third order nonlinear elasticity  $D$  can be extracted by fitting the stress-strain relation to the function  $\sigma = E\epsilon + \frac{1}{2}D\epsilon^2$  with  $E$  as the Young's modulus. The values of  $D$  from the present SW potential are -219.6 N/m and -256.6 N/m along the armchair and zigzag directions, respectively. The ultimate stress is about 9.0 Nm<sup>-1</sup> at the ultimate strain of 0.24 in the armchair direction at the low temperature of 1 K. The ultimate stress is about 8.6 Nm<sup>-1</sup> at the ultimate strain of 0.28 in the zigzag direction at the low temperature of 1 K.

### LVIII. 1T-ZRTE<sub>2</sub>

Most existing theoretical studies on the single-layer 1T-ZrTe<sub>2</sub> are based on the first-principles calculations. In this section, we will develop the SW potential for the single-layer 1T-ZrTe<sub>2</sub>.

The structure for the single-layer 1T-ZrTe<sub>2</sub> is shown in Fig. 71 (with M=Zr and X=Te). Each Zr atom is surrounded by six Te atoms. These Te atoms are categorized into the top group (eg. atoms 1, 3, and 5) and bottom group (eg. atoms 2, 4, and 6). Each Te atom is connected to three Zr atoms. The structural parameters are from the first-principles calculations,<sup>48</sup> including the lattice constant  $a = 4.0064$  Å, and the bond length  $d_{\text{Zr-Te}} = 2.9021$  Å, which is derived from the angle  $\theta_{\text{TeZrZr}} = 87.3^\circ$ . The other angle is

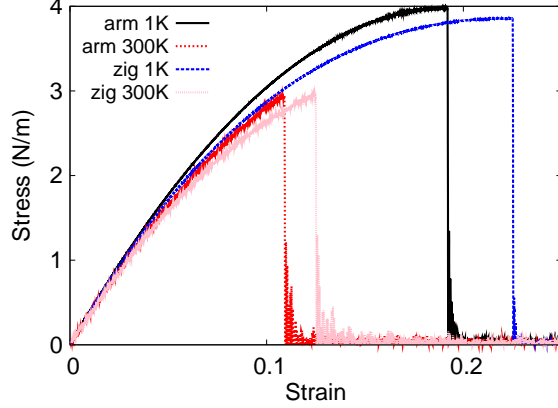


FIG. 114: (Color online) Stress-strain for single-layer 1T-ZrTe<sub>2</sub> of dimension  $100 \times 100 \text{ \AA}$  along the armchair and zigzag directions.

TABLE CCXXX: The VFF model for single-layer 1T-ZrTe<sub>2</sub>. The second line gives an explicit expression for each VFF term. The third line is the force constant parameters. Parameters are in the unit of  $\frac{\text{eV}}{\text{\AA}^2}$  for the bond stretching interactions, and in the unit of eV for the angle bending interaction. The fourth line gives the initial bond length (in unit of  $\text{\AA}$ ) for the bond stretching interaction and the initial angle (in unit of degrees) for the angle bending interaction. The angle  $\theta_{ijk}$  has atom  $i$  as the apex.

VFF type	bond stretching	angle bending	
expression	$\frac{1}{2}K_{\text{Zr-Te}}(\Delta r)^2$	$\frac{1}{2}K_{\text{Zr-Te-Te}}(\Delta\theta)^2$	$\frac{1}{2}K_{\text{Te-Zr-Zr}}(\Delta\theta)^2$
parameter	2.974	3.681	3.681
$r_0$ or $\theta_0$	2.902	87.301	87.301

$\theta_{\text{ZrTeTe}} = 87.3^\circ$  with Te atoms from the same (top or bottom) group.

Table CCXXX shows three VFF terms for the single-layer 1T-ZrTe<sub>2</sub>, one of which is the bond stretching interaction shown by Eq. (1) while the other two terms are the angle bending interaction shown by Eq. (2). We note that the angle bending term  $K_{\text{Zr-Te-Te}}$  is for the angle  $\theta_{\text{Zr-Te-Te}}$  with both Te atoms from the same (top or bottom) group. We find that there are actually only two parameters in the VFF model, so we can determine their value by fitting to the Young's modulus and the Poisson's ratio of the system. The *ab initio* calculations have predicted the Young's modulus to be 44 N/m and the Poisson's ratio as

TABLE CCXXXI: Two-body SW potential parameters for single-layer 1T-ZrTe<sub>2</sub> used by GULP<sup>8</sup> as expressed in Eq. (3).

	$A$ (eV)	$\rho$ (Å)	$B$ (Å <sup>4</sup> )	$r_{\min}$ (Å)	$r_{\max}$ (Å)
Zr-Te	3.493	1.441	35.467	0.0	3.925

TABLE CCXXXII: Three-body SW potential parameters for single-layer 1T-ZrTe<sub>2</sub> used by GULP<sup>8</sup> as expressed in Eq. (4). The angle  $\theta_{ijk}$  in the first line indicates the bending energy for the angle with atom  $i$  as the apex.

	$K$ (eV)	$\theta_0$ (degree)	$\rho_1$ (Å)	$\rho_2$ (Å)	$r_{\min12}$ (Å)	$r_{\max12}$ (Å)	$r_{\min13}$ (Å)	$r_{\max13}$ (Å)	$r_{\min23}$ (Å)	$r_{\max23}$ (Å)
$\theta_{\text{Zr-Te-Te}}$	30.905	87.301	1.441	1.441	0.0	3.925	0.0	3.925	0.0	5.473
$\theta_{\text{Te-Zr-Zr}}$	30.905	87.301	1.441	1.441	0.0	3.925	0.0	3.925	0.0	5.473

0.13.<sup>48</sup>

The parameters for the two-body SW potential used by GULP are shown in Tab. CCXXXI. The parameters for the three-body SW potential used by GULP are shown in Tab. CCXXXII. Some representative parameters for the SW potential used by LAMMPS are listed in Tab. CCXXXIII.

We use LAMMPS to perform MD simulations for the mechanical behavior of the single-layer 1T-ZrTe<sub>2</sub> under uniaxial tension at 1.0 K and 300.0 K. Fig. 114 shows the stress-strain curve for the tension of a single-layer 1T-ZrTe<sub>2</sub> of dimension  $100 \times 100$  Å. Periodic boundary conditions are applied in both armchair and zigzag directions. The single-layer 1T-ZrTe<sub>2</sub> is stretched uniaxially along the armchair or zigzag direction. The stress is calculated without involving the actual thickness of the quasi-two-dimensional structure of the single-layer 1T-ZrTe<sub>2</sub>. The Young's modulus can be obtained by a linear fitting of the stress-strain relation in the small strain range of  $[0, 0.01]$ . The Young's modulus are 39.2 N/m and 39.1 N/m along the armchair and zigzag directions, respectively. The Young's modulus is essentially

TABLE CCXXXIII: SW potential parameters for single-layer 1T-ZrTe<sub>2</sub> used by LAMMPS<sup>9</sup> as expressed in Eqs. (9) and (10).

	$\epsilon$ (eV)	$\sigma$ (Å)	$a$	$\lambda$	$\gamma$	$\cos \theta_0$	$A_L$	$B_L$	$p$	$q$	tol
Zr-Te <sub>1</sub> -Te <sub>1</sub>	1.000	1.441	2.723	30.905	1.000	0.047	3.493	8.225	4	0	0.0

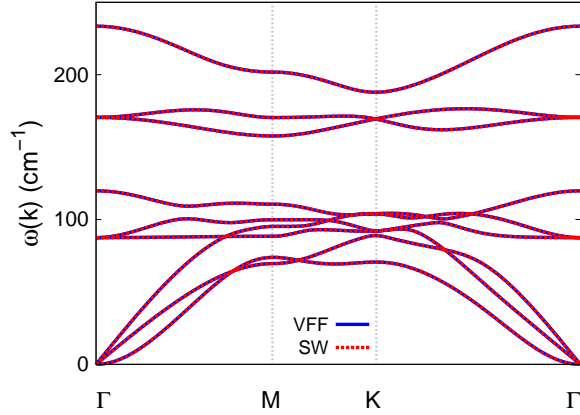


FIG. 115: (Color online) Phonon spectrum for single-layer 1T-ZrTe<sub>2</sub> along the  $\Gamma$ MK $\Gamma$  direction in the Brillouin zone. The phonon dispersion from the SW potential is exactly the same as that from the VFF model.

isotropic in the armchair and zigzag directions. The Poisson's ratio from the VFF model and the SW potential is  $\nu_{xy} = \nu_{yx} = 0.10$ . The fitted Young's modulus value is about 10% smaller than the *ab initio* result of 44 N/m,<sup>48</sup> as only short-range interactions are considered in the present work. The long-range interactions are ignored, which typically leads to about 10% underestimation for the value of the Young's modulus.

There is no available value for nonlinear quantities in the single-layer 1T-ZrTe<sub>2</sub>. We have thus used the nonlinear parameter  $B = 0.5d^4$  in Eq. (5), which is close to the value of  $B$  in most materials. The value of the third order nonlinear elasticity  $D$  can be extracted by fitting the stress-strain relation to the function  $\sigma = E\epsilon + \frac{1}{2}D\epsilon^2$  with  $E$  as the Young's modulus. The values of  $D$  from the present SW potential are -187.2 N/m and -201.1 N/m along the armchair and zigzag directions, respectively. The ultimate stress is about 4.0 Nm<sup>-1</sup> at the ultimate strain of 0.19 in the armchair direction at the low temperature of 1 K. The ultimate stress is about 3.9 Nm<sup>-1</sup> at the ultimate strain of 0.22 in the zigzag direction at the low temperature of 1 K.

Fig. 115 shows that the VFF model and the SW potential give exactly the same phonon dispersion, as the SW potential is derived from the VFF model.

TABLE CCXXXIV: The VFF model for single-layer 1T-NbS<sub>2</sub>. The second line gives an explicit expression for each VFF term. The third line is the force constant parameters. Parameters are in the unit of  $\frac{\text{eV}}{\text{Å}^2}$  for the bond stretching interactions, and in the unit of eV for the angle bending interaction. The fourth line gives the initial bond length (in unit of Å) for the bond stretching interaction and the initial angle (in unit of degrees) for the angle bending interaction. The angle  $\theta_{ijk}$  has atom i as the apex.

VFF type	bond stretching		angle bending	
expression	$\frac{1}{2}K_{\text{Nb-S}}(\Delta r)^2$	$\frac{1}{2}K_{\text{Nb-S-S}}(\Delta\theta)^2$	$\frac{1}{2}K_{\text{S-Nb-Nb}}(\Delta\theta)^2$	
parameter	7.930	4.283	4.283	
$r_0$ or $\theta_0$	2.450	84.671	84.671	

TABLE CCXXXV: Two-body SW potential parameters for single-layer 1T-NbS<sub>2</sub> used by GULP<sup>8</sup> as expressed in Eq. (3).

	$A$ (eV)	$\rho$ (Å)	$B$ (Å <sup>4</sup> )	$r_{\min}$ (Å)	$r_{\max}$ (Å)
Nb-S	6.192	1.125	18.015	0.0	3.280

TABLE CCXXXVI: Three-body SW potential parameters for single-layer 1T-NbS<sub>2</sub> used by GULP<sup>8</sup> as expressed in Eq. (4). The angle  $\theta_{ijk}$  in the first line indicates the bending energy for the angle with atom i as the apex.

	$K$ (eV)	$\theta_0$ (degree)	$\rho_1$ (Å)	$\rho_2$ (Å)	$r_{\min12}$ (Å)	$r_{\max12}$ (Å)	$r_{\min13}$ (Å)	$r_{\max13}$ (Å)	$r_{\min23}$ (Å)	$r_{\max23}$ (Å)
$\theta_{\text{Nb-S-S}}$	32.472	84.671	1.125	1.125	0.0	3.280	0.0	3.280	0.0	4.508
$\theta_{\text{S-Nb-Nb}}$	32.472	84.671	1.125	1.125	0.0	3.280	0.0	3.280	0.0	4.508

TABLE CCXXXVII: SW potential parameters for single-layer 1T-NbS<sub>2</sub> used by LAMMPS<sup>9</sup> as expressed in Eqs. (9) and (10).

	$\epsilon$ (eV)	$\sigma$ (Å)	$a$	$\lambda$	$\gamma$	$\cos\theta_0$	$A_L$	$B_L$	$p$	$q$	tol
Nb-S <sub>1</sub> -S <sub>1</sub>	1.000	1.125	2.916	32.472	1.000	0.093	6.192	11.247	4	0	0.0
S <sub>1</sub> -Nb-Nb	1.000	1.125	2.916	32.472	1.000	0.093	6.192	11.247	4	0	0.0

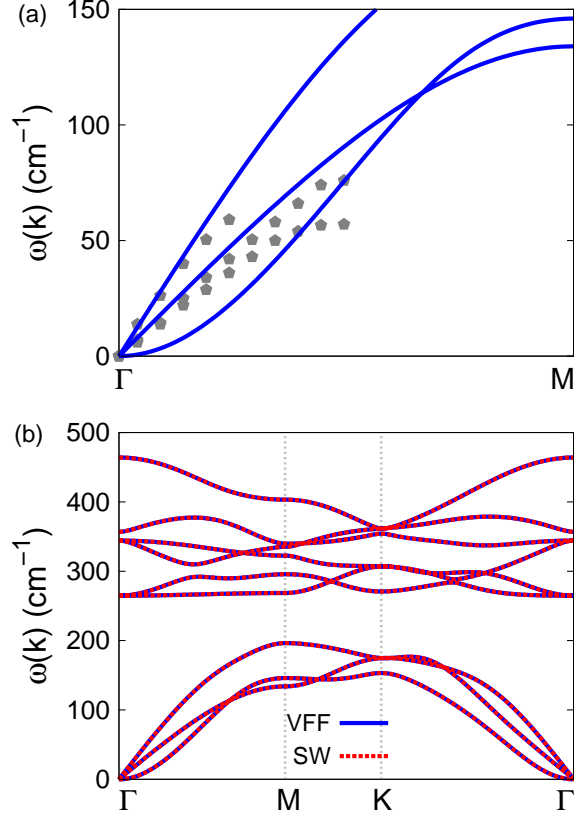


FIG. 116: (Color online) Phonon spectrum for single-layer 1T-NbS<sub>2</sub>. (a) Phonon dispersion along the  $\Gamma$ M direction in the Brillouin zone. The results from the VFF model (lines) are comparable with the experiment data (pentagons) from Ref. 12. (b) The phonon dispersion from the SW potential is exactly the same as that from the VFF model.

### LIX. 1T-NbS<sub>2</sub>

Most existing theoretical studies on the single-layer 1T-NbS<sub>2</sub> are based on the first-principles calculations. In this section, we will develop the SW potential for the single-layer 1T-NbS<sub>2</sub>.

The structure for the single-layer 1T-NbS<sub>2</sub> is shown in Fig. 71 (with M=Nb and X=S). Each Nb atom is surrounded by six S atoms. These S atoms are categorized into the top group (eg. atoms 1, 3, and 5) and bottom group (eg. atoms 2, 4, and 6). Each S atom is connected to three Nb atoms. The structural parameters are from the first-principles calculations,<sup>12</sup> including the lattice constant  $a = 3.30 \text{ \AA}$  and the bond length  $d_{\text{Nb-S}} = 2.45 \text{ \AA}$ .

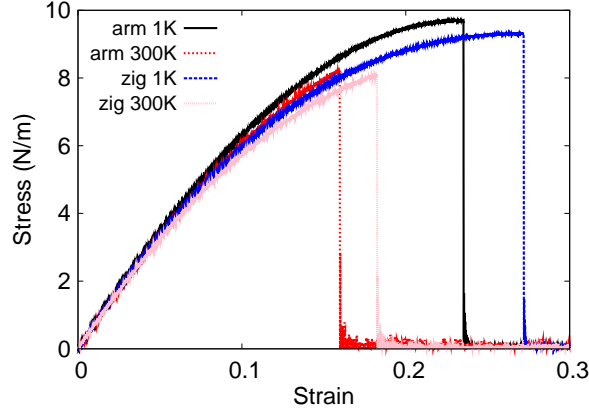


FIG. 117: (Color online) Stress-strain for single-layer 1T-NbS<sub>2</sub> of dimension 100 × 100 Å along the armchair and zigzag directions.

The resultant angles are  $\theta_{\text{NbSS}} = 84.671^\circ$  with S atoms from the same (top or bottom) group, and  $\theta_{\text{SNbNb}} = 84.671^\circ$ .

Table CCXXXIV shows three VFF terms for the single-layer 1T-NbS<sub>2</sub>, one of which is the bond stretching interaction shown by Eq. (1) while the other two terms are the angle bending interaction shown by Eq. (2). We note that the angle bending term  $K_{\text{Nb-S-S}}$  is for the angle  $\theta_{\text{Nb-S-S}}$  with both S atoms from the same (top or bottom) group. These force constant parameters are determined by fitting to the three acoustic branches in the phonon dispersion along the  $\Gamma\text{M}$  as shown in Fig. 116 (a). The *ab initio* calculations for the phonon dispersion are from Ref. 12. The lowest acoustic branch (flexural mode) is linear and very close to the inplane transverse acoustic branch in the *ab initio* calculations, which may due to the violation of the rigid rotational invariance.<sup>20</sup> Fig. 116 (b) shows that the VFF model and the SW potential give exactly the same phonon dispersion, as the SW potential is derived from the VFF model.

The parameters for the two-body SW potential used by GULP are shown in Tab. CCXXXV. The parameters for the three-body SW potential used by GULP are shown in Tab. CCXXXVI. Some representative parameters for the SW potential used by LAMMPS are listed in Tab. CCXXXVII.

We use LAMMPS to perform MD simulations for the mechanical behavior of the single-layer 1T-NbS<sub>2</sub> under uniaxial tension at 1.0 K and 300.0 K. Fig. 117 shows the stress-strain curve for the tension of a single-layer 1T-NbS<sub>2</sub> of dimension 100 × 100 Å. Periodic boundary

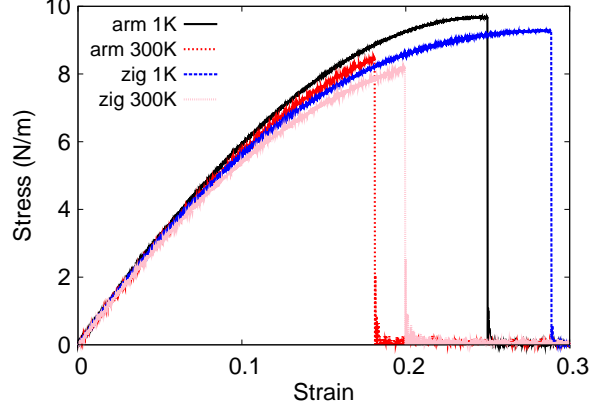


FIG. 118: (Color online) Stress-strain for single-layer 1T-NbSe<sub>2</sub> of dimension  $100 \times 100 \text{ \AA}$  along the armchair and zigzag directions.

conditions are applied in both armchair and zigzag directions. The single-layer 1T-NbS<sub>2</sub> is stretched uniaxially along the armchair or zigzag direction. The stress is calculated without involving the actual thickness of the quasi-two-dimensional structure of the single-layer 1T-NbS<sub>2</sub>. The Young's modulus can be obtained by a linear fitting of the stress-strain relation in the small strain range of  $[0, 0.01]$ . The Young's modulus are 73.8 N/m and 73.4 N/m along the armchair and zigzag directions, respectively. The Young's modulus is essentially isotropic in the armchair and zigzag directions. The Poisson's ratio from the VFF model and the SW potential is  $\nu_{xy} = \nu_{yx} = 0.18$ .

There is no available value for nonlinear quantities in the single-layer 1T-NbS<sub>2</sub>. We have thus used the nonlinear parameter  $B = 0.5d^4$  in Eq. (5), which is close to the value of  $B$  in most materials. The value of the third order nonlinear elasticity  $D$  can be extracted by fitting the stress-strain relation to the function  $\sigma = E\epsilon + \frac{1}{2}D\epsilon^2$  with  $E$  as the Young's modulus. The values of  $D$  from the present SW potential are -250.5 N/m and -290.4 N/m along the armchair and zigzag directions, respectively. The ultimate stress is about  $9.7 \text{ Nm}^{-1}$  at the ultimate strain of 0.23 in the armchair direction at the low temperature of 1 K. The ultimate stress is about  $9.4 \text{ Nm}^{-1}$  at the ultimate strain of 0.27 in the zigzag direction at the low temperature of 1 K.

TABLE CCXXXVIII: The VFF model for single-layer 1T-NbSe<sub>2</sub>. The second line gives an explicit expression for each VFF term. The third line is the force constant parameters. Parameters are in the unit of  $\frac{\text{eV}}{\text{\AA}^2}$  for the bond stretching interactions, and in the unit of eV for the angle bending interaction. The fourth line gives the initial bond length (in unit of \AA) for the bond stretching interaction and the initial angle (in unit of degrees) for the angle bending interaction. The angle  $\theta_{ijk}$  has atom i as the apex.

VFF type	bond stretching	angle bending	
expression	$\frac{1}{2}K_{\text{Nb-Se}}(\Delta r)^2$	$\frac{1}{2}K_{\text{Nb-Se-Se}}(\Delta\theta)^2$	$\frac{1}{2}K_{\text{Se-Nb-Nb}}(\Delta\theta)^2$
parameter	7.930	4.283	4.283
$r_0$ or $\theta_0$	2.570	82.529	82.529

TABLE CCXXXIX: Two-body SW potential parameters for single-layer 1T-NbSe<sub>2</sub> used by GULP<sup>8</sup> as expressed in Eq. (3).

	$A$ (eV)	$\rho$ (\AA)	$B$ (\AA <sup>4</sup> )	$r_{\text{min}}$ (\AA)	$r_{\text{max}}$ (\AA)
Nb-Se	6.430	1.104	21.812	0.0	3.412

## LX. 1T-NBSE<sub>2</sub>

Most existing theoretical studies on the single-layer 1T-NbSe<sub>2</sub> are based on the first-principles calculations. In this section, we will develop the SW potential for the single-layer 1T-NbSe<sub>2</sub>.

The structure for the single-layer 1T-NbSe<sub>2</sub> is shown in Fig. 71 (with M=Nb and X=Se). Each Nb atom is surrounded by six Se atoms. These Se atoms are categorized into the top group (eg. atoms 1, 3, and 5) and bottom group (eg. atoms 2, 4, and 6). Each

TABLE CCXL: Three-body SW potential parameters for single-layer 1T-NbSe<sub>2</sub> used by GULP<sup>8</sup> as expressed in Eq. (4). The angle  $\theta_{ijk}$  in the first line indicates the bending energy for the angle with atom i as the apex.

	$K$ (eV)	$\theta_0$ (degree)	$\rho_1$ (\AA)	$\rho_2$ (\AA)	$r_{\text{min}12}$ (\AA)	$r_{\text{max}12}$ (\AA)	$r_{\text{min}13}$ (\AA)	$r_{\text{max}13}$ (\AA)	$r_{\text{min}23}$ (\AA)	$r_{\text{max}23}$ (\AA)
$\theta_{\text{Nb-Se-Se}}$	29.956	82.528	1.104	1.104	0.0	3.412	0.0	3.412	0.0	4.631
$\theta_{\text{Se-Nb-Nb}}$	29.956	82.528	1.104	1.104	0.0	3.412	0.0	3.412	0.0	4.631

TABLE CCXLI: SW potential parameters for single-layer 1T-NbSe<sub>2</sub> used by LAMMPS<sup>9</sup> as expressed in Eqs. (9) and (10).

	$\epsilon$ (eV)	$\sigma$ (Å)	$a$	$\lambda$	$\gamma$	$\cos \theta_0$	$A_L$	$B_L$	$p$	$q$	tol
Nb-Se <sub>1</sub> -Se <sub>1</sub>	1.000	1.104	3.092	29.956	1.000	0.130	6.430	14.706	4	0	0.0

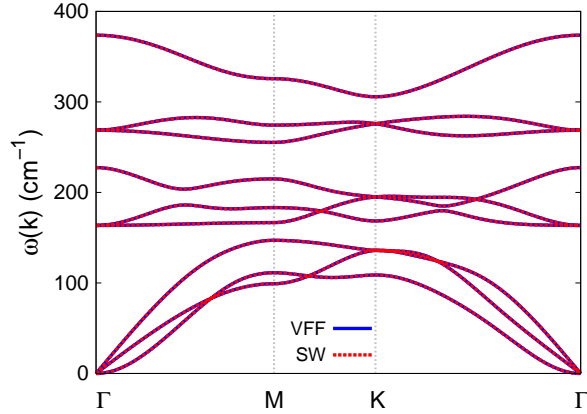


FIG. 119: (Color online) Phonon spectrum for single-layer 1T-NbSe<sub>2</sub> along the  $\Gamma$ MKT direction in the Brillouin zone. The phonon dispersion from the SW potential is exactly the same as that from the VFF model.

Se atom is connected to three Nb atoms. The structural parameters are from the first-principles calculations,<sup>12</sup> including the lattice constant  $a = 3.39$  Å and the bond length  $d_{\text{Nb-Se}} = 2.57$  Å. The resultant angles are  $\theta_{\text{NbSeSe}} = 82.529^\circ$  with Se atoms from the same (top or bottom) group, and  $\theta_{\text{SeNbNb}} = 82.529^\circ$ .

Table CCXXXVIII shows three VFF terms for the single-layer 1T-NbSe<sub>2</sub>, one of which is the bond stretching interaction shown by Eq. (1) while the other two terms are the angle bending interaction shown by Eq. (2). We note that the angle bending term  $K_{\text{Nb-Se-Se}}$  is for the angle  $\theta_{\text{Nb-Se-Se}}$  with both Se atoms from the same (top or bottom) group. We find that there are actually only two parameters in the VFF model, so we can determine their value by fitting to the Young's modulus and the Poisson's ratio of the system. The *ab initio* calculations have predicted the Young's modulus to be 73 N/m and the Poisson's ratio as 0.20.<sup>48</sup>

The parameters for the two-body SW potential used by GULP are shown in Tab. CCXXXIX. The parameters for the three-body SW potential used by GULP are shown

in Tab. CCXL. Some representative parameters for the SW potential used by LAMMPS are listed in Tab. CCXLI.

We use LAMMPS to perform MD simulations for the mechanical behavior of the single-layer 1T-NbSe<sub>2</sub> under uniaxial tension at 1.0 K and 300.0 K. Fig. 118 shows the stress-strain curve for the tension of a single-layer 1T-NbSe<sub>2</sub> of dimension 100 × 100 Å. Periodic boundary conditions are applied in both armchair and zigzag directions. The single-layer 1T-NbSe<sub>2</sub> is stretched uniaxially along the armchair or zigzag direction. The stress is calculated without involving the actual thickness of the quasi-two-dimensional structure of the single-layer 1T-NbSe<sub>2</sub>. The Young's modulus can be obtained by a linear fitting of the stress-strain relation in the small strain range of [0, 0.01]. The Young's modulus are 67.1 N/m and 66.8 N/m along the armchair and zigzag directions, respectively. The Young's modulus is essentially isotropic in the armchair and zigzag directions. The Poisson's ratio from the VFF model and the SW potential is  $\nu_{xy} = \nu_{yx} = 0.20$ . The fitted Young's modulus value is about 10% smaller than the *ab initio* result of 73 N/m,<sup>48</sup> as only short-range interactions are considered in the present work. The long-range interactions are ignored, which typically lead to about 10% underestimation for the Young's modulus value.

There is no available value for nonlinear quantities in the single-layer 1T-NbSe<sub>2</sub>. We have thus used the nonlinear parameter  $B = 0.5d^4$  in Eq. (5), which is close to the value of  $B$  in most materials. The value of the third order nonlinear elasticity  $D$  can be extracted by fitting the stress-strain relation to the function  $\sigma = E\epsilon + \frac{1}{2}D\epsilon^2$  with  $E$  as the Young's modulus. The values of  $D$  from the present SW potential are -193.5 N/m and -233.4 N/m along the armchair and zigzag directions, respectively. The ultimate stress is about 9.7 Nm<sup>-1</sup> at the ultimate strain of 0.25 in the armchair direction at the low temperature of 1 K. The ultimate stress is about 9.3 Nm<sup>-1</sup> at the ultimate strain of 0.29 in the zigzag direction at the low temperature of 1 K.

Fig. 119 shows that the VFF model and the SW potential give exactly the same phonon dispersion, as the SW potential is derived from the VFF model.

## LXI. 1T-NbTe<sub>2</sub>

Most existing theoretical studies on the single-layer 1T-NbTe<sub>2</sub> are based on the first-principles calculations. In this section, we will develop the SW potential for the single-layer

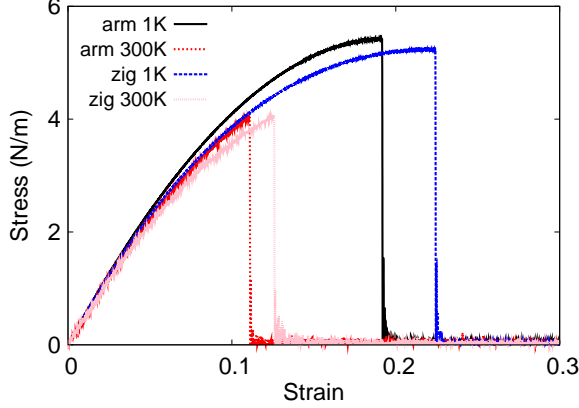


FIG. 120: (Color online) Stress-strain for single-layer 1T-NbTe<sub>2</sub> of dimension  $100 \times 100 \text{ \AA}$  along the armchair and zigzag directions.

TABLE CCXLII: The VFF model for single-layer 1T-NbTe<sub>2</sub>. The second line gives an explicit expression for each VFF term. The third line is the force constant parameters. Parameters are in the unit of  $\frac{eV}{\text{Å}^2}$  for the bond stretching interactions, and in the unit of eV for the angle bending interaction. The fourth line gives the initial bond length (in unit of Å) for the bond stretching interaction and the initial angle (in unit of degrees) for the angle bending interaction. The angle  $\theta_{ijk}$  has atom  $i$  as the apex.

VFF type	bond stretching	angle bending	
expression	$\frac{1}{2}K_{\text{Nb-Te}}(\Delta r)^2$	$\frac{1}{2}K_{\text{Nb-Te-Te}}(\Delta\theta)^2$	$\frac{1}{2}K_{\text{Te-Nb-Nb}}(\Delta\theta)^2$
parameter	3.559	4.863	4.863
$r_0$ or $\theta_0$	2.770	79.972	79.972

1T-NbTe<sub>2</sub>.

The structure for the single-layer 1T-NbTe<sub>2</sub> is shown in Fig. 71 (with M=Nb and X=Te). Each Nb atom is surrounded by six Te atoms. These Te atoms are categorized into the top group (eg. atoms 1, 3, and 5) and bottom group (eg. atoms 2, 4, and 6). Each Te atom is connected to three Nb atoms. The structural parameters are from the first-principles calculations,<sup>12</sup> including the lattice constant  $a = 3.56 \text{ \AA}$  and the bond length  $d_{\text{Nb-Te}} = 2.77 \text{ \AA}$ . The resultant angles are  $\theta_{\text{NbTeTe}} = 79.972^\circ$  with Te atoms from the same (top or bottom) group, and  $\theta_{\text{TeNbNb}} = 79.972^\circ$ .

TABLE CCXLIII: Two-body SW potential parameters for single-layer 1T-NbTe<sub>2</sub> used by GULP<sup>8</sup> as expressed in Eq. (3).

	$A$ (eV)	$\rho$ (Å)	$B$ (Å <sup>4</sup> )	$r_{\min}$ (Å)	$r_{\max}$ (Å)
Nb-Te	3.123	1.094	29.437	0.0	3.640

TABLE CCXLIV: Three-body SW potential parameters for single-layer 1T-NbTe<sub>2</sub> used by GULP<sup>8</sup> as expressed in Eq. (4). The angle  $\theta_{ijk}$  in the first line indicates the bending energy for the angle with atom  $i$  as the apex.

	$K$ (eV)	$\theta_0$ (degree)	$\rho_1$ (Å)	$\rho_2$ (Å)	$r_{\min12}$ (Å)	$r_{\max12}$ (Å)	$r_{\min13}$ (Å)	$r_{\max13}$ (Å)	$r_{\min23}$ (Å)	$r_{\max23}$ (Å)
$\theta_{\text{Nb-Te-Te}}$	30.968	79.972	1.094	1.094	0.0	3.640	0.0	3.640	0.0	4.863
$\theta_{\text{Te-Nb-Nb}}$	30.968	79.972	1.094	1.094	0.0	3.640	0.0	3.640	0.0	4.863

Table CCXLII shows three VFF terms for the single-layer 1T-NbTe<sub>2</sub>, one of which is the bond stretching interaction shown by Eq. (1) while the other two terms are the angle bending interaction shown by Eq. (2). We note that the angle bending term  $K_{\text{Nb-Te-Te}}$  is for the angle  $\theta_{\text{Nb-Te-Te}}$  with both Te atoms from the same (top or bottom) group. We find that there are actually only two parameters in the VFF model, so we can determine their value by fitting to the Young's modulus and the Poisson's ratio of the system. The *ab initio* calculations have predicted the Young's modulus to be 56 N/m and the Poisson's ratio as 0.11.<sup>48</sup>

The parameters for the two-body SW potential used by GULP are shown in Tab. CCXLIII. The parameters for the three-body SW potential used by GULP are shown in Tab. CCXLIV. Some representative parameters for the SW potential used by LAMMPS are listed in Tab. CCXLV.

We use LAMMPS to perform MD simulations for the mechanical behavior of the single-layer 1T-NbTe<sub>2</sub> under uniaxial tension at 1.0 K and 300.0 K. Fig. 120 shows the stress-strain

TABLE CCXLV: SW potential parameters for single-layer 1T-NbTe<sub>2</sub> used by LAMMPS<sup>9</sup> as expressed in Eqs. (9) and (10).

	$\epsilon$ (eV)	$\sigma$ (Å)	$a$	$\lambda$	$\gamma$	$\cos \theta_0$	$A_L$	$B_L$	$p$	$q$	tol
Nb-Te <sub>1</sub> -Te <sub>1</sub>	1.000	1.094	3.328	30.968	1.000	0.174	3.123	20.560	4	0	0.0

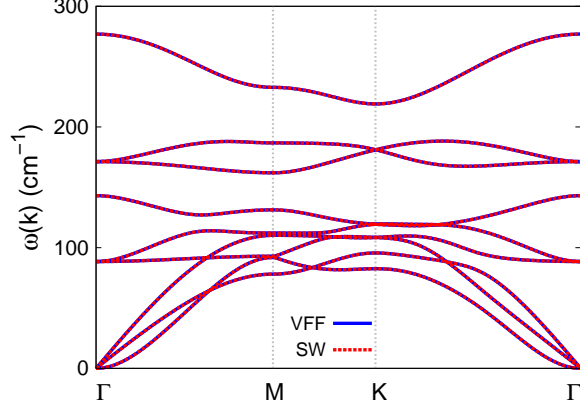


FIG. 121: (Color online) Phonon spectrum for single-layer 1T-NbTe<sub>2</sub> along the  $\Gamma$ MK $\Gamma$  direction in the Brillouin zone. The phonon dispersion from the SW potential is exactly the same as that from the VFF model.

curve for the tension of a single-layer 1T-NbTe<sub>2</sub> of dimension  $100 \times 100$  Å. Periodic boundary conditions are applied in both armchair and zigzag directions. The single-layer 1T-NbTe<sub>2</sub> is stretched uniaxially along the armchair or zigzag direction. The stress is calculated without involving the actual thickness of the quasi-two-dimensional structure of the single-layer 1T-NbTe<sub>2</sub>. The Young's modulus can be obtained by a linear fitting of the stress-strain relation in the small strain range of  $[0, 0.01]$ . The Young's modulus are 52.2 N/m and 51.9 N/m along the armchair and zigzag directions, respectively. The Young's modulus is essentially isotropic in the armchair and zigzag directions. The Poisson's ratio from the VFF model and the SW potential is  $\nu_{xy} = \nu_{yx} = 0.11$ . The fitted Young's modulus value is about 10% smaller than the *ab initio* result of 56 N/m,<sup>48</sup> as only short-range interactions are considered in the present work. The long-range interactions are ignored, which typically leads to about 10% underestimation for the value of the Young's modulus.

There is no available value for nonlinear quantities in the single-layer 1T-NbTe<sub>2</sub>. We have thus used the nonlinear parameter  $B = 0.5d^4$  in Eq. (5), which is close to the value of  $B$  in most materials. The value of the third order nonlinear elasticity  $D$  can be extracted by fitting the stress-strain relation to the function  $\sigma = E\epsilon + \frac{1}{2}D\epsilon^2$  with  $E$  as the Young's modulus. The values of  $D$  from the present SW potential are -237.7 N/m and -265.0 N/m along the armchair and zigzag directions, respectively. The ultimate stress is about 5.4 Nm<sup>-1</sup> at the ultimate strain of 0.19 in the armchair direction at the low temperature of 1 K. The

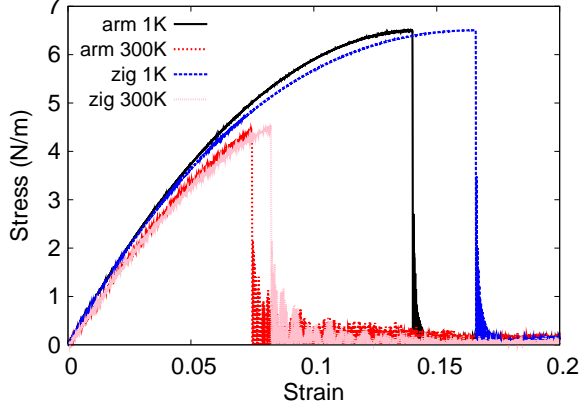


FIG. 122: (Color online) Stress-strain for single-layer 1T-MoS<sub>2</sub> of dimension  $100 \times 100 \text{ \AA}$  along the armchair and zigzag directions.

TABLE CCXLVI: The VFF model for single-layer 1T-MoS<sub>2</sub>. The second line gives an explicit expression for each VFF term. The third line is the force constant parameters. Parameters are in the unit of  $\frac{\text{eV}}{\text{\AA}^2}$  for the bond stretching interactions, and in the unit of eV for the angle bending interaction. The fourth line gives the initial bond length (in unit of  $\text{\AA}$ ) for the bond stretching interaction and the initial angle (in unit of degrees) for the angle bending interaction. The angle  $\theta_{ijk}$  has atom  $i$  as the apex.

VFF type	bond stretching	angle bending	
expression	$\frac{1}{2}K_{\text{Mo-S}}(\Delta r)^2$	$\frac{1}{2}K_{\text{Mo-S-S}}(\Delta\theta)^2$	$\frac{1}{2}K_{\text{S-Mo-Mo}}(\Delta\theta)^2$
parameter	3.523	10.394	10.394
$r_0$ or $\theta_0$	2.419	82.799	82.799

ultimate stress is about  $5.2 \text{ Nm}^{-1}$  at the ultimate strain of 0.22 in the zigzag direction at the low temperature of 1 K.

Fig. 121 shows that the VFF model and the SW potential give exactly the same phonon dispersion, as the SW potential is derived from the VFF model.

## LXII. 1T-MOS<sub>2</sub>

Most existing theoretical studies on the single-layer 1T-MoS<sub>2</sub> are based on the first-principles calculations. In this section, we will develop the SW potential for the single-layer

TABLE CCXLVII: Two-body SW potential parameters for single-layer 1T-MoS<sub>2</sub> used by GULP<sup>8</sup> as expressed in Eq. (3).

	$A$ (eV)	$\rho$ (Å)	$B$ (Å <sup>4</sup> )	$r_{\min}$ (Å)	$r_{\max}$ (Å)
Mo-S	2.550	1.048	17.129	0.0	3.215

TABLE CCXLVIII: Three-body SW potential parameters for single-layer 1T-MoS<sub>2</sub> used by GULP<sup>8</sup> as expressed in Eq. (4). The angle  $\theta_{ijk}$  in the first line indicates the bending energy for the angle with atom  $i$  as the apex.

	$K$ (eV)	$\theta_0$ (degree)	$\rho_1$ (Å)	$\rho_2$ (Å)	$r_{\min12}$ (Å)	$r_{\max12}$ (Å)	$r_{\min13}$ (Å)	$r_{\max13}$ (Å)	$r_{\min23}$ (Å)	$r_{\max23}$ (Å)
$\theta_{\text{Mo-S-S}}$	73.436	82.799	1.048	1.048	0.0	3.215	0.0	3.215	0.0	4.371
$\theta_{\text{S-Mo-Mo}}$	73.436	82.799	1.048	1.048	0.0	3.215	0.0	3.215	0.0	4.371

1T-MoS<sub>2</sub>.

The structure for the single-layer 1T-MoS<sub>2</sub> is shown in Fig. 71 (with M=Mo and X=S). Each Mo atom is surrounded by six S atoms. These S atoms are categorized into the top group (eg. atoms 1, 3, and 5) and bottom group (eg. atoms 2, 4, and 6). Each S atom is connected to three Mo atoms. The structural parameters are from the first-principles calculations,<sup>48</sup> including the lattice constant  $a = 3.1998$  Å, and the bond length  $d_{\text{Mo-S}} = 2.4193$  Å, which is derived from the angle  $\theta_{\text{SMoMo}} = 82.8^\circ$ . The other angle is  $\theta_{\text{MoSS}} = 82.8^\circ$  with S atoms from the same (top or bottom) group.

Table CCXLVI shows three VFF terms for the single-layer 1T-MoS<sub>2</sub>, one of which is the bond stretching interaction shown by Eq. (1) while the other two terms are the angle bending interaction shown by Eq. (2). We note that the angle bending term  $K_{\text{Mo-S-S}}$  is for the angle  $\theta_{\text{Mo-S-S}}$  with both S atoms from the same (top or bottom) group. We find that there are actually only two parameters in the VFF model, so we can determine their value by fitting to the Young's modulus and the Poisson's ratio of the system. The *ab initio*

TABLE CCXLIX: SW potential parameters for single-layer 1T-MoS<sub>2</sub> used by LAMMPS<sup>9</sup> as expressed in Eqs. (9) and (10).

	$\epsilon$ (eV)	$\sigma$ (Å)	$a$	$\lambda$	$\gamma$	$\cos \theta_0$	$A_L$	$B_L$	$p$	$q$	tol
Mo-S <sub>1</sub> -S <sub>1</sub>	1.000	1.048	3.069	73.436	1.000	0.125	2.550	14.207	4	0	0.0

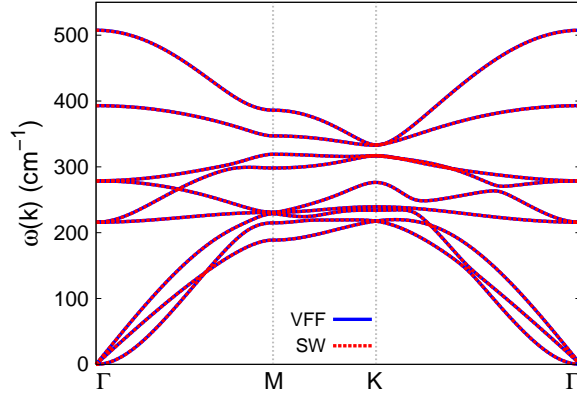


FIG. 123: (Color online) Phonon spectrum for single-layer 1T-MoS<sub>2</sub> along the  $\Gamma$ MK $\Gamma$  direction in the Brillouin zone. The phonon dispersion from the SW potential is exactly the same as that from the VFF model.

calculations have predicted the Young's modulus to be 103 N/m and the Poisson's ratio as -0.07.<sup>48</sup> The *ab initio* calculations have predicted a negative Poisson's ratio in the 1T-MoS<sub>2</sub>, which was attributed to the orbital coupling in this material. The orbital coupling enhances the angle bending interaction in the VFF model. As a result, the value of the angle bending parameter is much larger than the bond stretching force constant parameter, which is typical in auxetic materials with negative Poisson's ratio.<sup>52</sup>

The parameters for the two-body SW potential used by GULP are shown in Tab. CCXLVII. The parameters for the three-body SW potential used by GULP are shown in Tab. CCXLVIII. Some representative parameters for the SW potential used by LAMMPS are listed in Tab. CCXLIX.

We use LAMMPS to perform MD simulations for the mechanical behavior of the single-layer 1T-MoS<sub>2</sub> under uniaxial tension at 1.0 K and 300.0 K. Fig. 122 shows the stress-strain curve for the tension of a single-layer 1T-MoS<sub>2</sub> of dimension  $100 \times 100$  Å. Periodic boundary conditions are applied in both armchair and zigzag directions. The single-layer 1T-MoS<sub>2</sub> is stretched uniaxially along the armchair or zigzag direction. The stress is calculated without involving the actual thickness of the quasi-two-dimensional structure of the single-layer 1T-MoS<sub>2</sub>. The Young's modulus can be obtained by a linear fitting of the stress-strain relation in the small strain range of [0, 0.01]. The Young's modulus are 88.7 N/m and 88.3 N/m along the armchair and zigzag directions, respectively. The Young's modulus is essentially

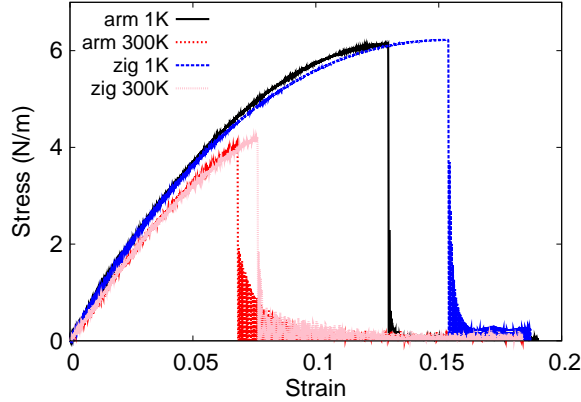


FIG. 124: (Color online) Stress-strain for single-layer 1T-MoSe<sub>2</sub> of dimension  $100 \times 100 \text{ \AA}$  along the armchair and zigzag directions.

isotropic in the armchair and zigzag directions. The Poisson's ratio from the VFF model and the SW potential is  $\nu_{xy} = \nu_{yx} = -0.07$ . The fitted Young's modulus value is about 10% smaller than the *ab initio* result of 103 N/m,<sup>48</sup> as only short-range interactions are considered in the present work. The long-range interactions are ignored, which typically leads to about 10% underestimation for the value of the Young's modulus.

There is no available value for nonlinear quantities in the single-layer 1T-MoS<sub>2</sub>. We have thus used the nonlinear parameter  $B = 0.5d^4$  in Eq. (5), which is close to the value of  $B$  in most materials. The value of the third order nonlinear elasticity  $D$  can be extracted by fitting the stress-strain relation to the function  $\sigma = E\epsilon + \frac{1}{2}D\epsilon^2$  with  $E$  as the Young's modulus. The values of  $D$  from the present SW potential are -595.2 N/m and -624.1 N/m along the armchair and zigzag directions, respectively. The ultimate stress is about  $6.5 \text{ Nm}^{-1}$  at the ultimate strain of 0.14 in the armchair direction at the low temperature of 1 K. The ultimate stress is about  $6.5 \text{ Nm}^{-1}$  at the ultimate strain of 0.16 in the zigzag direction at the low temperature of 1 K.

Fig. 123 shows that the VFF model and the SW potential give exactly the same phonon dispersion, as the SW potential is derived from the VFF model.

TABLE CCL: The VFF model for single-layer 1T-MoSe<sub>2</sub>. The second line gives an explicit expression for each VFF term. The third line is the force constant parameters. Parameters are in the unit of  $\frac{\text{eV}}{\text{\AA}^2}$  for the bond stretching interactions, and in the unit of eV for the angle bending interaction. The fourth line gives the initial bond length (in unit of \AA) for the bond stretching interaction and the initial angle (in unit of degrees) for the angle bending interaction. The angle  $\theta_{ijk}$  has atom i as the apex.

VFF type	bond stretching	angle bending	
expression	$\frac{1}{2}K_{\text{Mo-Se}}(\Delta r)^2$	$\frac{1}{2}K_{\text{Mo-Se-Se}}(\Delta\theta)^2$	$\frac{1}{2}K_{\text{Se-Mo-Mo}}(\Delta\theta)^2$
parameter	2.964	14.753	14.753
$r_0$ or $\theta_0$	2.529	80.501	80.501

TABLE CCLI: Two-body SW potential parameters for single-layer 1T-MoSe<sub>2</sub> used by GULP<sup>8</sup> as expressed in Eq. (3).

	$A$ (eV)	$\rho$ (\AA)	$B$ (\AA <sup>4</sup> )	$r_{\text{min}}$ (\AA)	$r_{\text{max}}$ (\AA)
Mo-Se	2.201	1.017	20.463	0.0	3.331

### LXIII. 1T-MOSE<sub>2</sub>

Most existing theoretical studies on the single-layer 1T-MoSe<sub>2</sub> are based on the first-principles calculations. In this section, we will develop the SW potential for the single-layer 1T-MoSe<sub>2</sub>.

The structure for the single-layer 1T-MoSe<sub>2</sub> is shown in Fig. 71 (with M=Mo and X=Se). Each Mo atom is surrounded by six Se atoms. These Se atoms are categorized into the top group (eg. atoms 1, 3, and 5) and bottom group (eg. atoms 2, 4, and 6). Each

TABLE CCLII: Three-body SW potential parameters for single-layer 1T-MoSe<sub>2</sub> used by GULP<sup>8</sup> as expressed in Eq. (4). The angle  $\theta_{ijk}$  in the first line indicates the bending energy for the angle with atom i as the apex.

	$K$ (eV)	$\theta_0$ (degree)	$\rho_1$ (\AA)	$\rho_2$ (\AA)	$r_{\text{min}12}$ (\AA)	$r_{\text{max}12}$ (\AA)	$r_{\text{min}13}$ (\AA)	$r_{\text{max}13}$ (\AA)	$r_{\text{min}23}$ (\AA)	$r_{\text{max}23}$ (\AA)
$\theta_{\text{Mo-Se-Se}}$	95.770	80.501	1.017	1.017	0.0	3.331	0.0	3.331	0.0	4.465
$\theta_{\text{Se-Mo-Mo}}$	95.770	80.501	1.017	1.017	0.0	3.331	0.0	3.331	0.0	4.465

TABLE CCLIII: SW potential parameters for single-layer 1T-MoSe<sub>2</sub> used by LAMMPS<sup>9</sup> as expressed in Eqs. (9) and (10).

	$\epsilon$ (eV)	$\sigma$ (Å)	$a$	$\lambda$	$\gamma$	$\cos \theta_0$	$A_L$	$B_L$	$p$	$q$	tol
Mo-Se <sub>1</sub> -Se <sub>1</sub>	1.000	1.017	3.276	95.770	1.000	0.165	2.201	19.152	4	0	0.0

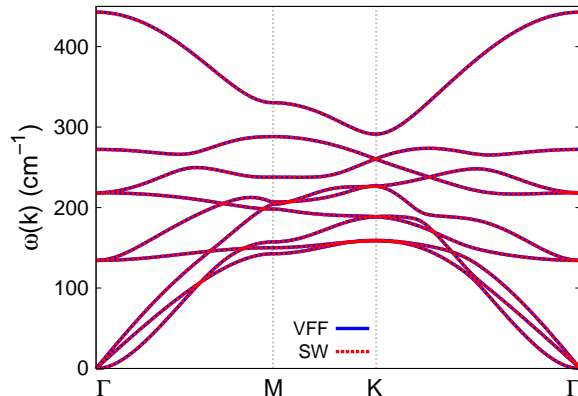


FIG. 125: (Color online) Phonon spectrum for single-layer 1T-MoSe<sub>2</sub> along the  $\Gamma$ MK $\Gamma$  direction in the Brillouin zone. The phonon dispersion from the SW potential is exactly the same as that from the VFF model.

Se atom is connected to three Mo atoms. The structural parameters are from the first-principles calculations,<sup>48</sup> including the lattice constant  $a = 3.2685$  Å, and the bond length  $d_{\text{Mo-Se}} = 2.5293$  Å, which is derived from the angle  $\theta_{\text{SeMoMo}} = 80.5^\circ$ . The other angle is  $\theta_{\text{MoSeSe}} = 80.5^\circ$  with Se atoms from the same (top or bottom) group.

Table CCL shows three VFF terms for the single-layer 1T-MoSe<sub>2</sub>, one of which is the bond stretching interaction shown by Eq. (1) while the other two terms are the angle bending interaction shown by Eq. (2). We note that the angle bending term  $K_{\text{Mo-Se-Se}}$  is for the angle  $\theta_{\text{Mo-Se-Se}}$  with both Se atoms from the same (top or bottom) group. We find that there are actually only two parameters in the VFF model, so we can determine their value by fitting to the Young's modulus and the Poisson's ratio of the system. The *ab initio* calculations have predicted the Young's modulus to be 104 N/m and the Poisson's ratio as -0.13.<sup>48</sup> The *ab initio* calculations have predicted a negative Poisson's ratio in the 1T-MoSe<sub>2</sub>, which was attributed to the orbital coupling in this material. The orbital coupling enhances the angle bending interaction in the VFF model. As a result, the value of the angle bending

parameter is much larger than the bond stretching force constant parameter, which is typical in auxetic materials with negative Poisson’s ratio.<sup>52</sup>

The parameters for the two-body SW potential used by GULP are shown in Tab. CCLI. The parameters for the three-body SW potential used by GULP are shown in Tab. CCLII. Some representative parameters for the SW potential used by LAMMPS are listed in Tab. CCLIII.

We use LAMMPS to perform MD simulations for the mechanical behavior of the single-layer 1T-MoSe<sub>2</sub> under uniaxial tension at 1.0 K and 300.0 K. Fig. 124 shows the stress-strain curve for the tension of a single-layer 1T-MoSe<sub>2</sub> of dimension 100 × 100 Å. Periodic boundary conditions are applied in both armchair and zigzag directions. The single-layer 1T-MoSe<sub>2</sub> is stretched uniaxially along the armchair or zigzag direction. The stress is calculated without involving the actual thickness of the quasi-two-dimensional structure of the single-layer 1T-MoSe<sub>2</sub>. The Young’s modulus can be obtained by a linear fitting of the stress-strain relation in the small strain range of [0, 0.01]. The Young’s modulus are 88.2 N/m and 87.9 N/m along the armchair and zigzag directions, respectively. The Young’s modulus is essentially isotropic in the armchair and zigzag directions. The Poisson’s ratio from the VFF model and the SW potential is  $\nu_{xy} = \nu_{yx} = -0.13$ . The fitted Young’s modulus value is about 10% smaller than the *ab initio* result of 104 N/m,<sup>48</sup> as only short-range interactions are considered in the present work. The long-range interactions are ignored, which typically leads to about 10% underestimation for the value of the Young’s modulus.

There is no available value for nonlinear quantities in the single-layer 1T-MoSe<sub>2</sub>. We have thus used the nonlinear parameter  $B = 0.5d^4$  in Eq. (5), which is close to the value of  $B$  in most materials. The value of the third order nonlinear elasticity  $D$  can be extracted by fitting the stress-strain relation to the function  $\sigma = E\epsilon + \frac{1}{2}D\epsilon^2$  with  $E$  as the Young’s modulus. The values of  $D$  from the present SW potential are -632.6 N/m and -629.7 N/m along the armchair and zigzag directions, respectively. The ultimate stress is about 6.1 Nm<sup>-1</sup> at the ultimate strain of 0.13 in the armchair direction at the low temperature of 1 K. The ultimate stress is about 6.2 Nm<sup>-1</sup> at the ultimate strain of 0.15 in the zigzag direction at the low temperature of 1 K.

Fig. 125 shows that the VFF model and the SW potential give exactly the same phonon dispersion, as the SW potential is derived from the VFF model.

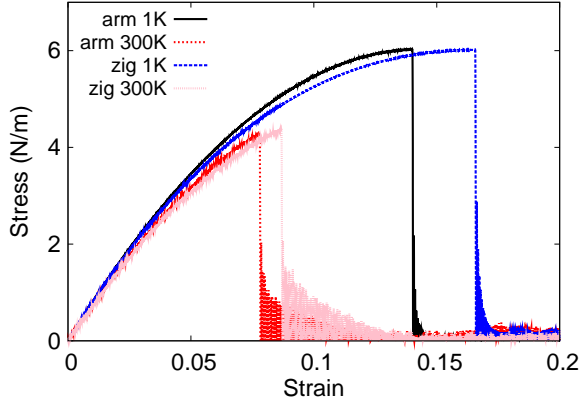


FIG. 126: (Color online) Stress-strain for single-layer 1T-MoTe<sub>2</sub> of dimension  $100 \times 100 \text{ \AA}$  along the armchair and zigzag directions.

TABLE CCLIV: The VFF model for single-layer 1T-MoTe<sub>2</sub>. The second line gives an explicit expression for each VFF term. The third line is the force constant parameters. Parameters are in the unit of  $\frac{\text{eV}}{\text{A}^2}$  for the bond stretching interactions, and in the unit of eV for the angle bending interaction. The fourth line gives the initial bond length (in unit of  $\text{\AA}$ ) for the bond stretching interaction and the initial angle (in unit of degrees) for the angle bending interaction. The angle  $\theta_{ijk}$  has atom  $i$  as the apex.

VFF type	bond stretching	angle bending	
expression	$\frac{1}{2}K_{\text{Mo-Te}}(\Delta r)^2$	$\frac{1}{2}K_{\text{Mo-Te-Te}}(\Delta\theta)^2$	$\frac{1}{2}K_{\text{Te-Mo-Mo}}(\Delta\theta)^2$
parameter	3.074	12.516	12.516
$r_0$ or $\theta_0$	2.729	79.700	79.700

#### LXIV. 1T-MOTE<sub>2</sub>

Most existing theoretical studies on the single-layer 1T-MoTe<sub>2</sub> are based on the first-principles calculations. In this section, we will develop the SW potential for the single-layer 1T-MoTe<sub>2</sub>.

The structure for the single-layer 1T-MoTe<sub>2</sub> is shown in Fig. 71 (with M=Mo and X=Te). Each Mo atom is surrounded by six Te atoms. These Te atoms are categorized into the top group (eg. atoms 1, 3, and 5) and bottom group (eg. atoms 2, 4, and 6). Each Te atom is connected to three Mo atoms. The structural parameters are from the first-

TABLE CCLV: Two-body SW potential parameters for single-layer 1T-MoTe<sub>2</sub> used by GULP<sup>8</sup> as expressed in Eq. (3).

	$A$ (eV)	$\rho$ (Å)	$B$ (Å <sup>4</sup> )	$r_{\min}$ (Å)	$r_{\max}$ (Å)
Mo-Te	2.597	1.068	27.720	0.0	3.582

TABLE CCLVI: Three-body SW potential parameters for single-layer 1T-MoTe<sub>2</sub> used by GULP<sup>8</sup> as expressed in Eq. (4). The angle  $\theta_{ijk}$  in the first line indicates the bending energy for the angle with atom  $i$  as the apex.

	$K$ (eV)	$\theta_0$ (degree)	$\rho_1$ (Å)	$\rho_2$ (Å)	$r_{\min12}$ (Å)	$r_{\max12}$ (Å)	$r_{\min13}$ (Å)	$r_{\max13}$ (Å)	$r_{\min23}$ (Å)	$r_{\max23}$ (Å)
$\theta_{\text{Mo-Te-Te}}$	78.925	79.700	1.068	1.068	0.0	3.582	0.0	3.582	0.0	4.777
$\theta_{\text{Te-Mo-Mo}}$	78.925	79.700	1.068	1.068	0.0	3.582	0.0	3.582	0.0	4.777

principles calculations,<sup>48</sup> including the lattice constant  $a = 3.4970$  Å, and the bond length  $d_{\text{Mo-Te}} = 2.7287$  Å, which is derived from the angle  $\theta_{\text{TeMoMo}} = 79.7^\circ$ . The other angle is  $\theta_{\text{MoTeTe}} = 79.7^\circ$  with Te atoms from the same (top or bottom) group.

Table CCLIV shows three VFF terms for the single-layer 1T-MoTe<sub>2</sub>, one of which is the bond stretching interaction shown by Eq. (1) while the other two terms are the angle bending interaction shown by Eq. (2). We note that the angle bending term  $K_{\text{Mo-Te-Te}}$  is for the angle  $\theta_{\text{Mo-Te-Te}}$  with both Te atoms from the same (top or bottom) group. We find that there are actually only two parameters in the VFF model, so we can determine their value by fitting to the Young's modulus and the Poisson's ratio of the system. The *ab initio* calculations have predicted the Young's modulus to be 92 N/m and the Poisson's ratio as -0.07.<sup>48</sup> The *ab initio* calculations have predicted a negative Poisson's ratio in the 1T-MoTe<sub>2</sub>, which was attributed to the orbital coupling in this material. The orbital coupling enhances the angle bending interaction in the VFF model. As a result, the value of the angle bending parameter is much larger than the bond stretching force constant parameter, which is typical

TABLE CCLVII: SW potential parameters for single-layer 1T-MoTe<sub>2</sub> used by LAMMPS<sup>9</sup> as expressed in Eqs. (9) and (10).

	$\epsilon$ (eV)	$\sigma$ (Å)	$a$	$\lambda$	$\gamma$	$\cos \theta_0$	$A_L$	$B_L$	$p$	$q$	tol
Mo-Te <sub>1</sub> -Te <sub>1</sub>	1.000	1.068	3.355	78.925	1.000	0.179	2.597	21.328	4	0	0.0

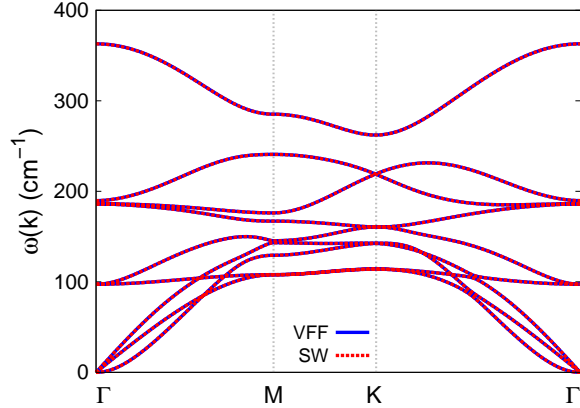


FIG. 127: (Color online) Phonon spectrum for single-layer 1T-MoTe<sub>2</sub> along the  $\Gamma$ MK $\Gamma$  direction in the Brillouin zone. The phonon dispersion from the SW potential is exactly the same as that from the VFF model.

in auxetic materials with negative Poisson's ratio.<sup>52</sup>

The parameters for the two-body SW potential used by GULP are shown in Tab. CCLV. The parameters for the three-body SW potential used by GULP are shown in Tab. CCLVI. Some representative parameters for the SW potential used by LAMMPS are listed in Tab. CCLVII.

We use LAMMPS to perform MD simulations for the mechanical behavior of the single-layer 1T-MoTe<sub>2</sub> under uniaxial tension at 1.0 K and 300.0 K. Fig. 126 shows the stress-strain curve for the tension of a single-layer 1T-MoTe<sub>2</sub> of dimension  $100 \times 100 \text{ \AA}$ . Periodic boundary conditions are applied in both armchair and zigzag directions. The single-layer 1T-MoTe<sub>2</sub> is stretched uniaxially along the armchair or zigzag direction. The stress is calculated without involving the actual thickness of the quasi-two-dimensional structure of the single-layer 1T-MoTe<sub>2</sub>. The Young's modulus can be obtained by a linear fitting of the stress-strain relation in the small strain range of  $[0, 0.01]$ . The Young's modulus are 81.6 N/m and 81.2 N/m along the armchair and zigzag directions, respectively. The Young's modulus is essentially isotropic in the armchair and zigzag directions. The Poisson's ratio from the VFF model and the SW potential is  $\nu_{xy} = \nu_{yx} = -0.07$ . The fitted Young's modulus value is about 10% smaller than the *ab initio* result of 92 N/m,<sup>48</sup> as only short-range interactions are considered in the present work. The long-range interactions are ignored, which typically leads to about 10% underestimation for the value of the Young's modulus.

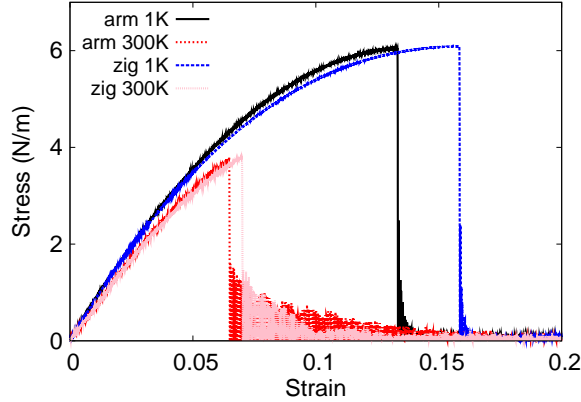


FIG. 128: (Color online) Stress-strain for single-layer 1T-TcS<sub>2</sub> of dimension  $100 \times 100 \text{ \AA}$  along the armchair and zigzag directions.

There is no available value for nonlinear quantities in the single-layer 1T-MoTe<sub>2</sub>. We have thus used the nonlinear parameter  $B = 0.5d^4$  in Eq. (5), which is close to the value of  $B$  in most materials. The value of the third order nonlinear elasticity  $D$  can be extracted by fitting the stress-strain relation to the function  $\sigma = E\epsilon + \frac{1}{2}D\epsilon^2$  with  $E$  as the Young's modulus. The values of  $D$  from the present SW potential are  $-543.1 \text{ N/m}$  and  $-558.6 \text{ N/m}$  along the armchair and zigzag directions, respectively. The ultimate stress is about  $6.0 \text{ Nm}^{-1}$  at the ultimate strain of  $0.14$  in the armchair direction at the low temperature of  $1 \text{ K}$ . The ultimate stress is about  $6.0 \text{ Nm}^{-1}$  at the ultimate strain of  $0.16$  in the zigzag direction at the low temperature of  $1 \text{ K}$ .

Fig. 127 shows that the VFF model and the SW potential give exactly the same phonon dispersion, as the SW potential is derived from the VFF model.

## LXV. 1T-TCS<sub>2</sub>

Most existing theoretical studies on the single-layer 1T-TcS<sub>2</sub> are based on the first-principles calculations. In this section, we will develop the SW potential for the single-layer 1T-TcS<sub>2</sub>.

The structure for the single-layer 1T-TcS<sub>2</sub> is shown in Fig. 71 (with  $M=\text{Tc}$  and  $X=\text{S}$ ). Each Tc atom is surrounded by six S atoms. These S atoms are categorized into the top group (eg. atoms 1, 3, and 5) and bottom group (eg. atoms 2, 4, and 6). Each S atom is connected

TABLE CCLVIII: The VFF model for single-layer 1T-TcS<sub>2</sub>. The second line gives an explicit expression for each VFF term. The third line is the force constant parameters. Parameters are in the unit of  $\frac{\text{eV}}{\text{Å}^2}$  for the bond stretching interactions, and in the unit of eV for the angle bending interaction. The fourth line gives the initial bond length (in unit of Å) for the bond stretching interaction and the initial angle (in unit of degrees) for the angle bending interaction. The angle  $\theta_{ijk}$  has atom i as the apex.

VFF type	bond stretching	angle bending	
expression	$\frac{1}{2}K_{\text{Tc-S}}(\Delta r)^2$	$\frac{1}{2}K_{\text{Tc-S-S}}(\Delta\theta)^2$	$\frac{1}{2}K_{\text{S-Tc-Tc}}(\Delta\theta)^2$
parameter	2.986	11.141	11.141
$r_0$ or $\theta_0$	2.392	79.800	79.800

TABLE CCLIX: Two-body SW potential parameters for single-layer 1T-TcS<sub>2</sub> used by GULP<sup>8</sup> as expressed in Eq. (3).

	$A$ (eV)	$\rho$ (Å)	$B$ (Å <sup>4</sup> )	$r_{\text{min}}$ (Å)	$r_{\text{max}}$ (Å)
Tc-S	1.945	0.939	16.380	0.0	3.142

to three Tc atoms. The structural parameters are from the first-principles calculations,<sup>48</sup> including the lattice constant  $a = 3.0692$  Å, and the bond length  $d_{\text{Tc-S}} = 2.3924$  Å, which is derived from the angle  $\theta_{\text{STcTc}} = 79.8^\circ$ . The other angle is  $\theta_{\text{TcSS}} = 79.8^\circ$  with S atoms from the same (top or bottom) group.

Table CCLVIII shows three VFF terms for the single-layer 1T-TcS<sub>2</sub>, one of which is the bond stretching interaction shown by Eq. (1) while the other two terms are the angle bending interaction shown by Eq. (2). We note that the angle bending term  $K_{\text{Tc-S-S}}$  is for the angle

TABLE CCLX: Three-body SW potential parameters for single-layer 1T-TcS<sub>2</sub> used by GULP<sup>8</sup> as expressed in Eq. (4). The angle  $\theta_{ijk}$  in the first line indicates the bending energy for the angle with atom i as the apex.

	$K$ (eV)	$\theta_0$ (degree)	$\rho_1$ (Å)	$\rho_2$ (Å)	$r_{\text{min}12}$ (Å)	$r_{\text{max}12}$ (Å)	$r_{\text{min}13}$ (Å)	$r_{\text{max}13}$ (Å)	$r_{\text{min}23}$ (Å)	$r_{\text{max}23}$ (Å)
$\theta_{\text{Tc-S-S}}$	70.512	79.800	0.939	0.939	0.0	3.142	0.0	3.142	0.0	4.193
$\theta_{\text{S-Tc-Tc}}$	70.512	79.800	0.939	0.939	0.0	3.142	0.0	3.142	0.0	4.193

TABLE CCLXI: SW potential parameters for single-layer 1T-TcS<sub>2</sub> used by LAMMPS<sup>9</sup> as expressed in Eqs. (9) and (10).

	$\epsilon$ (eV)	$\sigma$ (Å)	$a$	$\lambda$	$\gamma$	$\cos \theta_0$	$A_L$	$B_L$	$p$	$q$	tol
Tc-S <sub>1</sub> -S <sub>1</sub>	1.000	0.939	3.345	70.512	1.000	0.177	1.945	21.038	4	0	0.0

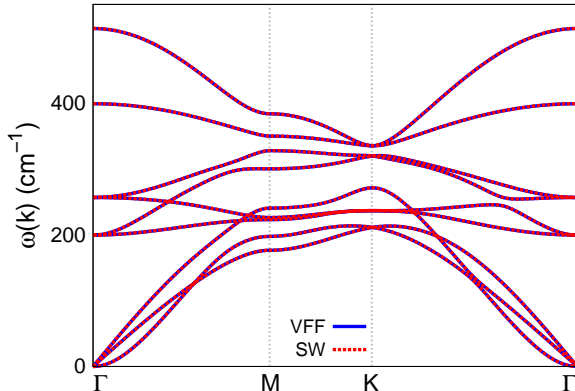


FIG. 129: (Color online) Phonon spectrum for single-layer 1T-TcS<sub>2</sub> along the  $\Gamma$ MK $\Gamma$  direction in the Brillouin zone. The phonon dispersion from the SW potential is exactly the same as that from the VFF model.

$\theta_{\text{Tc-S-S}}$  with both S atoms from the same (top or bottom) group. We find that there are actually only two parameters in the VFF model, so we can determine their value by fitting to the Young's modulus and the Poisson's ratio of the system. The *ab initio* calculations have predicted the Young's modulus to be 94 N/m and the Poisson's ratio as -0.10.<sup>48</sup> The *ab initio* calculations have predicted a negative Poisson's ratio in the 1T-TcS<sub>2</sub>, which was attributed to the orbital coupling in this material. The orbital coupling enhances the angle bending interaction in the VFF model. As a result, the value of the angle bending parameter is much larger than the bond stretching force constant parameter, which is typical in auxetic materials with negative Poisson's ratio.<sup>52</sup>

The parameters for the two-body SW potential used by GULP are shown in Tab. CCLIX. The parameters for the three-body SW potential used by GULP are shown in Tab. CCLX. Some representative parameters for the SW potential used by LAMMPS are listed in Tab. CCLXI.

We use LAMMPS to perform MD simulations for the mechanical behavior of the single-

layer 1T-TcS<sub>2</sub> under uniaxial tension at 1.0 K and 300.0 K. Fig. 128 shows the stress-strain curve for the tension of a single-layer 1T-TcS<sub>2</sub> of dimension 100 × 100 Å. Periodic boundary conditions are applied in both armchair and zigzag directions. The single-layer 1T-TcS<sub>2</sub> is stretched uniaxially along the armchair or zigzag direction. The stress is calculated without involving the actual thickness of the quasi-two-dimensional structure of the single-layer 1T-TcS<sub>2</sub>. The Young's modulus can be obtained by a linear fitting of the stress-strain relation in the small strain range of [0, 0.01]. The Young's modulus are 84.3 N/m and 84.0 N/m along the armchair and zigzag directions, respectively. The Young's modulus is essentially isotropic in the armchair and zigzag directions. The Poisson's ratio from the VFF model and the SW potential is  $\nu_{xy} = \nu_{yx} = -0.10$ . The fitted Young's modulus value is about 10% smaller than the *ab initio* result of 94 N/m,<sup>48</sup> as only short-range interactions are considered in the present work. The long-range interactions are ignored, which typically leads to about 10% underestimation for the value of the Young's modulus.

There is no available value for nonlinear quantities in the single-layer 1T-TcS<sub>2</sub>. We have thus used the nonlinear parameter  $B = 0.5d^4$  in Eq. (5), which is close to the value of  $B$  in most materials. The value of the third order nonlinear elasticity  $D$  can be extracted by fitting the stress-strain relation to the function  $\sigma = E\epsilon + \frac{1}{2}D\epsilon^2$  with  $E$  as the Young's modulus. The values of  $D$  from the present SW potential are -572.0 N/m and -588.6 N/m along the armchair and zigzag directions, respectively. The ultimate stress is about 6.0 Nm<sup>-1</sup> at the ultimate strain of 0.13 in the armchair direction at the low temperature of 1 K. The ultimate stress is about 6.1 Nm<sup>-1</sup> at the ultimate strain of 0.16 in the zigzag direction at the low temperature of 1 K.

Fig. 129 shows that the VFF model and the SW potential give exactly the same phonon dispersion, as the SW potential is derived from the VFF model.

## LXVI. 1T-TCSE<sub>2</sub>

Most existing theoretical studies on the single-layer 1T-TcSe<sub>2</sub> are based on the first-principles calculations. In this section, we will develop the SW potential for the single-layer 1T-TcSe<sub>2</sub>.

The structure for the single-layer 1T-TcSe<sub>2</sub> is shown in Fig. 71 (with M=Tc and X=Se). Each Tc atom is surrounded by six Se atoms. These Se atoms are categorized into the

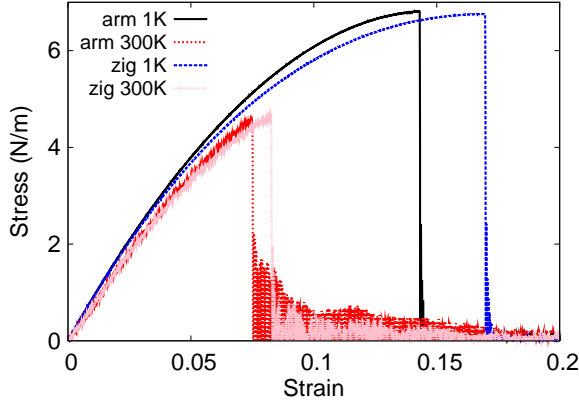


FIG. 130: (Color online) Stress-strain for single-layer 1T-TcSe<sub>2</sub> of dimension  $100 \times 100 \text{ \AA}$  along the armchair and zigzag directions.

TABLE CCLXII: The VFF model for single-layer 1T-TcSe<sub>2</sub>. The second line gives an explicit expression for each VFF term. The third line is the force constant parameters. Parameters are in the unit of  $\frac{\text{eV}}{\text{A}^2}$  for the bond stretching interactions, and in the unit of eV for the angle bending interaction. The fourth line gives the initial bond length (in unit of  $\text{\AA}$ ) for the bond stretching interaction and the initial angle (in unit of degrees) for the angle bending interaction. The angle  $\theta_{ijk}$  has atom  $i$  as the apex.

VFF type	bond stretching	angle bending	
expression	$\frac{1}{2}K_{\text{Tc-Se}}(\Delta r)^2$	$\frac{1}{2}K_{\text{Tc-Se-Se}}(\Delta\theta)^2$	$\frac{1}{2}K_{\text{Se-Tc-Tc}}(\Delta\theta)^2$
parameter	3.467	10.636	10.636
$r_0$ or $\theta_0$	2.506	78.001	78.001

top group (eg. atoms 1, 3, and 5) and bottom group (eg. atoms 2, 4, and 6). Each Se atom is connected to three Tc atoms. The structural parameters are from the first-principles calculations,<sup>48</sup> including the lattice constant  $a = 3.1543 \text{ \AA}$ , and the bond length  $d_{\text{Tc-Se}} = 2.5061 \text{ \AA}$ , which is derived from the angle  $\theta_{\text{SeTcTc}} = 78^\circ$ . The other angle is  $\theta_{\text{TcSeSe}} = 78^\circ$  with Se atoms from the same (top or bottom) group.

Table CCLXII shows three VFF terms for the single-layer 1T-TcSe<sub>2</sub>, one of which is the bond stretching interaction shown by Eq. (1) while the other two terms are the angle bending interaction shown by Eq. (2). We note that the angle bending term  $K_{\text{Tc-Se-Se}}$  is

TABLE CCLXIII: Two-body SW potential parameters for single-layer 1T-TcSe<sub>2</sub> used by GULP<sup>8</sup> as expressed in Eq. (3).

	$A$ (eV)	$\rho$ (Å)	$B$ (Å <sup>4</sup> )	$r_{\min}$ (Å)	$r_{\max}$ (Å)
Tc-Se	2.355	0.925	19.723	0.0	3.267

TABLE CCLXIV: Three-body SW potential parameters for single-layer 1T-TcSe<sub>2</sub> used by GULP<sup>8</sup> as expressed in Eq. (4). The angle  $\theta_{ijk}$  in the first line indicates the bending energy for the angle with atom  $i$  as the apex.

	$K$ (eV)	$\theta_0$ (degree)	$\rho_1$ (Å)	$\rho_2$ (Å)	$r_{\min12}$ (Å)	$r_{\max12}$ (Å)	$r_{\min13}$ (Å)	$r_{\max13}$ (Å)	$r_{\min23}$ (Å)	$r_{\max23}$ (Å)
$\theta_{\text{Tc-Se-Se}}$	63.150	78.001	0.925	0.925	0.0	3.267	0.0	3.267	0.0	4.309
$\theta_{\text{Se-Tc-Tc}}$	63.150	78.001	0.925	0.925	0.0	3.267	0.0	3.267	0.0	4.309

for the angle  $\theta_{\text{Tc-Se-Se}}$  with both Se atoms from the same (top or bottom) group. We find that there are actually only two parameters in the VFF model, so we can determine their value by fitting to the Young's modulus and the Poisson's ratio of the system. The *ab initio* calculations have predicted the Young's modulus to be 104 N/m and the Poisson's ratio as -0.04.<sup>48</sup> The *ab initio* calculations have predicted a negative Poisson's ratio in the 1T-TcSe<sub>2</sub>, which was attributed to the orbital coupling in this material. The orbital coupling enhances the angle bending interaction in the VFF model. As a result, the value of the angle bending parameter is much larger than the bond stretching force constant parameter, which is typical in auxetic materials with negative Poisson's ratio.<sup>52</sup>

The parameters for the two-body SW potential used by GULP are shown in Tab. CCLXIII. The parameters for the three-body SW potential used by GULP are shown in Tab. CCLXIV. Some representative parameters for the SW potential used by LAMMPS are listed in Tab. CCLXV.

We use LAMMPS to perform MD simulations for the mechanical behavior of the single-

TABLE CCLXV: SW potential parameters for single-layer 1T-TcSe<sub>2</sub> used by LAMMPS<sup>9</sup> as expressed in Eqs. (9) and (10).

	$\epsilon$ (eV)	$\sigma$ (Å)	$a$	$\lambda$	$\gamma$	$\cos \theta_0$	$A_L$	$B_L$	$p$	$q$	tol
Tc-Se <sub>1</sub> -Se <sub>1</sub>	1.000	0.925	3.532	63.150	1.000	0.208	2.355	26.932	4	0	0.0

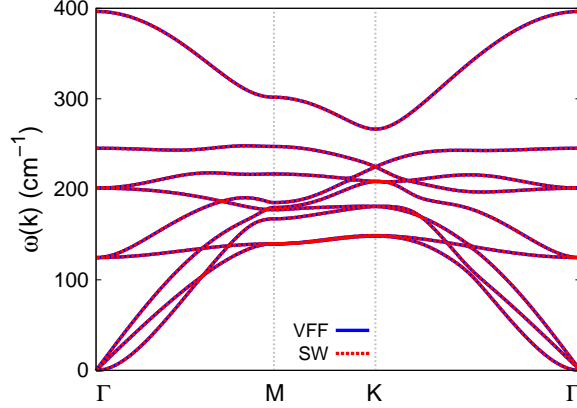


FIG. 131: (Color online) Phonon spectrum for single-layer 1T-TcSe<sub>2</sub> along the  $\Gamma$ MK $\Gamma$  direction in the Brillouin zone. The phonon dispersion from the SW potential is exactly the same as that from the VFF model.

layer 1T-TcSe<sub>2</sub> under uniaxial tension at 1.0 K and 300.0 K. Fig. 130 shows the stress-strain curve for the tension of a single-layer 1T-TcSe<sub>2</sub> of dimension  $100 \times 100$  Å. Periodic boundary conditions are applied in both armchair and zigzag directions. The single-layer 1T-TcSe<sub>2</sub> is stretched uniaxially along the armchair or zigzag direction. The stress is calculated without involving the actual thickness of the quasi-two-dimensional structure of the single-layer 1T-TcSe<sub>2</sub>. The Young's modulus can be obtained by a linear fitting of the stress-strain relation in the small strain range of  $[0, 0.01]$ . The Young's modulus are 88.8 N/m and 88.3 N/m along the armchair and zigzag directions, respectively. The Young's modulus is essentially isotropic in the armchair and zigzag directions. The Poisson's ratio from the VFF model and the SW potential is  $\nu_{xy} = \nu_{yx} = -0.04$ . The fitted Young's modulus value is about 10% smaller than the *ab initio* result of 104 N/m,<sup>48</sup> as only short-range interactions are considered in the present work. The long-range interactions are ignored, which typically leads to about 10% underestimation for the value of the Young's modulus.

There is no available value for nonlinear quantities in the single-layer 1T-TcSe<sub>2</sub>. We have thus used the nonlinear parameter  $B = 0.5d^4$  in Eq. (5), which is close to the value of  $B$  in most materials. The value of the third order nonlinear elasticity  $D$  can be extracted by fitting the stress-strain relation to the function  $\sigma = E\epsilon + \frac{1}{2}D\epsilon^2$  with  $E$  as the Young's modulus. The values of  $D$  from the present SW potential are -565.7 N/m and -587.3 N/m along the armchair and zigzag directions, respectively. The ultimate stress is about  $6.8 \text{ Nm}^{-1}$

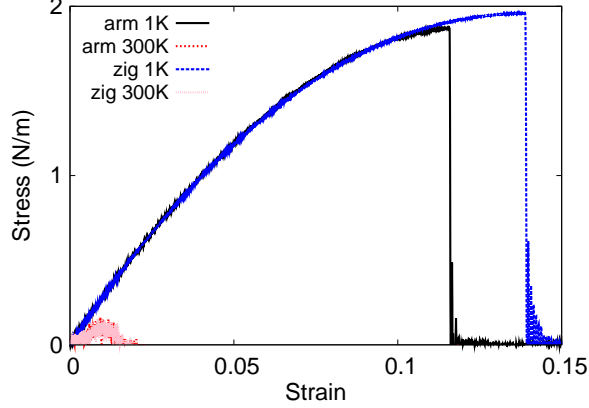


FIG. 132: (Color online) Stress-strain for single-layer 1T-TcTe<sub>2</sub> of dimension  $100 \times 100 \text{ \AA}$  along the armchair and zigzag directions.

TABLE CCLXVI: The VFF model for single-layer 1T-TcTe<sub>2</sub>. The second line gives an explicit expression for each VFF term. The third line is the force constant parameters. Parameters are in the unit of  $\frac{\text{eV}}{\text{\AA}^2}$  for the bond stretching interactions, and in the unit of eV for the angle bending interaction. The fourth line gives the initial bond length (in unit of  $\text{\AA}$ ) for the bond stretching interaction and the initial angle (in unit of degrees) for the angle bending interaction. The angle  $\theta_{ijk}$  has atom  $i$  as the apex.

VFF type	bond stretching	angle bending	
expression	$\frac{1}{2}K_{\text{Tc-Te}}(\Delta r)^2$	$\frac{1}{2}K_{\text{Tc-Te-Te}}(\Delta\theta)^2$	$\frac{1}{2}K_{\text{Te-Te-Tc}}(\Delta\theta)^2$
parameter	0.785	8.894	8.894
$r_0$ or $\theta_0$	2.690	78.801	78.801

at the ultimate strain of 0.14 in the armchair direction at the low temperature of 1 K. The ultimate stress is about  $6.8 \text{ Nm}^{-1}$  at the ultimate strain of 0.17 in the zigzag direction at the low temperature of 1 K.

Fig. 131 shows that the VFF model and the SW potential give exactly the same phonon dispersion, as the SW potential is derived from the VFF model.

TABLE CCLXVII: Two-body SW potential parameters for single-layer 1T-TcTe<sub>2</sub> used by GULP<sup>8</sup> as expressed in Eq. (3).

	$A$ (eV)	$\rho$ (Å)	$B$ (Å <sup>4</sup> )	$r_{\min}$ (Å)	$r_{\max}$ (Å)
Tc-Te	0.628	1.021	26.181	0.0	3.519

TABLE CCLXVIII: Three-body SW potential parameters for single-layer 1T-TcTe<sub>2</sub> used by GULP<sup>8</sup> as expressed in Eq. (4). The angle  $\theta_{ijk}$  in the first line indicates the bending energy for the angle with atom  $i$  as the apex.

	$K$ (eV)	$\theta_0$ (degree)	$\rho_1$ (Å)	$\rho_2$ (Å)	$r_{\min12}$ (Å)	$r_{\max12}$ (Å)	$r_{\min13}$ (Å)	$r_{\max13}$ (Å)	$r_{\min23}$ (Å)	$r_{\max23}$ (Å)
$\theta_{\text{Tc-Te-Te}}$	54.313	78.801	1.021	1.021	0.0	3.519	0.0	3.519	0.0	4.665
$\theta_{\text{Te-Tc-Tc}}$	54.313	78.801	1.021	1.021	0.0	3.519	0.0	3.519	0.0	4.665

## LXVII. 1T-TCTE<sub>2</sub>

Most existing theoretical studies on the single-layer 1T-TcTe<sub>2</sub> are based on the first-principles calculations. In this section, we will develop the SW potential for the single-layer 1T-TcTe<sub>2</sub>.

The structure for the single-layer 1T-TcTe<sub>2</sub> is shown in Fig. 71 (with M=Tc and X=Te). Each Tc atom is surrounded by six Te atoms. These Te atoms are categorized into the top group (eg. atoms 1, 3, and 5) and bottom group (eg. atoms 2, 4, and 6). Each Te atom is connected to three Tc atoms. The structural parameters are from the first-principles calculations,<sup>48</sup> including the lattice constant  $a = 3.4149$  Å, and the bond length  $d_{\text{Tc-Te}} = 2.6900$  Å, which is derived from the angle  $\theta_{\text{TeTcTc}} = 78.8^\circ$ . The other angle is  $\theta_{\text{TcTeTe}} = 78.8^\circ$  with Te atoms from the same (top or bottom) group.

Table CCLXVI shows three VFF terms for the single-layer 1T-TcTe<sub>2</sub>, one of which is the bond stretching interaction shown by Eq. (1) while the other two terms are the angle

TABLE CCLXIX: SW potential parameters for single-layer 1T-TcTe<sub>2</sub> used by LAMMPS<sup>9</sup> as expressed in Eqs. (9) and (10).

	$\epsilon$ (eV)	$\sigma$ (Å)	$a$	$\lambda$	$\gamma$	$\cos \theta_0$	$A_L$	$B_L$	$p$	$q$	tol
Tc-Te <sub>1</sub> -Te <sub>1</sub>	1.000	1.021	3.447	54.313	1.000	0.194	0.628	24.110	4	0	0.0

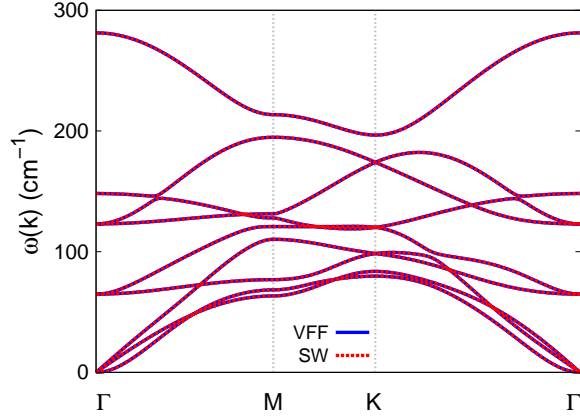


FIG. 133: (Color online) Phonon spectrum for single-layer 1T-TcTe<sub>2</sub> along the  $\Gamma$ MKT direction in the Brillouin zone. The phonon dispersion from the SW potential is exactly the same as that from the VFF model.

bending interaction shown by Eq. (2). We note that the angle bending term  $K_{\text{Tc-Te-Te}}$  is for the angle  $\theta_{\text{Tc-Te-Te}}$  with both Te atoms from the same (top or bottom) group. We find that there are actually only two parameters in the VFF model, so we can determine their value by fitting to the Young's modulus and the Poisson's ratio of the system. The *ab initio* calculations have predicted the Young's modulus to be 34 N/m and the Poisson's ratio as -0.36.<sup>48</sup> The *ab initio* calculations have predicted a negative Poisson's ratio in the 1T-TcTe<sub>2</sub>, which was attributed to the orbital coupling in this material. The orbital coupling enhances the angle bending interaction in the VFF model. As a result, the value of the angle bending parameter is much larger than the bond stretching force constant parameter, which is typical in auxetic materials with negative Poisson's ratio.<sup>52</sup>

The parameters for the two-body SW potential used by GULP are shown in Tab. CCLXVII. The parameters for the three-body SW potential used by GULP are shown in Tab. CCLXVIII. Some representative parameters for the SW potential used by LAMMPS are listed in Tab. CCLXIX.

We use LAMMPS to perform MD simulations for the mechanical behavior of the single-layer 1T-TcTe<sub>2</sub> under uniaxial tension at 1.0 K and 300.0 K. Fig. 132 shows the stress-strain curve for the tension of a single-layer 1T-TcTe<sub>2</sub> of dimension  $100 \times 100 \text{ \AA}$ . Periodic boundary conditions are applied in both armchair and zigzag directions. The single-layer 1T-TcTe<sub>2</sub> is stretched uniaxially along the armchair or zigzag direction. The stress is calculated without

involving the actual thickness of the quasi-two-dimensional structure of the single-layer 1T-TcTe<sub>2</sub>. The Young's modulus can be obtained by a linear fitting of the stress-strain relation in the small strain range of [0, 0.01]. The Young's modulus is 28.6 N/m along the armchair and zigzag directions. The Poisson's ratio from the VFF model and the SW potential is  $\nu_{xy} = \nu_{yx} = -0.21$ . The fitted Young's modulus value is about 10% smaller than the *ab initio* result of 34 N/m,<sup>48</sup> as only short-range interactions are considered in the present work. The long-range interactions are ignored, which typically leads to about 10% underestimation for the value of the Young's modulus.

There is no available value for nonlinear quantities in the single-layer 1T-TcTe<sub>2</sub>. We have thus used the nonlinear parameter  $B = 0.5d^4$  in Eq. (5), which is close to the value of  $B$  in most materials. The value of the third order nonlinear elasticity  $D$  can be extracted by fitting the stress-strain relation to the function  $\sigma = E\epsilon + \frac{1}{2}D\epsilon^2$  with  $E$  as the Young's modulus. The values of  $D$  from the present SW potential are -207.8 N/m and -208.7 N/m along the armchair and zigzag directions, respectively. The ultimate stress is about 1.9 Nm<sup>-1</sup> at the ultimate strain of 0.11 in the armchair direction at the low temperature of 1 K. The ultimate stress is about 2.0 Nm<sup>-1</sup> at the ultimate strain of 0.14 in the zigzag direction at the low temperature of 1 K. The ultimate strain decreases to be about 0.01 at 300 K, so the single-layer 1T-TcTe<sub>2</sub> is not very stable at higher temperature. It is because this material is very soft and the Poisson's ratio is very small (negative value).

Fig. 133 shows that the VFF model and the SW potential give exactly the same phonon dispersion, as the SW potential is derived from the VFF model.

## LXVIII. 1T-RhTe<sub>2</sub>

Most existing theoretical studies on the single-layer 1T-RhTe<sub>2</sub> are based on the first-principles calculations. In this section, we will develop the SW potential for the single-layer 1T-RhTe<sub>2</sub>.

The structure for the single-layer 1T-RhTe<sub>2</sub> is shown in Fig. 71 (with M=Rh and X=Te). Each Rh atom is surrounded by six Te atoms. These Te atoms are categorized into the top group (eg. atoms 1, 3, and 5) and bottom group (eg. atoms 2, 4, and 6). Each Te atom is connected to three Rh atoms. The structural parameters are from the first-principles calculations,<sup>48</sup> including the lattice constant  $a = 3.7563 \text{ \AA}$ , and the bond length

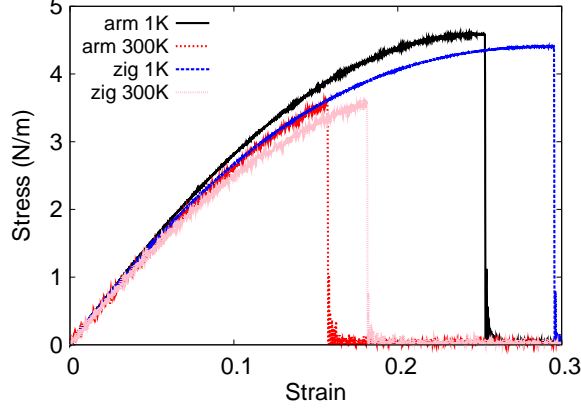


FIG. 134: (Color online) Stress-strain for single-layer 1T-RhTe<sub>2</sub> of dimension  $100 \times 100 \text{ \AA}$  along the armchair and zigzag directions.

TABLE CCLXX: The VFF model for single-layer 1T-RhTe<sub>2</sub>. The second line gives an explicit expression for each VFF term. The third line is the force constant parameters. Parameters are in the unit of  $\frac{eV}{\text{Å}^2}$  for the bond stretching interactions, and in the unit of eV for the angle bending interaction. The fourth line gives the initial bond length (in unit of Å) for the bond stretching interaction and the initial angle (in unit of degrees) for the angle bending interaction. The angle  $\theta_{ijk}$  has atom  $i$  as the apex.

VFF type	bond stretching	angle bending	
expression	$\frac{1}{2}K_{\text{Rh-Te}}(\Delta r)^2$	$\frac{1}{2}K_{\text{Rh-Te-Te}}(\Delta\theta)^2$	$\frac{1}{2}K_{\text{Te-Rh-Rh}}(\Delta\theta)^2$
parameter	4.366	1.869	1.869
$r_0$ or $\theta_0$	2.633	91.001	91.001

$d_{\text{Rh-Te}} = 2.6332 \text{ \AA}$ , which is derived from the angle  $\theta_{\text{TeRhRh}} = 91^\circ$ . The other angle is  $\theta_{\text{RhTeTe}} = 91^\circ$  with Te atoms from the same (top or bottom) group.

Table CCLXX shows three VFF terms for the single-layer 1T-RhTe<sub>2</sub>, one of which is the bond stretching interaction shown by Eq. (1) while the other two terms are the angle bending interaction shown by Eq. (2). We note that the angle bending term  $K_{\text{Rh-Te-Te}}$  is for the angle  $\theta_{\text{Rh-Te-Te}}$  with both Te atoms from the same (top or bottom) group. We find that there are actually only two parameters in the VFF model, so we can determine their value by fitting to the Young's modulus and the Poisson's ratio of the system. The *ab initio*

TABLE CCLXXI: Two-body SW potential parameters for single-layer 1T-RhTe<sub>2</sub> used by GULP<sup>8</sup> as expressed in Eq. (3).

	$A$ (eV)	$\rho$ (Å)	$B$ (Å <sup>4</sup> )	$r_{\min}$ (Å)	$r_{\max}$ (Å)
Rh-Te	4.640	1.450	24.038	0.0	3.610

TABLE CCLXXII: Three-body SW potential parameters for single-layer 1T-RhTe<sub>2</sub> used by GULP<sup>8</sup> as expressed in Eq. (4). The angle  $\theta_{ijk}$  in the first line indicates the bending energy for the angle with atom  $i$  as the apex.

	$K$ (eV)	$\theta_0$ (degree)	$\rho_1$ (Å)	$\rho_2$ (Å)	$r_{\min12}$ (Å)	$r_{\max12}$ (Å)	$r_{\min13}$ (Å)	$r_{\max13}$ (Å)	$r_{\min23}$ (Å)	$r_{\max23}$ (Å)
$\theta_{\text{Rh-Te-Te}}$	18.192	91.001	1.450	1.450	0.0	3.610	0.0	3.610	0.0	5.131
$\theta_{\text{Te-Rh-Rh}}$	18.192	91.001	1.450	1.450	0.0	3.610	0.0	3.610	0.0	5.131

calculations have predicted the Young's modulus to be 37 N/m and the Poisson's ratio as 0.20.<sup>48</sup>

The parameters for the two-body SW potential used by GULP are shown in Tab. CCLXXI. The parameters for the three-body SW potential used by GULP are shown in Tab. CCLXXII. Some representative parameters for the SW potential used by LAMMPS are listed in Tab. CCLXXIII.

We use LAMMPS to perform MD simulations for the mechanical behavior of the single-layer 1T-RhTe<sub>2</sub> under uniaxial tension at 1.0 K and 300.0 K. Fig. 134 shows the stress-strain curve for the tension of a single-layer 1T-RhTe<sub>2</sub> of dimension  $100 \times 100$  Å. Periodic boundary conditions are applied in both armchair and zigzag directions. The single-layer 1T-RhTe<sub>2</sub> is stretched uniaxially along the armchair or zigzag direction. The stress is calculated without involving the actual thickness of the quasi-two-dimensional structure of the single-layer 1T-RhTe<sub>2</sub>. The Young's modulus can be obtained by a linear fitting of the stress-strain relation in the small strain range of  $[0, 0.01]$ . The Young's modulus are 32.1 N/m and 32.0 N/m

TABLE CCLXXIII: SW potential parameters for single-layer 1T-RhTe<sub>2</sub> used by LAMMPS<sup>9</sup> as expressed in Eqs. (9) and (10).

	$\epsilon$ (eV)	$\sigma$ (Å)	$a$	$\lambda$	$\gamma$	$\cos \theta_0$	$A_L$	$B_L$	$p$	$q$	tol
Rh-Te <sub>1</sub> -Te <sub>1</sub>	1.000	1.450	2.490	18.192	1.000	-0.017	4.640	5.436	4	0	0.0

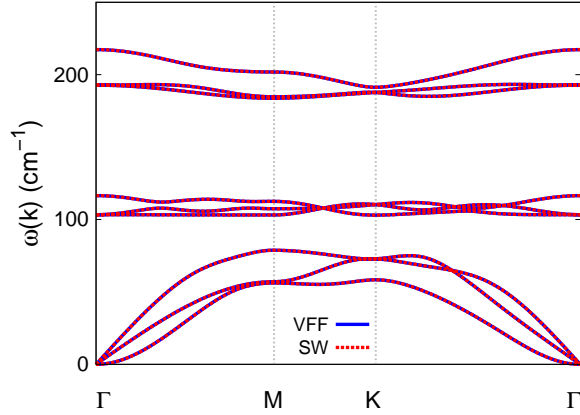


FIG. 135: (Color online) Phonon spectrum for single-layer 1T-RhTe<sub>2</sub> along the  $\Gamma$ MK $\Gamma$  direction in the Brillouin zone. The phonon dispersion from the SW potential is exactly the same as that from the VFF model.

along the armchair and zigzag directions, respectively. The Young's modulus is essentially isotropic in the armchair and zigzag directions. The Poisson's ratio from the VFF model and the SW potential is  $\nu_{xy} = \nu_{yx} = 0.20$ . The fitted Young's modulus value is about 10% smaller than the *ab initio* result of 37 N/m,<sup>48</sup> as only short-range interactions are considered in the present work. The long-range interactions are ignored, which typically leads to about 10% underestimation for the value of the Young's modulus.

There is no available value for nonlinear quantities in the single-layer 1T-RhTe<sub>2</sub>. We have thus used the nonlinear parameter  $B = 0.5d^4$  in Eq. (5), which is close to the value of  $B$  in most materials. The value of the third order nonlinear elasticity  $D$  can be extracted by fitting the stress-strain relation to the function  $\sigma = E\epsilon + \frac{1}{2}D\epsilon^2$  with  $E$  as the Young's modulus. The values of  $D$  from the present SW potential are -103.1 N/m and -116.5 N/m along the armchair and zigzag directions, respectively. The ultimate stress is about 4.6 Nm<sup>-1</sup> at the ultimate strain of 0.25 in the armchair direction at the low temperature of 1 K. The ultimate stress is about 4.4 Nm<sup>-1</sup> at the ultimate strain of 0.29 in the zigzag direction at the low temperature of 1 K.

Fig. 135 shows that the VFF model and the SW potential give exactly the same phonon dispersion, as the SW potential is derived from the VFF model.

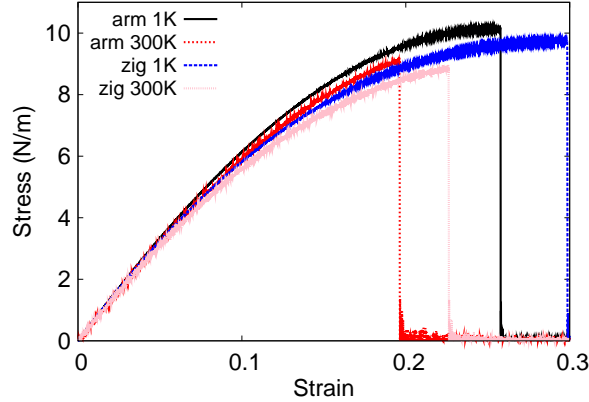


FIG. 136: (Color online) Stress-strain for single-layer 1T-PdS<sub>2</sub> of dimension  $100 \times 100 \text{ \AA}$  along the armchair and zigzag directions.

TABLE CCLXXIV: The VFF model for single-layer 1T-PdS<sub>2</sub>. The second line gives an explicit expression for each VFF term. The third line is the force constant parameters. Parameters are in the unit of  $\frac{\text{eV}}{\text{Å}^2}$  for the bond stretching interactions, and in the unit of eV for the angle bending interaction. The fourth line gives the initial bond length (in unit of Å) for the bond stretching interaction and the initial angle (in unit of degrees) for the angle bending interaction. The angle  $\theta_{ijk}$  has atom *i* as the apex.

VFF type	bond stretching	angle bending	
expression	$\frac{1}{2}K_{\text{Pd-S}}(\Delta r)^2$	$\frac{1}{2}K_{\text{Pd-S-S}}(\Delta\theta)^2$	$\frac{1}{2}K_{\text{S-Pd-Pd}}(\Delta\theta)^2$
parameter	10.374	3.122	3.122
$r_0$ or $\theta_0$	2.401	94.998	94.998

## LXIX. 1T-PDS<sub>2</sub>

Most existing theoretical studies on the single-layer 1T-PdS<sub>2</sub> are based on the first-principles calculations. In this section, we will develop the SW potential for the single-layer 1T-PdS<sub>2</sub>.

The structure for the single-layer 1T-PdS<sub>2</sub> is shown in Fig. 71 (with M=Pd and X=S). Each Pd atom is surrounded by six S atoms. These S atoms are categorized into the top group (eg. atoms 1, 3, and 5) and bottom group (eg. atoms 2, 4, and 6). Each S atom is connected to three Pd atoms. The structural parameters are from the first-principles calculations,<sup>48</sup>

TABLE CCLXXV: Two-body SW potential parameters for single-layer 1T-PdS<sub>2</sub> used by GULP<sup>8</sup> as expressed in Eq. (3).

	$A$ (eV)	$\rho$ (Å)	$B$ (Å <sup>4</sup> )	$r_{\min}$ (Å)	$r_{\max}$ (Å)
Pd-S	10.116	1.467	16.625	0.0	3.340

TABLE CCLXXVI: Three-body SW potential parameters for single-layer 1T-PdS<sub>2</sub> used by GULP<sup>8</sup> as expressed in Eq. (4). The angle  $\theta_{ijk}$  in the first line indicates the bending energy for the angle with atom  $i$  as the apex.

	$K$ (eV)	$\theta_0$ (degree)	$\rho_1$ (Å)	$\rho_2$ (Å)	$r_{\min12}$ (Å)	$r_{\max12}$ (Å)	$r_{\min13}$ (Å)	$r_{\max13}$ (Å)	$r_{\min23}$ (Å)	$r_{\max23}$ (Å)
$\theta_{\text{Pd-S-S}}$	35.859	94.998	1.467	1.467	0.0	3.340	0.0	3.340	0.0	4.837
$\theta_{\text{S-Pd-Pd}}$	35.859	94.998	1.467	1.467	0.0	3.340	0.0	3.340	0.0	4.837

including the lattice constant  $a = 3.5408$  Å, and the bond length  $d_{\text{Pd-S}} = 2.4013$  Å, which is derived from the angle  $\theta_{\text{SPdPd}} = 95^\circ$ . The other angle is  $\theta_{\text{PdSS}} = 95^\circ$  with S atoms from the same (top or bottom) group.

Table CCLXXIV shows three VFF terms for the single-layer 1T-PdS<sub>2</sub>, one of which is the bond stretching interaction shown by Eq. (1) while the other two terms are the angle bending interaction shown by Eq. (2). We note that the angle bending term  $K_{\text{Pd-S-S}}$  is for the angle  $\theta_{\text{Pd-S-S}}$  with both S atoms from the same (top or bottom) group. We find that there are actually only two parameters in the VFF model, so we can determine their value by fitting to the Young's modulus and the Poisson's ratio of the system. The *ab initio* calculations have predicted the Young's modulus to be 77 N/m and the Poisson's ratio as 0.53.<sup>48</sup>

The parameters for the two-body SW potential used by GULP are shown in Tab. CCLXXV. The parameters for the three-body SW potential used by GULP are shown in Tab. CCLXXVI. Some representative parameters for the SW potential used by LAMMPS

TABLE CCLXXVII: SW potential parameters for single-layer 1T-PdS<sub>2</sub> used by LAMMPS<sup>9</sup> as expressed in Eqs. (9) and (10).

	$\epsilon$ (eV)	$\sigma$ (Å)	$a$	$\lambda$	$\gamma$	$\cos \theta_0$	$A_L$	$B_L$	$p$	$q$	tol
Pd-S <sub>1</sub> -S <sub>1</sub>	1.000	1.467	2.276	35.859	1.000	-0.087	10.116	3.588	4	0	0.0

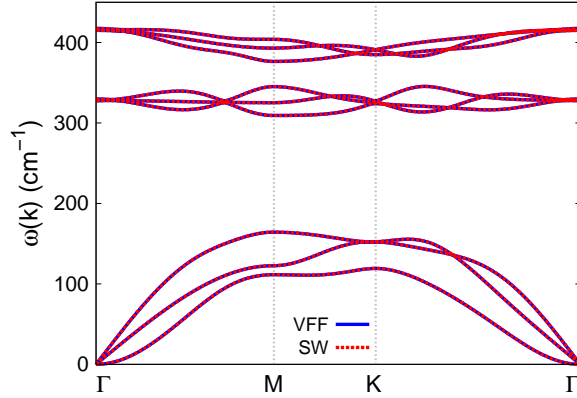


FIG. 137: (Color online) Phonon spectrum for single-layer 1T-PdS<sub>2</sub> along the  $\Gamma$ MK $\Gamma$  direction in the Brillouin zone. The phonon dispersion from the SW potential is exactly the same as that from the VFF model.

are listed in Tab. [CCLXXVII](#).

We use LAMMPS to perform MD simulations for the mechanical behavior of the single-layer 1T-PdS<sub>2</sub> under uniaxial tension at 1.0 K and 300.0 K. Fig. [136](#) shows the stress-strain curve for the tension of a single-layer 1T-PdS<sub>2</sub> of dimension  $100 \times 100 \text{ \AA}$ . Periodic boundary conditions are applied in both armchair and zigzag directions. The single-layer 1T-PdS<sub>2</sub> is stretched uniaxially along the armchair or zigzag direction. The stress is calculated without involving the actual thickness of the quasi-two-dimensional structure of the single-layer 1T-PdS<sub>2</sub>. The Young's modulus can be obtained by a linear fitting of the stress-strain relation in the small strain range of  $[0, 0.01]$ . The Young's modulus are 69.9 N/m and 69.5 N/m along the armchair and zigzag directions, respectively. The Young's modulus is essentially isotropic in the armchair and zigzag directions. The Poisson's ratio from the VFF model and the SW potential is  $\nu_{xy} = \nu_{yx} = 0.20$ . The fitted Young's modulus value is about 10% smaller than the *ab initio* result of 77 N/m,<sup>48</sup> as only short-range interactions are considered in the present work. The long-range interactions are ignored, which typically leads to about 10% underestimation for the value of the Young's modulus.

There is no available value for nonlinear quantities in the single-layer 1T-PdS<sub>2</sub>. We have thus used the nonlinear parameter  $B = 0.5d^4$  in Eq. (5), which is close to the value of  $B$  in most materials. The value of the third order nonlinear elasticity  $D$  can be extracted by fitting the stress-strain relation to the function  $\sigma = E\epsilon + \frac{1}{2}D\epsilon^2$  with  $E$  as the Young's modulus.

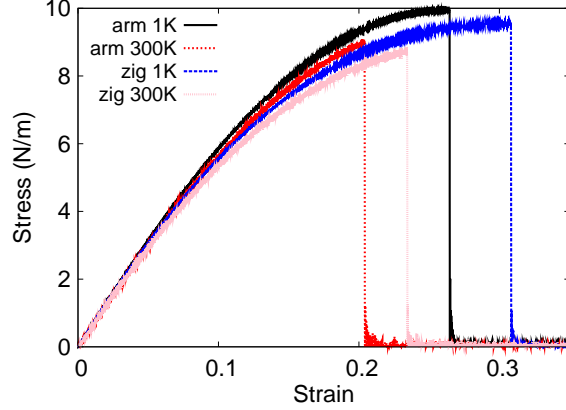


FIG. 138: (Color online) Stress-strain for single-layer 1T-PdSe<sub>2</sub> of dimension  $100 \times 100 \text{ \AA}$  along the armchair and zigzag directions.

The values of  $D$  from the present SW potential are  $-222.0 \text{ N/m}$  and  $-248.8 \text{ N/m}$  along the armchair and zigzag directions, respectively. The ultimate stress is about  $10.1 \text{ Nm}^{-1}$  at the ultimate strain of 0.25 in the armchair direction at the low temperature of 1 K. The ultimate stress is about  $9.7 \text{ Nm}^{-1}$  at the ultimate strain of 0.30 in the zigzag direction at the low temperature of 1 K.

Fig. 137 shows that the VFF model and the SW potential give exactly the same phonon dispersion, as the SW potential is derived from the VFF model.

## LXX. 1T-PDSE<sub>2</sub>

Most existing theoretical studies on the single-layer 1T-PdSe<sub>2</sub> are based on the first-principles calculations. In this section, we will develop the SW potential for the single-layer 1T-PdSe<sub>2</sub>.

The structure for the single-layer 1T-PdSe<sub>2</sub> is shown in Fig. 71 (with M=Pd and X=Se). Each Pd atom is surrounded by six Se atoms. These Se atoms are categorized into the top group (eg. atoms 1, 3, and 5) and bottom group (eg. atoms 2, 4, and 6). Each Se atom is connected to three Pd atoms. The structural parameters are from the first-principles calculations,<sup>48</sup> including the lattice constant  $a = 3.6759 \text{ \AA}$ , and the bond length  $d_{\text{Pd-Se}} = 2.4929 \text{ \AA}$ , which is derived from the angle  $\theta_{\text{SePdPd}} = 95^\circ$ . The other angle is  $\theta_{\text{PdSeSe}} = 95^\circ$  with Se atoms from the same (top or bottom) group.

TABLE CCLXXVIII: The VFF model for single-layer 1T-PdSe<sub>2</sub>. The second line gives an explicit expression for each VFF term. The third line is the force constant parameters. Parameters are in the unit of  $\frac{\text{eV}}{\text{\AA}^2}$  for the bond stretching interactions, and in the unit of eV for the angle bending interaction. The fourth line gives the initial bond length (in unit of \AA) for the bond stretching interaction and the initial angle (in unit of degrees) for the angle bending interaction. The angle  $\theta_{ijk}$  has atom *i* as the apex.

VFF type	bond stretching	angle bending	
expression	$\frac{1}{2}K_{\text{Pd-Se}}(\Delta r)^2$	$\frac{1}{2}K_{\text{Pd-Se-Se}}(\Delta\theta)^2$	$\frac{1}{2}K_{\text{Se-Pd-Pd}}(\Delta\theta)^2$
parameter	10.374	3.122	3.122
$r_0$ or $\theta_0$	2.493	94.999	94.999

TABLE CCLXXIX: Two-body SW potential parameters for single-layer 1T-PdSe<sub>2</sub> used by GULP<sup>8</sup> as expressed in Eq. (3).

	$A$ (eV)	$\rho$ (\AA)	$B$ (\AA <sup>4</sup> )	$r_{\text{min}}$ (\AA)	$r_{\text{max}}$ (\AA)
Pd-Se	10.902	1.523	19.310	0.0	3.467

Table CCLXXVIII shows three VFF terms for the single-layer 1T-PdSe<sub>2</sub>, one of which is the bond stretching interaction shown by Eq. (1) while the other two terms are the angle bending interaction shown by Eq. (2). We note that the angle bending term  $K_{\text{Pd-Se-Se}}$  is for the angle  $\theta_{\text{Pd-Se-Se}}$  with both Se atoms from the same (top or bottom) group. We find that there are actually only two parameters in the VFF model, so we can determine their value by fitting to the Young's modulus and the Poisson's ratio of the system. The *ab initio* calculations have predicted the Young's modulus to be 66 N/m and the Poisson's ratio as 0.45.<sup>48</sup>

TABLE CCLXXX: Three-body SW potential parameters for single-layer 1T-PdSe<sub>2</sub> used by GULP<sup>8</sup> as expressed in Eq. (4). The angle  $\theta_{ijk}$  in the first line indicates the bending energy for the angle with atom *i* as the apex.

	$K$ (eV)	$\theta_0$ (degree)	$\rho_1$ (\AA)	$\rho_2$ (\AA)	$r_{\text{min}12}$ (\AA)	$r_{\text{max}12}$ (\AA)	$r_{\text{min}13}$ (\AA)	$r_{\text{max}13}$ (\AA)	$r_{\text{min}23}$ (\AA)	$r_{\text{max}23}$ (\AA)
$\theta_{\text{Pd-Se-Se}}$	35.859	94.999	1.523	1.523	0.0	3.467	0.0	3.467	0.0	5.021
$\theta_{\text{Se-Pd-Pd}}$	35.859	94.999	1.523	1.523	0.0	3.467	0.0	3.467	0.0	5.021

TABLE CCLXXXI: SW potential parameters for single-layer 1T-PdSe<sub>2</sub> used by LAMMPS<sup>9</sup> as expressed in Eqs. (9) and (10).

	$\epsilon$ (eV)	$\sigma$ (Å)	$a$	$\lambda$	$\gamma$	$\cos \theta_0$	$A_L$	$B_L$	$p$	$q$	tol
Pd-Se <sub>1</sub> -Se <sub>1</sub>	1.000	1.523	2.276	35.859	1.000	-0.087	10.902	3.588	4	0	0.0

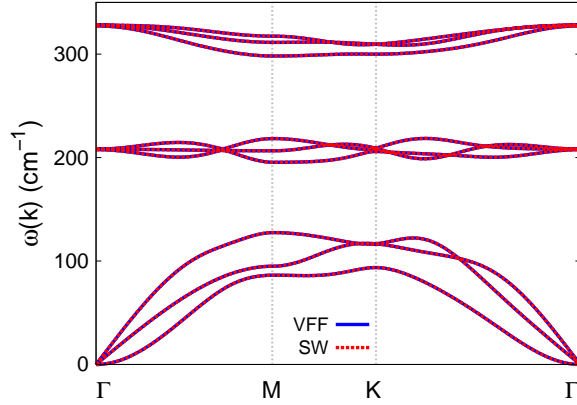


FIG. 139: (Color online) Phonon spectrum for single-layer 1T-PdSe<sub>2</sub> along the  $\Gamma$ MK $\Gamma$  direction in the Brillouin zone. The phonon dispersion from the SW potential is exactly the same as that from the VFF model.

The parameters for the two-body SW potential used by GULP are shown in Tab. CCLXXIX. The parameters for the three-body SW potential used by GULP are shown in Tab. CCLXXX. Some representative parameters for the SW potential used by LAMMPS are listed in Tab. CCLXXXI.

We use LAMMPS to perform MD simulations for the mechanical behavior of the single-layer 1T-PdSe<sub>2</sub> under uniaxial tension at 1.0 K and 300.0 K. Fig. 138 shows the stress-strain curve for the tension of a single-layer 1T-PdSe<sub>2</sub> of dimension  $100 \times 100$  Å. Periodic boundary conditions are applied in both armchair and zigzag directions. The single-layer 1T-PdSe<sub>2</sub> is stretched uniaxially along the armchair or zigzag direction. The stress is calculated without involving the actual thickness of the quasi-two-dimensional structure of the single-layer 1T-PdSe<sub>2</sub>. The Young's modulus can be obtained by a linear fitting of the stress-strain relation in the small strain range of  $[0, 0.01]$ . The Young's modulus are 65.5 N/m and 65.3 N/m along the armchair and zigzag directions, respectively. The Young's modulus is essentially isotropic in the armchair and zigzag directions. The Poisson's ratio from the VFF model

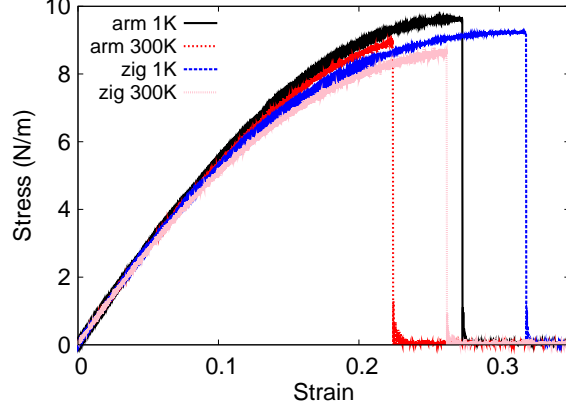


FIG. 140: (Color online) Stress-strain for single-layer 1T-PdTe<sub>2</sub> of dimension  $100 \times 100 \text{ \AA}$  along the armchair and zigzag directions.

and the SW potential is  $\nu_{xy} = \nu_{yx} = 0.21$ .

There is no available value for nonlinear quantities in the single-layer 1T-PdSe<sub>2</sub>. We have thus used the nonlinear parameter  $B = 0.5d^4$  in Eq. (5), which is close to the value of  $B$  in most materials. The value of the third order nonlinear elasticity  $D$  can be extracted by fitting the stress-strain relation to the function  $\sigma = E\epsilon + \frac{1}{2}D\epsilon^2$  with  $E$  as the Young's modulus. The values of  $D$  from the present SW potential are  $-194.7 \text{ N/m}$  and  $-222.8 \text{ N/m}$  along the armchair and zigzag directions, respectively. The ultimate stress is about  $9.9 \text{ Nm}^{-1}$  at the ultimate strain of 0.26 in the armchair direction at the low temperature of 1 K. The ultimate stress is about  $9.5 \text{ Nm}^{-1}$  at the ultimate strain of 0.31 in the zigzag direction at the low temperature of 1 K.

Fig. 139 shows that the VFF model and the SW potential give exactly the same phonon dispersion, as the SW potential is derived from the VFF model.

## LXXI. 1T-PDTE<sub>2</sub>

Most existing theoretical studies on the single-layer 1T-PdTe<sub>2</sub> are based on the first-principles calculations. In this section, we will develop the SW potential for the single-layer 1T-PdTe<sub>2</sub>.

The structure for the single-layer 1T-PdTe<sub>2</sub> is shown in Fig. 71 (with M=Pd and X=Te). Each Pd atom is surrounded by six Te atoms. These Te atoms are categorized into the

TABLE CCLXXXII: The VFF model for single-layer 1T-PdTe<sub>2</sub>. The second line gives an explicit expression for each VFF term. The third line is the force constant parameters. Parameters are in the unit of  $\frac{\text{eV}}{\text{\AA}^2}$  for the bond stretching interactions, and in the unit of eV for the angle bending interaction. The fourth line gives the initial bond length (in unit of  $\text{\AA}$ ) for the bond stretching interaction and the initial angle (in unit of degrees) for the angle bending interaction. The angle  $\theta_{ijk}$  has atom  $i$  as the apex.

VFF type	bond stretching	angle bending	
expression	$\frac{1}{2}K_{\text{Pd-Te}}(\Delta r)^2$	$\frac{1}{2}K_{\text{Pd-Te-Te}}(\Delta\theta)^2$	$\frac{1}{2}K_{\text{Te-Pd-Pd}}(\Delta\theta)^2$
parameter	10.374	3.122	3.122
$r_0$ or $\theta_0$	2.635	95.999	95.999

TABLE CCLXXXIII: Two-body SW potential parameters for single-layer 1T-PdTe<sub>2</sub> used by GULP<sup>8</sup> as expressed in Eq. (3).

	$A$ (eV)	$\rho$ ( $\text{\AA}$ )	$B$ ( $\text{\AA}^4$ )	$r_{\text{min}}$ ( $\text{\AA}$ )	$r_{\text{max}}$ ( $\text{\AA}$ )
Pd-Te	12.474	1.650	24.101	0.0	3.678

top group (eg. atoms 1, 3, and 5) and bottom group (eg. atoms 2, 4, and 6). Each Te atom is connected to three Pd atoms. The structural parameters are from the first-principles calculations,<sup>48</sup> including the lattice constant  $a = 3.9162 \text{ \AA}$ , and the bond length  $d_{\text{Pd-Te}} = 2.6349 \text{ \AA}$ , which is derived from the angle  $\theta_{\text{TePdPd}} = 96^\circ$ . The other angle is  $\theta_{\text{PdTeTe}} = 96^\circ$  with Te atoms from the same (top or bottom) group.

Table CCLXXXII shows three VFF terms for the single-layer 1T-PdTe<sub>2</sub>, one of which is the bond stretching interaction shown by Eq. (1) while the other two terms are the angle bending interaction shown by Eq. (2). We note that the angle bending term  $K_{\text{Pd-Te-Te}}$  is

TABLE CCLXXXIV: Three-body SW potential parameters for single-layer 1T-PdTe<sub>2</sub> used by GULP<sup>8</sup> as expressed in Eq. (4). The angle  $\theta_{ijk}$  in the first line indicates the bending energy for the angle with atom  $i$  as the apex.

	$K$ (eV)	$\theta_0$ (degree)	$\rho_1$ ( $\text{\AA}$ )	$\rho_2$ ( $\text{\AA}$ )	$r_{\text{min12}}$ ( $\text{\AA}$ )	$r_{\text{max12}}$ ( $\text{\AA}$ )	$r_{\text{min13}}$ ( $\text{\AA}$ )	$r_{\text{max13}}$ ( $\text{\AA}$ )	$r_{\text{min23}}$ ( $\text{\AA}$ )	$r_{\text{max23}}$ ( $\text{\AA}$ )
$\theta_{\text{Pd-Te-Te}}$	37.406	95.999	1.650	1.650	0.0	3.678	0.0	3.678	0.0	5.350
$\theta_{\text{Te-Pd-Pd}}$	37.406	95.999	1.650	1.650	0.0	3.678	0.0	3.678	0.0	5.350

TABLE CCLXXXV: SW potential parameters for single-layer 1T-PdTe<sub>2</sub> used by LAMMPS<sup>9</sup> as expressed in Eqs. (9) and (10).

	$\epsilon$ (eV)	$\sigma$ (Å)	$a$	$\lambda$	$\gamma$	$\cos \theta_0$	$A_L$	$B_L$	$p$	$q$	tol
Pd-Te <sub>1</sub> -Te <sub>1</sub>	1.000	1.650	2.229	37.406	1.000	-0.105	12.474	3.250	4	0	0.0

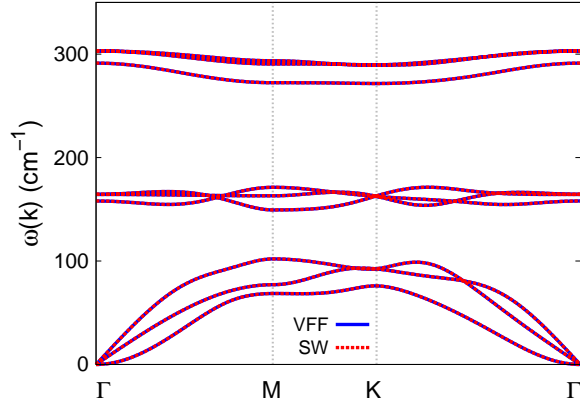


FIG. 141: (Color online) Phonon spectrum for single-layer 1T-PdTe<sub>2</sub> along the  $\Gamma$ MKT direction in the Brillouin zone. The phonon dispersion from the SW potential is exactly the same as that from the VFF model.

for the angle  $\theta_{\text{Pd-Te-Te}}$  with both Te atoms from the same (top or bottom) group. We find that there are actually only two parameters in the VFF model, so we can determine their value by fitting to the Young's modulus and the Poisson's ratio of the system. The *ab initio* calculations have predicted the Young's modulus to be 63 N/m and the Poisson's ratio as 0.35.<sup>48</sup>

The parameters for the two-body SW potential used by GULP are shown in Tab. CCLXXXIII. The parameters for the three-body SW potential used by GULP are shown in Tab. CCLXXXIV. Some representative parameters for the SW potential used by LAMMPS are listed in Tab. CCLXXXV.

We use LAMMPS to perform MD simulations for the mechanical behavior of the single-layer 1T-PdTe<sub>2</sub> under uniaxial tension at 1.0 K and 300.0 K. Fig. 140 shows the stress-strain curve for the tension of a single-layer 1T-PdTe<sub>2</sub> of dimension  $100 \times 100$  Å. Periodic boundary conditions are applied in both armchair and zigzag directions. The single-layer 1T-PdTe<sub>2</sub> is stretched uniaxially along the armchair or zigzag direction. The stress is calculated without

TABLE CCLXXXVI: The VFF model for single-layer 1T-SnS<sub>2</sub>. The second line gives an explicit expression for each VFF term. The third line is the force constant parameters. Parameters are in the unit of  $\frac{\text{eV}}{\text{Å}^2}$  for the bond stretching interactions, and in the unit of eV for the angle bending interaction. The fourth line gives the initial bond length (in unit of Å) for the bond stretching interaction and the initial angle (in unit of degrees) for the angle bending interaction. The angle  $\theta_{ijk}$  has atom i as the apex.

VFF type	bond stretching	angle bending	
expression	$\frac{1}{2}K_{\text{Sn-S}}(\Delta r)^2$	$\frac{1}{2}K_{\text{Sn-S-S}}(\Delta\theta)^2$	$\frac{1}{2}K_{\text{S-Sn-Sn}}(\Delta\theta)^2$
parameter	7.872	5.817	5.817
$r_0$ or $\theta_0$	2.570	90.173	90.173

involving the actual thickness of the quasi-two-dimensional structure of the single-layer 1T-PdTe<sub>2</sub>. The Young's modulus can be obtained by a linear fitting of the stress-strain relation in the small strain range of [0, 0.01]. The Young's modulus are 61.6 N/m and 61.4 N/m along the armchair and zigzag directions, respectively. The Young's modulus is essentially isotropic in the armchair and zigzag directions. The Poisson's ratio from the VFF model and the SW potential is  $\nu_{xy} = \nu_{yx} = 0.22$ .

There is no available value for nonlinear quantities in the single-layer 1T-PdTe<sub>2</sub>. We have thus used the nonlinear parameter  $B = 0.5d^4$  in Eq. (5), which is close to the value of  $B$  in most materials. The value of the third order nonlinear elasticity  $D$  can be extracted by fitting the stress-strain relation to the function  $\sigma = E\epsilon + \frac{1}{2}D\epsilon^2$  with  $E$  as the Young's modulus. The values of  $D$  from the present SW potential are -178.8 N/m and -203.8 N/m along the armchair and zigzag directions, respectively. The ultimate stress is about 9.6 Nm<sup>-1</sup> at the ultimate strain of 0.27 in the armchair direction at the low temperature of 1 K. The ultimate stress is about 9.2 Nm<sup>-1</sup> at the ultimate strain of 0.32 in the zigzag direction at the low temperature of 1 K.

Fig. 141 shows that the VFF model and the SW potential give exactly the same phonon dispersion, as the SW potential is derived from the VFF model.

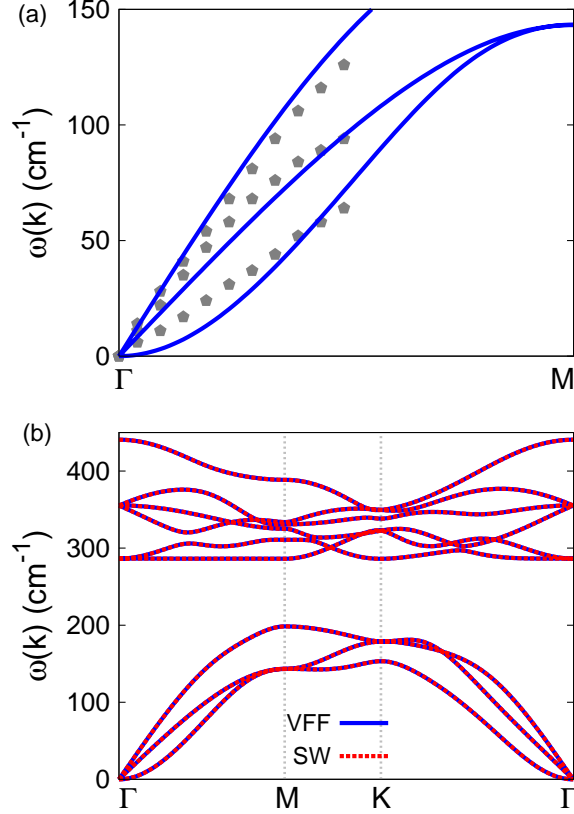


FIG. 142: (Color online) Phonon spectrum for single-layer 1T-SnS<sub>2</sub>. (a) Phonon dispersion along the  $\Gamma$ M direction in the Brillouin zone. The results from the VFF model (lines) are comparable with the *ab initio* results (pentagons) from Ref. 34. (b) The phonon dispersion from the SW potential is exactly the same as that from the VFF model.

TABLE CCLXXXVII: Two-body SW potential parameters for single-layer 1T-SnS<sub>2</sub> used by GULP<sup>8</sup> as expressed in Eq. (3).

	$A$ (eV)	$\rho$ ( $\text{\AA}$ )	$B$ ( $\text{\AA}^4$ )	$r_{\min}$ ( $\text{\AA}$ )	$r_{\max}$ ( $\text{\AA}$ )
Sn-S	7.805	1.384	21.812	0.0	3.513

## LXXII. 1T-SNS<sub>2</sub>

Most existing theoretical studies on the single-layer 1T-SnS<sub>2</sub> are based on the first-principles calculations. In this section, we will develop the SW potential for the single-layer 1T-SnS<sub>2</sub>.

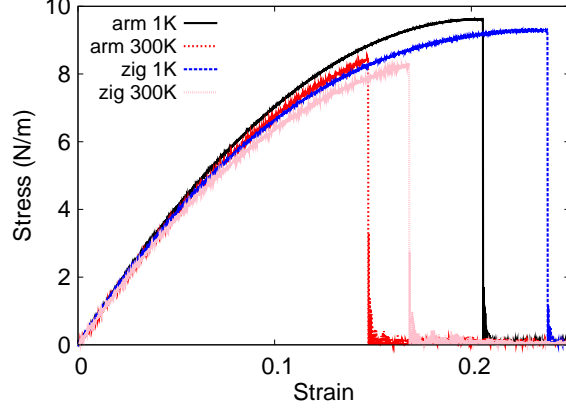


FIG. 143: (Color online) Stress-strain for single-layer 1T-SnS<sub>2</sub> of dimension 100 × 100 Å along the armchair and zigzag directions.

TABLE CCLXXXVIII: Three-body SW potential parameters for single-layer 1T-SnS<sub>2</sub> used by GULP<sup>8</sup> as expressed in Eq. (4). The angle  $\theta_{ijk}$  in the first line indicates the bending energy for the angle with atom *i* as the apex.

	$K$ (eV)	$\theta_0$ (degree)	$\rho_1$ (Å)	$\rho_2$ (Å)	$r_{\min 12}$ (Å)	$r_{\max 12}$ (Å)	$r_{\min 13}$ (Å)	$r_{\max 13}$ (Å)	$r_{\min 23}$ (Å)	$r_{\max 23}$ (Å)
$\theta_{\text{Sn-S-S}}$	54.748	90.173	1.384	1.384	0.0	3.513	0.0	3.513	0.0	4.972
$\theta_{\text{S-Sn-Sn}}$	54.748	90.173	1.384	1.384	0.0	3.513	0.0	3.513	0.0	4.972

The structure for the single-layer 1T-SnS<sub>2</sub> is shown in Fig. 71 (with M=Sn and X=S). Each Sn atom is surrounded by six S atoms. These S atoms are categorized into the top group (eg. atoms 1, 3, and 5) and bottom group (eg. atoms 2, 4, and 6). Each S atom is connected to three Sn atoms. The structural parameters are from the first-principles calculations,<sup>34</sup> including the lattice constant  $a = 3.640$  Å, and the bond length  $d_{\text{Sn-S}} = 2.570$  Å. The resultant angles are  $\theta_{\text{SSnSn}} = 90.173^\circ$ , and  $\theta_{\text{SnSS}} = 90.173^\circ$  with S atoms from the same (top or bottom) group.

TABLE CCLXXXIX: SW potential parameters for single-layer 1T-SnS<sub>2</sub> used by LAMMPS<sup>9</sup> as expressed in Eqs. (9) and (10).

	$\epsilon$ (eV)	$\sigma$ (Å)	$a$	$\lambda$	$\gamma$	$\cos \theta_0$	$A_L$	$B_L$	$p$	$q$	tol
Sn-S <sub>1</sub> -S <sub>1</sub>	1.000	1.384	2.539	54.748	1.000	-0.003	7.805	5.949	4	0	0.0

Table [CCLXXXVI](#) shows three VFF terms for the single-layer 1T-SnS<sub>2</sub>, one of which is the bond stretching interaction shown by Eq. (1) while the other two terms are the angle bending interaction shown by Eq. (2). We note that the angle bending term  $K_{\text{Sn-S-S}}$  is for the angle  $\theta_{\text{Sn-S-S}}$  with both S atoms from the same (top or bottom) group. These force constant parameters are determined by fitting to the acoustic branches in the phonon dispersion along the  $\Gamma\text{M}$  as shown in Fig. 142 (a). The *ab initio* calculations for the phonon dispersion are from Ref. 34. The lowest acoustic branch (flexural mode) is almost linear in the *ab initio* calculations, which may due to the violation of the rigid rotational invariance.<sup>20</sup> Fig. 142 (b) shows that the VFF model and the SW potential give exactly the same phonon dispersion, as the SW potential is derived from the VFF model.

The parameters for the two-body SW potential used by GULP are shown in Tab. [CCLXXXVII](#). The parameters for the three-body SW potential used by GULP are shown in Tab. [CCLXXXVIII](#). Some representative parameters for the SW potential used by LAMMPS are listed in Tab. [CCLXXXIX](#).

We use LAMMPS to perform MD simulations for the mechanical behavior of the single-layer 1T-SnS<sub>2</sub> under uniaxial tension at 1.0 K and 300.0 K. Fig. 143 shows the stress-strain curve for the tension of a single-layer 1T-SnS<sub>2</sub> of dimension  $100 \times 100 \text{ \AA}$ . Periodic boundary conditions are applied in both armchair and zigzag directions. The single-layer 1T-SnS<sub>2</sub> is stretched uniaxially along the armchair or zigzag direction. The stress is calculated without involving the actual thickness of the quasi-two-dimensional structure of the single-layer 1T-SnS<sub>2</sub>. The Young's modulus can be obtained by a linear fitting of the stress-strain relation in the small strain range of  $[0, 0.01]$ . The Young's modulus are 88.4 N/m and 87.9 N/m along the armchair and zigzag directions, respectively. The Young's modulus is essentially isotropic in the armchair and zigzag directions. The Poisson's ratio from the VFF model and the SW potential is  $\nu_{xy} = \nu_{yx} = 0.13$ .

There is no available value for nonlinear quantities in the single-layer 1T-SnS<sub>2</sub>. We have thus used the nonlinear parameter  $B = 0.5d^4$  in Eq. (5), which is close to the value of  $B$  in most materials. The value of the third order nonlinear elasticity  $D$  can be extracted by fitting the stress-strain relation to the function  $\sigma = E\epsilon + \frac{1}{2}D\epsilon^2$  with  $E$  as the Young's modulus. The values of  $D$  from the present SW potential are -392.8 N/m and -421.6 N/m along the armchair and zigzag directions, respectively. The ultimate stress is about  $9.6 \text{ Nm}^{-1}$  at the ultimate strain of 0.20 in the armchair direction at the low temperature of 1 K. The

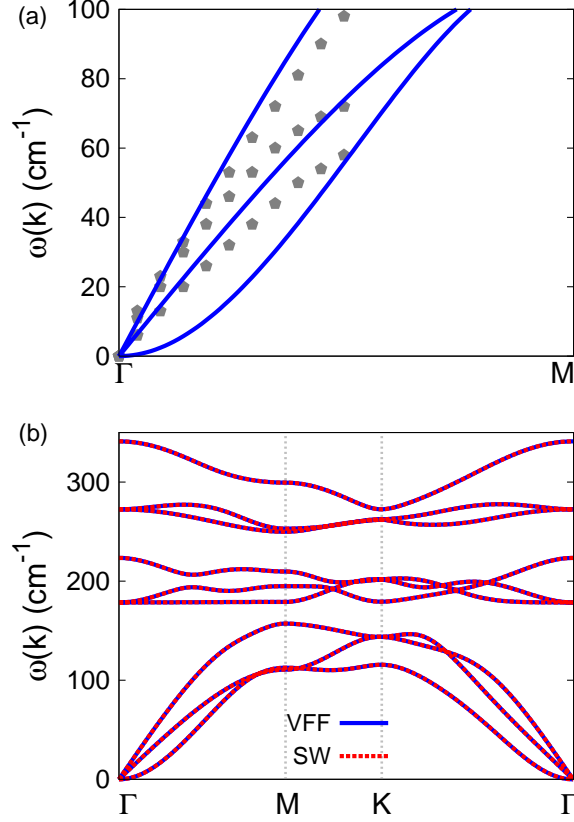


FIG. 144: (Color online) Phonon spectrum for single-layer 1T-SnSe<sub>2</sub>. (a) Phonon dispersion along the  $\Gamma$ M direction in the Brillouin zone. The results from the VFF model (lines) are comparable with the *ab initio* results (pentagons) from Ref. 34. (b) The phonon dispersion from the SW potential is exactly the same as that from the VFF model.

ultimate stress is about  $9.3 \text{ Nm}^{-1}$  at the ultimate strain of 0.24 in the zigzag direction at the low temperature of 1 K.

### LXXIII. 1T-SNSE<sub>2</sub>

Most existing theoretical studies on the single-layer 1T-SnSe<sub>2</sub> are based on the first-principles calculations. In this section, we will develop the SW potential for the single-layer 1T-SnSe<sub>2</sub>.

The structure for the single-layer 1T-SnSe<sub>2</sub> is shown in Fig. 71 (with M=Sn and X=Se). Each Sn atom is surrounded by six Se atoms. These Se atoms are categorized into the

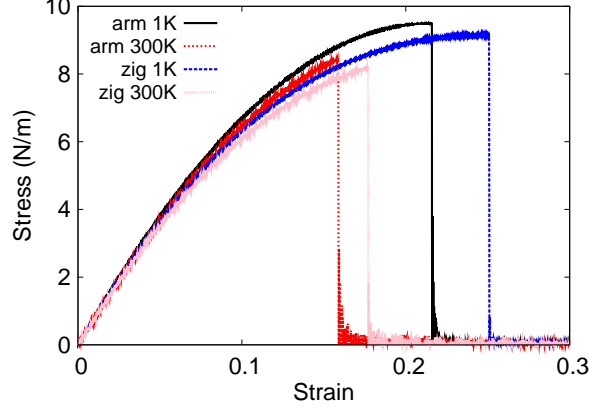


FIG. 145: (Color online) Stress-strain for single-layer 1T-SnSe<sub>2</sub> of dimension  $100 \times 100 \text{ \AA}$  along the armchair and zigzag directions.

TABLE CCXC: The VFF model for single-layer 1T-SnSe<sub>2</sub>. The second line gives an explicit expression for each VFF term. The third line is the force constant parameters. Parameters are in the unit of  $\frac{\text{eV}}{\text{\AA}^2}$  for the bond stretching interactions, and in the unit of eV for the angle bending interaction. The fourth line gives the initial bond length (in unit of  $\text{\AA}$ ) for the bond stretching interaction and the initial angle (in unit of degrees) for the angle bending interaction. The angle  $\theta_{ijk}$  has atom  $i$  as the apex.

VFF type	bond stretching	angle bending	
expression	$\frac{1}{2}K_{\text{Sn-Se}}(\Delta r)^2$	$\frac{1}{2}K_{\text{Sn-Se-Se}}(\Delta\theta)^2$	$\frac{1}{2}K_{\text{Se-Sn-Sn}}(\Delta\theta)^2$
parameter	7.872	5.817	5.817
$r_0$ or $\theta_0$	2.704	89.044	89.044

top group (eg. atoms 1, 3, and 5) and bottom group (eg. atoms 2, 4, and 6). Each Se atom is connected to three Sn atoms. The structural parameters are from the first-principles calculations,<sup>34</sup> including the lattice constant  $a = 3.792 \text{ \AA}$ , and the bond length  $d_{\text{Sn-Se}} = 2.704 \text{ \AA}$ . The resultant angles are  $\theta_{\text{SeSnSn}} = 89.044^\circ$ , and  $\theta_{\text{SnSeSe}} = 89.044^\circ$  with Se atoms from the same (top or bottom) group.

Table CCXC shows three VFF terms for the single-layer 1T-SnSe<sub>2</sub>, one of which is the bond stretching interaction shown by Eq. (1) while the other two terms are the angle bending interaction shown by Eq. (2). We note that the angle bending term  $K_{\text{Sn-Se-Se}}$  is for the angle

TABLE CCXCI: Two-body SW potential parameters for single-layer 1T-SnSe<sub>2</sub> used by GULP<sup>8</sup> as expressed in Eq. (3).

	$A$ (eV)	$\rho$ (Å)	$B$ (Å <sup>4</sup> )	$r_{\min}$ (Å)	$r_{\max}$ (Å)
Sn-Se	8.395	1.411	26.730	0.0	3.681

TABLE CCXCII: Three-body SW potential parameters for single-layer 1T-SnSe<sub>2</sub> used by GULP<sup>8</sup> as expressed in Eq. (4). The angle  $\theta_{ijk}$  in the first line indicates the bending energy for the angle with atom  $i$  as the apex.

	$K$ (eV)	$\theta_0$ (degree)	$\rho_1$ (Å)	$\rho_2$ (Å)	$r_{\min12}$ (Å)	$r_{\max12}$ (Å)	$r_{\min13}$ (Å)	$r_{\max13}$ (Å)	$r_{\min23}$ (Å)	$r_{\max23}$ (Å)
$\theta_{\text{Sn-Se-Se}}$	52.322	89.044	1.411	1.411	0.0	3.681	0.0	3.681	0.0	5.180
$\theta_{\text{Se-Sn-Sn}}$	52.322	89.044	1.411	1.411	0.0	3.681	0.0	3.681	0.0	5.180

$\theta_{\text{Sn-Se-Se}}$  with both Se atoms from the same (top or bottom) group. These force constant parameters are determined by fitting to the acoustic branches in the phonon dispersion along the  $\Gamma\text{M}$  as shown in Fig. 144 (a). The *ab initio* calculations for the phonon dispersion are from Ref. 34. The lowest acoustic branch (flexural mode) is almost linear in the *ab initio* calculations, which may due to the violation of the rigid rotational invariance.<sup>20</sup> Fig. 144 (b) shows that the VFF model and the SW potential give exactly the same phonon dispersion, as the SW potential is derived from the VFF model.

The parameters for the two-body SW potential used by GULP are shown in Tab. CCXCI. The parameters for the three-body SW potential used by GULP are shown in Tab. CCXCII. Some representative parameters for the SW potential used by LAMMPS are listed in Tab. CCXCIII.

We use LAMMPS to perform MD simulations for the mechanical behavior of the single-layer 1T-SnSe<sub>2</sub> under uniaxial tension at 1.0 K and 300.0 K. Fig. 145 shows the stress-strain curve for the tension of a single-layer 1T-SnSe<sub>2</sub> of dimension  $100 \times 100$  Å. Periodic boundary

TABLE CCXCIII: SW potential parameters for single-layer 1T-SnSe<sub>2</sub> used by LAMMPS<sup>9</sup> as expressed in Eqs. (9) and (10).

	$\epsilon$ (eV)	$\sigma$ (Å)	$a$	$\lambda$	$\gamma$	$\cos \theta_0$	$A_L$	$B_L$	$p$	$q$	tol
Sn-Se <sub>1</sub> -Se <sub>1</sub>	1.000	1.411	2.609	52.322	1.000	0.017	8.395	6.743	4	0	0.0

TABLE CCXCIV: The VFF model for single-layer 1T-HfS<sub>2</sub>. The second line gives an explicit expression for each VFF term. The third line is the force constant parameters. Parameters are in the unit of  $\frac{\text{eV}}{\text{\AA}^2}$  for the bond stretching interactions, and in the unit of eV for the angle bending interaction. The fourth line gives the initial bond length (in unit of \AA) for the bond stretching interaction and the initial angle (in unit of degrees) for the angle bending interaction. The angle  $\theta_{ijk}$  has atom i as the apex.

VFF type	bond stretching	angle bending	
expression	$\frac{1}{2}K_{\text{Hf-S}}(\Delta r)^2$	$\frac{1}{2}K_{\text{Hf-S-S}}(\Delta\theta)^2$	$\frac{1}{2}K_{\text{S-Hf-Hf}}(\Delta\theta)^2$
parameter	7.930	4.283	4.283
$r_0$ or $\theta_0$	2.550	91.078	91.078

conditions are applied in both armchair and zigzag directions. The single-layer 1T-SnSe<sub>2</sub> is stretched uniaxially along the armchair or zigzag direction. The stress is calculated without involving the actual thickness of the quasi-two-dimensional structure of the single-layer 1T-SnSe<sub>2</sub>. The Young's modulus can be obtained by a linear fitting of the stress-strain relation in the small strain range of [0, 0.01]. The Young's modulus are 82.0 N/m and 81.6 N/m along the armchair and zigzag directions, respectively. The Young's modulus is essentially isotropic in the armchair and zigzag directions. The Poisson's ratio from the VFF model and the SW potential is  $\nu_{xy} = \nu_{yx} = 0.15$ .

There is no available value for nonlinear quantities in the single-layer 1T-SnSe<sub>2</sub>. We have thus used the nonlinear parameter  $B = 0.5d^4$  in Eq. (5), which is close to the value of  $B$  in most materials. The value of the third order nonlinear elasticity  $D$  can be extracted by fitting the stress-strain relation to the function  $\sigma = E\epsilon + \frac{1}{2}D\epsilon^2$  with  $E$  as the Young's modulus. The values of  $D$  from the present SW potential are -339.2 N/m and -368.3 N/m along the armchair and zigzag directions, respectively. The ultimate stress is about 9.5 Nm<sup>-1</sup> at the ultimate strain of 0.21 in the armchair direction at the low temperature of 1 K. The ultimate stress is about 9.1 Nm<sup>-1</sup> at the ultimate strain of 0.25 in the zigzag direction at the low temperature of 1 K.

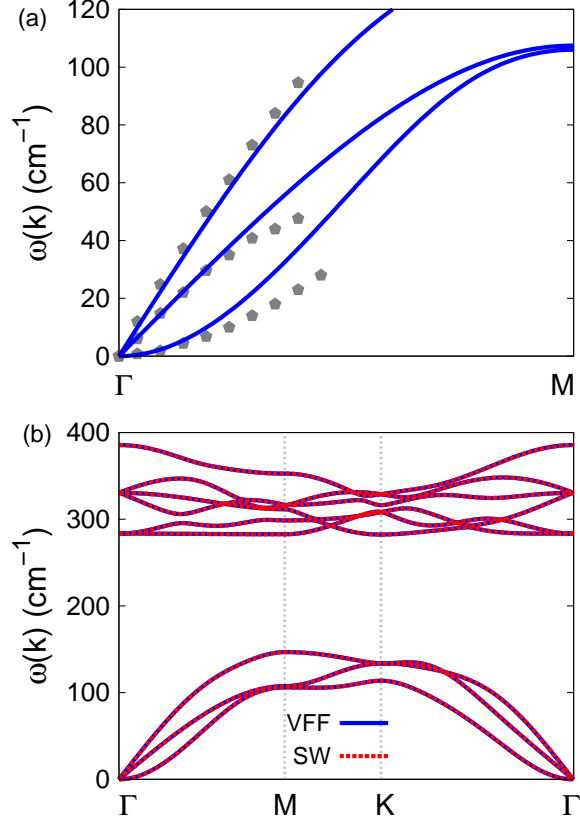


FIG. 146: (Color online) Phonon spectrum for single-layer 1T-HfS<sub>2</sub>. (a) Phonon dispersion along the  $\Gamma$ M direction in the Brillouin zone. The results from the VFF model (lines) are comparable with the experiment data (pentagons) from Ref. 38. (b) The phonon dispersion from the SW potential is exactly the same as that from the VFF model.

TABLE CCXCV: Two-body SW potential parameters for single-layer 1T-HfS<sub>2</sub> used by GULP<sup>8</sup> as expressed in Eq. (3).

	$A$ (eV)	$\rho$ ( $\text{\AA}$ )	$B$ ( $\text{\AA}^4$ )	$r_{\min}$ ( $\text{\AA}$ )	$r_{\max}$ ( $\text{\AA}$ )
Hf-S	7.917	1.407	21.141	0.0	3.497

#### LXXIV. 1T-HfS<sub>2</sub>

Most existing theoretical studies on the single-layer 1T-HfS<sub>2</sub> are based on the first-principles calculations. In this section, we will develop the SW potential for the single-layer 1T-HfS<sub>2</sub>.

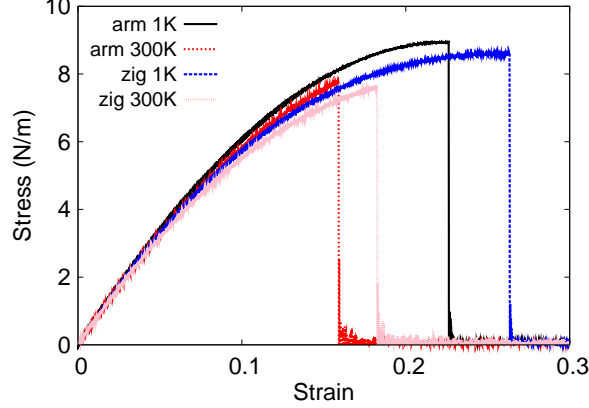


FIG. 147: (Color online) Stress-strain for single-layer 1T-HfS<sub>2</sub> of dimension 100 × 100 Å along the armchair and zigzag directions.

TABLE CCXCVI: Three-body SW potential parameters for single-layer 1T-HfS<sub>2</sub> used by GULP<sup>8</sup> as expressed in Eq. (4). The angle  $\theta_{ijk}$  in the first line indicates the bending energy for the angle with atom *i* as the apex.

	$K$ (eV)	$\theta_0$ (degree)	$\rho_1$ (Å)	$\rho_2$ (Å)	$r_{\min 12}$ (Å)	$r_{\max 12}$ (Å)	$r_{\min 13}$ (Å)	$r_{\max 13}$ (Å)	$r_{\min 23}$ (Å)	$r_{\max 23}$ (Å)
$\theta_{\text{Hf-S-S}}$	41.798	91.078	1.407	1.407	0.0	3.497	0.0	3.497	0.0	4.973
$\theta_{\text{S-Hf-Hf}}$	41.798	91.078	1.407	1.407	0.0	3.497	0.0	3.497	0.0	4.973

The structure for the single-layer 1T-HfS<sub>2</sub> is shown in Fig. 71 (with M=Hf and X=S). Each Hf atom is surrounded by six S atoms. These S atoms are categorized into the top group (eg. atoms 1, 3, and 5) and bottom group (eg. atoms 2, 4, and 6). Each S atom is connected to three Hf atoms. The structural parameters are from the first-principles calculations,<sup>53</sup> including the lattice constant  $a = 3.64$  Å and the bond length  $d_{\text{Hf-S}} = 2.55$  Å. The resultant angles are  $\theta_{\text{HfSS}} = 91.078^\circ$  with S atoms from the same (top or bottom) group,

TABLE CCXCVII: SW potential parameters for single-layer 1T-HfS<sub>2</sub> used by LAMMPS<sup>9</sup> as expressed in Eqs. (9) and (10).

	$\epsilon$ (eV)	$\sigma$ (Å)	$a$	$\lambda$	$\gamma$	$\cos \theta_0$	$A_L$	$B_L$	$p$	$q$	tol
Hf-S-S	1.000	1.407	2.485	41.798	1.000	-0.019	7.917	5.394	4	0	0.0
S-Hf-Hf	1.000	1.407	2.485	41.798	1.000	-0.019	7.917	5.394	4	0	0.0

and  $\theta_{\text{SHHf}} = 91.078^\circ$ .

Table [CCXCIV](#) shows three VFF terms for the single-layer 1T-HfS<sub>2</sub>, one of which is the bond stretching interaction shown by Eq. (1) while the other two terms are the angle bending interaction shown by Eq. (2). We note that the angle bending term  $K_{\text{Hf-S-S}}$  is for the angle  $\theta_{\text{Hf-S-S}}$  with both S atoms from the same (top or bottom) group. These force constant parameters are determined by fitting to the three acoustic branches in the phonon dispersion along the  $\Gamma\text{M}$  as shown in Fig. [146](#) (a). The *ab initio* calculations for the phonon dispersion are from Ref. 38. Similar phonon dispersion can also be found in other *ab initio* calculations.<sup>34,54</sup> Fig. [146](#) (b) shows that the VFF model and the SW potential give exactly the same phonon dispersion, as the SW potential is derived from the VFF model.

The parameters for the two-body SW potential used by GULP are shown in Tab. [CCXCV](#). The parameters for the three-body SW potential used by GULP are shown in Tab. [CCXCVI](#). Some representative parameters for the SW potential used by LAMMPS are listed in Tab. [CCXCVII](#).

We use LAMMPS to perform MD simulations for the mechanical behavior of the single-layer 1T-HfS<sub>2</sub> under uniaxial tension at 1.0 K and 300.0 K. Fig. [147](#) shows the stress-strain curve for the tension of a single-layer 1T-HfS<sub>2</sub> of dimension  $100 \times 100 \text{ \AA}$ . Periodic boundary conditions are applied in both armchair and zigzag directions. The single-layer 1T-HfS<sub>2</sub> is stretched uniaxially along the armchair or zigzag direction. The stress is calculated without involving the actual thickness of the quasi-two-dimensional structure of the single-layer 1T-HfS<sub>2</sub>. The Young's modulus can be obtained by a linear fitting of the stress-strain relation in the small strain range of  $[0, 0.01]$ . The Young's modulus are 73.3 N/m and 72.9 N/m along the armchair and zigzag directions, respectively. The Young's modulus is essentially isotropic in the armchair and zigzag directions. These values are close to the *ab initio* results at 0 K temperature, eg. 79.86 Nm<sup>-1</sup> in Ref. 53. The Poisson's ratio from the VFF model and the SW potential is  $\nu_{xy} = \nu_{yx} = 0.16$ , which agrees reasonably with the *ab initio* result<sup>53</sup> of 0.19.

There is no available value for nonlinear quantities in the single-layer 1T-HfS<sub>2</sub>. We have thus used the nonlinear parameter  $B = 0.5d^4$  in Eq. (5), which is close to the value of  $B$  in most materials. The value of the third order nonlinear elasticity  $D$  can be extracted by fitting the stress-strain relation to the function  $\sigma = E\epsilon + \frac{1}{2}D\epsilon^2$  with  $E$  as the Young's modulus. The values of  $D$  from the present SW potential are -280.9 N/m and -317.2 N/m

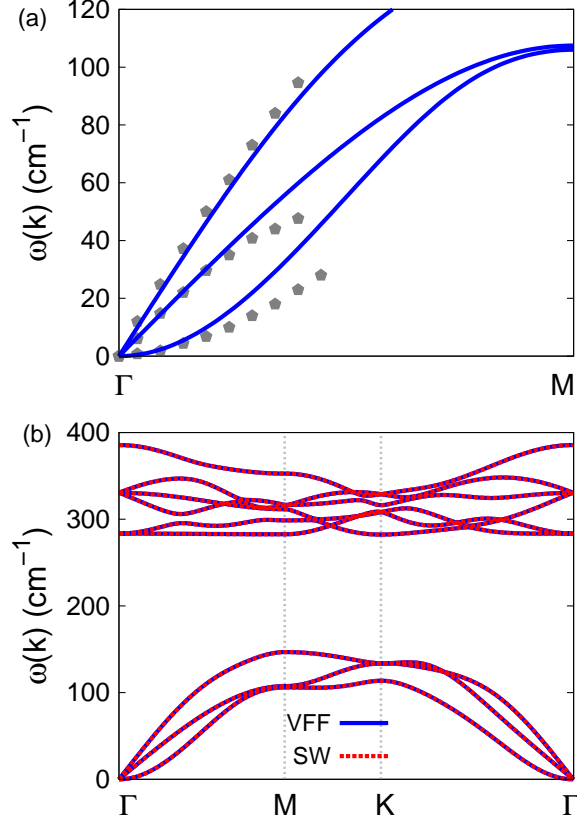


FIG. 148: (Color online) Phonon spectrum for single-layer 1T-HfSe<sub>2</sub>. (a) Phonon dispersion along the  $\Gamma$ M direction in the Brillouin zone. The results from the VFF model (lines) are comparable with the experiment data (pentagons) from Ref. 50. (b) The phonon dispersion from the SW potential is exactly the same as that from the VFF model.

along the armchair and zigzag directions, respectively. The ultimate stress is about  $8.9 \text{ Nm}^{-1}$  at the ultimate strain of 0.22 in the armchair direction at the low temperature of 1 K. The ultimate stress is about  $8.6 \text{ Nm}^{-1}$  at the ultimate strain of 0.26 in the zigzag direction at the low temperature of 1 K.

## LXXV. 1T-HFSE<sub>2</sub>

Most existing theoretical studies on the single-layer 1T-HfSe<sub>2</sub> are based on the first-principles calculations. In this section, we will develop the SW potential for the single-layer 1T-HfSe<sub>2</sub>.

TABLE CCXCVIII: The VFF model for single-layer 1T-HfSe<sub>2</sub>. The second line gives an explicit expression for each VFF term. The third line is the force constant parameters. Parameters are in the unit of  $\frac{\text{eV}}{\text{Å}^2}$  for the bond stretching interactions, and in the unit of eV for the angle bending interaction. The fourth line gives the initial bond length (in unit of Å) for the bond stretching interaction and the initial angle (in unit of degrees) for the angle bending interaction. The angle  $\theta_{ijk}$  has atom i as the apex.

VFF type	bond stretching	angle bending	
expression	$\frac{1}{2}K_{\text{Hf-Se}}(\Delta r)^2$	$\frac{1}{2}K_{\text{Hf-Se-Se}}(\Delta\theta)^2$	$\frac{1}{2}K_{\text{Se-Hf-Hf}}(\Delta\theta)^2$
parameter	7.930	4.283	4.283
$r_0$ or $\theta_0$	2.642	88.093	88.093

TABLE CCXCIX: Two-body SW potential parameters for single-layer 1T-HfSe<sub>2</sub> used by GULP<sup>8</sup> as expressed in Eq. (3).

	$A$ (eV)	$\rho$ (Å)	$B$ (Å <sup>4</sup> )	$r_{\min}$ (Å)	$r_{\max}$ (Å)
Hf-Se	7.871	1.341	24.361	0.0	3.583

TABLE CCC: Three-body SW potential parameters for single-layer 1T-HfSe<sub>2</sub> used by GULP<sup>8</sup> as expressed in Eq. (4). The angle  $\theta_{ijk}$  in the first line indicates the bending energy for the angle with atom i as the apex.

	$K$ (eV)	$\theta_0$ (degree)	$\rho_1$ (Å)	$\rho_2$ (Å)	$r_{\min12}$ (Å)	$r_{\max12}$ (Å)	$r_{\min13}$ (Å)	$r_{\max13}$ (Å)	$r_{\min23}$ (Å)	$r_{\max23}$ (Å)
$\theta_{\text{Hf-Se-Se}}$	37.039	88.093	1.341	1.341	0.0	3.583	0.0	3.583	0.0	5.018
$\theta_{\text{Se-Hf-Hf}}$	37.039	88.093	1.341	1.341	0.0	3.583	0.0	3.583	0.0	5.018

TABLE CCCI: SW potential parameters for single-layer 1T-HfSe<sub>2</sub> used by LAMMPS<sup>9</sup> as expressed in Eqs. (9) and (10).

	$\epsilon$ (eV)	$\sigma$ (Å)	$a$	$\lambda$	$\gamma$	$\cos\theta_0$	$A_L$	$B_L$	$p$	$q$	tol
Hf-Se-Se	1.000	1.341	2.672	37.039	1.000	0.033	7.871	7.533	4	0	0.0
Se-Hf-Hf	1.000	1.341	2.672	37.039	1.000	0.033	7.871	7.533	4	0	0.0

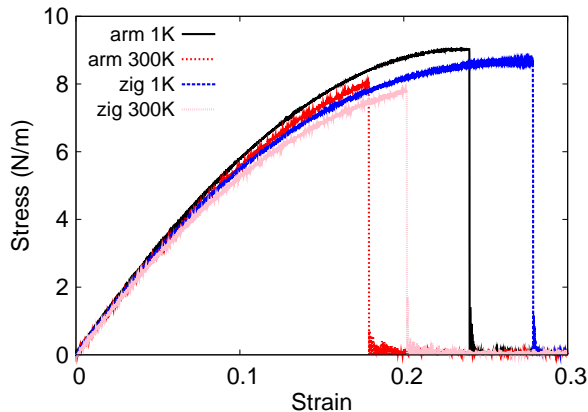


FIG. 149: (Color online) Stress-strain for single-layer 1T-HfSe<sub>2</sub> of dimension  $100 \times 100 \text{ \AA}$  along the armchair and zigzag directions.

The structure for the single-layer 1T-HfSe<sub>2</sub> is shown in Fig. 71 (with M=Hf and X=Se). Each Hf atom is surrounded by six Se atoms. These Se atoms are categorized into the top group (eg. atoms 1, 3, and 5) and bottom group (eg. atoms 2, 4, and 6). Each Se atom is connected to three Hf atoms. The structural parameters are from the first-principles calculations,<sup>51</sup> including the lattice constant  $a = 3.673 \text{ \AA}$ , and the position of the Se atom with respect to the Hf atomic plane  $h = 1.575 \text{ \AA}$ . The resultant angles are  $\theta_{\text{HfSeSe}} = 88.093^\circ$  with S atoms from the same (top or bottom) group, and  $\theta_{\text{SeHfHf}} = 88.093^\circ$ .

Table CCXCVIII shows three VFF terms for the single-layer 1T-HfSe<sub>2</sub>, one of which is the bond stretching interaction shown by Eq. (1) while the other two terms are the angle bending interaction shown by Eq. (2). We note that the angle bending term  $K_{\text{Hf-Se-Se}}$  is for the angle  $\theta_{\text{Hf-Se-Se}}$  with both Se atoms from the same (top or bottom) group. These force constant parameters are determined by fitting to the three acoustic branches in the phonon dispersion along the  $\Gamma\text{M}$  as shown in Fig. 148 (a). The *ab initio* calculations for the phonon dispersion are from Ref. 50. Similar phonon dispersion can also be found in other *ab initio* calculations.<sup>34</sup> Fig. 148 (b) shows that the VFF model and the SW potential give exactly the same phonon dispersion, as the SW potential is derived from the VFF model.

The parameters for the two-body SW potential used by GULP are shown in Tab. CCXCIX. The parameters for the three-body SW potential used by GULP are shown in Tab. CCC. Some representative parameters for the SW potential used by LAMMPS are listed in Tab. CCCI.

We use LAMMPS to perform MD simulations for the mechanical behavior of the single-layer 1T-HfSe<sub>2</sub> under uniaxial tension at 1.0 K and 300.0 K. Fig. 149 shows the stress-strain curve for the tension of a single-layer 1T-HfSe<sub>2</sub> of dimension 100 × 100 Å. Periodic boundary conditions are applied in both armchair and zigzag directions. The single-layer 1T-HfSe<sub>2</sub> is stretched uniaxially along the armchair or zigzag direction. The stress is calculated without involving the actual thickness of the quasi-two-dimensional structure of the single-layer 1T-HfSe<sub>2</sub>. The Young's modulus can be obtained by a linear fitting of the stress-strain relation in the small strain range of [0, 0.01]. The Young's modulus are 67.3 N/m and 67.0 N/m along the armchair and zigzag directions, respectively. The Young's modulus is essentially isotropic in the armchair and zigzag directions. The Poisson's ratio from the VFF model and the SW potential is  $\nu_{xy} = \nu_{yx} = 0.18$ .

There is no available value for nonlinear quantities in the single-layer 1T-HfSe<sub>2</sub>. We have thus used the nonlinear parameter  $B = 0.5d^4$  in Eq. (5), which is close to the value of  $B$  in most materials. The value of the third order nonlinear elasticity  $D$  can be extracted by fitting the stress-strain relation to the function  $\sigma = E\epsilon + \frac{1}{2}D\epsilon^2$  with  $E$  as the Young's modulus. The values of  $D$  from the present SW potential are -221.5 N/m and -258.6 N/m along the armchair and zigzag directions, respectively. The ultimate stress is about 9.0 Nm<sup>-1</sup> at the ultimate strain of 0.24 in the armchair direction at the low temperature of 1 K. The ultimate stress is about 8.7 Nm<sup>-1</sup> at the ultimate strain of 0.28 in the zigzag direction at the low temperature of 1 K.

## LXXVI. 1T-HfTe<sub>2</sub>

Most existing theoretical studies on the single-layer 1T-HfTe<sub>2</sub> are based on the first-principles calculations. In this section, we will develop the SW potential for the single-layer 1T-HfTe<sub>2</sub>.

The structure for the single-layer 1T-HfTe<sub>2</sub> is shown in Fig. 71 (with M=Hf and X=Te). Each Hf atom is surrounded by six Te atoms. These Te atoms are categorized into the top group (eg. atoms 1, 3, and 5) and bottom group (eg. atoms 2, 4, and 6). Each Te atom is connected to three Hf atoms. The structural parameters are from the first-principles calculations,<sup>48</sup> including the lattice constant  $a = 3.9606$  Å, and the bond length  $d_{\text{Hf-Te}} = 2.8559$  Å, which is derived from the angle  $\theta_{\text{TeHfHf}} = 87.8^\circ$ . The other angle is

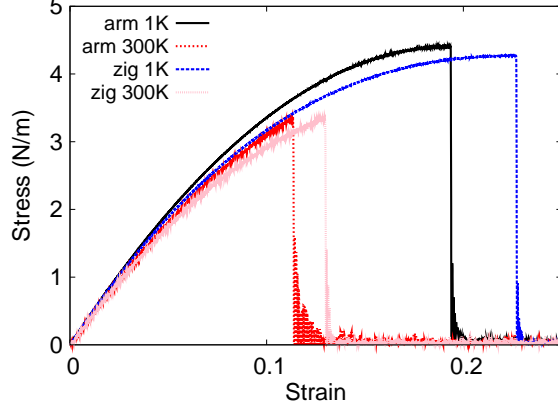


FIG. 150: (Color online) Stress-strain for single-layer 1T-HfTe<sub>2</sub> of dimension  $100 \times 100 \text{ \AA}$  along the armchair and zigzag directions.

TABLE CCCII: The VFF model for single-layer 1T-HfTe<sub>2</sub>. The second line gives an explicit expression for each VFF term. The third line is the force constant parameters. Parameters are in the unit of  $\frac{eV}{\text{Å}^2}$  for the bond stretching interactions, and in the unit of eV for the angle bending interaction. The fourth line gives the initial bond length (in unit of Å) for the bond stretching interaction and the initial angle (in unit of degrees) for the angle bending interaction. The angle  $\theta_{ijk}$  has atom  $i$  as the apex.

VFF type	bond stretching	angle bending	
expression	$\frac{1}{2}K_{\text{Hf-Te}}(\Delta r)^2$	$\frac{1}{2}K_{\text{Hf-Te-Te}}(\Delta\theta)^2$	$\frac{1}{2}K_{\text{Te-Hf-Hf}}(\Delta\theta)^2$
parameter	3.328	3.877	3.877
$r_0$ or $\theta_0$	2.856	87.801	87.801

$\theta_{\text{HfTeTe}} = 87.8^\circ$  with Te atoms from the same (top or bottom) group.

Table CCCII shows three VFF terms for the single-layer 1T-HfTe<sub>2</sub>, one of which is the bond stretching interaction shown by Eq. (1) while the other two terms are the angle bending interaction shown by Eq. (2). We note that the angle bending term  $K_{\text{Hf-Te-Te}}$  is for the angle  $\theta_{\text{Hf-Te-Te}}$  with both Te atoms from the same (top or bottom) group. We find that there are actually only two parameters in the VFF model, so we can determine their value by fitting to the Young's modulus and the Poisson's ratio of the system. The *ab initio* calculations have predicted the Young's modulus to be 50 N/m and the Poisson's ratio as

TABLE CCCIII: Two-body SW potential parameters for single-layer 1T-HfTe<sub>2</sub> used by GULP<sup>8</sup> as expressed in Eq. (3).

	$A$ (eV)	$\rho$ (Å)	$B$ (Å <sup>4</sup> )	$r_{\min}$ (Å)	$r_{\max}$ (Å)
Hf-Te	3.835	1.439	33.262	0.0	3.869

TABLE CCCIV: Three-body SW potential parameters for single-layer 1T-HfTe<sub>2</sub> used by GULP<sup>8</sup> as expressed in Eq. (4). The angle  $\theta_{ijk}$  in the first line indicates the bending energy for the angle with atom  $i$  as the apex.

	$K$ (eV)	$\theta_0$ (degree)	$\rho_1$ (Å)	$\rho_2$ (Å)	$r_{\min12}$ (Å)	$r_{\max12}$ (Å)	$r_{\min13}$ (Å)	$r_{\max13}$ (Å)	$r_{\min23}$ (Å)	$r_{\max23}$ (Å)
$\theta_{\text{Hf-Te-Te}}$	33.196	87.801	1.439	1.439	0.0	3.869	0.0	3.869	0.0	5.410
$\theta_{\text{Te-Hf-Hf}}$	33.196	87.801	1.439	1.439	0.0	3.869	0.0	3.869	0.0	5.410

0.10.<sup>48</sup>

The parameters for the two-body SW potential used by GULP are shown in Tab. CCCIII. The parameters for the three-body SW potential used by GULP are shown in Tab. CCCIV. Some representative parameters for the SW potential used by LAMMPS are listed in Tab. CCCV.

We use LAMMPS to perform MD simulations for the mechanical behavior of the single-layer 1T-HfTe<sub>2</sub> under uniaxial tension at 1.0 K and 300.0 K. Fig. 150 shows the stress-strain curve for the tension of a single-layer 1T-HfTe<sub>2</sub> of dimension  $100 \times 100$  Å. Periodic boundary conditions are applied in both armchair and zigzag directions. The single-layer 1T-HfTe<sub>2</sub> is stretched uniaxially along the armchair or zigzag direction. The stress is calculated without involving the actual thickness of the quasi-two-dimensional structure of the single-layer 1T-HfTe<sub>2</sub>. The Young's modulus can be obtained by a linear fitting of the stress-strain relation in the small strain range of  $[0, 0.01]$ . The Young's modulus is 43.1 N/m along the armchair and zigzag directions. The Poisson's ratio from the VFF model and the SW potential is

TABLE CCCV: SW potential parameters for single-layer 1T-HfTe<sub>2</sub> used by LAMMPS<sup>9</sup> as expressed in Eqs. (9) and (10).

	$\epsilon$ (eV)	$\sigma$ (Å)	$a$	$\lambda$	$\gamma$	$\cos \theta_0$	$A_L$	$B_L$	$p$	$q$	tol
Hf-Te <sub>1</sub> -Te <sub>1</sub>	1.000	1.439	2.690	33.196	1.000	0.038	3.835	7.764	4	0	0.0

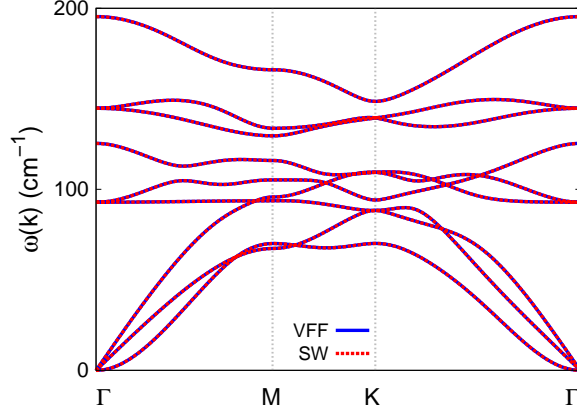


FIG. 151: (Color online) Phonon spectrum for single-layer 1T-HfTe<sub>2</sub> along the  $\Gamma$ MK $\Gamma$  direction in the Brillouin zone. The phonon dispersion from the SW potential is exactly the same as that from the VFF model.

$\nu_{xy} = \nu_{yx} = 0.10$ . The fitted Young's modulus value is about 10% smaller than the *ab initio* result of 50 N/m,<sup>48</sup> as only short-range interactions are considered in the present work. The long-range interactions are ignored, which typically leads to about 10% underestimation for the value of the Young's modulus.

There is no available value for nonlinear quantities in the single-layer 1T-HfTe<sub>2</sub>. We have thus used the nonlinear parameter  $B = 0.5d^4$  in Eq. (5), which is close to the value of  $B$  in most materials. The value of the third order nonlinear elasticity  $D$  can be extracted by fitting the stress-strain relation to the function  $\sigma = E\epsilon + \frac{1}{2}D\epsilon^2$  with  $E$  as the Young's modulus. The values of  $D$  from the present SW potential are -204.3 N/m and -220.7 N/m along the armchair and zigzag directions, respectively. The ultimate stress is about 4.4 Nm<sup>-1</sup> at the ultimate strain of 0.19 in the armchair direction at the low temperature of 1 K. The ultimate stress is about 4.3 Nm<sup>-1</sup> at the ultimate strain of 0.22 in the zigzag direction at the low temperature of 1 K.

Fig. 151 shows that the VFF model and the SW potential give exactly the same phonon dispersion, as the SW potential is derived from the VFF model.

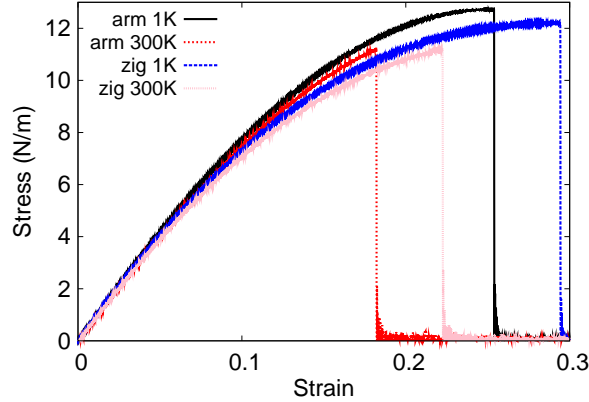


FIG. 152: (Color online) Stress-strain for single-layer 1T-TaS<sub>2</sub> of dimension  $100 \times 100 \text{ \AA}$  along the armchair and zigzag directions.

TABLE CCCVI: The VFF model for single-layer 1T-TaS<sub>2</sub>. The second line gives an explicit expression for each VFF term. The third line is the force constant parameters. Parameters are in the unit of  $\frac{eV}{\text{Å}^2}$  for the bond stretching interactions, and in the unit of eV for the angle bending interaction. The fourth line gives the initial bond length (in unit of Å) for the bond stretching interaction and the initial angle (in unit of degrees) for the angle bending interaction. The angle  $\theta_{ijk}$  has atom *i* as the apex.

VFF type	bond stretching	angle bending	
expression	$\frac{1}{2}K_{\text{Ta-S}}(\Delta r)^2$	$\frac{1}{2}K_{\text{Ta-S-S}}(\Delta\theta)^2$	$\frac{1}{2}K_{\text{S-Ta-Ta}}(\Delta\theta)^2$
parameter	11.192	4.774	4.774
$r_0$ or $\theta_0$	2.458	85.999	85.999

## LXXVII. 1T-TAS<sub>2</sub>

Most existing theoretical studies on the single-layer 1T-TaS<sub>2</sub> are based on the first-principles calculations. In this section, we will develop the SW potential for the single-layer 1T-TaS<sub>2</sub>.

The structure for the single-layer 1T-TaS<sub>2</sub> is shown in Fig. 71 (with M=Ta and X=S). Each Ta atom is surrounded by six S atoms. These S atoms are categorized into the top group (eg. atoms 1, 3, and 5) and bottom group (eg. atoms 2, 4, and 6). Each S atom is connected to three Ta atoms. The structural parameters are from the first-principles calculations,<sup>48</sup>

TABLE CCCVII: Two-body SW potential parameters for single-layer 1T-TaS<sub>2</sub> used by GULP<sup>8</sup> as expressed in Eq. (3).

	$A$ (eV)	$\rho$ (Å)	$B$ (Å <sup>4</sup> )	$r_{\min}$ (Å)	$r_{\max}$ (Å)
Ta-S	9.110	1.174	18.246	0.0	3.307

TABLE CCCVIII: Three-body SW potential parameters for single-layer 1T-TaS<sub>2</sub> used by GULP<sup>8</sup> as expressed in Eq. (4). The angle  $\theta_{ijk}$  in the first line indicates the bending energy for the angle with atom  $i$  as the apex.

	$K$ (eV)	$\theta_0$ (degree)	$\rho_1$ (Å)	$\rho_2$ (Å)	$r_{\min12}$ (Å)	$r_{\max12}$ (Å)	$r_{\min13}$ (Å)	$r_{\max13}$ (Å)	$r_{\min23}$ (Å)	$r_{\max23}$ (Å)
$\theta_{\text{Ta-S-S}}$	38.092	85.999	1.174	1.174	0.0	3.307	0.0	3.307	0.0	4.579
$\theta_{\text{S-Ta-Ta}}$	38.092	85.999	1.174	1.174	0.0	3.307	0.0	3.307	0.0	4.579

including the lattice constant  $a = 3.3524$  Å, and the bond length  $d_{\text{Ta-S}} = 2.4578$  Å, which is derived from the angle  $\theta_{\text{STaTa}} = 86^\circ$ . The other angle is  $\theta_{\text{TaSS}} = 86^\circ$  with S atoms from the same (top or bottom) group.

Table CCCVI shows three VFF terms for the single-layer 1T-TaS<sub>2</sub>, one of which is the bond stretching interaction shown by Eq. (1) while the other two terms are the angle bending interaction shown by Eq. (2). We note that the angle bending term  $K_{\text{Ta-S-S}}$  is for the angle  $\theta_{\text{Ta-S-S}}$  with both S atoms from the same (top or bottom) group. We find that there are actually only two parameters in the VFF model, so we can determine their value by fitting to the Young's modulus and the Poisson's ratio of the system. The *ab initio* calculations have predicted the Young's modulus to be 101 N/m and the Poisson's ratio as 0.20.<sup>48</sup>

The parameters for the two-body SW potential used by GULP are shown in Tab. CCCVII. The parameters for the three-body SW potential used by GULP are shown in Tab. CCCVIII. Some representative parameters for the SW potential used by LAMMPS are listed in Tab. CCCIX.

TABLE CCCIX: SW potential parameters for single-layer 1T-TaS<sub>2</sub> used by LAMMPS<sup>9</sup> as expressed in Eqs. (9) and (10).

	$\epsilon$ (eV)	$\sigma$ (Å)	$a$	$\lambda$	$\gamma$	$\cos \theta_0$	$A_L$	$B_L$	$p$	$q$	tol
Ta-S <sub>1</sub> -S <sub>1</sub>	1.000	1.174	2.816	38.092	1.000	0.070	9.110	9.589	4	0	0.0

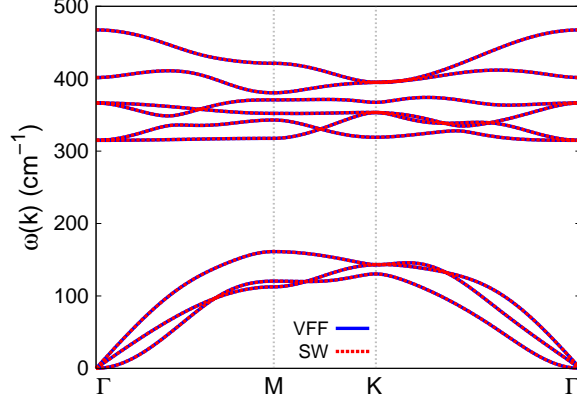


FIG. 153: (Color online) Phonon spectrum for single-layer 1T-TaS<sub>2</sub> along the  $\Gamma$ MK $\Gamma$  direction in the Brillouin zone. The phonon dispersion from the SW potential is exactly the same as that from the VFF model.

We use LAMMPS to perform MD simulations for the mechanical behavior of the single-layer 1T-TaS<sub>2</sub> under uniaxial tension at 1.0 K and 300.0 K. Fig. 152 shows the stress-strain curve for the tension of a single-layer 1T-TaS<sub>2</sub> of dimension  $100 \times 100$  Å. Periodic boundary conditions are applied in both armchair and zigzag directions. The single-layer 1T-TaS<sub>2</sub> is stretched uniaxially along the armchair or zigzag direction. The stress is calculated without involving the actual thickness of the quasi-two-dimensional structure of the single-layer 1T-TaS<sub>2</sub>. The Young's modulus can be obtained by a linear fitting of the stress-strain relation in the small strain range of  $[0, 0.01]$ . The Young's modulus are 87.8 N/m and 87.4 N/m along the armchair and zigzag directions, respectively. The Young's modulus is essentially isotropic in the armchair and zigzag directions. The Poisson's ratio from the VFF model and the SW potential is  $\nu_{xy} = \nu_{yx} = 0.20$ . The fitted Young's modulus value is about 10% smaller than the *ab initio* result of 101 N/m,<sup>48</sup> as only short-range interactions are considered in the present work. The long-range interactions are ignored, which typically leads to about 10% underestimation for the value of the Young's modulus.

There is no available value for nonlinear quantities in the single-layer 1T-TaS<sub>2</sub>. We have thus used the nonlinear parameter  $B = 0.5d^4$  in Eq. (5), which is close to the value of  $B$  in most materials. The value of the third order nonlinear elasticity  $D$  can be extracted by fitting the stress-strain relation to the function  $\sigma = E\epsilon + \frac{1}{2}D\epsilon^2$  with  $E$  as the Young's modulus. The values of  $D$  from the present SW potential are -276.3 N/m and -313.0 N/m along the

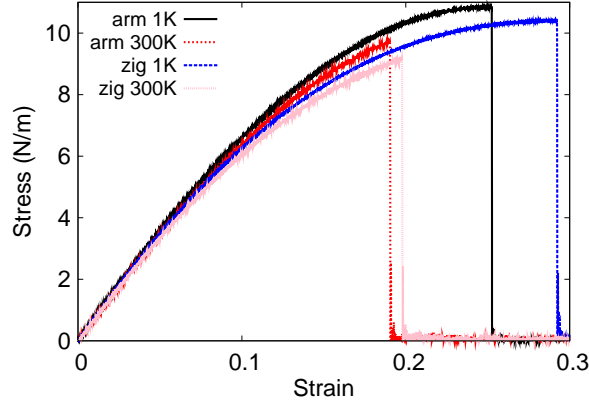


FIG. 154: (Color online) Stress-strain for single-layer 1T-TaSe<sub>2</sub> of dimension  $100 \times 100 \text{ \AA}$  along the armchair and zigzag directions.

TABLE CCCX: The VFF model for single-layer 1T-TaSe<sub>2</sub>. The second line gives an explicit expression for each VFF term. The third line is the force constant parameters. Parameters are in the unit of  $\frac{eV}{\text{Å}^2}$  for the bond stretching interactions, and in the unit of eV for the angle bending interaction. The fourth line gives the initial bond length (in unit of Å) for the bond stretching interaction and the initial angle (in unit of degrees) for the angle bending interaction. The angle  $\theta_{ijk}$  has atom *i* as the apex.

VFF type	bond stretching	angle bending	
expression	$\frac{1}{2}K_{\text{Ta-Se}}(\Delta r)^2$	$\frac{1}{2}K_{\text{Ta-Se-Se}}(\Delta\theta)^2$	$\frac{1}{2}K_{\text{Se-Ta-Ta}}(\Delta\theta)^2$
parameter	9.348	4.535	4.535
$r_0$ or $\theta_0$	2.561	84.999	84.999

armchair and zigzag directions, respectively. The ultimate stress is about  $12.7 \text{ Nm}^{-1}$  at the ultimate strain of 0.25 in the armchair direction at the low temperature of 1 K. The ultimate stress is about  $12.2 \text{ Nm}^{-1}$  at the ultimate strain of 0.29 in the zigzag direction at the low temperature of 1 K.

Fig. 153 shows that the VFF model and the SW potential give exactly the same phonon dispersion, as the SW potential is derived from the VFF model.

TABLE CCCXI: Two-body SW potential parameters for single-layer 1T-TaSe<sub>2</sub> used by GULP<sup>8</sup> as expressed in Eq. (3).

	$A$ (eV)	$\rho$ (Å)	$B$ (Å <sup>4</sup> )	$r_{\min}$ (Å)	$r_{\max}$ (Å)
Ta-Se	8.045	1.188	21.505	0.0	3.433

TABLE CCCXII: Three-body SW potential parameters for single-layer 1T-TaSe<sub>2</sub> used by GULP<sup>8</sup> as expressed in Eq. (4). The angle  $\theta_{ijk}$  in the first line indicates the bending energy for the angle with atom  $i$  as the apex.

	$K$ (eV)	$\theta_0$ (degree)	$\rho_1$ (Å)	$\rho_2$ (Å)	$r_{\min 12}$ (Å)	$r_{\max 12}$ (Å)	$r_{\min 13}$ (Å)	$r_{\max 13}$ (Å)	$r_{\min 23}$ (Å)	$r_{\max 23}$ (Å)
$\theta_{\text{Ta-Se-Se}}$	34.820	84.999	1.188	1.188	0.0	3.433	0.0	3.3433	0.0	4.727
$\theta_{\text{Se-Ta-Ta}}$	34.820	84.999	1.188	1.188	0.0	3.433	0.0	3.3433	0.0	4.727

### LXXVIII. 1T-TASE<sub>2</sub>

Most existing theoretical studies on the single-layer 1T-TaSe<sub>2</sub> are based on the first-principles calculations. In this section, we will develop the SW potential for the single-layer 1T-TaSe<sub>2</sub>.

The structure for the single-layer 1T-TaSe<sub>2</sub> is shown in Fig. 71 (with M=Ta and X=Se). Each Ta atom is surrounded by six Se atoms. These Se atoms are categorized into the top group (eg. atoms 1, 3, and 5) and bottom group (eg. atoms 2, 4, and 6). Each Se atom is connected to three Ta atoms. The structural parameters are from the first-principles calculations,<sup>48</sup> including the lattice constant  $a = 3.4602$  Å, and the bond length  $d_{\text{Ta-Se}} = 2.5609$  Å, which is derived from the angle  $\theta_{\text{SeTaTa}} = 85^\circ$ . The other angle is  $\theta_{\text{TaSeSe}} = 85^\circ$  with Se atoms from the same (top or bottom) group.

Table CCCX shows three VFF terms for the single-layer 1T-TaSe<sub>2</sub>, one of which is the bond stretching interaction shown by Eq. (1) while the other two terms are the angle bending

TABLE CCCXIII: SW potential parameters for single-layer 1T-TaSe<sub>2</sub> used by LAMMPS<sup>9</sup> as expressed in Eqs. (9) and (10).

	$\epsilon$ (eV)	$\sigma$ (Å)	$a$	$\lambda$	$\gamma$	$\cos \theta_0$	$A_L$	$B_L$	$p$	$q$	tol
Ta-Se <sub>1</sub> -Se <sub>1</sub>	1.000	1.188	2.891	34.820	1.000	0.087	8.045	10.813	4	0	0.0

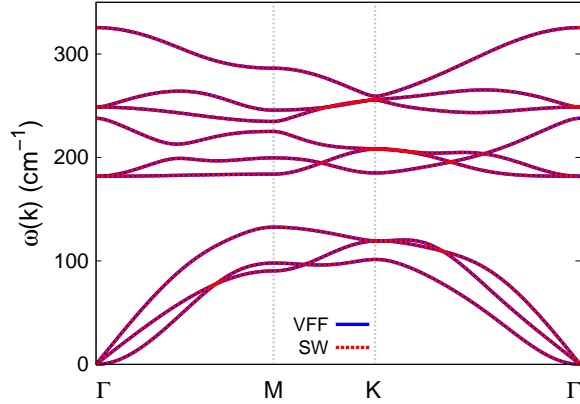


FIG. 155: (Color online) Phonon spectrum for single-layer 1T-TaSe<sub>2</sub> along the  $\Gamma$ MK $\Gamma$  direction in the Brillouin zone. The phonon dispersion from the SW potential is exactly the same as that from the VFF model.

interaction shown by Eq. (2). We note that the angle bending term  $K_{\text{Ta-Se-Se}}$  is for the angle  $\theta_{\text{Ta-Se-Se}}$  with both Se atoms from the same (top or bottom) group. We find that there are actually only two parameters in the VFF model, so we can determine their value by fitting to the Young's modulus and the Poisson's ratio of the system. The *ab initio* calculations have predicted the Young's modulus to be 85 N/m and the Poisson's ratio as 0.20.<sup>48</sup>

The parameters for the two-body SW potential used by GULP are shown in Tab. CCCXI. The parameters for the three-body SW potential used by GULP are shown in Tab. CCCXII. Some representative parameters for the SW potential used by LAMMPS are listed in Tab. CCCXIII.

We use LAMMPS to perform MD simulations for the mechanical behavior of the single-layer 1T-TaSe<sub>2</sub> under uniaxial tension at 1.0 K and 300.0 K. Fig. 154 shows the stress-strain curve for the tension of a single-layer 1T-TaSe<sub>2</sub> of dimension  $100 \times 100 \text{ \AA}$ . Periodic boundary conditions are applied in both armchair and zigzag directions. The single-layer 1T-TaSe<sub>2</sub> is stretched uniaxially along the armchair or zigzag direction. The stress is calculated without involving the actual thickness of the quasi-two-dimensional structure of the single-layer 1T-TaSe<sub>2</sub>. The Young's modulus can be obtained by a linear fitting of the stress-strain relation in the small strain range of  $[0, 0.01]$ . The Young's modulus are 74.6 N/m and 74.4 N/m along the armchair and zigzag directions, respectively. The Young's modulus is essentially isotropic in the armchair and zigzag directions. The Poisson's ratio from the VFF model

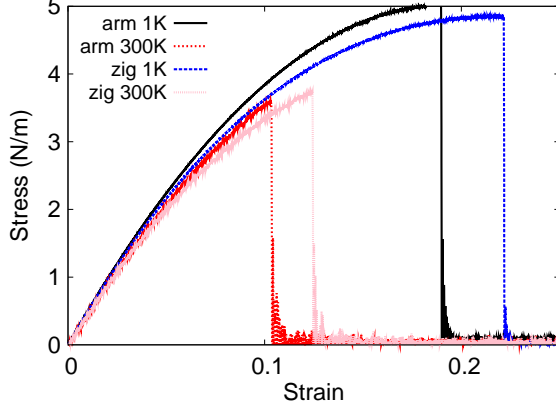


FIG. 156: (Color online) Stress-strain for single-layer 1T-TaTe<sub>2</sub> of dimension  $100 \times 100 \text{ \AA}$  along the armchair and zigzag directions.

and the SW potential is  $\nu_{xy} = \nu_{yx} = 0.20$ . The fitted Young's modulus value is about 10% smaller than the *ab initio* result of  $85 \text{ N/m}$ ,<sup>48</sup> as only short-range interactions are considered in the present work. The long-range interactions are ignored, which typically leads to about 10% underestimation for the value of the Young's modulus.

There is no available value for nonlinear quantities in the single-layer 1T-TaSe<sub>2</sub>. We have thus used the nonlinear parameter  $B = 0.5d^4$  in Eq. (5), which is close to the value of  $B$  in most materials. The value of the third order nonlinear elasticity  $D$  can be extracted by fitting the stress-strain relation to the function  $\sigma = E\epsilon + \frac{1}{2}D\epsilon^2$  with  $E$  as the Young's modulus. The values of  $D$  from the present SW potential are  $-231.7 \text{ N/m}$  and  $-265.4 \text{ N/m}$  along the armchair and zigzag directions, respectively. The ultimate stress is about  $10.8 \text{ Nm}^{-1}$  at the ultimate strain of 0.25 in the armchair direction at the low temperature of 1 K. The ultimate stress is about  $10.4 \text{ Nm}^{-1}$  at the ultimate strain of 0.29 in the zigzag direction at the low temperature of 1 K.

Fig. 155 shows that the VFF model and the SW potential give exactly the same phonon dispersion, as the SW potential is derived from the VFF model.

## LXXIX. 1T-TATE<sub>2</sub>

Most existing theoretical studies on the single-layer 1T-TaTe<sub>2</sub> are based on the first-principles calculations. In this section, we will develop the SW potential for the single-layer

TABLE CCCXIV: The VFF model for single-layer 1T-TaTe<sub>2</sub>. The second line gives an explicit expression for each VFF term. The third line is the force constant parameters. Parameters are in the unit of  $\frac{\text{eV}}{\text{\AA}^2}$  for the bond stretching interactions, and in the unit of eV for the angle bending interaction. The fourth line gives the initial bond length (in unit of  $\text{\AA}$ ) for the bond stretching interaction and the initial angle (in unit of degrees) for the angle bending interaction. The angle  $\theta_{ijk}$  has atom i as the apex.

VFF type	bond stretching	angle bending	
expression	$\frac{1}{2}K_{\text{Ta-Te}}(\Delta r)^2$	$\frac{1}{2}K_{\text{Ta-Te-Te}}(\Delta\theta)^2$	$\frac{1}{2}K_{\text{Te-Ta-Ta}}(\Delta\theta)^2$
parameter	3.442	4.516	4.516
$r_0$ or $\theta_0$	2.770	82.999	82.999

TABLE CCCXV: Two-body SW potential parameters for single-layer 1T-TaTe<sub>2</sub> used by GULP<sup>8</sup> as expressed in Eq. (3).

	$A$ (eV)	$\rho$ ( $\text{\AA}$ )	$B$ ( $\text{\AA}^4$ )	$r_{\text{min}}$ ( $\text{\AA}$ )	$r_{\text{max}}$ ( $\text{\AA}$ )
Ta-Te	3.283	1.207	29.415	0.0	3.684

1T-TaTe<sub>2</sub>.

The structure for the single-layer 1T-TaTe<sub>2</sub> is shown in Fig. 71 (with M=Ta and X=Te). Each Ta atom is surrounded by six Te atoms. These Te atoms are categorized into the top group (eg. atoms 1, 3, and 5) and bottom group (eg. atoms 2, 4, and 6). Each Te atom is connected to three Ta atoms. The structural parameters are from the first-principles calculations,<sup>48</sup> including the lattice constant  $a = 3.6702 \text{ \AA}$ , and the bond length  $d_{\text{Ta-Te}} = 2.7695 \text{ \AA}$ , which is derived from the angle  $\theta_{\text{TeTaTa}} = 83^\circ$ . The other angle is

TABLE CCCXVI: Three-body SW potential parameters for single-layer 1T-TaTe<sub>2</sub> used by GULP<sup>8</sup> as expressed in Eq. (4). The angle  $\theta_{ijk}$  in the first line indicates the bending energy for the angle with atom i as the apex.

	$K$ (eV)	$\theta_0$ (degree)	$\rho_1$ ( $\text{\AA}$ )	$\rho_2$ ( $\text{\AA}$ )	$r_{\text{min12}}$ ( $\text{\AA}$ )	$r_{\text{max12}}$ ( $\text{\AA}$ )	$r_{\text{min13}}$ ( $\text{\AA}$ )	$r_{\text{max13}}$ ( $\text{\AA}$ )	$r_{\text{min23}}$ ( $\text{\AA}$ )	$r_{\text{max23}}$ ( $\text{\AA}$ )
$\theta_{\text{Ta-Te-Te}}$	32.144	82.999	1.207	1.207	0.0	3.684	0.0	3.684	0.0	5.014
$\theta_{\text{Te-Ta-Ta}}$	32.144	82.999	1.207	1.207	0.0	3.684	0.0	3.684	0.0	5.014

TABLE CCCXVII: SW potential parameters for single-layer 1T-TaTe<sub>2</sub> used by LAMMPS<sup>9</sup> as expressed in Eqs. (9) and (10).

	$\epsilon$ (eV)	$\sigma$ (Å)	$a$	$\lambda$	$\gamma$	$\cos \theta_0$	$A_L$	$B_L$	$p$	$q$	tol
Ta-Se <sub>1</sub> -Se <sub>1</sub>	1.000	1.188	2.891	34.820	1.000	0.087	8.045	10.813	4	0	0.0

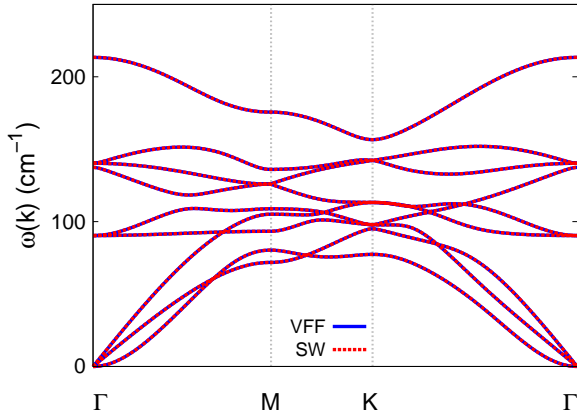


FIG. 157: (Color online) Phonon spectrum for single-layer 1T-TaTe<sub>2</sub> along the  $\Gamma$ MK $\Gamma$  direction in the Brillouin zone. The phonon dispersion from the SW potential is exactly the same as that from the VFF model.

$\theta_{\text{TaTeTe}} = 83^\circ$  with Te atoms from the same (top or bottom) group.

Table CCCXIV shows three VFF terms for the single-layer 1T-TaTe<sub>2</sub>, one of which is the bond stretching interaction shown by Eq. (1) while the other two terms are the angle bending interaction shown by Eq. (2). We note that the angle bending term  $K_{\text{Ta-Te-Te}}$  is for the angle  $\theta_{\text{Ta-Te-Te}}$  with both Te atoms from the same (top or bottom) group. We find that there are actually only two parameters in the VFF model, so we can determine their value by fitting to the Young's modulus and the Poisson's ratio of the system. The *ab initio* calculations have predicted the Young's modulus to be 57 N/m and the Poisson's ratio as 0.10.<sup>48</sup>

The parameters for the two-body SW potential used by GULP are shown in Tab. CCCXV. The parameters for the three-body SW potential used by GULP are shown in Tab. CCCXVI. Some representative parameters for the SW potential used by LAMMPS are listed in Tab. CCCXVII.

We use LAMMPS to perform MD simulations for the mechanical behavior of the single-

layer 1T-TaTe<sub>2</sub> under uniaxial tension at 1.0 K and 300.0 K. Fig. 156 shows the stress-strain curve for the tension of a single-layer 1T-TaTe<sub>2</sub> of dimension 100 × 100 Å. Periodic boundary conditions are applied in both armchair and zigzag directions. The single-layer 1T-TaTe<sub>2</sub> is stretched uniaxially along the armchair or zigzag direction. The stress is calculated without involving the actual thickness of the quasi-two-dimensional structure of the single-layer 1T-TaTe<sub>2</sub>. The Young's modulus can be obtained by a linear fitting of the stress-strain relation in the small strain range of [0, 0.01]. The Young's modulus are 50.3 N/m and 50.0 N/m along the armchair and zigzag directions, respectively. The Young's modulus is essentially isotropic in the armchair and zigzag directions. The Poisson's ratio from the VFF model and the SW potential is  $\nu_{xy} = \nu_{yx} = 0.10$ . The fitted Young's modulus value is about 10% smaller than the *ab initio* result of 57 N/m,<sup>48</sup> as only short-range interactions are considered in the present work. The long-range interactions are ignored, which typically leads to about 10% underestimation for the value of the Young's modulus.

There is no available value for nonlinear quantities in the single-layer 1T-TaTe<sub>2</sub>. We have thus used the nonlinear parameter  $B = 0.5d^4$  in Eq. (5), which is close to the value of  $B$  in most materials. The value of the third order nonlinear elasticity  $D$  can be extracted by fitting the stress-strain relation to the function  $\sigma = E\epsilon + \frac{1}{2}D\epsilon^2$  with  $E$  as the Young's modulus. The values of  $D$  from the present SW potential are -247.1 N/m and -262.2 N/m along the armchair and zigzag directions, respectively. The ultimate stress is about 5.0 Nm<sup>-1</sup> at the ultimate strain of 0.19 in the armchair direction at the low temperature of 1 K. The ultimate stress is about 4.9 Nm<sup>-1</sup> at the ultimate strain of 0.22 in the zigzag direction at the low temperature of 1 K.

Fig. 157 shows that the VFF model and the SW potential give exactly the same phonon dispersion, as the SW potential is derived from the VFF model.

## LXXX. 1T-WS<sub>2</sub>

Most existing theoretical studies on the single-layer 1T-WS<sub>2</sub> are based on the first-principles calculations. In this section, we will develop the SW potential for the single-layer 1T-WS<sub>2</sub>.

The structure for the single-layer 1T-WS<sub>2</sub> is shown in Fig. 71 (with M=W and X=S). Each W atom is surrounded by six S atoms. These S atoms are categorized into the top group

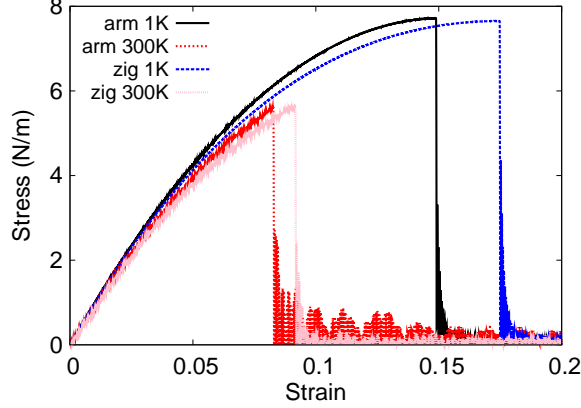


FIG. 158: (Color online) Stress-strain for single-layer 1T-WS<sub>2</sub> of dimension 100 × 100 Å along the armchair and zigzag directions.

TABLE CCCXVIII: The VFF model for single-layer 1T-WS<sub>2</sub>. The second line gives an explicit expression for each VFF term. The third line is the force constant parameters. Parameters are in the unit of  $\frac{\text{eV}}{\text{Å}^2}$  for the bond stretching interactions, and in the unit of eV for the angle bending interaction. The fourth line gives the initial bond length (in unit of Å) for the bond stretching interaction and the initial angle (in unit of degrees) for the angle bending interaction. The angle  $\theta_{ijk}$  has atom *i* as the apex.

VFF type	bond stretching	angle bending	
expression	$\frac{1}{2}K_{\text{W-S}}(\Delta r)^2$	$\frac{1}{2}K_{\text{W-S-S}}(\Delta\theta)^2$	$\frac{1}{2}K_{\text{S-W-W}}(\Delta\theta)^2$
parameter	4.395	10.087	10.087
$r_0$ or $\theta_0$	2.413	82.799	82.799

(eg. atoms 1, 3, and 5) and bottom group (eg. atoms 2, 4, and 6). Each S atom is connected to three W atoms. The structural parameters are from the first-principles calculations,<sup>48</sup> including the lattice constant  $a = 3.1908$  Å, and the bond length  $d_{\text{W-S}} = 2.4125$  Å, which is derived from the angle  $\theta_{\text{SWW}} = 82.8^\circ$ . The other angle is  $\theta_{\text{WSS}} = 82.8^\circ$  with S atoms from the same (top or bottom) group.

Table CCCXVIII shows three VFF terms for the single-layer 1T-WS<sub>2</sub>, one of which is the bond stretching interaction shown by Eq. (1) while the other two terms are the angle bending interaction shown by Eq. (2). We note that the angle bending term  $K_{\text{W-S-S}}$  is

TABLE CCCXIX: Two-body SW potential parameters for single-layer 1T-WS<sub>2</sub> used by GULP<sup>8</sup> as expressed in Eq. (3).

	$A$ (eV)	$\rho$ (Å)	$B$ (Å <sup>4</sup> )	$r_{\min}$ (Å)	$r_{\max}$ (Å)
W-S	3.163	1.045	16.937	0.0	3.206

TABLE CCCXX: Three-body SW potential parameters for single-layer 1T-WS<sub>2</sub> used by GULP<sup>8</sup> as expressed in Eq. (4). The angle  $\theta_{ijk}$  in the first line indicates the bending energy for the angle with atom  $i$  as the apex.

	$K$ (eV)	$\theta_0$ (degree)	$\rho_1$ (Å)	$\rho_2$ (Å)	$r_{\min12}$ (Å)	$r_{\max12}$ (Å)	$r_{\min13}$ (Å)	$r_{\max13}$ (Å)	$r_{\min23}$ (Å)	$r_{\max23}$ (Å)
$\theta_{W-S-S}$	71.264	82.799	1.045	1.045	0.0	3.206	0.0	3.206	0.0	4.359
$\theta_{S-W-W}$	71.264	82.799	1.045	1.045	0.0	3.206	0.0	3.206	0.0	4.359

for the angle  $\theta_{W-S-S}$  with both S atoms from the same (top or bottom) group. We find that there are actually only two parameters in the VFF model, so we can determine their value by fitting to the Young’s modulus and the Poisson’s ratio of the system. The *ab initio* calculations have predicted the Young’s modulus to be 113 N/m and the Poisson’s ratio as -0.03.<sup>48</sup> The *ab initio* calculations have predicted a negative Poisson’s ratio in the 1T-WS<sub>2</sub>, which was attributed to the orbital coupling in this material. The orbital coupling enhances the angle bending interaction in the VFF model. As a result, the value of the angle bending parameter is much larger than the bond stretching force constant parameter, which is typical in auxetic materials with negative Poisson’s ratio.<sup>52</sup>

The parameters for the two-body SW potential used by GULP are shown in Tab. CCCXIX. The parameters for the three-body SW potential used by GULP are shown in Tab. CCCXX. Some representative parameters for the SW potential used by LAMMPS are listed in Tab. CCCXXI.

We use LAMMPS to perform MD simulations for the mechanical behavior of the single-

TABLE CCCXXI: SW potential parameters for single-layer 1T-WS<sub>2</sub> used by LAMMPS<sup>9</sup> as expressed in Eqs. (9) and (10).

	$\epsilon$ (eV)	$\sigma$ (Å)	$a$	$\lambda$	$\gamma$	$\cos \theta_0$	$A_L$	$B_L$	$p$	$q$	tol
W-S <sub>1</sub> -S <sub>1</sub>	1.000	1.045	3.069	71.264	1.000	0.125	3.163	14.209	4	0	0.0

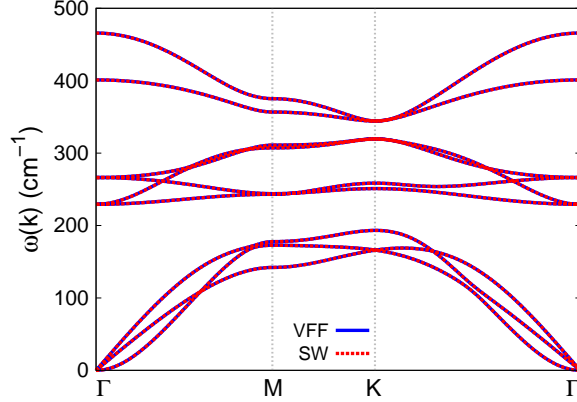


FIG. 159: (Color online) Phonon spectrum for single-layer 1T-WS<sub>2</sub> along the  $\Gamma$ MK $\Gamma$  direction in the Brillouin zone. The phonon dispersion from the SW potential is exactly the same as that from the VFF model.

layer 1T-WS<sub>2</sub> under uniaxial tension at 1.0 K and 300.0 K. Fig. 158 shows the stress-strain curve for the tension of a single-layer 1T-WS<sub>2</sub> of dimension  $100 \times 100 \text{ \AA}$ . Periodic boundary conditions are applied in both armchair and zigzag directions. The single-layer 1T-WS<sub>2</sub> is stretched uniaxially along the armchair or zigzag direction. The stress is calculated without involving the actual thickness of the quasi-two-dimensional structure of the single-layer 1T-WS<sub>2</sub>. The Young's modulus can be obtained by a linear fitting of the stress-strain relation in the small strain range of  $[0, 0.01]$ . The Young's modulus are 100.2 N/m and 99.5 N/m along the armchair and zigzag directions, respectively. The Young's modulus is essentially isotropic in the armchair and zigzag directions. The Poisson's ratio from the VFF model and the SW potential is  $\nu_{xy} = \nu_{yx} = -0.03$ . The fitted Young's modulus value is about 10% smaller than the *ab initio* result of 113 N/m,<sup>48</sup> as only short-range interactions are considered in the present work. The long-range interactions are ignored, which typically leads to about 10% underestimation for the value of the Young's modulus.

There is no available value for nonlinear quantities in the single-layer 1T-WS<sub>2</sub>. We have thus used the nonlinear parameter  $B = 0.5d^4$  in Eq. (5), which is close to the value of  $B$  in most materials. The value of the third order nonlinear elasticity  $D$  can be extracted by fitting the stress-strain relation to the function  $\sigma = E\epsilon + \frac{1}{2}D\epsilon^2$  with  $E$  as the Young's modulus. The values of  $D$  from the present SW potential are -666.6 N/m and -660.6 N/m along the armchair and zigzag directions, respectively. The ultimate stress is about  $7.7 \text{ Nm}^{-1}$

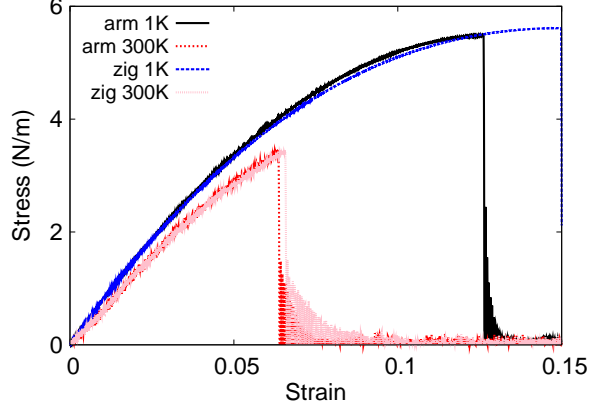


FIG. 160: (Color online) Stress-strain for single-layer 1T-WSe<sub>2</sub> of dimension  $100 \times 100 \text{ \AA}$  along the armchair and zigzag directions.

TABLE CCCXXII: The VFF model for single-layer 1T-WSe<sub>2</sub>. The second line gives an explicit expression for each VFF term. The third line is the force constant parameters. Parameters are in the unit of  $\frac{\text{eV}}{\text{Å}^2}$  for the bond stretching interactions, and in the unit of eV for the angle bending interaction. The fourth line gives the initial bond length (in unit of Å) for the bond stretching interaction and the initial angle (in unit of degrees) for the angle bending interaction. The angle  $\theta_{ijk}$  has atom *i* as the apex.

VFF type	bond stretching	angle bending	
expression	$\frac{1}{2}K_{\text{W-Se}}(\Delta r)^2$	$\frac{1}{2}K_{\text{W-Se-Se}}(\Delta\theta)^2$	$\frac{1}{2}K_{\text{Se-W-W}}(\Delta\theta)^2$
parameter	2.556	15.375	15.375
$r_0$ or $\theta_0$	2.521	80.501	80.501

at the ultimate strain of 0.15 in the armchair direction at the low temperature of 1 K. The ultimate stress is about  $7.7 \text{ Nm}^{-1}$  at the ultimate strain of 0.17 in the zigzag direction at the low temperature of 1 K.

Fig. 159 shows that the VFF model and the SW potential give exactly the same phonon dispersion, as the SW potential is derived from the VFF model.

TABLE CCCXXIII: Two-body SW potential parameters for single-layer 1T-WSe<sub>2</sub> used by GULP<sup>8</sup> as expressed in Eq. (3).

	$A$ (eV)	$\rho$ (Å)	$B$ (Å <sup>4</sup> )	$r_{\min}$ (Å)	$r_{\max}$ (Å)
W-Se	1.885	1.013	20.186	0.0	3.320

TABLE CCCXXIV: Three-body SW potential parameters for single-layer 1T-WSe<sub>2</sub> used by GULP<sup>8</sup> as expressed in Eq. (4). The angle  $\theta_{ijk}$  in the first line indicates the bending energy for the angle with atom  $i$  as the apex.

	$K$ (eV)	$\theta_0$ (degree)	$\rho_1$ (Å)	$\rho_2$ (Å)	$r_{\min12}$ (Å)	$r_{\max12}$ (Å)	$r_{\min13}$ (Å)	$r_{\max13}$ (Å)	$r_{\min23}$ (Å)	$r_{\max23}$ (Å)
$\theta_{W-Se-Se}$	99.800	80.501	1.013	1.013	0.0	3.320	0.0	3.320	0.0	4.450
$\theta_{Se-W-W}$	99.800	80.501	1.013	1.013	0.0	3.320	0.0	3.320	0.0	4.450

### LXXXI. 1T-WSe<sub>2</sub>

Most existing theoretical studies on the single-layer 1T-WSe<sub>2</sub> are based on the first-principles calculations. In this section, we will develop the SW potential for the single-layer 1T-WSe<sub>2</sub>.

The structure for the single-layer 1T-WSe<sub>2</sub> is shown in Fig. 71 (with M=W and X=Se). Each W atom is surrounded by six Se atoms. These Se atoms are categorized into the top group (eg. atoms 1, 3, and 5) and bottom group (eg. atoms 2, 4, and 6). Each Se atom is connected to three W atoms. The structural parameters are from the first-principles calculations,<sup>48</sup> including the lattice constant  $a = 3.2574$  Å, and the bond length  $d_{W-Se} = 2.5207$  Å, which is derived from the angle  $\theta_{SeWW} = 80.5^\circ$ . The other angle is  $\theta_{WSeSe} = 80.5^\circ$  with Se atoms from the same (top or bottom) group.

Table CCCXXII shows three VFF terms for the single-layer 1T-WSe<sub>2</sub>, one of which is the bond stretching interaction shown by Eq. (1) while the other two terms are the angle

TABLE CCCXXV: SW potential parameters for single-layer 1T-WSe<sub>2</sub> used by LAMMPS<sup>9</sup> as expressed in Eqs. (9) and (10).

	$\epsilon$ (eV)	$\sigma$ (Å)	$a$	$\lambda$	$\gamma$	$\cos \theta_0$	$A_L$	$B_L$	$p$	$q$	tol
W-Se <sub>1</sub> -Se <sub>1</sub>	1.000	1.013	3.277	99.800	1.000	0.165	1.885	19.156	4	0	0.0

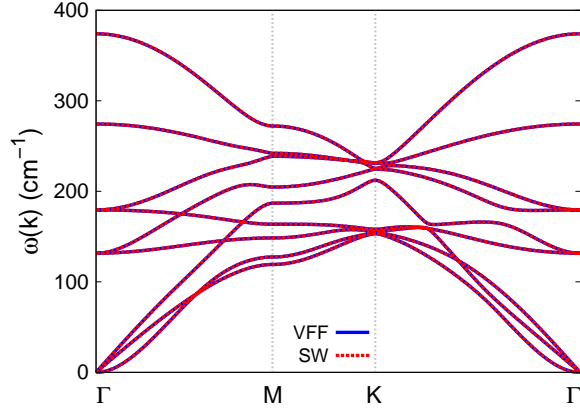


FIG. 161: (Color online) Phonon spectrum for single-layer 1T-WSe<sub>2</sub> along the  $\Gamma$ MK $\Gamma$  direction in the Brillouin zone. The phonon dispersion from the SW potential is exactly the same as that from the VFF model.

bending interaction shown by Eq. (2). We note that the angle bending term  $K_{\text{W-Se-Se}}$  is for the angle  $\theta_{\text{W-Se-Se}}$  with both Se atoms from the same (top or bottom) group. We find that there are actually only two parameters in the VFF model, so we can determine their value by fitting to the Young's modulus and the Poisson's ratio of the system. The *ab initio* calculations have predicted the Young's modulus to be 94 N/m and the Poisson's ratio as -0.15.<sup>48</sup> The *ab initio* calculations have predicted a negative Poisson's ratio in the 1T-WSe<sub>2</sub>, which was attributed to the orbital coupling in this material. The orbital coupling enhances the angle bending interaction in the VFF model. As a result, the value of the angle bending parameter is much larger than the bond stretching force constant parameter, which is typical in auxetic materials with negative Poisson's ratio.<sup>52</sup>

The parameters for the two-body SW potential used by GULP are shown in Tab. CCCXXIII. The parameters for the three-body SW potential used by GULP are shown in Tab. CCCXXIV. Some representative parameters for the SW potential used by LAMMPS are listed in Tab. CCCXXV.

We use LAMMPS to perform MD simulations for the mechanical behavior of the single-layer 1T-WSe<sub>2</sub> under uniaxial tension at 1.0 K and 300.0 K. Fig. 160 shows the stress-strain curve for the tension of a single-layer 1T-WSe<sub>2</sub> of dimension  $100 \times 100 \text{ \AA}$ . Periodic boundary conditions are applied in both armchair and zigzag directions. The single-layer 1T-WSe<sub>2</sub> is stretched uniaxially along the armchair or zigzag direction. The stress is calculated without

involving the actual thickness of the quasi-two-dimensional structure of the single-layer 1T-WSe<sub>2</sub>. The Young's modulus can be obtained by a linear fitting of the stress-strain relation in the small strain range of [0, 0.01]. The Young's modulus are 80.5 N/m and 80.3 N/m along the armchair and zigzag directions, respectively. The Young's modulus is essentially isotropic in the armchair and zigzag directions. The Poisson's ratio from the VFF model and the SW potential is  $\nu_{xy} = \nu_{yx} = -0.15$ . The fitted Young's modulus value is about 10% smaller than the *ab initio* result of 94 N/m,<sup>48</sup> as only short-range interactions are considered in the present work. The long-range interactions are ignored, which typically leads to about 10% underestimation for the value of the Young's modulus.

There is no available value for nonlinear quantities in the single-layer 1T-WSe<sub>2</sub>. We have thus used the nonlinear parameter  $B = 0.5d^4$  in Eq. (5), which is close to the value of  $B$  in most materials. The value of the third order nonlinear elasticity  $D$  can be extracted by fitting the stress-strain relation to the function  $\sigma = E\epsilon + \frac{1}{2}D\epsilon^2$  with  $E$  as the Young's modulus. The values of  $D$  from the present SW potential are -666.1 N/m and -580.1 N/m along the armchair and zigzag directions, respectively. The ultimate stress is about 5.5 Nm<sup>-1</sup> at the ultimate strain of 0.13 in the armchair direction at the low temperature of 1 K. The ultimate stress is about 5.6 Nm<sup>-1</sup> at the ultimate strain of 0.15 in the zigzag direction at the low temperature of 1 K.

Fig. 161 shows that the VFF model and the SW potential give exactly the same phonon dispersion, as the SW potential is derived from the VFF model.

## LXXXII. 1T-WTe<sub>2</sub>

Most existing theoretical studies on the single-layer 1T-WTe<sub>2</sub> are based on the first-principles calculations. In this section, we will develop the SW potential for the single-layer 1T-WTe<sub>2</sub>.

The structure for the single-layer 1T-WTe<sub>2</sub> is shown in Fig. 71 (with M=W and X=Te). Each W atom is surrounded by six Te atoms. These Te atoms are categorized into the top group (eg. atoms 1, 3, and 5) and bottom group (eg. atoms 2, 4, and 6). Each Te atom is connected to three W atoms. The structural parameters are from the first-principles calculations,<sup>48</sup> including the lattice constant  $a = 3.4970 \text{ \AA}$ , and the bond length  $d_{\text{W-Te}} = 2.7202 \text{ \AA}$ , which is derived from the angle  $\theta_{\text{TeWW}} = 80.0^\circ$ . The other angle is

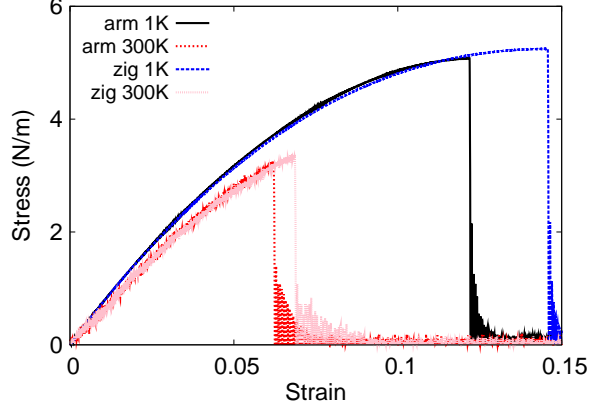


FIG. 162: (Color online) Stress-strain for single-layer 1T-WTe<sub>2</sub> of dimension  $100 \times 100 \text{ \AA}$  along the armchair and zigzag directions.

TABLE CCCXXVI: The VFF model for single-layer 1T-WTe<sub>2</sub>. The second line gives an explicit expression for each VFF term. The third line is the force constant parameters. Parameters are in the unit of  $\frac{eV}{\text{Å}^2}$  for the bond stretching interactions, and in the unit of eV for the angle bending interaction. The fourth line gives the initial bond length (in unit of Å) for the bond stretching interaction and the initial angle (in unit of degrees) for the angle bending interaction. The angle  $\theta_{ijk}$  has atom *i* as the apex.

VFF type	bond stretching	angle bending	
expression	$\frac{1}{2}K_{W-Te}(\Delta r)^2$	$\frac{1}{2}K_{W-Te-Te}(\Delta\theta)^2$	$\frac{1}{2}K_{Te-W-W}(\Delta\theta)^2$
parameter	2.272	19.437	19.437
$r_0$ or $\theta_0$	2.720	79.999	79.999

$\theta_{WTeTe} = 80.0^\circ$  with Te atoms from the same (top or bottom) group.

Table CCCXXVI shows three VFF terms for the single-layer 1T-WTe<sub>2</sub>, one of which is the bond stretching interaction shown by Eq. (1) while the other two terms are the angle bending interaction shown by Eq. (2). We note that the angle bending term  $K_{W-Te-Te}$  is for the angle  $\theta_{W-Te-Te}$  with both Te atoms from the same (top or bottom) group. We find that there are actually only two parameters in the VFF model, so we can determine their value by fitting to the Young's modulus and the Poisson's ratio of the system. The *ab initio* calculations have predicted the Young's modulus to be 88 N/m and the Poisson's ratio as

TABLE CCCXXVII: Two-body SW potential parameters for single-layer 1T-WTe<sub>2</sub> used by GULP<sup>8</sup> as expressed in Eq. (3).

	$A$ (eV)	$\rho$ (Å)	$B$ (Å <sup>4</sup> )	$r_{\min}$ (Å)	$r_{\max}$ (Å)
W-Te	1.924	1.075	27.376	0.0	3.575

TABLE CCCXXVIII: Three-body SW potential parameters for single-layer 1T-WTe<sub>2</sub> used by GULP<sup>8</sup> as expressed in Eq. (4). The angle  $\theta_{ijk}$  in the first line indicates the bending energy for the angle with atom  $i$  as the apex.

	$K$ (eV)	$\theta_0$ (degree)	$\rho_1$ (Å)	$\rho_2$ (Å)	$r_{\min12}$ (Å)	$r_{\max12}$ (Å)	$r_{\min13}$ (Å)	$r_{\max13}$ (Å)	$r_{\min23}$ (Å)	$r_{\max23}$ (Å)
$\theta_{W-Te-Te}$	123.899	79.999	1.075	1.075	0.0	3.575	0.0	3.575	0.0	4.777
$\theta_{Te-W-W}$	123.899	79.999	1.075	1.075	0.0	3.575	0.0	3.575	0.0	4.777

-0.18.<sup>48</sup> The *ab initio* calculations have predicted a negative Poisson's ratio in the 1T-WTe<sub>2</sub>, which was attributed to the orbital coupling in this material. The orbital coupling enhances the angle bending interaction in the VFF model. As a result, the value of the angle bending parameter is much larger than the bond stretching force constant parameter, which is typical in auxetic materials with negative Poisson's ratio.<sup>52</sup>

The parameters for the two-body SW potential used by GULP are shown in Tab. CCCXXVII. The parameters for the three-body SW potential used by GULP are shown in Tab. CCCXXVIII. Some representative parameters for the SW potential used by LAMMPS are listed in Tab. CCCXXIX.

We use LAMMPS to perform MD simulations for the mechanical behavior of the single-layer 1T-WTe<sub>2</sub> under uniaxial tension at 1.0 K and 300.0 K. Fig. 162 shows the stress-strain curve for the tension of a single-layer 1T-WTe<sub>2</sub> of dimension  $100 \times 100$  Å. Periodic boundary conditions are applied in both armchair and zigzag directions. The single-layer 1T-WTe<sub>2</sub> is stretched uniaxially along the armchair or zigzag direction. The stress is calculated without

TABLE CCCXXIX: SW potential parameters for single-layer 1T-WTe<sub>2</sub> used by LAMMPS<sup>9</sup> as expressed in Eqs. (9) and (10).

	$\epsilon$ (eV)	$\sigma$ (Å)	$a$	$\lambda$	$\gamma$	$\cos \theta_0$	$A_L$	$B_L$	$p$	$q$	tol
W-Te <sub>1</sub> -Te <sub>1</sub>	1.000	1.075	3.325	123.899	1.000	0.174	1.924	20.483	4	0	0.0

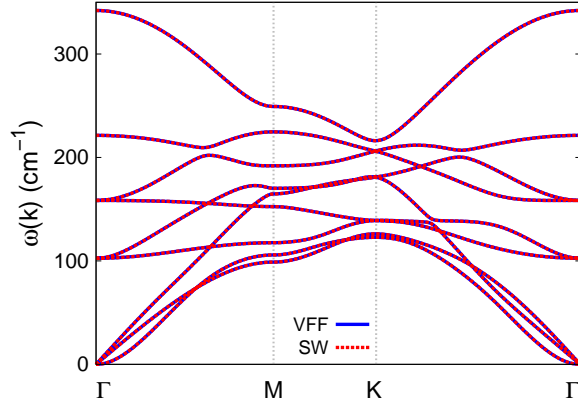


FIG. 163: (Color online) Phonon spectrum for single-layer 1T-WTe<sub>2</sub> along the  $\Gamma$ MK $\Gamma$  direction in the Brillouin zone. The phonon dispersion from the SW potential is exactly the same as that from the VFF model.

involving the actual thickness of the quasi-two-dimensional structure of the single-layer 1T-WTe<sub>2</sub>. The Young's modulus can be obtained by a linear fitting of the stress-strain relation in the small strain range of  $[0, 0.01]$ . The Young's modulus are 75.9 N/m and 75.8 N/m along the armchair and zigzag directions, respectively. The Young's modulus is essentially isotropic in the armchair and zigzag directions. The Poisson's ratio from the VFF model and the SW potential is  $\nu_{xy} = \nu_{yx} = -0.18$ . The fitted Young's modulus value is about 10% smaller than the *ab initio* result of 88 N/m,<sup>48</sup> as only short-range interactions are considered in the present work. The long-range interactions are ignored, which typically leads to about 10% underestimation for the value of the Young's modulus.

There is no available value for nonlinear quantities in the single-layer 1T-WTe<sub>2</sub>. We have thus used the nonlinear parameter  $B = 0.5d^4$  in Eq. (5), which is close to the value of  $B$  in most materials. The value of the third order nonlinear elasticity  $D$  can be extracted by fitting the stress-strain relation to the function  $\sigma = E\epsilon + \frac{1}{2}D\epsilon^2$  with  $E$  as the Young's modulus. The values of  $D$  from the present SW potential are -546.0 N/m and -551.5 N/m along the armchair and zigzag directions, respectively. The ultimate stress is about 5.1 Nm<sup>-1</sup> at the ultimate strain of 0.12 in the armchair direction at the low temperature of 1 K. The ultimate stress is about 5.2 Nm<sup>-1</sup> at the ultimate strain of 0.14 in the zigzag direction at the low temperature of 1 K.

Fig. 163 shows that the VFF model and the SW potential give exactly the same phonon

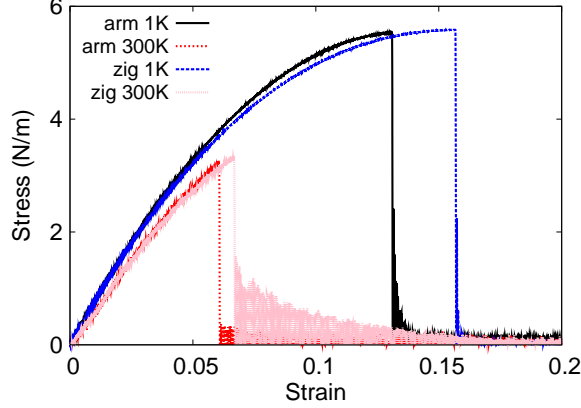


FIG. 164: (Color online) Stress-strain for single-layer 1T-ReS<sub>2</sub> of dimension  $100 \times 100 \text{ \AA}$  along the armchair and zigzag directions.

TABLE CCCXXX: The VFF model for single-layer 1T-ReS<sub>2</sub>. The second line gives an explicit expression for each VFF term. The third line is the force constant parameters. Parameters are in the unit of  $\frac{eV}{\text{Å}^2}$  for the bond stretching interactions, and in the unit of eV for the angle bending interaction. The fourth line gives the initial bond length (in unit of Å) for the bond stretching interaction and the initial angle (in unit of degrees) for the angle bending interaction. The angle  $\theta_{ijk}$  has atom *i* as the apex.

VFF type	bond stretching	angle bending	
expression	$\frac{1}{2}K_{\text{Re-S}}(\Delta r)^2$	$\frac{1}{2}K_{\text{Re-S-S}}(\Delta\theta)^2$	$\frac{1}{2}K_{\text{S-Re-Re}}(\Delta\theta)^2$
parameter	2.684	10.829	10.829
$r_0$ or $\theta_0$	2.405	79.498	79.498

dispersion, as the SW potential is derived from the VFF model.

### LXXXIII. 1T-RES<sub>2</sub>

Most existing theoretical studies on the single-layer 1T-ReS<sub>2</sub> are based on the first-principles calculations. In this section, we will develop the SW potential for the single-layer 1T-ReS<sub>2</sub>.

The structure for the single-layer 1T-ReS<sub>2</sub> is shown in Fig. 71 (with M=Re and X=S). Each Re atom is surrounded by six S atoms. These S atoms are categorized into the top group

TABLE CCCXXXI: Two-body SW potential parameters for single-layer 1T-ReS<sub>2</sub> used by GULP<sup>8</sup> as expressed in Eq. (3).

	$A$ (eV)	$\rho$ (Å)	$B$ (Å <sup>4</sup> )	$r_{\min}$ (Å)	$r_{\max}$ (Å)
Re-S	1.751	0.934	16.714	0.0	3.154

TABLE CCCXXXII: Three-body SW potential parameters for single-layer 1T-ReS<sub>2</sub> used by GULP<sup>8</sup> as expressed in Eq. (4). The angle  $\theta_{ijk}$  in the first line indicates the bending energy for the angle with atom  $i$  as the apex.

	$K$ (eV)	$\theta_0$ (degree)	$\rho_1$ (Å)	$\rho_2$ (Å)	$r_{\min12}$ (Å)	$r_{\max12}$ (Å)	$r_{\min13}$ (Å)	$r_{\max13}$ (Å)	$r_{\min23}$ (Å)	$r_{\max23}$ (Å)
$\theta_{\text{Re-S-S}}$	67.797	79.498	0.934	0.934	0.0	3.154	0.0	3.154	0.0	4.201
$\theta_{\text{S-Re-Re}}$	67.797	79.498	0.934	0.934	0.0	3.154	0.0	3.154	0.0	4.201

(eg. atoms 1, 3, and 5) and bottom group (eg. atoms 2, 4, and 6). Each S atom is connected to three Re atoms. The structural parameters are from the first-principles calculations,<sup>48</sup> including the lattice constant  $a = 3.0750$  Å, and the bond length  $d_{\text{Re-S}} = 2.4045$  Å, which is derived from the angle  $\theta_{\text{SReRe}} = 79.5^\circ$ . The other angle is  $\theta_{\text{ReSS}} = 79.5^\circ$  with S atoms from the same (top or bottom) group.

Table CCCXXX shows three VFF terms for the single-layer 1T-ReS<sub>2</sub>, one of which is the bond stretching interaction shown by Eq. (1) while the other two terms are the angle bending interaction shown by Eq. (2). We note that the angle bending term  $K_{\text{Re-S-S}}$  is for the angle  $\theta_{\text{Re-S-S}}$  with both S atoms from the same (top or bottom) group. We find that there are actually only two parameters in the VFF model, so we can determine their value by fitting to the Young's modulus and the Poisson's ratio of the system. The *ab initio* calculations have predicted the Young's modulus to be 90 N/m and the Poisson's ratio as -0.11.<sup>48</sup> The *ab initio* calculations have predicted a negative Poisson's ratio in the 1T-ReS<sub>2</sub>, which was attributed to the orbital coupling in this material. The orbital coupling enhances

TABLE CCCXXXIII: SW potential parameters for single-layer 1T-ReS<sub>2</sub> used by LAMMPS<sup>9</sup> as expressed in Eqs. (9) and (10).

	$\epsilon$ (eV)	$\sigma$ (Å)	$a$	$\lambda$	$\gamma$	$\cos \theta_0$	$A_L$	$B_L$	$p$	$q$	tol
Re-S <sub>1</sub> -S <sub>1</sub>	1.000	0.934	3.375	67.797	1.000	0.182	1.751	21.916	4	0	0.0

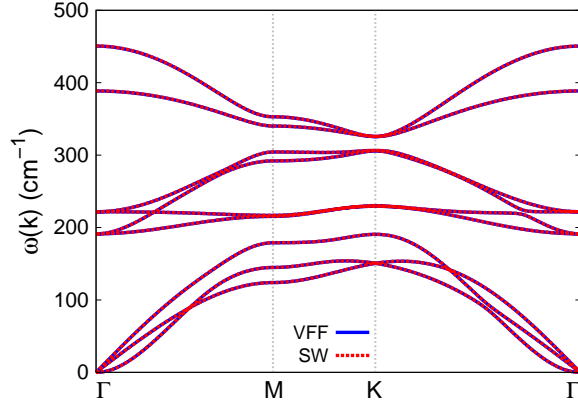


FIG. 165: (Color online) Phonon spectrum for single-layer 1T-ReS<sub>2</sub> along the  $\Gamma$ MK $\Gamma$  direction in the Brillouin zone. The phonon dispersion from the SW potential is exactly the same as that from the VFF model.

the angle bending interaction in the VFF model. As a result, the value of the angle bending parameter is much larger than the bond stretching force constant parameter, which is typical in auxetic materials with negative Poisson's ratio.<sup>52</sup>

The parameters for the two-body SW potential used by GULP are shown in Tab. CCCXXXI. The parameters for the three-body SW potential used by GULP are shown in Tab. CCCXXXII. Some representative parameters for the SW potential used by LAMMPS are listed in Tab. CCCXXXIII.

We use LAMMPS to perform MD simulations for the mechanical behavior of the single-layer 1T-ReS<sub>2</sub> under uniaxial tension at 1.0 K and 300.0 K. Fig. 164 shows the stress-strain curve for the tension of a single-layer 1T-ReS<sub>2</sub> of dimension  $100 \times 100 \text{ \AA}$ . Periodic boundary conditions are applied in both armchair and zigzag directions. The single-layer 1T-ReS<sub>2</sub> is stretched uniaxially along the armchair or zigzag direction. The stress is calculated without involving the actual thickness of the quasi-two-dimensional structure of the single-layer 1T-ReS<sub>2</sub>. The Young's modulus can be obtained by a linear fitting of the stress-strain relation in the small strain range of  $[0, 0.01]$ . The Young's modulus are 78.1 N/m and 77.8 N/m along the armchair and zigzag directions, respectively. The Young's modulus is essentially isotropic in the armchair and zigzag directions. The Poisson's ratio from the VFF model and the SW potential is  $\nu_{xy} = \nu_{yx} = -0.11$ . The fitted Young's modulus value is about 10% smaller than the *ab initio* result of 90 N/m,<sup>48</sup> as only short-range interactions are considered

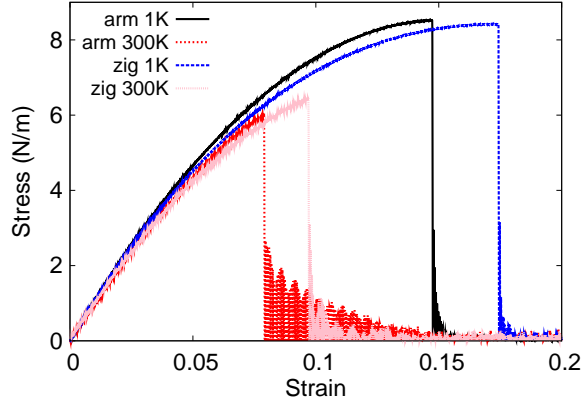


FIG. 166: (Color online) Stress-strain for single-layer 1T-ReSe<sub>2</sub> of dimension  $100 \times 100 \text{ \AA}$  along the armchair and zigzag directions.

in the present work. The long-range interactions are ignored, which typically leads to about 10% underestimation for the value of the Young's modulus.

There is no available value for nonlinear quantities in the single-layer 1T-ReS<sub>2</sub>. We have thus used the nonlinear parameter  $B = 0.5d^4$  in Eq. (5), which is close to the value of  $B$  in most materials. The value of the third order nonlinear elasticity  $D$  can be extracted by fitting the stress-strain relation to the function  $\sigma = E\epsilon + \frac{1}{2}D\epsilon^2$  with  $E$  as the Young's modulus. The values of  $D$  from the present SW potential are  $-537.1 \text{ N/m}$  and  $-550.7 \text{ N/m}$  along the armchair and zigzag directions, respectively. The ultimate stress is about  $5.5 \text{ Nm}^{-1}$  at the ultimate strain of 0.13 in the armchair direction at the low temperature of 1 K. The ultimate stress is about  $5.6 \text{ Nm}^{-1}$  at the ultimate strain of 0.15 in the zigzag direction at the low temperature of 1 K.

Fig. 165 shows that the VFF model and the SW potential give exactly the same phonon dispersion, as the SW potential is derived from the VFF model.

#### LXXXIV. 1T-RESE<sub>2</sub>

Most existing theoretical studies on the single-layer 1T-ReSe<sub>2</sub> are based on the first-principles calculations. In this section, we will develop the SW potential for the single-layer 1T-ReSe<sub>2</sub>.

The structure for the single-layer 1T-ReSe<sub>2</sub> is shown in Fig. 71 (with M=Re and X=Se).

TABLE CCCXXXIV: The VFF model for single-layer 1T-ReSe<sub>2</sub>. The second line gives an explicit expression for each VFF term. The third line is the force constant parameters. Parameters are in the unit of  $\frac{\text{eV}}{\text{Å}^2}$  for the bond stretching interactions, and in the unit of eV for the angle bending interaction. The fourth line gives the initial bond length (in unit of Å) for the bond stretching interaction and the initial angle (in unit of degrees) for the angle bending interaction. The angle  $\theta_{ijk}$  has atom i as the apex.

VFF type	bond stretching	angle bending	
expression	$\frac{1}{2}K_{\text{Re-Se}}(\Delta r)^2$	$\frac{1}{2}K_{\text{Re-Se-Se}}(\Delta\theta)^2$	$\frac{1}{2}K_{\text{Se-Re-Re}}(\Delta\theta)^2$
parameter	4.313	12.674	12.674
$r_0$ or $\theta_0$	2.515	76.999	76.999

TABLE CCCXXXV: Two-body SW potential parameters for single-layer 1T-ReSe<sub>2</sub> used by GULP<sup>8</sup> as expressed in Eq. (3).

	$A$ (eV)	$\rho$ (Å)	$B$ (Å <sup>4</sup> )	$r_{\min}$ (Å)	$r_{\max}$ (Å)
Re-Se	2.866	0.896	20.001	0.0	3.265

Each Re atom is surrounded by six Se atoms. These Se atoms are categorized into the top group (eg. atoms 1, 3, and 5) and bottom group (eg. atoms 2, 4, and 6). Each Se atom is connected to three Re atoms. The structural parameters are from the first-principles calculations,<sup>48</sup> including the lattice constant  $a = 3.1311$  Å, and the bond length  $d_{\text{Re-Se}} = 2.5149$  Å, which is derived from the angle  $\theta_{\text{SeReRe}} = 77^\circ$ . The other angle is  $\theta_{\text{ReSeSe}} = 77^\circ$  with Se atoms from the same (top or bottom) group.

Table CCCXXXIV shows three VFF terms for the single-layer 1T-ReSe<sub>2</sub>, one of which

TABLE CCCXXXVI: Three-body SW potential parameters for single-layer 1T-ReSe<sub>2</sub> used by GULP<sup>8</sup> as expressed in Eq. (4). The angle  $\theta_{ijk}$  in the first line indicates the bending energy for the angle with atom i as the apex.

	$K$ (eV)	$\theta_0$ (degree)	$\rho_1$ (Å)	$\rho_2$ (Å)	$r_{\min12}$ (Å)	$r_{\max12}$ (Å)	$r_{\min13}$ (Å)	$r_{\max13}$ (Å)	$r_{\min23}$ (Å)	$r_{\max23}$ (Å)
$\theta_{\text{Re-Se-Se}}$	72.666	76.999	0.896	0.896	0.0	3.265	0.0	3.265	0.0	4.277
$\theta_{\text{Se-Re-Re}}$	72.666	76.999	0.896	0.896	0.0	3.265	0.0	3.265	0.0	4.277

TABLE CCCXXXVII: SW potential parameters for single-layer 1T-ReSe<sub>2</sub> used by LAMMPS<sup>9</sup> as expressed in Eqs. (9) and (10).

	$\epsilon$ (eV)	$\sigma$ (Å)	$a$	$\lambda$	$\gamma$	$\cos \theta_0$	$A_L$	$B_L$	$p$	$q$	tol
Re-Se <sub>1</sub> -Se <sub>1</sub>	1.000	0.896	3.645	72.666	1.000	0.225	2.866	31.036	4	0	0.0

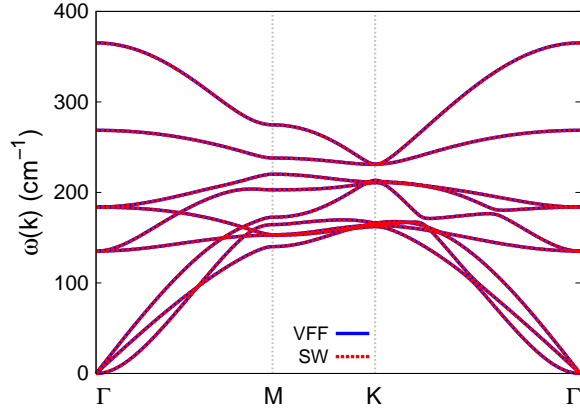


FIG. 167: (Color online) Phonon spectrum for single-layer 1T-ReSe<sub>2</sub> along the  $\Gamma$ MK $\Gamma$  direction in the Brillouin zone. The phonon dispersion from the SW potential is exactly the same as that from the VFF model.

is the bond stretching interaction shown by Eq. (1) while the other two terms are the angle bending interaction shown by Eq. (2). We note that the angle bending term  $K_{\text{Re-Se-Se}}$  is for the angle  $\theta_{\text{Re-Se-Se}}$  with both Se atoms from the same (top or bottom) group. We find that there are actually only two parameters in the VFF model, so we can determine their value by fitting to the Young's modulus and the Poisson's ratio of the system. The *ab initio* calculations have predicted the Young's modulus to be 123 N/m and the Poisson's ratio as -0.03.<sup>48</sup> The *ab initio* calculations have predicted a negative Poisson's ratio in the 1T-ReSe<sub>2</sub>, which was attributed to the orbital coupling in this material. The orbital coupling enhances the angle bending interaction in the VFF model. As a result, the value of the angle bending parameter is much larger than the bond stretching force constant parameter, which is typical in auxetic materials with negative Poisson's ratio.<sup>52</sup>

The parameters for the two-body SW potential used by GULP are shown in Tab. CCCXXXV. The parameters for the three-body SW potential used by GULP are shown in Tab. CCCXXXVI. Some representative parameters for the SW potential used by

LAMMPS are listed in Tab. [CCCXXXVII](#).

We use LAMMPS to perform MD simulations for the mechanical behavior of the single-layer 1T-ReSe<sub>2</sub> under uniaxial tension at 1.0 K and 300.0 K. Fig. [166](#) shows the stress-strain curve for the tension of a single-layer 1T-ReSe<sub>2</sub> of dimension 100 × 100 Å. Periodic boundary conditions are applied in both armchair and zigzag directions. The single-layer 1T-ReSe<sub>2</sub> is stretched uniaxially along the armchair or zigzag direction. The stress is calculated without involving the actual thickness of the quasi-two-dimensional structure of the single-layer 1T-ReSe<sub>2</sub>. The Young's modulus can be obtained by a linear fitting of the stress-strain relation in the small strain range of [0, 0.01]. The Young's modulus are 108.2 N/m and 107.7 N/m along the armchair and zigzag directions, respectively. The Young's modulus is essentially isotropic in the armchair and zigzag directions. The Poisson's ratio from the VFF model and the SW potential is  $\nu_{xy} = \nu_{yx} = -0.03$ . The fitted Young's modulus value is about 10% smaller than the *ab initio* result of 123 N/m,<sup>48</sup> as only short-range interactions are considered in the present work. The long-range interactions are ignored, which typically leads to about 10% underestimation for the value of the Young's modulus.

There is no available value for nonlinear quantities in the single-layer 1T-ReSe<sub>2</sub>. We have thus used the nonlinear parameter  $B = 0.5d^4$  in Eq. (5), which is close to the value of  $B$  in most materials. The value of the third order nonlinear elasticity  $D$  can be extracted by fitting the stress-strain relation to the function  $\sigma = E\epsilon + \frac{1}{2}D\epsilon^2$  with  $E$  as the Young's modulus. The values of  $D$  from the present SW potential are -669.3 N/m and -699.9 N/m along the armchair and zigzag directions, respectively. The ultimate stress is about 8.5 Nm<sup>-1</sup> at the ultimate strain of 0.14 in the armchair direction at the low temperature of 1 K. The ultimate stress is about 8.4 Nm<sup>-1</sup> at the ultimate strain of 0.17 in the zigzag direction at the low temperature of 1 K.

Fig. [167](#) shows that the VFF model and the SW potential give exactly the same phonon dispersion, as the SW potential is derived from the VFF model.

## LXXXV. 1T-RETE<sub>2</sub>

Most existing theoretical studies on the single-layer 1T-ReTe<sub>2</sub> are based on the first-principles calculations. In this section, we will develop the SW potential for the single-layer 1T-ReTe<sub>2</sub>.

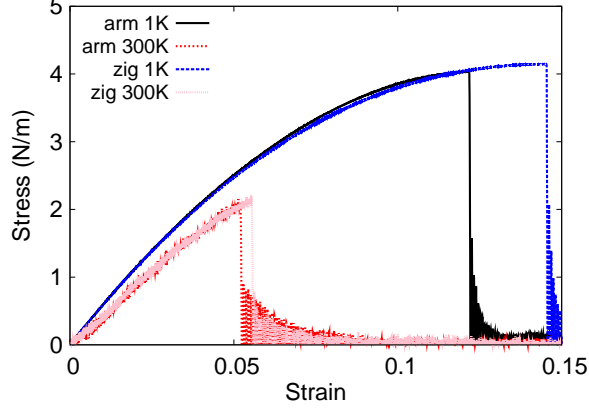


FIG. 168: (Color online) Stress-strain for single-layer 1T-ReTe<sub>2</sub> of dimension  $100 \times 100 \text{ \AA}$  along the armchair and zigzag directions.

TABLE CCCXXXVIII: The VFF model for single-layer 1T-ReTe<sub>2</sub>. The second line gives an explicit expression for each VFF term. The third line is the force constant parameters. Parameters are in the unit of  $\frac{eV}{\text{Å}^2}$  for the bond stretching interactions, and in the unit of eV for the angle bending interaction. The fourth line gives the initial bond length (in unit of Å) for the bond stretching interaction and the initial angle (in unit of degrees) for the angle bending interaction. The angle  $\theta_{ijk}$  has atom  $i$  as the apex.

VFF type	bond stretching	angle bending	
expression	$\frac{1}{2}K_{\text{Re-Te}}(\Delta r)^2$	$\frac{1}{2}K_{\text{Re-Te-Te}}(\Delta\theta)^2$	$\frac{1}{2}K_{\text{Te-Re-Te}}(\Delta\theta)^2$
parameter	1.724	14.812	14.812
$r_0$ or $\theta_0$	2.703	77.501	77.501

The structure for the single-layer 1T-ReTe<sub>2</sub> is shown in Fig. 71 (with M=Re and X=Te). Each Re atom is surrounded by six Te atoms. These Te atoms are categorized into the top group (eg. atoms 1, 3, and 5) and bottom group (eg. atoms 2, 4, and 6). Each Te atom is connected to three Re atoms. The structural parameters are from the first-principles calculations,<sup>48</sup> including the lattice constant  $a = 3.3834 \text{ \AA}$ , and the bond length  $d_{\text{Re-Te}} = 2.7027 \text{ \AA}$ , which is derived from the angle  $\theta_{\text{TeReRe}} = 77.5^\circ$ . The other angle is  $\theta_{\text{ReTeTe}} = 77.5^\circ$  with Te atoms from the same (top or bottom) group.

Table CCCXXXVIII shows three VFF terms for the single-layer 1T-ReTe<sub>2</sub>, one of which

TABLE CCCXXXIX: Two-body SW potential parameters for single-layer 1T-ReTe<sub>2</sub> used by GULP<sup>8</sup> as expressed in Eq. (3).

	$A$ (eV)	$\rho$ (Å)	$B$ (Å <sup>4</sup> )	$r_{\min}$ (Å)	$r_{\max}$ (Å)
Re-Te	1.343	0.980	26.678	0.0	3.517

TABLE CCCXL: Three-body SW potential parameters for single-layer 1T-ReTe<sub>2</sub> used by GULP<sup>8</sup> as expressed in Eq. (4). The angle  $\theta_{ijk}$  in the first line indicates the bending energy for the angle with atom  $i$  as the apex.

	$K$ (eV)	$\theta_0$ (degree)	$\rho_1$ (Å)	$\rho_2$ (Å)	$r_{\min12}$ (Å)	$r_{\max12}$ (Å)	$r_{\min13}$ (Å)	$r_{\max13}$ (Å)	$r_{\min23}$ (Å)	$r_{\max23}$ (Å)
$\theta_{\text{Re-Te-Te}}$	86.424	77.501	0.980	0.980	0.0	3.517	0.0	3.517	0.0	4.622
$\theta_{\text{Te-Re-Re}}$	86.424	77.501	0.980	0.980	0.0	3.517	0.0	3.517	0.0	4.622

is the bond stretching interaction shown by Eq. (1) while the other two terms are the angle bending interaction shown by Eq. (2). We note that the angle bending term  $K_{\text{Re-Te-Te}}$  is for the angle  $\theta_{\text{Re-Te-Te}}$  with both Te atoms from the same (top or bottom) group. We find that there are actually only two parameters in the VFF model, so we can determine their value by fitting to the Young's modulus and the Poisson's ratio of the system. The *ab initio* calculations have predicted the Young's modulus to be 71 N/m and the Poisson's ratio as -0.22.<sup>48</sup> The *ab initio* calculations have predicted a negative Poisson's ratio in the 1T-ReTe<sub>2</sub>, which was attributed to the orbital coupling in this material. The orbital coupling enhances the angle bending interaction in the VFF model. As a result, the value of the angle bending parameter is much larger than the bond stretching force constant parameter, which is typical in auxetic materials with negative Poisson's ratio.<sup>52</sup>

The parameters for the two-body SW potential used by GULP are shown in Tab. CCCXXXIX. The parameters for the three-body SW potential used by GULP are shown in Tab. CCCXL. Some representative parameters for the SW potential used by

TABLE CCCXLI: SW potential parameters for single-layer 1T-ReTe<sub>2</sub> used by LAMMPS<sup>9</sup> as expressed in Eqs. (9) and (10).

	$\epsilon$ (eV)	$\sigma$ (Å)	$a$	$\lambda$	$\gamma$	$\cos \theta_0$	$A_L$	$B_L$	$p$	$q$	tol
Re-Te <sub>1</sub> -Te <sub>1</sub>	1.000	0.980	3.587	86.424	1.000	0.216	1.343	28.891	4	0	0.0

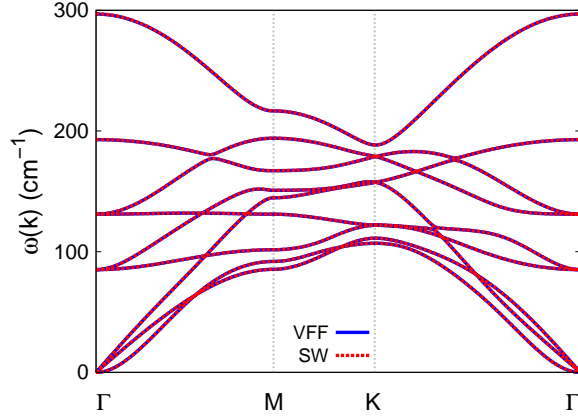


FIG. 169: (Color online) Phonon spectrum for single-layer 1T-ReTe<sub>2</sub> along the  $\Gamma$ MKT direction in the Brillouin zone. The phonon dispersion from the SW potential is exactly the same as that from the VFF model.

LAMMPS are listed in Tab. CCCXLI.

We use LAMMPS to perform MD simulations for the mechanical behavior of the single-layer 1T-ReTe<sub>2</sub> under uniaxial tension at 1.0 K and 300.0 K. Fig. 168 shows the stress-strain curve for the tension of a single-layer 1T-ReTe<sub>2</sub> of dimension  $100 \times 100 \text{ \AA}$ . Periodic boundary conditions are applied in both armchair and zigzag directions. The single-layer 1T-ReTe<sub>2</sub> is stretched uniaxially along the armchair or zigzag direction. The stress is calculated without involving the actual thickness of the quasi-two-dimensional structure of the single-layer 1T-ReTe<sub>2</sub>. The Young's modulus can be obtained by a linear fitting of the stress-strain relation in the small strain range of  $[0, 0.01]$ . The Young's modulus are 59.4 N/m and 59.3 N/m along the armchair and zigzag directions, respectively. The Young's modulus is essentially isotropic in the armchair and zigzag directions. The Poisson's ratio from the VFF model and the SW potential is  $\nu_{xy} = \nu_{yx} = -0.17$ . The fitted Young's modulus value is about 10% smaller than the *ab initio* result of 71 N/m,<sup>48</sup> as only short-range interactions are considered in the present work. The long-range interactions are ignored, which typically leads to about 10% underestimation for the value of the Young's modulus.

There is no available value for nonlinear quantities in the single-layer 1T-ReTe<sub>2</sub>. We have thus used the nonlinear parameter  $B = 0.5d^4$  in Eq. (5), which is close to the value of  $B$  in most materials. The value of the third order nonlinear elasticity  $D$  can be extracted by fitting the stress-strain relation to the function  $\sigma = E\epsilon + \frac{1}{2}D\epsilon^2$  with  $E$  as the Young's

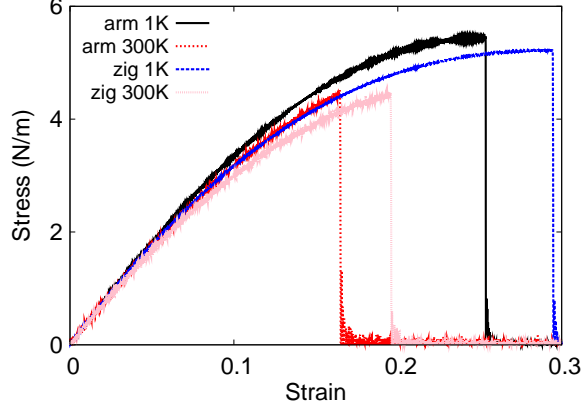


FIG. 170: (Color online) Stress-strain for single-layer 1T-IrTe<sub>2</sub> of dimension  $100 \times 100 \text{ \AA}$  along the armchair and zigzag directions.

modulus. The values of  $D$  from the present SW potential are  $-416.1 \text{ N/m}$  and  $-425.1 \text{ N/m}$  along the armchair and zigzag directions, respectively. The ultimate stress is about  $4.0 \text{ Nm}^{-1}$  at the ultimate strain of 0.12 in the armchair direction at the low temperature of 1 K. The ultimate stress is about  $4.1 \text{ Nm}^{-1}$  at the ultimate strain of 0.14 in the zigzag direction at the low temperature of 1 K.

Fig. 169 shows that the VFF model and the SW potential give exactly the same phonon dispersion, as the SW potential is derived from the VFF model.

## LXXXVI. 1T-IRTE<sub>2</sub>

Most existing theoretical studies on the single-layer 1T-IrTe<sub>2</sub> are based on the first-principles calculations. In this section, we will develop the SW potential for the single-layer 1T-IrTe<sub>2</sub>.

The structure for the single-layer 1T-IrTe<sub>2</sub> is shown in Fig. 71 (with M=Ir and X=Te). Each Ir atom is surrounded by six Te atoms. These Te atoms are categorized into the top group (eg. atoms 1, 3, and 5) and bottom group (eg. atoms 2, 4, and 6). Each Te atom is connected to three Ir atoms. The structural parameters are from the first-principles calculations,<sup>48</sup> including the lattice constant  $a = 3.8431 \text{ \AA}$ , and the bond length  $d_{\text{Ir-Te}} = 2.6490 \text{ \AA}$ , which is derived from the angle  $\theta_{\text{TeIrIr}} = 93^\circ$ . The other angle is  $\theta_{\text{IrTeTe}} = 93^\circ$  with Te atoms from the same (top or bottom) group.

TABLE CCCXLII: The VFF model for single-layer 1T-IrTe<sub>2</sub>. The second line gives an explicit expression for each VFF term. The third line is the force constant parameters. Parameters are in the unit of  $\frac{\text{eV}}{\text{\AA}^2}$  for the bond stretching interactions, and in the unit of eV for the angle bending interaction. The fourth line gives the initial bond length (in unit of \AA) for the bond stretching interaction and the initial angle (in unit of degrees) for the angle bending interaction. The angle  $\theta_{ijk}$  has atom i as the apex.

VFF type	bond stretching		angle bending	
expression	$\frac{1}{2}K_{\text{Ir-Te}}(\Delta r)^2$	$\frac{1}{2}K_{\text{Ir-Te-Te}}(\Delta\theta)^2$	$\frac{1}{2}K_{\text{Te-Ir-Ir}}(\Delta\theta)^2$	
parameter	5.334	2.182	2.182	
$r_0$ or $\theta_0$	2.649	93.002	93.002	

TABLE CCCXLIII: Two-body SW potential parameters for single-layer 1T-IrTe<sub>2</sub> used by GULP<sup>8</sup> as expressed in Eq. (3).

	$A$ (eV)	$\rho$ (\AA)	$B$ (\AA <sup>4</sup> )	$r_{\text{min}}$ (\AA)	$r_{\text{max}}$ (\AA)
Ir-Te	6.030	1.538	24.621	0.0	3.658

Table CCCXLII shows three VFF terms for the single-layer 1T-IrTe<sub>2</sub>, one of which is the bond stretching interaction shown by Eq. (1) while the other two terms are the angle bending interaction shown by Eq. (2). We note that the angle bending term  $K_{\text{Ir-Te-Te}}$  is for the angle  $\theta_{\text{Ir-Te-Te}}$  with both Te atoms from the same (top or bottom) group. We find that there are actually only two parameters in the VFF model, so we can determine their value by fitting to the Young's modulus and the Poisson's ratio of the system. The *ab initio* calculations have predicted the Young's modulus to be 45 N/m and the Poisson's ratio as 0.22.<sup>48</sup>

TABLE CCCXLIV: Three-body SW potential parameters for single-layer 1T-IrTe<sub>2</sub> used by GULP<sup>8</sup> as expressed in Eq. (4). The angle  $\theta_{ijk}$  in the first line indicates the bending energy for the angle with atom i as the apex.

	$K$ (eV)	$\theta_0$ (degree)	$\rho_1$ (\AA)	$\rho_2$ (\AA)	$r_{\text{min}12}$ (\AA)	$r_{\text{max}12}$ (\AA)	$r_{\text{min}13}$ (\AA)	$r_{\text{max}13}$ (\AA)	$r_{\text{min}23}$ (\AA)	$r_{\text{max}23}$ (\AA)
$\theta_{\text{Ir-Te-Te}}$	23.056	93.002	1.538	1.538	0.0	3.658	0.0	3.658	0.0	5.250
$\theta_{\text{Te-Ir-Ir}}$	23.056	93.002	1.538	1.538	0.0	3.658	0.0	3.658	0.0	5.250

TABLE CCCXLV: SW potential parameters for single-layer 1T-IrTe<sub>2</sub> used by LAMMPS<sup>9</sup> as expressed in Eqs. (9) and (10).

	$\epsilon$ (eV)	$\sigma$ (Å)	$a$	$\lambda$	$\gamma$	$\cos \theta_0$	$A_L$	$B_L$	$p$	$q$	tol
Ir-Te <sub>1</sub> -Te <sub>1</sub>	1.000	1.538	2.370	23.056	1.000	-0.052	6.030	4.398	4	0	0.0

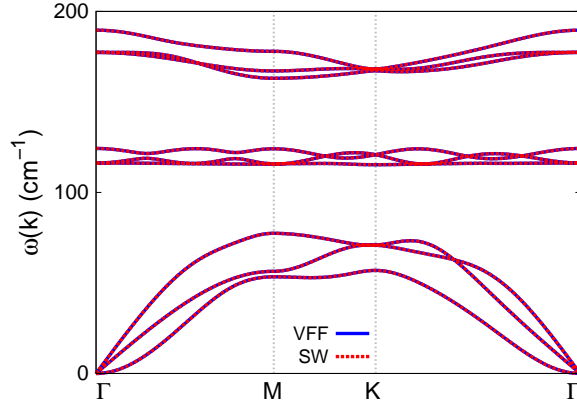


FIG. 171: (Color online) Phonon spectrum for single-layer 1T-IrTe<sub>2</sub> along the  $\Gamma$ MK $\Gamma$  direction in the Brillouin zone. The phonon dispersion from the SW potential is exactly the same as that from the VFF model.

The parameters for the two-body SW potential used by GULP are shown in Tab. CCCXLIII. The parameters for the three-body SW potential used by GULP are shown in Tab. CCCXLIV. Some representative parameters for the SW potential used by LAMMPS are listed in Tab. CCCXLV.

We use LAMMPS to perform MD simulations for the mechanical behavior of the single-layer 1T-IrTe<sub>2</sub> under uniaxial tension at 1.0 K and 300.0 K. Fig. 170 shows the stress-strain curve for the tension of a single-layer 1T-IrTe<sub>2</sub> of dimension  $100 \times 100$  Å. Periodic boundary conditions are applied in both armchair and zigzag directions. The single-layer 1T-IrTe<sub>2</sub> is stretched uniaxially along the armchair or zigzag direction. The stress is calculated without involving the actual thickness of the quasi-two-dimensional structure of the single-layer 1T-IrTe<sub>2</sub>. The Young's modulus can be obtained by a linear fitting of the stress-strain relation in the small strain range of  $[0, 0.01]$ . The Young's modulus are 38.6 N/m and 38.4 N/m along the armchair and zigzag directions, respectively. The Young's modulus is essentially isotropic in the armchair and zigzag directions. The Poisson's ratio from the VFF model

TABLE CCCXLVI: The VFF model for single-layer 1T-PtS<sub>2</sub>. The second line gives an explicit expression for each VFF term. The third line is the force constant parameters. Parameters are in the unit of  $\frac{\text{eV}}{\text{Å}^2}$  for the bond stretching interactions, and in the unit of eV for the angle bending interaction. The fourth line gives the initial bond length (in unit of Å) for the bond stretching interaction and the initial angle (in unit of degrees) for the angle bending interaction. The angle  $\theta_{ijk}$  has atom i as the apex.

VFF type	bond stretching	angle bending	
expression	$\frac{1}{2}K_{\text{Pt-S}}(\Delta r)^2$	$\frac{1}{2}K_{\text{Pt-S-S}}(\Delta\theta)^2$	$\frac{1}{2}K_{\text{S-Pt-Pt}}(\Delta\theta)^2$
parameter	12.128	4.975	4.975
$r_0$ or $\theta_0$	2.371	96.00	96.00

and the SW potential is  $\nu_{xy} = \nu_{yx} = 0.20$ . The fitted Young's modulus value is about 10% smaller than the *ab initio* result of 45 N/m,<sup>48</sup> as only short-range interactions are considered in the present work. The long-range interactions are ignored, which typically leads to about 10% underestimation for the value of the Young's modulus.

There is no available value for nonlinear quantities in the single-layer 1T-IrTe<sub>2</sub>. We have thus used the nonlinear parameter  $B = 0.5d^4$  in Eq. (5), which is close to the value of  $B$  in most materials. The value of the third order nonlinear elasticity  $D$  can be extracted by fitting the stress-strain relation to the function  $\sigma = E\epsilon + \frac{1}{2}D\epsilon^2$  with  $E$  as the Young's modulus. The values of  $D$  from the present SW potential are -127.7 N/m and -142.0 N/m along the armchair and zigzag directions, respectively. The ultimate stress is about 5.4 Nm<sup>-1</sup> at the ultimate strain of 0.25 in the armchair direction at the low temperature of 1 K. The ultimate stress is about 5.2 Nm<sup>-1</sup> at the ultimate strain of 0.29 in the zigzag direction at the low temperature of 1 K.

Fig. 171 shows that the VFF model and the SW potential give exactly the same phonon dispersion, as the SW potential is derived from the VFF model.

## LXXXVII. 1T-PTS<sub>2</sub>

Most existing theoretical studies on the single-layer 1T-PtS<sub>2</sub> are based on the first-principles calculations. In this section, we will develop the SW potential for the single-layer

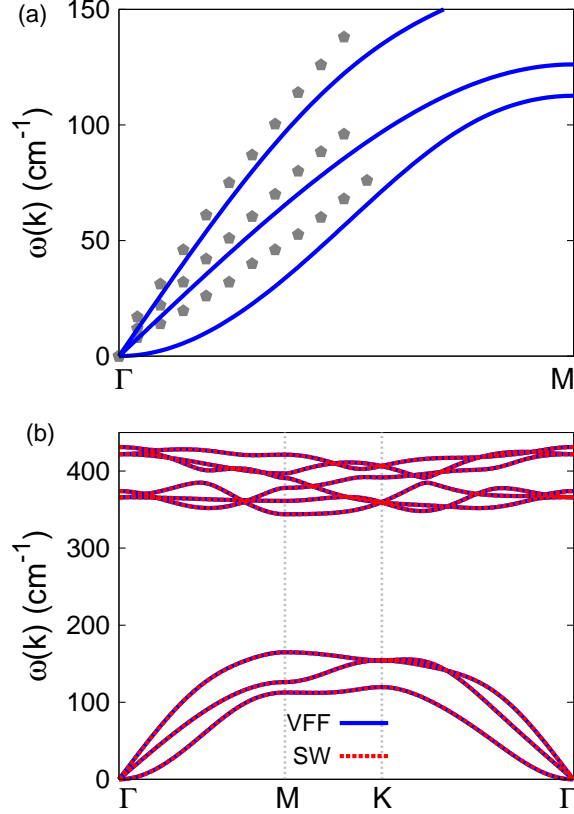


FIG. 172: (Color online) Phonon spectrum for single-layer 1T-PtS<sub>2</sub>. (a) Phonon dispersion along the  $\Gamma$ M direction in the Brillouin zone. The results from the VFF model (lines) are comparable with the *ab initio* results (pentagons) from Ref. 34. (b) The phonon dispersion from the SW potential is exactly the same as that from the VFF model.

TABLE CCCXLVII: Two-body SW potential parameters for single-layer 1T-PtS<sub>2</sub> used by GULP<sup>8</sup> as expressed in Eq. (3).

	$A$ (eV)	$\rho$ ( $\text{\AA}$ )	$B$ ( $\text{\AA}^4$ )	$r_{\min}$ ( $\text{\AA}$ )	$r_{\max}$ ( $\text{\AA}$ )
Pt-S	11.806	1.485	15.796	0.0	3.309

1T-PtS<sub>2</sub>.

The structure for the single-layer 1T-PtS<sub>2</sub> is shown in Fig. 71 (with M=Pt and X=S). Each Pt atom is surrounded by six S atoms. These S atoms are categorized into the top group (eg. atoms 1, 3, and 5) and bottom group (eg. atoms 2, 4, and 6). Each S atom is connected to three Pt atoms. The structural parameters are from the first-principles calculations,<sup>48</sup>

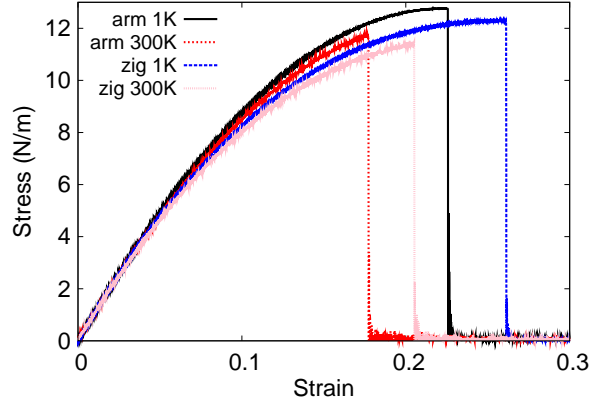


FIG. 173: (Color online) Stress-strain for single-layer 1T-PtS<sub>2</sub> of dimension  $100 \times 100 \text{ \AA}$  along the armchair and zigzag directions.

TABLE CCCXLVIII: Three-body SW potential parameters for single-layer 1T-PtS<sub>2</sub> used by GULP<sup>8</sup> as expressed in Eq. (4). The angle  $\theta_{ijk}$  in the first line indicates the bending energy for the angle with atom  $i$  as the apex.

	$K$ (eV)	$\theta_0$ (degree)	$\rho_1$ ( $\text{\AA}$ )	$\rho_2$ ( $\text{\AA}$ )	$r_{\min 12}$ ( $\text{\AA}$ )	$r_{\max 12}$ ( $\text{\AA}$ )	$r_{\min 13}$ ( $\text{\AA}$ )	$r_{\max 13}$ ( $\text{\AA}$ )	$r_{\min 23}$ ( $\text{\AA}$ )	$r_{\max 23}$ ( $\text{\AA}$ )
$\theta_{\text{Pt-S-S}}$	59.607	96.00	1.485	1.485	0.0	3.309	0.0	3.309	0.0	4.813
$\theta_{\text{S-Pt-Pt}}$	59.607	96.00	1.485	1.485	0.0	3.309	0.0	3.309	0.0	4.813

including the lattice constant  $a = 3.5237 \text{ \AA}$ , and the bond length  $d_{\text{Pt-S}} = 2.3708 \text{ \AA}$ , which is derived from the angle  $\theta_{\text{SPtPt}} = 96^\circ$ . The other angle is  $\theta_{\text{PtSS}} = 96^\circ$  with S atoms from the same (top or bottom) group.

Table CCCXLVI shows three VFF terms for the single-layer 1T-PtS<sub>2</sub>, one of which is the bond stretching interaction shown by Eq. (1) while the other two terms are the angle bending interaction shown by Eq. (2). We note that the angle bending term  $K_{\text{Pt-S-S}}$  is for the angle  $\theta_{\text{Pt-S-S}}$  with both S atoms from the same (top or bottom) group. These force

TABLE CCCXLIX: SW potential parameters for single-layer 1T-PtS<sub>2</sub> used by LAMMPS<sup>9</sup> as expressed in Eqs. (9) and (10).

	$\epsilon$ (eV)	$\sigma$ ( $\text{\AA}$ )	$a$	$\lambda$	$\gamma$	$\cos \theta_0$	$A_L$	$B_L$	$p$	$q$	tol
Pt-S <sub>1</sub> -S <sub>1</sub>	1.000	1.485	2.229	59.607	1.000	-0.105	11.806	3.250	4	0	0.0

constant parameters are determined by fitting to the three acoustic branches in the phonon dispersion along the  $\Gamma$ M as shown in Fig. 172 (a). The *ab initio* calculations for the phonon dispersion are from Ref. 34. The lowest acoustic branch (flexural mode) is almost linear in the *ab initio* calculations, which may be due to the violation of the rigid rotational invariance.<sup>20</sup> Fig. 172 (b) shows that the VFF model and the SW potential give exactly the same phonon dispersion, as the SW potential is derived from the VFF model.

The parameters for the two-body SW potential used by GULP are shown in Tab. CCCXLVII. The parameters for the three-body SW potential used by GULP are shown in Tab. CCCXLVIII. Some representative parameters for the SW potential used by LAMMPS are listed in Tab. CCCXLIX.

We use LAMMPS to perform MD simulations for the mechanical behavior of the single-layer 1T-PtS<sub>2</sub> under uniaxial tension at 1.0 K and 300.0 K. Fig. 173 shows the stress-strain curve for the tension of a single-layer 1T-PtS<sub>2</sub> of dimension 100 × 100 Å. Periodic boundary conditions are applied in both armchair and zigzag directions. The single-layer 1T-PtS<sub>2</sub> is stretched uniaxially along the armchair or zigzag direction. The stress is calculated without involving the actual thickness of the quasi-two-dimensional structure of the single-layer 1T-PtS<sub>2</sub>. The Young's modulus can be obtained by a linear fitting of the stress-strain relation in the small strain range of [0, 0.01]. The Young's modulus are 105.9 N/m and 105.4 N/m along the armchair and zigzag directions, respectively. The Young's modulus is essentially isotropic in the armchair and zigzag directions. The Poisson's ratio from the VFF model and the SW potential is  $\nu_{xy} = \nu_{yx} = 0.16$ .

There is no available value for nonlinear quantities in the single-layer 1T-PtS<sub>2</sub>. We have thus used the nonlinear parameter  $B = 0.5d^4$  in Eq. (5), which is close to the value of  $B$  in most materials. The value of the third order nonlinear elasticity  $D$  can be extracted by fitting the stress-strain relation to the function  $\sigma = E\epsilon + \frac{1}{2}D\epsilon^2$  with  $E$  as the Young's modulus. The values of  $D$  from the present SW potential are -420.6 N/m and -457.1 N/m along the armchair and zigzag directions, respectively. The ultimate stress is about 12.8 Nm<sup>-1</sup> at the ultimate strain of 0.22 in the armchair direction at the low temperature of 1 K. The ultimate stress is about 12.3 Nm<sup>-1</sup> at the ultimate strain of 0.26 in the zigzag direction at the low temperature of 1 K.

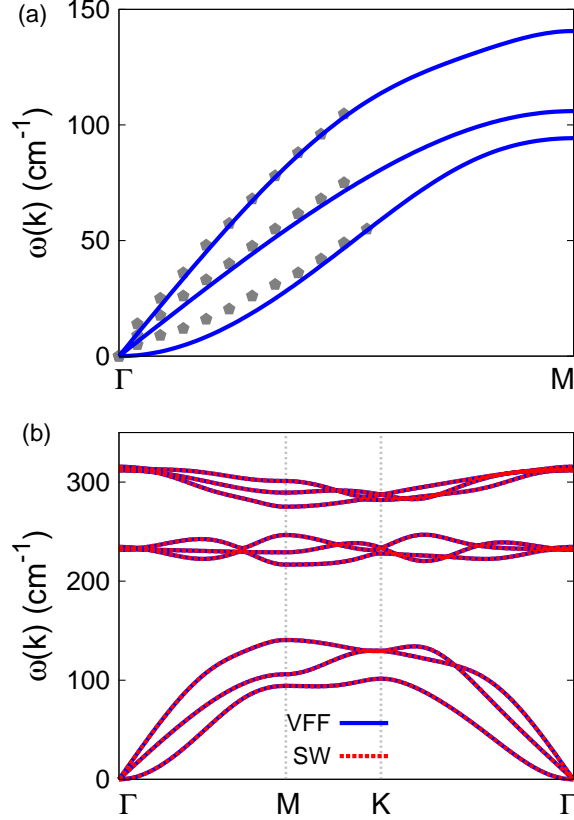


FIG. 174: (Color online) Phonon spectrum for single-layer 1T-PtSe<sub>2</sub>. (a) Phonon dispersion along the  $\Gamma$ M direction in the Brillouin zone. The results from the VFF model (lines) are comparable with the *ab initio* results (pentagons) from Ref. 34. (b) The phonon dispersion from the SW potential is exactly the same as that from the VFF model.

### LXXXVIII. 1T-PTSE<sub>2</sub>

Most existing theoretical studies on the single-layer 1T-PtSe<sub>2</sub> are based on the first-principles calculations. In this section, we will develop the SW potential for the single-layer 1T-PtSe<sub>2</sub>.

The structure for the single-layer 1T-PtSe<sub>2</sub> is shown in Fig. 71 (with M=Pt and X=Se). Each Pt atom is surrounded by six Se atoms. These Se atoms are categorized into the top group (eg. atoms 1, 3, and 5) and bottom group (eg. atoms 2, 4, and 6). Each Se atom is connected to three Pt atoms. The structural parameters are from the first-principles calculations,<sup>48</sup> including the lattice constant  $a = 3.6662 \text{ \AA}$ , and the bond length

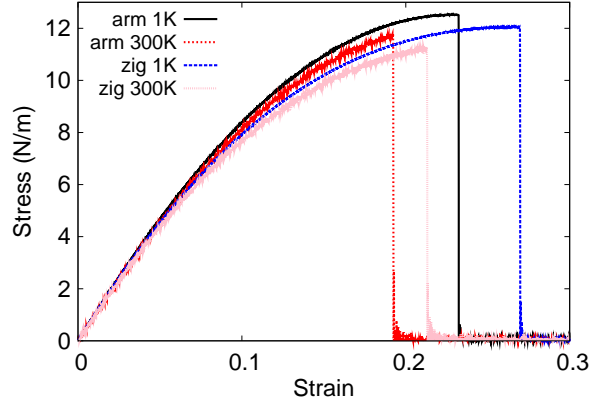


FIG. 175: (Color online) Stress-strain for single-layer 1T-PtSe<sub>2</sub> of dimension  $100 \times 100 \text{ \AA}$  along the armchair and zigzag directions.

TABLE CCCL: The VFF model for single-layer 1T-PtSe<sub>2</sub>. The second line gives an explicit expression for each VFF term. The third line is the force constant parameters. Parameters are in the unit of  $\frac{\text{eV}}{\text{A}^2}$  for the bond stretching interactions, and in the unit of eV for the angle bending interaction. The fourth line gives the initial bond length (in unit of  $\text{A}$ ) for the bond stretching interaction and the initial angle (in unit of degrees) for the angle bending interaction. The angle  $\theta_{ijk}$  has atom  $i$  as the apex.

VFF type	bond stretching	angle bending	
expression	$\frac{1}{2}K_{\text{Pt-Se}}(\Delta r)^2$	$\frac{1}{2}K_{\text{Pt-Se-Se}}(\Delta\theta)^2$	$\frac{1}{2}K_{\text{Se-Pt-Pt}}(\Delta\theta)^2$
parameter	12.128	4.975	4.975
$r_0$ or $\theta_0$	2.467	95.999	95.999

$d_{\text{Pt-Se}} = 2.4667 \text{ \AA}$ , which is derived from the angle  $\theta_{\text{SePtPt}} = 96^\circ$ . The other angle is  $\theta_{\text{PtSeSe}} = 96^\circ$  with Se atoms from the same (top or bottom) group.

Table CCCL shows three VFF terms for the single-layer 1T-PtSe<sub>2</sub>, one of which is the bond stretching interaction shown by Eq. (1) while the other two terms are the angle bending interaction shown by Eq. (2). We note that the angle bending term  $K_{\text{Pt-Se-Se}}$  is for the angle  $\theta_{\text{Pt-Se-Se}}$  with both Se atoms from the same (top or bottom) group. These force constant parameters are determined by fitting to the three acoustic branches in the phonon dispersion along the  $\Gamma\text{M}$  as shown in Fig. 174 (a). The *ab initio* calculations for the phonon dispersion

TABLE CCCLI: Two-body SW potential parameters for single-layer 1T-PtSe<sub>2</sub> used by GULP<sup>8</sup> as expressed in Eq. (3).

	$A$ (eV)	$\rho$ (Å)	$B$ (Å <sup>4</sup> )	$r_{\min}$ (Å)	$r_{\max}$ (Å)
Pt-Se	12.781	1.545	18.511	0.0	3.443

TABLE CCCLII: Three-body SW potential parameters for single-layer 1T-PtSe<sub>2</sub> used by GULP<sup>8</sup> as expressed in Eq. (4). The angle  $\theta_{ijk}$  in the first line indicates the bending energy for the angle with atom  $i$  as the apex.

	$K$ (eV)	$\theta_0$ (degree)	$\rho_1$ (Å)	$\rho_2$ (Å)	$r_{\min12}$ (Å)	$r_{\max12}$ (Å)	$r_{\min13}$ (Å)	$r_{\max13}$ (Å)	$r_{\min23}$ (Å)	$r_{\max23}$ (Å)
$\theta_{\text{Pt-Se-Se}}$	59.608	95.999	1.545	1.545	0.0	3.443	0.0	3.443	0.0	5.008
$\theta_{\text{Se-Pt-Pt}}$	59.608	95.999	1.545	1.545	0.0	3.443	0.0	3.443	0.0	5.008

are from Ref. 34. The lowest acoustic branch (flexural mode) is almost linear in the *ab initio* calculations, which may due to the violation of the rigid rotational invariance.<sup>20</sup> Fig. 174 (b) shows that the VFF model and the SW potential give exactly the same phonon dispersion, as the SW potential is derived from the VFF model.

The parameters for the two-body SW potential used by GULP are shown in Tab. CCCLI. The parameters for the three-body SW potential used by GULP are shown in Tab. CCCLII. Some representative parameters for the SW potential used by LAMMPS are listed in Tab. CCCLIII.

We use LAMMPS to perform MD simulations for the mechanical behavior of the single-layer 1T-PtSe<sub>2</sub> under uniaxial tension at 1.0 K and 300.0 K. Fig. 175 shows the stress-strain curve for the tension of a single-layer 1T-PtSe<sub>2</sub> of dimension  $100 \times 100$  Å. Periodic boundary conditions are applied in both armchair and zigzag directions. The single-layer 1T-PtSe<sub>2</sub> is stretched uniaxially along the armchair or zigzag direction. The stress is calculated without involving the actual thickness of the quasi-two-dimensional structure of the single-layer 1T-

TABLE CCCLIII: SW potential parameters for single-layer 1T-PtSe<sub>2</sub> used by LAMMPS<sup>9</sup> as expressed in Eqs. (9) and (10).

	$\epsilon$ (eV)	$\sigma$ (Å)	$a$	$\lambda$	$\gamma$	$\cos \theta_0$	$A_L$	$B_L$	$p$	$q$	tol
Pt-Se <sub>1</sub> -Se <sub>1</sub>	1.000	1.545	2.229	59.608	1.000	-0.105	12.781	3.250	4	0	0.0

TABLE CCCLIV: The VFF model for single-layer 1T-PtTe<sub>2</sub>. The second line gives an explicit expression for each VFF term. The third line is the force constant parameters. Parameters are in the unit of  $\frac{\text{eV}}{\text{Å}^2}$  for the bond stretching interactions, and in the unit of eV for the angle bending interaction. The fourth line gives the initial bond length (in unit of Å) for the bond stretching interaction and the initial angle (in unit of degrees) for the angle bending interaction. The angle  $\theta_{ijk}$  has atom i as the apex.

VFF type	bond stretching	angle bending	
expression	$\frac{1}{2}K_{\text{Pt-Te}}(\Delta r)^2$	$\frac{1}{2}K_{\text{Pt-Te-Te}}(\Delta\theta)^2$	$\frac{1}{2}K_{\text{Te-Pt-Pt}}(\Delta\theta)^2$
parameter	12.128	4.975	4.975
$r_0$ or $\theta_0$	2.661	95.998	95.998

PtSe<sub>2</sub>. The Young's modulus can be obtained by a linear fitting of the stress-strain relation in the small strain range of [0, 0.01]. The Young's modulus are 101.1 N/m and 100.5 N/m along the armchair and zigzag directions, respectively. The Young's modulus is essentially isotropic in the armchair and zigzag directions. The Poisson's ratio from the VFF model and the SW potential is  $\nu_{xy} = \nu_{yx} = 0.17$ .

There is no available value for nonlinear quantities in the single-layer 1T-PtSe<sub>2</sub>. We have thus used the nonlinear parameter  $B = 0.5d^4$  in Eq. (5), which is close to the value of  $B$  in most materials. The value of the third order nonlinear elasticity  $D$  can be extracted by fitting the stress-strain relation to the function  $\sigma = E\epsilon + \frac{1}{2}D\epsilon^2$  with  $E$  as the Young's modulus. The values of  $D$  from the present SW potential are -391.4 N/m and -424.0 N/m along the armchair and zigzag directions, respectively. The ultimate stress is about 12.5 Nm<sup>-1</sup> at the ultimate strain of 0.23 in the armchair direction at the low temperature of 1 K. The ultimate stress is about 12.1 Nm<sup>-1</sup> at the ultimate strain of 0.27 in the zigzag direction at the low temperature of 1 K.

### LXXXIX. 1T-PTTE<sub>2</sub>

Most existing theoretical studies on the single-layer 1T-PtTe<sub>2</sub> are based on the first-principles calculations. In this section, we will develop the SW potential for the single-layer 1T-PtTe<sub>2</sub>.

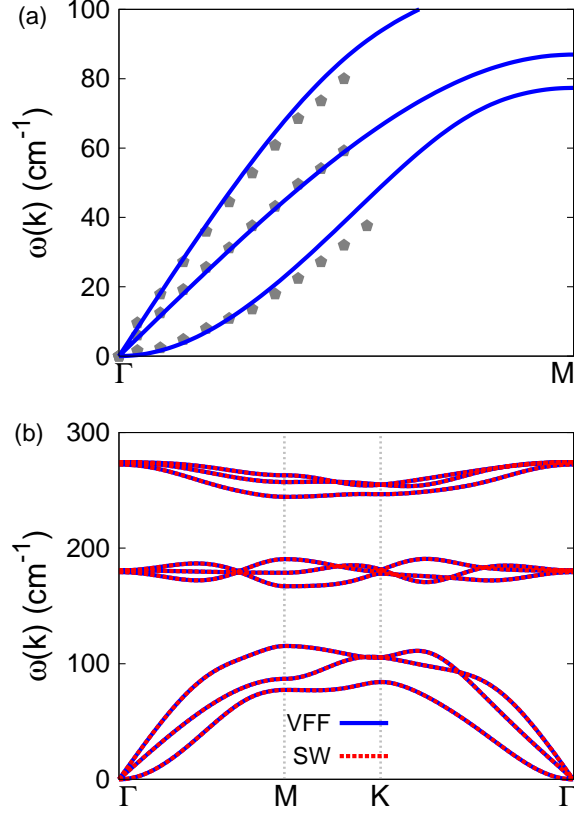


FIG. 176: (Color online) Phonon spectrum for single-layer 1T-PtTe<sub>2</sub>. (a) Phonon dispersion along the  $\Gamma$ M direction in the Brillouin zone. The results from the VFF model (lines) are comparable with the *ab initio* results (pentagons) from Ref. 34. (b) The phonon dispersion from the SW potential is exactly the same as that from the VFF model.

TABLE CCCLV: Two-body SW potential parameters for single-layer 1T-PtTe<sub>2</sub> used by GULP<sup>8</sup> as expressed in Eq. (3).

	$A$ (eV)	$\rho$ ( $\text{\AA}$ )	$B$ ( $\text{\AA}^4$ )	$r_{\min}$ ( $\text{\AA}$ )	$r_{\max}$ ( $\text{\AA}$ )
Pt-Te	14.877	1.667	25.081	0.0	3.714

The structure for the single-layer 1T-PtTe<sub>2</sub> is shown in Fig. 71 (with M=Pt and X=Te). Each Pt atom is surrounded by six Te atoms. These Te atoms are categorized into the top group (eg. atoms 1, 3, and 5) and bottom group (eg. atoms 2, 4, and 6). Each Te atom is connected to three Pt atoms. The structural parameters are from the first-principles calculations,<sup>48</sup> including the lattice constant  $a = 3.9554 \text{ \AA}$ , and the bond length

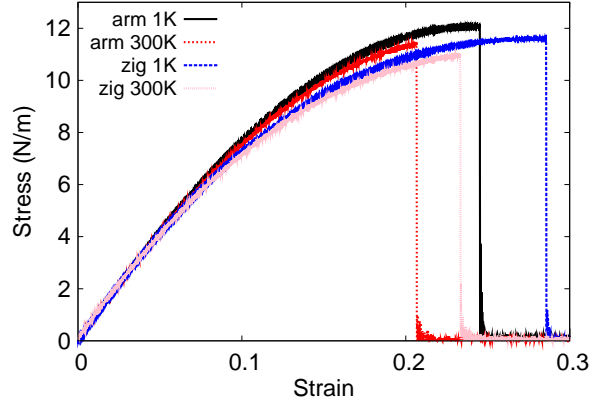


FIG. 177: (Color online) Stress-strain for single-layer 1T-PtTe<sub>2</sub> of dimension  $100 \times 100 \text{ \AA}$  along the armchair and zigzag directions.

TABLE CCCLVI: Three-body SW potential parameters for single-layer 1T-PtTe<sub>2</sub> used by GULP<sup>8</sup> as expressed in Eq. (4). The angle  $\theta_{ijk}$  in the first line indicates the bending energy for the angle with atom  $i$  as the apex.

	$K$ (eV)	$\theta_0$ (degree)	$\rho_1$ (Å)	$\rho_2$ (Å)	$r_{\min 12}$ (Å)	$r_{\max 12}$ (Å)	$r_{\min 13}$ (Å)	$r_{\max 13}$ (Å)	$r_{\min 23}$ (Å)	$r_{\max 23}$ (Å)
$\theta_{\text{Pt-Te-Te}}$	59.607	95.998	1.667	1.667	0.0	3.714	0.0	3.714	0.0	5.403
$\theta_{\text{Te-Pt-Pt}}$	59.607	95.998	1.667	1.667	0.0	3.714	0.0	3.714	0.0	5.403

$d_{\text{Pt-Te}} = 2.6613 \text{ \AA}$ , which is derived from the angle  $\theta_{\text{TePtPt}} = 96^\circ$ . The other angle is  $\theta_{\text{PtTeTe}} = 96^\circ$  with Te atoms from the same (top or bottom) group.

Table CCCLIV shows three VFF terms for the single-layer 1T-PtTe<sub>2</sub>, one of which is the bond stretching interaction shown by Eq. (1) while the other two terms are the angle bending interaction shown by Eq. (2). We note that the angle bending term  $K_{\text{Pt-Te-Te}}$  is for the angle  $\theta_{\text{Pt-Te-Te}}$  with both Te atoms from the same (top or bottom) group. These force constant parameters are determined by fitting to the three acoustic branches in the

TABLE CCCLVII: SW potential parameters for single-layer 1T-PtTe<sub>2</sub> used by LAMMPS<sup>9</sup> as expressed in Eqs. (9) and (10).

	$\epsilon$ (eV)	$\sigma$ (Å)	$a$	$\lambda$	$\gamma$	$\cos \theta_0$	$A_L$	$B_L$	$p$	$q$	tol
Pt-Te <sub>1</sub> -Te <sub>1</sub>	1.000	1.667	2.229	59.607	1.000	-0.104	14.877	3.250	4	0	0.0

phonon dispersion along the  $\Gamma$ M as shown in Fig. 176 (a). The *ab initio* calculations for the phonon dispersion are from Ref. 34. Fig. 176 (b) shows that the VFF model and the SW potential give exactly the same phonon dispersion, as the SW potential is derived from the VFF model.

The parameters for the two-body SW potential used by GULP are shown in Tab. CCCLV. The parameters for the three-body SW potential used by GULP are shown in Tab. CCCLVI. Some representative parameters for the SW potential used by LAMMPS are listed in Tab. CCCLVII.

We use LAMMPS to perform MD simulations for the mechanical behavior of the single-layer 1T-PtTe<sub>2</sub> under uniaxial tension at 1.0 K and 300.0 K. Fig. 177 shows the stress-strain curve for the tension of a single-layer 1T-PtTe<sub>2</sub> of dimension  $100 \times 100$  Å. Periodic boundary conditions are applied in both armchair and zigzag directions. The single-layer 1T-PtTe<sub>2</sub> is stretched uniaxially along the armchair or zigzag direction. The stress is calculated without involving the actual thickness of the quasi-two-dimensional structure of the single-layer 1T-PtTe<sub>2</sub>. The Young's modulus can be obtained by a linear fitting of the stress-strain relation in the small strain range of  $[0, 0.01]$ . The Young's modulus are 89.1 N/m and 88.7 N/m along the armchair and zigzag directions, respectively. The Young's modulus is essentially isotropic in the armchair and zigzag directions. The Poisson's ratio from the VFF model and the SW potential is  $\nu_{xy} = \nu_{yx} = 0.19$ .

There is no available value for nonlinear quantities in the single-layer 1T-PtTe<sub>2</sub>. We have thus used the nonlinear parameter  $B = 0.5d^4$  in Eq. (5), which is close to the value of  $B$  in most materials. The value of the third order nonlinear elasticity  $D$  can be extracted by fitting the stress-strain relation to the function  $\sigma = E\epsilon + \frac{1}{2}D\epsilon^2$  with  $E$  as the Young's modulus. The values of  $D$  from the present SW potential are -306.8 N/m and -340.9 N/m along the armchair and zigzag directions, respectively. The ultimate stress is about  $12.1 \text{ Nm}^{-1}$  at the ultimate strain of 0.24 in the armchair direction at the low temperature of 1 K. The ultimate stress is about  $11.6 \text{ Nm}^{-1}$  at the ultimate strain of 0.28 in the zigzag direction at the low temperature of 1 K.

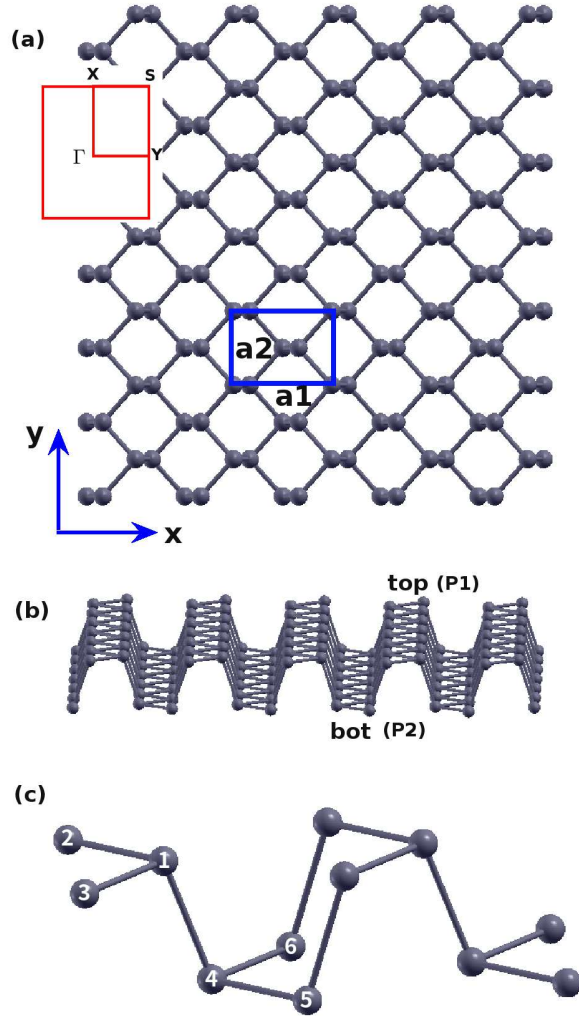


FIG. 178: (Color online) Structure for single-layer black phosphorus. (a) Top view. The armchair direction is along the x-axis, while the zigzag direction is along the y-axis. Inset shows the first Brillouin zone. (b) Perspective view illustrates the puckered configuration. The pucker is perpendicular to the x-axis and is parallel with the y-axis. Atoms are divided into the top (denoted by  $P_1$ ) and the bottom (denoted by  $P_2$ ) groups. (c) Atomic configuration.

### XC. BLACK PHOSPHORUS

The black phosphorus is also named the  $\alpha$  phosphorus. There are several empirical potentials available for the atomic interaction in the black phosphorus. A VFF model was proposed for the single-layer black phosphorus in 1982.<sup>56</sup> One of the present author (J.W.J.) simplified this VFF model by ignoring some angle-angle crossing terms, and use the

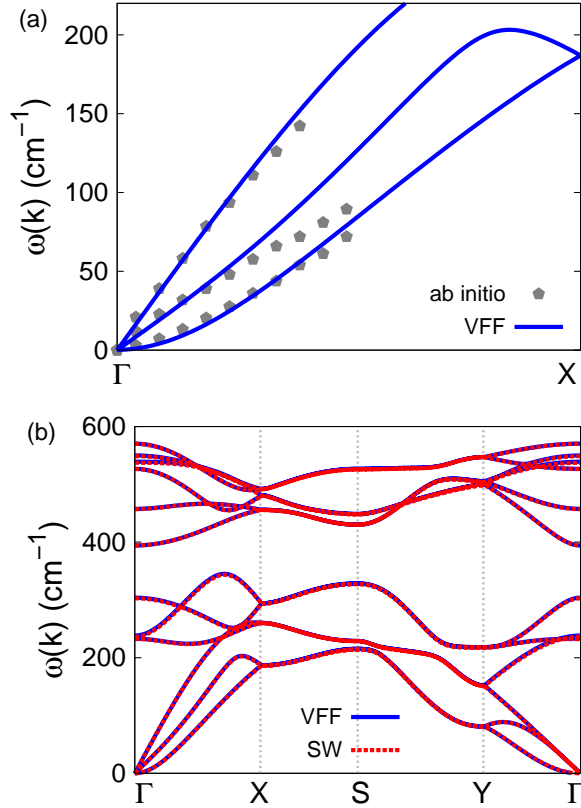


FIG. 179: (Color online) Phonon dispersion for the single-layer black phosphorus. (a) The VFF model is fitted to the three acoustic branches in the long wave limit along the  $\Gamma X$  direction. The *ab initio* results (gray pentagons) are from Ref. 55. (b) The VFF model (blue lines) and the SW potential (red lines) give the same phonon dispersion for the black phosphorus along  $\Gamma XSYT$ .

simplified VFF model to develop the SW potential for the black phosphorus.<sup>7</sup> However, the mechanical properties from this SW potential are smaller than first-principles calculations, as some angle-angle crossing VFF terms can not be implemented in the SW potential. We will thus propose a new set of SW potential for the single-layer black phosphorus in this section.

The structure of the single-layer black phosphorus is shown in Fig. 178, with structural parameters from the *ab initio* calculations.<sup>57</sup> The black phosphorus has a puckered configuration as shown in Fig. 178 (b), where the pucker is perpendicular to the x-direction. The bases for the rectangular unit cell are  $a_1 = 4.422 \text{ \AA}$  and  $a_2 = 3.348 \text{ \AA}$ . For bulk black phosphorus, the basis lattice vector in the third direction is  $a_3 = 10.587 \text{ \AA}$ . There are

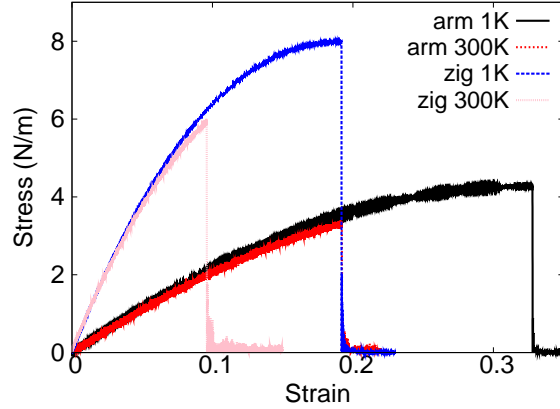


FIG. 180: (Color online) Stress-strain relations for the black phosphorus of size  $100 \times 100 \text{ \AA}$ . The black phosphorus is uniaxially stretched along the armchair or zigzag directions at temperatures 1 K and 300 K.

TABLE CCCLVIII: The VFF model for black phosphorus. The second line gives an explicit expression for each VFF term, where atom indexes are from Fig. 178 (c). The third line is the force constant parameters. Parameters are in the unit of  $\frac{eV}{\text{\AA}^2}$  for the bond stretching interactions, and in the unit of eV for the angle bending interaction. The fourth line gives the initial bond length (in unit of  $\text{\AA}$ ) for the bond stretching interaction and the initial angle (in unit of degrees) for the angle bending interaction. The angle  $\theta_{ijk}$  has atom  $i$  as the apex.

VFF type	bond stretching		angle bending	
expression	$\frac{1}{2}K_{12}(\Delta r_{12})^2$	$\frac{1}{2}K_{14}(\Delta r_{14})^2$	$\frac{1}{2}K_{123}(\Delta\theta_{123})^2$	$\frac{1}{2}K_{134}(\Delta\theta_{134})^2$
parameter	10.542	10.542	7.048	7.048
$r_0$ or $\theta_0$	2.238	2.260	96.581	102.307

four phosphorus atoms in the basic unit cell, and their relative coordinates are  $(-u, 0, -v)$ ,  $(u, 0, v)$ ,  $(0.5 - u, 0.5, v)$ , and  $(0.5 + u, 0.5, -v)$  with  $u = 0.0821$  and  $v = 0.1011$ . Atoms are categorized into the top and bottom groups. Atoms in the top group are denoted by  $P_1$ , while atoms in the bottom group are denoted by  $P_2$ .

Table CCCLVIII shows four VFF terms for the single-layer black phosphorus, two of which are the bond stretching interactions shown by Eq. (1) while the other two terms are the angle bending interaction shown by Eq. (2). The force constant parameters are reasonably chosen to be the same for the two bond stretching terms denoted by  $r_{12}$  and  $r_{14}$ ,

TABLE CCCLIX: Two-body SW potential parameters for black phosphorus used by GULP,<sup>8</sup> as expressed in Eq. (3). The quantity ( $r_{ij}$ ) in the first line lists one representative term for the two-body SW potential between atoms  $i$  and  $j$ . Atom indexes are from Fig. 178 (c).

	$A$ (eV)	$\rho$ (Å)	$B$ (Å <sup>4</sup> )	$r_{\min}$ (Å)	$r_{\max}$ (Å)
$r_{12}$	4.172	0.551	12.543	0.0	2.793
$r_{14}$	4.976	0.685	13.044	0.0	2.882

TABLE CCCLX: Three-body SW potential parameters for black phosphorus used by GULP,<sup>8</sup> as expressed in Eq. (4). The first line ( $\theta_{ijk}$ ) presents one representative term for the three-body SW potential. The angle  $\theta_{ijk}$  has the atom  $i$  as the apex. Atom indexes are from Fig. 178 (c).

	$K$ (eV)	$\theta_0$ (degree)	$\rho_1$ (Å)	$\rho_2$ (Å)	$r_{\min 12}$ (Å)	$r_{\max 12}$ (Å)	$r_{\min 13}$ (Å)	$r_{\max 13}$ (Å)	$r_{\min 23}$ (Å)	$r_{\max 23}$ (Å)
$\theta_{123}$	25.965	96.581	0.551	0.551	0.0	2.793	0.0	2.793	2.793	3.365
$\theta_{134}$	29.932	102.307	0.551	0.685	0.0	2.793	0.0	2.882	2.882	3.772

as these two bonds have very close bond length value. The force constant parameters are the same for the two angle bending terms  $\theta_{123}$  and  $\theta_{134}$ , which have very similar chemical environment. These force constant parameters are determined by fitting to the three acoustic branches in the phonon dispersion along the  $\Gamma X$  as shown in Fig. 179 (a). The *ab initio* calculations for the phonon dispersion are from Ref. 55. Similar phonon dispersion can also be found in other *ab initio* calculations.<sup>58-64</sup> Fig. 179 (b) shows that the VFF model and the SW potential give exactly the same phonon dispersion, as the SW potential is derived from the VFF model.

The parameters for the two-body SW potential used by GULP are shown in

TABLE CCCLXI: SW potential parameters for black phosphorus used by LAMMPS,<sup>9</sup> as expressed in Eqs. (9) and (10). Atom types ( $P_1$  and  $P_2$ ) in the first column are displayed in Fig. 178.

	$\epsilon$ (eV)	$\sigma$ (Å)	$a$	$\lambda$	$\gamma$	$\cos \theta_0$	$A_L$	$B_L$	$p$	$q$	tol
$P_1$ - $P_1$ - $P_1$	1.000	0.551	5.069	25.965	1.000	-0.115	4.172	136.080	4	0	0.0
$P_1$ - $P_2$ - $P_2$	1.000	0.685	4.207	0.000	1.000	0.000	4.976	59.245	4	0	0.0
$P_1$ - $P_1$ - $P_2$	1.000	0.000	0.000	29.932	1.000	-0.213	0.000	0.000	4	0	0.0

Tab. CCCLIX. The parameters for the three-body SW potential used by GULP are shown in Tab. CCCLX. Parameters for the SW potential used by LAMMPS are listed in Tab. CCCLXI.

Fig. 180 shows the stress strain relations for the black phosphorus of size  $100 \times 100 \text{ \AA}$ . The structure is uniaxially stretched in the armchair or zigzag directions at 1 K and 300 K. The Young's modulus is  $24.3 \text{ Nm}^{-1}$  and  $90.5 \text{ Nm}^{-1}$  in the armchair and zigzag directions respectively at 1 K, which are obtained by linear fitting of the stress strain relations in  $[0, 0.01]$ . These values agree quite well with previously reported *ab initio* results, eg.  $28.9 \text{ Nm}^{-1}$  and  $101.6 \text{ Nm}^{-1}$  from Ref. 65, or  $24.4 \text{ Nm}^{-1}$  and  $92.1 \text{ Nm}^{-1}$  from Ref. 66, or  $24.3 \text{ Nm}^{-1}$  and  $80.2 \text{ Nm}^{-1}$  from Ref. 58. The ultimate stress is about  $4.27 \text{ Nm}^{-1}$  at the critical strain of 0.33 in the armchair direction at the low temperature of 1 K. The ultimate stress is about  $8.0 \text{ Nm}^{-1}$  at the critical strain of 0.19 in the zigzag direction at the low temperature of 1 K. These values agree quite well with the *ab initio* results at 0 K.<sup>66</sup>

It should be noted that the Poisson's ratios from the VFF model and the SW potential are  $\nu_{xy} = 0.058$  and  $\nu_{yx} = 0.22$ . These values are obviously smaller than first-principles calculations results, eg. 0.4 and 0.93 from Ref. 67, or 0.17 and 0.62 from Ref. 58, or 0.24 and 0.81 from Ref. 59. The Poisson's ratio can not be obtained correctly by the VFF model proposed in 1982<sup>56</sup> and the SW potential<sup>7</sup> either.<sup>68</sup> These failures are due to the missing of one angle-angle crossing term,<sup>69</sup> which has not been implemented in the package LAMMPS and is not included in the present work.

## XCI. P-ARSENENE

Present studies on the puckered (p-) arsenene, also named  $\alpha$  arsenene, are based on first-principles calculations, and no empirical potential has been proposed for the p-arsenene. We will thus parametrize a set of VFF model for the single-layer p-arsenene in this section. We will also derive the SW potential based on the VFF model for the single-layer p-arsenene.

The structure of the single-layer p-arsenene is exactly the same as that of the black phosphorus as shown in Fig. 178. Structural parameters for p-arsenene are from the *ab initio* calculations.<sup>70</sup> The pucker of the p-arsenene is perpendicular to the x (armchair)-direction. The bases for the rectangular unit cell are  $a_1 = 4.77 \text{ \AA}$  and  $a_2 = 3.68 \text{ \AA}$ . There are four As atoms in the basic unit cell, and their relative coordinates are  $(-u, 0, -v)$ ,

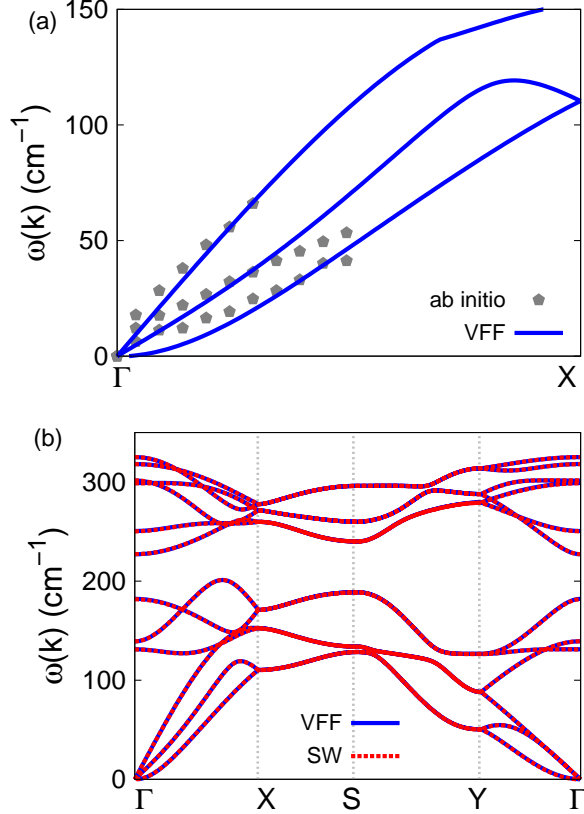


FIG. 181: (Color online) Phonon dispersion for the single-layer p-arsenene. (a) The VFF model is fitted to the three acoustic branches in the long wave limit along the  $\Gamma X$  direction. The *ab initio* results (gray pentagons) are from Ref. 70. (b) The VFF model (blue lines) and the SW potential (red lines) give the same phonon dispersion for the p-arsenene along  $\Gamma XSYT$ .

$(u, , v)$ ,  $(0.5 - u, 0.5, v)$ , and  $(0.5 + u, 0.5, -v)$  with  $u = 0.0714$  and  $v = 0.108$ . The value of the dimensionless parameter  $u$  is extracted from the geometrical parameters provided in Ref. 70. The other dimensionless parameter  $v$  is a ratio based on the lattice constant in the out-of-plane  $z$ -direction, so the other basis  $a_3 = 11.11 \text{ \AA}$  from Ref. 71 is also adopted in extracting the value of  $v$ . We note that the main purpose of the usage of  $u$  and  $v$  in representing atomic coordinates is to follow the same convention for all puckered structures. The resultant atomic coordinates are the same as that in Ref. 70.

Table CCCLXII shows four VFF terms for the single-layer p-arsenene, two of which are the bond stretching interactions shown by Eq. (1) while the other two terms are the angle bending interaction shown by Eq. (2). The force constant parameters are reasonably chosen

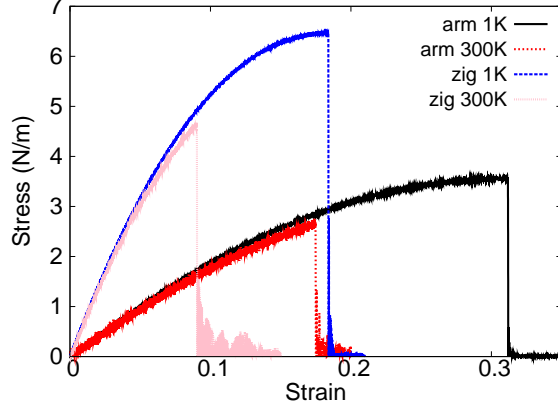


FIG. 182: (Color online) Stress-strain relations for the p-arsenene of size  $100 \times 100 \text{ \AA}$ . The p-arsenene is uniaxially stretched along the armchair or zigzag directions at temperatures 1 K and 300 K.

TABLE CCCLXII: The VFF model for p-arsenene. The second line gives an explicit expression for each VFF term, where atom indexes are from Fig. 178 (c). The third line is the force constant parameters. Parameters are in the unit of  $\frac{eV}{\text{Å}^2}$  for the bond stretching interactions, and in the unit of eV for the angle bending interaction. The fourth line gives the initial bond length (in unit of  $\text{Å}$ ) for the bond stretching interaction and the initial angle (in unit of degrees) for the angle bending interaction. The angle  $\theta_{ijk}$  has atom  $i$  as the apex.

VFF type	bond stretching		angle bending	
expression	$\frac{1}{2}K_{12} (\Delta r_{12})^2$	$\frac{1}{2}K_{14} (\Delta r_{14})^2$	$\frac{1}{2}K_{123} (\Delta \theta_{123})^2$	$\frac{1}{2}K_{134} (\Delta \theta_{134})^2$
parameter	7.936	7.936	7.456	7.456
$r_0$ or $\theta_0$	2.508	2.495	94.400	100.692

to be the same for the two bond stretching terms denoted by  $r_{12}$  and  $r_{14}$ , as these two bonds have very close bond length value. The force constant parameters happen to be the same for the two angle bending terms  $\theta_{123}$  and  $\theta_{134}$ . These force constant parameters are determined by fitting to the three acoustic branches in the phonon dispersion along the  $\Gamma X$  as shown in Fig. 181 (a). The *ab initio* calculations for the phonon dispersion are from Ref. 70. Similar phonon dispersion can also be found in other *ab initio* calculations.<sup>64,72–74</sup> We note that the lowest-frequency branch around the  $\Gamma$  point from the VFF model is lower than the *ab initio* results. This branch is the flexural branch, which should be a quadratic dispersion.

TABLE CCCLXIII: Two-body SW potential parameters for p-arsenene used by GULP,<sup>8</sup> as expressed in Eq. (3). The quantity ( $r_{ij}$ ) in the first line lists one representative term for the two-body SW potential between atoms  $i$  and  $j$ . Atom indexes are from Fig. 178 (c).

	$A$ (eV)	$\rho$ (Å)	$B$ (Å <sup>4</sup> )	$r_{\min}$ (Å)	$r_{\max}$ (Å)
$r_{12}$	3.180	0.455	19.782	0.0	3.042
$r_{14}$	4.477	0.737	19.375	0.0	3.173

TABLE CCCLXIV: Three-body SW potential parameters for p-arsenene used by GULP,<sup>8</sup> as expressed in Eq. (4). The first line ( $\theta_{ijk}$ ) presents one representative term for the three-body SW potential. The angle  $\theta_{ijk}$  has the atom  $i$  as the apex. Atom indexes are from Fig. 178 (c).

	$K$ (eV)	$\theta_0$ (degree)	$\rho_1$ (Å)	$\rho_2$ (Å)	$r_{\min 12}$ (Å)	$r_{\max 12}$ (Å)	$r_{\min 13}$ (Å)	$r_{\max 13}$ (Å)	$r_{\min 23}$ (Å)	$r_{\max 23}$ (Å)
$\theta_{123}$	20.597	94.400	0.455	0.455	0.0	3.042	0.0	3.042	3.628	4.225
$\theta_{134}$	26.831	100.692	0.455	0.737	0.0	3.042	0.0	3.173	3.173	4.149

However, the *ab initio* calculations give a linear dispersion for the flexural branch due to the violation of the rigid rotational invariance in the first-principles package,<sup>20</sup> so *ab initio* calculations typically overestimate the frequency of this branch. Fig. 181 (b) shows that the VFF model and the SW potential give exactly the same phonon dispersion, as the SW potential is derived from the VFF model.

The parameters for the two-body SW potential used by GULP are shown in Tab. CCCLXIII. The parameters for the three-body SW potential used by GULP are shown in Tab. CCCLXIV. Parameters for the SW potential used by LAMMPS are listed in

TABLE CCCLXV: SW potential parameters for p-arsenene used by LAMMPS,<sup>9</sup> as expressed in Eqs. (9) and (10). Atom types in the first column are displayed in Fig. 178 (b), with element symbol P substituted by As.

	$\epsilon$ (eV)	$\sigma$ (Å)	$a$	$\lambda$	$\gamma$	$\cos \theta_0$	$A_L$	$B_L$	$p$	$q$	tol
As <sub>1</sub> -As <sub>1</sub> -As <sub>1</sub>	1.000	0.455	6.686	20.597	1.000	-0.077	3.180	461.556	4	0	0.0
As <sub>1</sub> -As <sub>2</sub> -As <sub>2</sub>	1.000	0.737	4.305	0.000	1.000	0.000	4.477	65.671	4	0	0.0
As <sub>1</sub> -As <sub>1</sub> -As <sub>2</sub>	1.000	0.000	0.000	26.831	1.000	-0.186	0.000	0.000	4	0	0.0

TABLE CCCLXVI: The VFF model for p-antimonene. The second line gives an explicit expression for each VFF term, where atom indexes are from Fig. 183 (c). The third line is the force constant parameters. Parameters are in the unit of  $\frac{eV}{\text{\AA}^2}$  for the bond stretching interactions, and in the unit of eV for the angle bending interaction. The fourth line gives the initial bond length (in unit of  $\text{\AA}$ ) for the bond stretching interaction and the initial angle (in unit of degrees) for the angle bending interaction. The angle  $\theta_{ijk}$  has atom i as the apex.

VFF type	bond stretching		angle bending		
expression	$\frac{1}{2}K_{12}(\Delta r_{12})^2$	$\frac{1}{2}K_{14}(\Delta r_{14})^2$	$\frac{1}{2}K_{123}(\Delta\theta_{123})^2$	$\frac{1}{2}K_{134}(\Delta\theta_{134})^2$	$\frac{1}{2}K_{415}(\Delta\theta_{415})^2$
parameter	7.675	7.675	6.534	12.068	12.068
$r_0$ or $\theta_0$	2.950	2.870	95.380	88.300	102.800

Tab. CCCLXV.

Fig. 182 shows the stress strain relations for the p-arsenene of size  $100 \times 100 \text{ \AA}$ . The structure is uniaxially stretched in the armchair or zigzag directions at 1 K and 300 K. The Young's modulus is  $20.7 \text{ Nm}^{-1}$  and  $73.0 \text{ Nm}^{-1}$  in the armchair and zigzag directions respectively at 1 K, which are obtained by linear fitting of the stress strain relations in  $[0, 0.01]$ . The third-order nonlinear elastic constant  $D$  can be obtained by fitting the stress-strain relation to  $\sigma = E\epsilon + \frac{1}{2}D\epsilon^2$  with  $E$  as the Young's modulus. The values of  $D$  are  $-56.4 \text{ N/m}$  and  $-415.5 \text{ N/m}$  at 1 K along the armchair and zigzag directions, respectively. The ultimate stress is about  $3.5 \text{ Nm}^{-1}$  at the critical strain of 0.31 in the armchair direction at the low temperature of 1 K. The ultimate stress is about  $6.5 \text{ Nm}^{-1}$  at the critical strain of 0.18 in the zigzag direction at the low temperature of 1 K.

## XCII. P-ANTIMONENE

Present studies on the puckered (p-) antimonene, also named  $\alpha$  antimonene, are based on first-principles calculations, and no empirical potential has been proposed for the p-antimonene. We will thus parametrize a set of VFF model for the single-layer p-antimonene in this section. We will also derive the SW potential based on the VFF model for the single-layer p-antimonene.

The structure of the single-layer p-antimonene is shown in Fig. 183, which is similar as

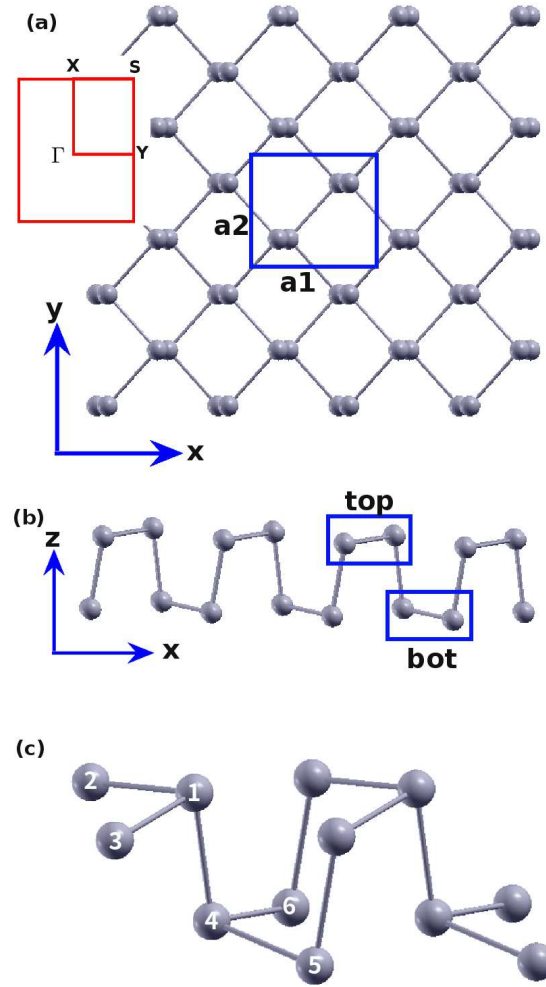


FIG. 183: (Color online) Structure for single-layer p-antimonene. (a) Top view. The armchair direction is along the x-axis, while the zigzag direction is along the y-axis. The first Brillouin zone is shown in the inset. (b) Side view illustrates the puckered configuration. The pucker is perpendicular to the x-axis and is parallel with the y-axis. Sb atoms in the top/bottom group have different z-coordinates. (c) Atomic configuration.

that of the black phosphorus as shown in Fig. 178. Structural parameters for p-antimonene are from the *ab initio* calculations.<sup>70</sup> The pucker of the p-antimonene is perpendicular to the x (armchair)-direction. The bases for the rectangular unit cell are  $a_1 = 4.73 \text{ \AA}$  and  $a_2 = 4.36 \text{ \AA}$ . There are four Sb atoms in the basic unit cell, and their relative coordinates are  $(-u, 0, -v)$ ,  $(u, 0, v)$ ,  $(0.5 - u, 0.5, v + w)$ , and  $(0.5 + u, 0.5, -v + w)$  with  $u = 0.044$ ,  $v = 0.128$  and  $w = 0.0338$ . The value of the dimensionless parameter  $u$  is extracted from

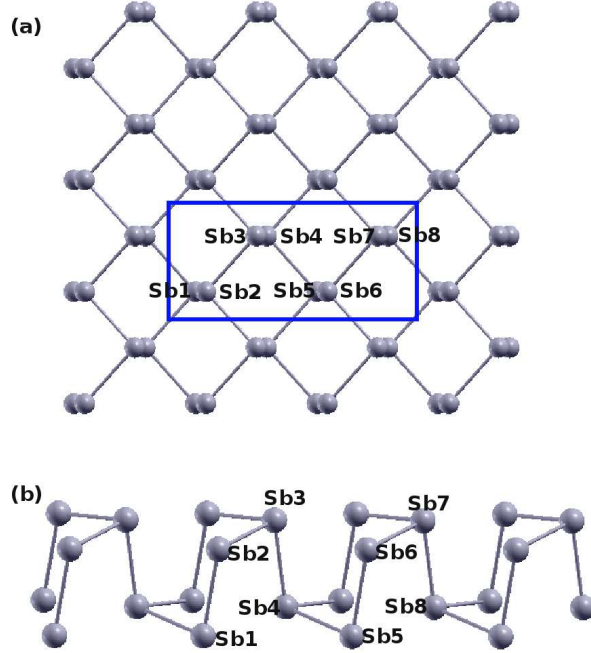


FIG. 184: (Color online) Eight atom types are introduced for the Sb atoms in the p-antimonene. (a) Top view. (b) Side view.

TABLE CCCLXVII: Two-body SW potential parameters for p-antimonene used by GULP,<sup>8</sup> as expressed in Eq. (3). The quantity  $(r_{ij})$  in the first line lists one representative term for the two-body SW potential between atoms  $i$  and  $j$ . Atom indexes are from Fig. 183 (c).

	$A$ (eV)	$\rho$ ( $\text{\AA}$ )	$B$ ( $\text{\AA}^4$ )	$r_{\min}$ ( $\text{\AA}$ )	$r_{\max}$ ( $\text{\AA}$ )
$r_{12}$	1.750	0.122	37.867	0.0	3.250
$r_{14}$	11.221	1.843	33.923	0.0	4.020

the geometrical parameters (bond lengths and bond angles) provided in Ref. 70. The dimensionless parameters  $v$  and  $w$  are ratios based on the lattice constant in the out-of-plane  $z$ -direction, so an arbitrary value of  $a_3 = 11.11 \text{ \AA}$  is adopted in extracting the values of  $v$  and  $w$ . The value of  $a_3$  has no effect on the actual position of each Sb atom. We note that the main purpose of the usage of  $u$ ,  $v$ , and  $w$  in representing atomic coordinates is to follow the same convention of black phosphorus. The resultant atomic coordinates are the same as that in Ref. 70.

As shown in Fig. 183 (b), a specific feature in the puckered configuration of the p-

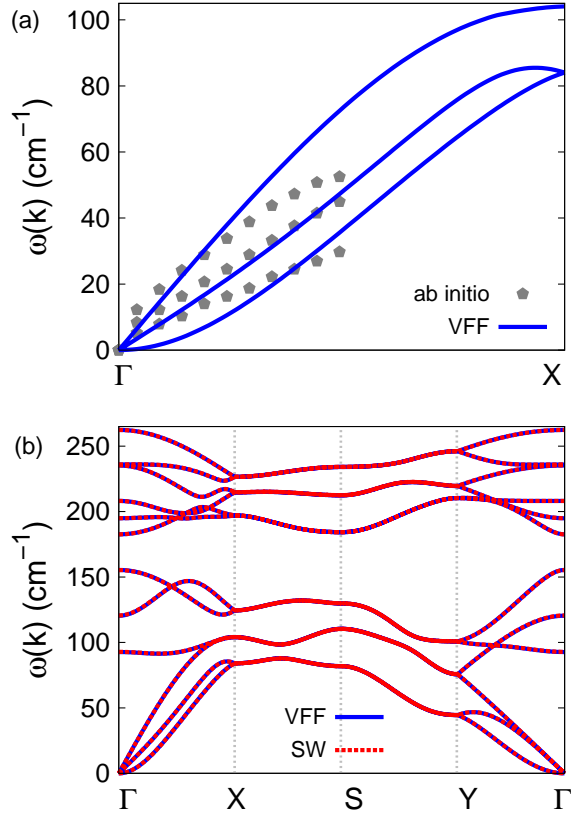


FIG. 185: (Color online) Phonon dispersion for the single-layer p-antimonene. (a) The VFF model is fitted to the three acoustic branches in the long wave limit along the  $\Gamma X$  direction. The *ab initio* results (gray pentagons) are from Ref. 70. (b) The VFF model (blue lines) and the SW potential (red lines) give the same phonon dispersion for the p-antimonene along  $\Gamma X S \bar{Y} \Gamma$ .

antimonene is that Sb atoms in the top/bottom group are further divided into two subgroups with different  $z$ -coordinates. Specifically, in Fig. 183 (c), there is a difference of  $wa_3$  between the  $z$ -coordinate of atom 1 and the  $z$ -coordinates of atoms 2 and 3. Similarly, atom 4 is higher than atoms 5 and 6 for  $wa_3$  along the  $z$ -direction. As a result of the nonzero value of  $w$ , there are two different inter-group angles, i.e.,  $\theta_{134} = 88.3^\circ$  and  $\theta_{415} = 102.8^\circ$ . We have  $w = 0$  for the ideal puckered configuration of the black phosphorus.

Table CCCLXVI shows five VFF terms for the single-layer p-antimonene, two of which are the bond stretching interactions shown by Eq. (1) while the other three terms are the angle bending interaction shown by Eq. (2). The force constant parameters are reasonably chosen to be the same for the two bond stretching terms denoted by  $r_{12}$  and  $r_{14}$ , as these two

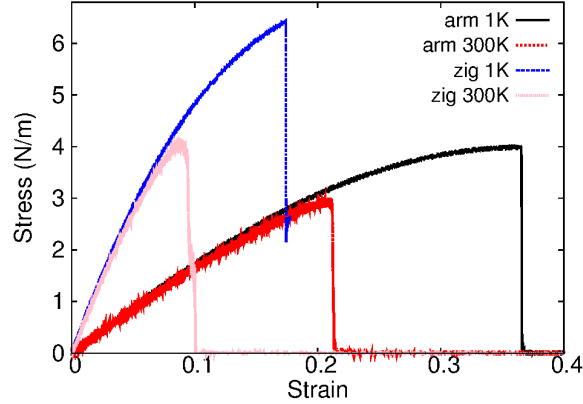


FIG. 186: (Color online) Stress-strain relations for the p-antimonene of size  $100 \times 100 \text{ \AA}$ . The p-antimonene is uniaxially stretched along the armchair or zigzag directions at temperatures 1 K and 300 K.

TABLE CCCLXVIII: Three-body SW potential parameters for p-antimonene used by GULP,<sup>8</sup> as expressed in Eq. (4). The first line ( $\theta_{ijk}$ ) presents one representative term for the three-body SW potential. The angle  $\theta_{ijk}$  has the atom  $i$  as the apex. Atom indexes are from Fig. 183 (c).

	$K$ (eV)	$\theta_0$ (degree)	$\rho_1$ ( $\text{\AA}$ )	$\rho_2$ ( $\text{\AA}$ )	$r_{\min 12}$ ( $\text{\AA}$ )	$r_{\max 12}$ ( $\text{\AA}$ )	$r_{\min 13}$ ( $\text{\AA}$ )	$r_{\max 13}$ ( $\text{\AA}$ )	$r_{\min 23}$ ( $\text{\AA}$ )	$r_{\max 23}$ ( $\text{\AA}$ )
$\theta_{123}$	7.435	95.380	0.122	0.122	0.0	3.250	0.0	3.250	0.0	4.545
$\theta_{134}$	45.054	88.380	1.843	0.122	0.0	4.020	0.0	3.250	0.0	5.715
$\theta_{415}$	47.338	102.800	1.843	0.122	0.0	4.020	0.0	3.250	0.0	6.105

bonds have very close bond length value. The force constant parameters are the same for the two angle bending terms  $\theta_{134}$  and  $\theta_{415}$ , which have the same arm lengths. As a result, there are only three force constant parameters, i.e.,  $K_{12} = K_{14}$ ,  $K_{123}$ , and  $K_{134} = K_{415}$ . These three force constant parameters are determined by fitting to the three acoustic branches in the phonon dispersion along the  $\Gamma X$  as shown in Fig. 185 (a). The *ab initio* calculations for the phonon dispersion are from Ref. 70. Similar phonon dispersion can also be found in other *ab initio* calculations.<sup>64,75,76</sup> We note that the lowest-frequency branch around the  $\Gamma$  point from the VFF model is lower than the *ab initio* results. This branch is the flexural branch, which should be a quadratic dispersion. However, the *ab initio* calculations give a linear dispersion for the flexural branch due to the violation of the rigid rotational invariance in the first-principles package,<sup>20</sup> so *ab initio* calculations typically overestimate the frequency

TABLE CCCLXIX: SW potential parameters for p-antimonene used by LAMMPS,<sup>9</sup> as expressed in Eqs. (9) and (10). Atom types in the first column are displayed in Fig. 184.

	$\epsilon$ (eV)	$\sigma$ (Å)	$a$	$\lambda$	$\gamma$	$\cos \theta_0$	$A_L$	$B_L$	$p$	$q$	tol
Sb <sub>5</sub> -Sb <sub>4</sub> -Sb <sub>4</sub>	1.000	5.103	0.958	635.059	1.000	-0.094	38.498	0.056	4	0	0.0
Sb <sub>1</sub> -Sb <sub>2</sub> -Sb <sub>2</sub>	1.000	1.924	2.102	0.000	1.000	0.000	11.708	2.476	4	0	0.0
Sb <sub>5</sub> -Sb <sub>4</sub> -Sb <sub>6</sub>	1.000	0.000	0.000	431.139	1.000	0.030	0.000	0.000	4	0	0.0
Sb <sub>2</sub> -Sb <sub>3</sub> -Sb <sub>1</sub>	1.000	0.000	0.000	452.994	1.000	-0.222	0.000	0.000	4	0	0.0

of this branch. Fig. 185 (b) shows that the VFF model and the SW potential give exactly the same phonon dispersion, as the SW potential is derived from the VFF model.

The parameters for the two-body SW potential used by GULP are shown in Tab. CCCLXVII. The parameters for the three-body SW potential used by GULP are shown in Tab. CCCLXVIII. Parameters for the SW potential used by LAMMPS are listed in Tab. CCCLXIX. Eight atom types have been introduced for writing the SW potential script used by LAMMPS as shown in Fig. 184, which technically increases the cutoff for the bond stretching interaction between atom 1 and atom 2 in Fig. 183 (c).

Fig. 186 shows the stress strain relations for the p-antimonene of size  $100 \times 100$  Å. The structure is uniaxially stretched in the armchair or zigzag directions at 1 K and 300 K. The Young's modulus is  $18.3 \text{ Nm}^{-1}$  and  $65.2 \text{ Nm}^{-1}$  in the armchair and zigzag directions respectively at 1 K, which are obtained by linear fitting of the stress strain relations in  $[0, 0.01]$ . The Poisson's ratios from the VFF model and the SW potential are  $\nu_{xy} = 0.08$  and  $\nu_{yx} = 0.29$ . The third-order nonlinear elastic constant  $D$  can be obtained by fitting the stress-strain relation to  $\sigma = E\epsilon + \frac{1}{2}D\epsilon^2$  with  $E$  as the Young's modulus. The values of  $D$  are  $-22.1 \text{ N/m}$  and  $-354.1 \text{ N/m}$  at 1 K along the armchair and zigzag directions, respectively. The ultimate stress is about  $3.7 \text{ Nm}^{-1}$  at the critical strain of 0.37 in the armchair direction at the low temperature of 1 K. The ultimate stress is about  $6.4 \text{ Nm}^{-1}$  at the critical strain of 0.17 in the zigzag direction at the low temperature of 1 K.

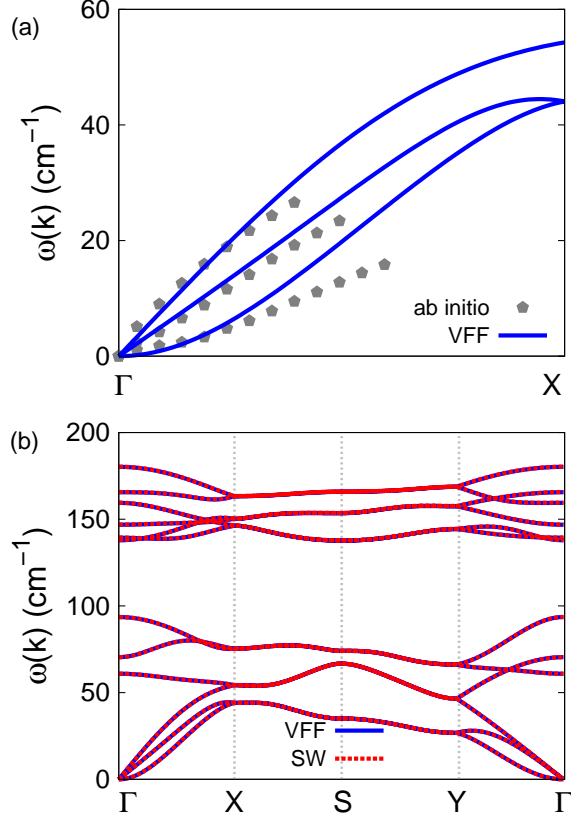


FIG. 187: (Color online) Phonon dispersion for the single-layer p-bismuthene. (a) The VFF model is fitted to the three acoustic branches in the long wave limit along the  $\Gamma$ X direction. The *ab initio* results (gray pentagons) are from Ref. 77. (b) The VFF model (blue lines) and the SW potential (red lines) give the same phonon dispersion for the p-bismuthene along  $\Gamma$ XSYT.

### XCI. P-BISMUTHENE

Present studies on the puckered (p-) bismuthene, which is also named  $\alpha$  bismuthene, are based on first-principles calculations, and no empirical potential has been proposed for the p-bismuthene. We will thus parametrize a set of VFF model for the single-layer p-bismuthene in this section. We will also derive the SW potential based on the VFF model for the single-layer p-bismuthene.

The structure of the single-layer p-bismuthene is the same as p-antimonene as shown in Fig. 183. Structural parameters for p-bismuthene are from the *ab initio* calculations.<sup>77</sup> The pucker of the p-bismuthene is perpendicular to the x (armchair)-direction. The bases for

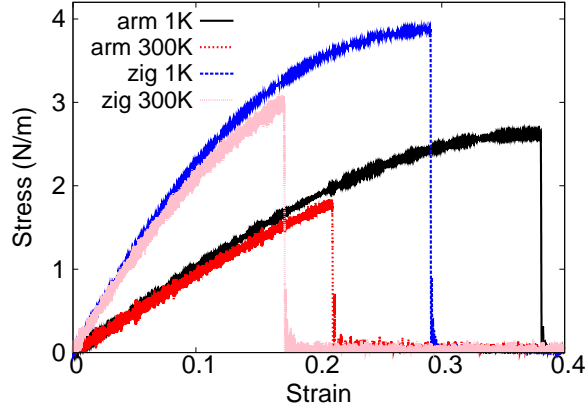


FIG. 188: (Color online) Stress-strain relations for the p-bismuthene of size  $100 \times 100 \text{ \AA}$ . The p-bismuthene is uniaxially stretched along the armchair or zigzag directions at temperatures 1 K and 300 K.

TABLE CCCLXX: The VFF model for p-bismuthene. The second line gives an explicit expression for each VFF term, where atom indexes are from Fig. 183 (c). The third line is the force constant parameters. Parameters are in the unit of  $\frac{eV}{\text{Å}^2}$  for the bond stretching interactions, and in the unit of eV for the angle bending interaction. The fourth line gives the initial bond length (in unit of  $\text{Å}$ ) for the bond stretching interaction and the initial angle (in unit of degrees) for the angle bending interaction. The angle  $\theta_{ijk}$  has atom  $i$  as the apex.

VFF type	bond stretching		angle bending		
expression	$\frac{1}{2}K_{12}(\Delta r_{12})^2$	$\frac{1}{2}K_{14}(\Delta r_{14})^2$	$\frac{1}{2}K_{123}(\Delta\theta_{123})^2$	$\frac{1}{2}K_{134}(\Delta\theta_{134})^2$	$\frac{1}{2}K_{415}(\Delta\theta_{415})^2$
parameter	7.675	7.675	2.267	8.347	8.347
$r_0$ or $\theta_0$	3.110	3.097	94.018	86.486	103.491

the rectangular unit cell are  $a_1 = 4.94 \text{ \AA}$  and  $a_2 = 4.55 \text{ \AA}$ . There are four Bi atoms in the basic unit cell, and their relative coordinates are  $(-u, 0, -v)$ ,  $(u, 0, v)$ ,  $(0.5 - u, 0.5, v + w)$ , and  $(0.5 + u, 0.5, -v + w)$  with  $u = 0.0405$ ,  $v = 0.130$  and  $w = 0.0391$ . The value of the dimensionless parameter  $u$  is extracted from the geometrical parameters provided in Ref. 77. The dimensionless parameters  $v$  and  $w$  are ratios based on the lattice constant in the out-of-plane  $z$ -direction, so an arbitrary value of  $a_3 = 11.81 \text{ \AA}$  is adopted in extracting the values of  $v$  and  $w$ . The value of  $a_3$  has no effect on the actual position of each Bi atom. We note that the main purpose of the usage of  $u$ ,  $v$ , and  $w$  in representing atomic coordinates is to

TABLE CCCLXXI: Two-body SW potential parameters for p-bismuthene used by GULP,<sup>8</sup> as expressed in Eq. (3). The quantity ( $r_{ij}$ ) in the first line lists one representative term for the two-body SW potential between atoms  $i$  and  $j$ . Atom indexes are from Fig. 183 (c).

	$A$ (eV)	$\rho$ (Å)	$B$ (Å <sup>4</sup> )	$r_{\min}$ (Å)	$r_{\max}$ (Å)
$r_{12}$	1.777	0.109	46.775	0.0	3.401
$r_{14}$	12.322	1.872	45.998	0.0	4.301

TABLE CCCLXXII: Three-body SW potential parameters for p-bismuthene used by GULP,<sup>8</sup> as expressed in Eq. (4). The first line ( $\theta_{ijk}$ ) presents one representative term for the three-body SW potential. The angle  $\theta_{ijk}$  has the atom  $i$  as the apex. Atom indexes are from Fig. 183 (c).

	$K$ (eV)	$\theta_0$ (degree)	$\rho_1$ (Å)	$\rho_2$ (Å)	$r_{\min12}$ (Å)	$r_{\max12}$ (Å)	$r_{\min13}$ (Å)	$r_{\max13}$ (Å)	$r_{\min23}$ (Å)	$r_{\max23}$ (Å)
$\theta_{123}$	2.408	94.018	0.109	0.109	0.0	3.401	0.0	3.401	0.0	4.745
$\theta_{134}$	28.842	86.486	1.872	0.109	0.0	4.301	0.0	3.401	0.0	5.982
$\theta_{415}$	30.388	103.491	1.872	0.109	0.0	4.301	0.0	3.401	0.0	6.473

follow the same convention of black phosphorus. The resultant atomic coordinates are the same as that in Ref. 77.

As shown in Fig. 183 (b), a specific feature in the puckered configuration of the p-bismuthene is that Bi atoms in the top/bottom group are further divided into two subgroups with different  $z$ -coordinates. Specifically, in Fig. 183 (c), there is a difference of  $wa_3$  between the  $z$ -coordinate of atom 1 and the  $z$ -coordinates of atoms 2 and 3. Similarly, atom 4 is

TABLE CCCLXXIII: SW potential parameters for p-bismuthene used by LAMMPS,<sup>9</sup> as expressed in Eqs. (9) and (10). Atom types in the first column are displayed in Fig. 184 with elemental symbol Sb substituted by Bi.

	$\epsilon$ (eV)	$\sigma$ (Å)	$a$	$\lambda$	$\gamma$	$\cos \theta_0$	$A_L$	$B_L$	$p$	$q$	tol
Bi <sub>1</sub> -Bi <sub>8</sub> -Bi <sub>8</sub>	1.000	2.737	1.571	112.813	1.000	-0.070	18.974	1.000	4	0	0.0
Bi <sub>1</sub> -Bi <sub>2</sub> -Bi <sub>2</sub>	1.000	2.808	1.532	0.000	1.000	0.000	19.577	0.888	4	0	0.0
Bi <sub>1</sub> -Bi <sub>8</sub> -Bi <sub>2</sub>	1.000	0.000	0.000	429.598	1.000	0.061	0.000	0.000	4	0	0.0
Bi <sub>2</sub> -Bi <sub>3</sub> -Bi <sub>1</sub>	1.000	0.000	0.000	452.618	1.000	-0.233	0.000	0.000	4	0	0.0

higher than atoms 5 and 6 for  $wa_3$  along the z-direction. As a result of the nonzero value of  $w$ , there are two different inter-group angles, i.e.,  $\theta_{134} = 86.486^\circ$  and  $\theta_{415} = 103.491^\circ$ . We have  $w = 0$  for the ideal puckered configuration of the black phosphorus.

Table CCCLXX shows five VFF terms for the single-layer p-bismuthene, two of which are the bond stretching interactions shown by Eq. (1) while the other three terms are the angle bending interaction shown by Eq. (2). The force constant parameters are reasonably chosen to be the same for the two bond stretching terms denoted by  $r_{12}$  and  $r_{14}$ , as these two bonds have very close bond length value. The force constant parameters are the same for the two angle bending terms  $\theta_{134}$  and  $\theta_{415}$ , which have the same arm lengths. As a result, there are only three force constant parameters, i.e.,  $K_{12} = K_{14}$ ,  $K_{123}$ , and  $K_{134} = K_{415}$ . These three force constant parameters are determined by fitting to the three acoustic branches in the phonon dispersion along the  $\Gamma X$  as shown in Fig. 187 (a). The *ab initio* calculations for the phonon dispersion are from Ref. 77. Similar phonon dispersion can also be found in other *ab initio* calculations.<sup>64</sup> Fig. 187 (b) shows that the VFF model and the SW potential give exactly the same phonon dispersion, as the SW potential is derived from the VFF model.

The parameters for the two-body SW potential used by GULP are shown in Tab. CCCLXXI. The parameters for the three-body SW potential used by GULP are shown in Tab. CCCLXXII. Parameters for the SW potential used by LAMMPS are listed in Tab. CCCLXXIII. Eight atom types have been introduced for writing the SW potential script used by LAMMPS as shown in Fig. 184, which helps to increase the cutoff for the bond stretching interaction between atoms like 1 and 2 in Fig. 183 (c).

Fig. 188 shows the stress strain relations for the p-bismuthene of size  $100 \times 100 \text{ \AA}$ . The structure is uniaxially stretched in the armchair or zigzag directions at 1 K and 300 K. The Young's modulus is  $10.2 \text{ Nm}^{-1}$  and  $26.2 \text{ Nm}^{-1}$  in the armchair and zigzag directions respectively at 1 K, which are obtained by linear fitting of the stress strain relations in  $[0, 0.01]$ . The Poisson's ratios from the VFF model and the SW potential are  $\nu_{xy} = 0.24$  and  $\nu_{yx} = 0.61$ . These values are very close to the *ab initio* calculations, eg.  $\nu_{xy} = 0.261$  and  $\nu_{yx} = 0.648$  in Ref. 77. The third-order nonlinear elastic constant  $D$  can be obtained by fitting the stress-strain relation to  $\sigma = E\epsilon + \frac{1}{2}D\epsilon^2$  with  $E$  as the Young's modulus. The values of  $D$  are  $-12.4 \text{ N/m}$  and  $-86.4 \text{ N/m}$  at 1 K along the armchair and zigzag directions, respectively. The ultimate stress is about  $2.6 \text{ Nm}^{-1}$  at the critical strain of 0.38 in the armchair direction at the low temperature of 1 K. The ultimate stress is about  $3.9 \text{ Nm}^{-1}$  at

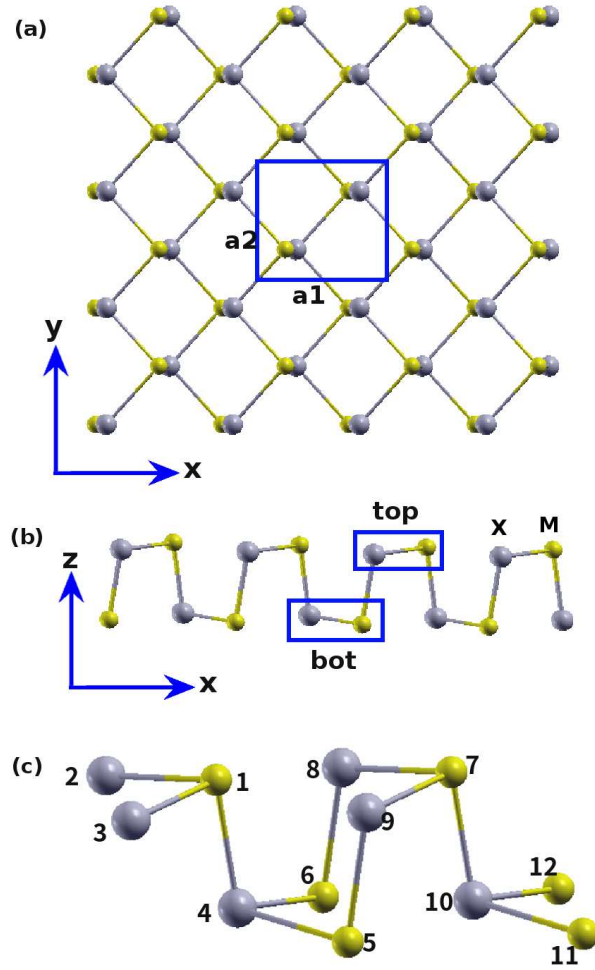


FIG. 189: (Color online) Structure for single-layer p-MX, with M from group IV and X from group VI. (a) Top view. The armchair direction is along the x-axis, while the zigzag direction is along the y-axis. Inset shows the first Brillouin zone. (b) Side view illustrates the puckered configuration. The pucker is perpendicular to the x-axis and is parallel with the y-axis. Sn and Se atoms in the top/bottom group have different z-coordinates. (c) Atomic configuration.

the critical strain of 0.29 in the zigzag direction at the low temperature of 1 K.

#### XCIV. P-SITE

Present studies on the puckered (p-) SiTe are based on first-principles calculations, and no empirical potential has been proposed for the p-SiTe. We will thus parametrize the SW potential for the single-layer p-SiTe in this section.

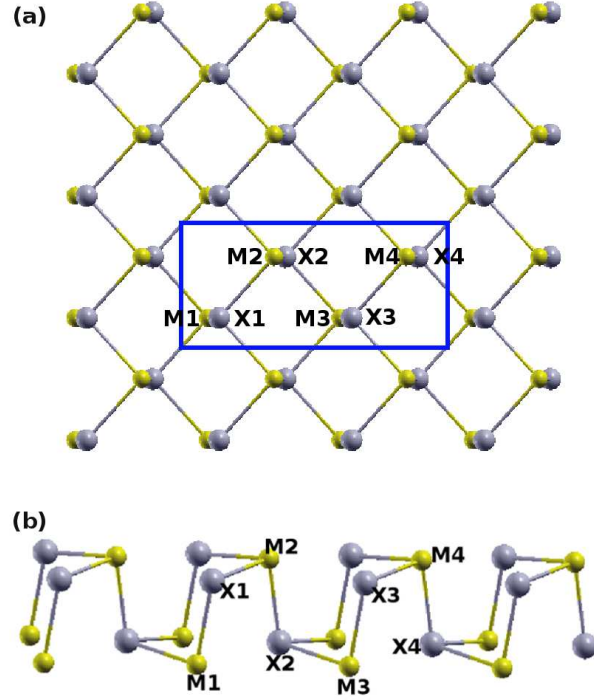


FIG. 190: (Color online) Eight atom types are introduced for atoms in the p-MX, with M from group IV and X from group VI. (a) Top view. (b) Side view.

The structure of the single-layer p-SiTe is shown in Fig. 189, with M=Si and X=Te. Structural parameters for p-SiTe are from the *ab initio* calculations.<sup>78</sup> The pucker of the p-SiTe is perpendicular to the x (armchair)-direction. The bases for the rectangular unit cell are  $a_1 = 4.29 \text{ \AA}$  and  $a_2 = 4.11 \text{ \AA}$ . There are two Te atoms and two Si atoms in the basic unit cell, and their relative coordinates are  $(-u, 0, -v)$ ,  $(u, 0, v)$ ,  $(0.5 - u, 0.5, v + w)$ , and  $(0.5 + u, 0.5, -v + w)$  with  $u = 0.03513$ ,  $v = 0.1211$  and  $w = 0.02745$ . The value of the dimensionless parameter  $u$  is extracted from the geometrical parameters (bond lengths and bond angles) provided in Ref. 78. The dimensionless parameters  $v$  and  $w$  are ratios based on the lattice constant in the out-of-plane z-direction, which is arbitrarily chosen as  $a_3 = 10.825 \text{ \AA}$ . We note that the main purpose of the usage of  $u$ ,  $v$ , and  $w$  in representing atomic coordinates is to follow the same convention for all puckered structures in the present work. The resultant atomic coordinates are the same as that in Ref. 78.

As shown in Fig. 189 (b), a specific feature in the puckered configuration of the p-SiTe is that Te and Si atoms in the top/bottom group have different z-coordinates. Atom Te is in

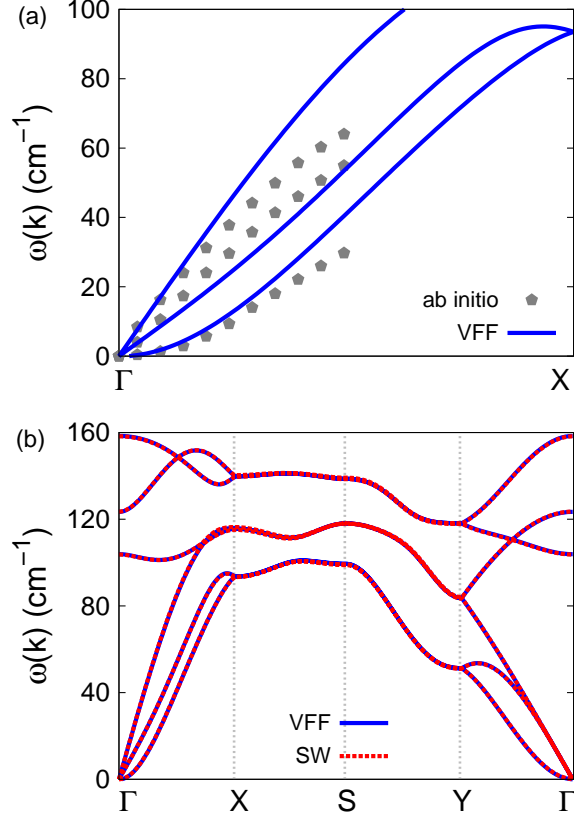


FIG. 191: (Color online) Phonon dispersion for the single-layer p-SiTe. (a) The VFF model is fitted to the three acoustic branches in the long wave limit along the  $\Gamma$ X direction. The *ab initio* calculations are from Ref. 78. (b) The VFF model (blue lines) and the SW potential (red lines) give the same phonon dispersion for the p-SiTe along  $\Gamma$ XSYT.

the top and bottom most position. Specifically, in Fig. 189 (c), there is a difference of  $wa_3$  between the  $z$ -coordinate of atom 1 and the  $z$ -coordinates of atoms 2 and 3. Similarly, atom 4 is higher than atoms 5 and 6 for  $wa_3$  along the  $z$ -direction. As a result of the nonzero value of  $w$ , there are two different inter-group angles, i.e.,  $\theta_{134} = 88.252^\circ$  and  $\theta_{415} = 100.496^\circ$  in Fig. 189 (c). We have  $w = 0$  for the ideal puckered configuration of materials like the black phosphorus.

Table CCCLXXIV shows five VFF terms for the single-layer p-SiTe, two of which are the bond stretching interactions shown by Eq. (1) while the other three terms are the angle bending interaction shown by Eq. (2). The force constant parameters are the same for the two angle bending terms  $\theta_{134}$  and  $\theta_{415}$ , which have the same arm lengths. All force

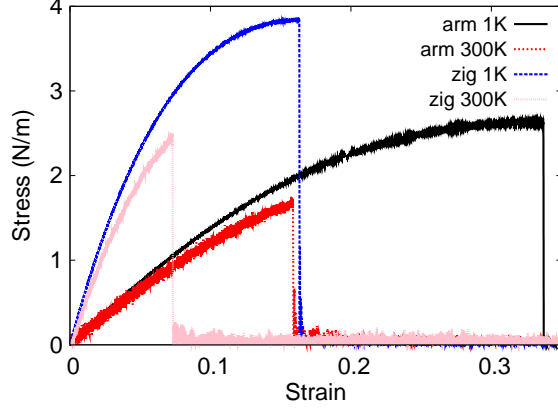


FIG. 192: (Color online) Stress-strain relations for the single-layer p-SiTe of size  $100 \times 100 \text{ \AA}$ . The single-layer p-SiTe is uniaxially stretched along the armchair or zigzag directions at temperatures 1 K and 300 K.

TABLE CCCLXXIV: The VFF model for the single-layer p-SiTe. The second line gives an explicit expression for each VFF term, where atom indexes are from Fig. 189 (c). The third line is the force constant parameters. Parameters are in the unit of  $\frac{eV}{\text{Å}^2}$  for the bond stretching interactions, and in the unit of eV for the angle bending interaction. The fourth line gives the initial bond length (in unit of  $\text{Å}$ ) for the bond stretching interaction and the initial angle (in unit of degrees) for the angle bending interaction. The angle  $\theta_{ijk}$  has atom  $i$  as the apex.

VFF type	bond stretching		angle bending		
expression	$\frac{1}{2}K_{12}(\Delta r_{12})^2$	$\frac{1}{2}K_{14}(\Delta r_{14})^2$	$\frac{1}{2}K_{123}(\Delta\theta_{123})^2$	$\frac{1}{2}K_{134}(\Delta\theta_{134})^2$	$\frac{1}{2}K_{415}(\Delta\theta_{415})^2$
parameter	5.420	7.913	6.059	9.182	9.182
$r_0$ or $\theta_0$	2.777	2.639	95.477	88.252	100.496

constant parameters are determined by fitting to the three acoustic branches in the phonon dispersion along the  $\Gamma X$  as shown in Fig. 191 (a). The *ab initio* calculations are from Ref. 78. Fig. 191 (b) shows that the VFF model and the SW potential give exactly the same phonon dispersion.

The parameters for the two-body SW potential used by GULP are shown in Tab. CCCLXXV. The parameters for the three-body SW potential used by GULP are shown in Tab. CCCLXXVI. Parameters for the SW potential used by LAMMPS are listed in Tab. CCCLXXVII. Eight atom types have been introduced for writing the SW potential

TABLE CCCLXXV: Two-body SW potential parameters for the single-layer p-SiTe used by GULP,<sup>8</sup> as expressed in Eq. (3). The quantity ( $r_{ij}$ ) in the first line lists one representative term for the two-body SW potential between atoms  $i$  and  $j$ . Atom indexes are from Fig. 189 (c).

	$A$ (eV)	$\rho$ (Å)	$B$ (Å <sup>4</sup> )	$r_{\min}$ (Å)	$r_{\max}$ (Å)
$r_{12}$	0.756	0.101	35.682	0.0	2.993
$r_{14}$	18.792	2.867	29.101	0.0	3.762

TABLE CCCLXXVI: Three-body SW potential parameters for the single-layer p-SiTe used by GULP,<sup>8</sup> as expressed in Eq. (4). The first line ( $\theta_{ijk}$ ) presents one representative term for the three-body SW potential. The angle  $\theta_{ijk}$  has the atom  $i$  as the apex. Atom indexes are from Fig. 189 (c).

	$K$ (eV)	$\theta_0$ (degree)	$\rho_1$ (Å)	$\rho_2$ (Å)	$r_{\min12}$ (Å)	$r_{\max12}$ (Å)	$r_{\min13}$ (Å)	$r_{\max13}$ (Å)	$r_{\min23}$ (Å)	$r_{\max23}$ (Å)
$\theta_{123}$	7.775	95.477	0.101	0.101	0.0	2.993	0.0	2.993	0.0	4.200
$\theta_{134}$	94.157	88.252	2.867	0.101	0.0	3.762	0.0	2.993	0.0	5.351
$\theta_{415}$	97.298	100.496	2.867	0.101	0.0	3.762	0.0	2.993	0.0	5.883

script used by LAMMPS as shown in Fig. 190 with  $M=Si$  and  $X=Te$ , which helps to increase the cutoff for the bond stretching interaction between atom 1 and atom 2 in Fig. 189 (c).

Fig. 192 shows the stress strain relations for the single-layer p-SiTe of size  $100 \times 100$  Å. The structure is uniaxially stretched in the armchair or zigzag directions at 1 K and 300 K. The Young's modulus is  $15.4 \text{ Nm}^{-1}$  and  $59.0 \text{ Nm}^{-1}$  in the armchair and zigzag directions respectively at 1 K, which are obtained by linear fitting of the stress strain relations in  $[0,$

TABLE CCCLXXVII: SW potential parameters for p-SiTe used by LAMMPS,<sup>9</sup> as expressed in Eqs. (9) and (10). Atom types in the first column are displayed in Fig. 190, with  $M=Si$  and  $X=Te$ .

	$\epsilon$ (eV)	$\sigma$ (Å)	$a$	$\lambda$	$\gamma$	$\cos \theta_0$	$A_L$	$B_L$	$p$	$q$	tol
Te <sub>1</sub> -Si <sub>4</sub> -Si <sub>4</sub>	1.000	7.259	0.635	8419.695	1.000	-0.095	65.141	0.013	4	0	0.0
Te <sub>1</sub> -Si <sub>1</sub> -Si <sub>1</sub>	1.000	2.867	1.312	0.000	1.000	0.000	18.792	0.431	4	0	0.0
Te <sub>1</sub> -Si <sub>4</sub> -Si <sub>1</sub>	1.000	0.000	0.000	3098.456	1.000	0.031	0.000	0.000	4	0	0.0
Se <sub>1</sub> -Ti <sub>2</sub> -Ti <sub>1</sub>	1.000	0.000	0.000	3201.825	1.000	-0.182	0.000	0.000	4	0	0.0

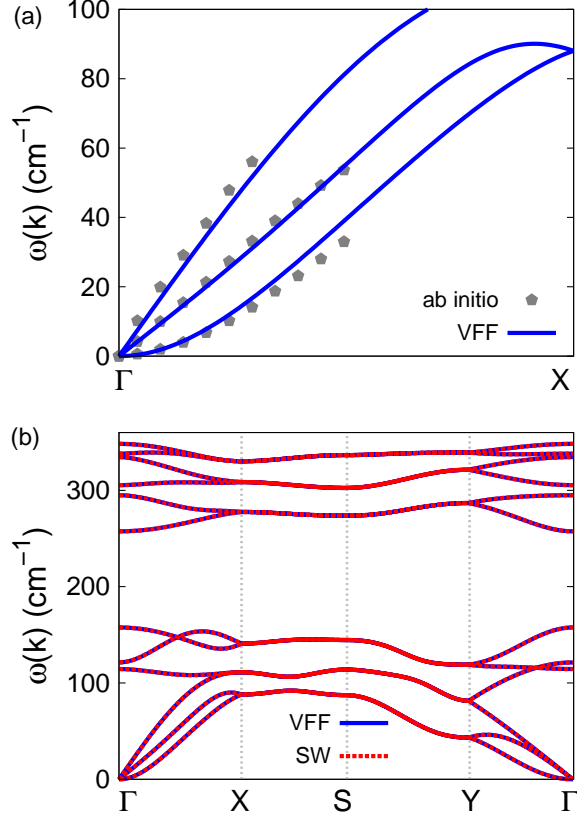


FIG. 193: (Color online) Phonon dispersion for the single-layer p-GeS. (a) The VFF model is fitted to the three acoustic branches in the long wave limit along the  $\Gamma X$  direction. The *ab initio* calculations are from Ref. 79. (b) The VFF model (blue lines) and the SW potential (red lines) give the same phonon dispersion for the p-GeS along  $\Gamma XSY\Gamma$ .

0.01]. The Poisson's ratios from the VFF model and the SW potential are  $\nu_{xy} = 0.04$  and  $\nu_{yx} = 0.17$ . The third-order nonlinear elastic constant  $D$  can be obtained by fitting the stress-strain relation to  $\sigma = E\epsilon + \frac{1}{2}D\epsilon^2$  with  $E$  as the Young's modulus. The values of  $D$  are  $-43.3 \text{ Nm}^{-1}$  and  $-468.3 \text{ Nm}^{-1}$  at 1 K along the armchair and zigzag directions, respectively. The ultimate stress is about  $2.6 \text{ Nm}^{-1}$  at the critical strain of 0.34 in the armchair direction at the low temperature of 1 K. The ultimate stress is about  $3.8 \text{ Nm}^{-1}$  at the critical strain of 0.16 in the zigzag direction at the low temperature of 1 K.

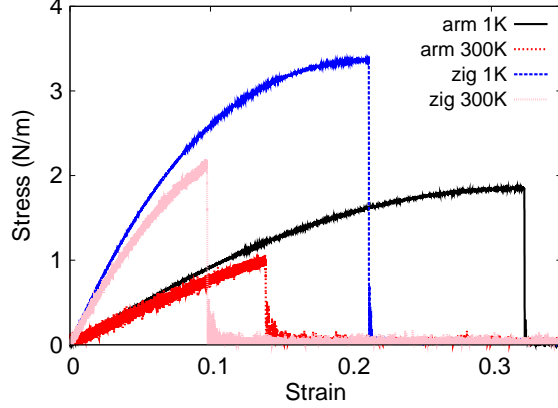


FIG. 194: (Color online) Stress-strain relations for the single-layer p-GeS of size  $100 \times 100 \text{ \AA}$ . The single-layer p-GeS is uniaxially stretched along the armchair or zigzag directions at temperatures 1 K and 300 K.

TABLE CCCLXXVIII: The VFF model for the single-layer p-GeS. The second line gives an explicit expression for each VFF term, where atom indexes are from Fig. 189 (c). The third line is the force constant parameters. Parameters are in the unit of  $\frac{eV}{\text{Å}^2}$  for the bond stretching interactions, and in the unit of eV for the angle bending interaction. The fourth line gives the initial bond length (in unit of  $\text{Å}$ ) for the bond stretching interaction and the initial angle (in unit of degrees) for the angle bending interaction. The angle  $\theta_{ijk}$  has atom  $i$  as the apex.

VFF type	bond stretching		angle bending		
expression	$\frac{1}{2}K_{12} (\Delta r_{12})^2$	$\frac{1}{2}K_{14} (\Delta r_{14})^2$	$\frac{1}{2}K_{123} (\Delta \theta_{123})^2$	$\frac{1}{2}K_{134} (\Delta \theta_{134})^2$	$\frac{1}{2}K_{415} (\Delta \theta_{415})^2$
parameter	6.364	6.364	2.153	3.896	3.896
$r_0$ or $\theta_0$	2.438	2.448	96.800	91.718	105.537

## XCV. P-GES

Present studies on the puckered (p-) GeS are based on first-principles calculations, and no empirical potential has been proposed for the p-GeS. We will thus parametrize the SW potential for the single-layer p-GeS in this section.

The structure of the single-layer p-GeS is shown in Fig. 189, with  $M=Ge$  and  $X=S$ . Structural parameters for p-GeS are from the experiment.<sup>80</sup> The experimental data are for the structure of bulk GeS, with GeS layers coupled through the weak van der Waals

TABLE CCCLXXIX: Two-body SW potential parameters for the single-layer p-GeS used by GULP,<sup>8</sup> as expressed in Eq. (3). The quantity ( $r_{ij}$ ) in the first line lists one representative term for the two-body SW potential between atoms  $i$  and  $j$ . Atom indexes are from Fig. 189 (c).

	$A$ (eV)	$\rho$ (Å)	$B$ (Å <sup>4</sup> )	$r_{\min}$ (Å)	$r_{\max}$ (Å)
$r_{12}$	1.960	0.434	21.198	0.0	2.858
$r_{14}$	10.732	2.316	21.547	0.0	3.420

TABLE CCCLXXX: Three-body SW potential parameters for the single-layer p-GeS used by GULP,<sup>8</sup> as expressed in Eq. (4). The first line ( $\theta_{ijk}$ ) presents one representative term for the three-body SW potential. The angle  $\theta_{ijk}$  has the atom  $i$  as the apex. Atom indexes are from Fig. 189 (c).

	$K$ (eV)	$\theta_0$ (degree)	$\rho_1$ (Å)	$\rho_2$ (Å)	$r_{\min12}$ (Å)	$r_{\max12}$ (Å)	$r_{\min13}$ (Å)	$r_{\max13}$ (Å)	$r_{\min23}$ (Å)	$r_{\max23}$ (Å)
$\theta_{123}$	8.629	96.800	0.434	0.434	0.0	2.858	0.0	2.858	0.0	3.973
$\theta_{134}$	59.369	91.718	2.316	0.434	0.0	3.420	0.0	2.858	0.0	4.871
$\theta_{415}$	63.895	105.537	2.316	0.434	0.0	3.420	0.0	2.858	0.0	5.175

interaction. We will use these structural data for the single-layer p-GeS, as the weak van der Waals interaction shall induce only neglectable effects on the structure within each p-GeS layer. The pucker of the p-GeS is perpendicular to the  $x$  (armchair)-direction. The bases for the rectangular unit cell are  $a_1 = 4.299$  Å and  $a_2 = 3.646$  Å. There are two Ge atoms and two S atoms in the basic unit cell, and their relative coordinates are  $(-u, 0, -v)$ ,  $(u, 0, v)$ ,  $(0.5 - u, 0.5, v + w)$ , and  $(0.5 + u, 0.5, -v + w)$  with  $u = 0.0650$ ,  $v = 0.1137$  and  $w = 0.02841$ .

TABLE CCCLXXXI: SW potential parameters for p-GeS used by LAMMPS,<sup>9</sup> as expressed in Eqs. (9) and (10). Atom types in the first column are displayed in Fig. 190 with M=Ge and X=S.

	$\epsilon$ (eV)	$\sigma$ (Å)	$a$	$\lambda$	$\gamma$	$\cos \theta_0$	$A_L$	$B_L$	$p$	$q$	tol
Ge <sub>1</sub> -S <sub>4</sub> -S <sub>4</sub>	1.000	6.563	0.620	3379.798	1.000	-0.118	62.700	0.011	4	0	0.0
Ge <sub>1</sub> -S <sub>1</sub> -S <sub>1</sub>	1.000	2.316	1.477	0.000	1.000	0.000	10.732	0.749	4	0	0.0
Ge <sub>1</sub> -S <sub>4</sub> -S <sub>1</sub>	1.000	0.000	0.000	1174.884	1.000	-0.030	0.000	0.000	4	0	0.0
S <sub>1</sub> -Ge <sub>2</sub> -Ge <sub>1</sub>	1.000	0.000	0.000	1264.559	1.000	-0.268	0.000	0.000	4	0	0.0

The value of the dimensionless parameter  $u$  is extracted from the geometrical parameters (bond lengths and bond angles) provided in Ref. 80. The dimensionless parameters  $v$  and  $w$  are ratios based on the lattice constant in the out-of-plane  $z$ -direction, i.e.,  $a_3 = 10.481 \text{ \AA}$ . We note that the main purpose of the usage of  $u$ ,  $v$ , and  $w$  in representing atomic coordinates is to follow the same convention for all puckered structures in the present work. The resultant atomic coordinates are the same as that in Ref. 80.

As shown in Fig. 189 (b), a specific feature in the puckered configuration of the p-GeS is that Ge and S atoms in the top/bottom group have different  $z$ -coordinates. Atom Ge is in the top and bottom most position. Specifically, in Fig. 189 (c), there is a difference of  $wa_3$  between the  $z$ -coordinate of atom 1 and the  $z$ -coordinates of atoms 2 and 3. Similarly, atom 4 is higher than atoms 5 and 6 for  $wa_3$  along the  $z$ -direction. As a result of the nonzero value of  $w$ , there are two different inter-group angles, i.e.,  $\theta_{134} = 91.718^\circ$  and  $\theta_{415} = 105.537^\circ$  in Fig. 189 (c). We have  $w = 0$  for the ideal puckered configuration of materials like the black phosphorus.

Table CCCLXXVIII shows five VFF terms for the single-layer p-GeS, two of which are the bond stretching interactions shown by Eq. (1) while the other three terms are the angle bending interaction shown by Eq. (2). The force constant parameters are reasonably chosen to be the same for the two bond stretching terms  $r_{12}$  and  $r_{14}$ , as these two bonds have almost the same bond length. The force constant parameters are the same for the two angle bending terms  $\theta_{134}$  and  $\theta_{415}$ , which have the same arm lengths. As a result, there are only three force constant parameters, i.e.,  $K_{12} = K_{14}$ ,  $K_{123}$ , and  $K_{134} = K_{415}$ . These three force constant parameters are determined by fitting to the three acoustic branches in the phonon dispersion along the  $\Gamma X$  as shown in Fig. 193 (a). The *ab initio* calculations are from Ref. 79. Similar phonon dispersion can also be found in other *ab initio* calculations.<sup>81</sup> Fig. 193 (b) shows that the VFF model and the SW potential give exactly the same phonon dispersion.

The parameters for the two-body SW potential used by GULP are shown in Tab. CCCLXXIX. The parameters for the three-body SW potential used by GULP are shown in Tab. CCCLXXX. Parameters for the SW potential used by LAMMPS are listed in Tab. CCCLXXXI. Eight atom types have been introduced for writing the SW potential script used by LAMMPS as shown in Fig. 190 with  $M=Ge$  and  $X=S$ , which helps to increase the cutoff for the bond stretching interaction between atom 1 and atom 2 in Fig. 189 (c).

Fig. 194 shows the stress strain relations for the single-layer p-GeS of size  $100 \times 100 \text{ \AA}$ .

TABLE CCCLXXXII: The VFF model for the single-layer p-GeSe. The second line gives an explicit expression for each VFF term, where atom indexes are from Fig. 189 (c). The third line is the force constant parameters. Parameters are in the unit of  $\frac{\text{eV}}{\text{\AA}^2}$  for the bond stretching interactions, and in the unit of eV for the angle bending interaction. The fourth line gives the initial bond length (in unit of  $\text{\AA}$ ) for the bond stretching interaction and the initial angle (in unit of degrees) for the angle bending interaction. The angle  $\theta_{ijk}$  has atom i as the apex.

VFF type	bond stretching		angle bending		
expression	$\frac{1}{2}K_{12}(\Delta r_{12})^2$	$\frac{1}{2}K_{14}(\Delta r_{14})^2$	$\frac{1}{2}K_{123}(\Delta\theta_{123})^2$	$\frac{1}{2}K_{134}(\Delta\theta_{134})^2$	$\frac{1}{2}K_{415}(\Delta\theta_{415})^2$
parameter	5.063	5.063	2.249	5.927	5.927
$r_0$ or $\theta_0$	2.574	2.564	96.228	91.296	103.481

TABLE CCCLXXXIII: Two-body SW potential parameters for the single-layer p-GeSe used by GULP,<sup>8</sup> as expressed in Eq. (3). The quantity ( $r_{ij}$ ) in the first line lists one representative term for the two-body SW potential between atoms i and j. Atom indexes are from Fig. 189 (c).

	$A$ (eV)	$\rho$ ( $\text{\AA}$ )	$B$ ( $\text{\AA}^4$ )	$r_{\min}$ ( $\text{\AA}$ )	$r_{\max}$ ( $\text{\AA}$ )
$r_{12}$	1.334	0.321	26.338	0.0	2.945
$r_{14}$	9.514	2.454	25.931	0.0	3.588

The structure is uniaxially stretched in the armchair or zigzag directions at 1 K and 300 K. The Young's modulus is  $9.9 \text{ Nm}^{-1}$  and  $36.5 \text{ Nm}^{-1}$  in the armchair and zigzag directions respectively at 1 K, which are obtained by linear fitting of the stress strain relations in  $[0, 0.01]$ . The Poisson's ratios from the VFF model and the SW potential are  $\nu_{xy} = 0.09$  and  $\nu_{yx} = 0.32$ . The third-order nonlinear elastic constant  $D$  can be obtained by fitting the stress-strain relation to  $\sigma = E\epsilon + \frac{1}{2}D\epsilon^2$  with  $E$  as the Young's modulus. The values of  $D$  are  $-22.7 \text{ Nm}^{-1}$  and  $-206.1 \text{ Nm}^{-1}$  at 1 K along the armchair and zigzag directions, respectively. The ultimate stress is about  $1.9 \text{ Nm}^{-1}$  at the critical strain of 0.32 in the armchair direction at the low temperature of 1 K. The ultimate stress is about  $3.4 \text{ Nm}^{-1}$  at the critical strain of 0.21 in the zigzag direction at the low temperature of 1 K.

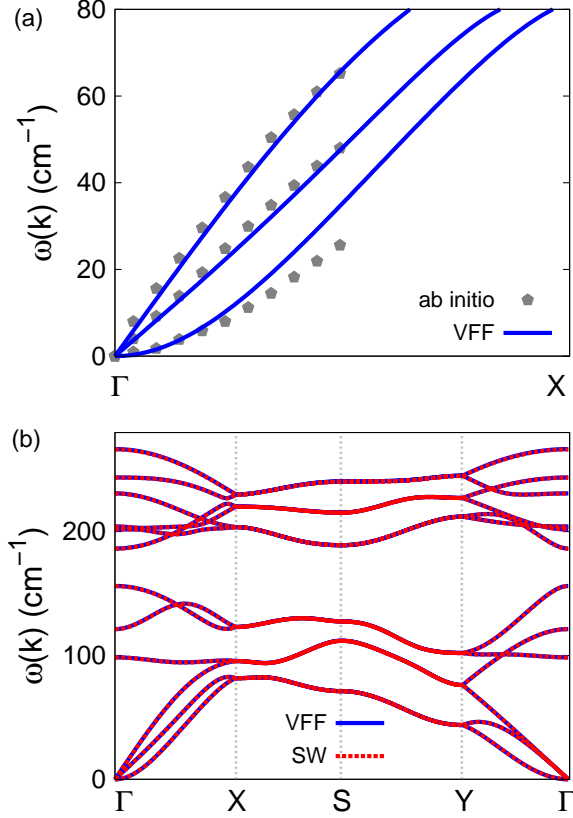


FIG. 195: (Color online) Phonon dispersion for the single-layer p-GeSe. (a) The VFF model is fitted to the three acoustic branches in the long wave limit along the  $\Gamma X$  direction. The *ab initio* calculations are from Ref. 79. (b) The VFF model (blue lines) and the SW potential (red lines) give the same phonon dispersion for the p-GeSe along  $\Gamma XSYT$ .

## XCVI. P-GESE

Present studies on the puckered (p-) GeSe are based on first-principles calculations, and no empirical potential has been proposed for the p-GeSe. We will thus parametrize the SW potential for the single-layer p-GeSe in this section.

The structure of the single-layer p-GeSe is shown in Fig. 189, with  $M=Ge$  and  $X=Se$ . Structural parameters for p-GeSe are from the experiment.<sup>80</sup> The experimental data are for the structure of bulk GeSe, with GeSe layers coupled through the weak van der Waals interaction. We will use these structural data for the single-layer p-GeSe, as the weak van der Waals interaction shall induce only neglectable effects on the structure within each p-GeSe

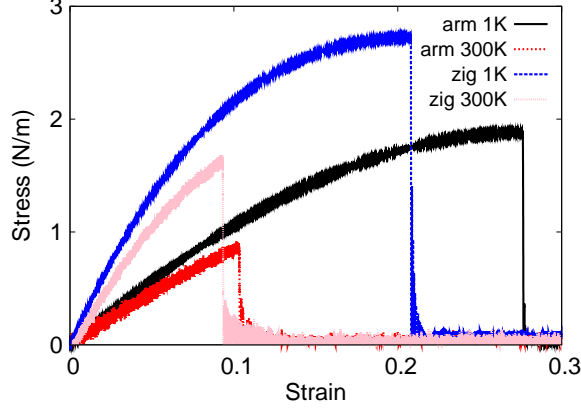


FIG. 196: (Color online) Stress-strain relations for the single-layer p-GeSe of size  $100 \times 100 \text{ \AA}$ . The single-layer p-GeSe is uniaxially stretched along the armchair or zigzag directions at temperatures 1 K and 300 K.

TABLE CCCLXXXIV: Three-body SW potential parameters for the single-layer p-GeSe used by GULP,<sup>8</sup> as expressed in Eq. (4). The first line ( $\theta_{ijk}$ ) presents one representative term for the three-body SW potential. The angle  $\theta_{ijk}$  has the atom  $i$  as the apex. Atom indexes are from Fig. 189 (c).

	$K$ (eV)	$\theta_0$ (degree)	$\rho_1$ ( $\text{\AA}$ )	$\rho_2$ ( $\text{\AA}$ )	$r_{\min 12}$ ( $\text{\AA}$ )	$r_{\max 12}$ ( $\text{\AA}$ )	$r_{\min 13}$ ( $\text{\AA}$ )	$r_{\max 13}$ ( $\text{\AA}$ )	$r_{\min 23}$ ( $\text{\AA}$ )	$r_{\max 23}$ ( $\text{\AA}$ )
$\theta_{123}$	6.416	96.228	0.321	0.321	0.0	2.945	0.0	2.945	0.0	4.111
$\theta_{134}$	77.319	91.296	2.454	0.321	0.0	3.588	0.0	2.945	0.0	5.112
$\theta_{415}$	81.721	103.481	2.454	0.321	0.0	3.588	0.0	2.945	0.0	5.397

layer. The pucker of the p-GeSe is perpendicular to the  $x$  (armchair)-direction. The bases for the rectangular unit cell are  $a_1 = 4.388 \text{ \AA}$  and  $a_2 = 3.833 \text{ \AA}$ . There are two Ge atoms and two Se atoms in the basic unit cell, and their relative coordinates are  $(-u, 0, -v)$ ,  $(u, 0, v)$ ,  $(0.5 - u, 0.5, v + w)$ , and  $(0.5 + u, 0.5, -v + w)$  with  $u = 0.0567$ ,  $v = 0.1162$  and  $w = 0.02551$ . The value of the dimensionless parameter  $u$  is extracted from the geometrical parameters (bond lengths and bond angles) provided in Ref. 80. The dimensionless parameters  $v$  and  $w$  are ratios based on the lattice constant in the out-of-plane  $z$ -direction, i.e.,  $a_3 = 10.825 \text{ \AA}$ . We note that the main purpose of the usage of  $u$ ,  $v$ , and  $w$  in representing atomic coordinates is to follow the same convention for all puckered structures in the present work. The resultant atomic coordinates are the same as that in Ref. 80.

TABLE CCCLXXXV: SW potential parameters for p-GeSe used by LAMMPS,<sup>9</sup> as expressed in Eqs. (9) and (10). Atom types in the first column are displayed in Fig. 190 with M=Ge and X=Se.

	$\epsilon$ (eV)	$\sigma$ (Å)	$a$	$\lambda$	$\gamma$	$\cos \theta_0$	$A_L$	$B_L$	$p$	$q$	tol
Ge <sub>1</sub> -Se <sub>4</sub> -Se <sub>4</sub>	1.000	6.848	0.626	3360.535	1.000	-0.108	54.241	0.012	4	0	0.0
Ge <sub>1</sub> -Se <sub>1</sub> -Se <sub>1</sub>	1.000	2.454	1.462	0.000	1.000	0.000	9.514	0.715	4	0	0.0
Ge <sub>1</sub> -Se <sub>4</sub> -Se <sub>1</sub>	1.000	0.000	0.000	1769.546	1.000	-0.023	0.000	0.000	4	0	0.0
Se <sub>1</sub> -Ge <sub>2</sub> -Ge <sub>1</sub>	1.000	0.000	0.000	1870.284	1.000	-0.233	0.000	0.000	4	0	0.0

As shown in Fig. 189 (b), a specific feature in the puckered configuration of the p-GeSe is that Ge and Se atoms in the top/bottom group have different z-coordinates. Atom Ge is in the top and bottom most position. Specifically, in Fig. 189 (c), there is a difference of  $wa_3$  between the z-coordinate of atom 1 and the z-coordinates of atoms 2 and 3. Similarly, atom 4 is higher than atoms 5 and 6 for  $wa_3$  along the z-direction. As a result of the nonzero value of  $w$ , there are two different inter-group angles, i.e.,  $\theta_{134} = 91.296^\circ$  and  $\theta_{415} = 103.481^\circ$  in Fig. 189 (c). We have  $w = 0$  for the ideal puckered configuration of materials like the black phosphorus.

Table CCCLXXXII shows five VFF terms for the single-layer p-GeSe, two of which are the bond stretching interactions shown by Eq. (1) while the other three terms are the angle bending interaction shown by Eq. (2). The force constant parameters are reasonably chosen to be the same for the two bond stretching terms  $r_{12}$  and  $r_{14}$ , as these two bonds have almost the same bond length. The force constant parameters are the same for the two angle bending terms  $\theta_{134}$  and  $\theta_{415}$ , which have the same arm lengths. As a result, there are only three force constant parameters, i.e.,  $K_{12} = K_{14}$ ,  $K_{123}$ , and  $K_{134} = K_{415}$ . These three force constant parameters are determined by fitting to the three acoustic branches in the phonon dispersion along the  $\Gamma X$  as shown in Fig. 195 (a). The *ab initio* calculations are from Ref. 79. Similar phonon dispersion can also be found in other *ab initio* calculations.<sup>81</sup> Fig. 195 (b) shows that the VFF model and the SW potential give exactly the same phonon dispersion.

The parameters for the two-body SW potential used by GULP are shown in Tab. CCCLXXXIII. The parameters for the three-body SW potential used by GULP are shown in Tab. CCCLXXXIV. Parameters for the SW potential used by LAMMPS are listed in Tab. CCCLXXXV. Eight atom types have been introduced for writing the SW potential

TABLE CCCLXXXVI: The VFF model for the single-layer p-SnS. The second line gives an explicit expression for each VFF term, where atom indexes are from Fig. 189 (c). The third line is the force constant parameters. Parameters are in the unit of  $\frac{\text{eV}}{\text{\AA}^2}$  for the bond stretching interactions, and in the unit of eV for the angle bending interaction. The fourth line gives the initial bond length (in unit of  $\text{\AA}$ ) for the bond stretching interaction and the initial angle (in unit of degrees) for the angle bending interaction. The angle  $\theta_{ijk}$  has atom i as the apex.

VFF type	bond stretching		angle bending		
expression	$\frac{1}{2}K_{12}(\Delta r_{12})^2$	$\frac{1}{2}K_{14}(\Delta r_{14})^2$	$\frac{1}{2}K_{123}(\Delta\theta_{123})^2$	$\frac{1}{2}K_{134}(\Delta\theta_{134})^2$	$\frac{1}{2}K_{415}(\Delta\theta_{415})^2$
parameter	4.163	4.163	1.776	5.841	5.841
$r_0$ or $\theta_0$	2.665	2.627	96.830	89.042	103.294

script used by LAMMPS as shown in Fig. 190 with M=Ge and X=Se, which helps to increase the cutoff for the bond stretching interaction between atom 1 and atom 2 in Fig. 189 (c).

Fig. 196 shows the stress strain relations for the single-layer p-GeSe of size  $100 \times 100 \text{\AA}$ . The structure is uniaxially stretched in the armchair or zigzag directions at 1 K and 300 K. The Young's modulus is  $11.7 \text{ Nm}^{-1}$  and  $31.1 \text{ Nm}^{-1}$  in the armchair and zigzag directions respectively at 1 K, which are obtained by linear fitting of the stress strain relations in  $[0, 0.01]$ . The Poisson's ratios from the VFF model and the SW potential are  $\nu_{xy} = 0.12$  and  $\nu_{yx} = 0.33$ . The third-order nonlinear elastic constant  $D$  can be obtained by fitting the stress-strain relation to  $\sigma = E\epsilon + \frac{1}{2}D\epsilon^2$  with E as the Young's modulus. The values of  $D$  are  $-29.0 \text{ Nm}^{-1}$  and  $-182.3 \text{ Nm}^{-1}$  at 1 K along the armchair and zigzag directions, respectively. The ultimate stress is about  $1.9 \text{ Nm}^{-1}$  at the critical strain of 0.28 in the armchair direction at the low temperature of 1 K. The ultimate stress is about  $2.7 \text{ Nm}^{-1}$  at the critical strain of 0.21 in the zigzag direction at the low temperature of 1 K.

## XCVII. P-SNS

Present studies on the puckered (p-) SnS are based on first-principles calculations, and no empirical potential has been proposed for the p-SnS. We will thus parametrize the SW potential for the single-layer p-SnS in this section.

The structure of the single-layer p-SnS is shown in Fig. 189, with M=Sn and X=S.

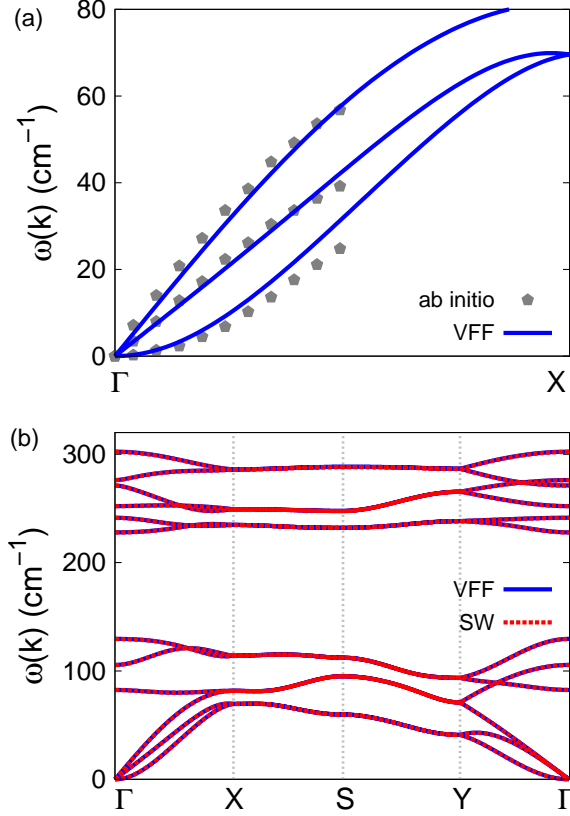


FIG. 197: (Color online) Phonon dispersion for the single-layer p-SnS. (a) The VFF model is fitted to the three acoustic branches in the long wave limit along the  $\Gamma X$  direction. The *ab initio* calculations are from Ref. 79. (b) The VFF model (blue lines) and the SW potential (red lines) give the same phonon dispersion for the p-SnS along  $\Gamma X S \bar{Y} T$ .

Structural parameters for p-SnS are from the experiment.<sup>80</sup> The experimental data are for the structure of bulk SnS, with p-SnS layers coupled through the weak van der Waals interaction. We will use these structural data for the single-layer p-SnS, as the weak van der Waals interaction shall induce only neglectable effects on the structure within each p-SnS layer. The pucker of the p-SnS is perpendicular to the x (armchair)-direction. The bases for the rectangular unit cell are  $a_1 = 4.334 \text{ \AA}$  and  $a_2 = 3.987 \text{ \AA}$ . There are two Sn atoms and two S atoms in the basic unit cell, and their relative coordinates are  $(-u, 0, -v)$ ,  $(u, 0, v)$ ,  $(0.5 - u, 0.5, v + w)$ , and  $(0.5 + u, 0.5, -v + w)$  with  $u = 0.04975$ ,  $v = 0.1157$  and  $w = 0.02975$ . The value of the dimensionless parameter  $u$  is extracted from the geometrical parameters (bond lengths and bond angles) provided in Ref. 80. The dimensionless parameters  $v$  and  $w$

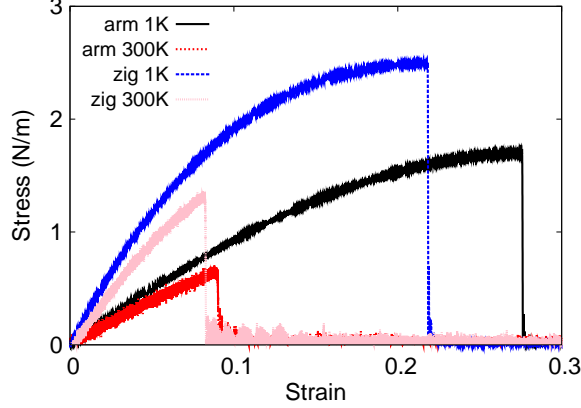


FIG. 198: (Color online) Stress-strain relations for the single-layer p-SnS of size  $100 \times 100 \text{ \AA}$ . The single-layer p-SnS is uniaxially stretched along the armchair or zigzag directions at temperatures 1 K and 300 K.

TABLE CCCLXXXVII: Two-body SW potential parameters for the single-layer p-SnS used by GULP,<sup>8</sup> as expressed in Eq. (3). The quantity  $(r_{ij})$  in the first line lists one representative term for the two-body SW potential between atoms  $i$  and  $j$ . Atom indexes are from Fig. 189 (c).

	$A$ (eV)	$\rho$ ( $\text{\AA}$ )	$B$ ( $\text{\AA}^4$ )	$r_{\min}$ ( $\text{\AA}$ )	$r_{\max}$ ( $\text{\AA}$ )
$r_{12}$	0.889	0.221	30.265	0.0	2.978
$r_{14}$	8.755	2.635	28.575	0.0	3.701

are ratios based on the lattice constant in the out-of-plane  $z$ -direction, i.e.,  $a_3 = 11.200 \text{ \AA}$ . We note that the main purpose of the usage of  $u$ ,  $v$ , and  $w$  in representing atomic coordinates is to follow the same convention for all puckered structures in the present work. The resultant atomic coordinates are the same as that in Ref. 80.

As shown in Fig. 189 (b), a specific feature in the puckered configuration of the p-SnS is that Sn and S atoms in the top/bottom group have different  $z$ -coordinates. Atom Sn is in the top and bottom most position. Specifically, in Fig. 189 (c), there is a difference of  $wa_3$  between the  $z$ -coordinate of atom 1 and the  $z$ -coordinates of atoms 2 and 3. Similarly, atom 4 is higher than atoms 5 and 6 for  $wa_3$  along the  $z$ -direction. As a result of the nonzero value of  $w$ , there are two different inter-group angles, i.e.,  $\theta_{134} = 89.042^\circ$  and  $\theta_{415} = 103.294^\circ$  in Fig. 189 (c). We have  $w = 0$  for the ideal puckered configuration of materials like the black phosphorus.

TABLE CCCLXXXVIII: Three-body SW potential parameters for the single-layer p-SnS used by GULP,<sup>8</sup> as expressed in Eq. (4). The first line ( $\theta_{ijk}$ ) presents one representative term for the three-body SW potential. The angle  $\theta_{ijk}$  has the atom i as the apex. Atom indexes are from Fig. 189 (c).

	$K$ (eV)	$\theta_0$ (degree)	$\rho_1$ (Å)	$\rho_2$ (Å)	$r_{\min 12}$ (Å)	$r_{\max 12}$ (Å)	$r_{\min 13}$ (Å)	$r_{\max 13}$ (Å)	$r_{\min 23}$ (Å)	$r_{\max 23}$ (Å)
$\theta_{123}$	3.687	96.830	0.221	0.221	0.0	2.978	0.0	2.978	0.0	4.161
$\theta_{134}$	68.698	89.042	2.635	0.221	0.0	3.701	0.0	2.978	0.0	5.231
$\theta_{415}$	72.512	103.294	2.635	0.221	0.0	3.701	0.0	2.978	0.0	5.576

TABLE CCCLXXXIX: SW potential parameters for p-SnS used by LAMMPS,<sup>9</sup> as expressed in Eqs. (9) and (10). Atom types in the first column are displayed in Fig. 190 with M=Sn and X=S.

	$\epsilon$ (eV)	$\sigma$ (Å)	$a$	$\lambda$	$\gamma$	$\cos \theta_0$	$A_L$	$B_L$	$p$	$q$	tol
Sn <sub>1</sub> -S <sub>4</sub> -S <sub>4</sub>	1.000	7.182	0.620	2800.319	1.000	-0.119	49.119	0.011	4	0	0.0
Sn <sub>1</sub> -S <sub>1</sub> -S <sub>1</sub>	1.000	2.635	1.405	0.000	1.000	0.000	8.755	0.593	4	0	0.0
Sn <sub>1</sub> -S <sub>4</sub> -S <sub>1</sub>	1.000	0.000	0.000	1893.224	1.000	0.017	0.000	0.000	4	0	0.0
S <sub>1</sub> -Sn <sub>2</sub> -Sn <sub>1</sub>	1.000	0.000	0.000	1998.361	1.000	-0.230	0.000	0.000	4	0	0.0

Table CCCLXXXVI shows five VFF terms for the single-layer p-SnS, two of which are the bond stretching interactions shown by Eq. (1) while the other three terms are the angle bending interaction shown by Eq. (2). The force constant parameters are reasonably chosen to be the same for the two bond stretching terms  $r_{12}$  and  $r_{14}$ , as these two bonds have almost the same bond length. The force constant parameters are the same for the two angle bending terms  $\theta_{134}$  and  $\theta_{415}$ , which have the same arm lengths. As a result, there are only three force constant parameters, i.e.,  $K_{12} = K_{14}$ ,  $K_{123}$ , and  $K_{134} = K_{415}$ . These three force constant parameters are determined by fitting to the three acoustic branches in the phonon dispersion along the  $\Gamma X$  as shown in Fig. 197 (a). The *ab initio* calculations are from Ref. 79. Similar phonon dispersion can also be found in other *ab initio* calculations.<sup>81</sup> Fig. 197 (b) shows that the VFF model and the SW potential give exactly the same phonon dispersion.

The parameters for the two-body SW potential used by GULP are shown in Tab. CCCLXXXVII. The parameters for the three-body SW potential used by GULP are shown in Tab. CCCLXXXVIII. Parameters for the SW potential used by LAMMPS are

TABLE CCCXC: The VFF model for the single-layer p-SnSe. The second line gives an explicit expression for each VFF term, where atom indexes are from Fig. 189 (c). The third line is the force constant parameters. Parameters are in the unit of  $\frac{\text{eV}}{\text{\AA}^2}$  for the bond stretching interactions, and in the unit of eV for the angle bending interaction. The fourth line gives the initial bond length (in unit of  $\text{\AA}$ ) for the bond stretching interaction and the initial angle (in unit of degrees) for the angle bending interaction. The angle  $\theta_{ijk}$  has atom i as the apex.

VFF type	bond stretching		angle bending		
expression	$\frac{1}{2}K_{12}(\Delta r_{12})^2$	$\frac{1}{2}K_{14}(\Delta r_{14})^2$	$\frac{1}{2}K_{123}(\Delta\theta_{123})^2$	$\frac{1}{2}K_{134}(\Delta\theta_{134})^2$	$\frac{1}{2}K_{415}(\Delta\theta_{415})^2$
parameter	3.872	3.872	3.157	7.674	7.674
$r_0$ or $\theta_0$	2.793	2.743	96.050	88.980	101.570

listed in Tab. CCCLXXXIX. Eight atom types have been introduced for writing the SW potential script used by LAMMPS as shown in Fig. 190 with M=Sn and X=S, which helps to increase the cutoff for the bond stretching interaction between atom 1 and atom 2 in Fig. 189 (c).

Fig. 198 shows the stress strain relations for the single-layer p-SnS of size  $100 \times 100 \text{ \AA}$ . The structure is uniaxially stretched in the armchair or zigzag directions at 1 K and 300 K. The Young's modulus is  $10.0 \text{ Nm}^{-1}$  and  $26.9 \text{ Nm}^{-1}$  in the armchair and zigzag directions respectively at 1 K, which are obtained by linear fitting of the stress strain relations in  $[0, 0.01]$ . The Poisson's ratios from the VFF model and the SW potential are  $\nu_{xy} = 0.16$  and  $\nu_{yx} = 0.42$ . The third-order nonlinear elastic constant  $D$  can be obtained by fitting the stress-strain relation to  $\sigma = E\epsilon + \frac{1}{2}D\epsilon^2$  with E as the Young's modulus. The values of  $D$  are  $-21.0 \text{ Nm}^{-1}$  and  $-149.8 \text{ Nm}^{-1}$  at 1 K along the armchair and zigzag directions, respectively. The ultimate stress is about  $1.7 \text{ Nm}^{-1}$  at the critical strain of 0.28 in the armchair direction at the low temperature of 1 K. The ultimate stress is about  $2.5 \text{ Nm}^{-1}$  at the critical strain of 0.22 in the zigzag direction at the low temperature of 1 K.

### XCVIII. P-SNSE

Present studies on the puckered (p-) SnSe are based on first-principles calculations, and no empirical potential has been proposed for the p-SnSe. We will thus parametrize the SW

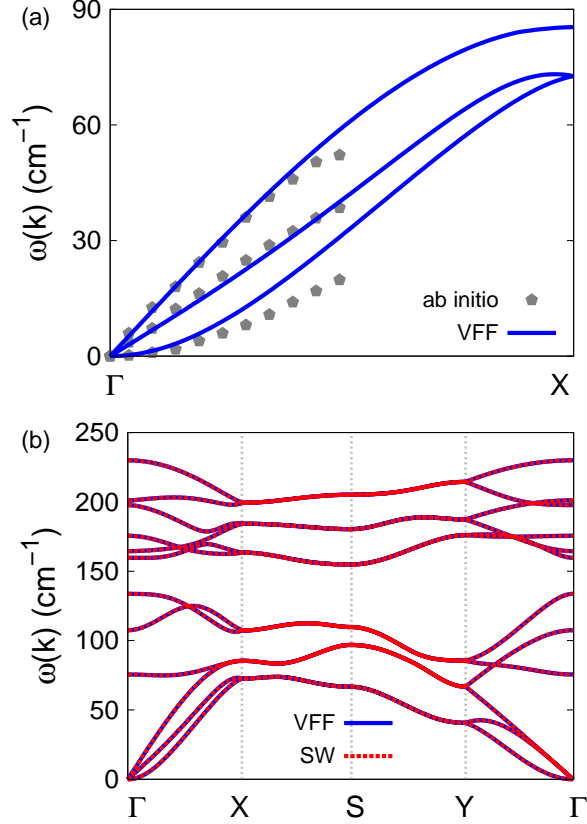


FIG. 199: (Color online) Phonon dispersion for the single-layer p-SnSe. (a) The VFF model is fitted to the three acoustic branches in the long wave limit along the  $\Gamma X$  direction. The *ab initio* calculations are from Ref. 82. (b) The VFF model (blue lines) and the SW potential (red lines) give the same phonon dispersion for the p-SnSe along  $\Gamma X S \bar{Y} \Gamma$ .

potential for the single-layer p-SnSe in this section.

The structure of the single-layer p-SnSe is shown in Fig. 189 with  $M=\text{Sn}$  and  $X=\text{Se}$ . Structural parameters for p-SnSe are from the experiment.<sup>80</sup> The experimental data are for the structure of bulk SnSe, with SnSe layers coupled through the weak van der Waals interaction. We will use these structural data for the single-layer p-SnSe, as the weak van der Waals interaction shall induce only neglectable effects on the structure within each p-SnSe layer. The pucker of the p-SnSe is perpendicular to the x (armchair)-direction. The bases for the rectangular unit cell are  $a_1 = 4.445 \text{ \AA}$  and  $a_2 = 4.153 \text{ \AA}$ . There are two Sn atoms and two Se atoms in the basic unit cell, and their relative coordinates are  $(-u, 0, -v)$ ,  $(u, 0, v)$ ,  $(0.5 - u, 0.5, v + w)$ , and  $(0.5 + u, 0.5, -v + w)$  with  $u = 0.0427$ ,  $v = 0.1181$  and  $w = 0.02678$ .

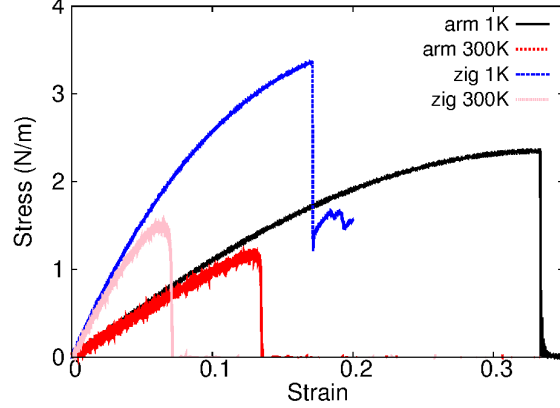


FIG. 200: (Color online) Stress-strain relations for the single-layer p-SnSe of size  $100 \times 100 \text{ \AA}$ . The single-layer p-SnSe is uniaxially stretched along the armchair or zigzag directions at temperatures 1 K and 300 K.

TABLE CCCXCI: Two-body SW potential parameters for the single-layer p-SnSe used by GULP,<sup>8</sup> as expressed in Eq. (3). The quantity  $(r_{ij})$  in the first line lists one representative term for the two-body SW potential between atoms  $i$  and  $j$ . Atom indexes are from Fig. 189 (c).

	$A$ (eV)	$\rho$ ( $\text{\AA}$ )	$B$ ( $\text{\AA}^4$ )	$r_{\min}$ ( $\text{\AA}$ )	$r_{\max}$ ( $\text{\AA}$ )
$r_{12}$	0.767	0.109	30.427	0.0	3.069
$r_{14}$	8.642	2.846	28.306	0.0	4.140

The value of the dimensionless parameter  $u$  is extracted from the geometrical parameters (bond lengths and bond angles) provided in Ref. 80. The dimensionless parameters  $v$  and  $w$  are ratios based on the lattice constant in the out-of-plane  $z$ -direction, i.e.,  $a_3 = 11.501 \text{ \AA}$ . We note that the main purpose of the usage of  $u$ ,  $v$ , and  $w$  in representing atomic coordinates is to follow the same convention for all puckered structures in the present work. The resultant atomic coordinates are the same as that in Ref. 80.

As shown in Fig. 189 (b), a specific feature in the puckered configuration of the p-SnSe is that Sn and Se atoms in the top/bottom group have different  $z$ -coordinates. Specifically, in Fig. 189 (c), there is a difference of  $wa_3$  between the  $z$ -coordinate of atom 1 and the  $z$ -coordinates of atoms 2 and 3. Similarly, atom 4 is higher than atoms 5 and 6 for  $wa_3$  along the  $z$ -direction. As a result of the nonzero value of  $w$ , there are two different inter-group angles, i.e.,  $\theta_{134} = 88.98^\circ$  and  $\theta_{415} = 101.57^\circ$  in Fig. 189 (c). We have  $w = 0$  for the ideal

TABLE CCCXCII: Three-body SW potential parameters for the single-layer p-SnSe used by GULP,<sup>8</sup> as expressed in Eq. (4). The first line ( $\theta_{ijk}$ ) presents one representative term for the three-body SW potential. The angle  $\theta_{ijk}$  has the atom i as the apex. Atom indexes are from Fig. 189 (c).

	$K$ (eV)	$\theta_0$ (degree)	$\rho_1$ (Å)	$\rho_2$ (Å)	$r_{\min 12}$ (Å)	$r_{\max 12}$ (Å)	$r_{\min 13}$ (Å)	$r_{\max 13}$ (Å)	$r_{\min 23}$ (Å)	$r_{\max 23}$ (Å)
$\theta_{123}$	3.519	96.050	0.109	0.109	0.0	3.069	0.0	3.069	0.0	4.229
$\theta_{134}$	43.705	88.980	2.846	0.109	0.0	4.140	0.0	3.069	0.0	5.634
$\theta_{415}$	45.523	101.570	2.846	0.109	0.0	3.069	0.0	4.140	0.0	5.950

TABLE CCCXCIII: SW potential parameters for p-SnSe used by LAMMPS,<sup>9</sup> as expressed in Eqs. (9) and (10). Atom types in the first column are displayed in Fig. 190, with M=Sn and X=Se.

	$\epsilon$ (eV)	$\sigma$ (Å)	$a$	$\lambda$	$\gamma$	$\cos \theta_0$	$A_L$	$B_L$	$p$	$q$	tol
Sn <sub>3</sub> -Se <sub>2</sub> -Se <sub>2</sub>	1.000	4.933	0.942	324.990	1.000	-0.105	17.943	0.051	4	0	0.0
Sn <sub>1</sub> -Se <sub>1</sub> -Se <sub>1</sub>	1.000	1.819	2.122	0.000	1.000	0.000	5.338	2.586	4	0	0.0
Sn <sub>3</sub> -Se <sub>2</sub> -Se <sub>3</sub>	1.000	0.000	0.000	279.207	0.000	0.018	0.000	0.000	4	0	0.0
Se <sub>1</sub> -Sn <sub>2</sub> -Sn <sub>1</sub>	1.000	0.000	0.000	290.818	0.000	-0.201	0.000	0.000	4	0	0.0

puckered configuration of materials like the black phosphorus.

Table CCCXC shows five VFF terms for the single-layer p-SnSe, two of which are the bond stretching interactions shown by Eq. (1) while the other three terms are the angle bending interaction shown by Eq. (2). The force constant parameters are reasonably chosen to be the same for the two bond stretching terms  $r_{12}$  and  $r_{14}$ , as these two bonds have almost the same bond length. The force constant parameters are the same for the two angle bending terms  $\theta_{134}$  and  $\theta_{415}$ , which have the same arm lengths. As a result, there are only three force constant parameters, i.e.,  $K_{12} = K_{14}$ ,  $K_{123}$ , and  $K_{134} = K_{415}$ . These three force constant parameters are determined by fitting to the three acoustic branches in the phonon dispersion along the  $\Gamma X$  as shown in Fig. 199 (a). The *ab initio* calculations are from Ref. 82. Fig. 199 (b) shows that the VFF model and the SW potential give exactly the same phonon dispersion.

The parameters for the two-body SW potential used by GULP are shown in Tab. CCCXCI. The parameters for the three-body SW potential used by GULP are shown

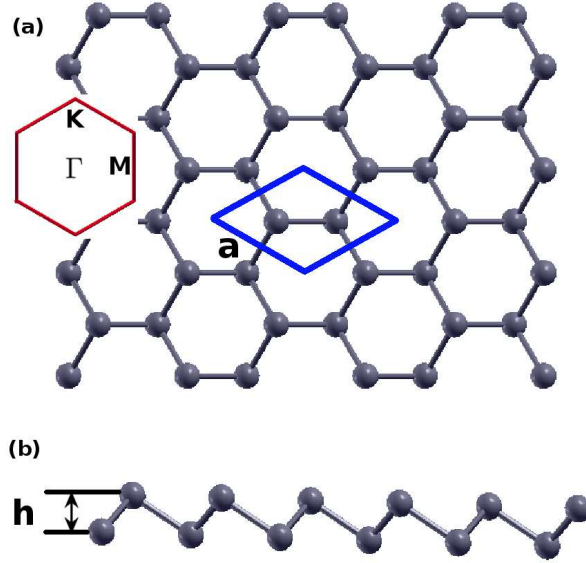


FIG. 201: (Color online) Structure for the buckled M, with M from group V. (a) Top view. The armchair direction is along the horizontal direction, while the zigzag direction is along the vertical direction. The unit cell is displayed by the blue rhombus. Inset shows the first Brillouin zone. (b) Side view illustrates the buckled configuration of height  $h$ .

in Tab. CCCXCII. Parameters for the SW potential used by LAMMPS are listed in Tab. CCCXCIII. Eight atom types have been introduced for writing the SW potential script used by LAMMPS as shown in Fig. 190 with M=Sn and X=Se, which technically increases the cutoff for the bond stretching interaction between atom 1 and atom 2 in Fig. 189 (c).

Fig. 200 shows the stress strain relations for the single-layer p-SnSe of size  $100 \times 100 \text{ \AA}$ . The structure is uniaxially stretched in the armchair or zigzag directions at 1 K and 300 K. The Young's modulus is  $11.9 \text{ Nm}^{-1}$  and  $35.7 \text{ Nm}^{-1}$  in the armchair and zigzag directions respectively at 1 K, which are obtained by linear fitting of the stress strain relations in  $[0, 0.01]$ . The Poisson's ratios from the VFF model and the SW potential are  $\nu_{xy} = 0.09$  and  $\nu_{yx} = 0.27$ . The third-order nonlinear elastic constant  $D$  can be obtained by fitting the stress-strain relation to  $\sigma = E\epsilon + \frac{1}{2}D\epsilon^2$  with E as the Young's modulus. The values of  $D$  are  $-25.9 \text{ Nm}^{-1}$  and  $-196.0 \text{ Nm}^{-1}$  at 1 K along the armchair and zigzag directions, respectively. The ultimate stress is about  $2.1 \text{ Nm}^{-1}$  at the critical strain of 0.33 in the armchair direction at the low temperature of 1 K. The ultimate stress is about  $3.4 \text{ Nm}^{-1}$  at the critical strain of 0.17 in the zigzag direction at the low temperature of 1 K.

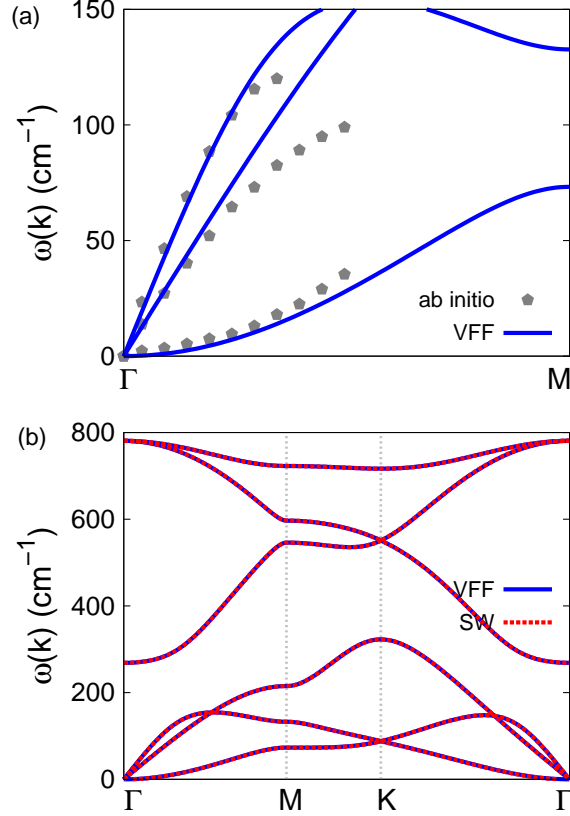


FIG. 202: (Color online) Phonon dispersion for the silicene. (a) The VFF model is fitted to the three acoustic branches in the long wave limit along the  $\Gamma M$  direction. The *ab initio* results (gray pentagons) are from Ref. 83. (b) The VFF model (blue lines) and the SW potential (red lines) give the same phonon dispersion for the silicene along  $\Gamma M K \Gamma$ .

## XCIX. SILICENE

There have been several empirical potentials available for the silicene. A many-body potential based on the Lennard-Jones and Axilrod-Teller functions was used to describe the interaction within the single-layer silicene.<sup>84</sup> The modified embedded-atom potential<sup>85</sup> was used by Pei et al to simulate the thermal transport in the single-layer silicene in 2013.<sup>86</sup> The environment-dependent interatomic potential<sup>87</sup> was also used to simulate the silicene.<sup>88</sup> In particular, the original set of SW parameters<sup>4</sup> for the silicon were found to be not suitable for the planar silicene, so two sets of optimized parameters for the SW potential were proposed to simulate the thermal conductivity in the single-layer silicene in 2014.<sup>89</sup> We will develop a

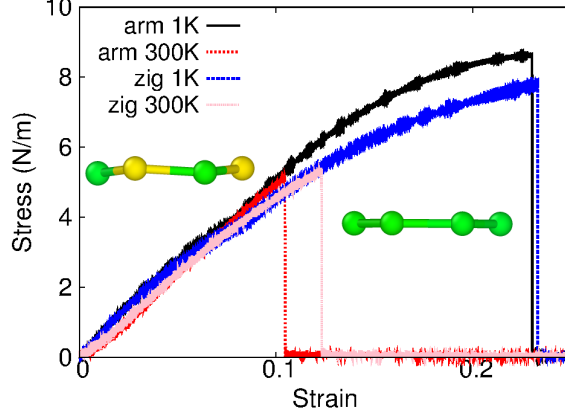


FIG. 203: (Color online) Stress-strain relations for the silicene of size  $100 \times 100 \text{ \AA}$ . The silicene is uniaxially stretched along the armchair or zigzag directions at temperatures 1 K and 300 K. Left inset shows the buckled configuration for the silicene at the uniaxial strain 0.07 at 1 K along the armchair direction. Right inset: the buckled configuration becomes planar for the silicene at the uniaxial strain of 0.08 at 1 K along the armchair direction.

TABLE CCCXCIV: The VFF model for silicene. The second line gives an explicit expression for each VFF term. The third line is the force constant parameters. Parameters are in the unit of  $\frac{eV}{\text{\AA}^2}$  for the bond stretching interactions, and in the unit of eV for the angle bending interaction. The fourth line gives the initial bond length (in unit of  $\text{\AA}$ ) for the bond stretching interaction and the initial angle (in unit of degrees) for the angle bending interaction.

VFF type	bond stretching	angle bending
expression	$\frac{1}{2}K_r (\Delta r)^2$	$\frac{1}{2}K_\theta (\Delta \theta)^2$
parameter	18.387	3.465
$r_0$ or $\theta_0$	2.279	116.218

new SW potential to describe the interaction within the silicene in this section, with specific focus on the mechanical properties of the silicene.

The structure of the silicene is shown in Fig. 201, with structural parameters from the *ab initio* calculations.<sup>83</sup> The silicene has a buckled configuration as shown in Fig. 201 (b), where the buckle is along the zigzag direction. The height of the buckle is  $h = 0.45 \text{ \AA}$  and the lattice constant is  $3.87 \text{ \AA}$ , which results in a bond length of  $2.279 \text{ \AA}$ .

TABLE CCCXCV: Two-body SW potential parameters for silicene used by GULP,<sup>8</sup> as expressed in Eq. (3).

	$A$ (eV)	$\rho$ (Å)	$B$ (Å <sup>4</sup> )	$r_{\min}$ (Å)	$r_{\max}$ (Å)
Si-Si	19.343	1.668	16.186	0.0	3.075

TABLE CCCXCVI: Three-body SW potential parameters for silicene used by GULP,<sup>8</sup> as expressed in Eq. (4).

	$K$ (eV)	$\theta_0$ (degree)	$\rho_1$ (Å)	$\rho_2$ (Å)	$r_{\min12}$ (Å)	$r_{\max12}$ (Å)	$r_{\min13}$ (Å)	$r_{\max13}$ (Å)	$r_{\min23}$ (Å)	$r_{\max23}$ (Å)
Si-Si-Si	142.310	116.218	1.668	1.668	0.0	3.075	0.0	3.075	3.075	4.181

Table CCCXCIV shows the VFF model for the silicene. The force constant parameters are determined by fitting to the three acoustic branches in the phonon dispersion along the  $\Gamma M$  as shown in Fig. 202 (a). The *ab initio* calculations for the phonon dispersion are from Ref. 83. Similar phonon dispersion can also be found in other *ab initio* calculations.<sup>83,90–101</sup> Fig. 202 (b) shows that the VFF model and the SW potential give exactly the same phonon dispersion, as the SW potential is derived from the VFF model.

We note that the present SW potential is fitted perfectly to the three acoustic phonon branches, so it can give a nice description for the elastic deformation of the silicene. As a trade off, the optical phonons are overestimated by the present SW potential. Hence, the present SW potential is in particular suitable for the simulation of mechanical or thermal processes which are dominated by acoustic phonons, while the present SW potential may cause a systematic error for the optical absorption process which mainly involves the optical phonons. One can introduce the long-range interactions (eg. the second-nearest-neighboring interaction) to give a good description for both acoustic and optical phonon branches, see one such example for borophene in Ref. 14. It is because the long-range interaction mainly contributes to the acoustic phonon branches, while it makes only neglectable contribution

TABLE CCCXCVII: SW potential parameters for silicene used by LAMMPS,<sup>9</sup> as expressed in Eqs. (9) and (10).

	$\epsilon$ (eV)	$\sigma$ (Å)	$a$	$\lambda$	$\gamma$	$\cos \theta_0$	$A_L$	$B_L$	$p$	$q$	tol
Si-Si-Si	1.000	1.668	1.844	142.310	1.000	-0.442	19.343	2.091	4	0	0.0

to the optical phonon branches. As another solution, the SW potential can give reasonable descriptions for the optical phonon branches by reducing its accuracy in describing acoustic phonon branches as done in Ref. 89.

The parameters for the two-body SW potential used by GULP are shown in Tab. CCCXCV. The parameters for the three-body SW potential used by GULP are shown in Tab. CCCXCVI. Parameters for the SW potential used by LAMMPS are listed in Tab. CCCXCVII.

Fig. 203 shows the stress strain relations for the silicene of size  $100 \times 100 \text{ \AA}$ . The structure is uniaxially stretched in the armchair or zigzag directions at 1 K and 300 K. The Young's modulus is  $63.3 \text{ Nm}^{-1}$  in both armchair and zigzag directions at 1 K, which are obtained by linear fitting of the stress strain relations in  $[0, 0.01]$ . The Young's modulus is isotropic for the silicene. The value of the Young's modulus agrees with the value of  $63.8 \text{ Nm}^{-1}$  from the *ab initio* calculations.<sup>102</sup> The Poisson's ratios from the VFF model and the SW potential are  $\nu_{xy} = \nu_{yx} = 0.15$ , which are smaller but comparable with the *ab initio* results of 0.325.<sup>102</sup> The third-order nonlinear elastic constant  $D$  can be obtained by fitting the stress-strain relation to  $\sigma = E\epsilon + \frac{1}{2}D\epsilon^2$  with  $E$  as the Young's modulus. The values of  $D$  are  $-212.5 \text{ Nm}^{-1}$  and  $-267.5 \text{ Nm}^{-1}$  at 1 K along the armchair and zigzag directions, respectively. The ultimate stress is about  $8.6 \text{ Nm}^{-1}$  at the critical strain of 0.23 in the armchair direction at the low temperature of 1 K. The ultimate stress is about  $7.8 \text{ Nm}^{-1}$  at the critical strain of 0.23 in the zigzag direction at the low temperature of 1 K.

The stress-strain curves shown in Fig. 203 disclose a structural transition at the strain around 0.076 for the silicene at the low temperature of 1 K. The buckled configuration of the silicene is flattened during this structural transition, which can be seen from these two insets in Fig. 203. This structural transition was also observed in the *ab initio* calculations,<sup>94</sup> where the critical strain for the structural transition is 0.2. At temperatures above 300 K, this structural transition is blurred by stronger thermal vibrations; i.e., the buckled configuration of the silicene can be strongly disturbed by the thermal vibration at higher temperatures.

### C. GERMANENE

In a recent work, the Tersoff potential was applied to simulate the thermal conductivity of the germanene nanoribbon.<sup>103</sup> We will provide the SW potential to describe the interaction

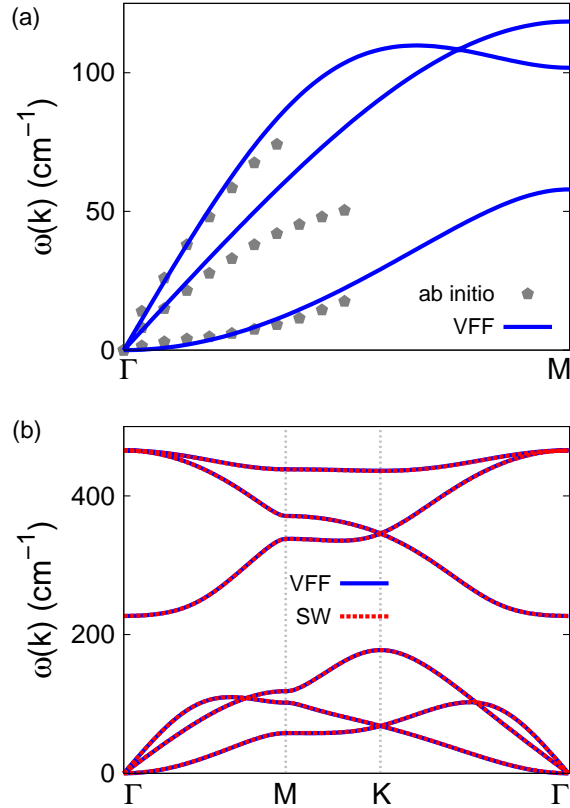


FIG. 204: (Color online) Phonon dispersion for the germanene. (a) The VFF model is fitted to the three acoustic branches in the long wave limit along the  $\Gamma\text{M}$  direction. The *ab initio* results (gray pentagons) are from Ref. 83. (b) The VFF model (blue lines) and the SW potential (red lines) give the same phonon dispersion for the germanene along  $\Gamma\text{MK}\Gamma$ .

within the germanene in this section.

The structure of the germanene is shown in Fig. 201, with structural parameters from the *ab initio* calculations.<sup>83</sup> The germanene has a buckled configuration as shown in Fig. 201 (b), where the buckle is along the zigzag direction. The height of the buckle is  $h = 0.69 \text{ \AA}$  and the lattice constant is  $4.06 \text{ \AA}$ , which results in a bond length of  $2.443 \text{ \AA}$ .

Table CCCXCVIII shows the VFF model for the germanene. The force constant parameters are determined by fitting to the three acoustic branches in the phonon dispersion along the  $\Gamma\text{M}$  as shown in Fig. 204 (a). The *ab initio* calculations for the phonon dispersion are from Ref. 83. Similar phonon dispersion can also be found in other *ab initio* calculations.<sup>83,91,92,97,100,101,104</sup> Fig. 204 (b) shows that the VFF model and the SW poten-

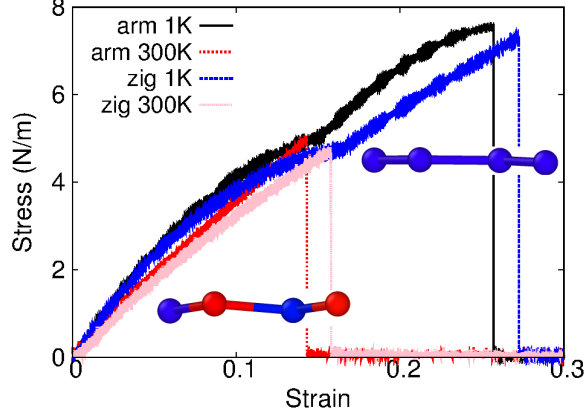


FIG. 205: (Color online) Stress-strain relations for the germanene of size  $100 \times 100 \text{ \AA}$ . The germanene is uniaxially stretched along the armchair or zigzag directions at temperatures 1 K and 300 K. Left bottom inset shows the buckled configuration for the germanene at the uniaxial strain 0.14 at 1 K along the armchair direction. Right top inset: the buckled configuration becomes planar for the germanene at the uniaxial strain of 0.16 at 1 K along the armchair direction.

TABLE CCCXCVIII: The VFF model for germanene. The second line gives an explicit expression for each VFF term. The third line is the force constant parameters. Parameters are in the unit of  $\frac{\text{eV}}{\text{\AA}^2}$  for the bond stretching interactions, and in the unit of eV for the angle bending interaction. The fourth line gives the initial bond length (in unit of  $\text{\AA}$ ) for the bond stretching interaction and the initial angle (in unit of degrees) for the angle bending interaction.

VFF type	bond stretching	angle bending
expression	$\frac{1}{2}K_r (\Delta r)^2$	$\frac{1}{2}K_\theta (\Delta \theta)^2$
parameter	18.387	3.465
$r_0$ or $\theta_0$	2.443	112.358

tial give exactly the same phonon dispersion, as the SW potential is derived from the VFF model.

The parameters for the two-body SW potential used by GULP are shown in Tab. CCCXCIX. The parameters for the three-body SW potential used by GULP are shown in Tab. CD. Parameters for the SW potential used by LAMMPS are listed in Tab. CDI.

Fig. 205 shows the stress strain relations for the germanene of size  $100 \times 100 \text{ \AA}$ . The

TABLE CCCXCIX: Two-body SW potential parameters for germanene used by GULP,<sup>8</sup> as expressed in Eq. (3).

	$A$ (eV)	$\rho$ (Å)	$B$ (Å <sup>4</sup> )	$r_{\min}$ (Å)	$r_{\max}$ (Å)
Ge-Ge	19.570	1.607	21.372	0.0	3.252

TABLE CD: Three-body SW potential parameters for germanene used by GULP,<sup>8</sup> as expressed in Eq. (4).

	$K$ (eV)	$\theta_0$ (degree)	$\rho_1$ (Å)	$\rho_2$ (Å)	$r_{\min12}$ (Å)	$r_{\max12}$ (Å)	$r_{\min13}$ (Å)	$r_{\max13}$ (Å)	$r_{\min23}$ (Å)	$r_{\max23}$ (Å)
Ge-Ge-Ge	107.735	112.358	1.607	1.607	0.0	3.252	0.0	3.252	3.252	4.4

structure is uniaxially stretched in the armchair or zigzag directions at 1 K and 300 K. The Young's modulus is 53.2 Nm<sup>-1</sup> in both armchair and zigzag directions at 1 K, which are obtained by linear fitting of the stress strain relations in [0, 0.01]. The Young's modulus is isotropic for the germanene. The Poisson's ratios from the VFF model and the SW potential are  $\nu_{xy} = \nu_{yx} = 0.19$ . The third-order nonlinear elastic constant  $D$  can be obtained by fitting the stress-strain relation to  $\sigma = E\epsilon + \frac{1}{2}D\epsilon^2$  with  $E$  as the Young's modulus. The values of  $D$  are -229.2 Nm<sup>-1</sup> and -278.2 Nm<sup>-1</sup> at 1 K along the armchair and zigzag directions, respectively. The ultimate stress is about 7.5 Nm<sup>-1</sup> at the critical strain of 0.26 in the armchair direction at the low temperature of 1 K. The ultimate stress is about 7.3 Nm<sup>-1</sup> at the critical strain of 0.27 in the zigzag direction at the low temperature of 1 K.

The stress-strain curves shown in Fig. 205 disclose a structural transition for the germanene at the low temperature of 1 K. The critical strains for the structural transition are 0.15 and 0.16 along the armchair and zigzag directions, respectively. The buckled configuration of the germanene is flattened during this structural transition, which can be seen from these two insets in Fig. 205. At temperatures above 300 K, this structural transition is blurred by stronger thermal vibrations; i.e., the buckled configuration of the germanene

TABLE CDI: SW potential parameters for germanene used by LAMMPS,<sup>9</sup> as expressed in Eqs. (9) and (10).

	$\epsilon$ (eV)	$\sigma$ (Å)	$a$	$\lambda$	$\gamma$	$\cos \theta_0$	$A_L$	$B_L$	$p$	$q$	tol
Ge-Ge-Ge	1.000	1.607	2.024	107.735	1.000	-0.380	19.570	3.205	4	0	0.0

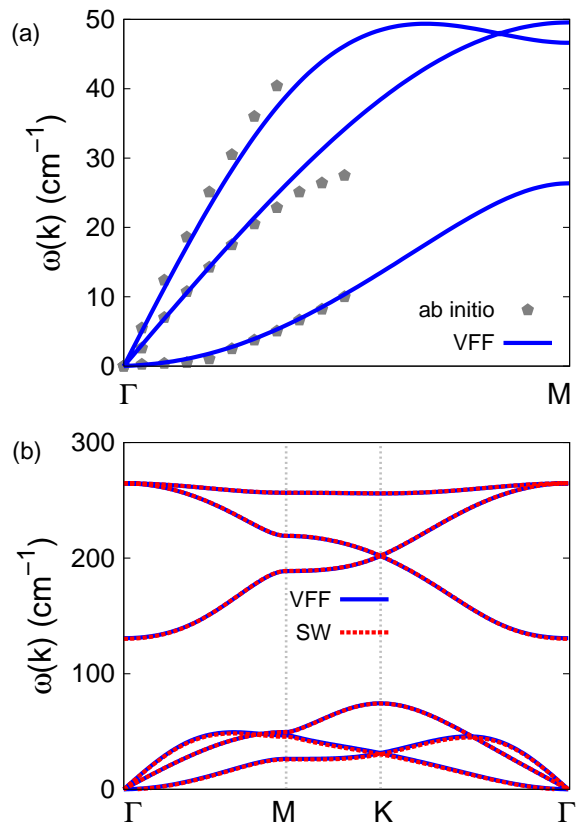


FIG. 206: (Color online) Phonon dispersion for the stanene. (a) The VFF model is fitted to the three acoustic branches in the long wave limit along the  $\Gamma$ M direction. The *ab initio* results (gray pentagons) are from Ref. 104. (b) The VFF model (blue lines) and the SW potential (red lines) give the same phonon dispersion for the stanene along  $\Gamma$ MKT.

can be strongly disturbed by the thermal vibration at higher temperatures.

## CI. STANENE

There are several available empirical potentials for the description of the interaction within the stanene. The modified embedded atom method potential was applied to simulate mechanical properties for the stanene.<sup>105</sup> A VFF model was fitted for the stanene in 2015.<sup>106</sup> The Tersoff potential was parameterized to describe the interaction for stanene.<sup>107</sup> In this section, we will develop the SW potential for the stanene.

The structure of the stanene is shown in Fig. 201, with structural parameters from the

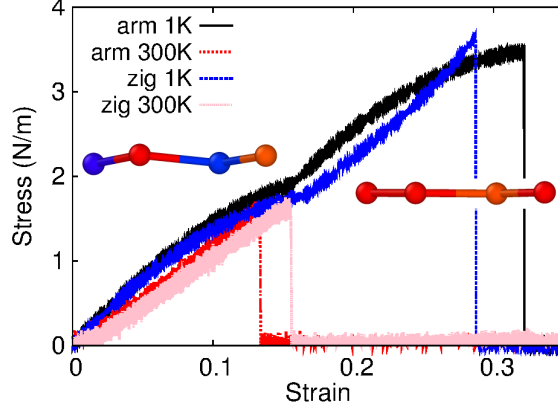


FIG. 207: (Color online) Stress-strain relations for the stanene of size  $100 \times 100 \text{ \AA}$ . The stanene is uniaxially stretched along the armchair or zigzag directions at temperatures 1 K and 300 K. Left inset: the buckled configuration for the stanene at the uniaxial strain 0.14 at 1 K along the armchair direction. Right inset: the buckled configuration becomes planar for the stanene at the uniaxial strain of 0.16 at 1 K along the armchair direction.

TABLE CDII: The VFF model for stanene. The second line gives an explicit expression for each VFF term. The third line is the force constant parameters. Parameters are in the unit of  $\frac{\text{eV}}{\text{\AA}^2}$  for the bond stretching interactions, and in the unit of eV for the angle bending interaction. The fourth line gives the initial bond length (in unit of  $\text{\AA}$ ) for the bond stretching interaction and the initial angle (in unit of degrees) for the angle bending interaction.

VFF type	bond stretching	angle bending
expression	$\frac{1}{2}K_r (\Delta r)^2$	$\frac{1}{2}K_\theta (\Delta\theta)^2$
parameter	10.489	1.372
$r_0$ or $\theta_0$	2.836	111.224

*ab initio* calculations.<sup>104</sup> The stanene has a buckled configuration as shown in Fig. 201 (b), where the buckle is along the zigzag direction. The height of the buckle is  $h = 0.86 \text{ \AA}$  and the lattice constant is  $4.68 \text{ \AA}$ , which results in a bond length of  $2.836 \text{ \AA}$ .

Table CDII shows the VFF model for the stanene. The force constant parameters are determined by fitting to the three acoustic branches in the phonon dispersion along the  $\Gamma\text{M}$  as shown in Fig. 206 (a). The *ab initio* calculations for the phonon dispersion are from

TABLE CDIII: Two-body SW potential parameters for stanene used by GULP,<sup>8</sup> as expressed in Eq. (3).

	$A$ (eV)	$\rho$ (Å)	$B$ (Å <sup>4</sup> )	$r_{\min}$ (Å)	$r_{\max}$ (Å)
Sn-Sn	19.542	2.227	42.047	0.0	3.758

TABLE CDIV: Three-body SW potential parameters for stanene used by GULP,<sup>8</sup> as expressed in Eq. (4).

	$K$ (eV)	$\theta_0$ (degree)	$\rho_1$ (Å)	$\rho_2$ (Å)	$r_{\min12}$ (Å)	$r_{\max12}$ (Å)	$r_{\min13}$ (Å)	$r_{\max13}$ (Å)	$r_{\min23}$ (Å)	$r_{\max23}$ (Å)
Sn-Sn-Sn	98.863	111.224	2.227	2.227	0.0	3.758	0.0	3.758	3.758	5.076

Ref. 104 with the spin-orbit coupling effect. Similar phonon dispersion can also be found in other *ab initio* calculations.<sup>100,101,104,108–110</sup> Fig. 206 (b) shows that the VFF model and the SW potential give exactly the same phonon dispersion, as the SW potential is derived from the VFF model.

The parameters for the two-body SW potential used by GULP are shown in Tab. CDIII. The parameters for the three-body SW potential used by GULP are shown in Tab. CDIV. Parameters for the SW potential used by LAMMPS are listed in Tab. CDV.

Fig. 207 shows the stress strain relations for the stanene of size  $100 \times 100$  Å. The structure is uniaxially stretched in the armchair or zigzag directions at 1 K and 300 K. The Young's modulus is  $17.0 \text{ Nm}^{-1}$  in both armchair and zigzag directions at 1 K, which are obtained by linear fitting of the stress strain relations in  $[0, 0.01]$ . The Young's modulus is isotropic for the stanene. The Poisson's ratios from the VFF model and the SW potential are  $\nu_{xy} = \nu_{yx} = 0.29$ . The third-order nonlinear elastic constant  $D$  can be obtained by fitting the stress-strain relation to  $\sigma = E\epsilon + \frac{1}{2}D\epsilon^2$  with  $E$  as the Young's modulus. The values of  $D$  are  $-37.2 \text{ Nm}^{-1}$  and  $-69.4 \text{ Nm}^{-1}$  at 1 K along the armchair and zigzag directions, respectively. The ultimate stress is about  $3.5 \text{ Nm}^{-1}$  at the critical strain of 0.32 in the armchair direction

TABLE CDV: SW potential parameters for stanene used by LAMMPS,<sup>9</sup> as expressed in Eqs. (9) and (10).

	$\epsilon$ (eV)	$\sigma$ (Å)	$a$	$\lambda$	$\gamma$	$\cos \theta_0$	$A_L$	$B_L$	$p$	$q$	tol
Sn-Sn-Sn	1.000	2.227	1.687	98.863	1.000	-0.362	19.542	1.709	4	0	0.0

TABLE CDVI: The VFF model for indiene. The second line gives an explicit expression for each VFF term. The third line is the force constant parameters. Parameters are in the unit of  $\frac{\text{eV}}{\text{\AA}^2}$  for the bond stretching interactions, and in the unit of eV for the angle bending interaction. The fourth line gives the initial bond length (in unit of  $\text{\AA}$ ) for the bond stretching interaction and the initial angle (in unit of degrees) for the angle bending interaction.

VFF type	bond stretching	angle bending
expression	$\frac{1}{2}K_r (\Delta r)^2$	$\frac{1}{2}K_\theta (\Delta\theta)^2$
parameter	2.128	1.175
$r_0$ or $\theta_0$	2.890	94.372

TABLE CDVII: Two-body SW potential parameters for indiene used by GULP,<sup>8</sup> as expressed in Eq. (3).

	$A$ (eV)	$\rho$ ( $\text{\AA}$ )	$B$ ( $\text{\AA}^4$ )	$r_{\min}$ ( $\text{\AA}$ )	$r_{\max}$ ( $\text{\AA}$ )
In-In	1.537	0.946	41.855	0.0	3.565

at the low temperature of 1 K. The ultimate stress is about  $3.6 \text{ Nm}^{-1}$  at the critical strain of 0.29 in the zigzag direction at the low temperature of 1 K.

The stress-strain curves shown in Fig. 207 disclose a structural transition for the stanene at the low temperature of 1 K. The critical strain for the structural transition is about 0.15 along the armchair and zigzag directions. The buckled configuration of the stanene is flattened during this structural transition, which can be seen from these two insets in Fig. 207. At temperatures above 300 K, this structural transition is blurred by stronger thermal vibrations; i.e., the buckled configuration of the stanene can be strongly disturbed by the thermal vibration at higher temperatures.

## CII. INDIENE

In this section, we will develop the SW potential for the indiene, i.e., the single layer of Indium atoms. The structure of the indiene is shown in Fig. 201, with structural parameters from the *ab initio* calculations.<sup>111</sup> The indiene has a buckled configuration as shown in Fig. 201 (b), where the buckle is along the zigzag direction. The lattice constant is  $4.24 \text{ \AA}$

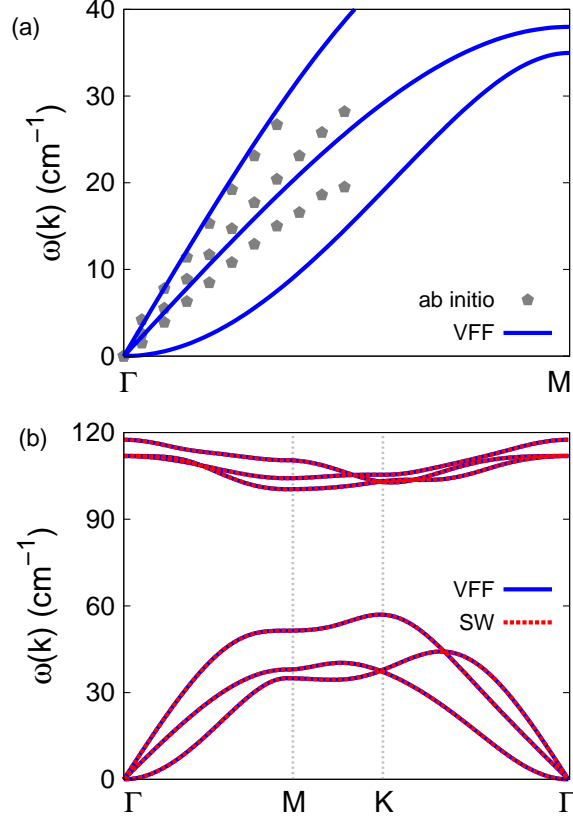


FIG. 208: (Color online) Phonon dispersion for the indiene. (a) The VFF model is fitted to the three acoustic branches in the long wave limit along the  $\Gamma M$  direction. The *ab initio* results (gray pentagons) are from Ref. 111. (b) The VFF model (blue lines) and the SW potential (red lines) give the same phonon dispersion for the indiene along  $\Gamma M K \Gamma$ .

TABLE CDVIII: Three-body SW potential parameters for indiene used by GULP,<sup>8</sup> as expressed in Eq. (4).

	$K$ (eV)	$\theta_0$ (degree)	$\rho_1$ (Å)	$\rho_2$ (Å)	$r_{\min 12}$ (Å)	$r_{\max 12}$ (Å)	$r_{\min 13}$ (Å)	$r_{\max 13}$ (Å)	$r_{\min 23}$ (Å)	$r_{\max 23}$ (Å)
In-In-In	9.745	94.372	0.946	0.946	0.0	3.565	0.0	4.565	3.565	4.686

and the bond length is 2.89 Å, which results in the buckling height of  $h = 1.536$  Å.

Table CDVI shows the VFF model for the indiene. The force constant parameters are determined by fitting to the three acoustic branches in the phonon dispersion along the  $\Gamma M$  as shown in Fig. 208 (a). The *ab initio* calculations for the phonon dispersion are from Ref. 111. We note that the lowest-frequency branch around the  $\Gamma$  point from the VFF model is lower

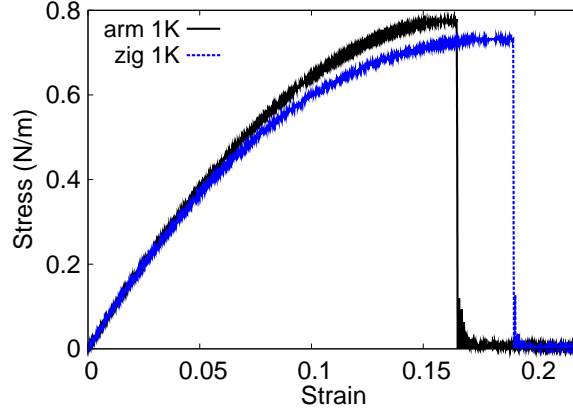


FIG. 209: (Color online) Stress-strain relations for the indiene of size  $100 \times 100 \text{ \AA}$ . The indiene is uniaxially stretched along the armchair or zigzag directions at temperatures 1 K.

TABLE CDIX: SW potential parameters for indiene used by LAMMPS,<sup>9</sup> as expressed in Eqs. (9) and (10).

	$\epsilon$ (eV)	$\sigma$ ( $\text{\AA}$ )	$a$	$\lambda$	$\gamma$	$\cos \theta_0$	$A_L$	$B_L$	$p$	$q$	tol
In-In-In	1.000	0.946	3.768	9.745	1.000	-0.076	1.537	52.262	4	0	0.0

than the *ab initio* results. This branch is the flexural branch, which should be a quadratic dispersion. However, the *ab initio* calculations give a linear dispersion for the flexural branch due to the violation of the rigid rotational invariance in the first-principles package,<sup>20</sup> so *ab initio* calculations typically overestimate the frequency of this branch. Fig. 208 (b) shows that the VFF model and the SW potential give exactly the same phonon dispersion, as the SW potential is derived from the VFF model.

The parameters for the two-body SW potential used by GULP are shown in Tab. CDVII. The parameters for the three-body SW potential used by GULP are shown in Tab. CDVIII. Parameters for the SW potential used by LAMMPS are listed in Tab. CDIX.

Fig. 209 shows the stress strain relations for the indiene of size  $100 \times 100 \text{ \AA}$ . The structure is uniaxially stretched in the armchair or zigzag directions at 1 K. The Young's modulus is  $8.4 \text{ Nm}^{-1}$  in both armchair and zigzag directions at 1 K, which are obtained by linear fitting of the stress strain relations in  $[0, 0.01]$ . The Young's modulus of the indiene is very small; i.e., the indiene is very soft. As a result, we find that the structure becomes unstable at room temperature. The Poisson's ratios from the VFF model and the SW potential are

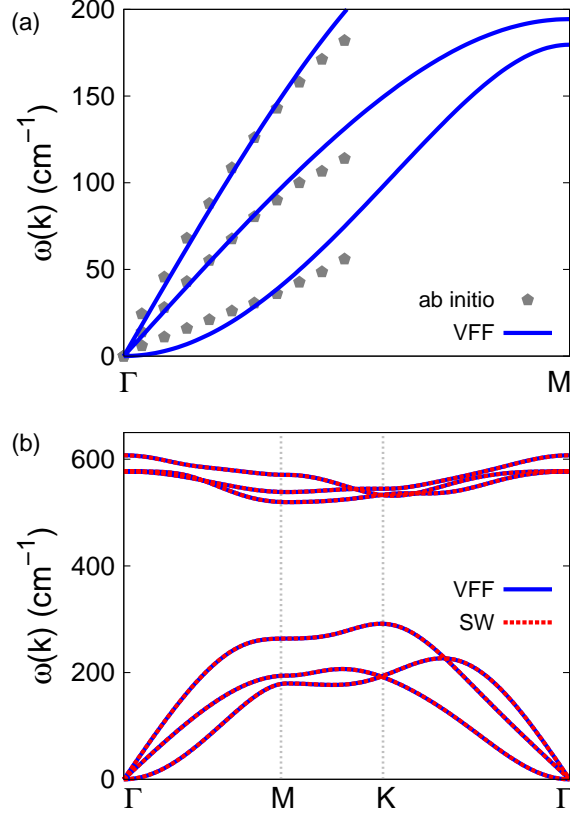


FIG. 210: (Color online) Phonon dispersion for the single-layer blue phosphorus. (a) The VFF model is fitted to the three acoustic branches in the long wave limit along the  $\Gamma$ M direction. The *ab initio* results (gray pentagons) are from Ref. 55. (b) The VFF model (blue lines) and the SW potential (red lines) give the same phonon dispersion for the blue phosphorus along  $\Gamma$ MKT.

$\nu_{xy} = \nu_{yx} = 0.18$ . The third-order nonlinear elastic constant  $D$  can be obtained by fitting the stress-strain relation to  $\sigma = E\epsilon + \frac{1}{2}D\epsilon^2$  with  $E$  as the Young's modulus. The values of  $D$  are  $-42.0 \text{ Nm}^{-1}$  and  $-50.2 \text{ Nm}^{-1}$  at 1 K along the armchair and zigzag directions, respectively. The ultimate stress is about  $0.77 \text{ Nm}^{-1}$  at the critical strain of 0.16 in the armchair direction at the low temperature of 1 K. The ultimate stress is about  $0.73 \text{ Nm}^{-1}$  at the critical strain of 0.19 in the zigzag direction at the low temperature of 1 K.

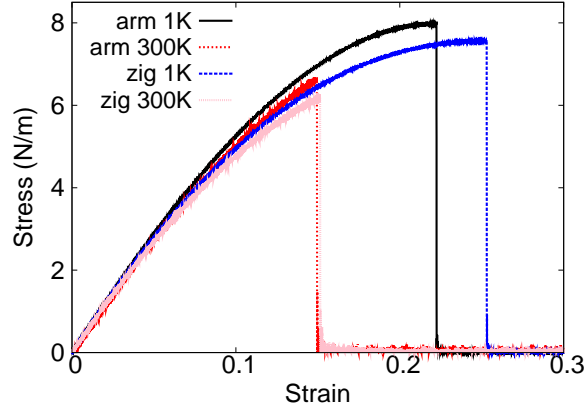


FIG. 211: (Color online) Stress-strain relations for the blue phosphorus of size  $100 \times 100 \text{ \AA}$ . The blue phosphorus is uniaxially stretched along the armchair or zigzag directions at temperatures 1 K and 300 K.

TABLE CDX: The VFF model for blue phosphorus. The second line gives an explicit expression for each VFF term. The third line is the force constant parameters. Parameters are in the unit of  $\frac{\text{eV}}{\text{\AA}^2}$  for the bond stretching interactions, and in the unit of eV for the angle bending interaction. The fourth line gives the initial bond length (in unit of  $\text{\AA}$ ) for the bond stretching interaction and the initial angle (in unit of degrees) for the angle bending interaction.

VFF type	bond stretching	angle bending
expression	$\frac{1}{2}K_r (\Delta r)^2$	$\frac{1}{2}K_\theta (\Delta \theta)^2$
parameter	15.372	5.138
$r_0$ or $\theta_0$	2.270	94.209

TABLE CDXI: Two-body SW potential parameters for blue phosphorus used by GULP,<sup>8</sup> as expressed in Eq. (3).

	$A$ (eV)	$\rho$ ( $\text{\AA}$ )	$B$ ( $\text{\AA}^4$ )	$r_{\min}$ ( $\text{\AA}$ )	$r_{\max}$ ( $\text{\AA}$ )
P-P	5.706	0.491	13.276	0.0	2.798

TABLE CDXII: Three-body SW potential parameters for blue phosphorus used by GULP,<sup>8</sup> as expressed in Eq. (4).

	$K$ (eV)	$\theta_0$ (degree)	$\rho_1$ (Å)	$\rho_2$ (Å)	$r_{\min 12}$ (Å)	$r_{\max 12}$ (Å)	$r_{\min 13}$ (Å)	$r_{\max 13}$ (Å)	$r_{\min 23}$ (Å)	$r_{\max 23}$ (Å)
P-P-P	16.605	94.209	0.491	0.491	0.0	2.798	0.0	2.798	2.798	3.677

TABLE CDXIII: SW potential parameters for blue phosphorus used by LAMMPS,<sup>9</sup> as expressed in Eqs. (9) and (10).

	$\epsilon$ (eV)	$\sigma$ (Å)	$a$	$\lambda$	$\gamma$	$\cos \theta_0$	$A_L$	$B_L$	$p$	$q$	tol
P-P-P	1.000	0.491	5.699	16.605	1.000	-0.073	5.706	228.424	4	0	0.0

### CIII. BLUE PHOSPHORUS

The blue phosphorus is also named  $\beta$ -phosphorus. Present studies on the blue phosphorus are based on first-principles calculations, and no empirical potential has been proposed for the blue phosphorus. We will thus parametrize a set of VFF model for the single-layer blue phosphorus in this section. We will also derive the SW potential based on the VFF model for the single-layer blue phosphorus.

The structure of the single-layer blue phosphorus is shown in Fig. 201, with structural parameters from the *ab initio* calculations.<sup>55</sup> The blue phosphorus has a buckled configuration as shown in Fig. 201 (b), where the buckle is along the zigzag direction. The height of the buckle is  $h = 1.211$  Å. The lattice constant is 3.326 Å, and the bond length is 2.270 Å.

Table CDX shows the VFF model for the single-layer blue phosphorus. The force constant parameters are determined by fitting to the three acoustic branches in the phonon dispersion along the  $\Gamma M$  as shown in Fig. 210 (a). The *ab initio* calculations for the phonon dispersion are from Ref. 55. Similar phonon dispersion can also be found in other *ab initio* calculations.<sup>61,64,83</sup> Fig. 210 (b) shows that the VFF model and the SW potential give exactly the same phonon dispersion, as the SW potential is derived from the VFF model.

The parameters for the two-body SW potential used by GULP are shown in Tab. CDXI. The parameters for the three-body SW potential used by GULP are shown in Tab. CDXII. Parameters for the SW potential used by LAMMPS are listed in Tab. CDXIII.

Fig. 211 shows the stress strain relations for the single-layer blue phosphorus of size  $100 \times 100$  Å. The structure is uniaxially stretched in the armchair or zigzag directions at

TABLE CDXIV: The VFF model for b-arsenene. The second line gives an explicit expression for each VFF term. The third line is the force constant parameters. Parameters are in the unit of  $\frac{eV}{\text{\AA}^2}$  for the bond stretching interactions, and in the unit of eV for the angle bending interaction. The fourth line gives the initial bond length (in unit of  $\text{\AA}$ ) for the bond stretching interaction and the initial angle (in unit of degrees) for the angle bending interaction.

VFF type	bond stretching	angle bending
expression	$\frac{1}{2}K_r (\Delta r)^2$	$\frac{1}{2}K_\theta (\Delta\theta)^2$
parameter	15.372	5.138
$r_0$ or $\theta_0$	2.510	91.964

TABLE CDXV: Two-body SW potential parameters for b-arsenene used by GULP,<sup>8</sup> as expressed in Eq. (3).

	$A$ (eV)	$\rho$ ( $\text{\AA}$ )	$B$ ( $\text{\AA}^4$ )	$r_{\min}$ ( $\text{\AA}$ )	$r_{\max}$ ( $\text{\AA}$ )
As-As	6.418	0.482	19.846	0.0	3.060

1 K and 300 K. The Young's modulus is  $60.5 \text{ Nm}^{-1}$  and  $60.6 \text{ Nm}^{-1}$  in the armchair and zigzag directions respectively at 1 K, which are obtained by linear fitting of the stress strain relations in  $[0, 0.01]$ . The Young's modulus is isotropic for the blue phosphorus. The Poisson's ratios from the VFF model and the SW potential are  $\nu_{xy} = \nu_{yx} = 0.18$ . The third-order nonlinear elastic constant  $D$  can be obtained by fitting the stress-strain relation to  $\sigma = E\epsilon + \frac{1}{2}D\epsilon^2$  with  $E$  as the Young's modulus. The values of  $D$  are  $-195.3 \text{ Nm}^{-1}$  and  $-237.0 \text{ Nm}^{-1}$  at 1 K along the armchair and zigzag directions, respectively. The ultimate stress is about  $8.0 \text{ Nm}^{-1}$  at the critical strain of 0.22 in the armchair direction at the low temperature of 1 K. The ultimate stress is about  $7.6 \text{ Nm}^{-1}$  at the critical strain of 0.25 in the zigzag direction at the low temperature of 1 K.

#### CIV. B-ARSENENE

Present studies on the buckled (b-) arsenene, which is also named  $\beta$  arsenene, are based on first-principles calculations, and no empirical potential has been proposed for the b-arsenene. We will thus parametrize a set of VFF model for the single-layer b-arsenene in this section.

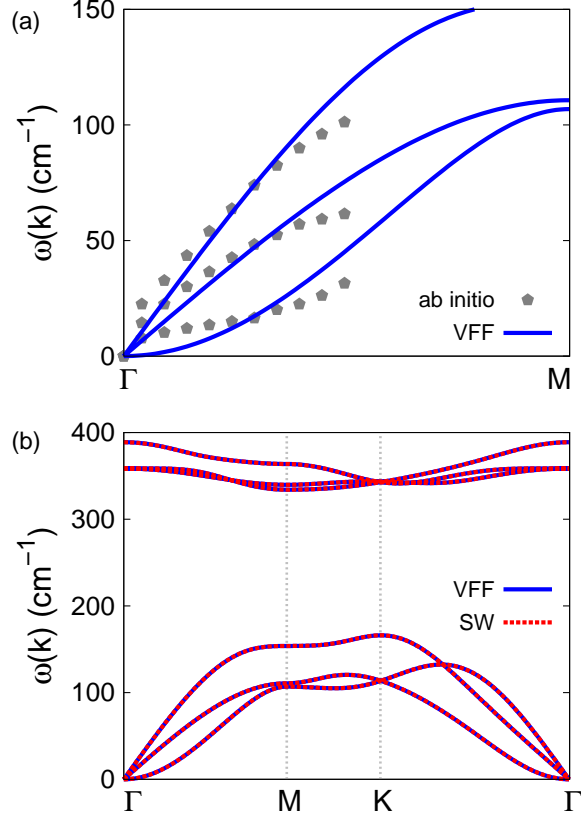


FIG. 212: (Color online) Phonon dispersion for the single-layer b-arsenene. (a) The VFF model is fitted to the three acoustic branches in the long wave limit along the  $\Gamma$ M direction. The *ab initio* results (gray pentagons) are from Ref. 70. (b) The VFF model (blue lines) and the SW potential (red lines) give the same phonon dispersion for the b-arsenene along  $\Gamma$ MK $\Gamma$ .

TABLE CDXVI: Three-body SW potential parameters for b-arsenene used by GULP,<sup>8</sup> as expressed in Eq. (4).

	$K$ (eV)	$\theta_0$ (degree)	$\rho_1$ (Å)	$\rho_2$ (Å)	$r_{\min 12}$ (Å)	$r_{\max 12}$ (Å)	$r_{\min 13}$ (Å)	$r_{\max 13}$ (Å)	$r_{\min 23}$ (Å)	$r_{\max 23}$ (Å)
As-As-As	14.845	91.964	0.482	0.482	0.0	3.060	0.0	3.060	3.060	4.004

We will also derive the SW potential based on the VFF model for the single-layer b-arsenene.

The structure of the single-layer b-arsenene is shown in Fig. 201, with structural parameters from the *ab initio* calculations.<sup>70</sup> The b-arsenene has a buckled configuration as shown in Fig. 201 (b), where the buckle is along the zigzag direction. The height of the buckle is  $h = 1.40$  Å. The lattice constant is 3.61 Å, and the bond length is 2.51 Å.

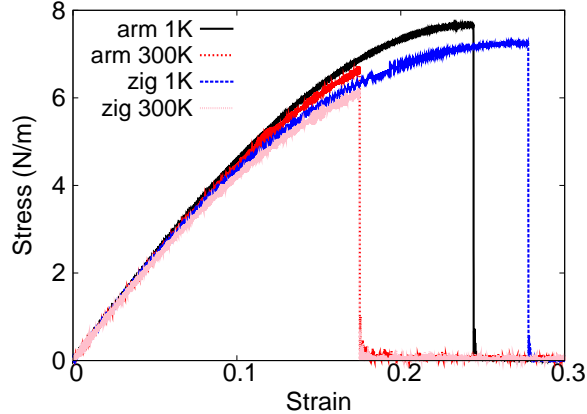


FIG. 213: (Color online) Stress-strain relations for the b-arsenene of size  $100 \times 100 \text{ \AA}$ . The b-arsenene is uniaxially stretched along the armchair or zigzag directions at temperatures 1 K and 300 K.

TABLE CDXVII: SW potential parameters for b-arsenene used by LAMMPS,<sup>9</sup> as expressed in Eqs. (9) and (10).

	$\epsilon$ (eV)	$\sigma$ ( $\text{\AA}$ )	$a$	$\lambda$	$\gamma$	$\cos \theta_0$	$A_L$	$B_L$	$p$	$q$	tol
As-As-As	1.000	0.482	6.349	14.845	1.000	-0.034	6.418	367.693	4	0	0.0

Table CDXIV shows the VFF model for the single-layer b-arsenene. The force constant parameters are determined by fitting to the three acoustic branches in the phonon dispersion along the  $\Gamma M$  as shown in Fig. 212 (a). The *ab initio* calculations for the phonon dispersion are from Ref. 70. Similar phonon dispersion can also be found in other *ab initio* calculations.<sup>64,72,73</sup> We note that the lowest-frequency branch around the  $\Gamma$  point from the VFF model is lower than the *ab initio* results. This branch is the flexural branch, which should be a quadratic dispersion. However, the *ab initio* calculations give a linear dispersion for the flexural branch due to the violation of the rigid rotational invariance in the first-principles package,<sup>20</sup> so *ab initio* calculations typically overestimate the frequency of this branch. Fig. 212 (b) shows that the VFF model and the SW potential give exactly the same phonon dispersion, as the SW potential is derived from the VFF model.

The parameters for the two-body SW potential used by GULP are shown in Tab. CDXV. The parameters for the three-body SW potential used by GULP are shown in Tab. CDXVI. Parameters for the SW potential used by LAMMPS are listed in Tab. CDXVII.

TABLE CDXVIII: The VFF model for b-antimonene. The second line gives an explicit expression for each VFF term. The third line is the force constant parameters. Parameters are in the unit of  $\frac{\text{eV}}{\text{\AA}^2}$  for the bond stretching interactions, and in the unit of eV for the angle bending interaction. The fourth line gives the initial bond length (in unit of  $\text{\AA}$ ) for the bond stretching interaction and the initial angle (in unit of degrees) for the angle bending interaction.

VFF type	bond stretching	angle bending
expression	$\frac{1}{2}K_r (\Delta r)^2$	$\frac{1}{2}K_\theta (\Delta\theta)^2$
parameter	15.372	5.138
$r_0$ or $\theta_0$	2.890	90.927

TABLE CDXIX: Two-body SW potential parameters for b-antimonene used by GULP,<sup>8</sup> as expressed in Eq. (3).

	$A$ (eV)	$\rho$ ( $\text{\AA}$ )	$B$ ( $\text{\AA}^4$ )	$r_{\min}$ ( $\text{\AA}$ )	$r_{\max}$ ( $\text{\AA}$ )
Sb-Sb	8.173	0.523	34.879	0.0	3.505

Fig. 213 shows the stress strain relations for the single-layer b-arsenene of size  $100 \times 100 \text{\AA}$ . The structure is uniaxially stretched in the armchair or zigzag directions at 1 K and 300 K. The Young's modulus is  $50.8 \text{ Nm}^{-1}$  and  $49.9 \text{ Nm}^{-1}$  in the armchair and zigzag directions respectively at 1 K, which are obtained by linear fitting of the stress strain relations in  $[0, 0.01]$ . The Young's modulus is isotropic for the b-arsenene. The Poisson's ratios from the VFF model and the SW potential are  $\nu_{xy} = \nu_{yx} = 0.21$ . The third-order nonlinear elastic constant  $D$  can be obtained by fitting the stress-strain relation to  $\sigma = E\epsilon + \frac{1}{2}D\epsilon^2$  with  $E$  as the Young's modulus. The values of  $D$  are  $-127.6 \text{ Nm}^{-1}$  and  $-153.6 \text{ Nm}^{-1}$  at 1 K along the armchair and zigzag directions, respectively. The ultimate stress is about  $7.6 \text{ Nm}^{-1}$  at the critical strain of 0.24 in the armchair direction at the low temperature of 1 K. The ultimate stress is about  $7.2 \text{ Nm}^{-1}$  at the critical strain of 0.28 in the zigzag direction at the low temperature of 1 K.

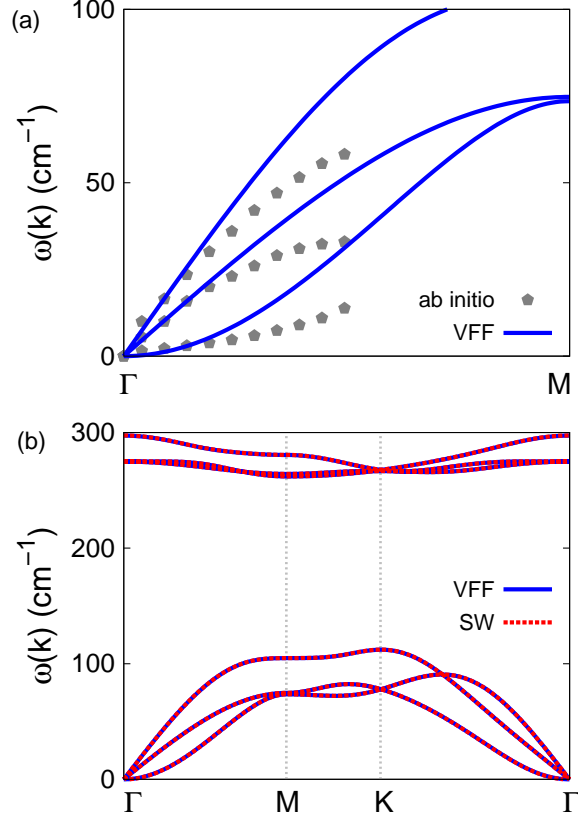


FIG. 214: (Color online) Phonon dispersion for the single-layer b-antimonene. (a) The VFF model is fitted to the three acoustic branches in the long wave limit along the  $\Gamma M$  direction. The *ab initio* results (gray pentagons) are from Ref. 70. (b) The VFF model (blue lines) and the SW potential (red lines) give the same phonon dispersion for the b-antimonene along  $\Gamma M K \Gamma$ .

TABLE CDXX: Three-body SW potential parameters for b-antimonene used by GULP,<sup>8</sup> as expressed in Eq. (4).

	$K$ (eV)	$\theta_0$ (degree)	$\rho_1$ ( $\text{\AA}$ )	$\rho_2$ ( $\text{\AA}$ )	$r_{\min 12}$ ( $\text{\AA}$ )	$r_{\max 12}$ ( $\text{\AA}$ )	$r_{\min 13}$ ( $\text{\AA}$ )	$r_{\max 13}$ ( $\text{\AA}$ )	$r_{\min 23}$ ( $\text{\AA}$ )	$r_{\max 23}$ ( $\text{\AA}$ )
Sb-Sb-Sb	14.100	90.927	0.523	0.523	0.0	3.505	0.0	3.503	3.505	4.577

## CV. B-ANTIMONENE

The buckled (b-) antimonene is a Sb allotrope, which is also named  $\beta$  antimonene. Present studies on the b-antimonene are based on first-principles calculations, and no empirical potential has been proposed for the b-antimonene. We will thus parametrize a set of VFF

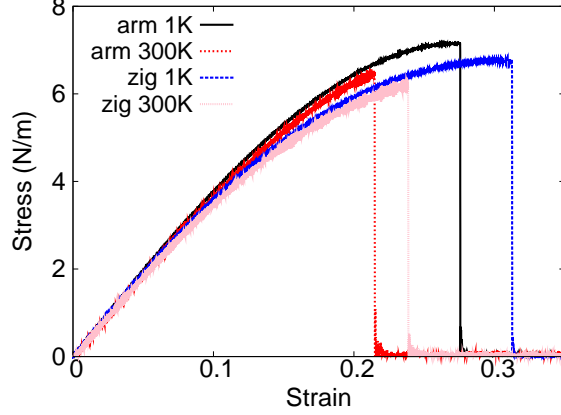


FIG. 215: (Color online) Stress-strain relations for the b-antimonene of size  $100 \times 100 \text{ \AA}$ . The b-antimonene is uniaxially stretched along the armchair or zigzag directions at temperatures 1 K and 300 K.

TABLE CDXXI: SW potential parameters for b-antimonene used by LAMMPS,<sup>9</sup> as expressed in Eqs. (9) and (10).

	$\epsilon$ (eV)	$\sigma$ ( $\text{\AA}$ )	$a$	$\lambda$	$\gamma$	$\cos \theta_0$	$A_L$	$B_L$	$p$	$q$	tol
Sb-Sb-Sb	1.000	0.523	6.702	14.100	1.000	-0.016	8.173	466.184	4	0	0.0

model for the single-layer b-antimonene in this section. We will also derive the SW potential based on the VFF model for the single-layer b-antimonene.

The structure of the single-layer b-antimonene is shown in Fig. 201, with structural parameters from the *ab initio* calculations.<sup>70</sup> The b-antimonene has a buckled configuration as shown in Fig. 201 (b), where the buckle is along the zigzag direction. The height of the buckle is  $h = 1.65 \text{ \AA}$ . The lattice constant is  $4.12 \text{ \AA}$ , and the bond length is  $2.89 \text{ \AA}$ .

Table CDXVIII shows the VFF model for the single-layer b-antimonene. The force constant parameters are determined by fitting to the three acoustic branches in the phonon dispersion along the  $\Gamma M$  as shown in Fig. 214 (a). The *ab initio* calculations for the phonon dispersion are from Ref. 70. Similar phonon dispersion can also be found in other *ab initio* calculations.<sup>64,72,73</sup> Fig. 214 (b) shows that the VFF model and the SW potential give exactly the same phonon dispersion, as the SW potential is derived from the VFF model.

The parameters for the two-body SW potential used by GULP are shown in Tab. CDXIX. The parameters for the three-body SW potential used by GULP are shown in Tab. CDXX.

TABLE CDXXII: The VFF model for b-bismuthene. The second line gives an explicit expression for each VFF term. The third line is the force constant parameters. Parameters are in the unit of  $\frac{\text{eV}}{\text{\AA}^2}$  for the bond stretching interactions, and in the unit of eV for the angle bending interaction. The fourth line gives the initial bond length (in unit of  $\text{\AA}$ ) for the bond stretching interaction and the initial angle (in unit of degrees) for the angle bending interaction.

VFF type	bond stretching	angle bending
expression	$\frac{1}{2}K_r (\Delta r)^2$	$\frac{1}{2}K_\theta (\Delta\theta)^2$
parameter	11.529	3.853
$r_0$ or $\theta_0$	3.045	90.901

TABLE CDXXIII: Two-body SW potential parameters for b-bismuthene used by GULP,<sup>8</sup> as expressed in Eq. (3).

	$A$ (eV)	$\rho$ ( $\text{\AA}$ )	$B$ ( $\text{\AA}^4$ )	$r_{\min}$ ( $\text{\AA}$ )	$r_{\max}$ ( $\text{\AA}$ )
Bi-Bi	6.805	0.552	42.985	0.0	3.693

Parameters for the SW potential used by LAMMPS are listed in Tab. CDXXI.

Fig. 215 shows the stress strain relations for the single-layer b-antimonene of size  $100 \times 100 \text{\AA}$ . The structure is uniaxially stretched in the armchair or zigzag directions at 1 K and 300 K. The Young's modulus is  $39.6 \text{ Nm}^{-1}$  in both armchair and zigzag directions at 1 K, which are obtained by linear fitting of the stress strain relations in  $[0, 0.01]$ . The Young's modulus is isotropic for the b-antimonene. The Poisson's ratios from the VFF model and the SW potential are  $\nu_{xy} = \nu_{yx} = 0.24$ . The third-order nonlinear elastic constant  $D$  can be obtained by fitting the stress-strain relation to  $\sigma = E\epsilon + \frac{1}{2}D\epsilon^2$  with  $E$  as the Young's modulus. The values of  $D$  are  $-62.6 \text{ Nm}^{-1}$  and  $-91.5 \text{ Nm}^{-1}$  at 1 K along the armchair and zigzag directions, respectively. The ultimate stress is about  $7.1 \text{ Nm}^{-1}$  at the critical strain of 0.28 in the armchair direction at the low temperature of 1 K. The ultimate stress is about  $6.7 \text{ Nm}^{-1}$  at the critical strain of 0.31 in the zigzag direction at the low temperature of 1 K.

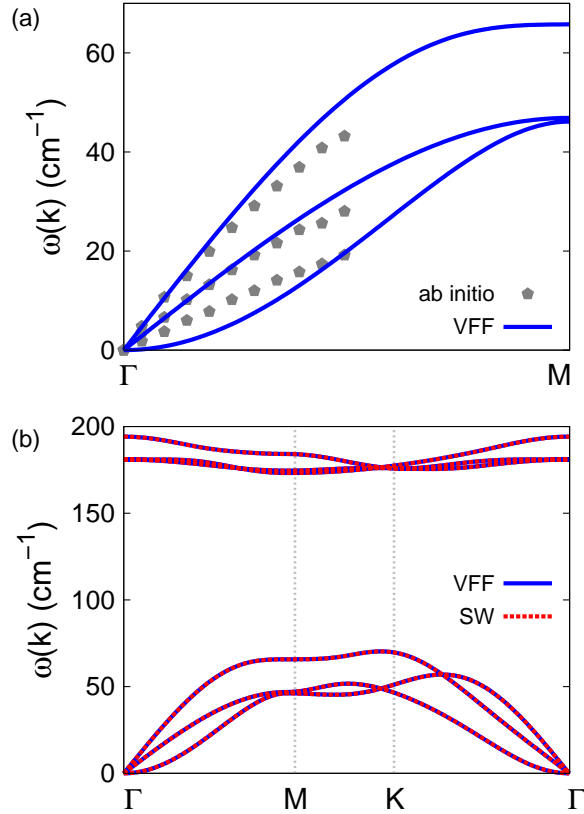


FIG. 216: (Color online) Phonon dispersion for the single-layer b-bismuthene. (a) The VFF model is fitted to the three acoustic branches in the long wave limit along the  $\Gamma M$  direction. The *ab initio* results (gray pentagons) are from Ref. 64. (b) The VFF model (blue lines) and the SW potential (red lines) give the same phonon dispersion for the b-bismuthene along  $\Gamma M K \Gamma$ .

TABLE CDXXIV: Three-body SW potential parameters for b-bismuthene used by GULP,<sup>8</sup> as expressed in Eq. (4).

	$K$ (eV)	$\theta_0$ (degree)	$\rho_1$ ( $\text{\AA}$ )	$\rho_2$ ( $\text{\AA}$ )	$r_{\min 12}$ ( $\text{\AA}$ )	$r_{\max 12}$ ( $\text{\AA}$ )	$r_{\min 13}$ ( $\text{\AA}$ )	$r_{\max 13}$ ( $\text{\AA}$ )	$r_{\min 23}$ ( $\text{\AA}$ )	$r_{\max 23}$ ( $\text{\AA}$ )
Bi-Bi-Bi	10.574	90.901	0.552	0.552	0.0	3.693	0.0	3.693	3.693	4.821

## CVI. B-BISMUTHENE

The buckled (b-) bismuthene is a Bi allotrope, which is also named *beta* bismuthene. Most studies on the b-bismuthene are based on first-principles calculations, while a modified Morse potential was proposed for the b-bismuthene in 2013.<sup>112</sup> We will parametrize a set of VFF

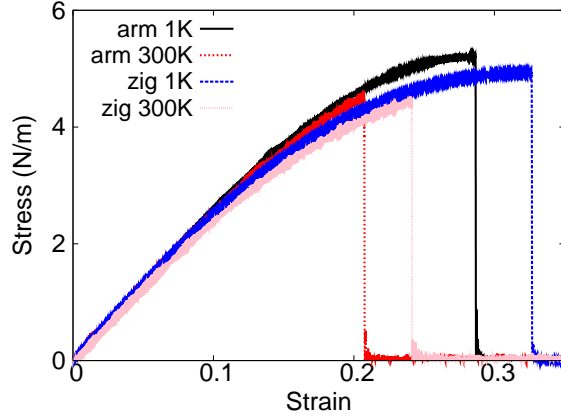


FIG. 217: (Color online) Stress-strain relations for the b-bismuthene of size  $100 \times 100 \text{ \AA}$ . The b-bismuthene is uniaxially stretched along the armchair or zigzag directions at temperatures 1 K and 300 K.

TABLE CDXXV: SW potential parameters for b-bismuthene used by LAMMPS,<sup>9</sup> as expressed in Eqs. (9) and (10).

	$\epsilon$ (eV)	$\sigma$ ( $\text{\AA}$ )	$a$	$\lambda$	$\gamma$	$\cos \theta_0$	$A_L$	$B_L$	$p$	$q$	tol
Bi-Bi-Bi	1.000	0.552	6.690	10.574	1.000	-0.016	6.805	462.978	4	0	0.0

model for the single-layer b-bismuthene in this section. We will also derive the SW potential based on the VFF model for the single-layer b-bismuthene.

The structure of the single-layer b-bismuthene is shown in Fig. 201, with structural parameters from the *ab initio* calculations.<sup>70</sup> The b-bismuthene has a buckled configuration as shown in Fig. 201 (b), where the buckle is along the zigzag direction. The height of the buckle is  $h = 1.73 \text{ \AA}$ . The lattice constant is  $4.34 \text{ \AA}$ , and the bond length is  $3.045 \text{ \AA}$ .

Table CDXXII shows the VFF model for the single-layer b-bismuthene. The force constant parameters are determined by fitting to the three acoustic branches in the phonon dispersion along the  $\Gamma$ M as shown in Fig. 216 (a). The *ab initio* calculations for the phonon dispersion are from Ref. 64. Similar phonon dispersion can also be found in other *ab initio* calculations.<sup>77</sup> We note that the lowest-frequency branch around the  $\Gamma$  point from the VFF model is lower than the *ab initio* results. This branch is the flexural branch, which should be a quadratic dispersion. However, the *ab initio* calculations give a linear dispersion for the flexural branch due to the violation of the rigid rotational invariance in the first-

principles package,<sup>20</sup> so *ab initio* calculations typically overestimate the frequency of this branch. Fig. 216 (b) shows that the VFF model and the SW potential give exactly the same phonon dispersion, as the SW potential is derived from the VFF model.

The parameters for the two-body SW potential used by GULP are shown in Tab. CDXXIII. The parameters for the three-body SW potential used by GULP are shown in Tab. CDXXIV. Parameters for the SW potential used by LAMMPS are listed in Tab. CDXXV.

Fig. 217 shows the stress strain relations for the single-layer b-bismuthene of size  $100 \times 100$  Å. The structure is uniaxially stretched in the armchair or zigzag directions at 1 K and 300 K. The Young's modulus is  $27.0 \text{ Nm}^{-1}$  in both armchair and zigzag directions at 1 K, which are obtained by linear fitting of the stress strain relations in  $[0, 0.01]$ . The Young's modulus is isotropic for the b-bismuthene. The value of the Young's modulus is close to the value of  $23.9 \text{ Nm}^{-1}$  from the *ab initio* calculations.<sup>77</sup> The Poisson's ratios from the VFF model and the SW potential are  $\nu_{xy} = \nu_{yx} = 0.25$ , which are comparable with the *ab initio* results of 0.327.<sup>77</sup> The third-order nonlinear elastic constant  $D$  can be obtained by fitting the stress-strain relation to  $\sigma = E\epsilon + \frac{1}{2}D\epsilon^2$  with  $E$  as the Young's modulus. The values of  $D$  are  $-34.3 \text{ Nm}^{-1}$  and  $-54.5 \text{ Nm}^{-1}$  at 1 K along the armchair and zigzag directions, respectively. The ultimate stress is about  $5.2 \text{ Nm}^{-1}$  at the critical strain of 0.29 in the armchair direction at the low temperature of 1 K. The ultimate stress is about  $4.9 \text{ Nm}^{-1}$  at the critical strain of 0.33 in the zigzag direction at the low temperature of 1 K.

## CVII. B-SITE

Present studies on the buckled (b-) SiTe are based on first-principles calculations, and no empirical potential has been proposed for the b-SiTe. We will thus parametrize a set of SW potential for the single-layer b-SiTe in this section.

The structure of the single-layer b-SiTe is shown in Fig. 218. The structural parameters are from the *ab initio* calculations.<sup>78</sup> The b-SiTe has a buckled configuration as shown in Fig. 218 (b), where the buckle is along the zigzag direction. This structure can be determined by two independent geometrical parameters, eg. the lattice constant  $3.83$  Å and the bond length  $2.689$  Å. The resultant height of the buckle is  $h = 1.53$  Å.

Table CDXXVI shows the VFF model for the single-layer b-SiTe. The force constant

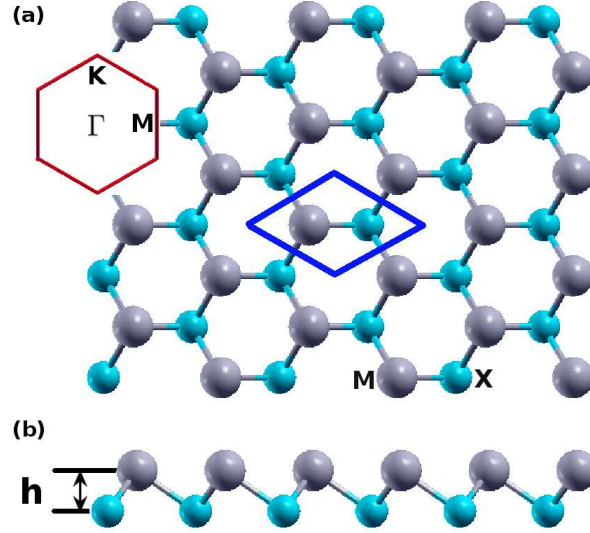


FIG. 218: (Color online) Structure for single-layer buckled MX (b-MX), with M from group IV and X from group VI, or both M and X from group IV, or M from group III and X from group V. (a) Top view. The armchair direction is along the horizontal direction, while the zigzag direction is along the vertical direction. The unit cell is displayed by the blue rhombus. Inset shows the first Brillouin zone. (b) Side view illustrates the buckled configuration of height  $h$ .

TABLE CDXXVI: The VFF model for b-SiTe. The second line gives an explicit expression for each VFF term. The third line is the force constant parameters. Parameters are in the unit of  $\frac{\text{eV}}{\text{\AA}^2}$  for the bond stretching interactions, and in the unit of eV for the angle bending interaction. The fourth line gives the initial bond length (in unit of  $\text{\AA}$ ) for the bond stretching interaction and the initial angle (in unit of degrees) for the angle bending interaction.

VFF type	bond stretching	angle bending
expression	$\frac{1}{2}K_r (\Delta r)^2$	$\frac{1}{2}K_\theta (\Delta \theta)^2$
parameter	8.418	4.349
$r_0$ or $\theta_0$	2.690	90.779

parameters are determined by fitting to the acoustic branches in the phonon dispersion along the  $\Gamma\text{M}$  as shown in Fig. 219 (a). The *ab initio* calculations for the phonon dispersion are from Ref. 78. Fig. 219 (b) shows that the VFF model and the SW potential give exactly the same phonon dispersion, as the SW potential is derived from the VFF model.

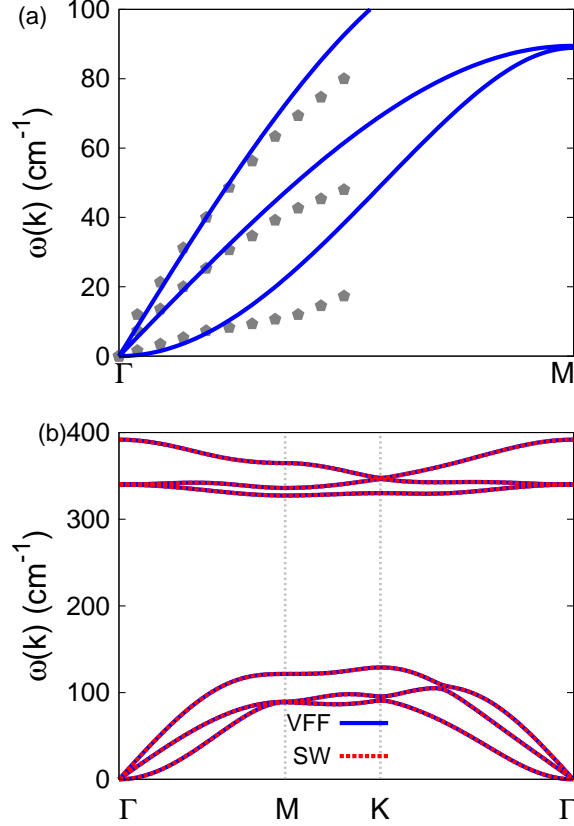


FIG. 219: (Color online) Phonon dispersion for the single-layer b-SiTe. (a) The VFF model is fitted to the three acoustic branches in the long wave limit along the  $\Gamma$ M direction. The *ab initio* results (gray pentagons) are from Ref. 78. (b) The VFF model (blue lines) and the SW potential (red lines) give the same phonon dispersion for the b-SiTe along  $\Gamma$ MK $\Gamma$ .

TABLE CDXXVII: Two-body SW potential parameters for b-SiTe used by GULP,<sup>8</sup> as expressed in Eq. (3).

	$A$ (eV)	$\rho$ ( $\text{\AA}$ )	$B$ ( $\text{\AA}^4$ )	$r_{\min}$ ( $\text{\AA}$ )	$r_{\max}$ ( $\text{\AA}$ )
Si-Te	9.285	1.473	26.181	0.0	3.685

The parameters for the two-body SW potential used by GULP are shown in Tab. CDXXVII. The parameters for the three-body SW potential used by GULP are shown in Tab. CDXXVIII. Parameters for the SW potential used by LAMMPS are listed in Tab. CDXXIX.

We use LAMMPS to perform MD simulations for the mechanical behavior of the single-

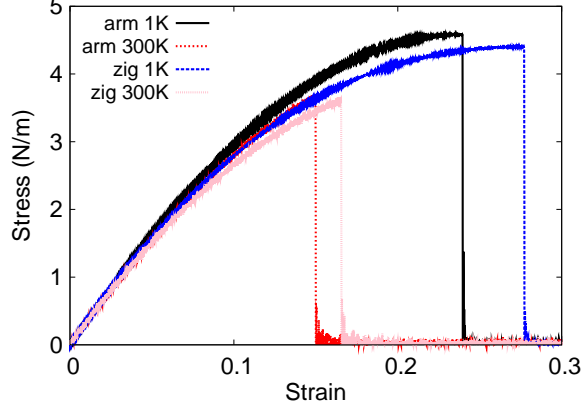


FIG. 220: (Color online) Stress-strain relations for the b-SiTe of size  $100 \times 100 \text{ \AA}$ . The b-SiTe is uniaxially stretched along the armchair or zigzag directions at temperatures 1 K and 300 K.

TABLE CDXXVIII: Three-body SW potential parameters for b-SiTe used by GULP,<sup>8</sup> as expressed in Eq. (4).

	$K$ (eV)	$\theta_0$ (degree)	$\rho_1$ ( $\text{\AA}$ )	$\rho_2$ ( $\text{\AA}$ )	$r_{\min 12}$ ( $\text{\AA}$ )	$r_{\max 12}$ ( $\text{\AA}$ )	$r_{\min 13}$ ( $\text{\AA}$ )	$r_{\max 13}$ ( $\text{\AA}$ )	$r_{\min 23}$ ( $\text{\AA}$ )	$r_{\max 23}$ ( $\text{\AA}$ )
Si-Te-Te	41.952	90.779	1.473	1.473	0.0	3.685	0.0	3.685	0.0	5.232
Te-Si-Si	41.952	90.779	1.473	1.473	0.0	3.685	0.0	3.685	0.0	5.232

layer b-SiTe under uniaxial tension at 1.0 K and 300.0 K. Fig. 220 shows the stress-strain curve for the tension of a single-layer b-SiTe of dimension  $100 \times 100 \text{ \AA}$ . Periodic boundary conditions are applied in both armchair and zigzag directions. The single-layer b-SiTe is stretched uniaxially along the armchair or zigzag direction. The stress is calculated without involving the actual thickness of the quasi-two-dimensional structure of the single-layer b-SiTe. The Young's modulus can be obtained by a linear fitting of the stress-strain relation in the small strain range of  $[0, 0.01]$ . The Young's modulus are 34.3 N/m and 34.6 N/m

TABLE CDXXIX: SW potential parameters for b-SiTe used by LAMMPS,<sup>9</sup> as expressed in Eqs. (9) and (10).

	$\epsilon$ (eV)	$\sigma$ ( $\text{\AA}$ )	$a$	$\lambda$	$\gamma$	$\cos \theta_0$	$A_L$	$B_L$	$p$	$q$	tol
Si-Te-Te	1.000	0.725	4.497	27.653	1.000	-0.014	4.428	113.714	4	0	0.0
Te-Si-Si	1.000	0.725	4.497	27.653	1.000	-0.014	4.428	113.714	4	0	0.0

TABLE CDXXX: The VFF model for b-SnGe. The second line gives an explicit expression for each VFF term. The third line is the force constant parameters. Parameters are in the unit of  $\frac{\text{eV}}{\text{\AA}^2}$  for the bond stretching interactions, and in the unit of eV for the angle bending interaction. The fourth line gives the initial bond length (in unit of  $\text{\AA}$ ) for the bond stretching interaction and the initial angle (in unit of degrees) for the angle bending interaction.

VFF type	bond stretching	angle bending
expression	$\frac{1}{2}K_r (\Delta r)^2$	$\frac{1}{2}K_\theta (\Delta\theta)^2$
parameter	8.390	3.112
$r_0$ or $\theta_0$	2.570	112.350

TABLE CDXXXI: Two-body SW potential parameters for b-SnGe used by GULP,<sup>8</sup> as expressed in Eq. (3).

	$A$ (eV)	$\rho$ ( $\text{\AA}$ )	$B$ ( $\text{\AA}^4$ )	$r_{\min}$ ( $\text{\AA}$ )	$r_{\max}$ ( $\text{\AA}$ )
Sn-Ge	13.674	2.267	21.812	0.0	3.777

along the armchair and zigzag directions, respectively. The Young's modulus is essentially isotropic in the armchair and zigzag directions. These values agrees with the *ab initio* result at 0 K temperature, eg.  $34.1 \text{ Nm}^{-1}$  in Ref. 78. The Poisson's ratio from the VFF model and the SW potential is  $\nu_{xy} = \nu_{yx} = 0.18$ , which agrees with the *ab initio* result<sup>78</sup> of 0.18.

There is no available value for nonlinear quantities in the single-layer b-SiTe. We have thus used the nonlinear parameter  $B = 0.5d^4$  in Eq. (5), which is close to the value of  $B$  in most materials. The value of the third order nonlinear elasticity  $D$  can be extracted by fitting the stress-strain relation to the function  $\sigma = E\epsilon + \frac{1}{2}D\epsilon^2$  with  $E$  as the Young's modulus. The values of  $D$  from the present SW potential are  $-119.3 \text{ N/m}$  and  $-137.2 \text{ N/m}$  along the armchair and zigzag directions, respectively. The ultimate stress is about  $4.6 \text{ Nm}^{-1}$  at the ultimate strain of 0.24 in the armchair direction at the low temperature of 1 K. The ultimate stress is about  $4.4 \text{ Nm}^{-1}$  at the ultimate strain of 0.27 in the zigzag direction at the low temperature of 1 K.

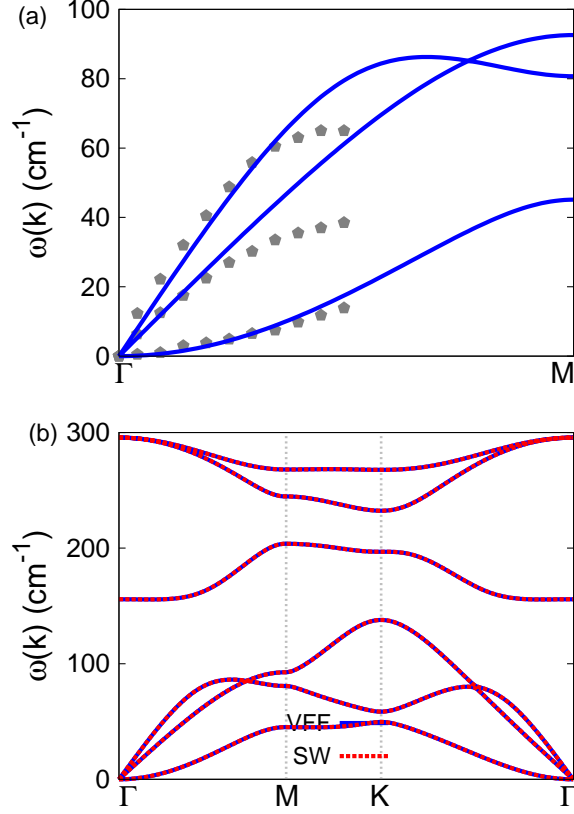


FIG. 221: (Color online) Phonon dispersion for the single-layer b-SnGe. (a) The VFF model is fitted to the three acoustic branches in the long wave limit along the  $\Gamma M$  direction. The *ab initio* results (gray pentagons) are from Ref. 113. (b) The VFF model (blue lines) and the SW potential (red lines) give the same phonon dispersion for the b-SnGe along  $\Gamma MK\Gamma$ .

TABLE CDXXXII: Three-body SW potential parameters for b-SnGe used by GULP,<sup>8</sup> as expressed in Eq. (4).

	$K$ (eV)	$\theta_0$ (degree)	$\rho_1$ ( $\text{\AA}$ )	$\rho_2$ ( $\text{\AA}$ )	$r_{\min 12}$ ( $\text{\AA}$ )	$r_{\max 12}$ ( $\text{\AA}$ )	$r_{\min 13}$ ( $\text{\AA}$ )	$r_{\max 13}$ ( $\text{\AA}$ )	$r_{\min 23}$ ( $\text{\AA}$ )	$r_{\max 23}$ ( $\text{\AA}$ )
Sn-Ge-Ge	77.881	112.350	2.267	2.267	0.0	3.777	0.0	3.777	0.0	5.833
Ge-Sn-Sn	77.881	112.350	2.267	2.267	0.0	3.777	0.0	3.777	0.0	5.833

### CVIII. B-SNGE

Present studies on the buckled SnGe (b-SnGe) are based on first-principles calculations, and no empirical potential has been proposed for the b-SnGe. We will thus parametrize a

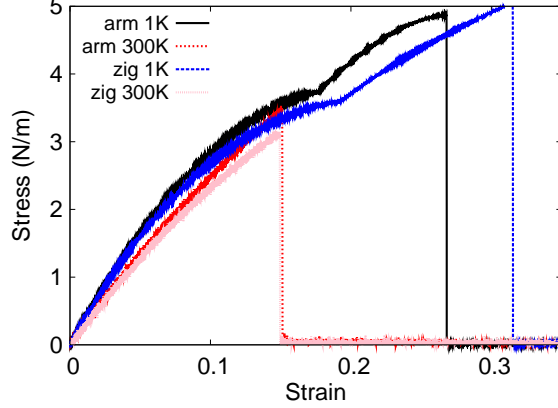


FIG. 222: (Color online) Stress-strain relations for the b-SnGe of size  $100 \times 100 \text{ \AA}$ . The b-SnGe is uniaxially stretched along the armchair or zigzag directions at temperatures 1 K and 300 K.

TABLE CDXXXIII: SW potential parameters for b-SnGe used by LAMMPS,<sup>9</sup> as expressed in Eqs. (9) and (10).

	$\epsilon$ (eV)	$\sigma$ ( $\text{\AA}$ )	$a$	$\lambda$	$\gamma$	$\cos \theta_0$	$A_L$	$B_L$	$p$	$q$	tol
Sn-Ge-Ge	1.000	2.267	1.666	77.881	1.000	-0.380	13.674	0.826	4	0	0.0
Ge-Sn-Sn	1.000	2.267	1.666	77.881	1.000	-0.380	13.674	0.826	4	0	0.0

set of SW potential for the single-layer b-SnGe in this section.

The structure of the single-layer b-SnGe is shown in Fig. 218. The structural parameters are from the *ab initio* calculations.<sup>113</sup> The b-SnGe has a buckled configuration as shown in Fig. 218 (b), where the buckle is along the zigzag direction. This structure can be determined by two independent geometrical parameters, eg. the lattice constant  $4.27 \text{ \AA}$  and the bond length  $2.57 \text{ \AA}$ . The resultant height of the buckle is  $h = 0.73 \text{ \AA}$ .

Table CDXXX shows the VFF model for the single-layer b-SnGe. The force constant parameters are determined by fitting to the acoustic branches in the phonon dispersion along the  $\Gamma M$  as shown in Fig. 221 (a). The *ab initio* calculations for the phonon dispersion are from Ref. 113. Fig. 221 (b) shows that the VFF model and the SW potential give exactly the same phonon dispersion, as the SW potential is derived from the VFF model.

The parameters for the two-body SW potential used by GULP are shown in Tab. CDXXXI. The parameters for the three-body SW potential used by GULP are shown in Tab. CDXXXII. Parameters for the SW potential used by LAMMPS are listed in

Tab. [CDXXXIII](#).

We use LAMMPS to perform MD simulations for the mechanical behavior of the single-layer b-SnGe under uniaxial tension at 1.0 K and 300.0 K. Fig. [222](#) shows the stress-strain curve for the tension of a single-layer b-SnGe of dimension  $100 \times 100 \text{ \AA}$ . Periodic boundary conditions are applied in both armchair and zigzag directions. The single-layer b-SnGe is stretched uniaxially along the armchair or zigzag direction. The stress is calculated without involving the actual thickness of the quasi-two-dimensional structure of the single-layer b-SnGe. The Young's modulus can be obtained by a linear fitting of the stress-strain relation in the small strain range of  $[0, 0.01]$ . The Young's modulus is 36.8 N/m along both armchair and zigzag directions. The Poisson's ratio from the VFF model and the SW potential is  $\nu_{xy} = \nu_{yx} = 0.11$ .

There is no available value for nonlinear quantities in the single-layer b-SnGe. We have thus used the nonlinear parameter  $B = 0.5d^4$  in Eq. (5), which is close to the value of  $B$  in most materials. The value of the third order nonlinear elasticity  $D$  can be extracted by fitting the stress-strain relation to the function  $\sigma = E\epsilon + \frac{1}{2}D\epsilon^2$  with  $E$  as the Young's modulus. The values of  $D$  from the present SW potential are -171.6 N/m and -197.0 N/m along the armchair and zigzag directions, respectively. The ultimate stress is about  $4.9 \text{ Nm}^{-1}$  at the ultimate strain of 0.27 in the armchair direction at the low temperature of 1 K. The ultimate stress is about  $5.0 \text{ Nm}^{-1}$  at the ultimate strain of 0.31 in the zigzag direction at the low temperature of 1 K.

## CIX. B-SiGe

Present studies on the buckled SiGe (b-SiGe) are based on first-principles calculations, and no empirical potential has been proposed for the b-SiGe. We will thus parametrize a set of SW potential for the single-layer b-SiGe in this section.

The structure of the single-layer b-SiGe is shown in Fig. [218](#). The structural parameters are from the *ab initio* calculations.<sup>113</sup> The b-SiGe has a buckled configuration as shown in Fig. [218](#) (b), where the buckle is along the zigzag direction. This structure can be determined by two independent geometrical parameters, eg. the lattice constant  $3.89 \text{ \AA}$  and the bond length  $2.31 \text{ \AA}$ . The resultant height of the buckle is  $h = 0.55 \text{ \AA}$ .

Table [CDXXXIV](#) shows the VFF model for the single-layer b-SiGe. The force constant

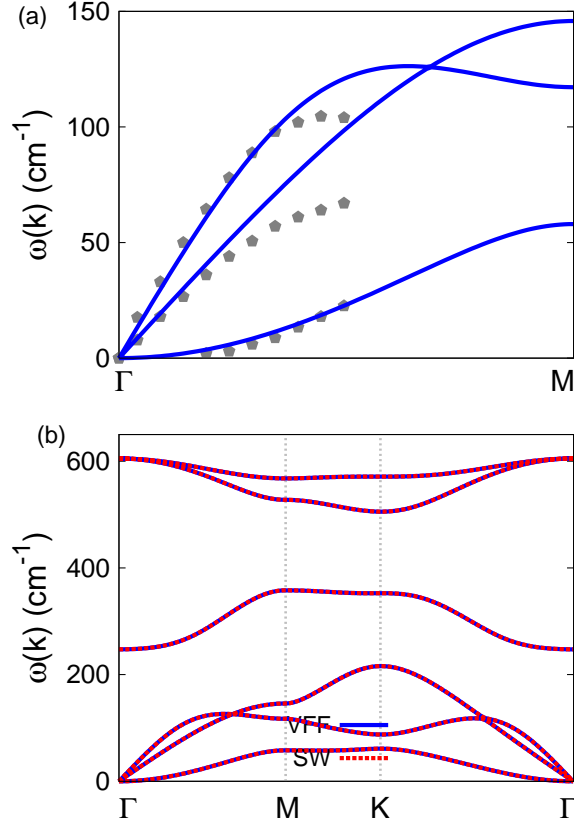


FIG. 223: (Color online) Phonon dispersion for the single-layer b-SiGe. (a) The VFF model is fitted to the three acoustic branches in the long wave limit along the  $\Gamma$ M direction. The *ab initio* results (gray pentagons) are from Ref. 113. (b) The VFF model (blue lines) and the SW potential (red lines) give the same phonon dispersion for the b-SiGe along  $\Gamma$ MK $\Gamma$ .

parameters are determined by fitting to the acoustic branches in the phonon dispersion along the  $\Gamma$ M as shown in Fig. 223 (a). The *ab initio* calculations for the phonon dispersion are from Ref. 113. Fig. 223 (b) shows that the VFF model and the SW potential give exactly the same phonon dispersion, as the SW potential is derived from the VFF model.

The parameters for the two-body SW potential used by GULP are shown in Tab. CDXXXV. The parameters for the three-body SW potential used by GULP are shown in Tab. CDXXXVI. Parameters for the SW potential used by LAMMPS are listed in Tab. CDXXXVII.

We use LAMMPS to perform MD simulations for the mechanical behavior of the single-layer b-SiGe under uniaxial tension at 1.0 K and 300.0 K. Fig. 224 shows the stress-strain

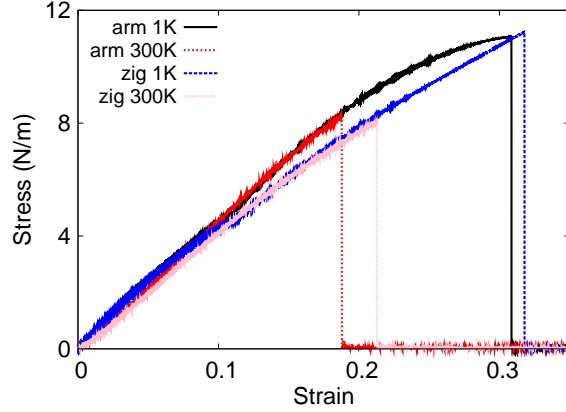


FIG. 224: (Color online) Stress-strain relations for the b-SiGe of size  $100 \times 100 \text{ \AA}$ . The b-SiGe is uniaxially stretched along the armchair or zigzag directions at temperatures 1 K and 300 K.

TABLE CDXXXIV: The VFF model for b-SiGe. The second line gives an explicit expression for each VFF term. The third line is the force constant parameters. Parameters are in the unit of  $\frac{eV}{\text{\AA}^2}$  for the bond stretching interactions, and in the unit of eV for the angle bending interaction. The fourth line gives the initial bond length (in unit of  $\text{\AA}$ ) for the bond stretching interaction and the initial angle (in unit of degrees) for the angle bending interaction.

VFF type	bond stretching	angle bending
expression	$\frac{1}{2}K_r (\Delta r)^2$	$\frac{1}{2}K_\theta (\Delta\theta)^2$
parameter	16.390	3.112
$r_0$ or $\theta_0$	2.310	114.702

curve for the tension of a single-layer b-SiGe of dimension  $100 \times 100 \text{ \AA}$ . Periodic boundary conditions are applied in both armchair and zigzag directions. The single-layer b-SiGe is stretched uniaxially along the armchair or zigzag direction. The stress is calculated without involving the actual thickness of the quasi-two-dimensional structure of the single-layer b-

TABLE CDXXXV: Two-body SW potential parameters for b-SiGe used by GULP,<sup>8</sup> as expressed in Eq. (3).

	$A$ (eV)	$\rho$ ( $\text{\AA}$ )	$B$ ( $\text{\AA}^4$ )	$r_{\min}$ ( $\text{\AA}$ )	$r_{\max}$ ( $\text{\AA}$ )
Si-Ge	22.576	2.122	14.237	0.0	3.417

TABLE CDXXXVI: Three-body SW potential parameters for b-SiGe used by GULP,<sup>8</sup> as expressed in Eq. (4).

	$K$ (eV)	$\theta_0$ (degree)	$\rho_1$ (Å)	$\rho_2$ (Å)	$r_{\min 12}$ (Å)	$r_{\max 12}$ (Å)	$r_{\min 13}$ (Å)	$r_{\max 13}$ (Å)	$r_{\min 23}$ (Å)	$r_{\max 23}$ (Å)
Si-Ge-Ge	87.197	114.702	2.122	2.122	0.0	3.417	0.0	3.417	0.0	5.314
Ge-Si-Si	87.197	114.702	2.122	2.122	0.0	3.417	0.0	3.417	0.0	5.314

TABLE CDXXXVII: SW potential parameters for b-SiGe used by LAMMPS,<sup>9</sup> as expressed in Eqs. (9) and (10).

	$\epsilon$ (eV)	$\sigma$ (Å)	$a$	$\lambda$	$\gamma$	$\cos \theta_0$	$A_L$	$B_L$	$p$	$q$	tol
Si-Ge-Ge	1.000	2.122	1.610	87.197	1.000	-0.418	22.576	0.702	4	0	0.0
Ge-Si-Si	1.000	2.122	1.610	87.197	1.000	-0.418	22.576	0.702	4	0	0.0

SiGe. The Young's modulus can be obtained by a linear fitting of the stress-strain relation in the small strain range of  $[0, 0.01]$ . The Young's modulus is 54.6 N/m and 54.3 N/m along the armchair and zigzag directions, respectively. The Poisson's ratio from the VFF model and the SW potential is  $\nu_{xy} = \nu_{yx} = 0.16$ .

There is no available value for nonlinear quantities in the single-layer b-SiGe. We have thus used the nonlinear parameter  $B = 0.5d^4$  in Eq. (5), which is close to the value of  $B$  in most materials. The value of the third order nonlinear elasticity  $D$  can be extracted by fitting the stress-strain relation to the function  $\sigma = E\epsilon + \frac{1}{2}D\epsilon^2$  with  $E$  as the Young's modulus. The values of  $D$  from the present SW potential are -186.7 N/m and -233.5 N/m along the armchair and zigzag directions, respectively. The ultimate stress is about  $11.0 \text{ Nm}^{-1}$  at the ultimate strain of 0.31 in the armchair direction at the low temperature of 1 K. The ultimate stress is about  $11.2 \text{ Nm}^{-1}$  at the ultimate strain of 0.31 in the zigzag direction at the low temperature of 1 K.

## CX. B-SNSI

Present studies on the buckled SnSi (b-SnSi) are based on first-principles calculations, and no empirical potential has been proposed for the b-SnSi. We will thus parametrize a set of SW potential for the single-layer b-SnSi in this section.

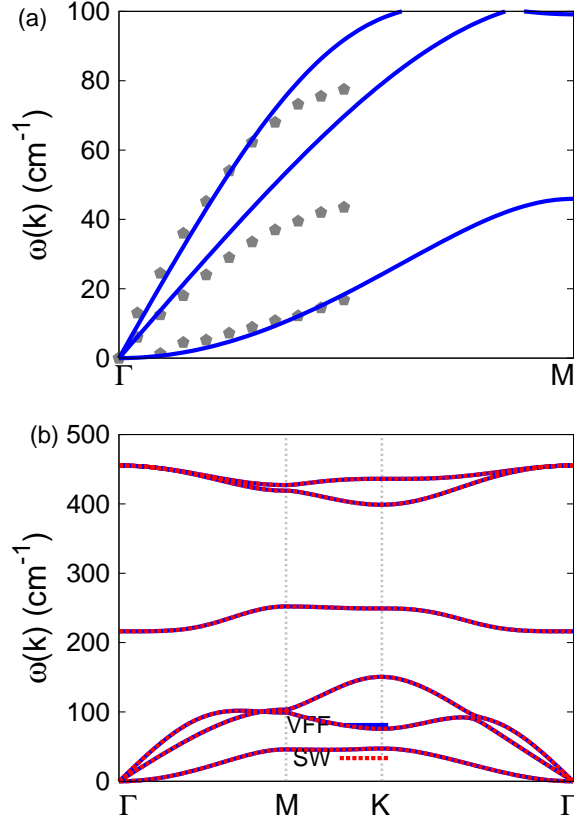


FIG. 225: (Color online) Phonon dispersion for the single-layer b-SnSi. (a) The VFF model is fitted to the three acoustic branches in the long wave limit along the  $\Gamma$ M direction. The *ab initio* results (gray pentagons) are from Ref. 113. (b) The VFF model (blue lines) and the SW potential (red lines) give the same phonon dispersion for the b-SnSi along  $\Gamma$ MKT.

The structure of the single-layer b-SnSi is shown in Fig. 218. The structural parameters are from the *ab initio* calculations.<sup>113</sup> The b-SnSi has a buckled configuration as shown in Fig. 218 (b), where the buckle is along the zigzag direction. This structure can be determined by two independent geometrical parameters, eg. the lattice constant 4.21 Å and the bond length 2.52 Å. The resultant height of the buckle is  $h = 0.67$  Å.

Table CDXXXVIII shows the VFF model for the single-layer b-SnSi. The force constant parameters are determined by fitting to the acoustic branches in the phonon dispersion along the  $\Gamma$ M as shown in Fig. 225 (a). The *ab initio* calculations for the phonon dispersion are from Ref. 113. Fig. 225 (b) shows that the VFF model and the SW potential give exactly the same phonon dispersion, as the SW potential is derived from the VFF model.

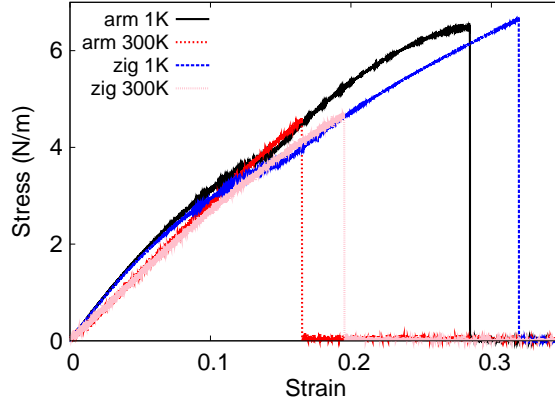


FIG. 226: (Color online) Stress-strain relations for the b-SnSi of size  $100 \times 100 \text{ \AA}$ . The b-SnSi is uniaxially stretched along the armchair or zigzag directions at temperatures 1 K and 300 K.

TABLE CDXXXVIII: The VFF model for b-SnSi. The second line gives an explicit expression for each VFF term. The third line is the force constant parameters. Parameters are in the unit of  $\frac{eV}{\text{\AA}^2}$  for the bond stretching interactions, and in the unit of eV for the angle bending interaction. The fourth line gives the initial bond length (in unit of  $\text{\AA}$ ) for the bond stretching interaction and the initial angle (in unit of degrees) for the angle bending interaction.

VFF type	bond stretching	angle bending
expression	$\frac{1}{2}K_r(\Delta r)^2$	$\frac{1}{2}K_\theta(\Delta\theta)^2$
parameter	10.315	2.880
$r_0$ or $\theta_0$	2.520	113.298

The parameters for the two-body SW potential used by GULP are shown in Tab. CDXXXIX. The parameters for the three-body SW potential used by GULP are shown in Tab. CDXL. Parameters for the SW potential used by LAMMPS are listed in Tab. CDXLI.

We use LAMMPS to perform MD simulations for the mechanical behavior of the single-

TABLE CDXXXIX: Two-body SW potential parameters for b-SnSi used by GULP,<sup>8</sup> as expressed in Eq. (3).

	$A$ (eV)	$\rho$ ( $\text{\AA}$ )	$B$ ( $\text{\AA}^4$ )	$r_{\min}$ ( $\text{\AA}$ )	$r_{\max}$ ( $\text{\AA}$ )
Sn-Si	16.463	2.260	20.164	0.0	3.713

TABLE CDXL: Three-body SW potential parameters for b-SnSi used by GULP,<sup>8</sup> as expressed in Eq. (4).

	$K$ (eV)	$\theta_0$ (degree)	$\rho_1$ (Å)	$\rho_2$ (Å)	$r_{\min 12}$ (Å)	$r_{\max 12}$ (Å)	$r_{\min 13}$ (Å)	$r_{\max 13}$ (Å)	$r_{\min 23}$ (Å)	$r_{\max 23}$ (Å)
Sn-Si-Si	75.415	113.298	2.260	2.260	0.0	3.713	0.0	3.713	0.0	5.751
Si-Sn-Sn	75.415	113.298	2.260	2.260	0.0	3.713	0.0	3.713	0.0	5.751

TABLE CDXLI: SW potential parameters for b-SnSi used by LAMMPS,<sup>9</sup> as expressed in Eqs. (9) and (10).

	$\epsilon$ (eV)	$\sigma$ (Å)	$a$	$\lambda$	$\gamma$	$\cos \theta_0$	$A_L$	$B_L$	$p$	$q$	tol
Sn-Si-Si	1.000	2.260	1.643	75.415	1.000	-0.396	16.463	0.773	4	0	0.0
Si-Sn-Sn	1.000	2.260	1.643	75.415	1.000	-0.396	16.463	0.773	4	0	0.0

layer b-SnSi under uniaxial tension at 1.0 K and 300.0 K. Fig. 226 shows the stress-strain curve for the tension of a single-layer b-SnSi of dimension  $100 \times 100$  Å. Periodic boundary conditions are applied in both armchair and zigzag directions. The single-layer b-SnSi is stretched uniaxially along the armchair or zigzag direction. The stress is calculated without involving the actual thickness of the quasi-two-dimensional structure of the single-layer b-SnSi. The Young's modulus can be obtained by a linear fitting of the stress-strain relation in the small strain range of  $[0, 0.01]$ . The Young's modulus is 39.0 N/m and 38.4 N/m along the armchair and zigzag directions, respectively. The Poisson's ratio from the VFF model and the SW potential is  $\nu_{xy} = \nu_{yx} = 0.14$ .

There is no available value for nonlinear quantities in the single-layer b-SnSi. We have thus used the nonlinear parameter  $B = 0.5d^4$  in Eq. (5), which is close to the value of  $B$  in most materials. The value of the third order nonlinear elasticity  $D$  can be extracted by fitting the stress-strain relation to the function  $\sigma = E\epsilon + \frac{1}{2}D\epsilon^2$  with  $E$  as the Young's modulus. The values of  $D$  from the present SW potential are -150.5 N/m and -174.8 N/m along the armchair and zigzag directions, respectively. The ultimate stress is about  $6.5 \text{ Nm}^{-1}$  at the ultimate strain of 0.28 in the armchair direction at the low temperature of 1 K. The ultimate stress is about  $6.6 \text{ Nm}^{-1}$  at the ultimate strain of 0.32 in the zigzag direction at the low temperature of 1 K.

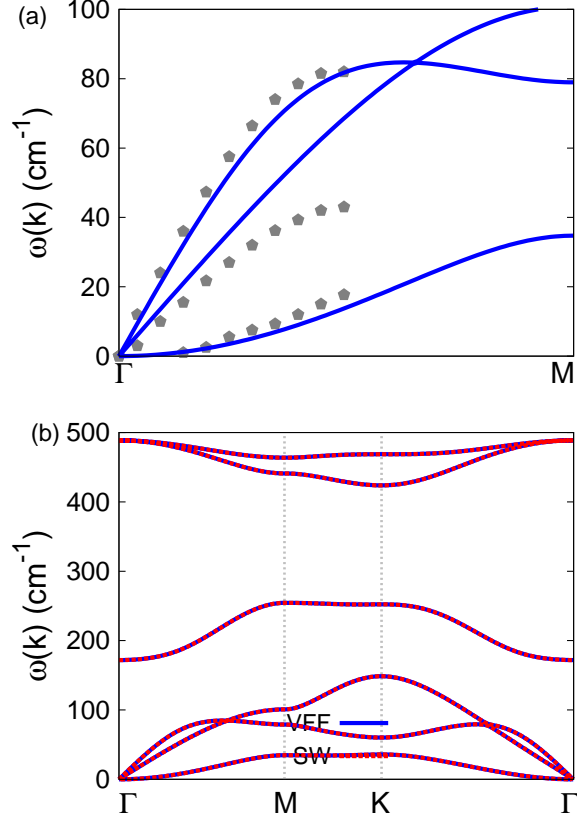


FIG. 227: (Color online) Phonon dispersion for the single-layer b-InP. (a) The VFF model is fitted to the three acoustic branches in the long wave limit along the  $\Gamma\text{M}$  direction. The *ab initio* results (gray pentagons) are from Ref. 113. (b) The VFF model (blue lines) and the SW potential (red lines) give the same phonon dispersion for the b-InP along  $\Gamma\text{MK}\Gamma$ .

### CXI. B-INP

Present studies on the buckled InP (b-InP) are based on first-principles calculations, and no empirical potential has been proposed for the b-InP. We will thus parametrize a set of SW potential for the single-layer b-InP in this section.

The structure of the single-layer b-InP is shown in Fig. 218. The structural parameters are from the *ab initio* calculations.<sup>113</sup> The b-InP has a buckled configuration as shown in Fig. 218 (b), where the buckle is along the zigzag direction. This structure can be determined by two independent geometrical parameters, eg. the lattice constant  $4.17 \text{ \AA}$  and the bond length  $2.46 \text{ \AA}$ . The resultant height of the buckle is  $h = 0.51 \text{ \AA}$ .

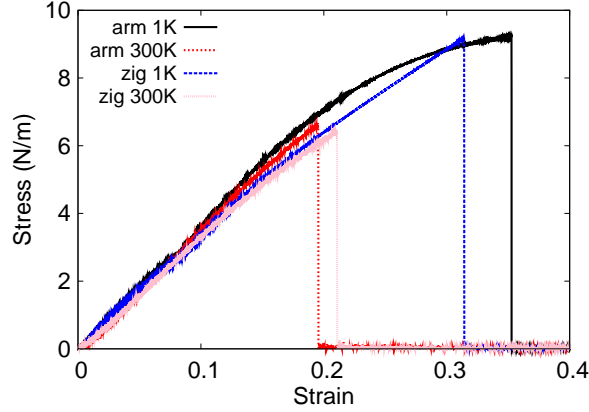


FIG. 228: (Color online) Stress-strain relations for the b-InP of size  $100 \times 100 \text{ \AA}$ . The b-InP is uniaxially stretched along the armchair or zigzag directions at temperatures 1 K and 300 K.

TABLE CDXLII: The VFF model for b-InP. The second line gives an explicit expression for each VFF term. The third line is the force constant parameters. Parameters are in the unit of  $\frac{\text{eV}}{\text{\AA}^2}$  for the bond stretching interactions, and in the unit of eV for the angle bending interaction. The fourth line gives the initial bond length (in unit of  $\text{\AA}$ ) for the bond stretching interaction and the initial angle (in unit of degrees) for the angle bending interaction.

VFF type	bond stretching	angle bending
expression	$\frac{1}{2}K_r (\Delta r)^2$	$\frac{1}{2}K_\theta (\Delta \theta)^2$
parameter	12.903	2.384
$r_0$ or $\theta_0$	2.460	115.895

Table CDXLII shows the VFF model for the single-layer b-InP. The force constant parameters are determined by fitting to the acoustic branches in the phonon dispersion along the  $\Gamma M$  as shown in Fig. 227 (a). The *ab initio* calculations for the phonon dispersion are from Ref. 113. Fig. 227 (b) shows that the VFF model and the SW potential give exactly

TABLE CDXLIII: Two-body SW potential parameters for b-InP used by GULP,<sup>8</sup> as expressed in Eq. (3).

	$A$ (eV)	$\rho$ ( $\text{\AA}$ )	$B$ ( $\text{\AA}^4$ )	$r_{\min}$ ( $\text{\AA}$ )	$r_{\max}$ ( $\text{\AA}$ )
In-P	20.610	2.306	18.311	0.0	3.651

TABLE CDXLIV: Three-body SW potential parameters for b-InP used by GULP,<sup>8</sup> as expressed in Eq. (4).

	$K$ (eV)	$\theta_0$ (degree)	$\rho_1$ (Å)	$\rho_2$ (Å)	$r_{\min 12}$ (Å)	$r_{\max 12}$ (Å)	$r_{\min 13}$ (Å)	$r_{\max 13}$ (Å)	$r_{\min 23}$ (Å)	$r_{\max 23}$ (Å)
In-P-P	70.782	115.895	2.306	2.306	0.0	3.651	0.0	3.651	0.0	5.696
P-In-In	70.782	115.895	2.306	2.306	0.0	3.651	0.0	3.651	0.0	5.696

TABLE CDXLV: SW potential parameters for b-InP used by LAMMPS,<sup>9</sup> as expressed in Eqs. (9) and (10).

	$\epsilon$ (eV)	$\sigma$ (Å)	$a$	$\lambda$	$\gamma$	$\cos \theta_0$	$A_L$	$B_L$	$p$	$q$	tol
In-P-P	1.000	2.306	1.583	70.782	1.000	-0.437	20.610	0.648	4	0	0.0
P-In-In	1.000	2.306	1.583	70.782	1.000	-0.437	20.610	0.648	4	0	0.0

the same phonon dispersion, as the SW potential is derived from the VFF model.

The parameters for the two-body SW potential used by GULP are shown in Tab. CDXLIII. The parameters for the three-body SW potential used by GULP are shown in Tab. CDXLIV. Parameters for the SW potential used by LAMMPS are listed in Tab. CDXLV.

We use LAMMPS to perform MD simulations for the mechanical behavior of the single-layer b-InP under uniaxial tension at 1.0 K and 300.0 K. Fig. 228 shows the stress-strain curve for the tension of a single-layer b-InP of dimension  $100 \times 100$  Å. Periodic boundary conditions are applied in both armchair and zigzag directions. The single-layer b-InP is stretched uniaxially along the armchair or zigzag direction. The stress is calculated without involving the actual thickness of the quasi-two-dimensional structure of the single-layer b-InP. The Young's modulus can be obtained by a linear fitting of the stress-strain relation in the small strain range of  $[0, 0.01]$ . The Young's modulus is 39.3 N/m and 38.3 N/m along the armchair and zigzag directions, respectively. The Poisson's ratio from the VFF model and the SW potential is  $\nu_{xy} = \nu_{yx} = 0.17$ .

There is no available value for nonlinear quantities in the single-layer b-InP. We have thus used the nonlinear parameter  $B = 0.5d^4$  in Eq. (5), which is close to the value of  $B$  in most materials. The value of the third order nonlinear elasticity  $D$  can be extracted by fitting the stress-strain relation to the function  $\sigma = E\epsilon + \frac{1}{2}D\epsilon^2$  with  $E$  as the Young's modulus.

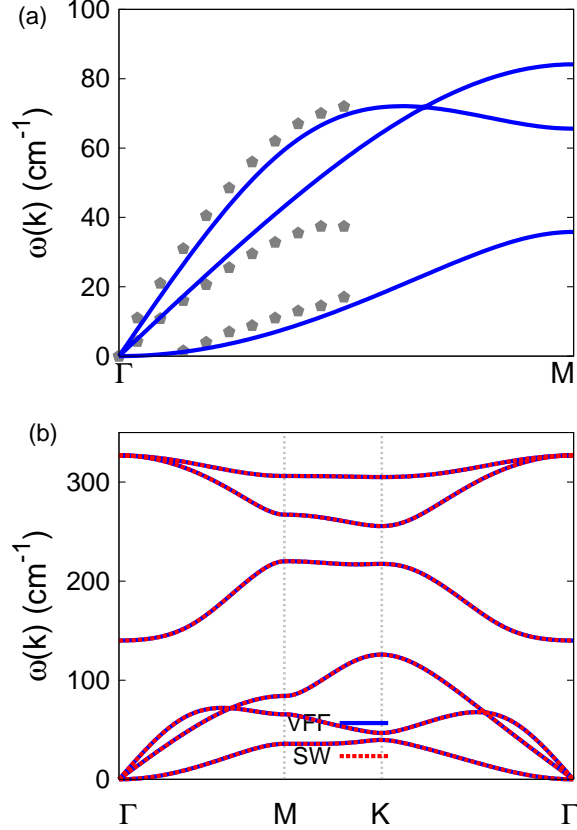


FIG. 229: (Color online) Phonon dispersion for the single-layer b-InAs. (a) The VFF model is fitted to the three acoustic branches in the long wave limit along the  $\Gamma$ M direction. The *ab initio* results (gray pentagons) are from Ref. 113. (b) The VFF model (blue lines) and the SW potential (red lines) give the same phonon dispersion for the b-InAs along  $\Gamma$ MK $\Gamma$ .

The values of  $D$  from the present SW potential are  $-119.3$  N/m and  $-132.0$  N/m along the armchair and zigzag directions, respectively. The ultimate stress is about  $9.2$  Nm $^{-1}$  at the ultimate strain of  $0.35$  in the armchair direction at the low temperature of  $1$  K. The ultimate stress is about  $9.1$  Nm $^{-1}$  at the ultimate strain of  $0.31$  in the zigzag direction at the low temperature of  $1$  K.

## CXII. B-INAS

Present studies on the buckled InAs (b-InAs) are based on first-principles calculations, and no empirical potential has been proposed for the b-InAs. We will thus parametrize a

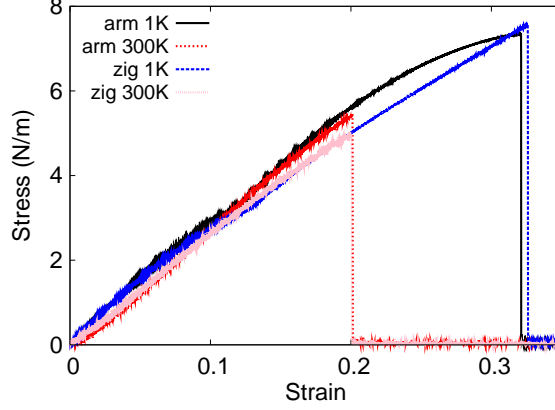


FIG. 230: (Color online) Stress-strain relations for the b-InAs of size  $100 \times 100 \text{ \AA}$ . The b-InAs is uniaxially stretched along the armchair or zigzag directions at temperatures 1 K and 300 K.

TABLE CDXLVI: The VFF model for b-InAs. The second line gives an explicit expression for each VFF term. The third line is the force constant parameters. Parameters are in the unit of  $\frac{eV}{\text{\AA}^2}$  for the bond stretching interactions, and in the unit of eV for the angle bending interaction. The fourth line gives the initial bond length (in unit of  $\text{\AA}$ ) for the bond stretching interaction and the initial angle (in unit of degrees) for the angle bending interaction.

VFF type	bond stretching	angle bending
expression	$\frac{1}{2}K_r(\Delta r)^2$	$\frac{1}{2}K_\theta(\Delta\theta)^2$
parameter	10.903	2.384
$r_0$ or $\theta_0$	2.550	114.115

set of SW potential for the single-layer b-InAs in this section.

The structure of the single-layer b-InAs is shown in Fig. 218. The structural parameters are from the *ab initio* calculations.<sup>113</sup> The b-InAs has a buckled configuration as shown in Fig. 218 (b), where the buckle is along the zigzag direction. This structure can be determined

TABLE CDXLVII: Two-body SW potential parameters for b-InAs used by GULP,<sup>8</sup> as expressed in Eq. (3).

	$A$ (eV)	$\rho$ ( $\text{\AA}$ )	$B$ ( $\text{\AA}^4$ )	$r_{\min}$ ( $\text{\AA}$ )	$r_{\max}$ ( $\text{\AA}$ )
In-As	18.099	2.320	21.141	0.0	3.766

TABLE CDXLVIII: Three-body SW potential parameters for b-InAs used by GULP,<sup>8</sup> as expressed in Eq. (4).

	$K$ (eV)	$\theta_0$ (degree)	$\rho_1$ (Å)	$\rho_2$ (Å)	$r_{\min 12}$ (Å)	$r_{\max 12}$ (Å)	$r_{\min 13}$ (Å)	$r_{\max 13}$ (Å)	$r_{\min 23}$ (Å)	$r_{\max 23}$ (Å)
In-As-As	64.931	114.115	2.320	2.320	0.0	3.766	0.0	3.766	0.0	5.847
As-In-In	64.931	114.115	2.320	2.320	0.0	3.766	0.0	3.766	0.0	5.847

TABLE CDXLIX: SW potential parameters for b-InAs used by LAMMPS,<sup>9</sup> as expressed in Eqs. (9) and (10).

	$\epsilon$ (eV)	$\sigma$ (Å)	$a$	$\lambda$	$\gamma$	$\cos \theta_0$	$A_L$	$B_L$	$p$	$q$	tol
In-As-As	1.000	2.320	1.624	64.931	1.000	-0.409	18.099	0.730	4	0	0.0
As-In-In	1.000	2.320	1.624	64.931	1.000	-0.409	18.099	0.730	4	0	0.0

by two independent geometrical parameters, eg. the lattice constant 4.28 Å and the bond length 2.55 Å. The resultant height of the buckle is  $h = 0.62$  Å.

Table CDXLVI shows the VFF model for the single-layer b-InAs. The force constant parameters are determined by fitting to the acoustic branches in the phonon dispersion along the  $\Gamma M$  as shown in Fig. 229 (a). The *ab initio* calculations for the phonon dispersion are from Ref. 113. Fig. 229 (b) shows that the VFF model and the SW potential give exactly the same phonon dispersion, as the SW potential is derived from the VFF model.

The parameters for the two-body SW potential used by GULP are shown in Tab. CDXLVII. The parameters for the three-body SW potential used by GULP are shown in Tab. CDXLVIII. Parameters for the SW potential used by LAMMPS are listed in Tab. CDXLIX.

We use LAMMPS to perform MD simulations for the mechanical behavior of the single-layer b-InAs under uniaxial tension at 1.0 K and 300.0 K. Fig. 230 shows the stress-strain curve for the tension of a single-layer b-InAs of dimension  $100 \times 100$  Å. Periodic boundary conditions are applied in both armchair and zigzag directions. The single-layer b-InAs is stretched uniaxially along the armchair or zigzag direction. The stress is calculated without involving the actual thickness of the quasi-two-dimensional structure of the single-layer b-InAs. The Young's modulus can be obtained by a linear fitting of the stress-strain relation in the small strain range of  $[0, 0.01]$ . The Young's modulus is 33.9 N/m and 34.2 N/m along

TABLE CDL: The VFF model for b-InSb. The second line gives an explicit expression for each VFF term. The third line is the force constant parameters. Parameters are in the unit of  $\frac{\text{eV}}{\text{\AA}^2}$  for the bond stretching interactions, and in the unit of eV for the angle bending interaction. The fourth line gives the initial bond length (in unit of  $\text{\AA}$ ) for the bond stretching interaction and the initial angle (in unit of degrees) for the angle bending interaction.

VFF type	bond stretching	angle bending
expression	$\frac{1}{2}K_r (\Delta r)^2$	$\frac{1}{2}K_\theta (\Delta\theta)^2$
parameter	8.903	2.384
$r_0$ or $\theta_0$	2.740	113.012

TABLE CDLI: Two-body SW potential parameters for b-InSb used by GULP,<sup>8</sup> as expressed in Eq. (3).

	$A$ (eV)	$\rho$ ( $\text{\AA}$ )	$B$ ( $\text{\AA}^4$ )	$r_{\min}$ ( $\text{\AA}$ )	$r_{\max}$ ( $\text{\AA}$ )
In-Sb	16.706	2.445	28.182	0.0	4.034

the armchair and zigzag directions, respectively. The Poisson's ratio from the VFF model and the SW potential is  $\nu_{xy} = \nu_{yx} = 0.17$ .

There is no available value for nonlinear quantities in the single-layer b-InAs. We have thus used the nonlinear parameter  $B = 0.5d^4$  in Eq. (5), which is close to the value of  $B$  in most materials. The value of the third order nonlinear elasticity  $D$  can be extracted by fitting the stress-strain relation to the function  $\sigma = E\epsilon + \frac{1}{2}D\epsilon^2$  with  $E$  as the Young's modulus. The values of  $D$  from the present SW potential are -85.0 N/m and -130.2 N/m along the armchair and zigzag directions, respectively. The ultimate stress is about  $7.3 \text{ Nm}^{-1}$  at the ultimate strain of 0.32 in the armchair direction at the low temperature of 1 K. The ultimate stress is about  $7.5 \text{ Nm}^{-1}$  at the ultimate strain of 0.32 in the zigzag direction at the low temperature of 1 K.

### CXIII. B-INSB

Present studies on the buckled InSb (b-InSb) are based on first-principles calculations, and no empirical potential has been proposed for the b-InSb. We will thus parametrize a

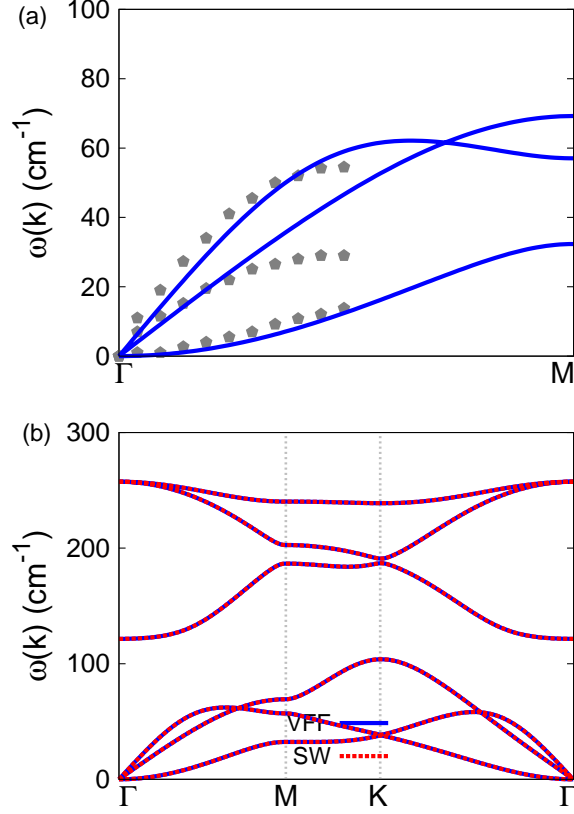


FIG. 231: (Color online) Phonon dispersion for the single-layer b-InSb. (a) The VFF model is fitted to the three acoustic branches in the long wave limit along the  $\Gamma$ M direction. The *ab initio* results (gray pentagons) are from Ref. 113. (b) The VFF model (blue lines) and the SW potential (red lines) give the same phonon dispersion for the b-InSb along  $\Gamma$ MKT.

TABLE CDLII: Three-body SW potential parameters for b-InSb used by GULP,<sup>8</sup> as expressed in Eq. (4).

	$K$ (eV)	$\theta_0$ (degree)	$\rho_1$ ( $\text{\AA}$ )	$\rho_2$ ( $\text{\AA}$ )	$r_{\min 12}$ ( $\text{\AA}$ )	$r_{\max 12}$ ( $\text{\AA}$ )	$r_{\min 13}$ ( $\text{\AA}$ )	$r_{\max 13}$ ( $\text{\AA}$ )	$r_{\min 23}$ ( $\text{\AA}$ )	$r_{\max 23}$ ( $\text{\AA}$ )
In-Sb-Sb	61.578	113.012	2.445	2.445	0.0	4.034	0.0	4.034	0.0	6.243
Sb-In-In	61.578	113.012	2.445	2.445	0.0	4.034	0.0	4.034	0.0	6.243

set of SW potential for the single-layer b-InSb in this section.

The structure of the single-layer b-InSb is shown in Fig. 218. The structural parameters are from the *ab initio* calculations.<sup>113</sup> The b-InSb has a buckled configuration as shown in Fig. 218 (b), where the buckle is along the zigzag direction. This structure can be determined

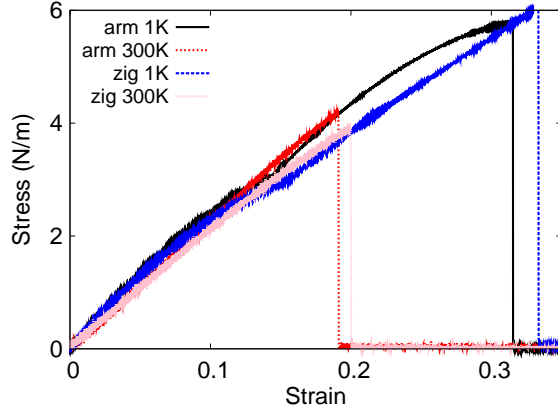


FIG. 232: (Color online) Stress-strain relations for the b-InSb of size  $100 \times 100 \text{ \AA}$ . The b-InSb is uniaxially stretched along the armchair or zigzag directions at temperatures 1 K and 300 K.

TABLE CDLIII: SW potential parameters for b-InSb used by LAMMPS,<sup>9</sup> as expressed in Eqs. (9) and (10).

	$\epsilon$ (eV)	$\sigma$ ( $\text{\AA}$ )	$a$	$\lambda$	$\gamma$	$\cos \theta_0$	$A_L$	$B_L$	$p$	$q$	tol
In-Sb-Sb	1.000	2.445	1.650	61.578	1.000	-0.391	16.706	0.788	4	0	0.0
Sb-In-In	1.000	2.445	1.650	61.578	1.000	-0.391	16.706	0.788	4	0	0.0

by two independent geometrical parameters, eg. the lattice constant  $4.57 \text{ \AA}$  and the bond length  $2.74 \text{ \AA}$ . The resultant height of the buckle is  $h = 0.73 \text{ \AA}$ .

Table CDL shows the VFF model for the single-layer b-InSb. The force constant parameters are determined by fitting to the acoustic branches in the phonon dispersion along the  $\Gamma M$  as shown in Fig. 231 (a). The *ab initio* calculations for the phonon dispersion are from Ref. 113. Fig. 231 (b) shows that the VFF model and the SW potential give exactly the same phonon dispersion, as the SW potential is derived from the VFF model.

The parameters for the two-body SW potential used by GULP are shown in Tab. CDLI. The parameters for the three-body SW potential used by GULP are shown in Tab. CDLII. Parameters for the SW potential used by LAMMPS are listed in Tab. CDLIII.

We use LAMMPS to perform MD simulations for the mechanical behavior of the single-layer b-InSb under uniaxial tension at 1.0 K and 300.0 K. Fig. 232 shows the stress-strain curve for the tension of a single-layer b-InSb of dimension  $100 \times 100 \text{ \AA}$ . Periodic boundary conditions are applied in both armchair and zigzag directions. The single-layer b-InSb is

TABLE CDLIV: The VFF model for b-GaAs. The second line gives an explicit expression for each VFF term. The third line is the force constant parameters. Parameters are in the unit of  $\frac{\text{eV}}{\text{\AA}^2}$  for the bond stretching interactions, and in the unit of eV for the angle bending interaction. The fourth line gives the initial bond length (in unit of  $\text{\AA}$ ) for the bond stretching interaction and the initial angle (in unit of degrees) for the angle bending interaction.

VFF type	bond stretching	angle bending
expression	$\frac{1}{2}K_r (\Delta r)^2$	$\frac{1}{2}K_\theta (\Delta\theta)^2$
parameter	12.903	3.284
$r_0$ or $\theta_0$	2.360	114.513

stretched uniaxially along the armchair or zigzag direction. The stress is calculated without involving the actual thickness of the quasi-two-dimensional structure of the single-layer b-InSb. The Young's modulus can be obtained by a linear fitting of the stress-strain relation in the small strain range of  $[0, 0.01]$ . The Young's modulus is 28.6 N/m and 28.9 N/m along the armchair and zigzag directions, respectively. The Poisson's ratio from the VFF model and the SW potential is  $\nu_{xy} = \nu_{yx} = 0.17$ .

There is no available value for nonlinear quantities in the single-layer b-InSb. We have thus used the nonlinear parameter  $B = 0.5d^4$  in Eq. (5), which is close to the value of  $B$  in most materials. The value of the third order nonlinear elasticity  $D$  can be extracted by fitting the stress-strain relation to the function  $\sigma = E\epsilon + \frac{1}{2}D\epsilon^2$  with  $E$  as the Young's modulus. The values of  $D$  from the present SW potential are -85.4 N/m and -121.0 N/m along the armchair and zigzag directions, respectively. The ultimate stress is about  $5.8 \text{ Nm}^{-1}$  at the ultimate strain of 0.31 in the armchair direction at the low temperature of 1 K. The ultimate stress is about  $6.0 \text{ Nm}^{-1}$  at the ultimate strain of 0.33 in the zigzag direction at the low temperature of 1 K.

#### CXIV. B-GAAS

Present studies on the buckled GaAs (b-GaAs) are based on first-principles calculations, and no empirical potential has been proposed for the b-GaAs. We will thus parametrize a set of SW potential for the single-layer b-GaAs in this section.

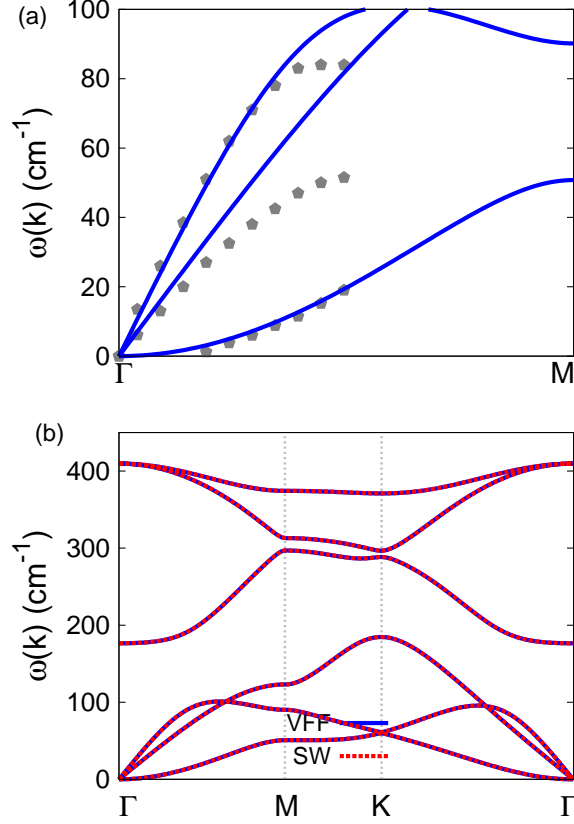


FIG. 233: (Color online) Phonon dispersion for the single-layer b-GaAs. (a) The VFF model is fitted to the three acoustic branches in the long wave limit along the  $\Gamma$ M direction. The *ab initio* results (gray pentagons) are from Ref. 113. (b) The VFF model (blue lines) and the SW potential (red lines) give the same phonon dispersion for the b-GaAs along  $\Gamma$ MK $\Gamma$ .

TABLE CDLV: Two-body SW potential parameters for b-GaAs used by GULP,<sup>8</sup> as expressed in Eq. (3).

	$A$ (eV)	$\rho$ ( $\text{\AA}$ )	$B$ ( $\text{\AA}^4$ )	$r_{\min}$ ( $\text{\AA}$ )	$r_{\max}$ ( $\text{\AA}$ )
Ga-As	18.485	2.161	15.510	0.0	3.489

The structure of the single-layer b-GaAs is shown in Fig. 218. The structural parameters are from the *ab initio* calculations.<sup>113</sup> The b-GaAs has a buckled configuration as shown in Fig. 218 (b), where the buckle is along the zigzag direction. This structure can be determined by two independent geometrical parameters, eg. the lattice constant  $3.97 \text{ \AA}$  and the bond length  $2.36 \text{ \AA}$ . The resultant height of the buckle is  $h = 0.55 \text{ \AA}$ .

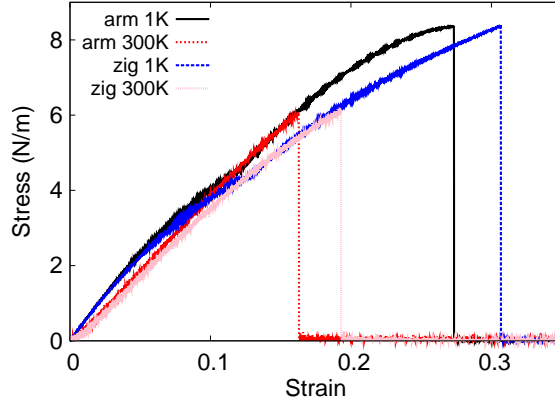


FIG. 234: (Color online) Stress-strain relations for the b-GaAs of size  $100 \times 100 \text{ \AA}$ . The b-GaAs is uniaxially stretched along the armchair or zigzag directions at temperatures 1 K and 300 K.

TABLE CDLVI: Three-body SW potential parameters for b-GaAs used by GULP,<sup>8</sup> as expressed in Eq. (4).

	$K$ (eV)	$\theta_0$ (degree)	$\rho_1$ ( $\text{\AA}$ )	$\rho_2$ ( $\text{\AA}$ )	$r_{\min 12}$ ( $\text{\AA}$ )	$r_{\max 12}$ ( $\text{\AA}$ )	$r_{\min 13}$ ( $\text{\AA}$ )	$r_{\max 13}$ ( $\text{\AA}$ )	$r_{\min 23}$ ( $\text{\AA}$ )	$r_{\max 23}$ ( $\text{\AA}$ )
Ga-As-As	91.177	114.513	2.161	2.161	0.0	3.489	0.0	3.489	0.0	5.423
As-Ga-Ga	91.177	114.513	2.161	2.161	0.0	3.489	0.0	3.489	0.0	5.423

Table CDLIV shows the VFF model for the single-layer b-GaAs. The force constant parameters are determined by fitting to the acoustic branches in the phonon dispersion along the  $\Gamma M$  as shown in Fig. 233 (a). The *ab initio* calculations for the phonon dispersion are from Ref. 113. Fig. 233 (b) shows that the VFF model and the SW potential give exactly the same phonon dispersion, as the SW potential is derived from the VFF model.

The parameters for the two-body SW potential used by GULP are shown in Tab. CDLV. The parameters for the three-body SW potential used by GULP are shown in Tab. CDLVI.

TABLE CDLVII: SW potential parameters for b-GaAs used by LAMMPS,<sup>9</sup> as expressed in Eqs. (9) and (10).

	$\epsilon$ (eV)	$\sigma$ ( $\text{\AA}$ )	$a$	$\lambda$	$\gamma$	$\cos \theta_0$	$A_L$	$B_L$	$p$	$q$	tol
Ga-As-As	1.000	2.161	1.614	91.177	1.000	-0.415	18.485	0.711	4	0	0.0
As-Ga-Ga	1.000	2.161	1.614	91.177	1.000	-0.415	18.485	0.711	4	0	0.0

Parameters for the SW potential used by LAMMPS are listed in Tab. [CDLVII](#).

We use LAMMPS to perform MD simulations for the mechanical behavior of the single-layer b-GaAs under uniaxial tension at 1.0 K and 300.0 K. Fig. [234](#) shows the stress-strain curve for the tension of a single-layer b-GaAs of dimension  $100 \times 100 \text{ \AA}$ . Periodic boundary conditions are applied in both armchair and zigzag directions. The single-layer b-GaAs is stretched uniaxially along the armchair or zigzag direction. The stress is calculated without involving the actual thickness of the quasi-two-dimensional structure of the single-layer b-GaAs. The Young's modulus can be obtained by a linear fitting of the stress-strain relation in the small strain range of  $[0, 0.01]$ . The Young's modulus is 50.5 N/m and 50.9 N/m along the armchair and zigzag directions, respectively. The Poisson's ratio from the VFF model and the SW potential is  $\nu_{xy} = \nu_{yx} = 0.13$ .

There is no available value for nonlinear quantities in the single-layer b-GaAs. We have thus used the nonlinear parameter  $B = 0.5d^4$  in Eq. (5), which is close to the value of  $B$  in most materials. The value of the third order nonlinear elasticity  $D$  can be extracted by fitting the stress-strain relation to the function  $\sigma = E\epsilon + \frac{1}{2}D\epsilon^2$  with  $E$  as the Young's modulus. The values of  $D$  from the present SW potential are -199.5 N/m and -258.6 N/m along the armchair and zigzag directions, respectively. The ultimate stress is about  $8.3 \text{ Nm}^{-1}$  at the ultimate strain of 0.27 in the armchair direction at the low temperature of 1 K. The ultimate stress is about  $8.3 \text{ Nm}^{-1}$  at the ultimate strain of 0.30 in the zigzag direction at the low temperature of 1 K.

## CXV. B-GAP

Present studies on the buckled GaP (b-GaP) are based on first-principles calculations, and no empirical potential has been proposed for the b-GaP. We will thus parametrize a set of SW potential for the single-layer b-GaP in this section.

The structure of the single-layer b-GaP is shown in Fig. [218](#). The structural parameters are from the *ab initio* calculations.<sup>113</sup> The b-GaP has a buckled configuration as shown in Fig. [218](#) (b), where the buckle is along the zigzag direction. This structure can be determined by two independent geometrical parameters, eg. the lattice constant  $3.84 \text{ \AA}$  and the bond length  $2.25 \text{ \AA}$ . The resultant height of the buckle is  $h = 0.40 \text{ \AA}$ .

Table [CDLVIII](#) shows the VFF model for the single-layer b-GaP. The force constant

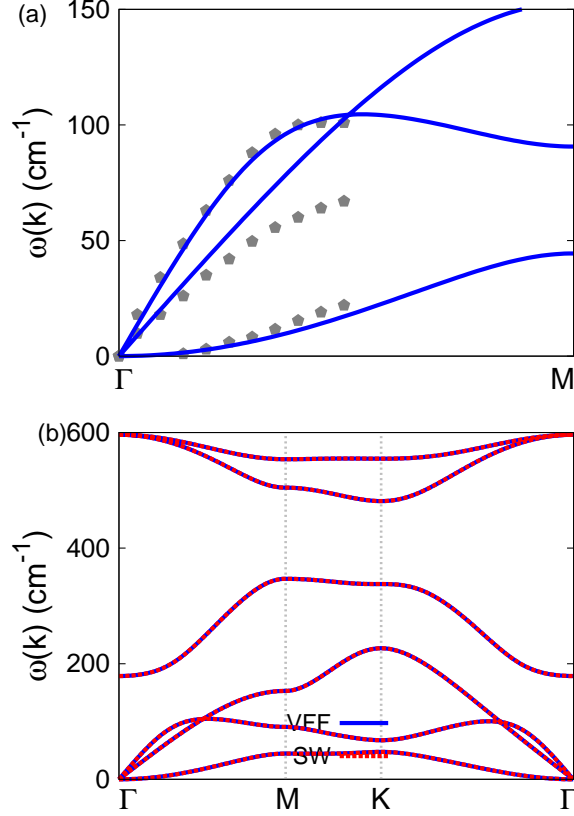


FIG. 235: (Color online) Phonon dispersion for the single-layer b-GaP. (a) The VFF model is fitted to the three acoustic branches in the long wave limit along the  $\Gamma M$  direction. The *ab initio* results (gray pentagons) are from Ref. 113. (b) The VFF model (blue lines) and the SW potential (red lines) give the same phonon dispersion for the b-GaP along  $\Gamma M K T \Gamma$ .

parameters are determined by fitting to the acoustic branches in the phonon dispersion along the  $\Gamma M$  as shown in Fig. 235 (a). The *ab initio* calculations for the phonon dispersion are from Ref. 113. Fig. 235 (b) shows that the VFF model and the SW potential give exactly the same phonon dispersion, as the SW potential is derived from the VFF model.

The parameters for the two-body SW potential used by GULP are shown in Tab. CDLIX. The parameters for the three-body SW potential used by GULP are shown in Tab. CDLX. Parameters for the SW potential used by LAMMPS are listed in Tab. CDLXI.

We use LAMMPS to perform MD simulations for the mechanical behavior of the single-layer b-GaP under uniaxial tension at 1.0 K and 300.0 K. Fig. 236 shows the stress-strain curve for the tension of a single-layer b-GaP of dimension  $100 \times 100 \text{ \AA}$ . Periodic boundary

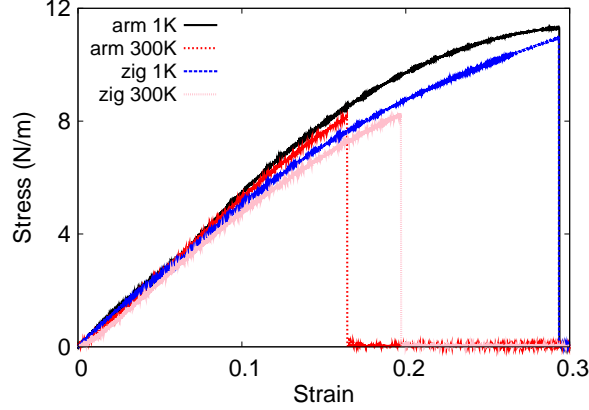


FIG. 236: (Color online) Stress-strain relations for the b-GaP of size  $100 \times 100 \text{ \AA}$ . The b-GaP is uniaxially stretched along the armchair or zigzag directions at temperatures 1 K and 300 K.

TABLE CDLVIII: The VFF model for b-GaP. The second line gives an explicit expression for each VFF term. The third line is the force constant parameters. Parameters are in the unit of  $\frac{\text{eV}}{\text{\AA}^2}$  for the bond stretching interactions, and in the unit of eV for the angle bending interaction. The fourth line gives the initial bond length (in unit of  $\text{\AA}$ ) for the bond stretching interaction and the initial angle (in unit of degrees) for the angle bending interaction.

VFF type	bond stretching	angle bending
expression	$\frac{1}{2}K_r(\Delta r)^2$	$\frac{1}{2}K_\theta(\Delta\theta)^2$
parameter	16.050	3.022
$r_0$ or $\theta_0$	2.250	117.152

conditions are applied in both armchair and zigzag directions. The single-layer b-GaP is stretched uniaxially along the armchair or zigzag direction. The stress is calculated without involving the actual thickness of the quasi-two-dimensional structure of the single-layer b-GaP. The Young's modulus can be obtained by a linear fitting of the stress-strain relation

TABLE CDLIX: Two-body SW potential parameters for b-GaP used by GULP,<sup>8</sup> as expressed in Eq. (3).

	$A$ (eV)	$\rho$ ( $\text{\AA}$ )	$B$ ( $\text{\AA}^4$ )	$r_{\min}$ ( $\text{\AA}$ )	$r_{\max}$ ( $\text{\AA}$ )
Ga-P	21.948	2.152	12.814	0.0	3.350

TABLE CDLX: Three-body SW potential parameters for b-GaP used by GULP,<sup>8</sup> as expressed in Eq. (4).

	$K$ (eV)	$\theta_0$ (degree)	$\rho_1$ (Å)	$\rho_2$ (Å)	$r_{\min 12}$ (Å)	$r_{\max 12}$ (Å)	$r_{\min 13}$ (Å)	$r_{\max 13}$ (Å)	$r_{\min 23}$ (Å)	$r_{\max 23}$ (Å)
Ga-P-P	95.438	117.152	2.152	2.152	0.0	3.350	0.0	3.350	0.0	5.246
P-Ga-Ga	95.438	117.152	2.152	2.152	0.0	3.350	0.0	3.350	0.0	5.246

TABLE CDLXI: SW potential parameters for b-GaP used by LAMMPS,<sup>9</sup> as expressed in Eqs. (9) and (10).

	$\epsilon$ (eV)	$\sigma$ (Å)	$a$	$\lambda$	$\gamma$	$\cos \theta_0$	$A_L$	$B_L$	$p$	$q$	tol
Ga-P-P	1.000	2.152	1.557	95.438	1.000	-0.456	21.948	0.597	4	0	0.0
P-Ga-Ga	1.000	2.152	1.557	95.438	1.000	-0.456	21.948	0.597	4	0	0.0

in the small strain range of  $[0, 0.01]$ . The Young's modulus is 57.2 N/m and 57.4 N/m along the armchair and zigzag directions, respectively. The Poisson's ratio from the VFF model and the SW potential is  $\nu_{xy} = \nu_{yx} = 0.14$ .

There is no available value for nonlinear quantities in the single-layer b-GaP. We have thus used the nonlinear parameter  $B = 0.5d^4$  in Eq. (5), which is close to the value of  $B$  in most materials. The value of the third order nonlinear elasticity  $D$  can be extracted by fitting the stress-strain relation to the function  $\sigma = E\epsilon + \frac{1}{2}D\epsilon^2$  with  $E$  as the Young's modulus. The values of  $D$  from the present SW potential are -186.4 N/m and -261.6 N/m along the armchair and zigzag directions, respectively. The ultimate stress is about 11.3 Nm<sup>-1</sup> at the ultimate strain of 0.29 in the armchair direction at the low temperature of 1 K. The ultimate stress is about 10.9 Nm<sup>-1</sup> at the ultimate strain of 0.29 in the zigzag direction at the low temperature of 1 K.

## CXVI. B-ALSB

Present studies on the buckled AlSb (b-AlSb) are based on first-principles calculations, and no empirical potential has been proposed for the b-AlSb. We will thus parametrize a set of SW potential for the single-layer b-AlSb in this section.

The structure of the single-layer b-AlSb is shown in Fig. 218. The structural parameters

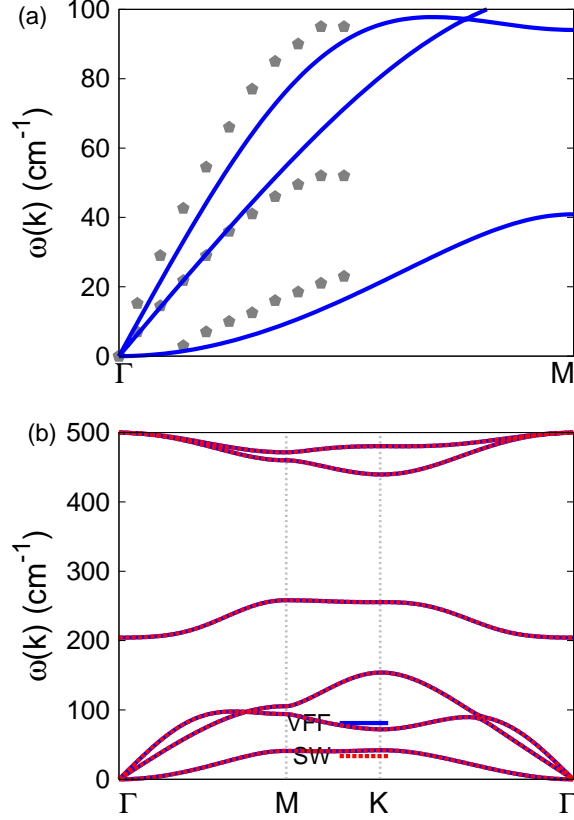


FIG. 237: (Color online) Phonon dispersion for the single-layer b-AlSb. (a) The VFF model is fitted to the three acoustic branches in the long wave limit along the  $\Gamma$ M direction. The *ab initio* results (gray pentagons) are from Ref. 113. (b) The VFF model (blue lines) and the SW potential (red lines) give the same phonon dispersion for the b-AlSb along  $\Gamma$ MK $\Gamma$ .

are from the *ab initio* calculations.<sup>113</sup> The b-AlSb has a buckled configuration as shown in Fig. 218 (b), where the buckle is along the zigzag direction. This structure can be determined by two independent geometrical parameters, eg. the lattice constant 4.33 Å and the bond length 2.57 Å. The resultant height of the buckle is  $h = 0.60$  Å.

Table CDLXII shows the VFF model for the single-layer b-AlSb. The force constant parameters are determined by fitting to the acoustic branches in the phonon dispersion along the  $\Gamma$ M as shown in Fig. 237 (a). The *ab initio* calculations for the phonon dispersion are from Ref. 113. Fig. 237 (b) shows that the VFF model and the SW potential give exactly the same phonon dispersion, as the SW potential is derived from the VFF model.

The parameters for the two-body SW potential used by GULP are shown in

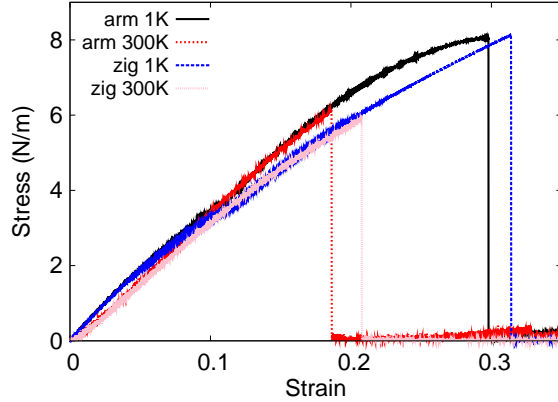


FIG. 238: (Color online) Stress-strain relations for the b-AlSb of size  $100 \times 100 \text{ \AA}$ . The b-AlSb is uniaxially stretched along the armchair or zigzag directions at temperatures 1 K and 300 K.

TABLE CDLXII: The VFF model for b-AlSb. The second line gives an explicit expression for each VFF term. The third line is the force constant parameters. Parameters are in the unit of  $\frac{\text{eV}}{\text{\AA}^2}$  for the bond stretching interactions, and in the unit of eV for the angle bending interaction. The fourth line gives the initial bond length (in unit of  $\text{\AA}$ ) for the bond stretching interaction and the initial angle (in unit of degrees) for the angle bending interaction.

VFF type	bond stretching	angle bending
expression	$\frac{1}{2}K_r(\Delta r)^2$	$\frac{1}{2}K_\theta(\Delta\theta)^2$
parameter	12.050	3.022
$r_0$ or $\theta_0$	2.570	114.791

Tab. CDLXIII. The parameters for the three-body SW potential used by GULP are shown in Tab. CDLXIV. Parameters for the SW potential used by LAMMPS are listed in Tab. CDLXV.

We use LAMMPS to perform MD simulations for the mechanical behavior of the single-

TABLE CDLXIII: Two-body SW potential parameters for b-AlSb used by GULP,<sup>8</sup> as expressed in Eq. (3).

	$A$ (eV)	$\rho$ ( $\text{\AA}$ )	$B$ ( $\text{\AA}^4$ )	$r_{\min}$ ( $\text{\AA}$ )	$r_{\max}$ ( $\text{\AA}$ )
Al-Sb	20.580	2.365	21.812	0.0	3.803

TABLE CDLXIV: Three-body SW potential parameters for b-AlSb used by GULP,<sup>8</sup> as expressed in Eq. (4).

	$K$ (eV)	$\theta_0$ (degree)	$\rho_1$ (Å)	$\rho_2$ (Å)	$r_{\min 12}$ (Å)	$r_{\max 12}$ (Å)	$r_{\min 13}$ (Å)	$r_{\max 13}$ (Å)	$r_{\min 23}$ (Å)	$r_{\max 23}$ (Å)
Al-Sb-Sb	85.046	114.791	2.365	2.365	0.0	3.803	0.0	3.803	0.0	5.915
Sb-Al-Al	85.046	114.791	2.365	2.365	0.0	3.803	0.0	3.803	0.0	5.915

TABLE CDLXV: SW potential parameters for b-AlSb used by LAMMPS,<sup>9</sup> as expressed in Eqs. (9) and (10).

	$\epsilon$ (eV)	$\sigma$ (Å)	$a$	$\lambda$	$\gamma$	$\cos \theta_0$	$A_L$	$B_L$	$p$	$q$	tol
Al-Sb-Sb	1.000	2.365	1.608	85.046	1.000	-0.419	20.580	0.697	4	0	0.0
Sb-Al-Al	1.000	2.365	1.608	85.046	1.000	-0.419	20.580	0.697	4	0	0.0

layer b-AlSb under uniaxial tension at 1.0 K and 300.0 K. Fig. 238 shows the stress-strain curve for the tension of a single-layer b-AlSb of dimension  $100 \times 100$  Å. Periodic boundary conditions are applied in both armchair and zigzag directions. The single-layer b-AlSb is stretched uniaxially along the armchair or zigzag direction. The stress is calculated without involving the actual thickness of the quasi-two-dimensional structure of the single-layer b-AlSb. The Young's modulus can be obtained by a linear fitting of the stress-strain relation in the small strain range of  $[0, 0.01]$ . The Young's modulus is 41.7 N/m and 42.0 N/m along the armchair and zigzag directions, respectively. The Poisson's ratio from the VFF model and the SW potential is  $\nu_{xy} = \nu_{yx} = 0.15$ .

There is no available value for nonlinear quantities in the single-layer b-AlSb. We have thus used the nonlinear parameter  $B = 0.5d^4$  in Eq. (5), which is close to the value of  $B$  in most materials. The value of the third order nonlinear elasticity  $D$  can be extracted by fitting the stress-strain relation to the function  $\sigma = E\epsilon + \frac{1}{2}D\epsilon^2$  with  $E$  as the Young's modulus. The values of  $D$  from the present SW potential are -142.4 N/m and -190.8 N/m along the armchair and zigzag directions, respectively. The ultimate stress is about  $8.1 \text{ Nm}^{-1}$  at the ultimate strain of 0.29 in the armchair direction at the low temperature of 1 K. The ultimate stress is about  $8.1 \text{ Nm}^{-1}$  at the ultimate strain of 0.31 in the zigzag direction at the low temperature of 1 K.

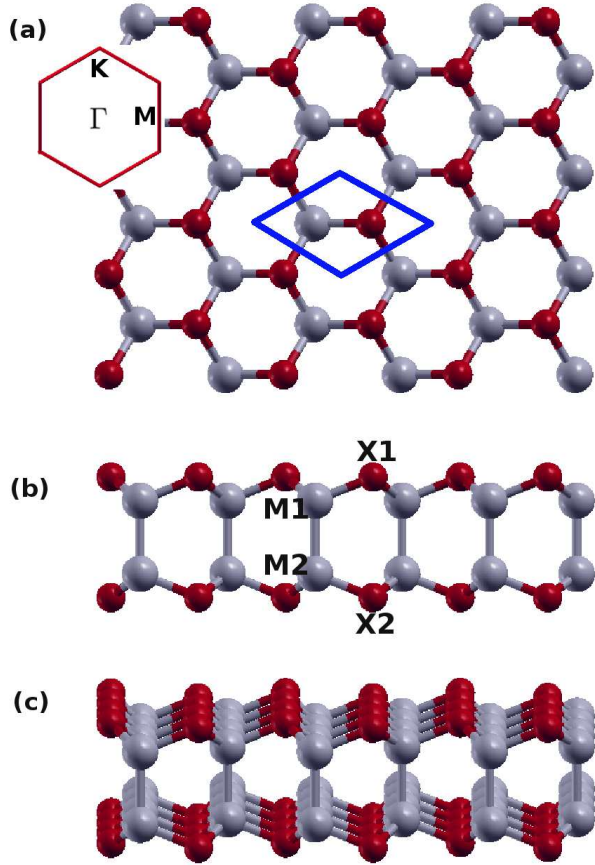


FIG. 239: (Color online) Structure of bi-buckled MX crystal, with M from group III and X from group VI. (a) Top view. The unit cell is highlighted by a blue parallelogram. Inset shows the first Brillouin zone of the reciprocal lattice space. (b) Side view displays the bi-buckled configuration. (c) Perspective view. M atoms are represented by larger gray balls. X atoms are represented by smaller red balls.

## CXVII. BO

Present studies on the BO are based on first-principles calculations, and no empirical potential has been proposed for the BO. We will thus parametrize a set of SW potential for the single-layer BO in this section.

The structure of the single-layer BO is shown in Fig. 239 with M=B and X=O. The structural parameters are from the *ab initio* calculations.<sup>114</sup> The BO has a bi-buckled configuration as shown in Fig. 239 (b), where the buckle is along the zigzag direction. Two buckling layers are symmetrically integrated through the interior B-B bonds, forming a bi-

TABLE CDLXVI: The VFF model for BO. The second line gives an explicit expression for each VFF term. The third line is the force constant parameters. Parameters are in the unit of  $\frac{eV}{\text{\AA}^2}$  for the bond stretching interactions, and in the unit of eV for the angle bending interaction. The fourth line gives the initial bond length (in unit of  $\text{\AA}$ ) for the bond stretching interaction and the initial angle (in unit of degrees) for the angle bending interaction.

VFF type	bond stretching		angle bending	
expression	$\frac{1}{2}K_{B-O}(\Delta r)^2$	$\frac{1}{2}K_{B-B}(\Delta r)^2$	$\frac{1}{2}K_{BOO}(\Delta\theta)^2$	$\frac{1}{2}K_{BBO}(\Delta\theta)^2$
parameter	23.030	15.512	5.577	6.209
$r_0$ or $\theta_0$	1.520	1.770	106.764	112.059

TABLE CDLXVII: Two-body SW potential parameters for BO used by GULP,<sup>8</sup> as expressed in Eq. (3).

	$A$ (eV)	$\rho$ ( $\text{\AA}$ )	$B$ ( $\text{\AA}^4$ )	$r_{\min}$ ( $\text{\AA}$ )	$r_{\max}$ ( $\text{\AA}$ )
B <sub>1</sub> -O <sub>1</sub>	11.725	1.207	2.669	0.0	2.197
B <sub>1</sub> -B <sub>2</sub>	6.749	0.875	4.908	0.0	2.392

TABLE CDLXVIII: Three-body SW potential parameters for BO used by GULP,<sup>8</sup> as expressed in Eq. (4).

	$K$ (eV)	$\theta_0$ (degree)	$\rho_1$ ( $\text{\AA}$ )	$\rho_2$ ( $\text{\AA}$ )	$r_{\min12}$ ( $\text{\AA}$ )	$r_{\max12}$ ( $\text{\AA}$ )	$r_{\min13}$ ( $\text{\AA}$ )	$r_{\max13}$ ( $\text{\AA}$ )	$r_{\min23}$ ( $\text{\AA}$ )	$r_{\max23}$ ( $\text{\AA}$ )
B <sub>1</sub> -O <sub>1</sub> -O <sub>1</sub>	107.486	106.764	1.207	1.207	0.0	2.197	0.0	2.197	0.0	3.333
B <sub>1</sub> -B <sub>2</sub> -O <sub>1</sub>	87.662	112.059	0.875	1.207	0.0	2.392	0.0	2.197	0.0	3.198

TABLE CDLXIX: SW potential parameters for BO used by LAMMPS,<sup>9</sup> as expressed in Eqs. (9) and (10).

	$\epsilon$ (eV)	$\sigma$ ( $\text{\AA}$ )	$a$	$\lambda$	$\gamma$	$\cos\theta_0$	$A_L$	$B_L$	$p$	$q$	tol
B <sub>1</sub> -O <sub>1</sub> -O <sub>1</sub>	1.000	1.207	1.820	107.486	1.000	-0.288	11.725	1.256	4	0	0.0
B <sub>1</sub> -B <sub>2</sub> -B <sub>2</sub>	1.000	0.875	2.734	0.000	1.000	0.000	6.749	8.377	4	0	0.0
B <sub>1</sub> -B <sub>2</sub> -O <sub>1</sub>	1.000	0.000	0.000	87.662	1.000	-0.376	0.000	0.000	4	0	0.0

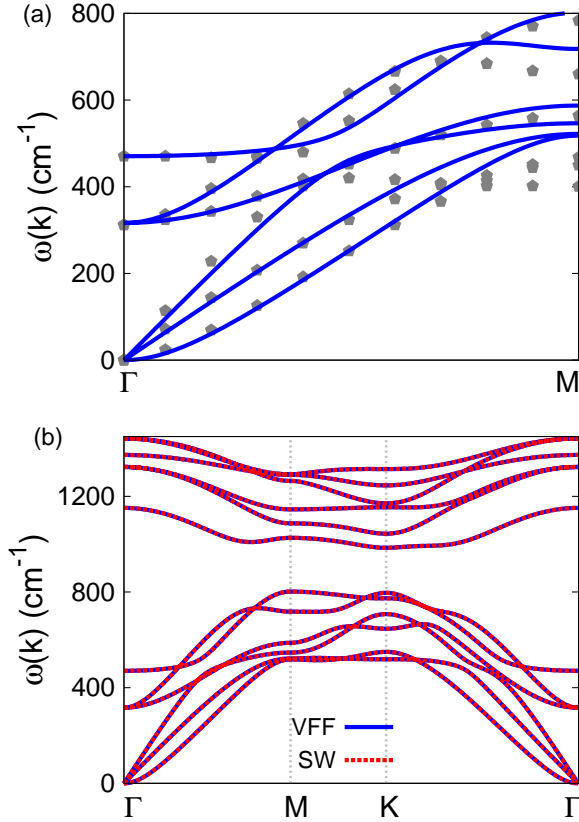


FIG. 240: (Color online) Phonon dispersion for the single-layer BO. (a) The VFF model is fitted to the six low-frequency branches along the  $\Gamma$ M direction. The *ab initio* results (gray pentagons) are from Ref. 114. (b) The VFF model (blue lines) and the SW potential (red lines) give the same phonon dispersion for the BO along  $\Gamma$ MK $\Gamma$ .

buckled configuration. This structure can be determined by three independent geometrical parameters, eg. the lattice constant  $2.44 \text{ \AA}$ , the bond length  $d_{\text{B-O}} = 1.52 \text{ \AA}$ , and the bond length  $d_{\text{B-B}} = 1.77 \text{ \AA}$ .

Table CDLXVI shows the VFF model for the single-layer BO. The force constant parameters are determined by fitting to the six low-frequency branches in the phonon dispersion along the  $\Gamma$ M as shown in Fig. 240 (a). The *ab initio* calculations for the phonon dispersion are from Ref. 114. Fig. 240 (b) shows that the VFF model and the SW potential give exactly the same phonon dispersion, as the SW potential is derived from the VFF model.

The parameters for the two-body SW potential used by GULP are shown in Tab. CDLXVII. The parameters for the three-body SW potential used by GULP are

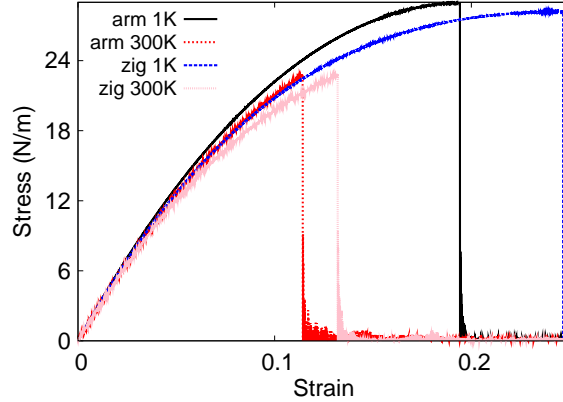


FIG. 241: (Color online) Stress-strain relations for the BO of size  $100 \times 100 \text{ \AA}$ . The BO is uniaxially stretched along the armchair or zigzag directions at temperatures 1 K and 300 K.

shown in Tab. CDLXVIII. Parameters for the SW potential used by LAMMPS are listed in Tab. CDLXIX.

We use LAMMPS to perform MD simulations for the mechanical behavior of the single-layer BO under uniaxial tension at 1.0 K and 300.0 K. Fig. 241 shows the stress-strain curve for the tension of a single-layer BO of dimension  $100 \times 100 \text{ \AA}$ . Periodic boundary conditions are applied in both armchair and zigzag directions. The single-layer BO is stretched uniaxially along the armchair or zigzag direction. The stress is calculated without involving the actual thickness of the quasi-two-dimensional structure of the single-layer BO. The Young's modulus can be obtained by a linear fitting of the stress-strain relation in the small strain range of  $[0, 0.01]$ . The Young's modulus is 299.6 N/m and 297.7 N/m along the armchair and zigzag directions, respectively. The Poisson's ratio from the VFF model and the SW potential is  $\nu_{xy} = \nu_{yx} = 0.11$ .

There is no available value for nonlinear quantities in the single-layer BO. We have thus used the nonlinear parameter  $B = 0.5d^4$  in Eq. (5), which is close to the value of  $B$  in most materials. The value of the third order nonlinear elasticity  $D$  can be extracted by fitting the stress-strain relation to the function  $\sigma = E\epsilon + \frac{1}{2}D\epsilon^2$  with  $E$  as the Young's modulus. The values of  $D$  from the present SW potential are -1554.7 N/m and -1585.2 N/m along the armchair and zigzag directions, respectively. The ultimate stress is about  $28.9 \text{ Nm}^{-1}$  at the ultimate strain of 0.19 in the armchair direction at the low temperature of 1 K. The ultimate stress is about  $28.2 \text{ Nm}^{-1}$  at the ultimate strain of 0.24 in the zigzag direction at

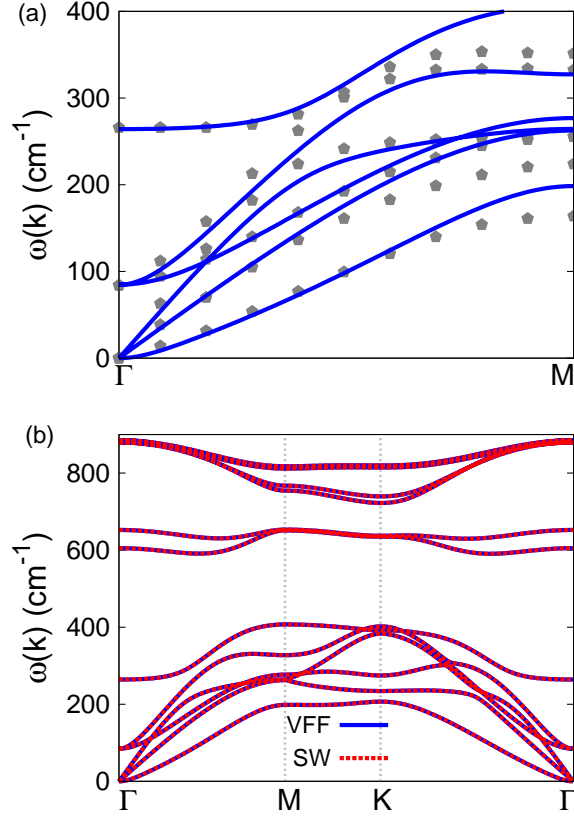


FIG. 242: (Color online) Phonon dispersion for the single-layer AIO. (a) The VFF model is fitted to the six low-frequency branches along the  $\Gamma$ M direction. The *ab initio* results (gray pentagons) are from Ref. 114. (b) The VFF model (blue lines) and the SW potential (red lines) give the same phonon dispersion for the AIO along  $\Gamma$ MKT $\Gamma$ .

the low temperature of 1 K.

### CXVIII. ALO

Present studies on the AIO are based on first-principles calculations, and no empirical potential has been proposed for the AIO. We will thus parametrize a set of SW potential for the single-layer AIO in this section.

The structure of the single-layer AIO is shown in Fig. 239 with M=Al and X=O. The structural parameters are from the *ab initio* calculations.<sup>114</sup> The AIO has a bi-buckled configuration as shown in Fig. 239 (b), where the buckle is along the zigzag direction. Two

TABLE CDLXX: The VFF model for AlO. The second line gives an explicit expression for each VFF term. The third line is the force constant parameters. Parameters are in the unit of  $\frac{eV}{\text{\AA}^2}$  for the bond stretching interactions, and in the unit of eV for the angle bending interaction. The fourth line gives the initial bond length (in unit of  $\text{\AA}$ ) for the bond stretching interaction and the initial angle (in unit of degrees) for the angle bending interaction.

VFF type	bond stretching		angle bending	
expression	$\frac{1}{2}K_{\text{Al-O}}(\Delta r)^2$	$\frac{1}{2}K_{\text{Al-Al}}(\Delta r)^2$	$\frac{1}{2}K_{\text{AlOO}}(\Delta\theta)^2$	$\frac{1}{2}K_{\text{AlAlO}}(\Delta\theta)^2$
parameter	18.189	6.410	3.182	1.318
$r_0$ or $\theta_0$	1.830	2.620	107.947	110.956

TABLE CDLXXI: Two-body SW potential parameters for AlO used by GULP,<sup>8</sup> as expressed in Eq. (3).

	$A$ (eV)	$\rho$ ( $\text{\AA}$ )	$B$ ( $\text{\AA}^4$ )	$r_{\min}$ ( $\text{\AA}$ )	$r_{\max}$ ( $\text{\AA}$ )
Al <sub>1</sub> -O <sub>1</sub>	13.758	1.488	5.608	0.0	2.655
Al <sub>1</sub> -Al <sub>2</sub>	3.609	0.678	23.560	0.0	3.287

TABLE CDLXXII: Three-body SW potential parameters for AlO used by GULP,<sup>8</sup> as expressed in Eq. (4).

	$K$ (eV)	$\theta_0$ (degree)	$\rho_1$ ( $\text{\AA}$ )	$\rho_2$ ( $\text{\AA}$ )	$r_{\min12}$ ( $\text{\AA}$ )	$r_{\max12}$ ( $\text{\AA}$ )	$r_{\min13}$ ( $\text{\AA}$ )	$r_{\max13}$ ( $\text{\AA}$ )	$r_{\min23}$ ( $\text{\AA}$ )	$r_{\max23}$ ( $\text{\AA}$ )
Al <sub>1</sub> -O <sub>1</sub> -O <sub>1</sub>	64.759	107.947	1.488	1.488	0.0	2.655	0.0	2.655	0.0	4.043
Al <sub>1</sub> -O <sub>1</sub> -Al <sub>2</sub>	12.688	110.956	1.488	0.678	0.0	2.655	0.0	3.287	0.0	4.213

TABLE CDLXXIII: SW potential parameters for AlO used by LAMMPS,<sup>9</sup> as expressed in Eqs. (9) and (10).

	$\epsilon$ (eV)	$\sigma$ ( $\text{\AA}$ )	$a$	$\lambda$	$\gamma$	$\cos\theta_0$	$A_L$	$B_L$	$p$	$q$	tol
Al <sub>1</sub> -O <sub>1</sub> -O <sub>1</sub>	1.000	1.488	1.785	64.759	1.000	-0.308	13.758	1.145	4	0	0.0
Al <sub>1</sub> -Al <sub>2</sub> -Al <sub>2</sub>	1.000	0.678	4.846	0.000	1.000	0.000	3.609	111.363	4	0	0.0
Al <sub>1</sub> -Al <sub>2</sub> -O <sub>1</sub>	1.000	0.000	0.000	12.688	1.000	-0.358	0.000	0.000	4	0	0.0

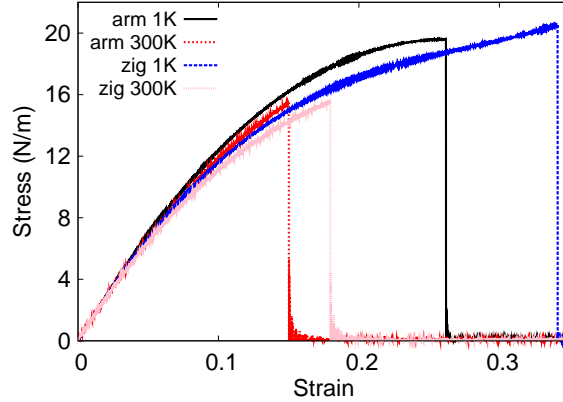


FIG. 243: (Color online) Stress-strain relations for the AlO of size  $100 \times 100 \text{ \AA}$ . The AlO is uniaxially stretched along the armchair or zigzag directions at temperatures 1 K and 300 K.

buckling layers are symmetrically integrated through the interior Al-Al bonds, forming a bi-buckled configuration. This structure can be determined by three independent geometrical parameters, eg. the lattice constant  $2.96 \text{ \AA}$ , the bond length  $d_{\text{Al-O}} = 1.83 \text{ \AA}$ , and the bond length  $d_{\text{Al-Al}} = 2.62 \text{ \AA}$ .

Table CDLXX shows the VFF model for the single-layer AlO. The force constant parameters are determined by fitting to the six low-frequency branches in the phonon dispersion along the  $\Gamma\text{M}$  as shown in Fig. 242 (a). The *ab initio* calculations for the phonon dispersion are from Ref. 114. Fig. 242 (b) shows that the VFF model and the SW potential give exactly the same phonon dispersion, as the SW potential is derived from the VFF model.

The parameters for the two-body SW potential used by GULP are shown in Tab. CDLXXI. The parameters for the three-body SW potential used by GULP are shown in Tab. CDLXXII. Parameters for the SW potential used by LAMMPS are listed in Tab. CDLXXIII.

We use LAMMPS to perform MD simulations for the mechanical behavior of the single-layer AlO under uniaxial tension at 1.0 K and 300.0 K. Fig. 243 shows the stress-strain curve for the tension of a single-layer AlO of dimension  $100 \times 100 \text{ \AA}$ . Periodic boundary conditions are applied in both armchair and zigzag directions. The single-layer AlO is stretched uniaxially along the armchair or zigzag direction. The stress is calculated without involving the actual thickness of the quasi-two-dimensional structure of the single-layer AlO. The Young's modulus can be obtained by a linear fitting of the stress-strain relation in the

TABLE CDLXXIV: The VFF model for GaO. The second line gives an explicit expression for each VFF term. The third line is the force constant parameters. Parameters are in the unit of  $\frac{eV}{\text{\AA}^2}$  for the bond stretching interactions, and in the unit of eV for the angle bending interaction. The fourth line gives the initial bond length (in unit of  $\text{\AA}$ ) for the bond stretching interaction and the initial angle (in unit of degrees) for the angle bending interaction.

VFF type	bond stretching		angle bending	
expression	$\frac{1}{2}K_{\text{Ga-O}}(\Delta r)^2$	$\frac{1}{2}K_{\text{Ga-Ga}}(\Delta r)^2$	$\frac{1}{2}K_{\text{GaOO}}(\Delta\theta)^2$	$\frac{1}{2}K_{\text{GaGaO}}(\Delta\theta)^2$
parameter	18.189	6.410	3.182	1.628
$r_0$ or $\theta_0$	1.940	2.510	107.051	111.794

TABLE CDLXXV: Two-body SW potential parameters for GaO used by GULP,<sup>8</sup> as expressed in Eq. (3).

	$A$ (eV)	$\rho$ ( $\text{\AA}$ )	$B$ ( $\text{\AA}^4$ )	$r_{\min}$ ( $\text{\AA}$ )	$r_{\max}$ ( $\text{\AA}$ )
Ga <sub>1</sub> -O <sub>1</sub>	15.178	1.550	7.082	0.0	2.807
Ga <sub>1</sub> -Ga <sub>2</sub>	4.225	0.890	19.846	0.0	3.257

small strain range of  $[0, 0.01]$ . The Young's modulus is 149.3 N/m and 148.2 N/m along the armchair and zigzag directions, respectively. The Poisson's ratio from the VFF model and the SW potential is  $\nu_{xy} = \nu_{yx} = 0.19$ .

There is no available value for nonlinear quantities in the single-layer AlO. We have thus used the nonlinear parameter  $B = 0.5d^4$  in Eq. (5), which is close to the value of  $B$  in most materials. The value of the third order nonlinear elasticity  $D$  can be extracted by fitting the stress-strain relation to the function  $\sigma = E\epsilon + \frac{1}{2}D\epsilon^2$  with  $E$  as the Young's modulus. The values of  $D$  from the present SW potential are -563.9 N/m and -565.6 N/m along the armchair and zigzag directions, respectively. The ultimate stress is about  $19.6 \text{ Nm}^{-1}$  at the ultimate strain of 0.26 in the armchair direction at the low temperature of 1 K. The ultimate stress is about  $20.4 \text{ Nm}^{-1}$  at the ultimate strain of 0.34 in the zigzag direction at the low temperature of 1 K.

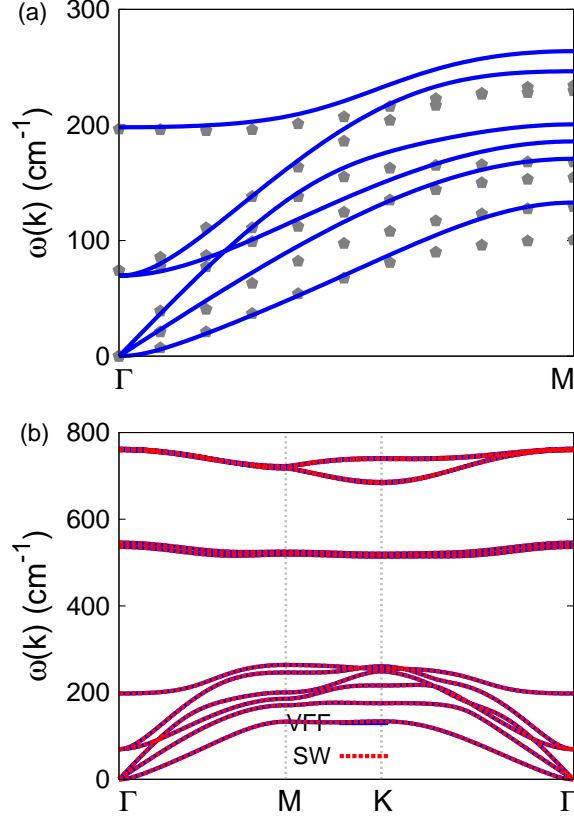


FIG. 244: (Color online) Phonon dispersion for the single-layer GaO. (a) The VFF model is fitted to the six low-frequency branches along the  $\Gamma$ M direction. The *ab initio* results (gray pentagons) are from Ref. 114. (b) The VFF model (blue lines) and the SW potential (red lines) give the same phonon dispersion for the GaO along  $\Gamma$ MK $\Gamma$ .

TABLE CDLXXVI: Three-body SW potential parameters for GaO used by GULP,<sup>8</sup> as expressed in Eq. (4).

	$K$ (eV)	$\theta_0$ (degree)	$\rho_1$ ( $\text{\AA}$ )	$\rho_2$ ( $\text{\AA}$ )	$r_{\min 12}$ ( $\text{\AA}$ )	$r_{\max 12}$ ( $\text{\AA}$ )	$r_{\min 13}$ ( $\text{\AA}$ )	$r_{\max 13}$ ( $\text{\AA}$ )	$r_{\min 23}$ ( $\text{\AA}$ )	$r_{\max 23}$ ( $\text{\AA}$ )
Ga <sub>1</sub> -O <sub>1</sub> -O <sub>1</sub>	62.149	107.051	1.550	1.550	0.0	2.807	0.0	2.807	0.0	4.262
Ga <sub>1</sub> -O <sub>1</sub> -Ga <sub>2</sub>	18.443	111.794	1.550	0.890	0.0	2.807	0.0	3.257	0.0	4.269

## CXIX. GAO

Present studies on the GaO are based on first-principles calculations, and no empirical potential has been proposed for the GaO. We will thus parametrize a set of SW potential

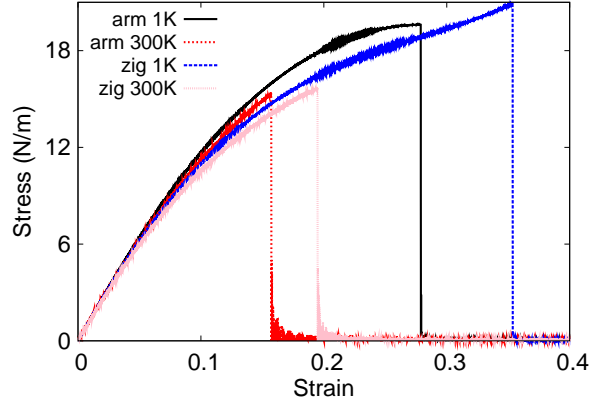


FIG. 245: (Color online) Stress-strain relations for the GaO of size  $100 \times 100 \text{ \AA}$ . The GaO is uniaxially stretched along the armchair or zigzag directions at temperatures 1 K and 300 K.

TABLE CDLXXVII: SW potential parameters for GaO used by LAMMPS,<sup>9</sup> as expressed in Eqs. (9) and (10).

	$\epsilon$ (eV)	$\sigma$ ( $\text{\AA}$ )	$a$	$\lambda$	$\gamma$	$\cos \theta_0$	$A_L$	$B_L$	$p$	$q$	tol
Ga <sub>1</sub> -O <sub>1</sub> -O <sub>1</sub>	1.000	1.550	1.811	62.149	1.000	-0.293	15.178	1.227	4	0	0.0
Ga <sub>1</sub> -Ga <sub>2</sub> -Ga <sub>2</sub>	1.000	0.890	3.661	0.000	1.000	0.000	4.225	31.685	4	0	0.0
Ga <sub>1</sub> -Ga <sub>2</sub> -O <sub>1</sub>	1.000	0.000	0.000	18.443	1.000	-0.371	0.000	0.000	4	0	0.0

for the single-layer GaO in this section.

The structure of the single-layer GaO is shown in Fig. 239 with M=Ga and X=O. The structural parameters are from the *ab initio* calculations.<sup>114</sup> The GaO has a bi-buckled configuration as shown in Fig. 239 (b), where the buckle is along the zigzag direction. Two buckling layers are symmetrically integrated through the interior Ga-Ga bonds, forming a bi-buckled configuration. This structure can be determined by three independent geometrical parameters, eg. the lattice constant  $3.12 \text{ \AA}$ , the bond length  $d_{\text{Ga-O}} = 1.94 \text{ \AA}$ , and the bond length  $d_{\text{Ga-Ga}} = 2.51 \text{ \AA}$ .

Table CDLXXIV shows the VFF model for the single-layer GaO. The force constant parameters are determined by fitting to the six low-frequency branches in the phonon dispersion along the  $\Gamma\text{M}$  as shown in Fig. 244 (a). The *ab initio* calculations for the phonon dispersion are from Ref. 114. Fig. 244 (b) shows that the VFF model and the SW potential give exactly the same phonon dispersion, as the SW potential is derived from the VFF

model.

The parameters for the two-body SW potential used by GULP are shown in Tab. CDLXXV. The parameters for the three-body SW potential used by GULP are shown in Tab. CDLXXVI. Parameters for the SW potential used by LAMMPS are listed in Tab. CDLXXVII.

We use LAMMPS to perform MD simulations for the mechanical behavior of the single-layer GaO under uniaxial tension at 1.0 K and 300.0 K. Fig. 245 shows the stress-strain curve for the tension of a single-layer GaO of dimension  $100 \times 100$  Å. Periodic boundary conditions are applied in both armchair and zigzag directions. The single-layer GaO is stretched uniaxially along the armchair or zigzag direction. The stress is calculated without involving the actual thickness of the quasi-two-dimensional structure of the single-layer GaO. The Young's modulus can be obtained by a linear fitting of the stress-strain relation in the small strain range of  $[0, 0.01]$ . The Young's modulus is 137.2 N/m and 136.6 N/m along the armchair and zigzag directions, respectively. The Poisson's ratio from the VFF model and the SW potential is  $\nu_{xy} = \nu_{yx} = 0.22$ .

There is no available value for nonlinear quantities in the single-layer GaO. We have thus used the nonlinear parameter  $B = 0.5d^4$  in Eq. (5), which is close to the value of  $B$  in most materials. The value of the third order nonlinear elasticity  $D$  can be extracted by fitting the stress-strain relation to the function  $\sigma = E\epsilon + \frac{1}{2}D\epsilon^2$  with  $E$  as the Young's modulus. The values of  $D$  from the present SW potential are -467.5 N/m and -529.6 N/m along the armchair and zigzag directions, respectively. The ultimate stress is about  $19.6 \text{ Nm}^{-1}$  at the ultimate strain of 0.28 in the armchair direction at the low temperature of 1 K. The ultimate stress is about  $20.8 \text{ Nm}^{-1}$  at the ultimate strain of 0.35 in the zigzag direction at the low temperature of 1 K.

## CXX. INO

Present studies on the InO are based on first-principles calculations, and no empirical potential has been proposed for the InO. We will thus parametrize a set of SW potential for the single-layer InO in this section.

The structure of the single-layer InO is shown in Fig. 239 with M=In and X=O. The structural parameters are from the *ab initio* calculations.<sup>114</sup> The InO has a bi-buckled con-

TABLE CDLXXVIII: The VFF model for InO. The second line gives an explicit expression for each VFF term. The third line is the force constant parameters. Parameters are in the unit of  $\frac{eV}{\text{\AA}^2}$  for the bond stretching interactions, and in the unit of eV for the angle bending interaction. The fourth line gives the initial bond length (in unit of  $\text{\AA}$ ) for the bond stretching interaction and the initial angle (in unit of degrees) for the angle bending interaction.

VFF type	bond stretching		angle bending	
expression	$\frac{1}{2}K_{\text{In-O}}(\Delta r)^2$	$\frac{1}{2}K_{\text{In-In}}(\Delta r)^2$	$\frac{1}{2}K_{\text{InOO}}(\Delta\theta)^2$	$\frac{1}{2}K_{\text{InInO}}(\Delta\theta)^2$
parameter	16.916	4.250	2.171	1.138
$r_0$ or $\theta_0$	2.160	2.860	107.328	111.538

TABLE CDLXXIX: Two-body SW potential parameters for InO used by GULP,<sup>8</sup> as expressed in Eq. (3).

	$A$ (eV)	$\rho$ ( $\text{\AA}$ )	$B$ ( $\text{\AA}^4$ )	$r_{\min}$ ( $\text{\AA}$ )	$r_{\max}$ ( $\text{\AA}$ )
In <sub>1</sub> -O <sub>1</sub>	17.600	1.735	10.884	0.0	3.128
In <sub>1</sub> -In <sub>2</sub>	3.440	0.945	33.453	0.0	3.682

TABLE CDLXXX: Three-body SW potential parameters for InO used by GULP,<sup>8</sup> as expressed in Eq. (4).

	$K$ (eV)	$\theta_0$ (degree)	$\rho_1$ ( $\text{\AA}$ )	$\rho_2$ ( $\text{\AA}$ )	$r_{\min12}$ ( $\text{\AA}$ )	$r_{\max12}$ ( $\text{\AA}$ )	$r_{\min13}$ ( $\text{\AA}$ )	$r_{\max13}$ ( $\text{\AA}$ )	$r_{\min23}$ ( $\text{\AA}$ )	$r_{\max23}$ ( $\text{\AA}$ )
In <sub>1</sub> -O <sub>1</sub> -O <sub>1</sub>	42.946	107.328	1.735	1.735	0.0	3.128	0.0	3.128	0.0	4.754
In <sub>1</sub> -O <sub>1</sub> -In <sub>2</sub>	12.470	111.538	1.735	0.945	0.0	3.128	0.0	3.682	0.0	4.800

TABLE CDLXXXI: SW potential parameters for InO used by LAMMPS,<sup>9</sup> as expressed in Eqs. (9) and (10).

	$\epsilon$ (eV)	$\sigma$ ( $\text{\AA}$ )	$a$	$\lambda$	$\gamma$	$\cos\theta_0$	$A_L$	$B_L$	$p$	$q$	tol
In <sub>1</sub> -O <sub>1</sub> -O <sub>1</sub>	1.000	1.735	1.803	42.946	1.000	-0.298	17.600	1.201	4	0	0.0
In <sub>1</sub> -In <sub>2</sub> -In <sub>2</sub>	1.000	0.945	3.895	0.000	1.000	0.000	3.440	41.864	4	0	0.0
In <sub>1</sub> -In <sub>2</sub> -O <sub>1</sub>	1.000	0.000	0.000	12.470	1.000	-0.367	0.000	0.000	4	0	0.0

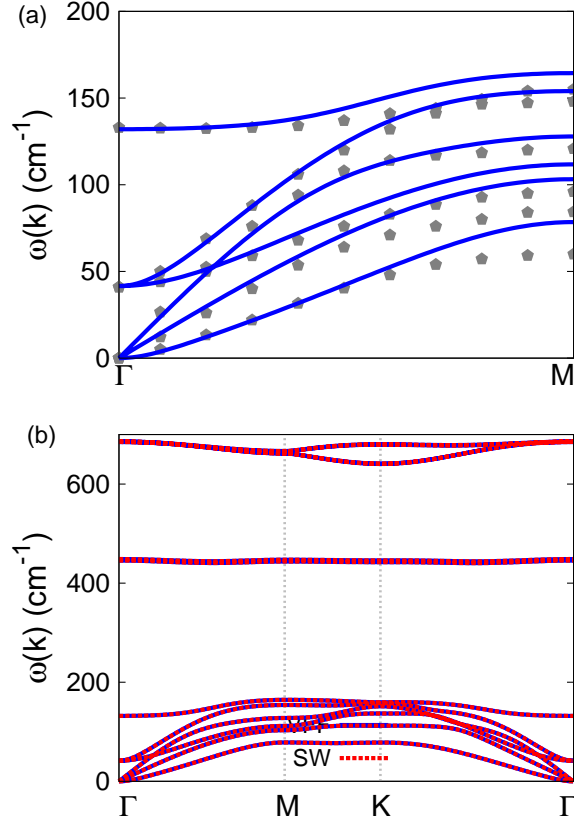


FIG. 246: (Color online) Phonon dispersion for the single-layer InO. (a) The VFF model is fitted to the six low-frequency branches along the  $\Gamma$ M direction. The *ab initio* results (gray pentagons) are from Ref. 114. (b) The VFF model (blue lines) and the SW potential (red lines) give the same phonon dispersion for the InO along  $\Gamma$ MK $\Gamma$ .

figuration as shown in Fig. 239 (b), where the buckle is along the zigzag direction. Two buckling layers are symmetrically integrated through the interior In-In bonds, forming a bi-buckled configuration. This structure can be determined by three independent geometrical parameters, eg. the lattice constant 3.48 Å, the bond length  $d_{\text{In-O}} = 2.16$  Å, and the bond length  $d_{\text{In-In}} = 2.86$  Å.

Table CDLXXVIII shows the VFF model for the single-layer InO. The force constant parameters are determined by fitting to the six low-frequency branches in the phonon dispersion along the  $\Gamma$ M as shown in Fig. 246 (a). The *ab initio* calculations for the phonon dispersion are from Ref. 114. Fig. 246 (b) shows that the VFF model and the SW potential give exactly the same phonon dispersion, as the SW potential is derived from the VFF

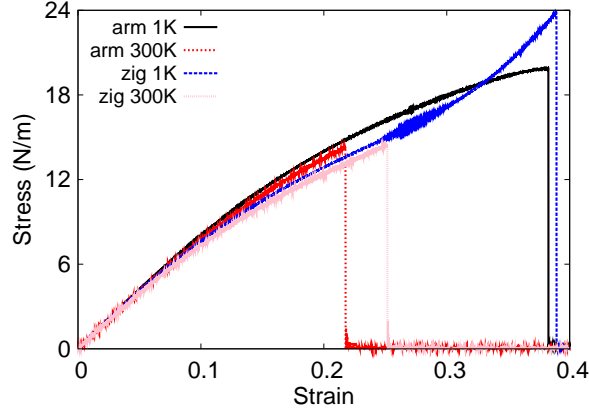


FIG. 247: (Color online) Stress-strain relations for the InO of size  $100 \times 100 \text{ \AA}$ . The InO is uniaxially stretched along the armchair or zigzag directions at temperatures 1 K and 300 K.

model.

The parameters for the two-body SW potential used by GULP are shown in Tab. CDLXXIX. The parameters for the three-body SW potential used by GULP are shown in Tab. CDLXXX. Parameters for the SW potential used by LAMMPS are listed in Tab. CDLXXXI.

We use LAMMPS to perform MD simulations for the mechanical behavior of the single-layer InO under uniaxial tension at 1.0 K and 300.0 K. Fig. 247 shows the stress-strain curve for the tension of a single-layer InO of dimension  $100 \times 100 \text{ \AA}$ . Periodic boundary conditions are applied in both armchair and zigzag directions. The single-layer InO is stretched uniaxially along the armchair or zigzag direction. The stress is calculated without involving the actual thickness of the quasi-two-dimensional structure of the single-layer InO. The Young's modulus can be obtained by a linear fitting of the stress-strain relation in the small strain range of  $[0, 0.01]$ . The Young's modulus is 85.7 N/m along the armchair and zigzag directions. The Poisson's ratio from the VFF model and the SW potential is  $\nu_{xy} = \nu_{yx} = 0.29$ .

There is no available value for nonlinear quantities in the single-layer InO. We have thus used the nonlinear parameter  $B = 0.5d^4$  in Eq. (5), which is close to the value of  $B$  in most materials. The value of the third order nonlinear elasticity  $D$  can be extracted by fitting the stress-strain relation to the function  $\sigma = E\epsilon + \frac{1}{2}D\epsilon^2$  with  $E$  as the Young's modulus. The values of  $D$  from the present SW potential are -157.3 N/m and -210.9 N/m along the

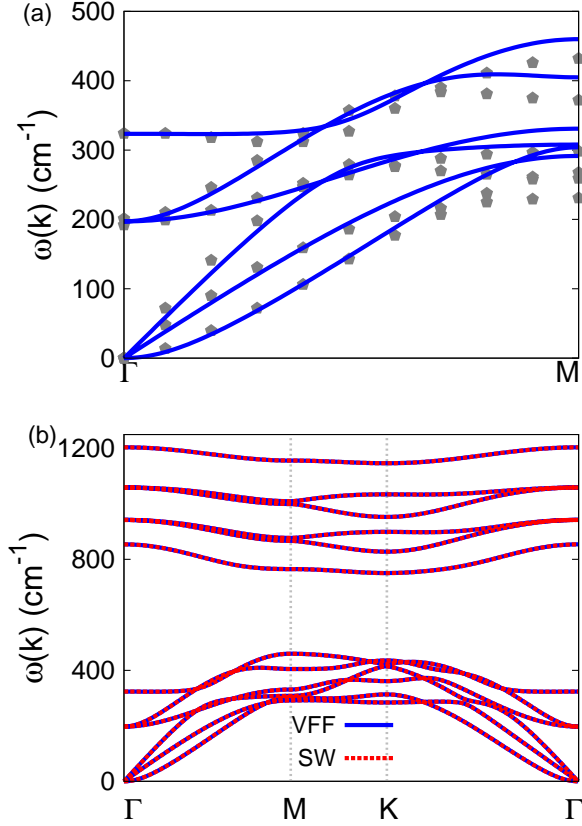


FIG. 248: (Color online) Phonon dispersion for the single-layer BS. (a) The VFF model is fitted to the six low-frequency branches along the  $\Gamma$ M direction. The *ab initio* results (gray pentagons) are from Ref. 114. (b) The VFF model (blue lines) and the SW potential (red lines) give the same phonon dispersion for the BS along  $\Gamma$ MK $\Gamma$ .

armchair and zigzag directions, respectively. The ultimate stress is about  $19.9 \text{ Nm}^{-1}$  at the ultimate strain of 0.38 in the armchair direction at the low temperature of 1 K. The ultimate stress is about  $23.6 \text{ Nm}^{-1}$  at the ultimate strain of 0.39 in the zigzag direction at the low temperature of 1 K.

## CXXI. BS

Present studies on the BS are based on first-principles calculations, and no empirical potential has been proposed for the BS. We will thus parametrize a set of SW potential for the single-layer BS in this section.

TABLE CDLXXXII: The VFF model for BS. The second line gives an explicit expression for each VFF term. The third line is the force constant parameters. Parameters are in the unit of  $\frac{eV}{\text{\AA}^2}$  for the bond stretching interactions, and in the unit of eV for the angle bending interaction. The fourth line gives the initial bond length (in unit of  $\text{\AA}$ ) for the bond stretching interaction and the initial angle (in unit of degrees) for the angle bending interaction.

VFF type	bond stretching		angle bending	
expression	$\frac{1}{2}K_{B-S}(\Delta r)^2$	$\frac{1}{2}K_{B-B}(\Delta r)^2$	$\frac{1}{2}K_{BSS}(\Delta\theta)^2$	$\frac{1}{2}K_{BBS}(\Delta\theta)^2$
parameter	17.138	16.385	5.144	3.861
$r_0$ or $\theta_0$	1.940	1.720	102.691	115.613

TABLE CDLXXXIII: Two-body SW potential parameters for BS used by GULP,<sup>8</sup> as expressed in Eq. (3).

	$A$ (eV)	$\rho$ ( $\text{\AA}$ )	$B$ ( $\text{\AA}^4$ )	$r_{\min}$ ( $\text{\AA}$ )	$r_{\max}$ ( $\text{\AA}$ )
B <sub>1</sub> -S <sub>1</sub>	13.021	1.417	7.082	0.0	2.769
B <sub>1</sub> -B <sub>2</sub>	14.613	1.809	4.376	0.0	2.602

TABLE CDLXXXIV: Three-body SW potential parameters for BS used by GULP,<sup>8</sup> as expressed in Eq. (4).

	$K$ (eV)	$\theta_0$ (degree)	$\rho_1$ ( $\text{\AA}$ )	$\rho_2$ ( $\text{\AA}$ )	$r_{\min12}$ ( $\text{\AA}$ )	$r_{\max12}$ ( $\text{\AA}$ )	$r_{\min13}$ ( $\text{\AA}$ )	$r_{\max13}$ ( $\text{\AA}$ )	$r_{\min23}$ ( $\text{\AA}$ )	$r_{\max23}$ ( $\text{\AA}$ )
B <sub>1</sub> -S <sub>1</sub> -S <sub>1</sub>	82.459	102.691	1.417	1.417	0.0	2.769	0.0	2.769	0.0	4.139
B <sub>1</sub> -B <sub>2</sub> -S <sub>1</sub>	102.002	115.613	1.809	1.417	0.0	2.602	0.0	2.769	0.0	3.717

TABLE CDLXXXV: SW potential parameters for BS used by LAMMPS,<sup>9</sup> as expressed in Eqs. (9) and (10).

	$\epsilon$ (eV)	$\sigma$ ( $\text{\AA}$ )	$a$	$\lambda$	$\gamma$	$\cos\theta_0$	$A_L$	$B_L$	$p$	$q$	tol
B <sub>1</sub> -S <sub>1</sub> -S <sub>1</sub>	1.000	1.417	1.955	82.459	1.000	-0.220	13.021	1.758	4	0	0.0
B <sub>1</sub> -B <sub>2</sub> -B <sub>2</sub>	1.000	1.809	1.438	0.000	1.000	0.000	14.613	0.408	4	0	0.0
B <sub>1</sub> -B <sub>2</sub> -S <sub>1</sub>	1.000	0.000	0.000	102.002	1.000	-0.432	0.000	0.000	4	0	0.0

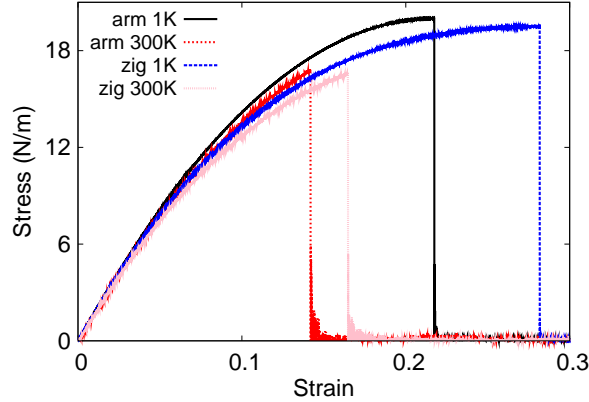


FIG. 249: (Color online) Stress-strain relations for the BS of size  $100 \times 100 \text{ \AA}$ . The BS is uniaxially stretched along the armchair or zigzag directions at temperatures 1 K and 300 K.

The structure of the single-layer BS is shown in Fig. 239 with  $M=B$  and  $X=S$ . The structural parameters are from the *ab initio* calculations.<sup>114</sup> The BS has a bi-buckled configuration as shown in Fig. 239 (b), where the buckle is along the zigzag direction. Two buckling layers are symmetrically integrated through the interior B-B bonds, forming a bi-buckled configuration. This structure can be determined by three independent geometrical parameters, eg. the lattice constant  $3.03 \text{ \AA}$ , the bond length  $d_{B-S} = 1.94 \text{ \AA}$ , and the bond length  $d_{B-B} = 1.72 \text{ \AA}$ .

Table CDLXXXII shows the VFF model for the single-layer BS. The force constant parameters are determined by fitting to the six low-frequency branches in the phonon dispersion along the  $\Gamma M$  as shown in Fig. 248 (a). The *ab initio* calculations for the phonon dispersion are from Ref. 114. Fig. 248 (b) shows that the VFF model and the SW potential give exactly the same phonon dispersion, as the SW potential is derived from the VFF model.

The parameters for the two-body SW potential used by GULP are shown in Tab. CDLXXXIII. The parameters for the three-body SW potential used by GULP are shown in Tab. CDLXXXIV. Parameters for the SW potential used by LAMMPS are listed in Tab. CDLXXXV.

We use LAMMPS to perform MD simulations for the mechanical behavior of the single-layer BS under uniaxial tension at 1.0 K and 300.0 K. Fig. 249 shows the stress-strain curve for the tension of a single-layer BS of dimension  $100 \times 100 \text{ \AA}$ . Periodic boundary conditions are applied in both armchair and zigzag directions. The single-layer BS is stretched uniaxially

TABLE CDLXXXVI: The VFF model for AIS. The second line gives an explicit expression for each VFF term. The third line is the force constant parameters. Parameters are in the unit of  $\frac{\text{eV}}{\text{\AA}^2}$  for the bond stretching interactions, and in the unit of eV for the angle bending interaction. The fourth line gives the initial bond length (in unit of  $\text{\AA}$ ) for the bond stretching interaction and the initial angle (in unit of degrees) for the angle bending interaction.

VFF type	bond stretching		angle bending	
expression	$\frac{1}{2}K_{\text{Al-S}}(\Delta r)^2$	$\frac{1}{2}K_{\text{Al-Al}}(\Delta r)^2$	$\frac{1}{2}K_{\text{AlSS}}(\Delta\theta)^2$	$\frac{1}{2}K_{\text{AlAIS}}(\Delta\theta)^2$
parameter	11.065	4.912	3.210	1.900
$r_0$ or $\theta_0$	2.320	2.590	100.600	117.324

along the armchair or zigzag direction. The stress is calculated without involving the actual thickness of the quasi-two-dimensional structure of the single-layer BS. The Young's modulus can be obtained by a linear fitting of the stress-strain relation in the small strain range of  $[0, 0.01]$ . The Young's modulus is 179.4 N/m and 178.5 N/m along the armchair and zigzag directions, respectively. The Poisson's ratio from the VFF model and the SW potential is  $\nu_{xy} = \nu_{yx} = 0.16$ .

There is no available value for nonlinear quantities in the single-layer BS. We have thus used the nonlinear parameter  $B = 0.5d^4$  in Eq. (5), which is close to the value of  $B$  in most materials. The value of the third order nonlinear elasticity  $D$  can be extracted by fitting the stress-strain relation to the function  $\sigma = E\epsilon + \frac{1}{2}D\epsilon^2$  with  $E$  as the Young's modulus. The values of  $D$  from the present SW potential are -793.2 N/m and -823.2 N/m along the armchair and zigzag directions, respectively. The ultimate stress is about 20.0  $\text{Nm}^{-1}$  at the ultimate strain of 0.21 in the armchair direction at the low temperature of 1 K. The ultimate stress is about 19.5  $\text{Nm}^{-1}$  at the ultimate strain of 0.28 in the zigzag direction at the low temperature of 1 K.

## CXXII. ALS

Present studies on the AIS are based on first-principles calculations, and no empirical potential has been proposed for the AIS. We will thus parametrize a set of SW potential for the single-layer AIS in this section.

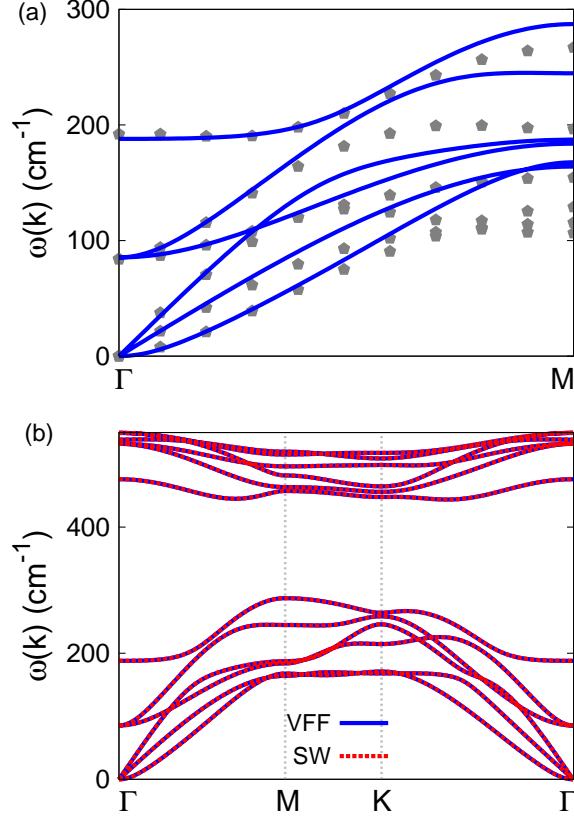


FIG. 250: (Color online) Phonon dispersion for the single-layer AIS. (a) The VFF model is fitted to the six low-frequency branches along the  $\Gamma$ M direction. The *ab initio* results (gray pentagons) are from Ref. 114. (b) The VFF model (blue lines) and the SW potential (red lines) give the same phonon dispersion for the AIS along  $\Gamma$ MK $\Gamma$ .

TABLE CDLXXXVII: Two-body SW potential parameters for AIS used by GULP,<sup>8</sup> as expressed in Eq. (3).

	$A$ (eV)	$\rho$ ( $\text{\AA}$ )	$B$ ( $\text{\AA}^4$ )	$r_{\min}$ ( $\text{\AA}$ )	$r_{\max}$ ( $\text{\AA}$ )
Al <sub>1</sub> -S <sub>1</sub>	11.476	1.618	14.485	0.0	3.289
Al <sub>1</sub> -Al <sub>2</sub>	4.575	1.280	22.499	0.0	3.500

The structure of the single-layer AIS is shown in Fig. 239 with M=Al and X=S. The structural parameters are from the *ab initio* calculations.<sup>114</sup> The AIS has a bi-buckled configuration as shown in Fig. 239 (b), where the buckle is along the zigzag direction. Two buckling layers are symmetrically integrated through the interior Al-Al bonds, forming a bi-

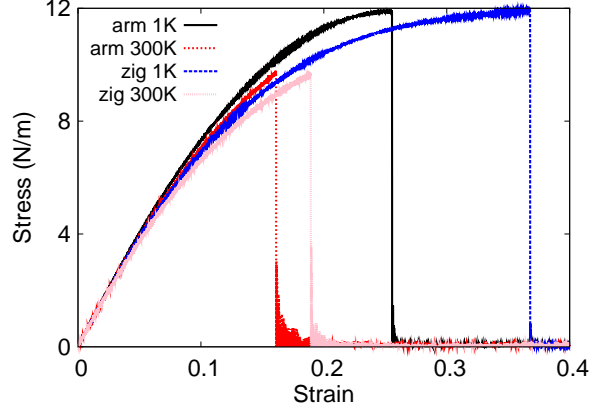


FIG. 251: (Color online) Stress-strain relations for the AlS of size  $100 \times 100 \text{ \AA}$ . The AlS is uniaxially stretched along the armchair or zigzag directions at temperatures 1 K and 300 K.

TABLE CDLXXXVIII: Three-body SW potential parameters for AlS used by GULP,<sup>8</sup> as expressed in Eq. (4).

	$K$ (eV)	$\theta_0$ (degree)	$\rho_1$ ( $\text{\AA}$ )	$\rho_2$ ( $\text{\AA}$ )	$r_{\min 12}$ ( $\text{\AA}$ )	$r_{\max 12}$ ( $\text{\AA}$ )	$r_{\min 13}$ ( $\text{\AA}$ )	$r_{\max 13}$ ( $\text{\AA}$ )	$r_{\min 23}$ ( $\text{\AA}$ )	$r_{\max 23}$ ( $\text{\AA}$ )
Al <sub>1</sub> -S <sub>1</sub> -S <sub>1</sub>	46.910	100.600	1.618	1.618	0.0	3.289	0.0	3.289	0.0	4.877
Al <sub>1</sub> -S <sub>1</sub> -Al <sub>2</sub>	26.090	117.324	1.280	1.618	0.0	3.500	0.0	3.289	0.0	4.853

buckled configuration. This structure can be determined by three independent geometrical parameters, eg. the lattice constant  $3.57 \text{ \AA}$ , the bond length  $d_{\text{Al-S}} = 2.32 \text{ \AA}$ , and the bond length  $d_{\text{Al-Al}} = 2.59 \text{ \AA}$ .

Table CDLXXXVI shows the VFF model for the single-layer AlS. The force constant parameters are determined by fitting to the six low-frequency branches in the phonon dispersion along the  $\Gamma\text{M}$  as shown in Fig. 250 (a). The *ab initio* calculations for the phonon

TABLE CDLXXXIX: SW potential parameters for AlS used by LAMMPS,<sup>9</sup> as expressed in Eqs. (9) and (10).

	$\epsilon$ (eV)	$\sigma$ ( $\text{\AA}$ )	$a$	$\lambda$	$\gamma$	$\cos \theta_0$	$A_L$	$B_L$	$p$	$q$	tol
Al <sub>1</sub> -S <sub>1</sub> -S <sub>1</sub>	1.000	1.618	2.032	46.910	1.000	-0.184	11.476	2.112	4	0	0.0
Al <sub>1</sub> -Al <sub>2</sub> -Al <sub>2</sub>	1.000	1.280	2.735	0.000	1.000	0.000	4.575	8.388	4	0	0.0
Al <sub>1</sub> -Al <sub>2</sub> -S <sub>1</sub>	1.000	0.000	0.000	26.090	1.000	-0.459	0.000	0.000	4	0	0.0

dispersion are from Ref. 114. Fig. 250 (b) shows that the VFF model and the SW potential give exactly the same phonon dispersion, as the SW potential is derived from the VFF model.

The parameters for the two-body SW potential used by GULP are shown in Tab. CDLXXXVII. The parameters for the three-body SW potential used by GULP are shown in Tab. CDLXXXVIII. Parameters for the SW potential used by LAMMPS are listed in Tab. CDLXXXIX.

We use LAMMPS to perform MD simulations for the mechanical behavior of the single-layer AIS under uniaxial tension at 1.0 K and 300.0 K. Fig. 251 shows the stress-strain curve for the tension of a single-layer AIS of dimension  $100 \times 100 \text{ \AA}$ . Periodic boundary conditions are applied in both armchair and zigzag directions. The single-layer AIS is stretched uniaxially along the armchair or zigzag direction. The stress is calculated without involving the actual thickness of the quasi-two-dimensional structure of the single-layer AIS. The Young's modulus can be obtained by a linear fitting of the stress-strain relation in the small strain range of  $[0, 0.01]$ . The Young's modulus is 85.2 N/m and 84.6 N/m along the armchair and zigzag directions, respectively. The Poisson's ratio from the VFF model and the SW potential is  $\nu_{xy} = \nu_{yx} = 0.22$ .

There is no available value for nonlinear quantities in the single-layer AIS. We have thus used the nonlinear parameter  $B = 0.5d^4$  in Eq. (5), which is close to the value of  $B$  in most materials. The value of the third order nonlinear elasticity  $D$  can be extracted by fitting the stress-strain relation to the function  $\sigma = E\epsilon + \frac{1}{2}D\epsilon^2$  with  $E$  as the Young's modulus. The values of  $D$  from the present SW potential are -289.7 N/m and -302.4 N/m along the armchair and zigzag directions, respectively. The ultimate stress is about  $11.9 \text{ Nm}^{-1}$  at the ultimate strain of 0.25 in the armchair direction at the low temperature of 1 K. The ultimate stress is about  $11.9 \text{ Nm}^{-1}$  at the ultimate strain of 0.36 in the zigzag direction at the low temperature of 1 K.

### CXXIII. GaS

Present studies on the GaS are based on first-principles calculations, and no empirical potential has been proposed for the GaS. We will thus parametrize a set of SW potential for the single-layer GaS in this section.

TABLE CDXC: The VFF model for GaS. The second line gives an explicit expression for each VFF term. The third line is the force constant parameters. Parameters are in the unit of  $\frac{\text{eV}}{\text{\AA}^2}$  for the bond stretching interactions, and in the unit of eV for the angle bending interaction. The fourth line gives the initial bond length (in unit of  $\text{\AA}$ ) for the bond stretching interaction and the initial angle (in unit of degrees) for the angle bending interaction.

VFF type	bond stretching		angle bending	
expression	$\frac{1}{2}K_{\text{Ga-S}}(\Delta r)^2$	$\frac{1}{2}K_{\text{Ga-Ga}}(\Delta r)^2$	$\frac{1}{2}K_{\text{GaSS}}(\Delta\theta)^2$	$\frac{1}{2}K_{\text{GaGaS}}(\Delta\theta)^2$
parameter	10.014	6.133	2.925	1.900
$r_0$ or $\theta_0$	2.360	2.470	100.921	117.065

TABLE CDXCI: Two-body SW potential parameters for GaS used by GULP,<sup>8</sup> as expressed in Eq. (3).

	$A$ (eV)	$\rho$ ( $\text{\AA}$ )	$B$ ( $\text{\AA}^4$ )	$r_{\min}$ ( $\text{\AA}$ )	$r_{\max}$ ( $\text{\AA}$ )
Ga <sub>1</sub> -S <sub>1</sub>	10.825	1.658	15.510	0.0	3.349
Ga <sub>1</sub> -Ga <sub>2</sub>	6.316	1.506	18.610	0.0	3.434

TABLE CDXCII: Three-body SW potential parameters for GaS used by GULP,<sup>8</sup> as expressed in Eq. (4).

	$K$ (eV)	$\theta_0$ (degree)	$\rho_1$ ( $\text{\AA}$ )	$\rho_2$ ( $\text{\AA}$ )	$r_{\min12}$ ( $\text{\AA}$ )	$r_{\max12}$ ( $\text{\AA}$ )	$r_{\min13}$ ( $\text{\AA}$ )	$r_{\max13}$ ( $\text{\AA}$ )	$r_{\min23}$ ( $\text{\AA}$ )	$r_{\max23}$ ( $\text{\AA}$ )
Ga <sub>1</sub> -S <sub>1</sub> -S <sub>1</sub>	43.355	100.921	1.658	1.658	0.0	3.349	0.0	3.349	0.0	4.972
Ga <sub>1</sub> -S <sub>1</sub> -Ga <sub>2</sub>	30.536	117.065	1.658	1.506	0.0	3.349	0.0	3.434	0.0	4.809

TABLE CDXCIII: SW potential parameters for GaS used by LAMMPS,<sup>9</sup> as expressed in Eqs. (9) and (10).

	$\epsilon$ (eV)	$\sigma$ ( $\text{\AA}$ )	$a$	$\lambda$	$\gamma$	$\cos\theta_0$	$A_L$	$B_L$	$p$	$q$	tol
Ga <sub>1</sub> -S <sub>1</sub> -S <sub>1</sub>	1.000	1.658	2.020	43.355	1.000	-0.189	10.825	2.052	4	0	0.0
Ga <sub>1</sub> -Ga <sub>2</sub> -Ga <sub>2</sub>	1.000	1.506	2.280	0.000	1.000	0.000	6.316	3.615	4	0	0.0
Ga <sub>1</sub> -Ga <sub>2</sub> -S <sub>1</sub>	1.000	0.000	0.000	30.536	1.000	-0.455	0.000	0.000	4	0	0.0

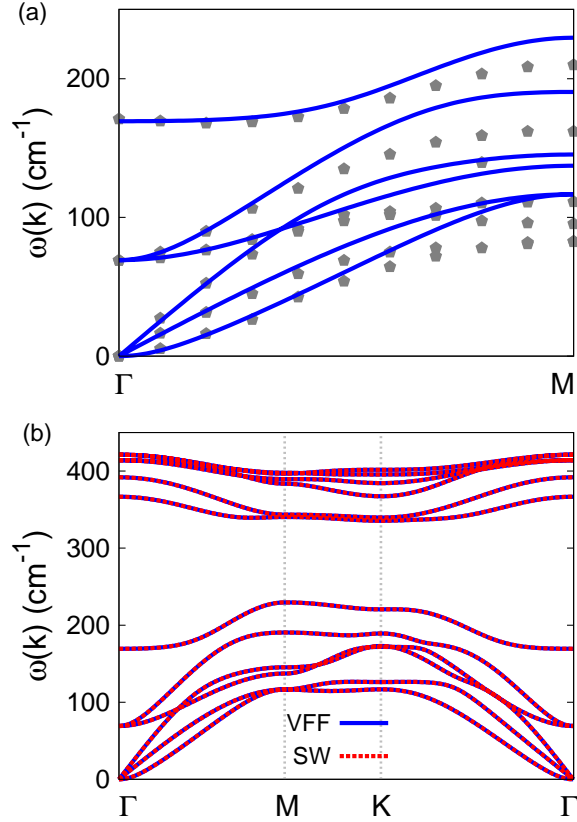


FIG. 252: (Color online) Phonon dispersion for the single-layer GaS. (a) The VFF model is fitted to the six low-frequency branches along the  $\Gamma$ M direction. The *ab initio* results (gray pentagons) are from Ref. 114. (b) The VFF model (blue lines) and the SW potential (red lines) give the same phonon dispersion for the GaS along  $\Gamma$ MKT.

The structure of the single-layer GaS is shown in Fig. 239 with M=Ga and X=S. The structural parameters are from the *ab initio* calculations.<sup>114</sup> The GaS has a bi-buckled configuration as shown in Fig. 239 (b), where the buckle is along the zigzag direction. Two buckling layers are symmetrically integrated through the interior Ga-Ga bonds, forming a bi-buckled configuration. This structure can be determined by three independent geometrical parameters, eg. the lattice constant  $3.64 \text{ \AA}$ , the bond length  $d_{\text{Ga-S}} = 2.36 \text{ \AA}$ , and the bond length  $d_{\text{Ga-Ga}} = 2.47 \text{ \AA}$ .

Table CDXC shows the VFF model for the single-layer GaS. The force constant parameters are determined by fitting to the six low-frequency branches in the phonon dispersion along the  $\Gamma$ M as shown in Fig. 252 (a). The *ab initio* calculations for the phonon dispersion

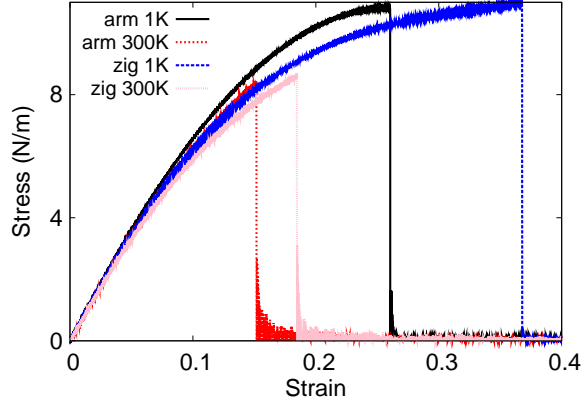


FIG. 253: (Color online) Stress-strain relations for the GaS of size  $100 \times 100 \text{ \AA}$ . The GaS is uniaxially stretched along the armchair or zigzag directions at temperatures 1 K and 300 K.

are from Ref. 114. Fig. 252 (b) shows that the VFF model and the SW potential give exactly the same phonon dispersion, as the SW potential is derived from the VFF model.

The parameters for the two-body SW potential used by GULP are shown in Tab. CDXCI. The parameters for the three-body SW potential used by GULP are shown in Tab. CDXCII. Parameters for the SW potential used by LAMMPS are listed in Tab. CDXCIII.

We use LAMMPS to perform MD simulations for the mechanical behavior of the single-layer GaS under uniaxial tension at 1.0 K and 300.0 K. Fig. 253 shows the stress-strain curve for the tension of a single-layer GaS of dimension  $100 \times 100 \text{ \AA}$ . Periodic boundary conditions are applied in both armchair and zigzag directions. The single-layer GaS is stretched uniaxially along the armchair or zigzag direction. The stress is calculated without involving the actual thickness of the quasi-two-dimensional structure of the single-layer GaS. The Young's modulus can be obtained by a linear fitting of the stress-strain relation in the small strain range of  $[0, 0.01]$ . The Young's modulus is 76.2 N/m along the armchair and zigzag directions. The Poisson's ratio from the VFF model and the SW potential is  $\nu_{xy} = \nu_{yx} = 0.23$ .

There is no available value for nonlinear quantities in the single-layer GaS. We have thus used the nonlinear parameter  $B = 0.5d^4$  in Eq. (5), which is close to the value of  $B$  in most materigas. The value of the third order nonlinear elasticity  $D$  can be extracted by fitting the stress-strain relation to the function  $\sigma = E\epsilon + \frac{1}{2}D\epsilon^2$  with  $E$  as the Young's modulus. The values of  $D$  from the present SW potential are -254.5 N/m and -269.8 N/m along the

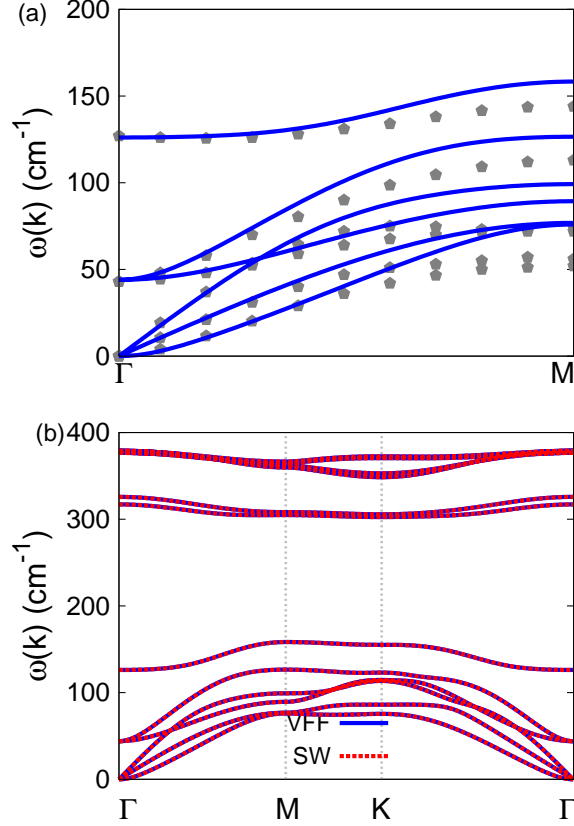


FIG. 254: (Color online) Phonon dispersion for the single-layer InS. (a) The VFF model is fitted to the six low-frequency branches along the  $\Gamma$ M direction. The *ab initio* results (gray pentagons) are from Ref. 114. (b) The VFF model (blue lines) and the SW potential (red lines) give the same phonon dispersion for the InS along  $\Gamma$ MK $\Gamma$ .

armchair and zigzag directions, respectively. The ultimate stress is about  $10.8 \text{ Nm}^{-1}$  at the ultimate strain of 0.26 in the armchair direction at the low temperature of 1 K. The ultimate stress is about  $11.0 \text{ Nm}^{-1}$  at the ultimate strain of 0.36 in the zigzag direction at the low temperature of 1 K.

#### CXXIV. INS

Present studies on the InS are based on first-principles calculations, and no empirical potential has been proposed for the InS. We will thus parametrize a set of SW potential for the single-layer InS in this section.

TABLE CDXCIV: The VFF model for InS. The second line gives an explicit expression for each VFF term. The third line is the force constant parameters. Parameters are in the unit of  $\frac{eV}{\text{\AA}^2}$  for the bond stretching interactions, and in the unit of eV for the angle bending interaction. The fourth line gives the initial bond length (in unit of  $\text{\AA}$ ) for the bond stretching interaction and the initial angle (in unit of degrees) for the angle bending interaction.

VFF type	bond stretching		angle bending	
expression	$\frac{1}{2}K_{\text{In-S}}(\Delta r)^2$	$\frac{1}{2}K_{\text{In-In}}(\Delta r)^2$	$\frac{1}{2}K_{\text{InSS}}(\Delta\theta)^2$	$\frac{1}{2}K_{\text{InInS}}(\Delta\theta)^2$
parameter	10.014	4.533	2.179	1.412
$r_0$ or $\theta_0$	2.560	2.820	100.624	117.305

TABLE CDXCV: Two-body SW potential parameters for InS used by GULP,<sup>8</sup> as expressed in Eq. (3).

	$A$ (eV)	$\rho$ ( $\text{\AA}$ )	$B$ ( $\text{\AA}^4$ )	$r_{\min}$ ( $\text{\AA}$ )	$r_{\max}$ ( $\text{\AA}$ )
In <sub>1</sub> -S <sub>1</sub>	12.652	1.787	21.475	0.0	3.629
In <sub>1</sub> -In <sub>2</sub>	5.202	1.454	31.620	0.0	3.833

TABLE CDXCVI: Three-body SW potential parameters for InS used by GULP,<sup>8</sup> as expressed in Eq. (4).

	$K$ (eV)	$\theta_0$ (degree)	$\rho_1$ ( $\text{\AA}$ )	$\rho_2$ ( $\text{\AA}$ )	$r_{\min12}$ ( $\text{\AA}$ )	$r_{\max12}$ ( $\text{\AA}$ )	$r_{\min13}$ ( $\text{\AA}$ )	$r_{\max13}$ ( $\text{\AA}$ )	$r_{\min23}$ ( $\text{\AA}$ )	$r_{\max23}$ ( $\text{\AA}$ )
In <sub>1</sub> -S <sub>1</sub> -S <sub>1</sub>	31.876	100.624	1.787	1.787	0.0	3.629	0.0	3.629	0.0	5.382
In <sub>1</sub> -S <sub>1</sub> -In <sub>2</sub>	19.900	117.305	1.787	1.454	0.0	3.629	0.0	3.833	0.0	5.325

TABLE CDXCVII: SW potential parameters for InS used by LAMMPS,<sup>9</sup> as expressed in Eqs. (9) and (10).

	$\epsilon$ (eV)	$\sigma$ ( $\text{\AA}$ )	$a$	$\lambda$	$\gamma$	$\cos\theta_0$	$A_L$	$B_L$	$p$	$q$	tol
In <sub>1</sub> -S <sub>1</sub> -S <sub>1</sub>	1.000	1.787	2.031	31.876	1.000	-0.184	12.652	2.108	4	0	0.0
In <sub>1</sub> -In <sub>2</sub> -In <sub>2</sub>	1.000	1.454	2.635	0.000	1.000	0.000	5.202	7.067	4	0	0.0
In <sub>1</sub> -In <sub>2</sub> -S <sub>1</sub>	1.000	0.000	0.000	19.990	1.000	-0.459	0.000	0.000	4	0	0.0

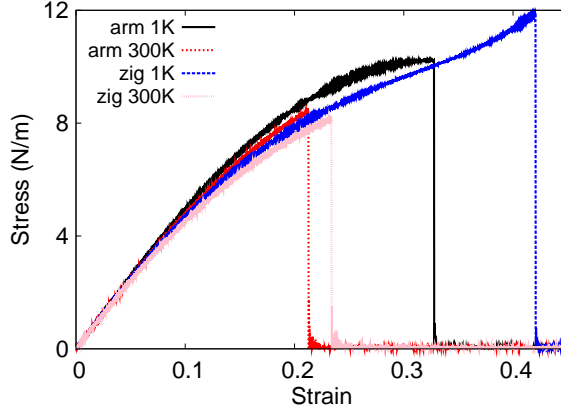


FIG. 255: (Color online) Stress-strain relations for the InS of size  $100 \times 100 \text{ \AA}$ . The InS is uniaxially stretched along the armchair or zigzag directions at temperatures 1 K and 300 K.

The structure of the single-layer InS is shown in Fig. 239 with  $M=\text{In}$  and  $X=\text{S}$ . The structural parameters are from the *ab initio* calculations.<sup>114</sup> The InS has a bi-buckled configuration as shown in Fig. 239 (b), where the buckle is along the zigzag direction. Two buckling layers are symmetrically integrated through the interior In-In bonds, forming a bi-buckled configuration. This structure can be determined by three independent geometrical parameters, eg. the lattice constant  $3.94 \text{ \AA}$ , the bond length  $d_{\text{In-S}} = 2.56 \text{ \AA}$ , and the bond length  $d_{\text{In-In}} = 2.82 \text{ \AA}$ .

Table CDXCIV shows the VFF model for the single-layer InS. The force constant parameters are determined by fitting to the six low-frequency branches in the phonon dispersion along the  $\Gamma\text{M}$  as shown in Fig. 254 (a). The *ab initio* calculations for the phonon dispersion are from Ref. 114. Fig. 254 (b) shows that the VFF model and the SW potential give exactly the same phonon dispersion, as the SW potential is derived from the VFF model.

The parameters for the two-body SW potential used by GULP are shown in Tab. CDXCV. The parameters for the three-body SW potential used by GULP are shown in Tab. CDXCVI. Parameters for the SW potential used by LAMMPS are listed in Tab. CDXCVII.

We use LAMMPS to perform MD simulations for the mechanical behavior of the single-layer InS under uniaxial tension at 1.0 K and 300.0 K. Fig. 255 shows the stress-strain curve for the tension of a single-layer InS of dimension  $100 \times 100 \text{ \AA}$ . Periodic boundary conditions are applied in both armchair and zigzag directions. The single-layer InS is stretched uniaxially along the armchair or zigzag direction. The stress is calculated without involving the

TABLE CDXCVIII: The VFF model for BSe. The second line gives an explicit expression for each VFF term. The third line is the force constant parameters. Parameters are in the unit of  $\frac{eV}{\text{Å}^2}$  for the bond stretching interactions, and in the unit of eV for the angle bending interaction. The fourth line gives the initial bond length (in unit of Å) for the bond stretching interaction and the initial angle (in unit of degrees) for the angle bending interaction.

VFF type	bond stretching		angle bending	
expression	$\frac{1}{2}K_{B-Se}(\Delta r)^2$	$\frac{1}{2}K_{B-B}(\Delta r)^2$	$\frac{1}{2}K_{BSeSe}(\Delta\theta)^2$	$\frac{1}{2}K_{BBSe}(\Delta\theta)^2$
parameter	17.138	15.227	5.144	3.113
$r_0$ or $\theta_0$	2.100	1.710	101.394	116.681

actual thickness of the quasi-two-dimensional structure of the single-layer InS. The Young's modulus can be obtained by a linear fitting of the stress-strain relation in the small strain range of  $[0, 0.01]$ . The Young's modulus is 52.9 N/m and 53.2 N/m along the armchair and zigzag directions, respectively. The Poisson's ratio from the VFF model and the SW potential is  $\nu_{xy} = \nu_{yx} = 0.29$ .

There is no available value for nonlinear quantities in the single-layer InS. We have thus used the nonlinear parameter  $B = 0.5d^4$  in Eq. (5), which is close to the value of  $B$  in most materials. The value of the third order nonlinear elasticity  $D$  can be extracted by fitting the stress-strain relation to the function  $\sigma = E\epsilon + \frac{1}{2}D\epsilon^2$  with  $E$  as the Young's modulus. The values of  $D$  from the present SW potential are -115.9 N/m and -141.1 N/m along the armchair and zigzag directions, respectively. The ultimate stress is about  $10.2 \text{ Nm}^{-1}$  at the ultimate strain of 0.32 in the armchair direction at the low temperature of 1 K. The ultimate stress is about  $11.8 \text{ Nm}^{-1}$  at the ultimate strain of 0.42 in the zigzag direction at the low temperature of 1 K.

## CXXV. BSE

Present studies on the BSe are based on first-principles calculations, and no empirical potential has been proposed for the BSe. We will thus parametrize a set of SW potential for the single-layer BSe in this section.

The structure of the single-layer BSe is shown in Fig. 239 with M=B and X=Se. The

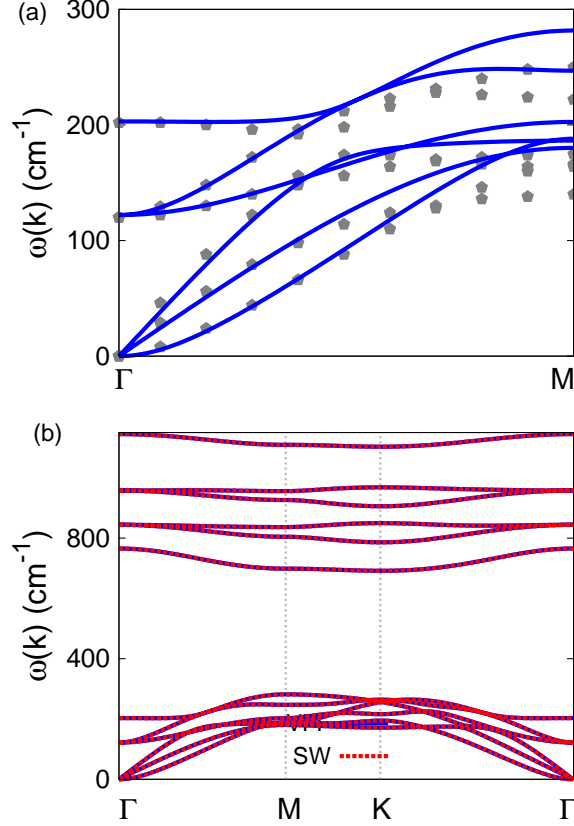


FIG. 256: (Color online) Phonon dispersion for the single-layer BSe. (a) The VFF model is fitted to the six low-frequency branches along the  $\Gamma$ M direction. The *ab initio* results (gray pentagons) are from Ref. 114. (b) The VFF model (blue lines) and the SW potential (red lines) give the same phonon dispersion for the BSe along  $\Gamma$ MK $\Gamma$ .

TABLE CDXCIX: Two-body SW potential parameters for BSe used by GULP,<sup>8</sup> as expressed in Eq. (3).

	$A$ (eV)	$\rho$ ( $\text{\AA}$ )	$B$ ( $\text{\AA}^4$ )	$r_{\min}$ ( $\text{\AA}$ )	$r_{\max}$ ( $\text{\AA}$ )
B <sub>1</sub> -Se <sub>1</sub>	14.825	1.491	9.724	0.0	2.985
B <sub>1</sub> -B <sub>2</sub>	17.700	2.252	4.275	0.0	2.691

structural parameters are from the *ab initio* calculations.<sup>114</sup> The BSe has a bi-buckled configuration as shown in Fig. 239 (b), where the buckle is along the zigzag direction. Two buckling layers are symmetrically integrated through the interior B-B bonds, forming a bi-buckled configuration. This structure can be determined by three independent geometrical

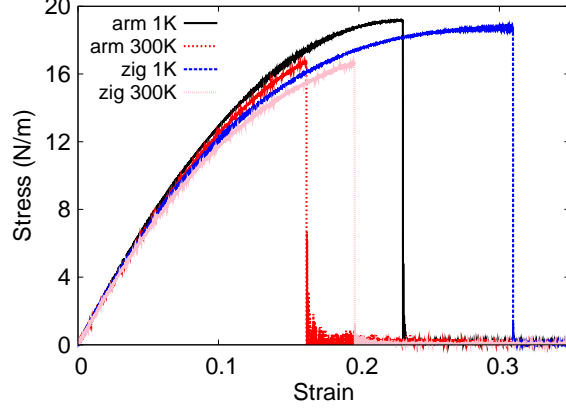


FIG. 257: (Color online) Stress-strain relations for the BSe of size  $100 \times 100 \text{ \AA}$ . The BSe is uniaxially stretched along the armchair or zigzag directions at temperatures 1 K and 300 K.

TABLE D: Three-body SW potential parameters for BSe used by GULP,<sup>8</sup> as expressed in Eq. (4).

	$K$ (eV)	$\theta_0$ (degree)	$\rho_1$ ( $\text{\AA}$ )	$\rho_2$ ( $\text{\AA}$ )	$r_{\min 12}$ ( $\text{\AA}$ )	$r_{\max 12}$ ( $\text{\AA}$ )	$r_{\min 13}$ ( $\text{\AA}$ )	$r_{\max 13}$ ( $\text{\AA}$ )	$r_{\min 23}$ ( $\text{\AA}$ )	$r_{\max 23}$ ( $\text{\AA}$ )
B <sub>1</sub> -S <sub>1</sub> -Se <sub>1</sub>	77.850	101.394	1.491	1.491	0.0	2.985	0.0	2.985	0.0	4.440
B <sub>1</sub> -B <sub>2</sub> -Se <sub>1</sub>	104.372	116.681	2.252	1.491	0.0	2.691	0.0	2.985	0.0	3.923

parameters, eg. the lattice constant  $3.25 \text{ \AA}$ , the bond length  $d_{\text{B-Se}} = 2.10 \text{ \AA}$ , and the bond length  $d_{\text{B-B}} = 1.71 \text{ \AA}$ .

Table CDXCVIII shows the VFF model for the single-layer BSe. The force constant parameters are determined by fitting to the six low-frequency branches in the phonon dispersion along the  $\Gamma\text{M}$  as shown in Fig. 256 (a). The *ab initio* calculations for the phonon dispersion are from Ref. 114. Fig. 256 (b) shows that the VFF model and the SW potential give exactly the same phonon dispersion, as the SW potential is derived from the VFF model.

TABLE DI: SW potential parameters for BSe used by LAMMPS,<sup>9</sup> as expressed in Eqs. (9) and (10).

	$\epsilon$ (eV)	$\sigma$ ( $\text{\AA}$ )	$a$	$\lambda$	$\gamma$	$\cos \theta_0$	$A_L$	$B_L$	$p$	$q$	tol
B <sub>1</sub> -Se <sub>1</sub> -Se <sub>1</sub>	1.000	1.491	2.002	77.850	1.000	-0.198	14.825	1.968	4	0	0.0
B <sub>1</sub> -B <sub>2</sub> -B <sub>2</sub>	1.000	2.252	1.195	0.000	1.000	0.000	17.700	0.166	4	0	0.0
B <sub>1</sub> -B <sub>2</sub> -Se <sub>1</sub>	1.000	0.000	0.000	104.372	1.000	-0.449	0.000	0.000	4	0	0.0

The parameters for the two-body SW potential used by GULP are shown in Tab. CDXCIX. The parameters for the three-body SW potential used by GULP are shown in Tab. D. Parameters for the SW potential used by LAMMPS are listed in Tab. DI.

We use LAMMPS to perform MD simulations for the mechanical behavior of the single-layer BSe under uniaxial tension at 1.0 K and 300.0 K. Fig. 257 shows the stress-strain curve for the tension of a single-layer BSe of dimension  $100 \times 100 \text{ \AA}$ . Periodic boundary conditions are applied in both armchair and zigzag directions. The single-layer BSe is stretched uniaxially along the armchair or zigzag direction. The stress is calculated without involving the actual thickness of the quasi-two-dimensional structure of the single-layer BSe. The Young's modulus can be obtained by a linear fitting of the stress-strain relation in the small strain range of  $[0, 0.01]$ . The Young's modulus is 157.3 N/m and 156.4 N/m along the armchair and zigzag directions, respectively. The Poisson's ratio from the VFF model and the SW potential is  $\nu_{xy} = \nu_{yx} = 0.19$ .

There is no available value for nonlinear quantities in the single-layer BSe. We have thus used the nonlinear parameter  $B = 0.5d^4$  in Eq. (5), which is close to the value of  $B$  in most materials. The value of the third order nonlinear elasticity  $D$  can be extracted by fitting the stress-strain relation to the function  $\sigma = E\epsilon + \frac{1}{2}D\epsilon^2$  with  $E$  as the Young's modulus. The values of  $D$  from the present SW potential are -627.0 N/m and -655.6 N/m along the armchair and zigzag directions, respectively. The ultimate stress is about  $19.2 \text{ Nm}^{-1}$  at the ultimate strain of 0.23 in the armchair direction at the low temperature of 1 K. The ultimate stress is about  $18.7 \text{ Nm}^{-1}$  at the ultimate strain of 0.31 in the zigzag direction at the low temperature of 1 K.

## CXXVI. ALSE

Present studies on the AlSe are based on first-principles calculations, and no empirical potential has been proposed for the AlSe. We will thus parametrize a set of SW potential for the single-layer AlSe in this section.

The structure of the single-layer AlSe is shown in Fig. 239 with M=Al and X=Se. The structural parameters are from the *ab initio* calculations.<sup>114</sup> The AlSe has a bi-buckled configuration as shown in Fig. 239 (b), where the buckle is along the zigzag direction. Two buckling layers are symmetrically integrated through the interior Al-Al bonds, forming a bi-

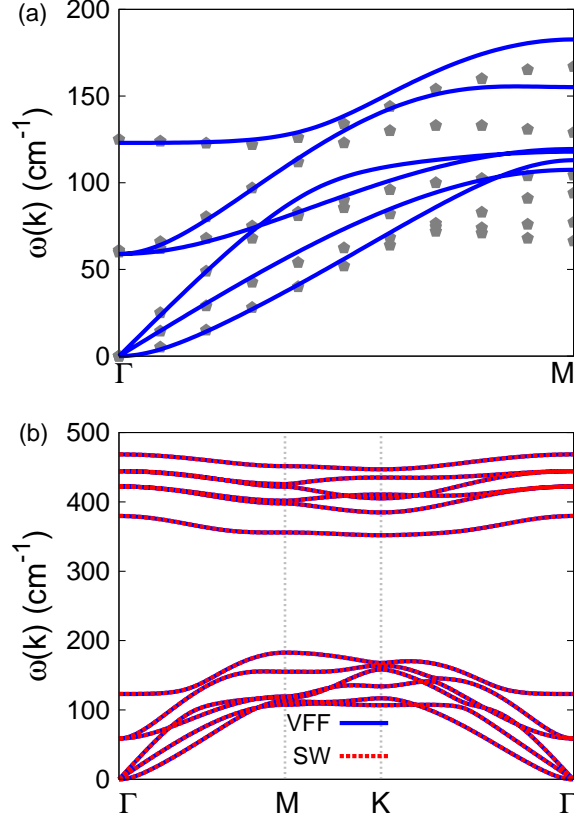


FIG. 258: (Color online) Phonon dispersion for the single-layer AlSe. (a) The VFF model is fitted to the six low-frequency branches along the  $\Gamma$ M direction. The *ab initio* results (gray pentagons) are from Ref. 114. (b) The VFF model (blue lines) and the SW potential (red lines) give the same phonon dispersion for the AlSe along  $\Gamma$ MKT $\Gamma$ .

buckled configuration. This structure can be determined by three independent geometrical parameters, eg. the lattice constant  $3.78 \text{ \AA}$ , the bond length  $d_{\text{Al-Se}} = 2.47 \text{ \AA}$ , and the bond length  $d_{\text{Al-Al}} = 2.57 \text{ \AA}$ .

Table DII shows the VFF model for the single-layer AlSe. The force constant parameters are determined by fitting to the six low-frequency branches in the phonon dispersion along the  $\Gamma$ M as shown in Fig. 258 (a). The *ab initio* calculations for the phonon dispersion are from Ref. 114. Fig. 258 (b) shows that the VFF model and the SW potential give exactly the same phonon dispersion, as the SW potential is derived from the VFF model.

The parameters for the two-body SW potential used by GULP are shown in Tab. DIII. The parameters for the three-body SW potential used by GULP are shown in Tab. DIV.

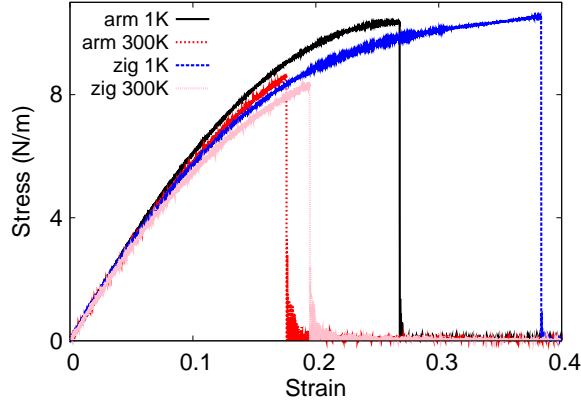


FIG. 259: (Color online) Stress-strain relations for the AlSe of size  $100 \times 100 \text{ \AA}$ . The AlSe is uniaxially stretched along the armchair or zigzag directions at temperatures 1 K and 300 K.

TABLE DII: The VFF model for AlSe. The second line gives an explicit expression for each VFF term. The third line is the force constant parameters. Parameters are in the unit of  $\frac{eV}{\text{\AA}^2}$  for the bond stretching interactions, and in the unit of eV for the angle bending interaction. The fourth line gives the initial bond length (in unit of  $\text{\AA}$ ) for the bond stretching interaction and the initial angle (in unit of degrees) for the angle bending interaction.

VFF type	bond stretching		angle bending	
expression	$\frac{1}{2}K_{Al-Se}(\Delta r)^2$	$\frac{1}{2}K_{Al-Al}(\Delta r)^2$	$\frac{1}{2}K_{AlSeSe}(\Delta\theta)^2$	$\frac{1}{2}K_{AlAlSe}(\Delta\theta)^2$
parameter	9.831	4.487	2.916	1.659
$r_0$ or $\theta_0$	2.470	2.570	99.846	117.926

Parameters for the SW potential used by LAMMPS are listed in Tab. DV.

We use LAMMPS to perform MD simulations for the mechanical behavior of the single-layer AlSe under uniaxial tension at 1.0 K and 300.0 K. Fig. 259 shows the stress-strain curve for the tension of a single-layer AlSe of dimension  $100 \times 100 \text{ \AA}$ . Periodic boundary

TABLE DIII: Two-body SW potential parameters for AlSe used by GULP,<sup>8</sup> as expressed in Eq. (3).

	$A$ (eV)	$\rho$ ( $\text{\AA}$ )	$B$ ( $\text{\AA}^4$ )	$r_{\min}$ ( $\text{\AA}$ )	$r_{\max}$ ( $\text{\AA}$ )
Al <sub>1</sub> -Se <sub>1</sub>	11.362	1.694	18.610	0.0	3.493
Al <sub>1</sub> -Al <sub>2</sub>	4.974	1.558	21.812	0.0	3.570

TABLE DIV: Three-body SW potential parameters for AlSe used by GULP,<sup>8</sup> as expressed in Eq. (4).

	$K$ (eV)	$\theta_0$ (degree)	$\rho_1$ (Å)	$\rho_2$ (Å)	$r_{\min 12}$ (Å)	$r_{\max 12}$ (Å)	$r_{\min 13}$ (Å)	$r_{\max 13}$ (Å)	$r_{\min 23}$ (Å)	$r_{\max 23}$ (Å)
Al <sub>1</sub> -Se <sub>1</sub> -Se <sub>1</sub>	41.235	99.846	1.694	1.694	0.0	3.493	0.0	3.493	0.0	5.164
Al <sub>1</sub> -Se <sub>1</sub> -Al <sub>2</sub>	26.418	117.926	1.558	1.694	0.0	3.570	0.0	3.493	0.0	5.029

TABLE DV: SW potential parameters for AlSe used by LAMMPS,<sup>9</sup> as expressed in Eqs. (9) and (10).

	$\epsilon$ (eV)	$\sigma$ (Å)	$a$	$\lambda$	$\gamma$	$\cos \theta_0$	$A_L$	$B_L$	$p$	$q$	tol
Al <sub>1</sub> -Se <sub>1</sub> -Se <sub>1</sub>	1.000	1.694	2.062	41.235	1.000	-0.171	11.362	2.260	4	0	0.0
Al <sub>1</sub> -Al <sub>2</sub> -Al <sub>2</sub>	1.000	1.558	2.292	0.000	1.000	0.000	4.974	3.704	4	0	0.0
Al <sub>1</sub> -Al <sub>2</sub> -Se <sub>1</sub>	1.000	0.000	0.000	26.418	1.000	-0.468	0.000	0.000	4	0	0.0

conditions are applied in both armchair and zigzag directions. The single-layer AlSe is stretched uniaxially along the armchair or zigzag direction. The stress is calculated without involving the actual thickness of the quasi-two-dimensional structure of the single-layer AlSe. The Young's modulus can be obtained by a linear fitting of the stress-strain relation in the small strain range of  $[0, 0.01]$ . The Young's modulus is 69.4 N/m and 69.2 N/m along the armchair and zigzag directions, respectively. The Poisson's ratio from the VFF model and the SW potential is  $\nu_{xy} = \nu_{yx} = 0.24$ .

There is no available value for nonlinear quantities in the single-layer AlSe. We have thus used the nonlinear parameter  $B = 0.5d^4$  in Eq. (5), which is close to the value of  $B$  in most materials. The value of the third order nonlinear elasticity  $D$  can be extracted by fitting the stress-strain relation to the function  $\sigma = E\epsilon + \frac{1}{2}D\epsilon^2$  with  $E$  as the Young's modulus. The values of  $D$  from the present SW potential are -217.3 N/m and -231.9 N/m along the armchair and zigzag directions, respectively. The ultimate stress is about 10.4 Nm<sup>-1</sup> at the ultimate strain of 0.27 in the armchair direction at the low temperature of 1 K. The ultimate stress is about 10.5 Nm<sup>-1</sup> at the ultimate strain of 0.38 in the zigzag direction at the low temperature of 1 K.

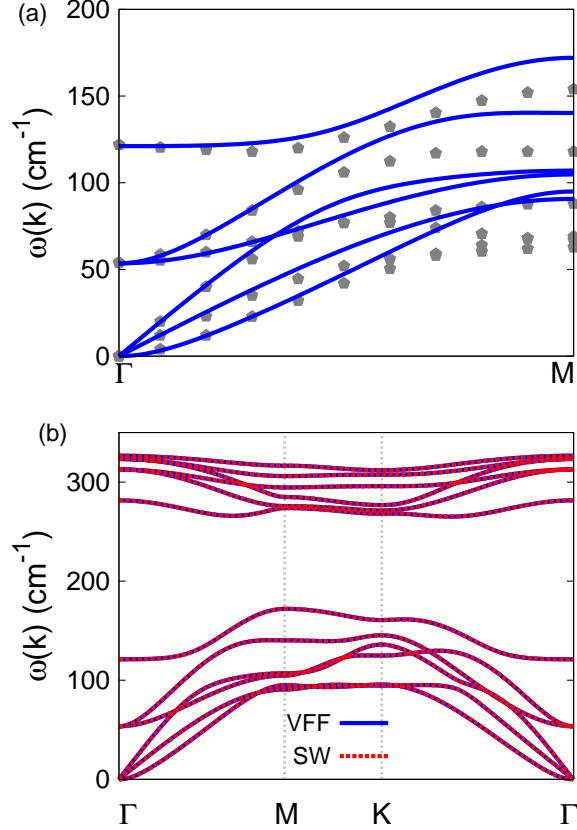


FIG. 260: (Color online) Phonon dispersion for the single-layer GaSe. (a) The VFF model is fitted to the six low-frequency branches along the  $\Gamma$ M direction. The *ab initio* results (gray pentagons) are from Ref. 114. (b) The VFF model (blue lines) and the SW potential (red lines) give the same phonon dispersion for the GaSe along  $\Gamma$ MK $\Gamma$ .

## CXXVII. GASE

Present studies on the GaSe are based on first-principles calculations, and no empirical potential has been proposed for the GaSe. We will thus parametrize a set of SW potential for the single-layer GaSe in this section.

The structure of the single-layer GaSe is shown in Fig. 239 with M=Ga and X=Se. The structural parameters are from the *ab initio* calculations.<sup>114</sup> The GaSe has a bi-buckled configuration as shown in Fig. 239 (b), where the buckle is along the zigzag direction. Two buckling layers are symmetrically integrated through the interior Ga-Ga bonds, forming a bi-buckled configuration. This structure can be determined by three independent geometrical

TABLE DVI: The VFF model for GaSe. The second line gives an explicit expression for each VFF term. The third line is the force constant parameters. Parameters are in the unit of  $\frac{\text{eV}}{\text{\AA}^2}$  for the bond stretching interactions, and in the unit of eV for the angle bending interaction. The fourth line gives the initial bond length (in unit of  $\text{\AA}$ ) for the bond stretching interaction and the initial angle (in unit of degrees) for the angle bending interaction.

VFF type	bond stretching		angle bending	
expression	$\frac{1}{2}K_{\text{Ga-Se}}(\Delta r)^2$	$\frac{1}{2}K_{\text{Ga-Ga}}(\Delta r)^2$	$\frac{1}{2}K_{\text{GaSeSe}}(\Delta\theta)^2$	$\frac{1}{2}K_{\text{GaGaSe}}(\Delta\theta)^2$
parameter	10.014	5.400	2.925	1.701
$r_0$ or $\theta_0$	2.500	2.460	99.636	118.092

TABLE DVII: Two-body SW potential parameters for GaSe used by GULP,<sup>8</sup> as expressed in Eq. (3).

	$A$ (eV)	$\rho$ ( $\text{\AA}$ )	$B$ ( $\text{\AA}^4$ )	$r_{\min}$ ( $\text{\AA}$ )	$r_{\max}$ ( $\text{\AA}$ )
Ga <sub>1</sub> -Se <sub>1</sub>	11.798	1.706	19.531	0.0	3.533
Ga <sub>1</sub> -Ga <sub>2</sub>	6.479	1.765	18.311	0.0	3.502

TABLE DVIII: Three-body SW potential parameters for GaSe used by GULP,<sup>8</sup> as expressed in Eq. (4).

	$K$ (eV)	$\theta_0$ (degree)	$\rho_1$ ( $\text{\AA}$ )	$\rho_2$ ( $\text{\AA}$ )	$r_{\min12}$ ( $\text{\AA}$ )	$r_{\max12}$ ( $\text{\AA}$ )	$r_{\min13}$ ( $\text{\AA}$ )	$r_{\max13}$ ( $\text{\AA}$ )	$r_{\min23}$ ( $\text{\AA}$ )	$r_{\max23}$ ( $\text{\AA}$ )
Ga <sub>1</sub> -Se <sub>1</sub> -Se <sub>1</sub>	40.978	99.636	1.706	1.706	0.0	3.533	0.0	3.533	0.0	5.218
Ga <sub>1</sub> -Se <sub>1</sub> -Ga <sub>2</sub>	31.031	118.092	1.765	1.706	0.0	3.502	0.0	3.533	0.0	4.985

TABLE DIX: SW potential parameters for GaSe used by LAMMPS,<sup>9</sup> as expressed in Eqs. (9) and (10).

	$\epsilon$ (eV)	$\sigma$ ( $\text{\AA}$ )	$a$	$\lambda$	$\gamma$	$\cos\theta_0$	$A_L$	$B_L$	$p$	$q$	tol
Ga <sub>1</sub> -Se <sub>1</sub> -Se <sub>1</sub>	1.000	1.706	2.070	40.978	1.000	-0.167	11.798	2.305	4	0	0.0
Ga <sub>1</sub> -Ga <sub>2</sub> -Ga <sub>2</sub>	1.000	1.765	1.984	0.000	1.000	0.000	6.479	1.888	4	0	0.0
Ga <sub>1</sub> -Ga <sub>2</sub> -Se <sub>1</sub>	1.000	0.000	0.000	31.031	1.000	-0.471	0.000	0.000	4	0	0.0

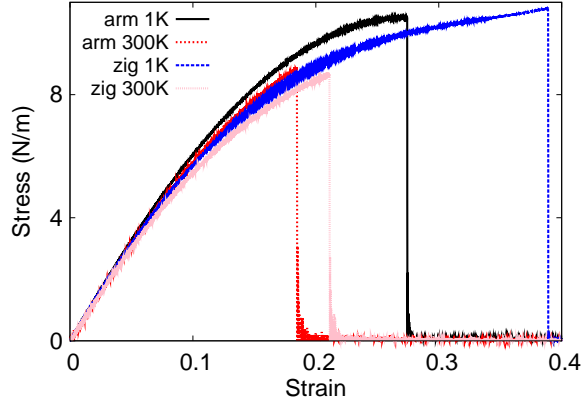


FIG. 261: (Color online) Stress-strain relations for the GaSe of size  $100 \times 100 \text{ \AA}$ . The GaSe is uniaxially stretched along the armchair or zigzag directions at temperatures 1 K and 300 K.

parameters, eg. the lattice constant  $3.82 \text{ \AA}$ , the bond length  $d_{\text{Ga-Se}} = 2.50 \text{ \AA}$ , and the bond length  $d_{\text{Ga-Ga}} = 2.46 \text{ \AA}$ .

Table DVI shows the VFF model for the single-layer GaSe. The force constant parameters are determined by fitting to the six low-frequency branches in the phonon dispersion along the  $\Gamma\text{M}$  as shown in Fig. 260 (a). The *ab initio* calculations for the phonon dispersion are from Ref. 114. Fig. 260 (b) shows that the VFF model and the SW potential give exactly the same phonon dispersion, as the SW potential is derived from the VFF model.

The parameters for the two-body SW potential used by GULP are shown in Tab. DVII. The parameters for the three-body SW potential used by GULP are shown in Tab. DVIII. Parameters for the SW potential used by LAMMPS are listed in Tab. DIX.

We use LAMMPS to perform MD simulations for the mechanical behavior of the single-layer GaSe under uniaxial tension at 1.0 K and 300.0 K. Fig. 261 shows the stress-strain curve for the tension of a single-layer GaSe of dimension  $100 \times 100 \text{ \AA}$ . Periodic boundary conditions are applied in both armchair and zigzag directions. The single-layer GaSe is stretched uniaxially along the armchair or zigzag direction. The stress is calculated without involving the actual thickness of the quasi-two-dimensional structure of the single-layer GaSe. The Young's modulus can be obtained by a linear fitting of the stress-strain relation in the small strain range of  $[0, 0.01]$ . The Young's modulus is  $68.3 \text{ N/m}$  and  $67.9 \text{ N/m}$  along the armchair and zigzag directions, respectively. The Poisson's ratio from the VFF model and the SW potential is  $\nu_{xy} = \nu_{yx} = 0.25$ .

TABLE DX: The VFF model for InSe. The second line gives an explicit expression for each VFF term. The third line is the force constant parameters. Parameters are in the unit of  $\frac{\text{eV}}{\text{\AA}^2}$  for the bond stretching interactions, and in the unit of eV for the angle bending interaction. The fourth line gives the initial bond length (in unit of  $\text{\AA}$ ) for the bond stretching interaction and the initial angle (in unit of degrees) for the angle bending interaction.

VFF type	bond stretching		angle bending	
expression	$\frac{1}{2}K_{\text{In-Se}}(\Delta r)^2$	$\frac{1}{2}K_{\text{In-In}}(\Delta r)^2$	$\frac{1}{2}K_{\text{InSeSe}}(\Delta\theta)^2$	$\frac{1}{2}K_{\text{InInSe}}(\Delta\theta)^2$
parameter	9.812	4.185	2.090	1.227
$r_0$ or $\theta_0$	2.690	2.810	99.296	118.361

TABLE DXI: Two-body SW potential parameters for InSe used by GULP,<sup>8</sup> as expressed in Eq. (3).

	$A$ (eV)	$\rho$ ( $\text{\AA}$ )	$B$ ( $\text{\AA}^4$ )	$r_{\text{min}}$ ( $\text{\AA}$ )	$r_{\text{max}}$ ( $\text{\AA}$ )
In <sub>1</sub> -Se <sub>1</sub>	13.281	1.822	26.181	0.0	3.797
In <sub>1</sub> -In <sub>2</sub>	5.414	1.661	31.174	0.0	2.890

There is no available value for nonlinear quantities in the single-layer GaSe. We have thus used the nonlinear parameter  $B = 0.5d^4$  in Eq. (5), which is close to the value of  $B$  in most materials. The value of the third order nonlinear elasticity  $D$  can be extracted by fitting the stress-strain relation to the function  $\sigma = E\epsilon + \frac{1}{2}D\epsilon^2$  with  $E$  as the Young's modulus. The values of  $D$  from the present SW potential are -206.1 N/m and -219.8 N/m along the armchair and zigzag directions, respectively. The ultimate stress is about  $10.5 \text{ Nm}^{-1}$  at the ultimate strain of 0.27 in the armchair direction at the low temperature of 1 K. The ultimate stress is about  $10.8 \text{ Nm}^{-1}$  at the ultimate strain of 0.39 in the zigzag direction at the low temperature of 1 K.

## CXXVIII. INSE

Present studies on the InSe are based on first-principles calculations, and no empirical potential has been proposed for the InSe. We will thus parametrize a set of SW potential for the single-layer InSe in this section.

The structure of the single-layer InSe is shown in Fig. 239 with M=In and X=Se. The

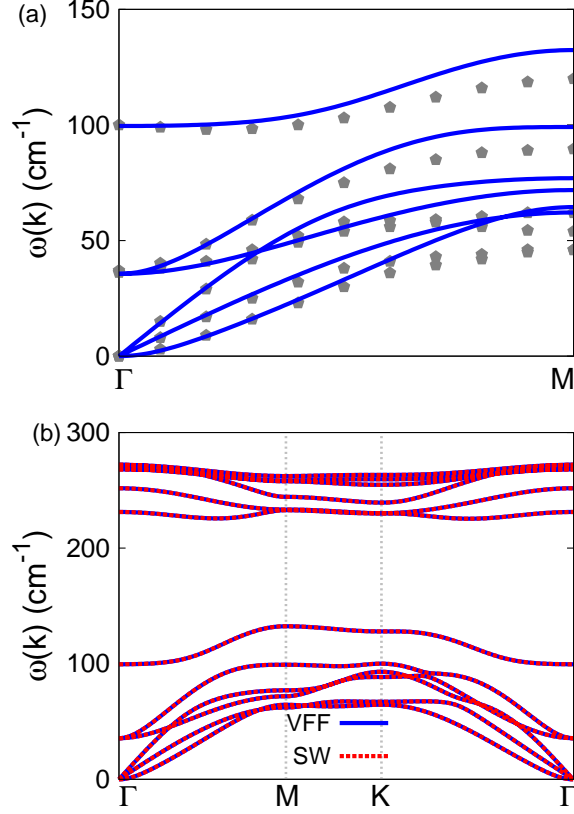


FIG. 262: (Color online) Phonon dispersion for the single-layer InSe. (a) The VFF model is fitted to the six low-frequency branches along the  $\Gamma$ M direction. The *ab initio* results (gray pentagons) are from Ref. 114. (b) The VFF model (blue lines) and the SW potential (red lines) give the same phonon dispersion for the InSe along  $\Gamma$ MKT $\Gamma$ .

TABLE DXII: Three-body SW potential parameters for InSe used by GULP,<sup>8</sup> as expressed in Eq. (4).

	$K$ (eV)	$\theta_0$ (degree)	$\rho_1$ ( $\text{\AA}$ )	$\rho_2$ ( $\text{\AA}$ )	$r_{\min 12}$ ( $\text{\AA}$ )	$r_{\max 12}$ ( $\text{\AA}$ )	$r_{\min 13}$ ( $\text{\AA}$ )	$r_{\max 13}$ ( $\text{\AA}$ )	$r_{\min 23}$ ( $\text{\AA}$ )	$r_{\max 23}$ ( $\text{\AA}$ )
In <sub>1</sub> -Se <sub>1</sub> -Se <sub>1</sub>	28.853	99.296	1.822	1.822	0.0	3.797	0.0	3.797	0.0	5.601
In <sub>1</sub> -Se <sub>1</sub> -In <sub>2</sub>	19.120	118.361	1.822	1.661	0.0	3.797	0.0	3.890	0.0	5.489

structural parameters are from the *ab initio* calculations.<sup>114</sup> The InSe has a bi-buckled configuration as shown in Fig. 239 (b), where the buckle is along the zigzag direction. Two buckling layers are symmetrically integrated through the interior In-In bonds, forming a bi-buckled configuration. This structure can be determined by three independent geometrical

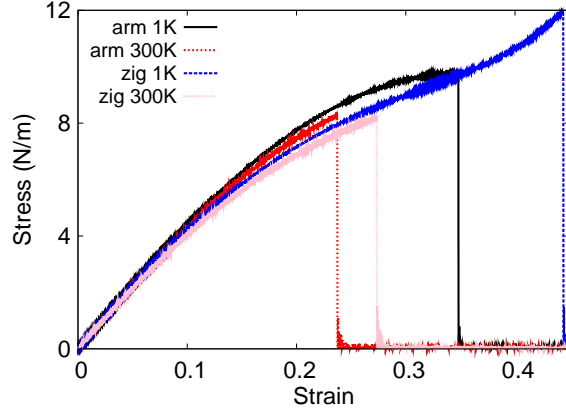


FIG. 263: (Color online) Stress-strain relations for the InSe of size  $100 \times 100 \text{ \AA}$ . The InSe is uniaxially stretched along the armchair or zigzag directions at temperatures 1 K and 300 K.

TABLE DXIII: SW potential parameters for InSe used by LAMMPS,<sup>9</sup> as expressed in Eqs. (9) and (10).

	$\epsilon$ (eV)	$\sigma$ ( $\text{\AA}$ )	$a$	$\lambda$	$\gamma$	$\cos \theta_0$	$A_L$	$B_L$	$p$	$q$	tol
In <sub>1</sub> -Se <sub>1</sub> -Se <sub>1</sub>	1.000	1.822	2.084	28.853	1.000	-0.162	13.281	2.377	4	0	0.0
In <sub>1</sub> -In <sub>2</sub> -In <sub>2</sub>	1.000	1.661	2.342	0.000	1.000	0.000	5.414	4.094	4	0	0.0
In <sub>1</sub> -In <sub>2</sub> -Se <sub>1</sub>	1.000	0.000	0.000	19.120	1.000	-0.475	0.000	0.000	4	0	0.0

parameters, eg. the lattice constant  $4.10 \text{ \AA}$ , the bond length  $d_{\text{In-Se}} = 2.69 \text{ \AA}$ , and the bond length  $d_{\text{In-In}} = 2.81 \text{ \AA}$ .

Table DX shows the VFF model for the single-layer InSe. The force constant parameters are determined by fitting to the six low-frequency branches in the phonon dispersion along the  $\Gamma\text{M}$  as shown in Fig. 262 (a). The *ab initio* calculations for the phonon dispersion are from Ref. 114. Fig. 262 (b) shows that the VFF model and the SW potential give exactly the same phonon dispersion, as the SW potential is derived from the VFF model.

The parameters for the two-body SW potential used by GULP are shown in Tab. DXI. The parameters for the three-body SW potential used by GULP are shown in Tab. DXII. Parameters for the SW potential used by LAMMPS are listed in Tab. DXIII.

We use LAMMPS to perform MD simulations for the mechanical behavior of the single-layer InSe under uniaxial tension at 1.0 K and 300.0 K. Fig. 263 shows the stress-strain curve for the tension of a single-layer InSe of dimension  $100 \times 100 \text{ \AA}$ . Periodic boundary

TABLE DXIV: The VFF model for BTe. The second line gives an explicit expression for each VFF term. The third line is the force constant parameters. Parameters are in the unit of  $\frac{\text{eV}}{\text{\AA}^2}$  for the bond stretching interactions, and in the unit of eV for the angle bending interaction. The fourth line gives the initial bond length (in unit of  $\text{\AA}$ ) for the bond stretching interaction and the initial angle (in unit of degrees) for the angle bending interaction.

VFF type	bond stretching		angle bending	
expression	$\frac{1}{2}K_{\text{B-Te}}(\Delta r)^2$	$\frac{1}{2}K_{\text{B-B}}(\Delta r)^2$	$\frac{1}{2}K_{\text{BTeTe}}(\Delta\theta)^2$	$\frac{1}{2}K_{\text{BBTe}}(\Delta\theta)^2$
parameter	13.287	14.502	5.466	2.515
$r_0$ or $\theta_0$	2.310	1.710	100.809	117.156

conditions are applied in both armchair and zigzag directions. The single-layer InSe is stretched uniaxially along the armchair or zigzag direction. The stress is calculated without involving the actual thickness of the quasi-two-dimensional structure of the single-layer InSe. The Young's modulus can be obtained by a linear fitting of the stress-strain relation in the small strain range of  $[0, 0.01]$ . The Young's modulus is 45.7 N/m and 45.8 N/m along the armchair and zigzag directions, respectively. The Poisson's ratio from the VFF model and the SW potential is  $\nu_{xy} = \nu_{yx} = 0.30$ .

There is no available value for nonlinear quantities in the single-layer InSe. We have thus used the nonlinear parameter  $B = 0.5d^4$  in Eq. (5), which is close to the value of  $B$  in most materials. The value of the third order nonlinear elasticity  $D$  can be extracted by fitting the stress-strain relation to the function  $\sigma = E\epsilon + \frac{1}{2}D\epsilon^2$  with  $E$  as the Young's modulus. The values of  $D$  from the present SW potential are -81.6 N/m and -103.5 N/m along the armchair and zigzag directions, respectively. The ultimate stress is about 9.8  $\text{Nm}^{-1}$  at the ultimate strain of 0.35 in the armchair direction at the low temperature of 1 K. The ultimate stress is about 11.9  $\text{Nm}^{-1}$  at the ultimate strain of 0.44 in the zigzag direction at the low temperature of 1 K.

## CXXIX. BTE

Present studies on the BTe are based on first-principles calculations, and no empirical potential has been proposed for the BTe. We will thus parametrize a set of SW potential

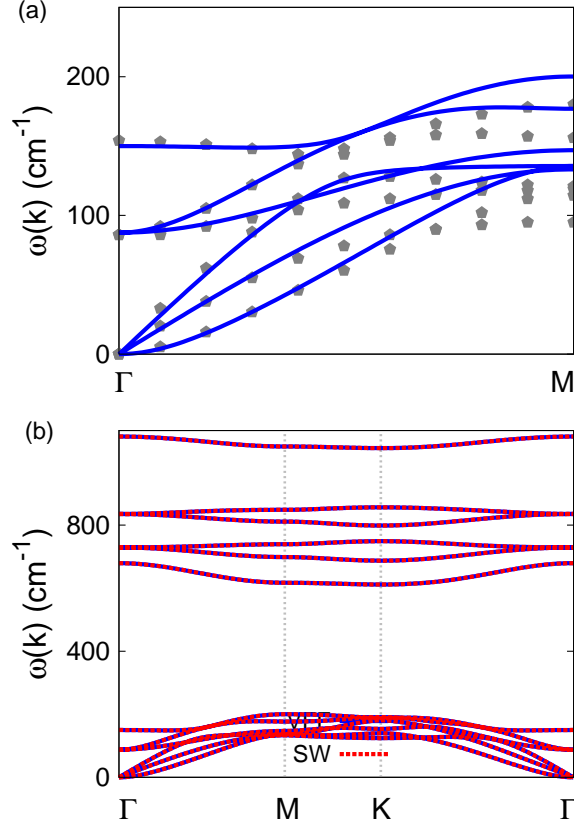


FIG. 264: (Color online) Phonon dispersion for the single-layer BTe. (a) The VFF model is fitted to the six low-frequency branches along the  $\Gamma$ M direction. The *ab initio* results (gray pentagons) are from Ref. 114. (b) The VFF model (blue lines) and the SW potential (red lines) give the same phonon dispersion for the BTe along  $\Gamma$ MK $\Gamma$ .

TABLE DXV: Two-body SW potential parameters for BTe used by GULP,<sup>8</sup> as expressed in Eq. (3).

	$A$ (eV)	$\rho$ ( $\text{\AA}$ )	$B$ ( $\text{\AA}^4$ )	$r_{\min}$ ( $\text{\AA}$ )	$r_{\max}$ ( $\text{\AA}$ )
B <sub>1</sub> -Te <sub>1</sub>	13.727	1.619	14.237	0.0	3.277
B <sub>1</sub> -B <sub>2</sub>	24.140	2.933	4.275	0.0	2.830

for the single-layer BTe in this section.

The structure of the single-layer BTe is shown in Fig. 239 with M=B and X=Te. The structural parameters are from the *ab initio* calculations.<sup>114</sup> The BTe has a bi-buckled configuration as shown in Fig. 239 (b), where the buckle is along the zigzag direction. Two buckling layers are symmetrically integrated through the interior B-B bonds, forming a bi-

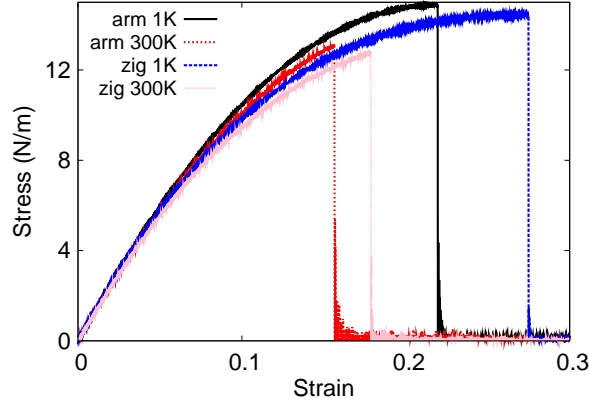


FIG. 265: (Color online) Stress-strain relations for the BTe of size  $100 \times 100 \text{ \AA}$ . The BTe is uniaxially stretched along the armchair or zigzag directions at temperatures 1 K and 300 K.

TABLE DXVI: Three-body SW potential parameters for BTe used by GULP,<sup>8</sup> as expressed in Eq. (4).

	$K$ (eV)	$\theta_0$ (degree)	$\rho_1$ ( $\text{\AA}$ )	$\rho_2$ ( $\text{\AA}$ )	$r_{\min 12}$ ( $\text{\AA}$ )	$r_{\max 12}$ ( $\text{\AA}$ )	$r_{\min 13}$ ( $\text{\AA}$ )	$r_{\max 13}$ ( $\text{\AA}$ )	$r_{\min 23}$ ( $\text{\AA}$ )	$r_{\max 23}$ ( $\text{\AA}$ )
B <sub>1</sub> -Te <sub>1</sub> -Te <sub>1</sub>	80.622	100.809	1.619	1.619	0.0	3.277	0.0	3.277	0.0	4.863
B <sub>1</sub> -B <sub>2</sub> -Te <sub>1</sub>	116.3301	117.156	2.933	1.619	0.0	2.830	0.0	3.277	0.0	4.199

buckled configuration. This structure can be determined by three independent geometrical parameters, eg. the lattice constant  $3.56 \text{ \AA}$ , the bond length  $d_{\text{B-Te}} = 2.31 \text{ \AA}$ , and the bond length  $d_{\text{B-B}} = 1.71 \text{ \AA}$ .

Table DXIV shows the VFF model for the single-layer BTe. The force constant parameters are determined by fitting to the six low-frequency branches in the phonon dispersion along the  $\Gamma\text{M}$  as shown in Fig. 264 (a). The *ab initio* calculations for the phonon dispersion

TABLE DXVII: SW potential parameters for BTe used by LAMMPS,<sup>9</sup> as expressed in Eqs. (9) and (10).

	$\epsilon$ (eV)	$\sigma$ ( $\text{\AA}$ )	$a$	$\lambda$	$\gamma$	$\cos \theta_0$	$A_L$	$B_L$	$p$	$q$	tol
B <sub>1</sub> -Te <sub>1</sub> -Te <sub>1</sub>	1.000	1.619	2.024	80.622	1.000	-0.188	13.727	2.073	4	0	0.0
B <sub>1</sub> -B <sub>2</sub> -B <sub>2</sub>	1.000	2.933	0.965	0.000	1.000	0.000	24.140	0.058	4	0	0.0
B <sub>1</sub> -B <sub>2</sub> -Te <sub>1</sub>	1.000	0.000	0.000	116.301	1.000	-0.456	0.000	0.000	4	0	0.0

are from Ref. 114. Fig. 264 (b) shows that the VFF model and the SW potential give exactly the same phonon dispersion, as the SW potential is derived from the VFF model.

The parameters for the two-body SW potential used by GULP are shown in Tab. DXV. The parameters for the three-body SW potential used by GULP are shown in Tab. DXVI. Parameters for the SW potential used by LAMMPS are listed in Tab. DXVII.

We use LAMMPS to perform MD simulations for the mechanical behavior of the single-layer BTe under uniaxial tension at 1.0 K and 300.0 K. Fig. 265 shows the stress-strain curve for the tension of a single-layer BTe of dimension  $100 \times 100$  Å. Periodic boundary conditions are applied in both armchair and zigzag directions. The single-layer BTe is stretched uniaxially along the armchair or zigzag direction. The stress is calculated without involving the actual thickness of the quasi-two-dimensional structure of the single-layer BTe. The Young's modulus can be obtained by a linear fitting of the stress-strain relation in the small strain range of  $[0, 0.01]$ . The Young's modulus is 130.6 N/m and 129.7 N/m along the armchair and zigzag directions, respectively. The Poisson's ratio from the VFF model and the SW potential is  $\nu_{xy} = \nu_{yx} = 0.16$ .

There is no available value for nonlinear quantities in the single-layer BTe. We have thus used the nonlinear parameter  $B = 0.5d^4$  in Eq. (5), which is close to the value of  $B$  in most materials. The value of the third order nonlinear elasticity  $D$  can be extracted by fitting the stress-strain relation to the function  $\sigma = E\epsilon + \frac{1}{2}D\epsilon^2$  with  $E$  as the Young's modulus. The values of  $D$  from the present SW potential are -560.4 N/m and -588.7 N/m along the armchair and zigzag directions, respectively. The ultimate stress is about  $14.9 \text{ Nm}^{-1}$  at the ultimate strain of 0.22 in the armchair direction at the low temperature of 1 K. The ultimate stress is about  $14.4 \text{ Nm}^{-1}$  at the ultimate strain of 0.27 in the zigzag direction at the low temperature of 1 K.

#### CXXX. ALTE

Present studies on the AlTe are based on first-principles calculations, and no empirical potential has been proposed for the AlTe. We will thus parametrize a set of SW potential for the single-layer AlTe in this section.

The structure of the single-layer AlTe is shown in Fig. 239 with M=Al and X=Te. The structural parameters are from the *ab initio* calculations.<sup>114</sup> The AlTe has a bi-buckled

TABLE DXVIII: The VFF model for AlTe. The second line gives an explicit expression for each VFF term. The third line is the force constant parameters. Parameters are in the unit of  $\frac{eV}{\text{\AA}^2}$  for the bond stretching interactions, and in the unit of eV for the angle bending interaction. The fourth line gives the initial bond length (in unit of  $\text{\AA}$ ) for the bond stretching interaction and the initial angle (in unit of degrees) for the angle bending interaction.

VFF type	bond stretching		angle bending	
expression	$\frac{1}{2}K_{\text{Al-Te}}(\Delta r)^2$	$\frac{1}{2}K_{\text{Al-Al}}(\Delta r)^2$	$\frac{1}{2}K_{\text{AlTeTe}}(\Delta\theta)^2$	$\frac{1}{2}K_{\text{AlAlTe}}(\Delta\theta)^2$
parameter	8.077	3.859	2.820	1.518
$r_0$ or $\theta_0$	2.700	2.580	99.124	118.495

TABLE DXIX: Two-body SW potential parameters for AlTe used by GULP,<sup>8</sup> as expressed in Eq. (3).

	$A$ (eV)	$\rho$ ( $\text{\AA}$ )	$B$ ( $\text{\AA}^4$ )	$r_{\min}$ ( $\text{\AA}$ )	$r_{\max}$ ( $\text{\AA}$ )
Al <sub>1</sub> -Te <sub>1</sub>	10.971	1.821	26.572	0.0	3.809
Al <sub>1</sub> -Al <sub>2</sub>	5.523	2.002	22.154	0.0	3.716

TABLE DXX: Three-body SW potential parameters for AlTe used by GULP,<sup>8</sup> as expressed in Eq. (4).

	$K$ (eV)	$\theta_0$ (degree)	$\rho_1$ ( $\text{\AA}$ )	$\rho_2$ ( $\text{\AA}$ )	$r_{\min12}$ ( $\text{\AA}$ )	$r_{\max12}$ ( $\text{\AA}$ )	$r_{\min13}$ ( $\text{\AA}$ )	$r_{\max13}$ ( $\text{\AA}$ )	$r_{\min23}$ ( $\text{\AA}$ )	$r_{\max23}$ ( $\text{\AA}$ )
Al <sub>1</sub> -Te <sub>1</sub> -Te <sub>1</sub>	38.638	99.124	1.821	1.821	0.0	3.809	0.0	3.809	0.0	5.614
Al <sub>1</sub> -Te <sub>1</sub> -Al <sub>2</sub>	29.574	118.495	2.002	1.821	0.0	3.716	0.0	3.809	0.0	5.330

TABLE DXXI: SW potential parameters for AlTe used by LAMMPS,<sup>9</sup> as expressed in Eqs. (9) and (10).

	$\epsilon$ (eV)	$\sigma$ ( $\text{\AA}$ )	$a$	$\lambda$	$\gamma$	$\cos\theta_0$	$A_L$	$B_L$	$p$	$q$	tol
Al <sub>1</sub> -Te <sub>1</sub> -Te <sub>1</sub>	1.000	1.821	2.091	38.638	1.000	-0.159	10.971	2.415	4	0	0.0
Al <sub>1</sub> -Al <sub>2</sub> -Al <sub>2</sub>	1.000	2.002	1.856	0.000	1.000	0.000	5.523	1.379	4	0	0.0
Al <sub>1</sub> -Al <sub>2</sub> -Te <sub>1</sub>	1.000	0.000	0.000	29.574	1.000	-0.477	0.000	0.000	4	0	0.0

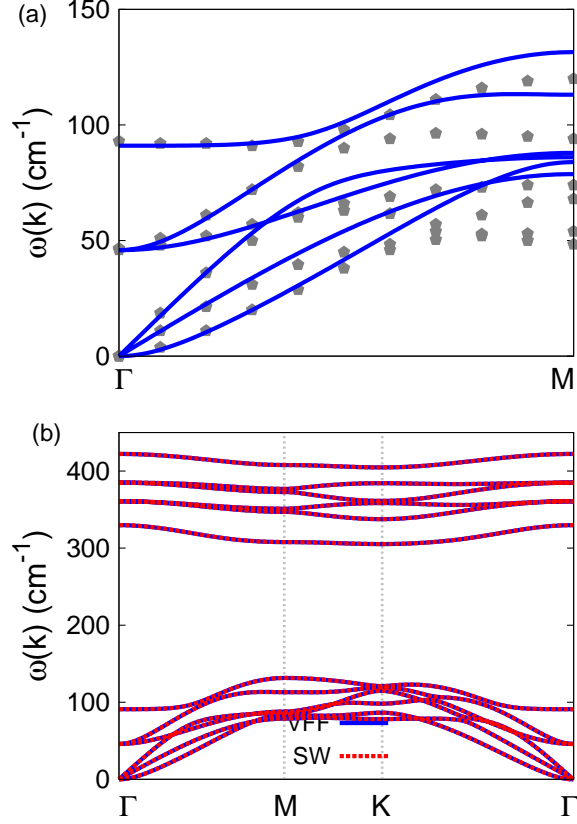


FIG. 266: (Color online) Phonon dispersion for the single-layer AlTe. (a) The VFF model is fitted to the six low-frequency branches along the  $\Gamma$ M direction. The *ab initio* results (gray pentagons) are from Ref. 114. (b) The VFF model (blue lines) and the SW potential (red lines) give the same phonon dispersion for the AlTe along  $\Gamma$ MK $\Gamma$ .

configuration as shown in Fig. 239 (b), where the buckle is along the zigzag direction. Two buckling layers are symmetrically integrated through the interior Al-Al bonds, forming a bi-buckled configuration. This structure can be determined by three independent geometrical parameters, eg. the lattice constant 4.11 Å, the bond length  $d_{\text{Al-Te}} = 2.70$  Å, and the bond length  $d_{\text{Al-Al}} = 2.58$  Å.

Table DXVIII shows the VFF model for the single-layer AlTe. The force constant parameters are determined by fitting to the six low-frequency branches in the phonon dispersion along the  $\Gamma$ M as shown in Fig. 266 (a). The *ab initio* calculations for the phonon dispersion are from Ref. 114. Fig. 266 (b) shows that the VFF model and the SW potential give exactly the same phonon dispersion, as the SW potential is derived from the VFF model.

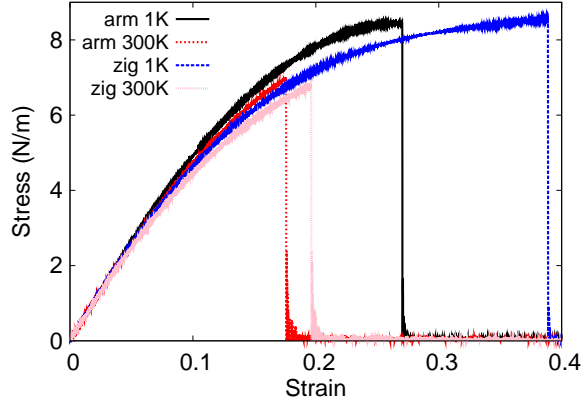


FIG. 267: (Color online) Stress-strain relations for the AlTe of size  $100 \times 100 \text{ \AA}$ . The AlTe is uniaxially stretched along the armchair or zigzag directions at temperatures 1 K and 300 K.

The parameters for the two-body SW potential used by GULP are shown in Tab. [DXIX](#). The parameters for the three-body SW potential used by GULP are shown in Tab. [DXX](#). Parameters for the SW potential used by LAMMPS are listed in Tab. [DXXI](#).

We use LAMMPS to perform MD simulations for the mechanical behavior of the single-layer AlTe under uniaxial tension at 1.0 K and 300.0 K. Fig. [267](#) shows the stress-strain curve for the tension of a single-layer AlTe of dimension  $100 \times 100 \text{ \AA}$ . Periodic boundary conditions are applied in both armchair and zigzag directions. The single-layer AlTe is stretched uniaxially along the armchair or zigzag direction. The stress is calculated without involving the actual thickness of the quasi-two-dimensional structure of the single-layer AlTe. The Young's modulus can be obtained by a linear fitting of the stress-strain relation in the small strain range of  $[0, 0.01]$ . The Young's modulus is 55.8 N/m and 54.9 N/m along the armchair and zigzag directions, respectively. The Poisson's ratio from the VFF model and the SW potential is  $\nu_{xy} = \nu_{yx} = 0.24$ .

There is no available value for nonlinear quantities in the single-layer AlTe. We have thus used the nonlinear parameter  $B = 0.5d^4$  in Eq. (5), which is close to the value of  $B$  in most materials. The value of the third order nonlinear elasticity  $D$  can be extracted by fitting the stress-strain relation to the function  $\sigma = E\epsilon + \frac{1}{2}D\epsilon^2$  with  $E$  as the Young's modulus. The values of  $D$  from the present SW potential are -171.4 N/m and -179.0 N/m along the armchair and zigzag directions, respectively. The ultimate stress is about  $8.4 \text{ Nm}^{-1}$  at the ultimate strain of 0.27 in the armchair direction at the low temperature of 1 K. The ultimate

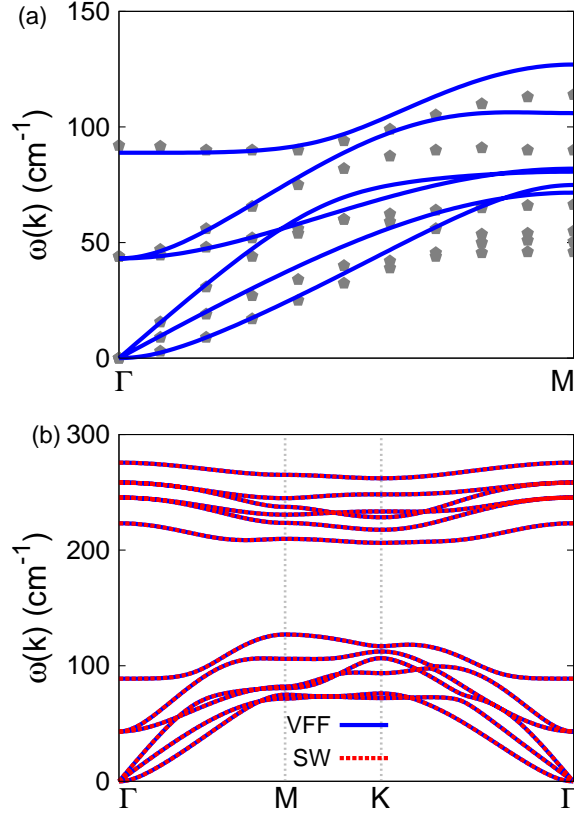


FIG. 268: (Color online) Phonon dispersion for the single-layer GaTe. (a) The VFF model is fitted to the six low-frequency branches along the  $\Gamma$ M direction. The *ab initio* results (gray pentagons) are from Ref. 114. (b) The VFF model (blue lines) and the SW potential (red lines) give the same phonon dispersion for the GaTe along  $\Gamma$ MK $\Gamma$ .

stress is about  $8.6 \text{ Nm}^{-1}$  at the ultimate strain of 0.39 in the zigzag direction at the low temperature of 1 K.

### CXXXI. GATE

Present studies on the GaTe are based on first-principles calculations, and no empirical potential has been proposed for the GaTe. We will thus parametrize a set of SW potential for the single-layer GaTe in this section.

The structure of the single-layer GaTe is shown in Fig. 239 with M=Ga and X=Te. The structural parameters are from the *ab initio* calculations.<sup>114</sup> The GaTe has a bi-buckled

TABLE DXXII: The VFF model for GaTe. The second line gives an explicit expression for each VFF term. The third line is the force constant parameters. Parameters are in the unit of  $\frac{eV}{\text{\AA}^2}$  for the bond stretching interactions, and in the unit of eV for the angle bending interaction. The fourth line gives the initial bond length (in unit of  $\text{\AA}$ ) for the bond stretching interaction and the initial angle (in unit of degrees) for the angle bending interaction.

VFF type	bond stretching		angle bending	
expression	$\frac{1}{2}K_{\text{Ga-Te}}(\Delta r)^2$	$\frac{1}{2}K_{\text{Ga-Ga}}(\Delta r)^2$	$\frac{1}{2}K_{\text{GaTeTe}}(\Delta\theta)^2$	$\frac{1}{2}K_{\text{GaGaTe}}(\Delta\theta)^2$
parameter	7.382	4.366	2.841	1.519
$r_0$ or $\theta_0$	2.700	2.460	99.781	117.978

TABLE DXXIII: Two-body SW potential parameters for GaTe used by GULP,<sup>8</sup> as expressed in Eq. (3).

	$A$ (eV)	$\rho$ ( $\text{\AA}$ )	$B$ ( $\text{\AA}^4$ )	$r_{\min}$ ( $\text{\AA}$ )	$r_{\max}$ ( $\text{\AA}$ )
Ga <sub>1</sub> -Te <sub>1</sub>	10.179	1.849	26.572	0.0	3.817
Ga <sub>1</sub> -Ga <sub>2</sub>	6.750	2.239	18.311	0.0	3.634

TABLE DXXIV: Three-body SW potential parameters for GaTe used by GULP,<sup>8</sup> as expressed in Eq. (4).

	$K$ (eV)	$\theta_0$ (degree)	$\rho_1$ ( $\text{\AA}$ )	$\rho_2$ ( $\text{\AA}$ )	$r_{\min12}$ ( $\text{\AA}$ )	$r_{\max12}$ ( $\text{\AA}$ )	$r_{\min13}$ ( $\text{\AA}$ )	$r_{\max13}$ ( $\text{\AA}$ )	$r_{\min23}$ ( $\text{\AA}$ )	$r_{\max23}$ ( $\text{\AA}$ )
Ga <sub>1</sub> -Te <sub>1</sub> -Te <sub>1</sub>	40.060	99.781	1.849	1.849	0.0	3.817	0.0	3.817	0.0	5.642
Ga <sub>1</sub> -Te <sub>1</sub> -Ga <sub>2</sub>	34.354	117.978	2.239	1.849	0.0	3.634	0.0	3.817	0.0	5.238

TABLE DXXV: SW potential parameters for GaTe used by LAMMPS,<sup>9</sup> as expressed in Eqs. (9) and (10).

	$\epsilon$ (eV)	$\sigma$ ( $\text{\AA}$ )	$a$	$\lambda$	$\gamma$	$\cos\theta_0$	$A_L$	$B_L$	$p$	$q$	tol
Ga <sub>1</sub> -Te <sub>1</sub> -Te <sub>1</sub>	1.000	1.849	2.065	40.060	1.000	-0.170	10.179	2.274	4	0	0.0
Ga <sub>1</sub> -Ga <sub>2</sub> -Ga <sub>2</sub>	1.000	2.239	1.623	0.000	1.000	0.000	6.750	0.728	4	0	0.0
Ga <sub>1</sub> -Ga <sub>2</sub> -Te <sub>1</sub>	1.000	0.000	0.000	34.354	1.000	-0.469	0.000	0.000	4	0	0.0

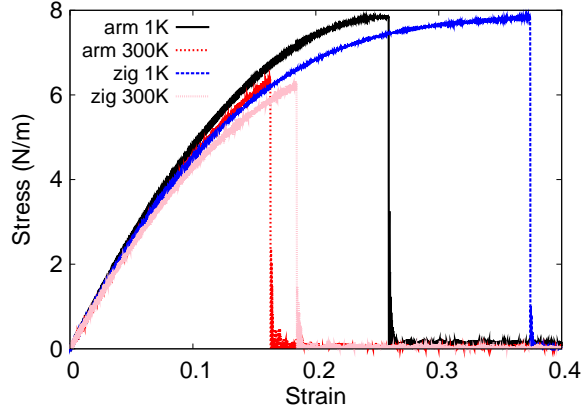


FIG. 269: (Color online) Stress-strain relations for the GaTe of size  $100 \times 100 \text{ \AA}$ . The GaTe is uniaxially stretched along the armchair or zigzag directions at temperatures 1 K and 300 K.

configuration as shown in Fig. 239 (b), where the buckle is along the zigzag direction. Two buckling layers are symmetrically integrated through the interior Ga-Ga bonds, forming a bi-buckled configuration. This structure can be determined by three independent geometrical parameters, eg. the lattice constant  $4.13 \text{ \AA}$ , the bond length  $d_{\text{Ga-Te}} = 2.70 \text{ \AA}$ , and the bond length  $d_{\text{Ga-Ga}} = 2.46 \text{ \AA}$ .

Table DXXII shows the VFF model for the single-layer GaTe. The force constant parameters are determined by fitting to the six low-frequency branches in the phonon dispersion along the  $\Gamma\text{M}$  as shown in Fig. 268 (a). The *ab initio* calculations for the phonon dispersion are from Ref. 114. Fig. 268 (b) shows that the VFF model and the SW potential give exactly the same phonon dispersion, as the SW potential is derived from the VFF model.

The parameters for the two-body SW potential used by GULP are shown in Tab. DXXIII. The parameters for the three-body SW potential used by GULP are shown in Tab. DXXIV. Parameters for the SW potential used by LAMMPS are listed in Tab. DXXV.

We use LAMMPS to perform MD simulations for the mechanical behavior of the single-layer GaTe under uniaxial tension at 1.0 K and 300.0 K. Fig. 269 shows the stress-strain curve for the tension of a single-layer GaTe of dimension  $100 \times 100 \text{ \AA}$ . Periodic boundary conditions are applied in both armchair and zigzag directions. The single-layer GaTe is stretched uniaxially along the armchair or zigzag direction. The stress is calculated without involving the actual thickness of the quasi-two-dimensional structure of the single-layer GaTe. The Young's modulus can be obtained by a linear fitting of the stress-strain relation in the small

TABLE DXXVI: The VFF model for InTe. The second line gives an explicit expression for each VFF term. The third line is the force constant parameters. Parameters are in the unit of  $\frac{eV}{\text{\AA}^2}$  for the bond stretching interactions, and in the unit of eV for the angle bending interaction. The fourth line gives the initial bond length (in unit of  $\text{\AA}$ ) for the bond stretching interaction and the initial angle (in unit of degrees) for the angle bending interaction.

VFF type	bond stretching		angle bending	
expression	$\frac{1}{2}K_{\text{In-Te}}(\Delta r)^2$	$\frac{1}{2}K_{\text{In-In}}(\Delta r)^2$	$\frac{1}{2}K_{\text{InTeTe}}(\Delta\theta)^2$	$\frac{1}{2}K_{\text{InInTe}}(\Delta\theta)^2$
parameter	5.592	3.928	2.419	1.227
$r_0$ or $\theta_0$	2.890	2.810	99.148	118.477

TABLE DXXVII: Two-body SW potential parameters for InTe used by GULP,<sup>8</sup> as expressed in Eq. (3).

	$A$ (eV)	$\rho$ ( $\text{\AA}$ )	$B$ ( $\text{\AA}^4$ )	$r_{\text{min}}$ ( $\text{\AA}$ )	$r_{\text{max}}$ ( $\text{\AA}$ )
In <sub>1</sub> -Te <sub>1</sub>	8.707	1.950	34.879	0.0	4.077
In <sub>1</sub> -In <sub>2</sub>	6.312	2.068	31.174	0.0	4.015

strain range of  $[0, 0.01]$ . The Young's modulus is 55.2 N/m and 55.3 N/m along the armchair and zigzag directions, respectively. The Poisson's ratio from the VFF model and the SW potential is  $\nu_{xy} = \nu_{yx} = 0.23$ .

There is no available value for nonlinear quantities in the single-layer GaTe. We have thus used the nonlinear parameter  $B = 0.5d^4$  in Eq. (5), which is close to the value of  $B$  in most materials. The value of the third order nonlinear elasticity  $D$  can be extracted by fitting the stress-strain relation to the function  $\sigma = E\epsilon + \frac{1}{2}D\epsilon^2$  with  $E$  as the Young's modulus. The values of  $D$  from the present SW potential are -183.2 N/m and -195.6 N/m along the armchair and zigzag directions, respectively. The ultimate stress is about 7.8  $\text{Nm}^{-1}$  at the ultimate strain of 0.26 in the armchair direction at the low temperature of 1 K. The ultimate stress is about 7.8  $\text{Nm}^{-1}$  at the ultimate strain of 0.37 in the zigzag direction at the low temperature of 1 K.

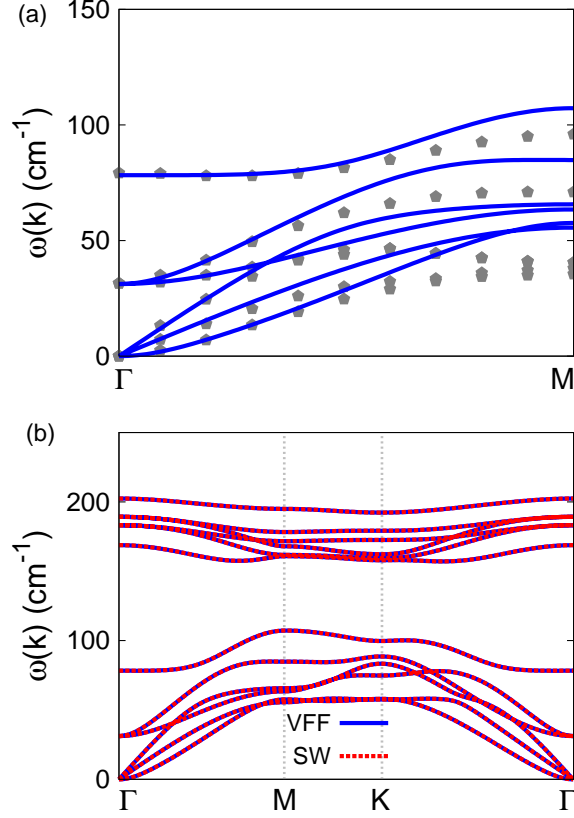


FIG. 270: (Color online) Phonon dispersion for the single-layer InTe. (a) The VFF model is fitted to the six low-frequency branches along the  $\Gamma$ M direction. The *ab initio* results (gray pentagons) are from Ref. 114. (b) The VFF model (blue lines) and the SW potential (red lines) give the same phonon dispersion for the InTe along  $\Gamma$ MK $\Gamma$ .

TABLE DXXVIII: Three-body SW potential parameters for InTe used by GULP,<sup>8</sup> as expressed in Eq. (4).

	$K$ (eV)	$\theta_0$ (degree)	$\rho_1$ (Å)	$\rho_2$ (Å)	$r_{\min 12}$ (Å)	$r_{\max 12}$ (Å)	$r_{\min 13}$ (Å)	$r_{\max 13}$ (Å)	$r_{\min 23}$ (Å)	$r_{\max 23}$ (Å)
In <sub>1</sub> -Te <sub>1</sub> -Te <sub>1</sub>	33.178	99.148	1.950	1.950	0.0	4.077	0.0	4.077	0.0	6.011
In <sub>1</sub> -Te <sub>1</sub> -In <sub>2</sub>	22.833	118.477	2.068	1.950	0.0	4.015	0.0	4.077	0.0	5.741

## CXXXII. INTE

Present studies on the InTe are based on first-principles calculations, and no empirical potential has been proposed for the InTe. We will thus parametrize a set of SW potential

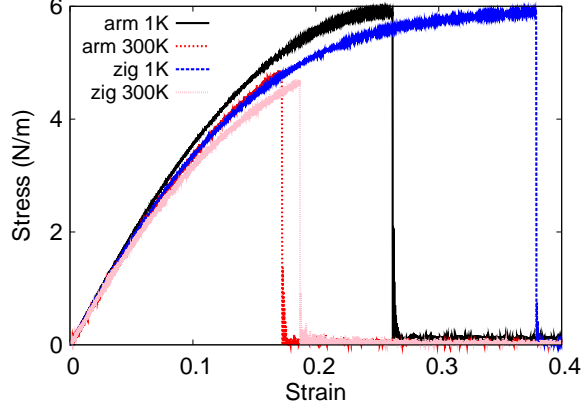


FIG. 271: (Color online) Stress-strain relations for the InTe of size  $100 \times 100 \text{ \AA}$ . The InTe is uniaxially stretched along the armchair or zigzag directions at temperatures 1 K and 300 K.

TABLE DXXIX: SW potential parameters for InTe used by LAMMPS,<sup>9</sup> as expressed in Eqs. (9) and (10).

	$\epsilon$ (eV)	$\sigma$ ( $\text{\AA}$ )	$a$	$\lambda$	$\gamma$	$\cos \theta_0$	$A_L$	$B_L$	$p$	$q$	tol
In <sub>1</sub> -Te <sub>1</sub> -Te <sub>1</sub>	1.000	1.950	2.090	33.178	1.000	-0.159	8.707	2.410	4	0	0.0
In <sub>1</sub> -In <sub>2</sub> -In <sub>2</sub>	1.000	2.068	1.942	0.000	1.000	0.000	6.312	1.704	4	0	0.0
In <sub>1</sub> -In <sub>2</sub> -Te <sub>1</sub>	1.000	0.000	0.000	22.833	1.000	-0.477	0.000	0.000	4	0	0.0

for the single-layer InTe in this section.

The structure of the single-layer InTe is shown in Fig. 239 with M=In and X=Te. The structural parameters are from the *ab initio* calculations.<sup>114</sup> The InTe has a bi-buckled configuration as shown in Fig. 239 (b), where the buckle is along the zigzag direction. Two buckling layers are symmetrically integrated through the interior In-In bonds, forming a bi-buckled configuration. This structure can be determined by three independent geometrical parameters, eg. the lattice constant  $4.40 \text{ \AA}$ , the bond length  $d_{\text{In-Te}} = 2.89 \text{ \AA}$ , and the bond length  $d_{\text{In-In}} = 2.81 \text{ \AA}$ .

Table DXXVI shows the VFF model for the single-layer InTe. The force constant parameters are determined by fitting to the six low-frequency branches in the phonon dispersion along the  $\Gamma\text{M}$  as shown in Fig. 270 (a). The *ab initio* calculations for the phonon dispersion are from Ref. 114. Fig. 270 (b) shows that the VFF model and the SW potential give exactly the same phonon dispersion, as the SW potential is derived from the VFF model.

The parameters for the two-body SW potential used by GULP are shown in Tab. [DXXVII](#). The parameters for the three-body SW potential used by GULP are shown in Tab. [DXXVIII](#). Parameters for the SW potential used by LAMMPS are listed in Tab. [DXXIX](#).

We use LAMMPS to perform MD simulations for the mechanical behavior of the single-layer InTe under uniaxial tension at 1.0 K and 300.0 K. Fig. [271](#) shows the stress-strain curve for the tension of a single-layer InTe of dimension  $100 \times 100 \text{ \AA}$ . Periodic boundary conditions are applied in both armchair and zigzag directions. The single-layer InTe is stretched uniaxially along the armchair or zigzag direction. The stress is calculated without involving the actual thickness of the quasi-two-dimensional structure of the single-layer InTe. The Young's modulus can be obtained by a linear fitting of the stress-strain relation in the small strain range of  $[0, 0.01]$ . The Young's modulus is 40.6 N/m and 40.9 N/m along the armchair and zigzag directions, respectively. The Poisson's ratio from the VFF model and the SW potential is  $\nu_{xy} = \nu_{yx} = 0.23$ .

There is no available value for nonlinear quantities in the single-layer InTe. We have thus used the nonlinear parameter  $B = 0.5d^4$  in Eq. (5), which is close to the value of  $B$  in most materials. The value of the third order nonlinear elasticity  $D$  can be extracted by fitting the stress-strain relation to the function  $\sigma = E\epsilon + \frac{1}{2}D\epsilon^2$  with  $E$  as the Young's modulus. The values of  $D$  from the present SW potential are -130.4 N/m and -142.2 N/m along the armchair and zigzag directions, respectively. The ultimate stress is about  $5.9 \text{ Nm}^{-1}$  at the ultimate strain of 0.26 in the armchair direction at the low temperature of 1 K. The ultimate stress is about  $5.9 \text{ Nm}^{-1}$  at the ultimate strain of 0.38 in the zigzag direction at the low temperature of 1 K.

### **CXXXIII. BOROPHENE**

Most existing theoretical studies on the monolayer of boron atoms (borophene) are based on the first-principles calculations. The ReaxFF force field model was developed for the borophene recently.<sup>116</sup> The present authors have provided the VFF model and the SW potential to describe the atomic interaction within the borophene,<sup>14</sup> which includes the second-nearest-neighboring interactions. In the present work, we present a more efficient SW potential with only the first-nearest-neighboring interactions.

The structure of the borophene is shown in Fig. [272](#), with structural parameters from the

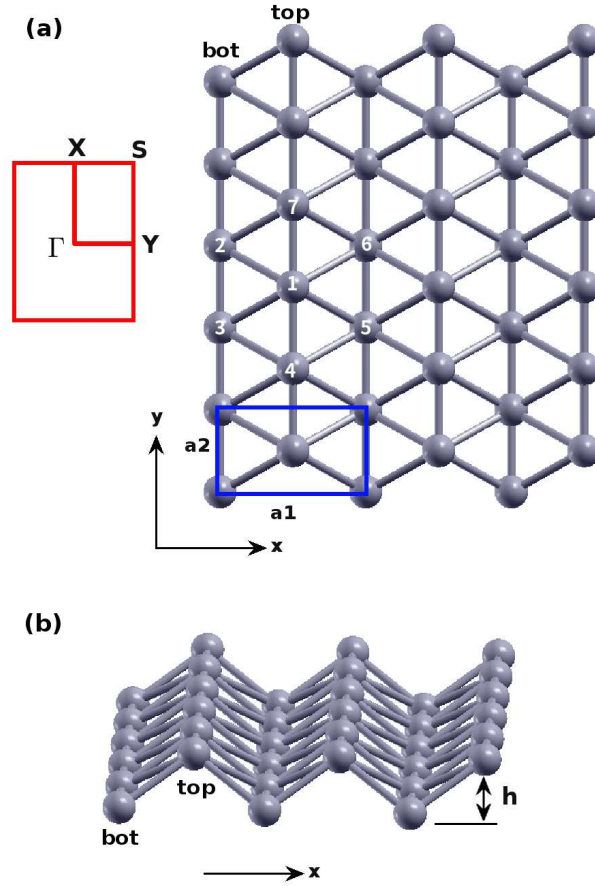


FIG. 272: (Color online) Structure for borophene. (a) Top view. Atoms are categorized into top chains and bottom chains. The top chain includes atoms like 1, 4, and 7. The bottom chain includes atoms like 2, 3, 5, and 6. The unit cell is shown by blue rectangle. The first Brillouin zone is shown by red rectangle on the left. (b) Perspective view illustrates the puckered configuration, with  $h$  as the distance between the top and bottom chains along the out-of-plane  $z$ -direction. The pucker is perpendicular to the  $x$ -axis and is parallel with the  $y$ -axis.

*ab initio* calculations.<sup>115</sup> Borophene has a puckered configuration as shown in Fig. 272 (b), where the pucker is perpendicular to the  $x$ -direction. The height of the pucker is  $h = 0.911 \text{ \AA}$ , which is the distance between the top chain and the bottom chain along the out-of-plane  $z$ -direction. The two lattice bases are  $a_1 = 2.866 \text{ \AA}$  and  $a_2 = 1.614 \text{ \AA}$  for the inplane rectangular unit cell. There are two inequivalent boron atoms in the unit cell. Boron atoms are categorized into the top chain and the bottom chain. The top chain includes atoms like 1, 4, and 7. The bottom chain includes atoms like 2, 3, 5, and 6.

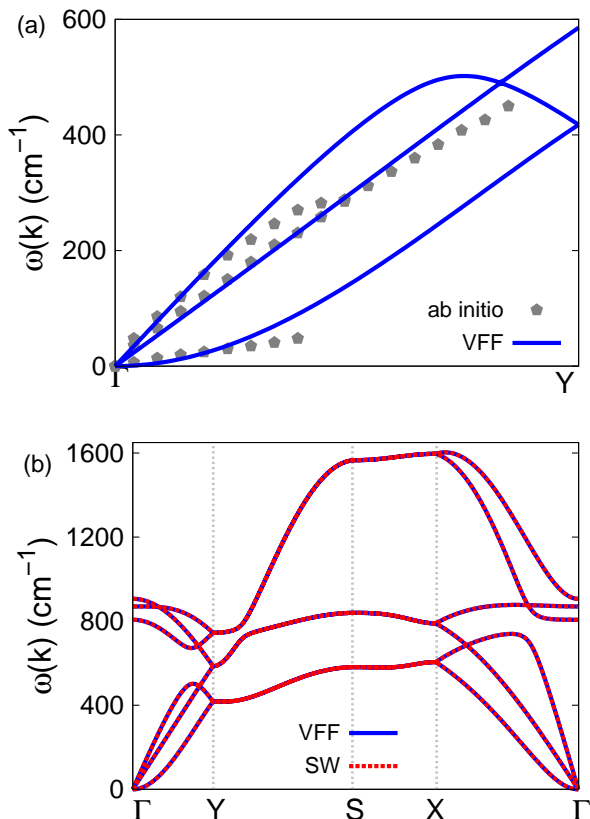


FIG. 273: (Color online) Phonon dispersion for the borophene. (a) The VFF model is fitted to the three acoustic branches in the long wave limit along the  $\Gamma Y$  direction. The *ab initio* results (gray pentagons) are from Ref. 115. (b) The VFF model (blue lines) and the SW potential (red lines) give the same phonon dispersion for the borophene along  $\Gamma Y S X \Gamma$ .

Table DXXX shows four VFF terms for the borophene, two of which are the bond stretching interaction shown by Eq. (1) while the other two terms are the angle bending interaction shown by Eq. (2). These force constant parameters are determined by fitting to the three acoustic branches in the phonon dispersion along the  $\Gamma X$  as shown in Fig. 273 (a). The *ab initio* calculations for the phonon dispersion are from Ref. 115. Similar phonon dispersion can also be found in other *ab initio* calculations.<sup>117</sup> Fig. 273 (b) shows that the VFF model and the SW potential give exactly the same phonon dispersion, as the SW potential is derived from the VFF model.

The parameters for the two-body SW potential used by GULP are shown in Tab. DXXXI. The parameters for the three-body SW potential used by GULP are shown in Tab. DXXXII.

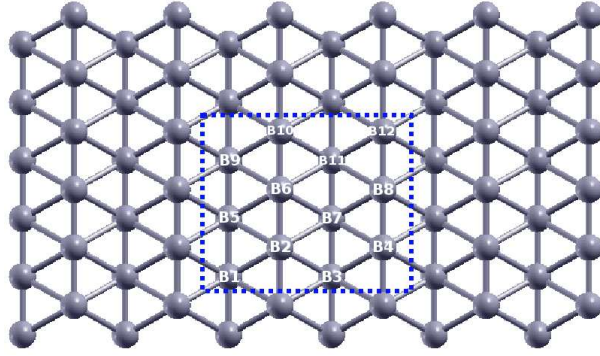


FIG. 274: (Color online) Twelve atom types are introduced for the boron atoms in the borophene. Atoms  $B_1$ ,  $B_3$ ,  $B_5$ ,  $B_7$ ,  $B_9$ , and  $B_{11}$  are from the bottom group. Atoms  $B_2$ ,  $B_4$ ,  $B_6$ ,  $B_8$ ,  $B_{10}$ , and  $B_{12}$  are from the top group.

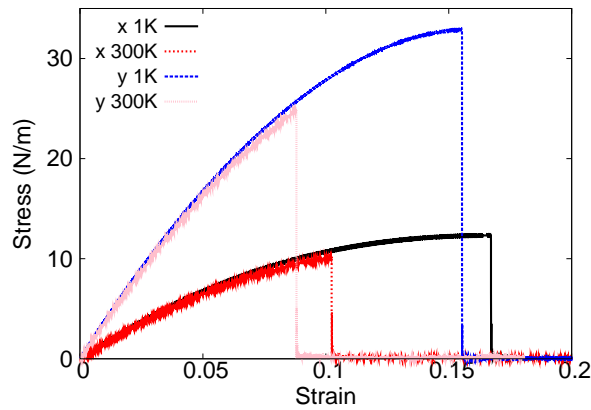


FIG. 275: (Color online) Stress-strain relations for the borophene of size  $100 \times 100 \text{ \AA}$ . The borophene is uniaxially stretched along the x or y directions at temperatures 1 K and 300 K.

Parameters for the SW potential used by LAMMPS are listed in Tab. [DXXXIII](#). We note that twelve atom types have been introduced for the simulation of borophene using LAMMPS, because the angles around atom 1 in Fig. [272](#) (a) are not distinguishable in LAMMPS. We thus need to differentiate these angles by assigning these six neighboring atoms (2, 3, 4, 5, 6, 7) with different atom types. Fig. [274](#) shows that twelve atom types are necessary for the purpose of differentiating all six neighbors around one B atom.

Fig. [275](#) shows the stress strain relations for the borophene of size  $100 \times 100 \text{ \AA}$ . The structure is uniaxially stretched in the x or y directions at 1 K and 300 K. The Young's

TABLE DXXX: The VFF model for borophene. The second line gives an explicit expression for each VFF term, where atom indexes are from Fig. 272 (a). The third line is the force constant parameters. Parameters are in the unit of  $\frac{\text{eV}}{\text{\AA}^2}$  for the bond stretching interactions, and in the unit of eV for the angle bending interaction. The fourth line gives the initial bond length (in unit of  $\text{\AA}$ ) for the bond stretching interaction and the initial angle (in unit of degrees) for the angle bending interaction. The angle  $\theta_{ijk}$  has atom i as the apex.

VFF type	bond stretching		angle bending	
expression	$\frac{1}{2}K_{14}(\Delta r_{14})^2$	$\frac{1}{2}K_{12}(\Delta r_{12})^2$	$\frac{1}{2}K_{134}(\Delta\theta_{134})^2$	$\frac{1}{2}K_{135}(\Delta\theta_{135})^2$
parameter	20.673	6.025	3.523	4.651
$r_0$ or $\theta_0$	1.614	1.880	64.581	99.318

TABLE DXXXI: Two-body SW potential parameters for borophene used by GULP,<sup>8</sup> as expressed in Eq. (3). The quantity  $(r_{ij})$  in the first line lists one representative term for the two-body SW potential between atoms i and j. Atom indexes are from Fig. 272 (a).

	$A$ (eV)	$\rho$ ( $\text{\AA}$ )	$B$ ( $\text{\AA}^4$ )	$r_{\min}$ ( $\text{\AA}$ )	$r_{\max}$ ( $\text{\AA}$ )
$r_{14}$	8.974	0.971	3.393	0.0	2.240
$r_{12}$	2.098	0.618	6.246	0.0	2.419

modulus is  $162.7 \text{ Nm}^{-1}$  and  $385.0 \text{ Nm}^{-1}$  in the x and y directions respectively at 1 K, which are obtained by linear fitting of the stress strain relations in  $[0, 0.01]$ . These values are in good agreement with the *ab initio* results at 0 K temperature, eg.  $170 \text{ Nm}^{-1}$  and  $398 \text{ Nm}^{-1}$  in Ref. 118, or  $166 \text{ Nm}^{-1}$  and  $389 \text{ Nm}^{-1}$  in Ref. 115, or  $163 \text{ Nm}^{-1}$  and  $399 \text{ Nm}^{-1}$  in Ref. 119. Previous *ab initio* calculations obtained negative Poisson's ratio for the uniaxial stretching

TABLE DXXXII: Three-body SW potential parameters for borophene used by GULP,<sup>8</sup> as expressed in Eq. (4). The first line  $(\theta_{ijk})$  presents one representative term for the three-body SW potential. The angle  $\theta_{ijk}$  has the atom i as the apex. Atom indexes are from Fig. 272 (a).

	$K$ (eV)	$\theta_0$ (degree)	$\rho_1$ ( $\text{\AA}$ )	$\rho_2$ ( $\text{\AA}$ )	$r_{\min12}$ ( $\text{\AA}$ )	$r_{\max12}$ ( $\text{\AA}$ )	$r_{\min13}$ ( $\text{\AA}$ )	$r_{\max13}$ ( $\text{\AA}$ )	$r_{\min23}$ ( $\text{\AA}$ )	$r_{\max23}$ ( $\text{\AA}$ )
$\theta_{134}$	32.074	64.581	0.971	0.618	0.0	2.240	0.0	2.419	0.0	2.419
$\theta_{135}$	23.668	99.318	0.618	0.618	0.0	2.419	0.0	2.410	2.240	3.047

TABLE DXXXIII: SW potential parameters for borophene used by LAMMPS,<sup>9</sup> as expressed in Eqs. (9) and (10). Atom types in the first column are displayed in Fig. 274.

	$\epsilon$ (eV)	$\sigma$ (Å)	$a$	$\lambda$	$\gamma$	$\cos \theta_0$	$A_L$	$B_L$	$p$	$q$	tol
B <sub>1</sub> -B <sub>5</sub> -B <sub>5</sub>	1.000	0.971	2.307	0.000	1.000	0.000	8.974	3.817	4	0	0.0
B <sub>1</sub> -B <sub>2</sub> -B <sub>2</sub>	1.000	0.618	3.914	0.000	1.000	0.000	2.098	42.820	4	0	0.0
B <sub>1</sub> -B <sub>2</sub> -B <sub>5</sub>	1.000	0.000	0.000	32.074	1.000	0.429	0.000	0.000	4	0	0.0
B <sub>1</sub> -B <sub>2</sub> -B <sub>4</sub>	1.000	0.000	0.000	23.668	1.000	-0.162	0.000	0.000	4	0	0.0

of the borophene in the x and y directions, e.g. -0.02 and -0.04 in Refs 118 and 115. The Poisson's ratio from the present SW potential are -0.03 and -0.07 along the x and y directions respectively, which are quite comparable with the *ab initio* results.

The third-order nonlinear constant ( $D$ ) can be obtained by fitting the stress strain relation to the function  $\sigma = E\epsilon + \frac{1}{2}D\epsilon^2$ , with  $E$  as the Young's modulus. The obtained values of  $D$  are -1100.1 Nm<sup>-1</sup> and -2173.6 Nm<sup>-1</sup> in the x and y directions, respectively. The ultimate stress is about 12.3 Nm<sup>-1</sup> at the critical strain of 0.17 in the x-direction at the low temperature of 1 K, which agree quite well with the *ab initio* results at 0 K.<sup>115,117,119</sup> The ultimate stress is about 32.9 Nm<sup>-1</sup> at the critical strain of 0.16 in the y-direction at the low temperature of 1 K, which are quite comparable with *ab initio* results at 0 K.<sup>115,117,119</sup>

#### CXXXIV. CONCLUSION REMARKS

As a final remark, we note some major advantages and deficiencies for the SW potential parameters provided in the present work. On the one hand, the key feature of the SW potential is its high efficiency, which is maintained by using minimum potential parameters in the present work, so the interaction range is limited to the first-nearest-neighboring atoms. As a result, the present SW potential parameters are of high computational efficiency. On the other hand, since the interaction is limited to short-range, the optical branches in the phonon spectrum are typically overestimated by the present SW potential. It is because we have ignored the long-range interactions, which contribute mostly to the acoustic phonon branches while have neglectable contribution to the optical phonon branches. The short-range interaction has thus been strengthened to give an accurate description for the acoustic

phonon branches and the elastic properties, which leads to the overestimation of the optical phonon branches as a trade off. Hence, there will be systematic overestimation for simulating optical processes using the present SW parameters.

We also note that the mathematical form of the SW potential is not suitable for the atomic-thick planar structures, such as graphene and b-BN, because the SW potential are not able to resist the bending motion of these real planar crystals.<sup>120,121</sup>

In conclusion, we have provided the SW potential parameters for 131 layered crystals. The supplemental resources for all simulations in the present work are available online in Ref. 1, including a fortran code to generate crystals' structures, files for molecular dynamics simulations using LAMMPS, files for phonon calculation with the SW potential using GULP, and files for phonon calculations with the valence force field model using GULP.

**Acknowledgements** The work is supported by the Recruitment Program of Global Youth Experts of China, the National Natural Science Foundation of China (NSFC) under Grant No. 11504225 and the start-up funding from Shanghai University.

---

\* Corresponding author: jiangjinwu@shu.edu.cn; jwjiang5918@hotmail.com

<sup>1</sup> <http://jiangjinwu.org/sw> .

<sup>2</sup> A. K. Geim and I. V. Grigorieva, *Nature* **499**, 419 (2013).

<sup>3</sup> P. Y. Yu, *Fundamentals of Semiconductors* (Springer, New York, 2010).

<sup>4</sup> F. H. Stillinger and T. A. Weber, *Physical Review B* **31**, 5262 (1985).

<sup>5</sup> J. Tersoff, *Physical Review Letters* **56**, 632 (1986).

<sup>6</sup> D. W. Brenner, O. A. Shenderova, J. A. Harrison, S. J. Stuart, B. Ni, and S. B. Sinnott, *Journal of Physics: Condensed Matter* **14**, 783 (2002).

<sup>7</sup> J.-W. Jiang, *Nanotechnology* **26**, 315706 (2015).

<sup>8</sup> J. D. Gale, *J. Chem. Soc., Faraday Trans.* **93**, 629 (1997).

<sup>9</sup> lammps, <http://www.cs.sandia.gov/~sjplimp/lammps.html> (2012).

<sup>10</sup> A. Stukowski, *Modelling and Simulation in Materials Science and Engineering* **18**, 015012 (2010).

<sup>11</sup> A. Kokalj, *Computational Materials Science* **28**, 155 (2003).

<sup>12</sup> C. Ataca, H. Sahin, and S. Ciraci, *Journal of Physical Chemistry C* **116**, 8983 (2012).

- <sup>13</sup> J.-W. Jiang, H. S. Park, and T. Rabczuk, *Journal of Applied Physics* **114**, 064307 (2013).
- <sup>14</sup> Y.-P. Zhou and J.-W. Jiang, *Scientific Reports* **7**, 45516 (2017).
- <sup>15</sup> J. L. Feldman, *Physical Review B* **25**, 7132 (1982).
- <sup>16</sup> E. B. Isaacs and C. A. Marianetti, *Physical Review B* **94**, 035120 (2016).
- <sup>17</sup> H. L. Zhuang, M. D. Johannes, M. N. Blonsky, and R. G. Hennig, *Applied Physics Letters* **104**, 022116 (2014).
- <sup>18</sup> D. Cakir, F. M. Peeters, and C. Sevik, *Applied Physics Letters* **104**, 203110 (2014).
- <sup>19</sup> M. M. Alyoruk, Y. Aierken, D. Cakir, F. M. Peeters, and C. Sevik, *Journal of Physical Chemistry C* **119**, 23231 (2015).
- <sup>20</sup> J.-W. Jiang, B.-S. Wang, J.-S. Wang, and H. S. Park, *Journal of Physics: Condensed Matter* **27**, 083001 (2015).
- <sup>21</sup> W. G. FlcMullan, thesis (1983).
- <sup>22</sup> N. Wakabayashi, H. G. Smith, and R. M. Nicklow, *Physical Review B* **12**, 659 (1975).
- <sup>23</sup> T. Liang, S. R. Phillpot, and S. B. Sinnott, *Physical Review B* **79**, 245110 (2009).
- <sup>24</sup> V. Varshney, S. S. Patnaik, C. Muratore, A. K. Roy, A. A. Voevodin, and B. L. Farmer, *Computational Materials Science* **48**, 101 (2010).
- <sup>25</sup> A. Kandemir, H. Yapicioglu, A. Kinaci, T. Cagin, and C. Sevik, *Nanotechnology* **27**, 055703 (2016).
- <sup>26</sup> A. Molina-Sánchez and L. Wirtz, *Physical Review B* **84**, 155413 (2011).
- <sup>27</sup> R. C. Cooper, C. Lee, C. A. Marianetti, X. Wei, J. Hone, and J. W. Kysar, *Physical Review B* **87**, 035423 (2013).
- <sup>28</sup> R. C. Cooper, C. Lee, C. A. Marianetti, X. Wei, J. Hone, and J. W. Kysar, *Physical Review B* **87**, 079901 (2013).
- <sup>29</sup> S. Bertolazzi, J. Brivio, and A. Kis, *ACS Nano* **5**, 9703 (2011).
- <sup>30</sup> S. Horzum, H. Sahin, S. Cahangirov, P. Cudazzo, A. Rubio, T. Serin, and F. M. Peeters, *Physical Review B* **87**, 125415 (2013).
- <sup>31</sup> W. Huang, H. Da, and G. Liang, *Journal of Applied Physics* **113**, 104304 (2013).
- <sup>32</sup> C. Sevik, *Physical Review B* **89**, 035422 (2014).
- <sup>33</sup> S. Kumar and U. Schwingenschlogl, *Chem. Mater.* **27**, 1278 (2015).
- <sup>34</sup> Z. Huang, W. Zhang, and W. Zhang, *Materials* **9**, 716 (2016).
- <sup>35</sup> J. Li, N. V. Medhekar, and V. B. Shenoy, *Journal of Physical Chemistry C* **117**, 15842 (2013).

- <sup>36</sup> H. Guo, T. Yang, M. Yamamoto, L. Zhou, R. Ishikawa, K. Ueno, K. Tsukagoshi, Z. Zhang, M. S. Dresselhaus, and R. Saito, *Physical Review B* **91**, 205415 (2015).
- <sup>37</sup> M. Kan, H. G. Nam, Y. H. Lee, and Q. Sun, *Phys. Chem. Chem. Phys.* **17**, 14866 (2015).
- <sup>38</sup> X. Gu and R. Yang, *Applied Physics Letters* **105**, 131903 (2014).
- <sup>39</sup> W. Huang, X. Luo, C. K. Gan, S. Y. Quek, and G. Liang, *Phys. Chem. Chem. Phys.* **16**, 10866 (2014).
- <sup>40</sup> P. Norouzzadeh and D. J. Singh, *Nanotechnology* **28**, 075708 (2017).
- <sup>41</sup> W.-X. Zhou and K.-Q. Chen, *Scientific Reports* **5**, 15070 (2015).
- <sup>42</sup> E. Torun, H. Sahin, S. Cahangirov, A. Rubio, and F. M. Peeters, *Journal of Applied Physics* **119**, 074307 (2016).
- <sup>43</sup> A. Mar, S. Jobic, and J. A. Ibers, *Journal of the American Chemical Society* **114**, 8963 (1992).
- <sup>44</sup> W. G. Dawson and D. W. Bullett, *Journal of Physics C: Solid State Physics* **20**, 6159 (1987).
- <sup>45</sup> B. E. Brown, *Acta Crystallographica* **20**, 268 (1996).
- <sup>46</sup> M. K. Jana, A. Singh, D. J. Late, C. Rajamathi, K. Biswas, C. Felser, U. V. Waghmare, and C. N. R. Rao, *Journal of Physics: Condensed Matter* **27**, 285401 (2015).
- <sup>47</sup> Y. C. Jiang, J. Gao, and L. Wang, *Scientific Reports* **6**, 19624 (2016).
- <sup>48</sup> L. Yu, Q. Yan, and A. Ruzsinszky, Preprint at <http://arxiv.org/abs/1701.06529> (2017).
- <sup>49</sup> Y. Li, J. Kang, and J. Li, *RSC Adv.* **4**, 7396 (2014).
- <sup>50</sup> G. Ding, G. Y. Gao, Z. Huang, W. Zhang, and K. Yao, *Nanotechnology* **27**, 375703 (2016).
- <sup>51</sup> W. Zhang, Z. Huang, W. Zhang, and Y. Li, *Nano Research* **7**, 1731 (2014).
- <sup>52</sup> J.-W. Jiang, T. Chang, X. Guo, and H. S. Park, *Nano Letters* **16**, 5286 (2016).
- <sup>53</sup> J. Kang, H. Sahin, and F. M. Peeters, *Phys. Chem. Chem. Phys.* **17**, 27742 (2015).
- <sup>54</sup> J. Chen, *Solid State Communications* **237-238**, 14 (2016).
- <sup>55</sup> Z. Zhu and D. Tomanek, *Physical Review Letters* **112**, 176802 (2014).
- <sup>56</sup> C. Kaneta, H. Katayama-Yoshida, and A. Morita, *Solid State Communications* **44**, 613 (1982).
- <sup>57</sup> Y. Du, C. Ouyang, S. Shi, and M. Lei, *Journal of Applied Physics* **107**, 093718 (2010).
- <sup>58</sup> G. Qin, Z. Qin, S.-Y. Yue, H.-J. Cui, Q.-R. Zheng, Q.-B. Yan, and G. Su, *Scientific Reports* **4**, 6946 (2014).
- <sup>59</sup> M. Elahi, K. Khaliji, S. M. Tabatabaei, M. Pourfath, and R. Asgari, *Physical Review B* **91**, 115412 (2014).
- <sup>60</sup> Z.-Y. Ong, Y. Cai, G. Zhang, and Y.-W. Zhang, *Journal of Physical Chemistry C* **118**, 25272

- (2014).
- <sup>61</sup> Y. Aierken, D. Cakir, C. Sevik, and F. M. Peeters, *Physical Review B* **92**, 081408 (2015).
- <sup>62</sup> J.-W. Jiang, *Nanotechnology* **26**, 055701 (2015).
- <sup>63</sup> A. Jain and A. J. H. McGaughey, *Scientific Reports* **5**, 8501 (2015).
- <sup>64</sup> S. Zhang, M. Xie, F. Li, Z. Yan, Y. Li, E. Kan, W. Liu, Z. Chen, and H. Zeng, *Angew. Chem. Int. Ed.* **55**, 1666 (2016).
- <sup>65</sup> J. Qiao, X. Kong, Z.-X. Hu, F. Yang, and W. Ji, *Nature Communications* **5**, 4475 (2014).
- <sup>66</sup> Q. Wei and X. Peng, *Applied Physics Letters* **104**, 251915 (2014).
- <sup>67</sup> J.-W. Jiang and H. S. Park, *Nature Communications* **5**, 4727 (2014).
- <sup>68</sup> D. Midtvedt and A. Croy, *Nanotechnology* **27**, 238001 (2016).
- <sup>69</sup> J.-W. Jiang, Preprint at <http://arxiv.org/abs/1605.02566v1> (2016).
- <sup>70</sup> Y. Xu, B. Peng, H. Zhang, H. Shao, R. Zhang, H. Lu, D. W. Zhang, and H. Zhu, Preprint at <http://arxiv.org/abs/1604.03422v1> (2016).
- <sup>71</sup> Z. Zhang, J. Xie, D. Yang, Y. Wang, M. Si, and D. Xue, *Applied Physics Express* **8**, 055201 (2015).
- <sup>72</sup> C. Kamal and M. Ezawa, *Physical Review B* **91**, 085423 (2015).
- <sup>73</sup> M. Zeraati, S. M. V. Allaei, I. A. Sarsari, M. Pourfath, and D. Donadio, *Physical Review B* **93**, 085424 (2015).
- <sup>74</sup> M. Yang and W.-M. Liu, Preprint at <http://arxiv.org/abs/1501.04350v1> (2016).
- <sup>75</sup> G. Wang, R. Pandey, and S. P. Karna, *ACS Appl. Mater. Interfaces* **7**, 11490 (2015).
- <sup>76</sup> G. Zheng, Y. Jia, S. Gao, and S.-H. Ke, *Physical Review B* **94**, 155448 (2016).
- <sup>77</sup> E. Akturk, O. U. Akturk, and S. Ciraci, *Physical Review B* **94**, 014115 (2016).
- <sup>78</sup> Y. Chen, Q. Sun, and P. Jena, *J. Mater. Chem. C* **4**, 6353 (2016).
- <sup>79</sup> G. Qin, Z. Qin, W.-Z. Fang, L.-C. Zhang, S.-Y. Yue, Q.-B. Yan, M. Hu, and G. Su, *Nanoscale* **8**, 11306 (2016).
- <sup>80</sup> H. Wiedemeier and H. G. von Schnering, *Zeitschrift für Kristallographie* **148**, 295 (1978).
- <sup>81</sup> A. K. Singh and R. G. Hennig, *Applied Physics Letters* **105**, 042103 (2014).
- <sup>82</sup> L.-C. Zhang, G. Qin, W.-Z. Fang, H.-J. Cui, Q.-R. Zheng, Q.-B. Yan, and G. Su, Preprint at <http://arxiv.org/abs/1505.04590> (2016).
- <sup>83</sup> X.-J. Ge, K.-L. Yao, and J.-T. Lu, *Physical Review B* **94**, 165433 (2016).
- <sup>84</sup> A. Ince and S. Erkoç, *Computational Materials Science* **50**, 865 (2011).

- <sup>85</sup> M. I. Baskes, *Physical Review B* **46**, 2727 (1992).
- <sup>86</sup> Q.-X. Pei, Y.-W. Zhang, Z.-D. Sha, and V. B. Shenoy, *Journal of Applied Physics* **114**, 033526 (2013).
- <sup>87</sup> J. F. Justo, M. Z. Bazant, E. Kaxiras, V. V. Bulatov, and S. Yip, *Physical Review B* **58**, 2539 (1998).
- <sup>88</sup> M. R. Chavez-Castillo, M. A. Rodriguez-Meza, and L. Meza-Montes, *RSC Adv.* **5**, 96052 (2015).
- <sup>89</sup> X. Zhang, H. Xie, M. Hu, H. Bao, S. Yu, G. Qin, and G. Su, *Physical Review B* **89**, 054310 (2014).
- <sup>90</sup> X. Li, J. T. Mullen, Z. Jin, K. M. Borysenko, M. B. Nardelli, and K. W. Kim, *Physical Review B* **87**, 115418 (2013).
- <sup>91</sup> E. Scalise, M. Houssa, G. Pourtois, B. van den Broek, V. Afanasev, and A. Stesmans, *Nano Research* **6**, 19 (2013).
- <sup>92</sup> N. J. Roome and J. D. Carey, *ACS Appl. Mater. Interfaces* **6**, 7743 (2014).
- <sup>93</sup> C. Yang, Z. Yu, P. Lu, Y. Liu, H. Ye, and T. Gao, *Computational Materials Science* **95**, 420 (2014).
- <sup>94</sup> B. Wang, J. Wu, X. Gu, H. Yin, Y. Wei, R. Yang, and M. Dresselhaus, *Applied Physics Letters* **104**, 081902 (2014).
- <sup>95</sup> H. Xie, M. Hu, and H. Bao, *Applied Physics Letters* **104**, 131906 (2014).
- <sup>96</sup> X. Gu and R. Yang, *Journal of Applied Physics* **117**, 025102 (2015).
- <sup>97</sup> L.-F. Huang, P.-L. Gong, and Z. Zeng, *Physical Review B* **91**, 205433 (2015).
- <sup>98</sup> Z. Wang, T. Feng, and X. Ruan, *Journal of Applied Physics* **117**, 084317 (2015).
- <sup>99</sup> H. Xie, T. Ouyang, E. Germaneau, G. Qin, M. Hu, and H. Bao, *Physical Review B* **93**, 075404 (2016).
- <sup>100</sup> Y. D. Kuang, L. Lindsay, S. Q. Shi, and G. P. Zheng, *Nanoscale* **8**, 3760 (2016).
- <sup>101</sup> B. Peng, H. Zhang, H. Shao, Y. Xu, and H. Zhu, Preprint at <http://arxiv.org/abs/1602.02266v1> (2016).
- <sup>102</sup> Q. Peng, X. Wen, and S. De, *RSC Advances* **3**, 13772 (2013).
- <sup>103</sup> M. A. Balatero, G. J. Paylaga, N. T. Paylaga, and R. V. Bantaculo, *Applied Mechanics and Materials* **772**, 67 (2015).
- <sup>104</sup> S. J. Zaveh, M. Roknabadi, and M. M. T. Morshedloo, *Superlattices and Microstructures* **91**,

- 383 (2016).
- <sup>105</sup> S. Mojumder, A. A. Amin, and M. M. Islam, *Journal of Applied Physics* **118**, 124305 (2015).
- <sup>106</sup> M. Modarresi, A. Kakoei, Y. Mogulkoc, and M. Roknabadi, *Computational Materials Science* **101**, 164 (2015).
- <sup>107</sup> M. J. Cherukara, B. Narayanan, A. Kinaci, K. Sasikumar, S. K. Gray, M. K. Chan, and S. K. R. S. Sankaranarayanan, *J. Phys. Chem. Lett.* **7**, 3752 (2016).
- <sup>108</sup> B. van den Broek, M. Houssa, E. Scalise, G. Pourtois, V. V. Afanasev, and A. Stesmans, *2D Mater.* **1**, 021004 (2014).
- <sup>109</sup> B. Peng, H. Zhang, H. Shao, Y. Xu, X. Zhang, and H. Zhu, *Scientific Reports* **6**, 20225 (2016).
- <sup>110</sup> H. Zhou, Y. Cai, G. Zhang, and Y.-W. Zhang, *Physical Review B* **94**, 045423 (2016).
- <sup>111</sup> D. Singh, S. K. Gupta, I. Lukacevic, and Y. Sonvane, *RSC Adv.* **6**, 8006 (2016).
- <sup>112</sup> L. Cheng, H. Liu, X. Tan, J. Zhang, J. Wei, H. L. J. Shi, and X. Tang, *Journal of Physical Chemistry C* **118**, 904 (2013).
- <sup>113</sup> H. Sahin, S. Cahangirov, M. Topsakal, E. Bekaroglu, E. Akturk, R. T. Senger, and S. Ciraci, *Physical Review B* **80**, 155453 (2009).
- <sup>114</sup> S. Demirci, N. Avazh, E. Durgun, and S. Cahangirov, *Physical Review B* **95**, 115409 (2017).
- <sup>115</sup> H. Wang, Q. Li, Y. Gao, F. Miao, X.-F. Zhou, and X. G. Wan, *New Journal of Physics* **18**, 73016 (2016).
- <sup>116</sup> M. Q. Le, B. Mortazavi, and T. Rabczuk, *Nanotechnology* **27**, 445709 (2016).
- <sup>117</sup> Z. Pang, X. Qian, R. Yang, and Y. Wei, Preprint at <http://arxiv.org/abs/1602.05370> (2016).
- <sup>118</sup> A. J. Mannix, X.-F. Zhou, B. Kiraly, J. D. Wood, D. Alducin, B. D. Myers, X. Liu, B. L. Fisher, U. Santiago, J. R. Guest, M. J. Yacaman, A. Ponce, A. R. Oganov, M. C. Hersam, and N. P. Guisinger, *Science* **350**, 1513 (2015).
- <sup>119</sup> Z. Zhang, Y. Yang, E. S. Penev, and B. I. Yakobson, *Advanced Functional Materials* **27**, 1605059 (2017).
- <sup>120</sup> M. Arroyo and T. Belytschko, *Physical Review B* **69**, 115415 (2004).
- <sup>121</sup> J.-W. Jiang, Z. Qi, H. S. Park, and T. Rabczuk, *Nanotechnology* **24**, 435705 (2013).